UiT The Arctic University of Norway

Faculty of health sciences

Department of medical biology

Biochemical characterization of Matrix Metalloproteinase-9

Binding interactions with two small non-peptide inhibitors and the proteoglycan serglycin

&

Processing of serglycin

Rangita Dawadi

A dissertation for the degree of Philosophiae Doctor, February 2020

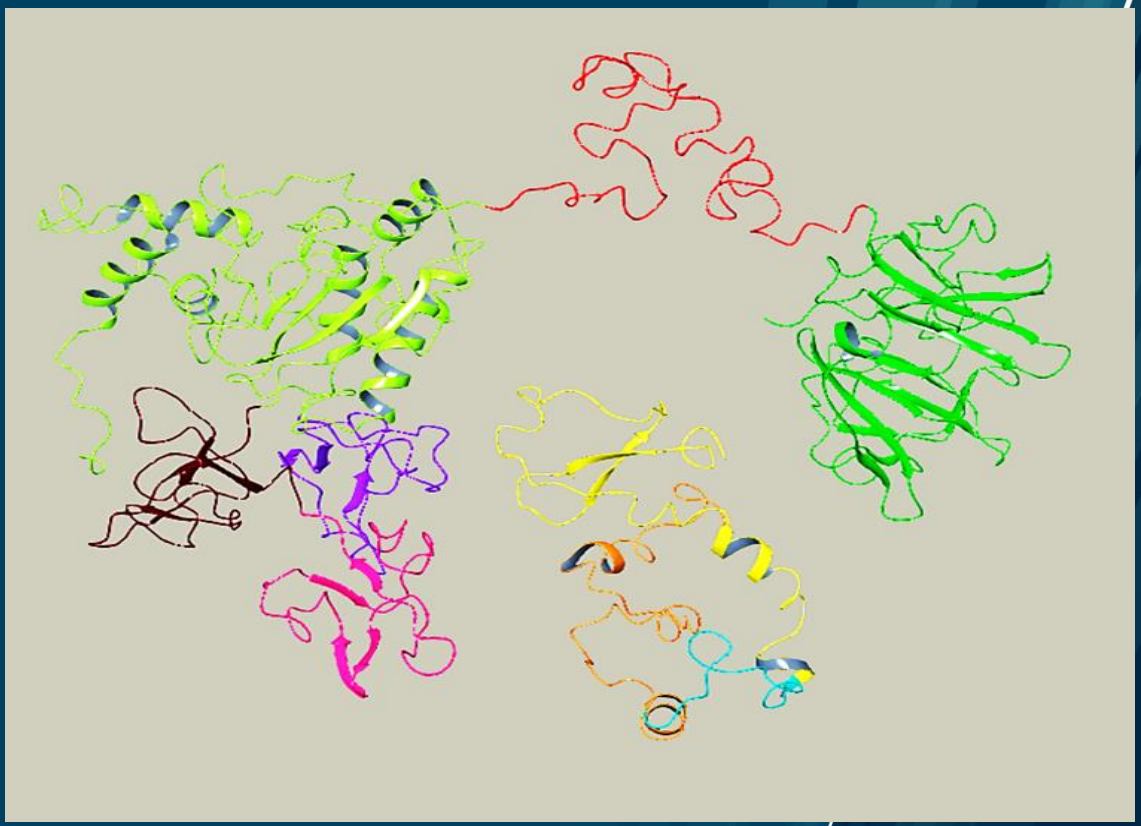

Biochemical characterization of Matrix Metalloproteinase-9

Binding interactions with two small non-peptide inhibitors and the proteoglycan serglycin

&

Processing of serglycin

By

Rangita Dawadi

A dissertation for the degree of Philosophiae Doctor

Tromsø, February 2020

Tumor Biology Research Group

Department of Medical Biology

Faculty of Health Sciences

UiT-The Arctic University of Norway

Title picture: Homology model of serglycin sandwiched between the two domains of full length MMP-9. Created with Maestro.

TABLE OF CONTENTS

Acknowledgements

Firstly, I would like to thank Norway and Norwegian people for inviting me into your beautiful country and giving this opportunity to pursue my educational ambitions. With this opportunity, I also got to experience both culture and environment so different yet so familiar to my own. Tromsø, you are beautiful and I will miss your ever-changing beauty and fierceness. People say if you can make it in New York, you can make it anywhere. I say if you can make it in the Arctic, you can make it anywhere. I tried. ☺

This work was carried out in the Tumor Biology Research group at the University of Tromsø starting from January 2016. I would like to give my regards to University of Tromsø for this opportunity.

My biggest acknowledgement goes to my main supervisor 'Joffe'. Your patience, humbleness and meticulousness with a combination of an immense knowledge and experience makes you an excellent supervisor. Thank you for your never-ending patience, even during the times when I have not given my best. Thank you for being like a guardian to me and always having your door open for any small questions and queries I had during these years. I would not have finished this work without your guidance so I really appreciate it.

Thank you to Gunbjørg, my co-supervisor. You have a very compassionate and optimistic nature and I appreciate that a lot. Your every suggestions be it work related or administrative or life related, all have been very helpful to me. Thank you very much for your support. I appreciate it.

I would also like to give my regards to my co-supervisor Ingebright Sylte. Your insights and valuable suggestions have really helped me to overcome any shortcomings I had regarding the molecular modelling part of the PhD study. Thank you for your constant support and positivity. Also thanks to Imin for teaching me the basics of molecular modelling and giving me the tips and tricks to tackle any problems I had during the last year of the PhD study. Thank you for making time for answering my questions and queries related to Maestro program.

My big appreciation to the TBG members for giving me such a supportive and encouraging environment to work and socialize. Eli, thank you for all your valuable help with the lab work and showing excitement for small things that happened in my life during these years. I have learnt a lot from you. Thank you to all the TBG members past and present. I really appreciate our chats and conversations of various kinds. One way or other, all of you have left an impact on me and I feel I have learnt something from all of you, mainly the work ethics, the balance of work and family and the value of teamwork. And thank you for the delicious friday cakes. *Tusen tusen takk.*

Dhanyawad to the Nepali community here in Tromsø for creating a home far away from home. Thankyou to all the friends I have made here in Tromsø. Thankyou Petja and Barbara, for letting me be the third Hamnanian ;). You guys rock!!

A big thanks to my soul sister Prapti. I wouldn't be in Tromsø if it wasn't for you. Literally!! Your encouragement and companionship has always kept me floating even during the times I felt like I was drowning.

Thanks to my Nepali gang: Priyanka, Shanti, Reeze, Dipesh, Swetadi, Roshanidi, Deepadi, Eman and Neha. So many delicious dinners, conversations and trips we shared together. Thank you guys for giving me this fun family.

My family!!! My life-support. Dhanyawad!!! Mummy and Buwa, I hope I can always carry the values and optimism that you two have passed down to me. Geetadi and Kriti, I hope we will never drift away

from each other and always have each other's back. The sisterhood we share is absolutely precious to me. Mahesh bhinaju and Suraj, you both are amazing additions to the family. Amogh, you are the best gift to our family and I am super proud to be your Hana. Thank you all for supporting me through thick and thin.

Lastly, to the love of my life, Salvador. You have nourished me with your delicious food and electric mind. Your vast knowledge makes me want to know more about the world. Thank you for sharing all those crazy trips, those late-night life-searching conversations and sharing this excitement for the future ahead - a life full of curiosity and creativity. I found my best companion to share this wild adventure called LIFE. *Obrigada e Adoro-te*.

Tromsø, February 2020

Rangita Dawadi

List of Papers

Paper I

Rangita Dawadi, Nabin Malla, Beate Hegge, Imin Wushur, Eli Berg, Gunbjørg Svineng, Ingebrigt Sylte, Jan-Olof Winberg.
Motifs and amino acids involved in the formation of complexes between pro-matrix metalloproteinase-9 and the proteoglycan serglycin core protein.
Manuscript

Paper II

Ingebrigt Sylte, Rangita Dawadi, Nabin Malla, Susannah von Hofsten, Tra-Mi Nguyen, Ann Iren Solli, Eli Berg, Olaylwola A. Adekoya, Gunbjørg Svineng, Jan-Olof Winberg (2018)**The selectivity of galardin and an azasugar-based hydroxamate compound for human matrix metalloproteases and bacterial metalloproteases.** PLoS ONE 13(8):e0200237. doi: 10.1371/journal.pone.0200237.eCollection 2018.

Paper III

Rangita Dawadi, Nabin Malla, Beate Hegge, Eli Berg, Gunbjørg Svineng and Jan-Olof Winberg
The Proteoglycan Serglycin is cleaved by Matrix Metalloproteinase-9
Manuscript

Abbreviations

ECM	- Extracellular Matrix
CD44	- Cluster of Differentiation 44
PG	- Proteoglycan
CSPG	- Chondroitin Sulfate proteoglycans
CS	- Chondrotin Sulfate
KS	- Keratin Sulfate
DS	- Dermatan Sulfate
HS	- Heparan Sulfate
SG	- Serglycin
GAG	- Glucosaminoglycan
THP-1	-Tamm-Horsfall Protein 1
MMP	- Matrix Metalloproteinase
TIMP	-Tissue Inhibitor of Matrixmetalloproteinase
HPX	- Hemopexin
FnII	- Fibronectin II
IL	- Interleukin
TNF	- Tumour Necrosis Factor
CNS	- Central Nervous System
mRNA	- Messenger Ribonucleic acid

DNA	- Deoxyribonucleic acid
SAXS	- Small Angle X-ray Scattering
AFM	- Atomic Force Microscopy
RECK	- Reversion inducing cysteine-rich protein with kazal motifs
HCLO	- Hypochlorous acid
APMA	- Amino phenyl mercury acetate
MI	- Myocardial Infarction
CAMs	- Cell Adhesion Molecules
BDNF	- Brain Derived Neurotropic Factor
NGF	- Nerve Growth Factor
GCP	- Granulocyte Chemotactic Protein
ENA	- Epithelial cell-derived neutrophil-activating peptide
B-CLL	- B-cell Lymphocytic Leukemia
DMP1	- Dentin matrix protein-1
SIBLINGs	- Small Integrin-Binding Ligands N-linked Glycoproteins
GPI	- Glycosylphosphatidylinositol
TPA	- Tissue Plasminogen activator
LPS	- Lipopolysaccharides
SDS-PAGE	- Sodium Dodecyl sulfate-plyacrylamide gel electrophoresis
NEM	- N-Ethylmaleimide
IA	- Iodacetate

EDTA	- Ethylenediaminetetraacetic acid
DMSO	- Dimethyl sulfoxide
NaCl	- Sodium chloride
PMA	- Phorbol 12-myristate 13-acetate
DMP	- Dimethylpimelimidate dihydrochloride
DTT	- Dithiothreitol
MDPF	- 2-Methoxy-2,4-diphenyl -3(2H)-furanone
UV	- Ultra violet
PVDF	- Polyvinylidene fluoride
OPLS3e	- Optimized potentials for liquid simulations
cABC	- Chondroitinase ABC
MD	- Molecular dynamics

Abstract

The present work has a focus on biochemical characterization of the human matrix metalloproteinase-9. One part of the investigation focuses on the enzymes ability to form a complex with the small proteoglycan serglycin. Previous studies showed that these two macromolecules form a very strong complex that is SDS-stable and reduction sensitive. Here, the focus was on which amino acids and regions in both proMMP-9 and serglycin are important for the complex formation. To obtain that, recombinant full-length proMMP-9 and various deletion variants of proMMP-9 were produced and purified. Serglycin was produced and purified from the monocytic cell line THP-1. *In vitro* reconstitution assays with the various proMMP-9 variants and serglycin have been performed to determine which domains of MMP-9 is involved in the complex formation. To get a further insight into which motifs and amino acids in these two macromolecules that interact, peptide arrays, homology modelling, protein-protein docking and molecular dynamic studies have been performed. The *in vitro* reconstitution studies showed that removing both the FnII module and the HPX domain from MMP-9 prevented the complex formation with serglycin. However, it was enough with one of these two regions present in order to form the complex. In serglycin, the chondroitin sulphate (CS) chains were not involved in the complex formation with the protease. Peptide arrays, docking and molecular dynamic simulations indicated that two blades in the FnII module, blade 1 and blade 2 interacted with the core protein of serglycin. This interaction involved the part of the FnII module that binds gelatin, which fits with a previous study that showed that gelatin inhibits the complex formation between proMMP-9 and serglycin. The present study also indicated that the FnII module interacted at the same time with two regions in serglycin, one in the N-terminal part and the other in the C-terminal part of this short core protein (131 amino acids). Of the four blades that make up the HPX domain in MMP-9, it was mainly blades III and IV that were involved in the interaction with serglycin. Another interesting finding was that proMMP-9, which is a very flexible protein could sandwich the serglycin core protein between the FnII module and the HPX domain. These studies also indicated that the forces that keep the two macromolecules together was a mixture of ionic and hydrophobic interactions along with hydrogen bonds.

The second study in this PhD thesis has a focus on the catalytic site in MMP-9. To which extent will different N- and C-terminal ends of the activated enzyme affect the enzymes binding of small non-peptide inhibitors and cleavage of a short quenched fluorescence substrate. In this study a recombinant full-length proMMP-9 variant produced in insect cells and proMMP-9

produced in THP-1 cells were used. The purified recombinant proMMP-9 was activated with the mercurial compound para-aminophenylmercuric acetate (APMA) as well as with the two enzymes trypsin and matrix metalloprotease-3 (MMP-3). The two enzymes removed the entire pro-domain from the enzyme and generated an identical N-terminal end. In the case of APMA, a part of the pro-domain remain bound to the enzyme. In all three cases, a large part of the C-terminal HPX domain was removed and all three activated forms was fully active. ProMMP-9 from THP-1 cells was activated with trypsin and had the same N-terminal end as the recombinant MMP-9 activated with trypsin and MMP-3. The main difference was that the C-terminal HPX domain remained intact. In spite of different N- and C-terminal ends, the K_m value for the small fluorescence quenched substrate was the same for all four MMP-9 variants. All four variants were tested for their ability to bind two slow tight binding inhibitors, galardin and an azasugar based hydroxamate compound, compound **1b**. The binding strength of galardin was approximately the same for all four activated variants of MMP-9 (51-69pM) indicating that the differences in N- and C-terminal residues did not affect the binding. Compound **1b** bound even stronger (6-11pM). The two hydroxamate inhibitors bound stronger to the various activated variants of MMP-9 than to human MMP-14 and to three bacterial metalloprotease, thermolysin, pseudolysin and auerolysin. Compound **1b** did not inhibit the three bacterial metalloproteases. Molecular modelling was used to determine why the two compounds bound with different strength to the enzymes. It was the shape and volume of the enzymes S'_1 subpocket that mainly determined the binding, and the size of the inhibitor moiety that entered the pocket.

A previous study and the present study of the complex formation between proMMP-9 and serglycin has indicated that serglycin is a likely substrate for MMP-9. The third study in this PhD thesis has focused on this and investigated whether an active MMP-9 can cleave the serglycin core protein. Will the presence or absence of bound CS-chains have an effect and will sites outside the catalytic site in MMP-9 (exosites) be of importance? Various activated variants of full-length MMP-9 and truncated variants of the enzyme were used. These were tested on a commercial his-tagged serglycin (Ht-SG) produced in E-Coli and hence lacked CS-chains. An active MMP-9 was also tested on intact and cABC treated serglycin from THP-1 cells. cABC degrades CS-chains and leaves a short stub on the core protein. Either SDS-PAGE or Western blotting determined the degradation products. It was shown that MMP-9 cleaves the serglycin core protein in the presence of intact CS-chains as well as in the presence of a short stub of CS-chains. In the Ht-SG, MMP-9 cleaved the core protein at several places generating several

cleavage products. In contrast to this, in the presence of CS-chains or a short CS-stub the active MMP-9 only generated a single cleavage product of approximately 10 kDa that lacked CS-chains. Thus, the presence of CS-chains affected where MMP-9 can process the core protein. The 10 kDa product without CS-chains was further cleaved by MMP-9. Furthermore, cleavage of Ht-SG by the various deletion variants of MMP-9 suggested that there is an exosite in the HPX domain presenting the serglycin to the active site of the enzyme. This is not the case for the degradation of the small quenched fluorescence substrate or the binding of the two hydroxamate compounds to MMP-9. Even if the full-length MMP-9 is extremely flexible, a certain size of a substrate or a substrate competitive inhibitor seems to be required for the HPX domain to be involved in presenting substrates or inhibitors to the catalytic site.

1. Introduction

1.1. Extracellular matrix environment

Our bodies are compositions of cells resulting in tissues and further tissues into organs. Moreover, to create this composition, extracellular matrix provides the perfect platform, as, not just a structural support, but also support for growth, migration, differentiation, survival, homeostasis and morphogenesis of millions of cells. The ECM comprises of a variety of matrix macromolecules, however, the major constituents are collagens, elastin, fibronectins, laminins, glycoproteins, proteoglycans and glycosaminoglycans, which are all fibrous-forming proteins [1]. Based on the composition and structure, ECMs can be classified into two major types, which are: the **interstitial,** that surrounds the cells and **pericellular,** that are in close contact with the cells. Basement membrane is a type of pericellular matrices found between parenchyma and connective tissues, where it acts as an anchor for parenchymal cells to be held together. Typically, basement membranes are composed of collagens which are also the most abundant proteins present and are mostly of type IV, XV and XVIII [2]. Apart from collagens, basement membranes also contains proteins such as laminins, nidogen 1 and 2, and the proteoglycans perlecan and agrin [1]. All these components provide bulk, shape and strength to the basement membrane. Various proteins have the capability of determining the behaviours, polarity, migration, differentiation, proliferation as well as survival of various cells and this is made possible via the intercellular communication and transmission of, for example growth factor signals, chemokines and cytokines [3]. For the free cellular movement and tissue remodelling in various physiological and pathological conditions, the controlled degradation of ECM is necessary, which is carried out vastly by various proteases such as matrix metalloproteases together with heparanases [3].

1.2. Proteoglycans and Glycosaminoglycans

Proteoglycans (PG) interact with various structural molecules in the ECM such as collagen, laminins, fibronectins, fibrin, elastin, fibrillin, hyaluronic acid as well as with the cell surface receptors CD44, epidermal growth factor receptor, intergins and selectins. All these interactions take place either through their core proteins or through the GAG chains present on their core proteins [4]. Proteoglycans are found both intracellularly, such as serglycin (SG) and extracellularaly, such as versican. Some PGs can also be found in the cell membrane due to the presence of a transmembrane domain in their core proteins, such as syndecans [5]. However,

these are all highly negatively charged molecules and are present in various forms ranging from tissue specific to cell-type specific [6, 7]. This diverse range of molecules represent different combinations of various core proteins with variety of GAG chains which are attached to them via serine residues [5]. GAGs are unbranched, linear glycosamine containing disaccharides in repeating order, which are negatively charged. This negative charge of GAGs contribute to the negative charge of PGs as well. Whichever proteoglycans GAGs are attached to, their biochemical behaviours are controlled by GAGs, which gives PGs similar fractionation properties [8]. In addition to that, since the PGs are mostly extracellular, their functions depend not just on their structure but also on the availability of various growth factors and receptors. This is because they are crucial for many signalling cascades, which, in turn can affect myriad of intracellular events that are driven by growth factors and receptors[5].

GAGs are generally divided into two different groups depending on their sulfation: 1) sulfated GAGs such as chondroitin sulfate (CS), keratin sulfate (KS), dermatan sulfate (DS), heparin, heparan sulfate (HS); and 2) non sulphated GAGs such as Hyaluronan [5]. In most animals, there are two types of GAG chains present; heparan sulphate (HS) and chondroitin sulphate (CS) and depending on which GAG is attached to various PGs, they can be called CSPG or HSPG. All the GAGs have the ability of interacting with various plasma proteins such as growth factors, cytokines, chemokines, proteases, protease inhibitors, coagulant and anticoagulant proteins, complement proteins, lipoproteins and lipolytic enzymes [9].

Functionally proteoglycans can be divided into those which are mediated by the core proteins and those which are primarily mediated by GAG chains [8]. Proteoglycans keep various tissues in our body healthy by ensuring their proper structural development, organization and hydration. Proteoglycans also exercise some functional effects to these tissues through interaction with various matrix structures, cells and cellular mediators. In a pathogenic state of a body, like in tumors, the proteoglycan expression is modified by the tumor cells, leading to facilitation of tumorigenesis through angiogenesis as well as changes in growth, and migration of tumor cells [10].

There is an estimation that there could be as many as 1 million syndecan-1 molecules at the surface of the epithelial cells. Syndecan is one of many proteoglycans and from this, we can take a hint that these molecules are found in abundance in our body. So, because of this abundancy, and their capability of binding proteins, it has been speculated that there is a high chance of their involvement in various molecular interactions at the cell-surface, such as; cell-matrix, cell-cell, or ligand-receptor interactions [11].

1.3. Chondrotin Sulfate Proteoglycans

The CS proteoglycans are involved in the proper organization of the ECM by working as key mediators, with an additional contribution to cell signalling [12]. Various leukemic monocyte cell lines such as THP-1, MonoMac and U937 produce various CSPGs. All three produce SG, glypican, syndecans -1, and -4. In addition to that, THP-1 and MonoMac both produce veriscan and perlecan as well. However, it has been shown from studies that the main CSPG produced by THP-1 monocytes is SG [13-15].

1.3.1. Serglycin

SG is a proteoglycan that is normally referred as an intracellular proteoglycan, however, it has been well established that SG acts more as a secretory product therefore having the ability to be incorporated into the ECM quite easily [6]. SG is expressed mainly in the secretory granules and vesicles in nucleated hematopoietic cells such as; neutrophils, lymphocytes, platelets, mast cells and megakaryocytes. Studies have also shown its presence in endothelial cells, uterine decidua, and embryonic stem cells [5, 16, 17]. However, SG has not been found to be stored in monocytes and macrophages, rather, they are constitutively secreted. Following inflammatory stimulation of these cells, SG secretion was shown to be increased, together with increase in the sulfation of the CS chains attached to it. The reason for this increase of SG might be due to its increased need in these inflammatory sites or due to increased in secretion of ligands that bind to SG. In addition, the increased sulfation pattern has been linked to the inflammatory conditions [6, 18].

As shown in **figure 1**, the structure of human SG comprises of a core protein of 17.6 kDa containing a 16-amino acid (Ser-Gly) repeat region where the glycosaminoglycan chains especially HS-chains (in case of connective tissue mast cells) or CS-chains (mucosal mast cells, monocytes and macrophages) are attached. In other species such as rat and mouse, this Ser-Gly repeat region is longer than human SG, where rat having the longest with 49 Ser-Gly repeats [17]. In cells like mast cells, SG is involved in storage and packaging of various cell mediators in storage granules and vesicles for secretion. Once they are secreted, SG is then involved in modulating activities of binding partners by either/or protecting, transporting, activating and interacting with target cells in the ECM [19]. In addition to that, SG is involved in homeostasis of secretory granules, apoptosis, blood coagulation and retention of major inflammatory mediators inside storage granules and secretory vesicles [6, 17]. When secreted from macrophages and platelets, SGs have been suspected to expedite transportation of chemokines

to the inflammatory sites [16]. The CS present in the SG with higher molecular mass compared to other GAGs such as HS, are efficient in inhibiting lysozyme activity [16].

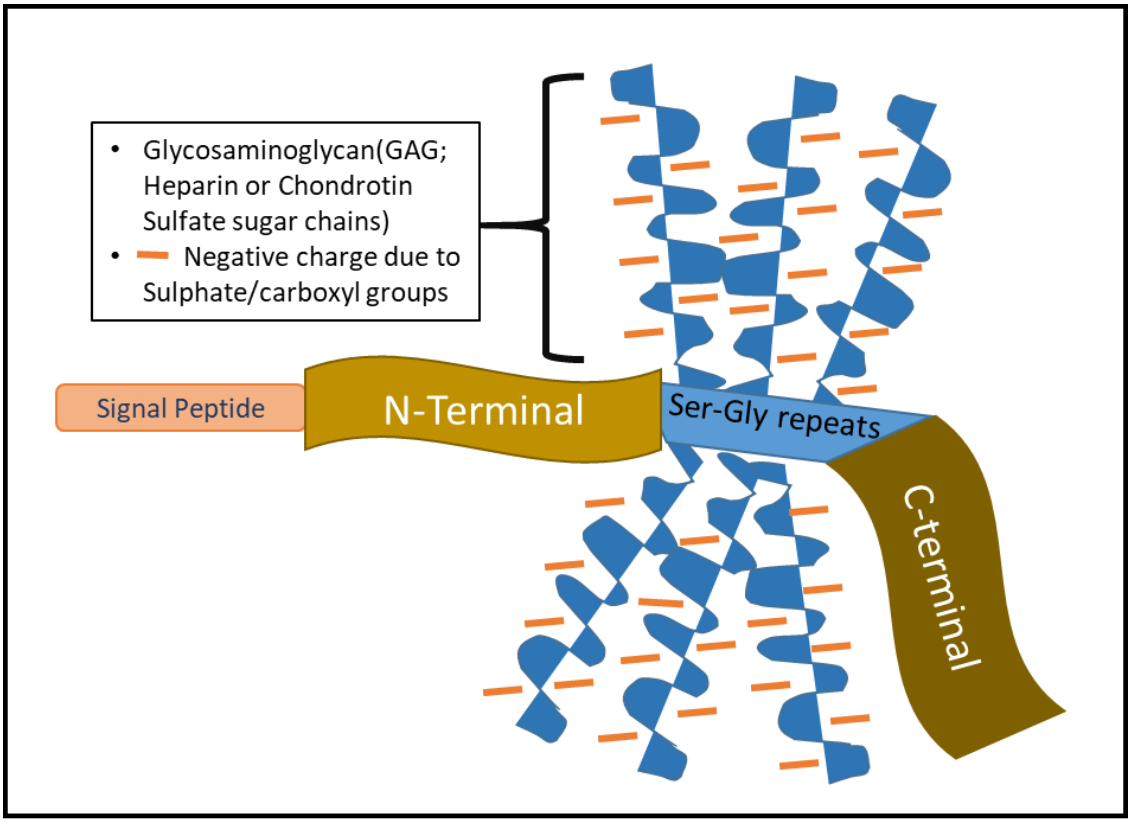

Fig.1. Structure of full-length SG. The full-length SG is composed of a signal peptide attached to the core-protein with the N-terminal region and C-terminal region with Ser-Gly repeat zone in between containing the negatively charged CS chains.

When expressed by different cells, SG has a unique ability of adopting highly divergent structures by glycosylation with help of different GAGs [20]. In pathological states, SG is expressed by many human leukaemia cells such as THP-1 and U-937. It is also expressed prominently in immature promyelocyte as well as myelocyte cells in bone marrow. Because of this high expression in leukemic cells, it can be used as a major biomarker for various human myeloid leukemia. In addition to that, it has also been linked with epithelial-mesenchymal transition in tissue samples of metastatic nasopharyngeal cells [17, 21, 22]. SG is highly expressed in human hematopoietic tumors as well as in non-hematopoietic tumors, and the expression has been found to be essential for metastatic growth and dispersion [19, 20]. In various diseased states, SG appears to act as a modulator within the complex tumor microenvironment where it appears to mediate interactions between tumor cells and the tumor microenvironment [23, 24]. Another study also shows that SG can be a potential prognostic

marker for glioma, as the level of SG expression is directly correlated with the human glioma malignancy grade, where the mast cells act as modulators of SG expression [20].

1.4. Proteolytic enzymes

Every single protein present in our body has to go through proteolysis, which takes place in different ways ranging from degradation of a protein into small fragments to cleavage of the pro-peptide leading to its activation [25]. Peptidases/Proteinases or proteolytic enzymes carry out proteolysis, an irreversible process, by hydrolysing the peptide bonds that make up a protein [25]. Based on this, proteinases can be divided into endopeptidases or exopeptidases depending upon the position in the target protein chain where the hydrolysis takes place. Endopeptidases cleave/hydrolyse the peptide bond within the protein structure while exopeptidases cleave proteins from the terminal ends of their peptide bonds.

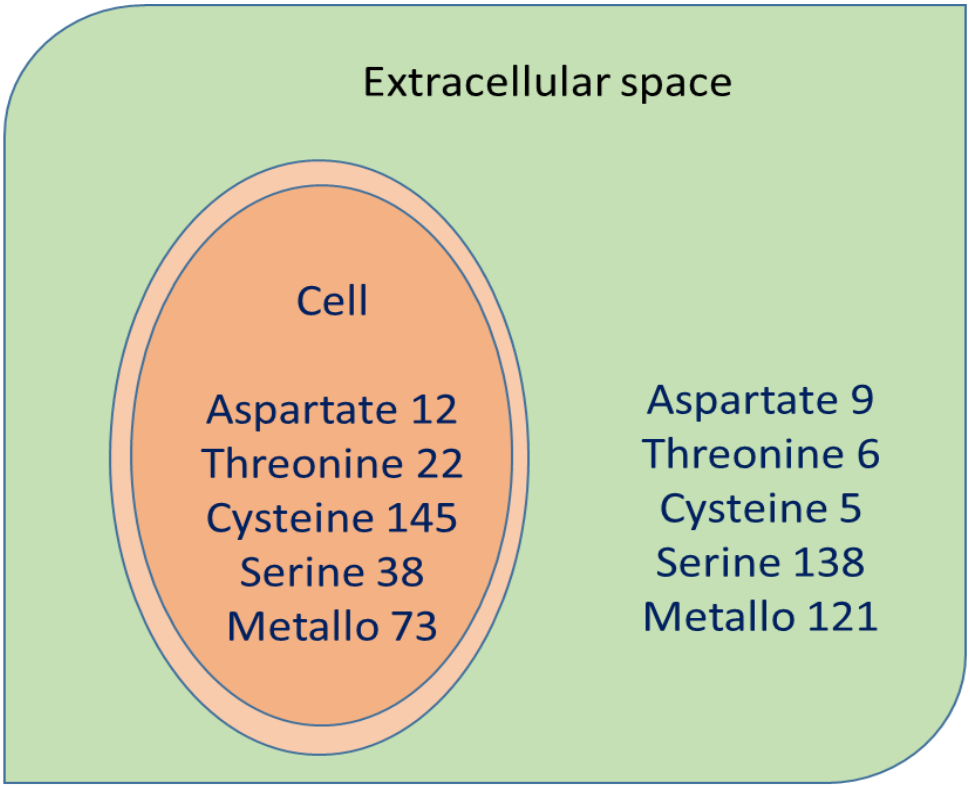

Fig.2. Cellular localization of the various classes of human proteases.

As seen in **figure 2 (**Modified from [26]**)** , there are at least 569 proteinases in humans as which are classified into two categories depending on where they are predominant. They are intracellular and extracellular types. There are 279 extracellular proteinases and 290

intracellular types. Of the intracellular localized proteases, 16 are estimated to be present within membranes [26]. Both extracellular and intracellular proteinases can be further divided into five different classes of proteinases. This division is based on the presence of chemical group/amino acid that participates in the hydrolysis of the peptide bonds as represented in **figure 3** (Figure modified from [27]). Aspartate, threonine and cysteine proteinases are commonly active intracellulary, at acidic environments, while serine and metalloproteinases are predominantly active extracellularly and at neutral pH [27]. For example; matrix metalloproteinases (MMPs) exhibit optimal proteolytic activity around pH 7.00 to 8.00 for most substrates with few exceptions where pH range is broader [28].

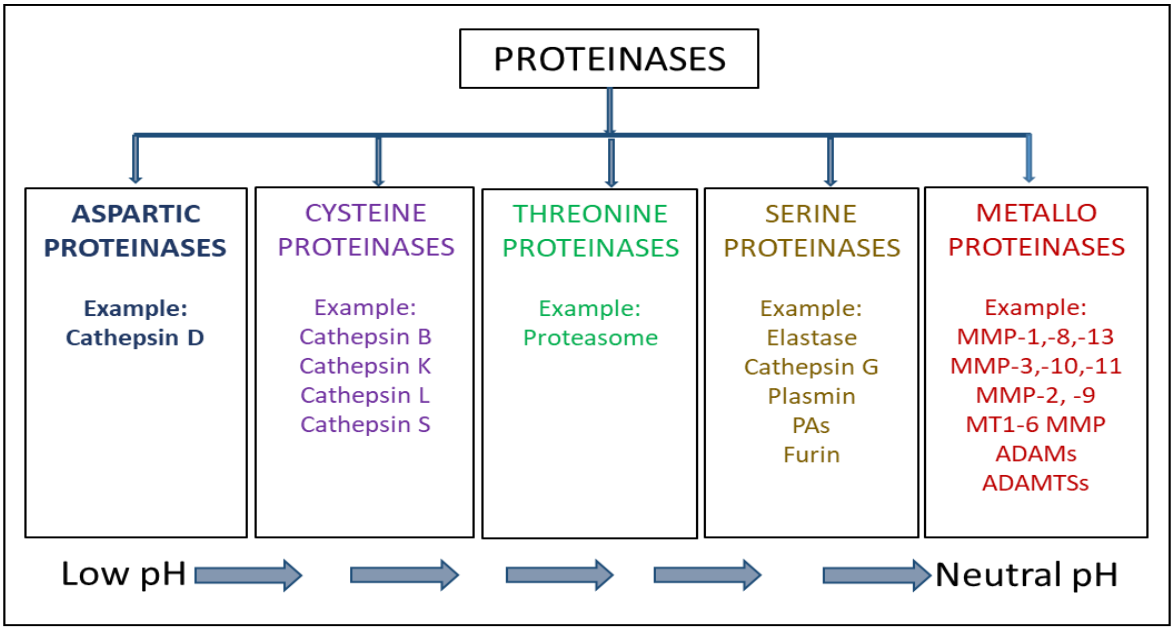

Fig.3. Five classes of proteinases with examples in each class and their pH sensitivity. These five classes are based on the presence of chemical group or amino acid residues that are involved in the hydrolysis of the peptide bonds in different extracellular and intracellular proteins.

1.4.1. Matrix Metalloproteinases (MMP): Structure and Classification

MMPs also called as matrixins are calcium and zinc dependent endopeptidases involved in the degradation and remodelling of various molecules in the ECM. These are multidomain proteins, organized into subgroups based on common domains and other motifs or based on shared substrates [29]. There are in total 23 human MMPs, which are numbered according to the chronology of their discovery and out of the 23 MMPs, MMP-4, -5,-6 and 22 are removed from the list as they have been found to be identical to other MMPs. They are classified based on the difference in their structures and main substrate preferences (**Fig.4.** Figure modified from [30])

[31]. The MMPs are made up of three basic and distinctive domains which are: an amino-terminal pro-peptide, a catalytic domain and a hemopexin-like domain at the carboxy-terminal end [30].

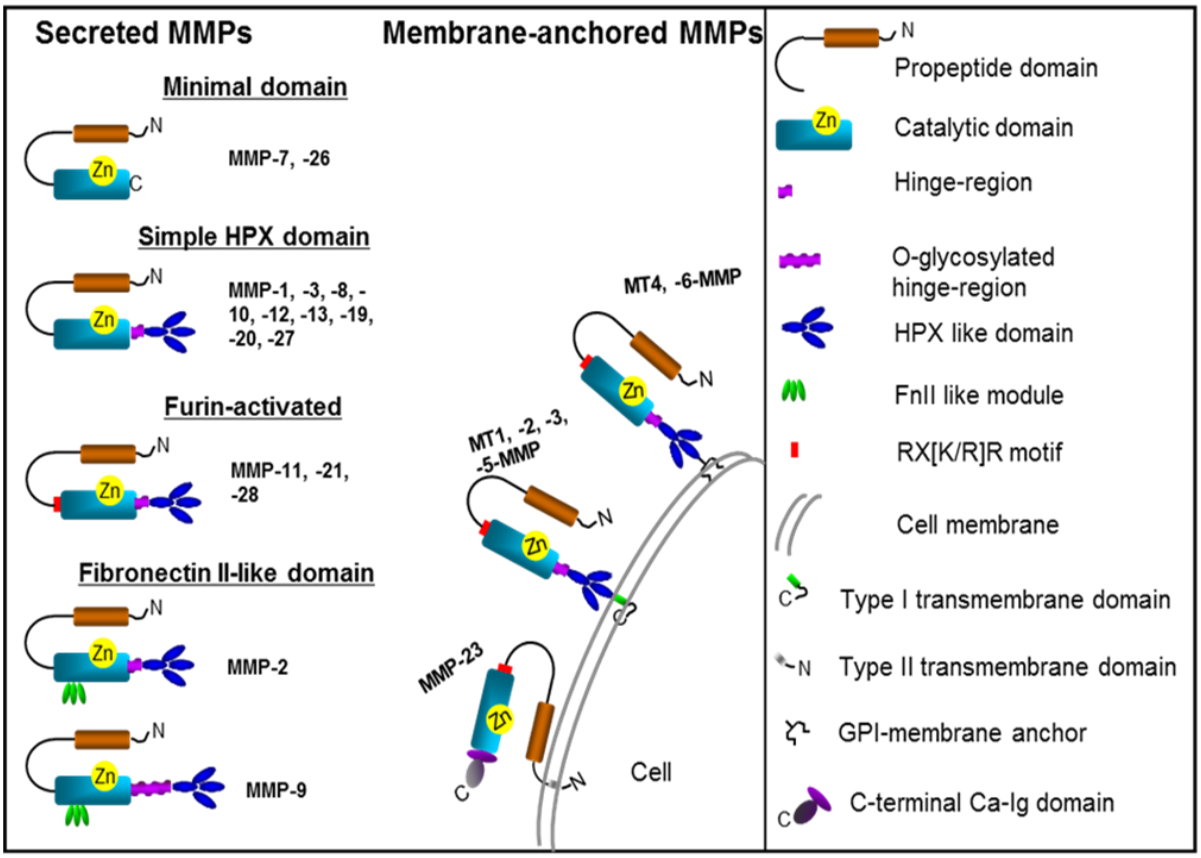

Fig. 4. Different MMPs with their domain structures. Almost all the MMPs contain four main components to their structures: propeptide domain, catalytic domain, hinge region and a HPX domain. MMPs lacking both the hinge and the hemopexin region are MMP-7 and -26. Despite most of the MMPs containing a hinge region, only MMP-9 has a heavily O-glycosylated hinge region. Only MMP-2 and MMP-9 contain a fibronectin module containing three fibronectin like repeats in the catalytic domain. The membrane-anchored MMPs and the three furin activated MMPs contain a motif called as RX(K/R)R motif at the C-terminal end of the prodomain.

In addition to these three domains, all inactive MMPs contain N-terminal signal peptide, which is cleaved off while they are in the endoplasmic reticulum, before they are secreted out of the cells [32]. The pro-peptide is made up of approximately 80-90 amino acids where a conserved motif containing a cysteine residue is present. This motif is called ‘’cysteine switch’’ and it is responsible for blocking the active site and thus maintaining the zymogen forms, or the latent forms of MMPs (proMMPs) [28]. The cysteine (PRCGV) in the pro-domain binds to the

catalytic zinc ion in the catalytic domain of the MMPs and hence a part of the pro-domain blocks the active site keeping the enzyme inactive. During activation, the pro-domain is physically removed and water molecule binds to the catalytic zinc ion [33]. In membrane-anchored MMPs, and three of the secreted MMPs, there is an additional proprotein processing motif called RX(K/R)R present in the C-terminal end of the pro-peptide (**Fig.4**.). This pro-peptide is cleaved by furin intracellularly, leading to activation of these MMPs. The catalytic domain has about 170 amino acids and contains two zinc ions (one is catalytic and the other is a structural), and three calcium ions. The catalytic zinc is bound to three histidines (imidazole side chain) in the HEXGHXXGXXH motif. The three calcium ions and the structural zinc ion are important for the stability and the expression of MMP activity [28, 34]. MMP-2 and -9 out of other MMPs are distinguishable due to presence of three fibronectin like repeats present in the catalytic domain. These repeats are responsible for interaction with collagens, gelatins and laminins [28].

Almost all MMPs contain a COOH-terminal hemopexin-like domain (HPX domain) except MMP-7, -23 and -26. The name of HPX domain is based on the similarity of its sequence with the sequence of the plasma protein hemopexin. It consists of about 190 amino acids and is attached to the catalytic domain through the hinge region. Structurally, the HPX domain is composed of a four bladed β-propellers, and its stability is maintained by the presence of a calcium ion and a disulphide bridge between blades I and IV [28]. Functionally, in the collagenases (MMP-1, MMP-8, and MMP-13) the presence of these blades are needed in order for these enzymes ability to cleave triple helical interstitial collagens [34, 35]. The HPX domains are highly conserved and functionally important for substrate binding, and in MMP-2 and MMP-9, the HPX domain also interacts with tissue inhibitors of MMPs (TIMPs) [27, 34, 35]. Furthermore, MMPs can also be divided into six groups based on the substrate specificity and homology as seen in **table 1**.

Even though initially the naming and classification of MMPs was based on their primary substrate specificity, we must acknowledge that, an immense amount of recent studies support the fact that all MMPs in general have broad substrate specificity and their functions are no longer limited to just the degradation of ECM. Recently, they have been recognized for both intracellular and extracellular activities ranging from signal transduction and transcription factor activity inside the cells, and as regulators of various bioactive molecules such as chemokines and cytokines in the ECM [36].

Table 1. Classification of MMPs based on substrate specificity [37, 38].

Class based on primary substrate	MMP name	Common name/ Descriptive name	Substrates
Collagenases	MMP-1	Collagenase-1 /	Aggrecan, nidogen, perlecan, versican casein, ovostatin, etc
	MMP-8	Collagenase-2 /	Aggrecan, elastin, fibronectin, laminin, etc
	MMP-13	Collagenase-3	Aggrecan, fibronectin, laminin, perlecan, casein, plasminogen activator 2, etc
	MMP-18	Collagenase 4	A1-antitrypsin
Gelatinases	MMP-2	Gelatinase-A	Aggrecan, elastin, fibronectin, laminin, THF-β, IL-1β, etc
	MMP-9	Gelatinase-B	Aggrecan, elastin, laminin, nidogen, versican, plasminogen, TGF-β, etc
Stromelysins	MMP-3	Stromelysin-1	Elastin, laminin, perlecan, casein, decorin, antithrombin III, TNF-α, etc
	MMP-10	Stromelysins-2	Elastin, fibronectin, laminin, casein, nidogen, etc
	MMP-11	Stromelysins-3	Fibronectin, laminin, α1-antitrypsin, etc
Matrilysins	MMP-7	Matrilysin	Elastin, enactin, laminin, decorin, integrin, etc
	MMP-26	Matrilysins-2	Fibronectin, fibrinogen, vitronectin, casein, fibrin, etc
MT-MMP (membrane type)	MMP-14	MT1-MMP	Elastin, fibrin, tenasin, perlecan CD44, etc
	MMP-15	MT2-MMP	Laminin, perlecan, tenasin, tissue transglutaminase, etc
	MMP-16	MT3-MMP	Fibronectin, laminin, perlecan, vitronectin, casein, etc
	MMP-17	MT4-MMP	Fibrin
	MMP-24	MT5-MMP	CS, DS, fibrin, fibronectin, etc
	MMP-25	MT6-MMP	Fibrin, fibronectin, α1-proteinase inhibitor,etc
Other enzymes	MMP-12	Macrophage elastase	Elastin, fibronectin, laminin, plasminogen, etc
	MMP-19	RASI 1 / RASI 6	Fibronectin, laminin, nidogen, tenascin, casein, etc
	MMP-20	Enamelysin	Aggrecan, amelogenin, etc
	MMP-21	MMP identified on chromosome 1	A1-antitrypsin
	MMP-23	From human ovary cDNA	
	MMP-22/MMP-27	Homology to Stromelysin-2	
	MMP-28	Epilysin	Casein

The first group collagenases comprises of MMP-1, -8, -13 and -18, which degrade collagens mainly the fibrillar collagens type 1, 2 and 3 **(Table.1.)**. They also cleave substrates such as: aggrecan, laminin, perlecan, casein. There are two Gelatinases: MMP-9 and MMP-2, whose primary substrates are gelatin and non-fibrillar collagens type 4 and 5. However, they also have a vast array of substrates some of which are: aggrecan, elastin, fibronectin, nidogen, TGF-α, TGF-β and IL-1β. Stromelysins are MMP-3, -10 and -11, and some of their substrates are proteoglycans, laminins, decorins, casein, fibronectins and non-fibrillar collagens. Matrilysins comprises of MMP-7 and -26, which degrade collagen type 4. Apart from that, they also cleave fibronectin, casein, vitronectin, enactin, etc. Another group of MMPs called the MT-MMPs consists of MMP-14, -15, -16, -17, -24 and -25. Some of their substrates are collagen 1, aggrecan, fibrin, nidogen, casein, etc. Other MMPs that do not fit in any of the above mentioned groups are: MMP-12, -19, -20, -21, -22/-27, 23, and -29 [39].

1.4.2. Expression, Regulation and Activation of MMPs

Whenever the ECM has to go through any kind of remodelling, expression of most of the MMPs take place, but this expression is usually very low in normal physiological conditions and is tightly controlled to maintain the homeostasis [40, 41]. As shown in **figure 5 (**Figure modified from [28]**)**, the expression of various MMPs takes place in fibroblasts, macrophages, neutrophils, epithelial and endothelial cells [28].

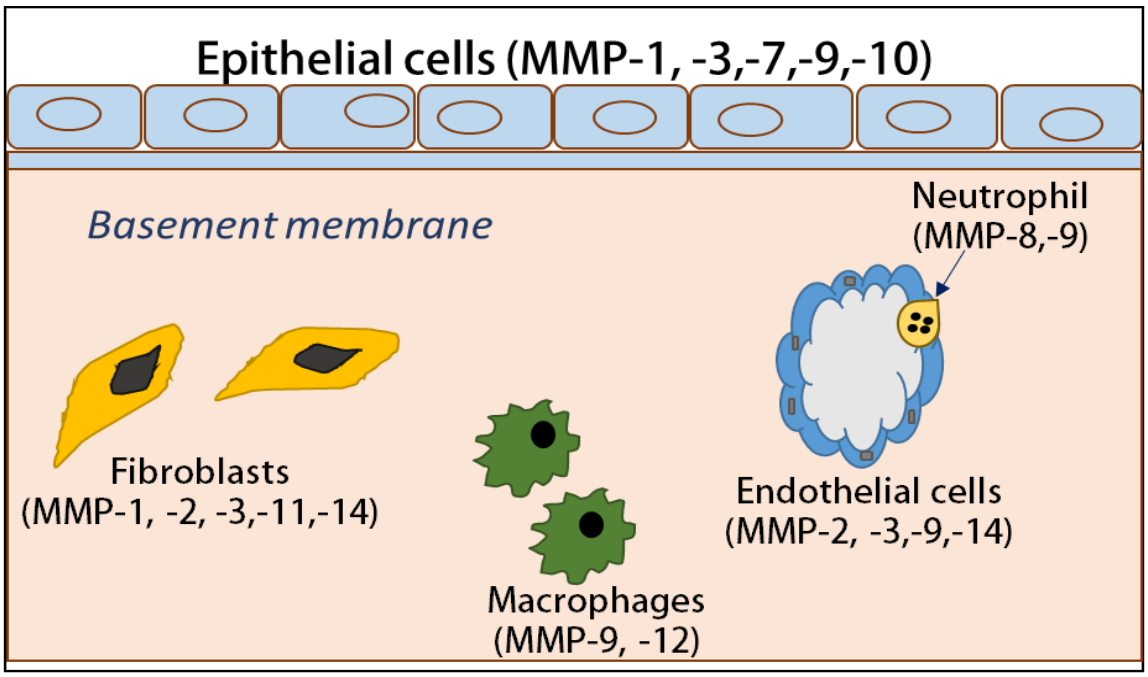

Fig.5. Tissue expression of MMPs in different cell types.

In a normal condition, expression of most MMPs occur only when the remodelling of ECM take place and the tight regulation of MMPs take place at several levels starting from the transcriptional level (**Fig.6.** Figure modified from [42]) [40]. Most MMPs require cellular activation for transcription as their expression is not constitutive, so this transcription is promoted by cytokines (interleukin (IL-1 and IL-17) and tumour necrosis factor (TNF-α)), growth factors and chemokines (**Fig.6**) which in turn induce the intercellular signalling and interactions between cells and the matrix [27, 31]. The expression of these MMPs, are further controlled by endogenous MMP inhibitors (MMPIs) and tissue inhibitors of MMPs (TIMPs) [41].

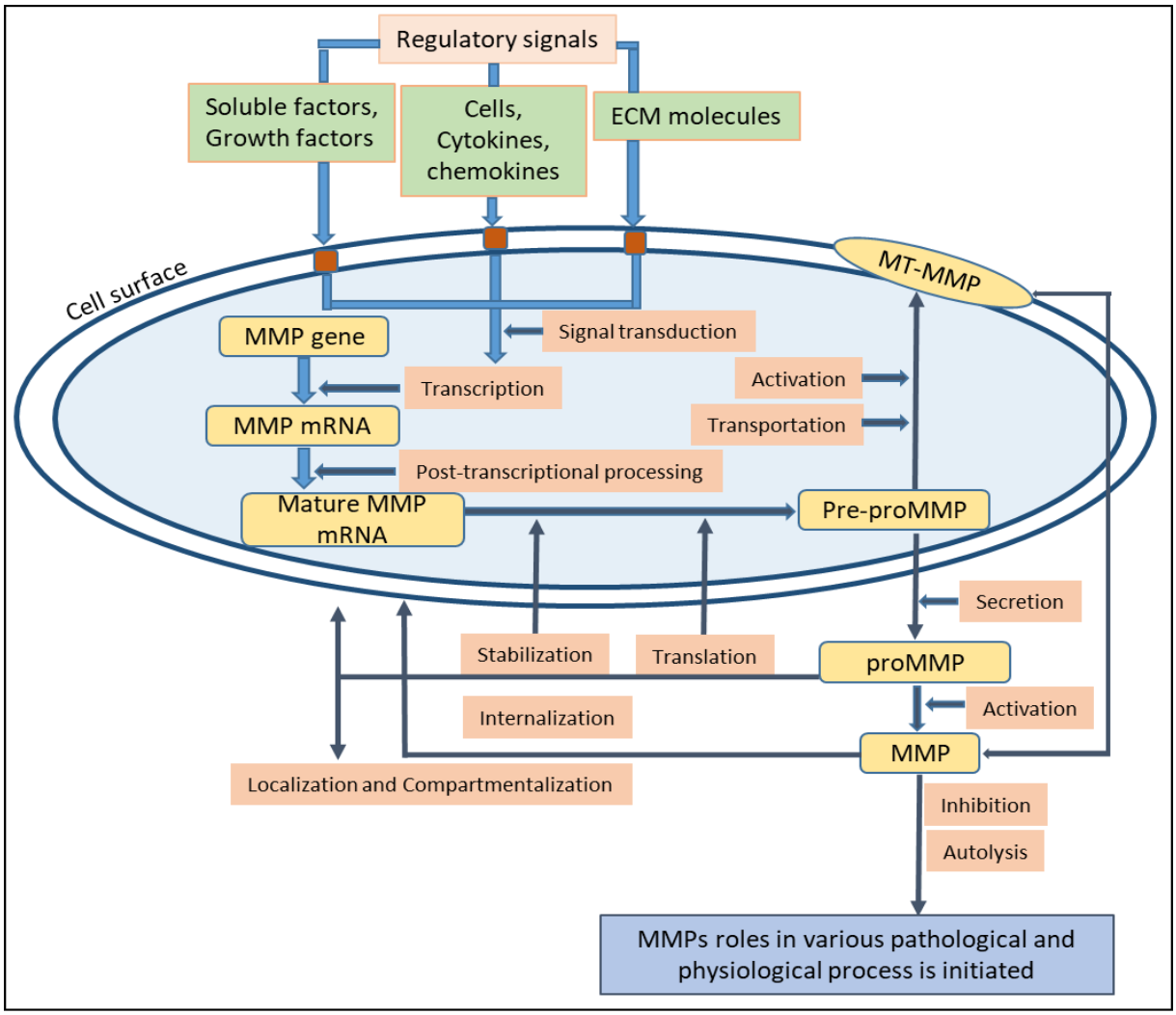

Fig.6. Different levels of MMP-9 expression and activity. Various regulatory signals are initiated due to the interactions between several cells, soluble factors and extracellular matrix cells with specific receptors in the cell surface. This leads to a cascade of events leading to the generation of functional matrix metalloproteinases (MMPs), which could either be localised in the cell surface (MT-MMPs) or secreted to the extracellular medium (proMMPs). Various events can activate proMMPs and these active enzymes then involve in numerous physiological and pathological processes.

Various regulatory signals of myriad origins initiate the synthesis and activity of the MMPs which takes place in various levels including transcription, activation, inhibition, complex formation as well as compartmentalization [43]. The transcriptional level where MMPs are synthesized is regulated by cellular interactions as well as interactions with ECM molecules, growth factors, soluble factors, cytokines and chemokines, as seen in **Fig.6**. The cytokines and growth factors have the ability to both upregulate and downregulate the MMP expression [43]. The MMP gene is expressed into MMP mRNA, which are then stabilized and translated in the pre-pro MMP. In some case, these pre-proMMPs are activated inside the cells and are transported to the cell membrane where they attach and perform their enzymatic actions there. These are the membrane bound MMPs. The rest of the pre-proMMPs are secreted when the secretory signals trigger their secretion. These proMMPs are either activated or inhibited by various molecules. When activated they initiate various biological processes. They are further controlled by inhibitors when they reach their maximum capacity.

1.4.3. MMPs in health and diseases

In the early days, studies on MMPs were labelled as destructive enzymes but that view has been changing, due to subsequent research findings showing myriad functions of MMPs from being regulators of cell behaviour and cell-signalling pathways to disease targets and anti-targets [44]. These matrixins were thought to be primarily involved in the degradation of various molecules in the ECM such as collagen and elastin, but studies have also shown them to process plenty of non-ECM molecules namely: cell surface receptors, growth factors, chemokines, cytokines. In addition, MMPs have also been found to influence cell proliferation, migration as well as differentiation [38]. As discussed above, recent studies have shown that these enzymes have a wide spectrum of activities with broad substrate specificity. Therefore, these enzymes are extremely important in both physiological and pathological states.

Various biological processes where they have been found to play critical roles are: connective tissue turnover, embryonic implantation/development, neurite growth, bone elongation/ossification, morphogenesis, ovulation, menstruation, mammary gland development, endometrial cycling, blastocyst implantation, cervical dilation, postpartum uterine involution, sperm maturation, reproduction, angiogenesis, enamel formation, antigen processing/presentation, hair follicle development, tissue resorption, wound healing/repair, blood vessel remodelling as well as innate immune defence [31, 38, 41, 44-49]. The

dysregulation of MMPs, can lead to various pathological states such as, arthritis, cirrhosis, aortic aneurysms and fibrosis, tumor growth and metastases and various diseases such as glaucoma, lupus scleroderma, multiple sclerosis and neurodegenerative diseases, etc [31].

Among the 23 MMPs, MMP-9, -13 and -14 have appeared to be prominently regulating cellular migration, ECM protein transformation, ECM degradation and apoptosis in the growth plate during bone remodelling [50]. In a pathological state of bone remodelling, MMPs influence diseases like rheumatoid arthritis, osteoarthritis and periodontal diseases. Since MMPs have myriad roles involving normal tissue maintenance functions, situations where altered expression and dysregulation of MMP activities occur, leads to the development of wide range of anomalies and pathologies, such as chronic inflammatory diseases and various stages of cancer, especially metastasis and angiogenesis [41, 44].

There are 10 different types of MMPs that can be detected at mRNA and protein levels in the mammalian central nervous system (CNS). Various studies have shown that MMPs such as MMP-2,-9,-11,-12,-13,-14,-15 and -24, are involved in the neural development and has the capability to respond against any neurological injury or disease [48]. Out of all these MMPs, MMP-2 and MMP-9 are present more profusely in the cortex, cerebellum as well as in the hippocampal region of the CNS. This clearly shows their critical roles in the neuronal biology [48]. In neurodegenerative disorders such as Parkinson's disease, Alzheimer's disease, Japanese encephalitis, several MMPs play various roles, either it is of protagonistic or antagonistic in nature. MMPs have also been found to be involved in the breakdown of the blood-brain barrier [41]. A Low level of MMP-1 has been found in the patients with Parkinson's disease and a significant correlation has been shown between the level of MMP-1 and the duration of this disease [51]. Whereas in Alzheimer's disease, MMPs have been found to play a dual role, on one hand they degrade the amyloid-β peptides (Aβ), a type of amyloid plagues that are hallmarks of this disease and on the other hand, MMPs have been found to contribute to the parenchymal destruction [48]. The expression of MMPs such as MMP-2, -7 and -9 have been found to increase significantly, leading to the severity of Japanese encephalitis [52].

Other pathological processes in which MMPs are involved are as follows; Atherosclerosis, cardiovascular diseases, corneal ulceration, emphysema, fibrotic lung diseases, gastric ulcer, Guillian-barre disease, liver cirrhosis, liver fibrosis, multiple sclerosis, nephritis, skin ulceration, Sorsby's fundus dystrophy and vascular diseases [41].

1.5. Gelatinases

Gelatins are the denatured collagens and since MMPs degrade collagens, it was discovered that certain MMPs also degraded gelatins, which is where the name ‘gelatinases’ come from [53]. MMPs that primarily degrade gelatins are of two types: Gelatinase A (MMP-2) and Gelatinase B (MMP-9). The main hallmark of gelatinases is the presence of three fibronectin-like repeats in their catalytic domain. Both gelatinases are structurally similar, but one of the main difference is the hinge region which connects the HPX domain to the catalytic domain. In MMP-9, the hinge region is much longer and heavily O-glycosylated. Therefore, the hinge region in MMP-9 is also called the OG domain [54]. Whereas, in MMP-2, the hinge region is small and unglycosylated. The size difference of the hinge region of these two enzymes are the main contributors to the size difference between the two enzymes, where proMMP-9 has an M_r of 72kDa and proMMP-9 of 92kDa [55]. Another difference between the two enzymes is in their HPX domains. TIMP-2 but not TIMP-1 binds to the HPX domain in proMMP-9 and links this heterodimer to a dimer of MMP-14 on the cell membrane. This results in the activation of proMMP-2 [56-59]. Whereas, TIMP-1 but not TIMP-2 bind to the HPX domain in proMP-9 [60, 61]. The biological functions of this complex is not fully understood but it is suggested that it prevents proMMP-9 from dimerization with proMMP-1 and the activation of proMMP-9 by MMP-3 [62].

1.6. MMP-9 and its characteristics

Like the other MMPs, MMP-9 is a multidomain enzyme which is encoded in the human genome by a gene located on chromosome 20 [63]. As we can see in **figure 7** (Figure taken from MEROPS database [37] and based on [64]), there are in total 707 amino acid residues present in a preproMMP-9, where the first 19 amino acids are the signal peptide that is removed during synthesis. There are 166 amino acid residues in FnII module and 187 amino acid residues in HPX domain.

It has a typical structure of a matrix metalloprotease as described under "Matrix metalloprotease”, section 1.4.1 in this thesis. The proMMP-9, during its synthesis, becomes heavily O-glycosylated and has a molecular weight of 92kDa. MMP-9 produced by neutrophils have been shown to have 85% of the glycosylation with O-glycans and the remaining 15% glycosylation with N-glycans [65]. Studies had determined that there was three possible N-

glycosylated sites in MMP-9, one located in prodomain (Asn38) and two in catalytic domain (Asn120 and Asn127) [54, 66]. However, Asn127 was not found to be glycosylated [66, 67].

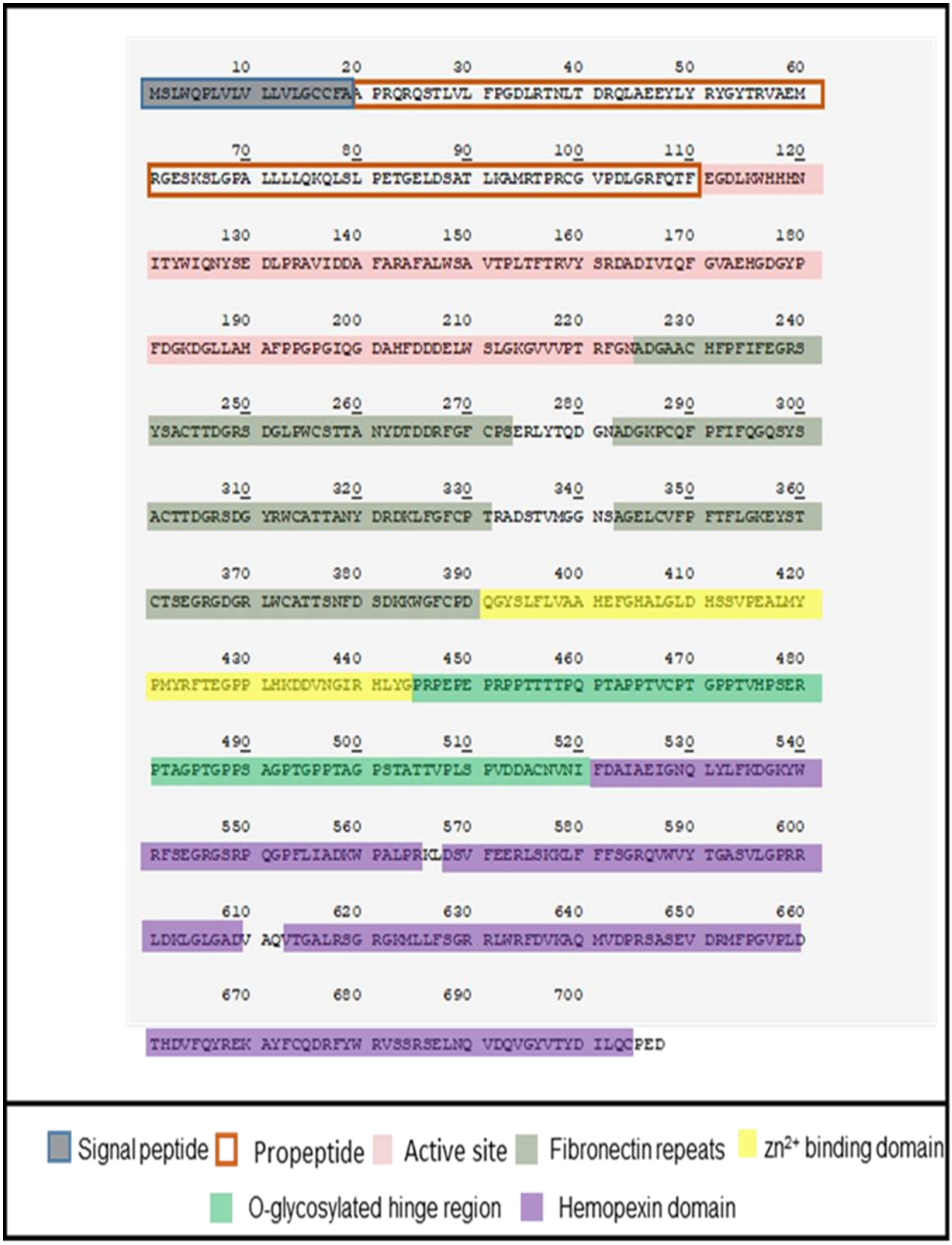

Fig.7. Amino acid sequence of MMP-9.

The N-terminal pro-domain is responsible for keeping the enzyme latent and is linked to the catalytic domain where three FnII like repeats are attached. The catalytic domain of MMP-9 consists of an active site containing Glu402, an important amino acid responsible for the catalytic property of the enzyme. In addition to that, it also contains a Zn^{2+} ion. The catalytic domain is linked with HPX domain with the help of a long and flexible hinge region [64].

MMP-9 is produced as monomers and multimers [13, 64, 68, 69]. Because of the long hinge region (OG-domain) between the catalytic domain and the HPX domain, MMP-9 has been found to have a very flexible structure [64]. This is possibly the reason why an X-ray structure of the full-length proMMP-9 lacks. However, there are partial MMP-9 crystal structures available. A crystallized structure of MMP-9 lacking the OG-domain and HPX domain has been imaged (PDB ID: 1l6j) [70]. In addition to that, recombinant MMP-9 HPX domain has also been crystalized (PDB ID: 1itv) [71]. Apart from these structures, a group has also attempted to create the three-dimensional structure of an inactive mutant full length MMP-9 monomer by combining two techniques called Small Angle X-ray Scattering (SAXS) and atomic force microscopy (AFM) [72]. They showed that the proMMP-9 contained an elongated structure with globular domains at its N- and C-terminal ends. This full length proMMP-9 structure was shown to be able to attain varied conformations (from elongated to compact) due to independent movements of the two globular domains which was possible due to the presence of a very flexible OG region [67, 72].

Normally, MMP-9 is stored in granules of neutrophils and its release only takes place after the influence of inflammatory mediators [73]. Apart from neutrophils, many other cell types such as epithelial cells, endothelial cells, stimulated macrophages, etc can synthesize MMP-9 as preproenzymes [42]. These forms of MMP-9 are secreted out of the cells as proenzymes. A previous study has shown that these secreted proMMP-9 are N-glycosylated at two sites, at Asn38 and Asn120 in pro-domain and catalytic domain respectively [66]. The glycosylation of proteins have been shown to be important for various reasons such as; promotion of proper protein folding and recognition of improper folding as well as possible protection from proteases after secretion, to state some few [67, 74]. The N-glycosylation in MMP-9 have been thought to provide a stabilizing effect to this enzyme and the glycosylation at the Asn120, especially has been demonstrated to be essential for its secretion [66]. In addition to that, a protein present in the plasma membrane called the membrane-anchored hRECK protein regulates the secretion of this proMMP-9. RECK has been found to negatively regulate MMP-9 in two ways; firstly, it supresses the secretion of MMP-9 from cells and secondly by

directly inhibiting MMP-9's activity. The downregulation of RECK gene can lead to increased secretion of MMP-9 which in turn can lead to morphological transformation [75, 76]. The down regulation of MMP-9 has also been shown to involve the internalisation and subsequent catabolism after binding to a cargo receptor lipoprotein receptor-related protein 1 (LRP-1) [77]. The overexpression of MMP-9 has been widely associated with various pathological states such as cell invasion, metastasis and tumour progression [78]. In the ECM, MMP-9 is known for cleaving denatured collagens, activating cytokines as well as growth factors, modulating chemokines and processing of the cell receptors [79].

1.6.1. Activators of MMP-9

MMP-9 has been found to be activated proteolytically by two major ways; 1) by naturally occurring proteases such as MMP-2, serine protease (trypsin), kallikrein, plasmin, neutrophil elastase, MMP-7, MMP-10, MMP-13 as well as MMP-3 (deemed as the most efficient activator of MMP-9), and 2) by organomercurial compounds, such as APMA (amino phenyl mercury acetate) and $HgCl_2$ (mercury chloride). Other activators of MMP-9 are hypochlorous acid (HCLO) as well as bacterial proteases such as thermolysin and pseudolysin [32, 64, 80-84]. CD44 has been found to stabilize/enhance MMP-9's activity [63].

1.6.2. Inhibitors of MMP-9

The natural inhibitors of MMPs in general are the tissue inhibitors of matrix metaloproteinases (TIMPs), which are secreted in a high-affinity, non-covalent complexes with MMPs, in a 1:1 enzyme:inhibitor ratio [85]. These are slow, tight-binding reversible inhibitors with dissociation constants in the pico-molar region and low dissociation rates of the formed complex [86]. Structurally, TIMPs consist of two domains: an N-terminal domain, which is around 125 amino acids long, and a C-terminal domain, which is around 65 amino acids long. There are four types of TIMPs: 1 to 4, out of which TIMP-1, an inducible protein, acts as the main inhibitor for MMP-9 [73]. The unique thing about TIMP-1 is that it can bind to both the active and inactive forms of MMP-9 **(Fig.8.** Figure modified from [43]).

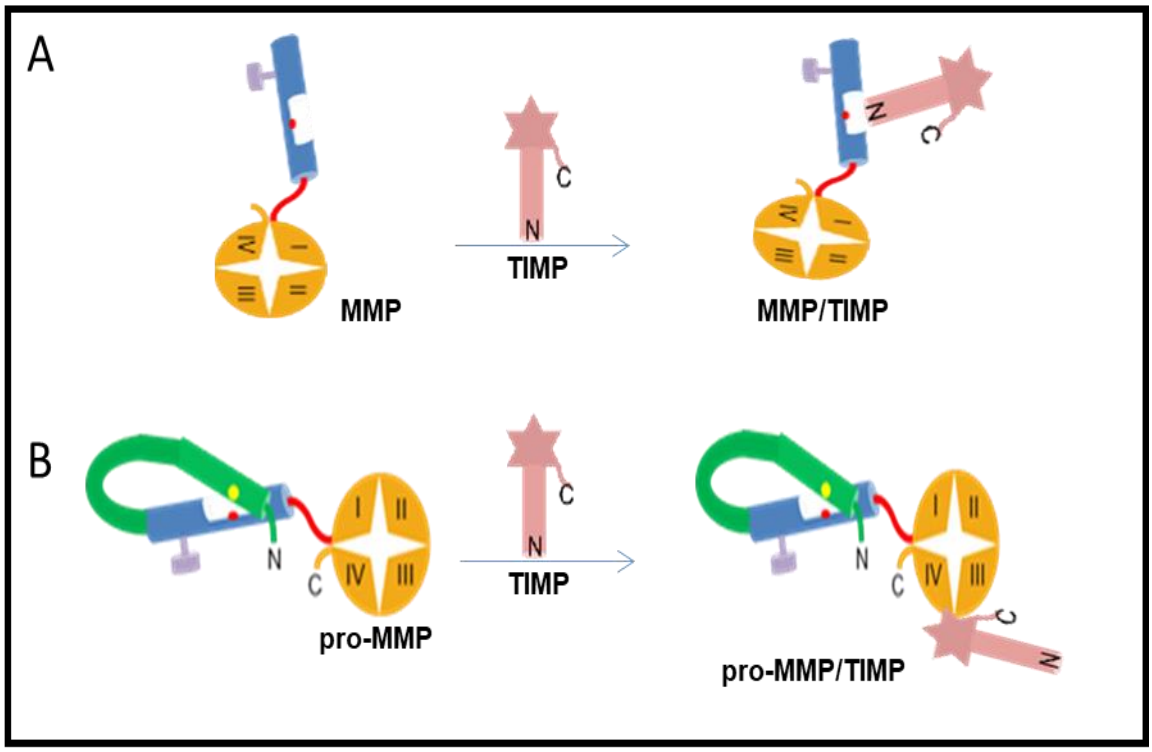

Fig. 8. Binding of TIMPs to MMPs.

The binding of N-terminal of TIMP-1 to the catalytic site of an active MMP-9 and binding of TIMP-1 to the C-terminal-HPX domain of the inactive MMP9 can lead to inhibition of the enzyme's proteolytic activities [62]. MMP-9 can also be inhibited by TIMP-2 and -3, however, they are much less effective than TIMP-1 [87].The activity of MMP-9 was also found to be inhibited by RECK as it inhibits the release of enzyme from the cells [75, 76]. Other compounds that can inhibit MMP-9 are galardin and compound 1b [32].

1.6.3. Domains of MMP-9

MMP-9 is a multidomain structure consisting of five domains before secretion. The first is a signal peptide, which directs the MMP-9 to secretory pathway. This is removed before the enzyme is secreted. This secreted enzyme structure, consists of a catalytic domain with pro-domain in its N-terminal and a HPX domain in its C-terminal that is attached with the help of another domain, the OG domain (**Fig.9**).

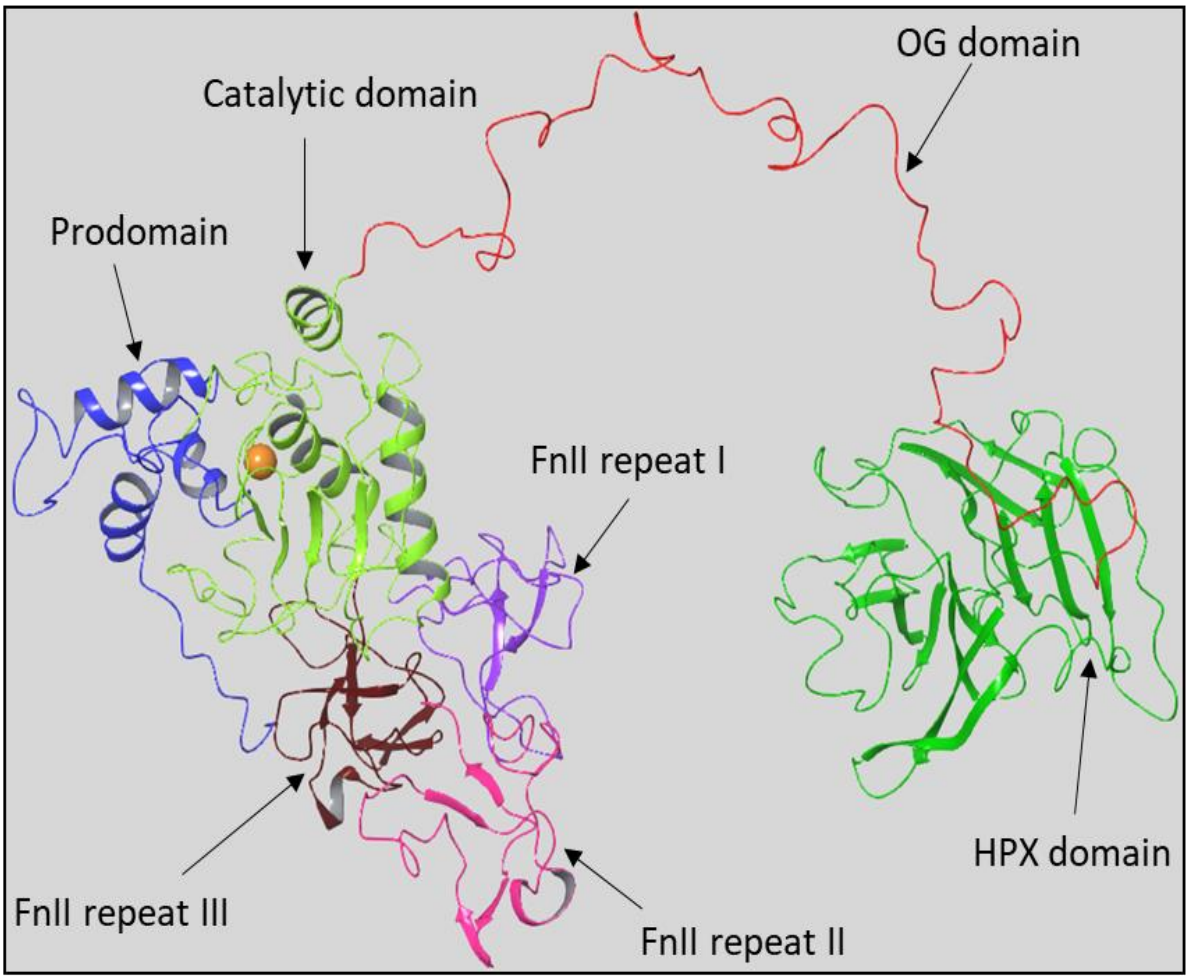

Fig.9. Predicted structure of full length MMP-9 by homology modelling. This full length homology model was predicted using available pdb structures 1itv and 1l6j, by using homology modelling tool in program Maestro in Schrödinger software package. Backbone MMP-9 prodomain (blue), zinc ion (Orange), catalytic domain (light green), FnII repeat I (purple), FnII repeat II (pink), FnII repeat III (brown), OG domain (red) and HPX domain (dark green).

This catalytic domain also contains a Fibronectin II (FnII) like module consisting of three repeats: FnII repeat I, FnII repeat II and FnII repeat III. Out of these domains, FnII and HPX have been studied in more detail as certain regions in both these domains might act as exosites for MMP-9. Here, exosites are simply secondary binding sites present in enzymes, which are located far away from the active site and have the capability of influencing its substrate specificity [88]. The five main domains of MMP-9 are discussed further.

1.6.3.1. Prodomain

As discussed earlier in the section of MMPs, the propeptide of MMP-9 also contain the similar propeptide region consisting of approximately 80 amino acids. The C-terminal region of this domain comprises of a ‘’cysteine switch’’ PRCGVPD, where the Cysteine residue coordinates with the catalytic zinc ion present in the active site of the catalytic region in MMP-9. This interaction keeps the MMP-9 in a latent stage [64]. However, the enzyme activation occurs when this interaction gets disrupted due to proteolytic processing or physical disruption by proteases, oxidants or denaturants. The disruption of cysteine-zinc ion then leaves zinc open, allowing it to coordinate with water molecule instead resulting in an active MMP-9 [89].

1.6.3.2. Catalytic domain

As with other MMPs, MMP-9 has an ellipsoidal shaped catalytic domain, which contains a small active cleft/pocket where a catalytic zinc is present. This catalytic zinc coordinates with three conserved histidine residues inside this pocket [36, 79]. As all other MMPs, MMP-9 also contains a highly conserved Glu- and Asp- rich region between Zn^{2+} binding site and the hinge region, which is thought to constitute Ca^{2+} binding sites [90]. Additionally, the catalytic domains in MMP-9, as with other MMPs contain various subsites labelled by unprimed and primed S, such as S_1, S_2, S_3 and S'_1, S'_2, S'_3 as seen in **figure 10 (**Figure part A modified from [91]. Out of these sites, S'_1 is present immediately to the right of catalytic Zn^{2+} and is the main subsite for substrate recognition in MMP-9 [79, 92]. It is specific for selective inhibition of various MMPs, including MMP-9 and this specificity comes due to the varied sizes and depth of these S'_1 sites in different MMPs which is why this site is targeted for designing synthetic MMP inhibitors [79].

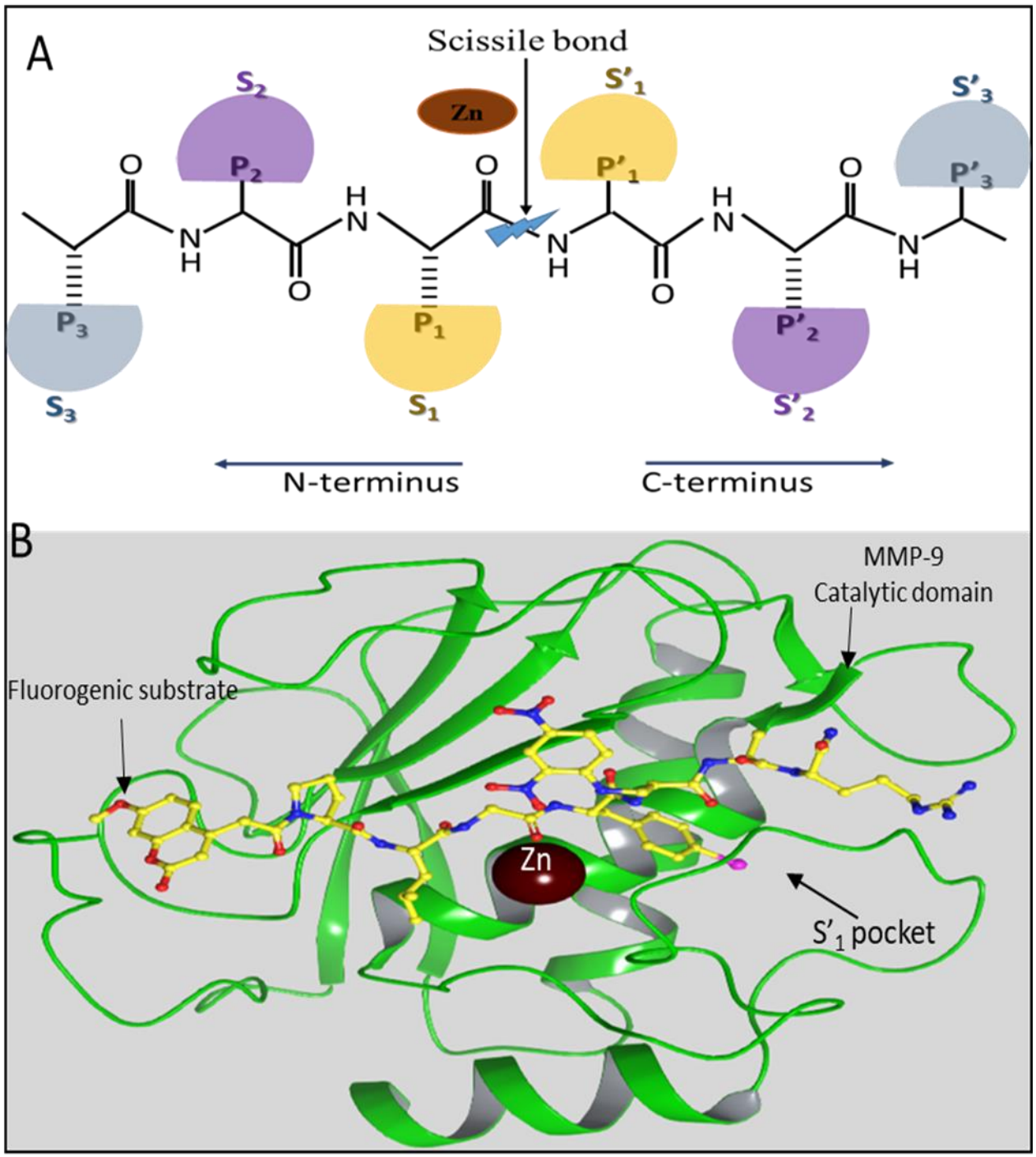

Fig. 10. The substrate-binding pocket of MMP-9 catalytic domain.

A. shows the nomenclature of the substrate binding pocket in the active site of MMP-9 catalytic domain. Non-primed sites: S_1-S_3, primed sites: S'_1-S'_3. Sciccile bond is a covalent chemical bond **B.** shows the fluorogenic synthetic peptidic substrate occupying the substrate binding site of MMP-9 in the catalytic domain of an inactive mutant of MMP-9 catalytic domain (crystal structure pdb id:4JIJ). MMP-9 catalytic domain (green), fluorogenic synthetic peptide (yellow), Catalytic zinc (Brown).

1.6.3.3. FnII domain

There are three repeats of fibronectin II module present in between the fifth β strand and the catalytic site helix and each of these three repeats of the FnII module in the catalytic domain of MMP-9 consists of two intramolecular disulphide bonds, helping to stabilize the structure. The second and third repeats in this domain are flexible and might interact with various sites of the ECM [33, 70]. Functionally, the FnII domain has been found to be responsible for binding and subsequent degradation of gelatin, elastin and native collagens especially collagen IV, V and XI. Studies have shown that this domain is responsible for enhancing the gelatinolytic nature of MMP-9 by 100-fold [54]. In addition, the lack of this domain in MMP-9 has been shown to lower the specific gelatinolytic activity down to 20% compared to the full length enzyme [93].

However, this domain does not influence the degradation of small chromogenic substances, as they directly bind to the active site of MMP-9 [13, 94-96]. There is also an estimation that this domain helps to enable localization of MMP-9 to the connective tissue matrices. Due to presence of certain motifs in the structure of this domain, these domain acts as an exosite, especially during the degradation of some substances [13].

1.6.3.4. O-glycosylated domain

MMP-9 contains a flexible 64 AA linker region between its catalytic and HPX domains. It is a central O-glycosylated (OG) domain, previously called as collagen V-like domain, containing abundant O-linked glycans and a single cysteine residue [54, 60]. Despite heavily O-glycosylated, MMP-9 also possesses N-linked oligosaccharides in this domain, which is also why, the size and much of the flexibility of MMP-9 is thought to be contributed by this domain [64]. To corroborate this, a study of OG domain with help of small angle X-ray crystallography and AFM have also shown the flexible nature of OG domain which is thought provide MMP-9 obtain varied enzyme conformations [72]. Due to lack of crystal structures of this domain, a combined study of *in silico* modelling and experimental analysis was done to obtain a three dimensional structure, which showed a unique and compact structure with the possibility of a disulphide bridge between the Cys468 in OG domain to the Cys674 in the hemopexin domain [54]. Studies have shown that deletion variants of MMP-9 lacking the OG domain can only be observed as monomers suggesting the importance of this domain in undergoing dimerization/multimerization [73]. The tertiary structure of OG domain has been shown to be important for orienting MMP-9 HPX-domain correctly for inhibition by TIMP-1 as well as for

the internalization by LRP-1 and LRP-2 (megalin). Thus, this domain is important for regulating the bioavailability of active MMP-9, as it seems to be responsible for orienting MMP-9 towards inhibitors and substrates [54].

1.6.3.5. Hemopexin domain

The MMP-9 HPX domain consists as a four-bladed propeller where blades I and IV are connected with each other by a single disulphide bridge and this domain lacks stabilizing elements unlike other related hemopexin-like structures (**Fig.8**.) [71]. Functionally, this domain has been shown to be responsible for the substrate specificity of MMP-9 and is important for linking MMP-9 with the CSPG core proteins [13, 97]. Due to the homological similarity of this domain with the plasma protein hemopexin, studies have been done to study the functional similarities between these two, which showed that, like the hemopexin protein, hemopexin domain in MMP-9 also binds to the cargo receptor called low density lipoprotein receptor-related protein-1 (LRP-1) [98]. Recently, it has also been found that megalin/LRP-2 is a functional receptor of MMP-9, which suggests that HPX domain has binding sites for these cargo receptors [54]. Additionally, due to the lower amino acid sequence homology of this domain compared to other MMP hemopexin domain, studies have also suggested the usefulness of targeting this domain as a mode of prevention against the MMP-9 mediated pathological functions [99].

Out of all the secreted MMPs only MMP-9 is capable to form a dimer and the blade IV of its HPX domain is found to be responsible for this dimerization [100]. The MMP-9 dimers are reduction sensitive and involves noncovalent and hydrophobic interactions and a salt bridge between the C-terminals of two subunits of MMP-9 [43]. In addition to that, this domain has been found to have binding sites for collagen type I and IV, elastin, fibronectin and gelatin [64, 97]. In a study done to examine whether a recombinant MMP-9HPX could inhibit the migration of colorectal cancer cells in a modified Boyden chamber assay, it was found that increasing the amount of recombinant HPX led to decreasing migration rate of these cells. Similarly, when adhesion studies on these colorectal cells were performed in the presence of recombinant HPX, inside a plate coated with various ECM components such as gelatin, collagen I and laminin, the binding of these cells reduced significantly [97]. An 85 kDa non-secreted form of proMMP-9 (which lacks N- or O- glycosylation) has been found to be associated with the cell membrane through the binding of the HPX domain to the Ku protein, which is a protein expressed inside

the cell and on the cell surface of macrophages as well as activated monocytes. It is involved in repairing DNA double-strand breaks [43].

1.6.4. Role of MMP-9 in pathological and physiological conditions

Because of MMP-9's involvement in wide range of pathological and physiological conditions, it is also regarded as a promising diagnostic and prognostic factor, which makes MMP-9 a significant biomarker with high potential [101]. MMP-9 is one of the enzymes that have prominent roles in brain physiology as well as pathology. The mRNA and protein expression of MMP-9 occurs in low levels in numerous structures of naive brain such as the hippocampus, cerebellum and cerebral cortex, especially in neurons. Its activity can generally be observed in the cell bodies and dendrites as well as excitatory synapses located in on dendritic spines [63]. For the control of synaptic plasticity as well as of synaptic cell adhesion molecules, MMP-9 has emerged to have a pivotal role. Apart from that, MMP-9 has been found to be important for postnatal brain development, adult brain neurogenesis, learning and memory. Studies have shown that, MMP-9 activates pro-inflammatory cytokines leading to neuro-inflammation, which is normally initiated in the brain as a favourable reaction to harmful stimuli. The upregulation of MMP-9 has also been associated with neurodegenerative and neoplastic conditions [63].

Stroke is another pathological state where MMP-9 seems to play a dual role. Enough evidence suggest its involvement in the injury process after the stroke onset. Whereas, MMP-9 has also been found to help the recovery process in the later stages of stroke, which makes it difficult to plan treatment strategies that involves targeting MMP-9 [102]. Other pathological conditions in brain, where MMP-9 seem to play important roles are lupus erythematosus, viral and bacterial meningitis, encephalitis, multiple sclerosis, brain injury, neuropathic pain and migraine, Alzheimer's disease, Parkinson's disease, Huntington's disease, Down's syndrome, epileptogenesis and epilepsy, bipolar disorder and brain tumours [63].

MMP-9 also has an important role to play in the cardiovascular health as well. A high level of serum MMP-9 has also been associated with the incidence of coronary heart disease, and this increased amount of MMP-9 have been found to be a predictor of increased mortality in these patients [103-105]. Hypertropic cardiomyopathy is another cardiovascular condition where the higher levels of MMP-9 can be observed and can be correlated with worsening of its prognosis [106]. This higher levels of MMP-9 is also associated with a higher risk of blood

pressure progression [107]. Studies have shown that, macrophages isolated from patients with acute Myocardial Infarction (MI) have a double amount of mRNA and protein levels of MMP-9 compared with a group with no MI [108]. Another study done on MI, MMP-9 deficient mice showed low level of macrophage infiltration that led to reduced rupture rate as well as reduced ventricular dilation [109]. In an experiment carried out on mice lacking apolipoprotein E (which is involved in metabolism of fats in the body), MMP-9 released by the macrophages contributed to an enhanced degradation of elastin and plaque disruption. In hypertension, MMP-9 contributes very early to breakdown of collagen and arterial distensibility [110]. MMP-9 activity has been found to be increased in arteries with high blood pressure compared to normal blood pressure [111].

The correlation between the level of MMP-9 in plasma and various cancers such as, head and neck squamous cell carcinoma, breast cancer, lung cancer, gastric cancer, hepatocellular carcinoma, colorectal cancer, ovarian cancer, have been shown by several research studies done in the past [43, 45, 112, 113]. Studies have shown that the overexpression of MMP-9 in the epithelial tumor of the ovary can contribute to metastases of ovarian carcinoma cells through the lymph nodes [114]. The increased serum and tissue expression of MMP-9 can also be associated with the worsening of prognosis in the patients with breast cancer [115]. In certain cases of patients with breast cancer, the zinc concentration in the blood was highly reduced and instead there was an increase in its concentration in the cellular compartments. This appeared to alter the activity of MMP-9 which contributed to the malignancy of breast cancer [116]. MMP-9 was found to be involved in the progression of colon cancer as well as the lymph node metastasis of colorectal cancers [97, 117].

MMP-9 seems to be involved in every physiological and pathological process that involves ECM remodelling, so it is of great interest to understand this enzyme both structurally and functionally. In addition to that, the dual nature of this enzyme in pathological processes makes it even more mysterious which requires more research.

1.6.5. Substrates of MMP-9

MMP-9 is one of many enzymes, which possess a wide range of potential substrates, which can be cleaved in the test tube but might not even interact in real life. This is because the biological specificity of MMP-9 and many other MMPs in general derive from the ‘’hic et nunc’’ approach, whose literal translation is ‘’here and now’’ and in enzymatic description, they are

active only very locally and briefly [63]. However, it has been known that MMP-9 targets various molecules ranging from growth factor and their precursors to cell surface receptors and cell adhesion molecules (CAMs) [63]. Additionally, recognized targets include gelatin, collagens IV, V, XI, XIV, elastin, aggrecan, decorin, laminin, entactin, human plasminogen, myelin basic protein, fibronectin, α_1Proteinase inhibitor (α_1PI) and Interleukin 8 [28, 110, 118]. In the brain, the substrates for MMP-9 include CAMs, the pro-form of brain-derived neurotrophic factor (BDNF) and mature nerve growth factor (NGF) [63]. MMP-9 has also been found to process denatured bovine collagen II and chemokines such as human and mouse granulocyte chemotactic protein-2 (GCP-2) as well as human epithelial-cell derived neutrophil activating peptide-78 (ENA-78) [118].

1.7. MMP-9, its complexes and their biological functions

Studies have suggested that the formation of MMP complexes might be linked to the regulation of its activity, substrate specificity, stability and localization [43]. A small fraction of acute myeloid leukemia displaying monocytic lineage markers were found to express the 85kDa proMMP-9, in complex with Ku protein, at the cell membrane. This complex has been found to be associated with cell invasion and has been found to be less sensitive to inhibition by TIMP1 when compared with a free 85kDa proMMP-9 [43]. B-cell lymphocytic leukemia (B-CLL) expresses isoforms of CD44 and integrins such as CD44v and integrin α4β1, and both these isoforms were found to form complex with active MMP-9 at the cell surface. Observation of these formed complexes in matrigel, showed induced cell migration through this gel [43]. Complex formation of proMMP-9 with the Dentin matrix protein-1 (DMP1) belonging to the family of small integrin-binding ligands N-linked glycoproteins (SIBLINGs) has been found to activate the enzyme where the prodomain is removed from the active site cleft without the presence of any chemical cleavage, i.e. due to conformational changes. In addition to that, there is an assumption that DMP1 can act as a mediator between proMMP-9 and various cell surface receptors such as CD44 and integrins [43]. Heparin and heparan sulfate can form complex with both the active and inactive MMP-9. This was discovered when active MMP-9 was found to be bound to HS chains of GPI-anchored glypican-like PGs on the cell surface of a highly metastatic clone isolated from murine colon adenocarcinoma. This interaction seemed to induce cell migration and cell invasion through matrigel [43].

Apart from these complexes with experimentally known biological functions, there are other complexes formed by MMP-9 whose functions are yet to be explored. One of such complexes is the complex formed with itself. These homodimers are formed only between two MMPs with high amount of O-glycosylates in their hinge regions and those lacking this glycosylation only appear as monomers [43, 71]. MMP-1 and MMP-8 are other MMPs that also seem to form a complex with MMP-9 but with unknown functions. A small amount of heterodimers between MMP-1 and MMP-9 were found to be produced together with proMMP-9, proMMP-1 and TIMP-1, when U937 cells (a monocytic leukemia cell line) was stimulated with a combination of a tumor promoter called phorbolester TPA and an endotoxin called lipopolysaccharide (LPS) [62]. This complex was formed with the help of the HPX domains of both proenzymes. When MMP-3 was added in this complex, it activated the proMMP-9 bound to MMP-1, leading to degradation of gelatin. Similarly, when only plasmin was added to this complex, it activated MMP-1, hence degrading interstitial collagen. Interestingly, when both MMP-3 and plasmin were added together with this complex, both MMP-1 and MMP-9 were activated leading to rapid degradation of both gelatin and interstitial collagen, suggesting an excellent cooperation between the two enzymes [43, 62]. THP-1 cells, which belongs to the leukemic monocyte cell lines, have been found to produce reduction sensitive heteromers between proMMP-9 and CSPGs, which will be discussed in next section.

1.7.1. ProMMP-9·CSPG complexes, their properties and their probable roles

MMP-9 can form complexes with chondroitin sulfate proteoglycans (CSPGs) [68]. The monocytic leukemia cell line THP-1 produces small amount of heteromers of proMMP-9 and CSPGs, where the proMMP-9 is linked to the core protein of one or more CSPGs [13, 62]. This production of heteromers increases significantly when these monocytic cells are stimulated with PMA. Two other cell lines U-937 and MonoMac have also been found to produce such complexes, but in a considerably lower amount than THP-1 and the amount do not vary even when these cells were stimulated with PMA. However, CSPGs isolated from all three cell lines can form complexes with proMMP-9 *in vitro* and this gave rise to two different types of complexes: SDS-stable and SDS-soluble complexes. As the name suggests, SDS-stable complexes are stable even in the presence of SDS and are reduction sensitive, and the SDS-soluble complexes dissolve and separate into individual components in the presence of SDS [13]. Both types of complex formation show alteration in the biochemical properties of

proMMP-9, such as the ability to bind to collagens and gelatins through the FnII repeats and also the ability to be activated by organomercurial compounds [13].

Previously, it was thought the reduction sensitivity of the SDS-stable complexes was due to the presence of disulphide bond between proMMP-9 and the core protein of CSPG/SG. However, when proMMP-9 and CSPG/SG were reconstituted in the presence of compounds such as: EDTA, IAc and NEM to counter the disulphide bridge formation, proMMP-9·CSPG/SG complexes still formed [13, 68]. This showed that the formation of SDS-stable complexes were not due to the formation of an intermolecular disulphide bond and its reduction sensitivity was rather due to intramolecular disulphide bridges present in the proMMP-9 itself [13]. This was supported when a study was conducted to examine the reduction sensitive nature of MMP-9 homodimers by examining formation of monomers and dimers of recombinant proMMP-9 HPX in presence and absence of DTT. The result clearly showed no formation of proMMP-9 HPX dimers in presence of DTT. This supports the fact that the reduction sensitive nature of SDS-stable proMMP-9·CSPG/SG complexes were due to the disulphide bridge within the HPX domain of proMMP-9. This disulphide bond was formed between Cys516 in blade 1 and Cys704 in blade 4 of HPX domain, which was shown by X-ray crystallography [71].

Further, the proMMP-9 and CSPG/SG could not be reconstituted in the presence of a mixture of 1% Triton X-100 and 1M NaCl, but 1% Triton X-100 or 1M NaCl alone could not prevent the *in vitro* reconstitution of the complexes. This suggested that the formation of both these complexes are due to compound forces [13].

The biochemical properties of proMMP-9 heteromers produced from stimulated THP-1 cells seemed to be different from the proMMP-9 in monomeric forms. This is supported by the binding patterns of monomeric forms and the heterodimeric forms of proMMP-9 with collagen I and gelatin [119] . The FnII module of proMMP-9 is involved in binding with both gelatin and collagen [96], however, it has been found that the proMMP-9 heteromer, cannot bind to gelatin as the formation of such complex leads to hiding of the FnII module in proMMP-9 [13]. This also suggests that the binding sites in the monomeric and heterodimeric forms of proMMP-9 for collagen I and gelatin seems to be the same or in overlapping regions. However, it appears that the proMMP-9 and proMMP-9/CSPG complex seems to bind to different and non-overlapping isotopes in gelatin [55].

Functionally, it is likely that the core protein of a proteoglycan might simply be acting as a carrier molecule for proMMP-9 in order to facilitate its localization to other substrates,

which might be in the surrounding area or attached to the GAGs of the proteoglycan itself [13]. The formation of proMMP-9/CSPGs complexes are possible at the pH range of 5.5 to 7.5 suggesting that these complexes might form inside the cells, in the extracellular matrix or in body fluids. However, this is only possible if both proMMP-9 and the CSPGs are housed in same environment. However, more studies need to be done to determine what type of conditions provide such environments for proMMP-9 and CSPGs to form such complexes and if its production is increased or decreased in diseased conditions [13].

1.7.2. MMP-9·Serglycin complex formation

SG is one of the CSPGs produced by THP-1, MonoMac and U937 cells in varying amounts and it has been found that is the major CSPG produced by THP-1 [13, 14]. From previous studies, we know that *in vitro* reconstitution of purified SG with proMMP-9 gave rise to proMMP-9·SG complexes [13]. Functionally, the role of proMMP-9·SG complex has been unknown but the suggestions are that, due to co-localization of both SG and proMMP-9 inside various cells, SG and its associated chondroitin sulfate chains might be allowing proMMP-9 to link to cell surface of both normal and malignant cells with the help of receptors like cD44. This might indicate the carrier functions of SG for proMMP-9 when they form such complexes [68]. Because very little is known about this complex formation our study has tried to understand more about this interaction.

2. Aims of the present study

Research on MMP-9 has grown exponentially since the early 2000s, and rightly so, given the fact that the biological functions of MMP-9 ranges from the brain physiology to the reproductive areas of the body. Alternatively, MMP-9 has also been shown to have various roles in myriad pathological conditions [64]. However, despite the increasing interest and foresight in academia over the possibilities of MMP-9 in advancing new technologies and applications, it has been found that the industry has been losing interest in using MMP-9 as possible biomarkers or even druggable targets [120]. This hints that there is a wide space between academia and industry, which needs to be abridged. This however, can be done with extensive biochemical characterization of MMP-9, which is what this thesis is attempting to do. By figuring out each and individual domains and modules of MMP-9, we can create a thorough understanding of MMP-9, which might also help solve missing links on structural studies of other related MMPs.

Hence, the overall aim of this thesis was to create a portfolio of MMP-9 that can provide a comprehensive understanding of its characteristics. This was done by studying the interactions of its individual domains and modules with inhibitors and substrates. For this, we had specific aims for each paper, which are summarized below:

Paper I:

- To determine whether both the FnII and HPX domains of MMP-9 are required for the complex formation between proMMP-9 and SG.
- To identify amino acids and regions of proMMP-9 (especially FnII module and HPX domain) and SG, that are important for the complex formation.
- To investigate which type of binding patterns are involved in the complex formation between proMMP-9 and SG.

Paper II:

- To examine the binding properties of MMP-9 and its variants with two hydroxamate. compounds called galardin and compound 1b and compare it with the binding of these two compounds with other human MMPs and three bacterial metalloproteases.
- To investigate if MMP-9 and its variants, activated by different activators such as trypsin, APMA and MMP-3 could affect their binding properties with galardin and

compound 1b and their ability to degrade the chromogenic substrate McPLGLDpaAR-NH_2.

Paper III:

- To determine if active MMP-9 can cleave the core protein in recombinant SG lacking CS-chains.
- To determine if active MMP-9 can cleave the core protein in native SG containing intact CS-chains.
- To determine if active MMP-9 can cleave the core protein in cABC treated SG, which contains just a short stub of CS-chains.
- If active MMP-9 cleaves the SG core protein, to what extent is the cleavage pattern be affected by the presence of CS-chains
- If active MMP-9 cleaves the SG core protein, are there exosites in MMP-9 that may affect the cleavage pattern.

3. Methods and methodological considerations

3.1. Production and purification of full lengthMMP-9 and its variants from THP-1 and insect cells

Our main goal for producing MMP-9 variants was to examine which parts of MMP-9 are important for complex formation with SG. For paper I-III, we needed to have a supply of full-length proMMP-9 and different recombinant variants. The full-length proMMP-9 was produced from PMA stimulated THP-1 cells and all the recombinant proMMP-9 variants were produced in two insect cell lines, either Sf-9 or High Five, using the Bacculo-virus expression system. After the production of our enzymes, we purified them from the cell media using various techniques, as discussed onwards. The THP-1 cells produce not just monomers of proMMP-9 but also the dimers as well as heterodimers and multimers of proMMP-9 with CSPGs in addition to various CSPGs and TIMP-1 [13, 68] . Because of this, our full-length proMMP-9 produced from PMA stimulated THP-1 cells needed to be separated out from all the extra molecules present in the cell media. For this, we first used an anion exchange chromatography (Q-Speharose column). This anion exchange chromatography is based on the technique of the isolation of proteins based on their charges using an ion-exchange resin containing positively charged groups (**Fig.11.).** Highly negatively charged macromolecules like proMMP-9·CSPG/SG and CSPGs binds to the Q-Sepharose column, under the conditions used.

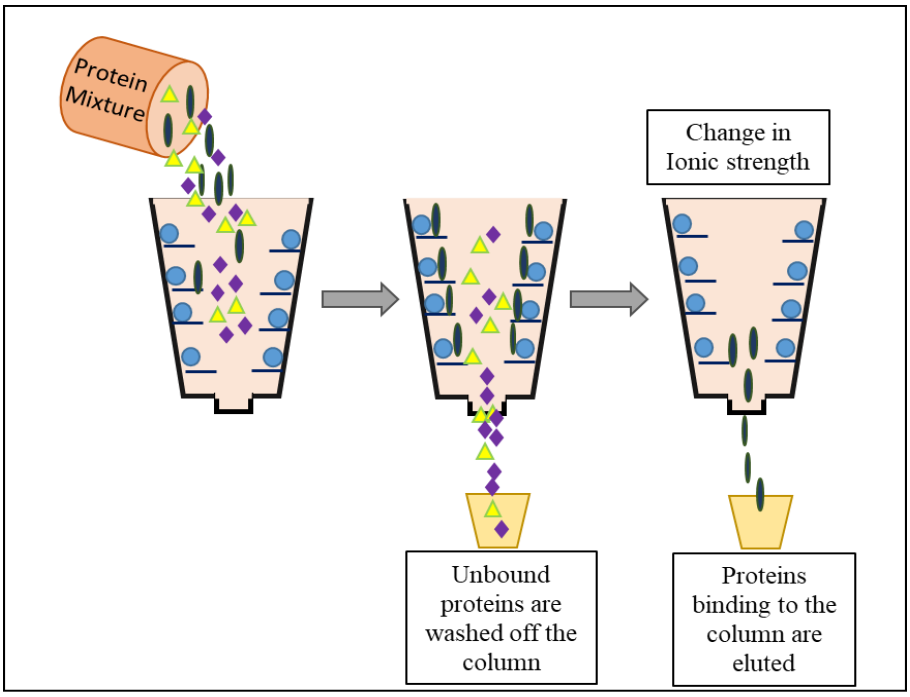

Fig.11. An overview of Ion exchange chromatography.

ProMMP-9 monomers, homomultimers and proMMP-9 with TIMP-1 bound to its HPX domain did not bind to the Q-Sepharose column and could be directly transferred to a Gelatin-Sepharose column.

The various recombinant variants containing FnII module such as recombinant full length proMMP-9 (rpMMP-9), recombinant variant lacking the hinge region (rpMMP-9ΔHPX) and the recombinant variant lacking the OG and HPX domain (rpMMP-9ΔOGHPX) were also purified using a one-step purification method using Gelatin-Sepharose affinity chromatography. Since these variants like the MMP-9 produced in THP-1 cells contained the FnII module, their purification was much simpler than those recombinant deletion variants that lacked the FnII module. The reason is that the FnII module has a high affinity to gelatin [54]. The affinity chromatography is based on the principle of isolation of proteins by utilizing their affinities for specific molecules ranging from substrates, inhibitors, ligands, antigens, antibodies and many other interacting molecules [121].

However, we suffered major setbacks while trying to purify our recombinant variant lacking the FnII module (rpMMP-9ΔFnII). First purification technique we used was the Gelatin-Sepharose affinity chromatography itself, as a previous study had showed that HPX domain in MMP-9 also binds to gelatin [99, 122]. Although, we failed to purify this variant using this technique. We then proceeded to try purifying it with other techniques. Some of the columns we tried using for purification of this variant were Heparin-Sepharose and Helix pomatia agglutinin (Lectin-Sepharose). However, even after trying various techniques, we were only able to obtain a partly purified enzyme.

Coincidentally, we managed to find another technique for purifying MMP-9ΔFnII and was based on the principle of salt precipitation, using ammonium sulfate as illustrated in **figure 12**. Salting out or salt precipitation is a technique that utilizes the solubility of proteins in various salt concentrations. Very few proteins can stay soluble in water so for most proteins, they require at least a small amount of salt to be able to remain folded and stable soluble in water. However, as the salt concentration increases, the protein start to lose their solubility, ultimately precipitating out at a high salt concentration [123, 124]. However, we need to keep in mind that while precipitating our protein of interest, other contaminants could also precipitate together so, it is important to use another application to further purify the proteins, which we did using a size exclusion chromatography (gel filtration) with Sephacryl 200 column. This technique is based on the separation of proteins from protein mixtures (containing various proteins and their complexes) based on their molecular sizes [125].

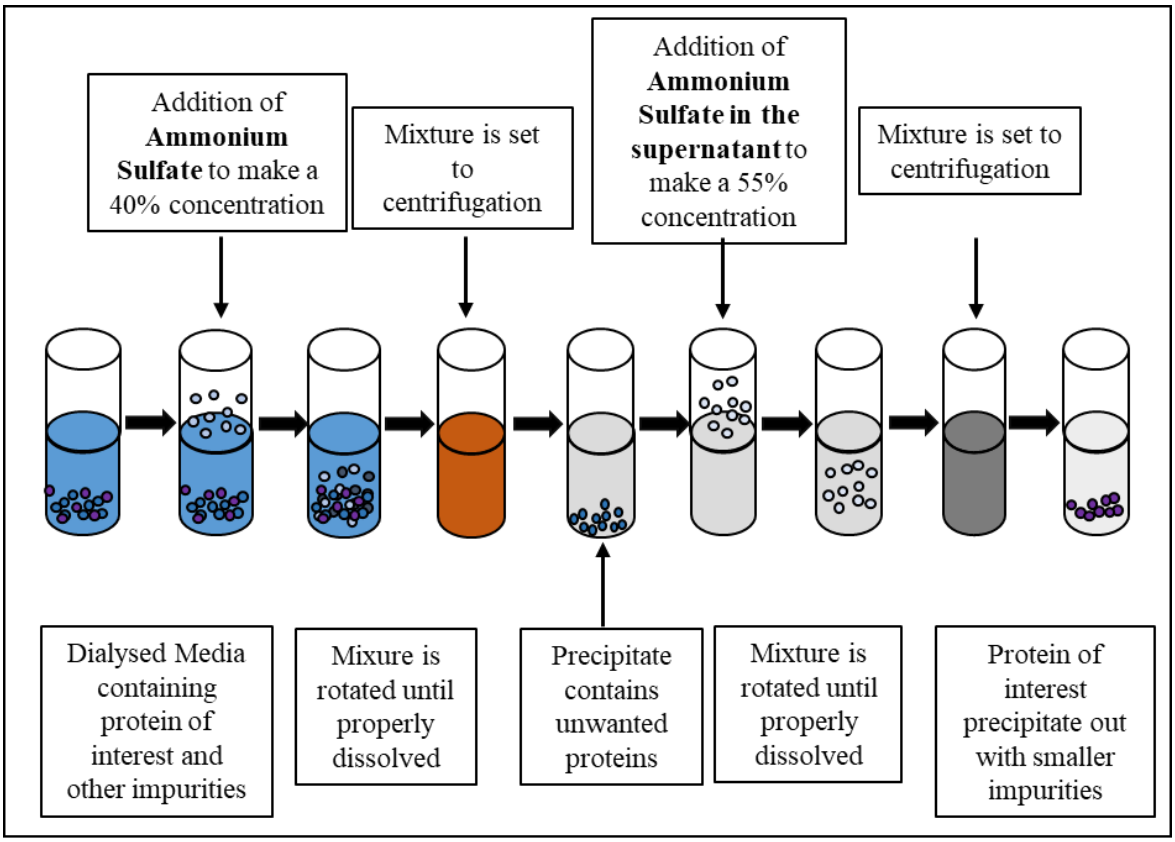

Fig.12. An overview of Ammonium sulfate precipitation as used in paper I.

Even after these processes, we still managed to obtain a partially pure rpMMP-9ΔFnII so, we decided not to follow these techniques to other variants of MMP-9 lacking the FnII module which were; recombinant proMMP-9 lacking the FnII module and HPX domain (rpMMP-9ΔFnIIHPX) and recombinant proMMP-9 lacking the FnII module, OG domain and HPX domain (rpMMP-9ΔFnIIOGHPX).

3.2. Production and purification of CSPGs and SG from unstimulated THP-1 cells

For **paper I and III**, we also needed a stock of CSPGs and SGs, which were produced from THP-1 without PMA stimulation. For the isolation of CSPGs and SG, PMA stimulation was avoided as it leads to high formation of proMMP-9/CSPG complexes and we would not be able to obtain desired amount of CSPGs and SG. Although the unstimulated THP-1 cell contains high percentage of CSPG/SG, it also contains small to negligible amount of proMMP-9, proMMP-9·CSPG/SG, TIMP-1 and proMMP-9·TIMP-1. As illustrated in **figure 13**, CSPSs/SG are separated from all the above mentioned molecules using two step Q-Sepharose purification affinity chromatography, with the removal of salt at the end, using Sephadex G-50 column. Purifying in the Q-Speharose column, it was important to maintain the pH of the buffer around 6, as higher pH would displace the positive charge of the Q-Sepharose column and our highly

negatively charged CSPGs would not be able to bind to this column, leading to problems with purification itself.

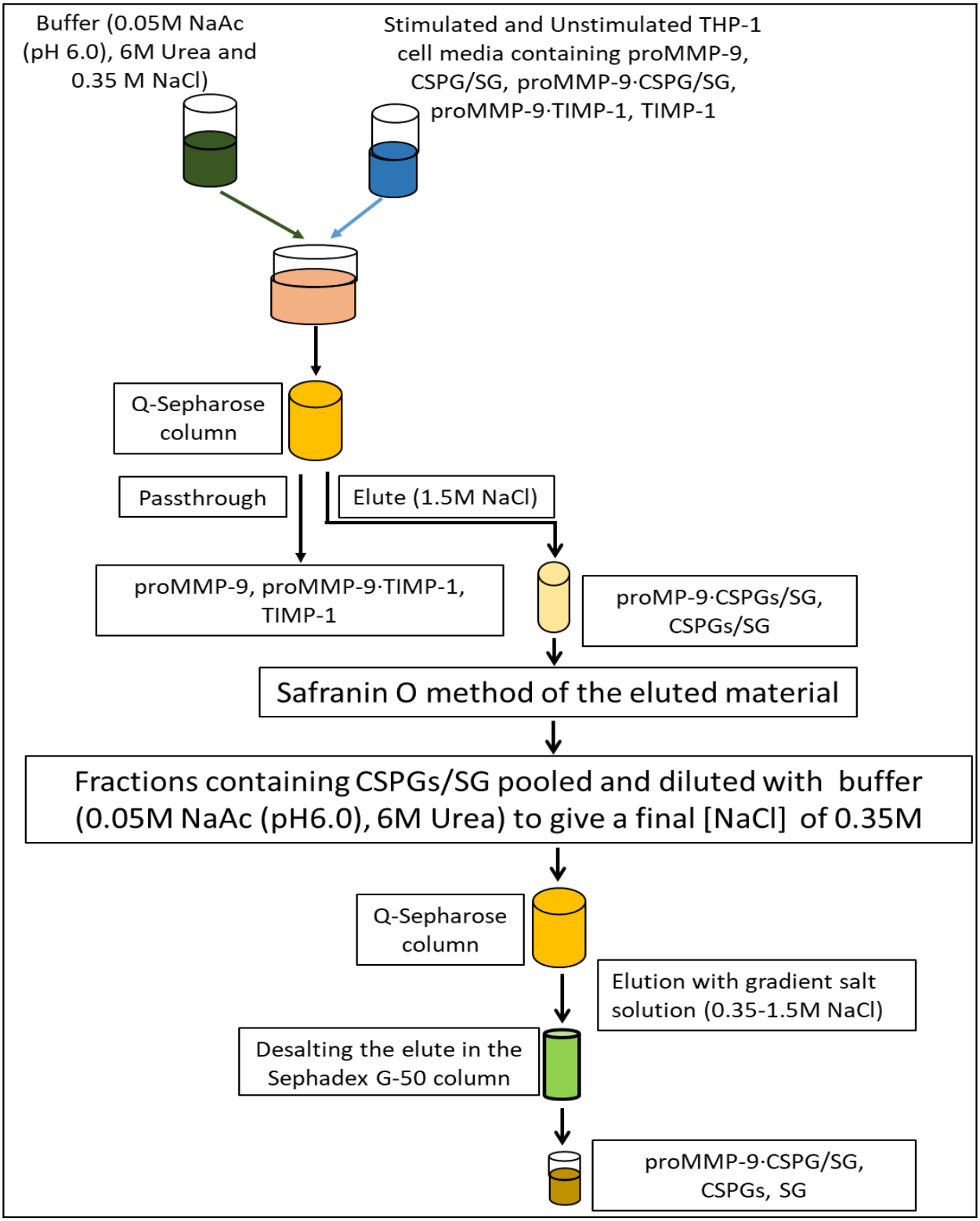

Fig.13. Illustration on the purification of CSPGs/SG from the stimulated and unstimulated THP-1 cell media.

The amount of proteoglycans were then quantified using Safranin O method after the first Q-Sepharose purification. This method is based on the quantification of the glycosaminoglycan chains bound to proteoglycans, with the help of cationic dye Safranin O. Adding this dye to the proteoglycans and its glycosaminoglycans, converts them into precipitates whose colour intensity is then used to measure their absorption at 536nm with a help of a standard spectrophotometer or a plate reader. The desalted CSPGs after second step Q-Sepharose purification were either used as it is for our further experiments or was further purified to extract SG from other putative CSPGs such as Versican, through size exclusion chromatography / gel filtration, using Sephacryl S-400 gel.

Since these purified CSPGs contained CS-chains, we wanted SGs without the CS-chains for examining the effect of CS-chains in complex formation between MMP-9 and SG, so His-tagged SG (Ht-SG) was commercially bought. However, it contained some amount of DTT, so before using it for our study, it was important to dialyse it to remove the DTT present, otherwise, it would result in broken disulphide bonds, denaturation of proMMP-9 and loss of enzymatic activity.

3.3. Gel Electrophoresis and Immunoblotting

For detecting our enzymes, we used a gel electrophoresis technique called gelatin zymography. This technique is quite a common technique used for detecting proteases and is based on the degradation of particular substrates [126]. In our case, we use gelatin embedded to the polyacrylamide as a substrate for detecting MMP-9 and its activities. Real time zymography is another type of electrophoresis where the gelatin is labelled with fluorescent dye 2-methoxy-2,4-diphenyl-3(2H)-furanone (MDPF). Since our variants lacking the FnII modules had 80% less activity on gelatin than the full length variants, their activity on gelatin zymography was often not as reliable, so we needed to use western blotting to detect whether these variants were able to form complexes with CSPG/SG, as we could observe these variants by using antibodies against them [93].

Western Blotting comprises of three main steps: separation of proteins by size using gel electrophoresis (SDS-PAGE), transfer to a solid support (eg: PVDF or nitrocellulose membranes) also called as blotting and the third is the usage of proper primary and secondary antibody to mark the target protein for visualization [127]. While observing the *in vitro* reconstituted complexes of proMMP-9 and its variants with cABC treated CSPG, by western

blotting, it was important to treat the SDS-PAGE gel with DTT before blotting as a previous study have shown that without this treatment, the complexes could not be transferred to the membrane [68].

3.4. Investigation of the complex formation between proMMP-9 and its variants with CSPG/SG

After we managed to produce and purify full length proMMP-9 and its variants as well as CSPGS and SGs, investigation of the binding patterns of proMMP-9 variants with CSPGs and SG was done by conducting three techniques: 1. *In vitro* reconstitution, 2. Peptide array studies and 3. Molecular modelling. All the results from these techniques were used for **paper I**.

3.4.1. *In vitro* reconstitution of proMMP-9 variants with CSPG/SG

Previous studies have shown that proMMP-9 (from THP-1 cells) and CSPG/SG could form complexes *in vitro,* and were of two types; a SDS-soluble and the other was a SDS-stable complex [13]. Hence, with this knowledge, we wanted to observe the complex formation between the variants of MMP-9 and the CSPG/SG. So, by conducting *in vitro* reconstitution studies, we were hoping to get answers for threes main questions: 1) Which of the deletion variants of MMP-9 form complex with CSPGS/SG 2) Which parts of these two molecules interact with each other? 3) What are the type of interactions that keep the two molecules together in the complex? The schematic diagram explaining the steps we took for conducting *in vitro* reconstitution is shown in **figure 14**.

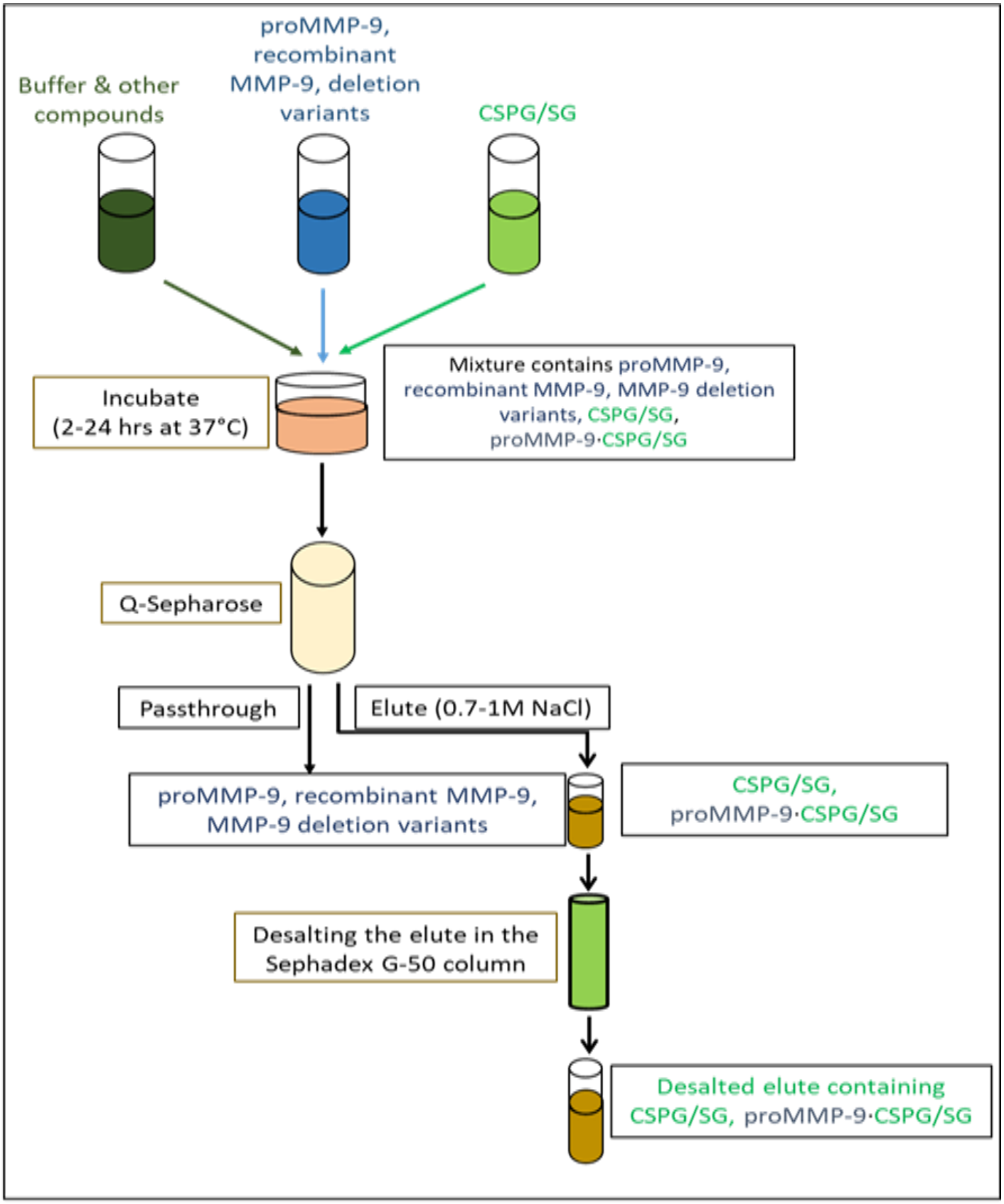

Fig.14. Illustration of *in vitro* reconstitution.

3.4.2. Peptide arrays and Mutation Peptide arrays

Peptide arrays gave us a wonderful second level approach to understand the binding patterns between proMMP-9 and SG. These arrays are generally made up of several immobilized peptides on filter papers, glass or monolayers. Peptides are normally preferred for this kind of immobilization as various protein binding and enzymatic activities are mostly directed towards peptides, so these arrays provide an excellent platform for the identification of protein-protein interactions as well as protein-peptide interactions. In addition to that, arrays are also important for identifying the actions of enzymes, adhesion of cells as well as the binding of metals [128]. However, the drawback of this technique is that we cannot duplicate many protein functions at the peptide level, as these peptides are just truncated forms of the original protein, so, they lack their original tertiary structures once immobilized in the arrays [129]. Therefore, we were aware that the peptides in these arrays are just planar/linear binding partners for our target proteins, thus, the binding patterns seen between our target proteins and their respective arrays might not reflect binding patterns in natural scenario, i.e. with the full length proteins. In addition to these peptide arrays, we decided to conduct mutation peptide arrays. These mutated peptide arrays were based on the amino acids in the peptides to which the target protein was bound. Mutating these amino acids in their respective peptide spots allowed us to confirm their importance in binding with their target proteins.

There was also a possibility of unspecific bindings from our polyclonal antibodies, so it was also necessary to conduct control experiments by incubating our arrays with respective primary antibodies and secondary antibodies.

The interpretation of the results was another issue, which had to be dealt with care. We selected the interacting spots based on the intensity of peptide spots after ruling out those spots that appeared after control experiments done with primary and secondary antibodies. Then we looked for common amino acids between binding spots, to see if we could isolate individual amino acids that might be more important for these bindings. An isolated peptide spot with a strong intensity was considered an artefact. However, there was also the possibility that such isolated peptide spots might come from the whole peptide sequence being involved in binding.

3.4.3. Molecular Modelling

After analysing the peptide arrays and the mutation peptide arrays, we were able to summarize amino acids that appeared to be important for binding between proMMP-9 and SG. However, we wanted to test another way to see if these amino acids would turn out to be really important or were they just coincident. So, we opted to use molecular modelling as a way to dissect the individual amino acid interactions between proMMP-9 and SG. Molecular modelling not only offered us a different perspective on our results obtained from wet lab experiments, it also provided us a creative visual stimuli which made it easier for us to visualize our proteins and their complexes, which was a bonus. The molecular modelling was done keeping the results from peptide arrays in mind so the selection of different docking models for conducting dynamic simulations were based on the results obtained from the peptide arrays. Therefore, the results from molecular modelling must only be taken as a complementary information on the binding between proMMP-9 and SG.

3.4.3.1. Homology modelling

Since we lacked full length crystal structures of both proMMP-9 and SG, we first had to create a homology model of these two proteins. For this, homology modelling provided us an excellent tool. This technique is based on the principle that if two or more sequences share high similarity then their structures will also share similarity. So, the structure of known or unknown proteins are based on the similarity of its sequence with other sequences of proteins with known structure [130]. Out of the homology models of full length MMP-9 and SG, the former has more accurate structure as it is based on already available X-ray structures of the catalytic domain (containing pro-domain and FnII domain) and the HPX domain. However, we must look at the SG with a bit more caution as the model created only had a 59% confidence. Nevertheless, since the molecular modelling study was just a complementary study to our previous works, we believe, future molecular modelling studies on this interaction might give more accurate and reliable results.

3.4.3.2. Binding mode prediction by using protein-protein docking

Protein complexes are known to have many biological functions so, understanding the interactions between the two units of a complex helps to gain valuable insights into the structural bases of these interactions and protein-protein docking provides a complementary

approach to do that. This technique, in the presence of known or even tentative 3D structures of proteins allows for, not just a visual understanding but also a comprehensive knowledge of how two proteins might affect each other's functions and mechanisms [131].

While conducting protein-protein docking, we selected MMP-9 FnII and MMP-9 HPX as the receptors and SG as the ligand. Normally, any computational docking program involves two major steps: 1) **Sampling;** a step where two protein molecule structures are used to search and generate a maximum number of near-native models based on the interaction between the two protein structures, 2) **Scoring;** a step of identification of the possible protein complex model that resembles the native model best. This is selected out of a big pool of models generated after the first step of sampling [131]. However, since we did not have any pre-formed X-ray structures of our proMMP-9/SG complexes, we could not score the best docking poses based on these pre-formed complexes. Therefore, to select the best docking models for conducting dynamics simulations we prepared our own selection process after the docking between proMMP-9 and SG was conducted, which is described in detail in **paper I**.

3.4.3.3. Molecular dynamics simulation

Molecular dynamics simulation is normally used for simulating an interaction between two molecules, with respect to time. It is used in various fields from structural biochemistry to biotechnology, and is commonly used for the investigation of dynamic properties between various molecules. This technique is based on molecular mechanics which is based on the principle that proteins are simply a collection of atomic masses and when they interact with each other, it is the collection of atomic masses that are interacting with each other through harmonic forces which is why, to study the dynamics in this system between these proteins, force needs to be applied [132].

The molecular dynamics studies of the protein interactions occur in an aqueous environment, mainly in a water body as seen in **figure 15**. To be able to simulate such a system for studying the protein interactions, it is important to understand the interaction between the particles at the surface and particles within, as the forces experienced by the particles at the surface can surpass the system to eventually influence the forces experienced by the particles within the system [132]. This tool provides a progession of simulated structure or interaction between structures with respect to time and this simulation is generated into a trajectory which

can be studied for further analysing the interactions between these structures in respect to time which is in nano second level [132].

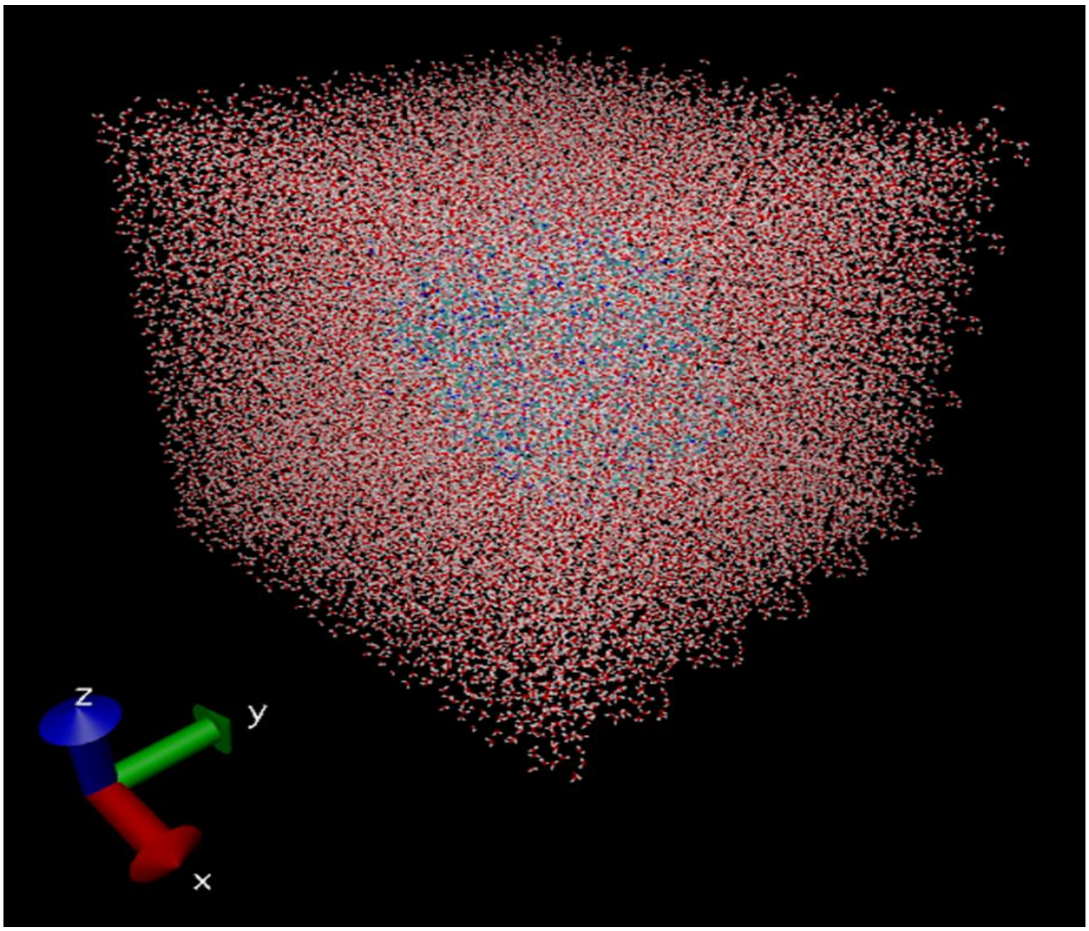

Fig.15. An example of the 3D aqueous system used for conducting molecular dynamics simulation. The system is used for creating an environment for allowing dynamic interaction between molecules. Picture taken from google stock files.

However, no tools are without limitations. A good dynamics simulation of a complex depends on two criteria. One is the accuray of the force field used. This is the equation used for deriving the forces interacting on all the atoms of a system. We have used OPLS3e, which is a modern force field credited with greater accuracy against the performance standards set by previous versions of force fields [133]. Another aspect to consider was the total computing time. Since, we are creating a simulation of interaction of two proteins, acquiring every nano second of this interaction was valuable. Due to economic reasons and time constraints we have tried to conduct dynamic simulations with an adequate sampling time of 100-500ns. Conducting dynamic simulations with longer sampling time meant, longer waiting periods to obtain results and higher energy usages. So, the obtained results in **paper I**, definitely needs to be analyzed keeping these issues in mind.

3.5. Activation, active site titration and calculation of the kinetic coefficients (K_m and K_i) of proMMP-9 and its variants for chromogenic substrate and inhibitors

For understanding the properties of enzyme, understanding its kinetic properties is quintessential. Since the main objective of an enzyme is to catalyse a reaction, it is important to examine how the velocity of this catalytic reaction changes with changes in the concentration of both enzyme and available substrate. In addition to this, we also need to be aware of the concentration of inhibitors that might be present while the reaction is taking place, as even a small amount of inhibitors might affect the activity of enzymes, in turn affecting the rate of the catalytic reaction itself. For this, it is important to know the exact amount of active enzyme available to us which can be known by titrating its active sites [134]. The concentration of our active enzyme variants was especially important to know in order to be able to compare their degradation of CSPG/SG and Ht-SG, which was done for **paper III**. This method of calculating the concentration of active enzyme is simply called active site titration, which was used in **papers II and III**.

However, before we could conduct an active titration of our enzymes, we needed to activate them, which we did with three different activators namely: trypsin/trypsin linked to magnetic beads (Mag.Trypsin), APMA and MMP-3. These different activators were used because they activate our enzymes differently resulting in enzymes with different N- and C-terminal residues. This was particularly important to see if these differently activated enzymes bind to inhibitors, degrade a small chromogenic substrate or CSPG/SG in a similar manner or not. Out of these activators, Magnetic Trypsin, was the easiest activator to use, as we could separate the activated enzyme from trypsin by simply using a magnet. This separation is instantaneous. For stopping the activation with normal trypsin, soyabean trypsin inhibitor (SBTI) was used and for stopping the activation with both APMA and MMP-3, we used EDTA. In case of MMP-3 activation, the activated MMP-9 was separated from MMP-3 using a Gelatin-Sepharose column. As gelatin is a MMP-9 substrate it was necessary to use EDTA during the entire purification, including the elution with DMSO as explained in detail in **paper II**. The presence of EDTA inhibits the activated MMP-9, so it needs to be removed. EDTA, DMSO and APMA were removed from MMP-9 by using a spin column with a 30kDA cut-off and washing as described in **paper II**. To acquire enzymes with maximum activity, it is important to follow the activation process with these activators closely by determining the enzymatic activity at different time points during the activation using the fluorescence quenched substrate Mca-PLGLDpaAR-NH_2. This allowed us to stop the activation process at the right time with

correct methods. This is important, as the activation process actually is a balance between activation and degradation.

Now, after these enzymes were activated, we conducted the active site titration of these activated enzymes by mixing them with varying concentrations of the slow tight binding substrate competing inhibitor galardin (Gm6001) followed by addition of a fixed amount of chromogenic substrate in order to determine the enzymatic activity at the different inhibitor concentrations. By plotting a dose response plot of, v_i/v_0 (initial rate activity of enzyme in the presence and absence of inhibitor) vs the concentration of the inhibitor [I], using the Morrison equation [135] or the Henderson's plot [136], we could calculate the active enzyme concentration [E]. The Henderson's plot is based on the linearized equation of the Morrison equation and the advantage of using this plot is that, we do not need the K_m value to calculate the enzyme concentration. However, to calculate the binding coefficient (K_i) of the enzyme for a slow tight binding inhibitor like galardin, we needed to calculate the K_m value, which is the binding affinity of our enzymes with the chromogenic substrate (McaPLGLDpaAR-NH_2).

For this, we conducted another kinetic study to calculate the initial reaction rates of our active enzymes, by incubating them with increasing amounts of substrate. The data we obtained from this assay were plotted in a non-linear regression plot (concentration of substrate [S] vs initial reaction velocity (v_o)) by using the Michaelis-Menten equation. This was used to calculate the K_m values of our enzymes for the substrate and further to calculate the K_i values, which were used in **paper II and paper III**.

3.6. Degradation studies of CSPG/SG and Ht-SG using active MMP-9 variants

First, it was important to test if active MMP-9 could cleave Ht-SG. As the commercially obtained Ht-SG contained DTT, it was necessary to remove the DTT. This compound breaks disulphide bridges. MMP-9 contain 6 disulphide bridges in the catalytic site holding the FnII module together and one disulphide bridge linking blade I and blade IV in the HPX domain together. Breaking these disulphide bridges inactivates the enzyme. In order to compare different enzymes ability to cleave a substrate, it is important to know the exact concentration of the active enzymes.

4. Summary of the main results

PAPER I

Motifs and amino acids involved in the formation of complexes between pro-matrix metalloproteinase-9 and the proteoglycan serglycin core protein

In this paper, we conducted *in vitro* reconstitution of the purified proMMP-9 variants and purified CSPG/SG. In addition, we conducted peptide arrays and mutation peptide arrays studies followed by molecular modelling. All these studies were done to examine the interaction modes between various amino acids and regions between proMMP-9 variants and CSPG/SG. The main findings were:

1. The proMMP-9 enzyme needs the presence of at least the HPX domain or the FnII module in order to form the proMMP-9/CSPG(SG) complex.

2. The FnII module at the same time interacted with the parts in SG located both to the N- and C-terminal side of the Ser-Gly repeats.

3. A stable ionic interaction was formed between Arg162 in the catalytic domain of the enzyme and Asp46 in SG, explaining why the SDS-stable complex CSPG/SG formed with the proMMP-9ΔHPX deletion variant.

4. At least a part of the SG core protein binds to the same or overlapping epitopes in the FnII module that bind gelatin.

5. HPX domain containing proMMP-9 variants formed SDS-stable complexes with CSPG/SG where the blade 3 and blade 4 appeared to be mainly involved in the HPX domain, and both the N- and C-terminal regions for the Ser-Gly repeats in SG.

6. The SG core protein at the same time can bind both the FnII module and the HPX domain but requires the enzyme to be in a closed conformation.

7. A single proMMP-9 molecule can sandwich one SG core protein between the two domains with the region in SG that binds the CS-chains points away from the enzyme.

PAPER II

The selectivity of galardin and an azasugar-based hydroxamate compound for human matrix metalloproteases and bacterial metalloproteases

In this paper, we activated our proMMP-9 variants and obtained the kinetic coefficients K_m and K_i of proMMP-9 for chromogenic substrate and inhibitors (galardin and compound 1b). This was done to examine the structural differences in activated proMMP-9 variants from different activators such as; trypsin, APMA and MMP-3. The main findings were:

1. Activation of the rpMMP-9 resulted in a largely truncated form in all scenarios, lacking most of or the entire HPX-domain but appearing to contain the entire O-glycosylated hinge region.

2. The trypsin and MMP-3 activated forms have Phe107 and the APMA activated form Met94 as the N-terminal residue.

3. The major form of the trypsin activated MMP-9 from THP-1 cells retained its C-terminal HPX-domain due to the presence of some TIMP-1 in the purified enzyme, with Phe107 as its N-terminal residue.

4. Despite structural differences of proMMP-9 variants from various activations, these activated forms had an almost identical K_m value for the quenched fluorescence substrate Mca-PLGLDpaAR-NH_2 and K_i values for galardin and compound **1b**.

5. Compound **1b** binds stronger than galardin to MMP-9 due to a larger part of compound 1b enters the S'_1 subpocket than galardin.

6. Both these compounds bind stronger to the various MMP-9 variants than to human MMP-14 or the three bacterial metalloproteses thermolysin, pseudolysin and auerolysin.

PAPER III

The Proteoglycan Serglycin is cleaved by Matrix Metalloproteinase-9

In this paper, we activated full length MMP-9 and its variants, determined their K_m values against Mca-PLGLDpaAR-NH_2, their K_i values for galardin and determined their active site concentration by active site titration. We conducted degradation studies of native SG and recombinant Ht-SG by the various activated MMP-9 variants. The main findings were:

1. All active MMP-9 variants showed approximately the same Km value for the chromogenic substrate.

2. All active MMP-9 variants bind galardin with approximately the same binding strength in the lower pM region.

3. Active MMP-9 cleaves the intact and cABC-treated SG from THP-1 cells. This results in a released peptide around 10 kDa based on SDS-PAGE. There were no difference whether intact SG or cABC treated SG was used.

4. The resultant 10kDa peptide was further degraded by MMP-9.

5. Ht-SG was cleaved by full length proMMP-9 and its variants.

6. All degradation studies showed very small variations in fragment sizes except with the trypsin-activated MMP-9 from THP-1 cells which showed distinct degradation products compared to the activated recombinant MMP-9 variants.

7. This suggested that proMMP-9 contain exosite for SG cleavage in the HPX domain.

5. General Discussion

The tissue distribution of MMP-9 ranges from endothelium cells, microvessels, macrophages to varicose veins, to name the few and its substrates range from ECM molecules to non-ECM molecules, for example; aggrecan, elastin, nidogen, fibronectin, laminins, TGF-β, IL-1β [38]. This type of tissue distribution and substrate specificity of MMP-9, its involvement in an array of physiological and pathological processes clearly makes it an easy target of study in various fields of biomedicine. However, due to limitations in time and resources, any new discoveries from these studies takes years, sometimes even decades. With this in mind, our study has tried to dissect this enzyme as much as it was possible, using as many tools and techniques we have had access to during these years.

The present thesis focuses on investigating the regions in both proMMP-9 and SG involved in forming complexes (paper I), examining the binding properties of proMMP-9 with substrates and inhibitors (paper II) and exploring the degradation process of SG by proMMP-9 and its recombinant variants (paper III).

5.1. Formation of proMMP-9·CSPG/SG complexes *in vitro*

Human leukemic monocytic cell line THP-1 has been found to produce proMMP-9·CSPG complexes and the stimulation of these cells with PMA has been shown to increase the synthesis of proMMP-9·CSPG heteromers [137]. The unstimulated THP-1 cells however has been shown to produce large number of uncomplexed CSPGs, especially SG and negligible amounts of proMMP-9 and proMMP-9·CSPG complexes [13, 14]. Aligning with this knowledge, **paper I** shows that most of the CSPGs we produced and purified from unstimulated THP-1 cells were SG. This was further verified when *in vitro* reconstitution of proMMP-9 with both the CSPGs and purified SG gave identical results. Previously, it was shown that the *in vitro* reconstitution of proMMP-9 and CSPG/SG isolated from THP-1 cells form two types of complexes; SDS-stable and SDS-soluble complexes [13]. We obtained similar complexes when conducting *in vitro* reconstitution of our full length proMMP-9 from THP-1 cells and its recombinant form produced from insect cells with CSPG/SG.

The binding of proMMP-9 to gelatin and collagen is mediated through its FnII module [138]. But, the interaction of the proMMP-9·CSPG/SG heteromers with gelatin was found to be weaker compared to the interaction of monomeric proMMP-9 with gelatin [119]. Previously

it was shown that the FnII module in proMMP-9 in complex with CSPG/SG remains hidden and their interactions with gelatin and collagen do not take place through this module. Although, a small amount of proMMP-9·CSPG/SG still interacted with gelatin and collagen, suggesting that the FnII module is not hidden in these heteromers or new interaction sites had been exposed in at least a subpopulation of the heteromers [119].

Our deletion variants containing FnII module; rpMMP-9ΔHPX and rpMMP-9ΔOGHPX, both formed SDS-stable as well as SDS-soluble complexes with CSPG/SG, highlighting the importance of this module in forming these complexes. Conversely, we could not observe any such complexes in gelatin zymography, when MMP-9 variants lacking the FnII module (rpMMP-9ΔFnII, rpMMP-9ΔFnIIHPX and rpMMP-9ΔFnIIOGHPX) were reconstituted with CSPG/SG. But since we had previous knowledge that the active MMP-9 lacking FnII module only shows 20% activity against gelatin compared to the full length MMP-9 [93], we conducted a western blotting of these complexes using antibodies against MMP-9. The results showed that except the variants lacking both FnII module and HPX domain, all other variants formed complexes. This shows the importance of both FnII and HPX domain in proMMP-9 for complex formation with CSPG/SG. From this, we can conclude that lacking either FnII or HPX does not affect the complex formation of proMMP-9 with CSPG/SG, however, lacking both leads to disability of proMMP-9 to form complexes with CSPG/SG. The fact that these complexes can be reconstituted *in vitro*, hints to a possibility that they also can form in the ECM during conditions when both these macromolecules occur in the same tissue. It is also possible that these complexes can form inside cells, especially if they are co-localized in the same secretory vesicles [13].

A previous study have shown that these proMMP-9·CSPG/SG heteromers can be activated by Ca^{2+} ions as the treatment of these complexes with calcium led to proteolytic cleavage followed by release of proMMP-9 from these complexes [119, 139]. The activation led to generation of N- and C-terminally truncated forms of MMP-9 which were both enzymatically active and it is suggested that this might be due to conformational changes in the proMMP-9 present in the complex with CSPG/SG, that goes through auto cleavage [139].

In most of our results, the THP-1 produced MMP-9 and all the recombinant variants containing the OG domain showed both monomers and reduction sensitive homomultimers. However, removing the OG domain showed only monomers suggesting the importance of this domain for forming homomultimers. This was supported by a previous study, which showed MMP-9 variants lacking this domain formed only monomers on non-reducing SDS-PAGE as

well as in analytical ultracentrifugation experiments, showing the importance of OG domain for dimerization/multimerization [54]. The dimers/trimers could be separated from the monomers and both forms were stable, which means that there are certain dimers/timers, which were formed already inside the THP-1 cells and could not be dismantled into monomers even when they are subjected to SDS. However, the OG domain was not necessary for the formation of the proMMP-9·CSPG/SG complexes, as the deletion variant that lacked both the OG and HPX domain (rpMMP-9ΔOGHPX) formed the complex. This shows that the different domains are important for the formation of different types of complexes.

An additional experiment was done to study the importance of the pro-domain in proMMP-9 for forming the complexes with SG. This was done by using pMMP-9 activated by trypsin (used in **paper II and III**), as it lacks the entire pro-domain. The *in vitro* reconstitution with this 83kDa form of MMP-9 with CSPG/SG resulted in formation of both SDS stable and soluble complexes despite the absence of pro-domain, suggesting that the pro-domain is not important in forming the complex formation. However, it was necessary with the presence of the MMP inhibitor EDTA in order to prevent the enzyme from processing the core protein as Paper III showed that SG is a MMP-9 substrate.

5.2. Regions in MMP-9 and SG involved in complex formation, from peptide arrays and molecular modelling

The peptide arrays and mutation peptide arrays were able to show us various amino acids and amino acid sequences that seem to involve in the complex formation between proMMP-9 and SG. The array of SG core protein incubated with proMMP-9 as well as rpMMP-9 showed identical binding patterns with small variations in intensities. Also, the binding of proMMP-9 to the region N- and C- terminal of the Ser-Gly repeat zone suggested that the whole core protein is involved in the binding of SG with proMMP-9. Molecular modelling studies of these complexes gave us glimpses into the possibilities of proMMP-9·SG complexes in a simulated system and it shed a light and helped us to gain an insight into the importance of different domains involved in these complex formations.

For **paper I**, we have used peptide array results and the molecular modelling results as complimentary to each other. From this, we observed that both FnII and HPX domains are involved in interactions with SG through a combination of ionic and hydrophobic interactions

together with hydrogen bonds. We also show that the full length MMP-9 is a flexible enzyme with the help of molecular modelling.

5.2.1. Involvement of catalytic domain with SG

From our *in vitro* reconstitution results, we were able to see that without the presence of both FnII module and HPX domain, no proMMP-9·CSPG/SG complexes were formed, so we did not have any expectations on the involvement of the MMP-9 catalytic domain in forming complexes with CSPG/SG. However, during the dynamics simulation of the model based on the SG docked to proMMP-9 FnII, we observed a stable ionic interaction between the catalytic domain of the enzyme with SG. In addition to that, while conducting MD of the full length MMP-9 with SG in near vicinity, we observed that the N-terminal of SG interacted closely with the catalytic domain of MMP-9 by forming two ionic interactions, one of which was stable throughout the DS. This suggests that there might be regions in catalytic domain, which might bind with SG, which are not necessarily involved in the complex formation. Another alternative is that the interaction with the catalytic domain is important for the complex formation, but alone it is not enough to form the strong proMMP-9·SG complex. This is a possibility as, in all the *in vitro* reconstitution studies conducted with both the full-length and deleted MMP-9 variants, the catalytic site was present. However, this provides an excellent basis for a future study to investigate whether certain regions of catalytic domain might be a necessity in combination with either FnII or HPX domains of proMMP-9 to form complexes with SG and possibly other substrates. A possible scheme would be to produce deletion variants of proMMP-9 lacking the regions in catalytic domain, which appeared to be involved in ionic interactions with SG based on the MD simulations. Then we could try to reconstitute these variants *in vitro* with SG. The results might give us a new paradigm into the complex formation of proMMP-9 with SG.

5.2.2. Involvement of FnII module with SG

We managed to settle with seventeen amino acid interactions between FnII module and SG, based on peptide arrays and molecular modelling, which gave a strong impression of the binding pattern between SG and the FnII module of MMP-9. The interacting amino acids in FnII module belonged to peptide spots; 19-22, 35 and 41-49. Most of these amino acids were

present in the second repeat of the FnII module. While the interacting amino acids in SG belonged to peptide spots: 14-15, 21, 47-48 and 51-54. These amino acids were located both N- and C-terminal to the Ser-Gly repeats. These interactions were a mixture of one ionic, 9 hydrophobic and 6 hydrogen bonds.

The peptide array results from the binding of rpMMP-9ΔHPX to the SG peptide array showed that FnII module of proMMP-9 can bind amino acids located both N- and C-terminal for the Ser-Gly repeats. In addition to that, MD simulations of the complex between SG and proMMP-9FnII suggested that the FnII module at the same time can bind amino acids in SG located both N- and C-terminal to the Ser-Gly repeats. This indicates that it is not possible for one SG molecule to bind two proMMP-9 molecules at the same time, i.e. one at both sides of the Ser-Gly repeats.

Previous studies have indicated that gelatin binds to the second FnII repeat, specifically to the amino acids: Arg307, Asp309, Asn319, Tyr320 and Asp323, which seem to be critical for binding [140]. These amino acids belong to the peptide spots 35 and 41-46, in our peptide array of MMP-9 FnII module, which we have found, all binds to SG. Our results from both peptide arrays and molecular modelling showed Arg307 and Tyr320 to be involved in binding with SG, further suggesting the presence of overlapping epitopes in the FnII module to which both SG and gelatin binds. These results line up with the previous results from *in vitro* reconstitution experiments which shows that gelatin inhibits the formation of the proMMP-9·CSPG/SG complex [13]. This alignment of our results with previous studies also strengthens the reliability of our results from both peptide arrays and molecular modelling.

5.2.3. Involvement of HPX domain with SG

When investigating the interaction of the MMP-9 HPX domain with the SG, we came up with two best models. In both models, 19 amino acid interactions gave strong impressions on the binding pattern between SG and the HPX module of MMP-9. In first model, all the interacting amino acids in HPX domain belonged to peptide spots; 69-71 and 76-85, all belonging to fourth blade. These amino acids interacted with the amino acids in SG belonging to peptide spots: 14, 15, 21, and 23-26, all present the N-terminal to the Ser-Gly repeat zone. While in the second model, the interacting amino acids present in HPX domain belonged to peptide spots; 53-54, 56, 57 and 75-85, almost all of which were present in the third blade. These amino acids interacted with the amino acids in SG belonging to peptide spots: 14, 15, 21, 47, 48 and 50-54,

most of which were present C-terminal to the Ser-Gly repeat and few N-terminal to the Ser-Gly repeat zone. In total from these two models, we observed 5 ionic and 30 hydrophobic interactions along with 10 hydrogen bonds. We must understand that a single amino acid might give two types of interaction at the same time, one from the side chains and the other main chain.

The MMP-9 HPX domain is mostly known for driving the non-catalytic functions of the enzyme. This is mainly due to the ability of this domain to interact with substrates, receptors and inhibitors [73, 97] . Studies have shown that HPX domain especially the blade I and IV are involved in binding with gelatin [99]. From our studies, we can see the involvement of blade IV in major interactions with SG, showing the importance of this blade, among others. As discussed before, the reduction sensitivity of the SDS-stable complexes comes from the intra-molecular disulphide bridges in the proMMP-9, one of which is present between the blade I and IV in HPX domain [68, 71].

5.2.4. The flexibility of full length MMP-9 changes in presence and absence of SG

A previous study conducted through a combination of small angle X-ray crystallography and AFM, showed that the full length MMP-9 had a flexible structure consisting of two domains at its terminal regions connected by the OG domain. This apparent flexibility was contributed to the OG domain [72]. In our hands, the MD simulation carried out using only the full length proMMP-9 also showed a very flexible enzyme where the OG domain either stretched out or coiled up, resulting in the two globular domains (catalytic and HPX domain) either close or far apart from each other. Again, this supports the reliability of the results we obtained from molecular modelling.

With this structural flexibility, MMP-9, unlike other MMPs, definitely has an advantage for accessing and interacting with various ECM and non-ECM molecules. For example, previous study on MMP-2 have shown that the first and second blades of its HPX domain was linked to the first FnII repeat. This shows that the relatively shorter OG domain in MMP-2 does not provide any flexibility as it does in MMP-9 [141]. Similarly, in case of MMP-1, the flexibility of its OG domain is also constrained due to the interactions between its HPX domain and the pro-domain [142].

When, SG was kept at close distance to the full length MMP-9, the MD simulations indicated that SG could either be sandwiched between the FnII module and the HPX domain or

bind to only one of these domains. These results also suggests that, both the domains are involved in complex formation with SG and both N- and C-terminal of Ser-Gly repeats in SG are involved in forming these complexes. Given the flexibility of MMP-9 and from what we have seen in MD simulations, we can conclude that SG can bind to FnII and HPX domain at the same time. Furthermore, when SG was placed between the FnII module and the HPX domain even at longer distances and the SG seemed to prefer to interact with the HPX domain, the flexibility of proMMP-9 was much less than without SG present. However, these results also raises questions such as; could two or more SG be involved in forming complexes with MMP-9 at the same time? Could different regions in SG be involved in binding with either FnII or HPX domain in proMMP-9?

As we can see from sections 5.1.1, 5.1.2. and 5.1.3 from this thesis, there are both common and different regions in SG that are involved in binding with catalytic domain, FnII module and the HPX domain, so the questions I have raised are plausible. The common interacting amino acids from SG for both FnII and HPX belong to peptide spots 14-15 and 21, all belonging to the N-terminal of the Ser-Gly repeats. With this information, we could conduct a future study by producing a variant of SG lacking the amino acids from these peptide spots and conducting an *in vitro* reconstitution with proMMP-9. It would also be interesting to study if the natural occurring splice variants of SG due to an alternative splice variant that lack exon two and hence a large part of the N-terminal region is lacking can form a complex with proMMP-9. The results might give answers to some of the questions being raised here.

5.3. Activation of MMP-9 and its recombinant variants

MMP-9 can be activated in various ways with proteases, non-proteases or through organomercurial compounds [64]. However, the enzyme proteolysis is the most studied MMP-9 activation mode so far, which have confirmed MMP-2, MMP-3, MMP-7, MMP-10, MMP-13 and trypsin to be *in vitro* activators of MMP-9 [64, 87]. Studies on the activation of proMMP-9 by trypsin and APMA have shown that the trypsin activated pMMP-9 loses the zinc binding motif (97-PRCGVPD) and has Phe107 as its N-terminal amino acid residue, while the APMA activated pMMP-9 has an intact zinc binding motif and has Met94 as its N-terminal amino acid residue [32, 143-146].

When we activated the proMMP-9 from THP-1 cells with trypsin the results coincided with results from these previous studies. The pro-domain was removed including the zinc

binding motif, which gave an enzyme with full activity. The main forms were observed at 84kDa and minor forms were around 60-80kDa, as described in **paper II**. When we activated the full length recombinant proMMP-9 with both trypsin and APMA, for **paper II and III**, we obtained main forms around 54kDa and minor forms appeared at 45, 49 and 61kDa with the APMA activation. The difference in these two activation was that the APMA activated MMP-9 showed no activity. This is because, APMA activation of MMP-9 also needs a presence of Ca^{2+}, as it leads to truncation of the C-terminal part of MMP-9, then a conformational change takes place that removes the interacting prodomain away from the catalytic domain of MMP-9, leading it its activated form [144, 147, 148].

For **paper II**, two other variants of MMP-9 (rpMMP-9ΔHPX and rpMMP-9ΔOGHPX) were also activated using APMA and trypsin respectively. The APMA activation of rpMMP-9ΔHPX lead to a main form at 118kDa and many minor forms around, 42, 48, 54 and 67kDa, which were basically lost parts from in OG domain and C-terminal. This activated form had intact zinc binding motif and had full enzymatic activity. The trypsin activation of rpMMP-9ΔOGHPX led to a main and minor forms around 39kDa and 35kDa, respectively. The pro-domain was removed during the activation and the enzyme had full activity.

MMP-3, another activator of MMP-9 has been shown to activate MMP-9 in two steps. First, it processes MMP-9 at Glu59-Met60, leading to the relaxing of the MMP-9 structure and then the second processing occurs at Arg106-Phe107, giving a 82kDa isoform of MMP-9 [87]. The activation of recombinant full length rpMMP-9 with MMP-3 in our case showed truncation of both the pro-domain and the C-terminal domain, with an active form around 54kDa together with two smaller forms. However, previous studies have not shown that the MMP-3 activation of MMP-9 also involves the C-terminal truncation, which we have shown in **paper II**. The recombinant rpMMP-9 was used for this activation with MMP-3. The reason for this is that proMMP-9 purified from THP-1 cells have TIMP-1 bound to the HPX domain, which prevents activation with MMP-3. This effect is through binding of the free N-terminal of TIMP-1 to the active sites of these proteases such as MMP-3, which leads to the formation of a ternary complex(s) [32, 62, 148]. This shows the complexity in activation of proMMP-9 depending on its cellular source. Also, it is complicated to try to activate this enzyme without removing the HPX domain. This complicates studies where the intention is to determine if the HPX domain contain exosites for a particular substrate.

5.4. The binding of small substrates and inhibitors to the MMP-9 active site

The knowledge on the subsite preferences of substrates for MMP-9 is important to know as the catalytic cleft of MMP-9 shares structural similarities with the other MMPs [149]. MMP-9 has been shown to have a deep hydrophobic S'_1 pocket in its catalytic cleft and is often the target of small peptide substrates or small inhibitors, [32, 149-152]. For **paper II and III**, we have examined the binding affinity (K_m) of MMP-9 and recombinant rpMMP-9 variants for a quenched fluorescence substrate McaPLGLDpaAR-NH2 (ES001). The MMP-9 and the rMMP-9 activated with APMA, trypsin and MMP-3 gave Km values between 3.0 ± 0.7μM to 4.5 ± 0.4μM. Similarly, for the APMA activated rMMP-9ΔHPX and trypsin-activated rMMP-9ΔOGHPX gave K_m 4.7 ± 1.2μM and 2.7 ± 0.5μM, respectively. This suggests that there is no significant difference in binding of ES001 to different MMP-9 variants, despite the differences in the N- and C-terminal amino acid residues due to different activations. However, as mentioned before this is because the chromogenic substrates only bind to the active site of MMP-9 and the domains of MMP-9 are involved in this binding [32]. However, we should not exclude the possibility that these domains might influence these interactions of small substrates to the catalytic site [32].

The binding of inhibitors to the catalytic site of MMPs, including MMP-9 has been thoroughly studied by using recombinant catalytic MMP domains, along with kinetic and X-ray crystallography [153, 154]. With the presence of the crystal structures of catalytic domain with or without FnII module of MMP-9, it is easy to conduct modelling studies to investigate the interactions of various inhibitors with the MMP-9 [32, 70]. For paper II, we studied the binding affinity of two hydroxamate compounds; 1b and galardin with proMMP-9 and rpMMP-9. These two compounds act as competitive inhibitors against the substrate ES001 when binding to MMP-9, so it was important to first calculate the K_m values of the enzymes which we had already done. To be able to obtain the most precise K_i values, we have used two methods and compared the results. One uses the Morrison equation for a dose response plot v_0/v_i vs [Inhibitor]. The other method uses the linear Henderson plot. The combination of these two plots are a good way of calculating the concentration of enzyme in assay and the K_i values for competitive slow tight binding inhibitors.

For **paper II and III**, the APMA, trypsin or MMP-3 activated MMP-9 or/and rMMP-9 variants, gave K_i values between 0.051 ± 0.003nM to 0.069 ± 0.001nM for galardin. Similarly, APMA activated rMMP-9ΔHPX and trypsin activated rMMP-9ΔOGHPX gave *K*i values of 67 ± 14pM and 55 ± 9pM, respectively. However, the trypsin and APMA activated MMP-9 or/and

rMMP-9, gave much lower K_i values for compound 1b, which came between 0.006 ± 0.000nM to 0.011 ± 0.001nM. This shows that very small amount of compound 1b is needed to inhibit our enzyme compared to galardin. The main reason for this variation in K_i values was that a larger part of compound 1b than of galardin bound to the S'_1 subpocket. Since the K_i values for all MMP-9 variants were more or less in the same range, we can say that no matter what domain MMP-9 lacks, it does not affect the binding of MMP-9 with galardin. From these results, we could say that MMP-9 and its variants binds very strongly to these hydroxamate inhibitors [32]. The binding of these two hydroxamate compounds to MMP-14 and bacterial metalloprotease was much weaker to MMP-9. Docking studies showed that the subsite S'_1 subpocket in MMP-9 is much deeper than in MMP-14.

5.5. MMP-9 cleaves the serglycin core protein

SG is a small proteoglycan, known to have various binders ranging from cell-surface receptors, chemokines, cytokines, compliment components, matrix molecules, proteolytic enzymes, neurotransmitters to intracellular proteins [23]. Even though these proteoglycans are produced intracellularly, they might be secreted constitutively or in a regulated manner, depending on where they are located and with what compounds they are in complex with [24]. These secreted proteins are expected to act as a vehicle for various compounds, proteases and cargo molecules such as chemokines that needs to be released out extracellularly so that they can be transported in a different location, presented to their substrates, or presented to their target cells, respectively [24, 155-157]. For this reason, it is likely that SG might have to protect these compounds from proteolytic attacks, giving them a resistance to protease degradation themselves [24].

Since our work has shown that the human monocytic leukemia cell line THP-1 produced proMMP-9·CSPG/SG complexes, it is natural to question, if the SG is a substrate for proMMP-9. This idea was first supported when the proMMP-9·CSPG/SG heteromers were activated in the presence of Ca^{2+}, even though it is known to stabilize proMMP-9. The presence of Ca^{2+} together with this heteromer led to the initiation of the cleavage of the C-terminal HPX domain of the enzyme and the core protein of PG, resulting in an activated enzyme [68, 139].

In **paper I**, an additional experiment was done to study the importance of prodomain of MMP-9 for forming the complexes with SG. This was done by using proMMP-9 activated by trypsin. Since, we know that trypsin activated pMMP-9 lacks the entire prodomain, we conducted *in vitro* reconstitution with this 83kDa form of MMP-9. Since this form of MMP-9

was already activated and had the possibility of cleaving CSPG/SG, we conducted experiments with and without the presence of EDTA as it is a known metalloproteinase inhibitor. This *in vitro* reconstitution resulted in formation of both SDS-stable and SDS-soluble complexes despite the absence of pro-domain, suggesting that the pro-domain is not important in forming the complexes. However, we also observed that much less complexes were formed in the absence of EDTA than compared to the presence of EDTA. This suggested that active MMP-9 could cleave intact SG.

Paper III, showed that both cABC treated and untreated SG purified from the THP-1 cells can be degraded by APMA activated recombinant MMP-9. The active MMP-9 also cleaved the SG core-protein whether it contained intact CS-chains or just a stub of the CS-chains remaining after cABC treatment. MMP-9 and its variants also cleaved and degraded Ht-SG with variations in the sizes of the cleaved products. These results clearly show that SG is a substrate of MMP-9. The two deletion variants rMMP-9ΔOGHPX activated with trypsin and rMMP-9ΔHPX activated with APMA, were also used to examine the degradation pattern of SG, to see the effect of the processing when the HPX and OG/HPX domains were absent. Similar degradation pattern was seen. Control degradation experiments with galardin was conducted to see the efficiency of this inhibitor at blocking the MMP-9 degradation of Ht-SG. As expected galardin totally blocked the degradation, leading to freezing of the level of degradation of SG by MMP-9 depending on what time point it was added. Similar experiments were conducted to see if small amounts of EDTA, another inhibitor of MMP-9, also could block the degradation of SG. Limited blockage was obtained after 180 min. However, in the presence of 10mM EDTA, full inhibition was obtained. These control experiments confirms that an active MMP-9 cleaves SG.

Since both MMP-9 and CSPG/SG can be isolated together from THP-1 cells, it is interesting to question how and where do these two proteins meet and form these complexes. As discussed above, perhaps the role of SG in proMMP-9·CSPG/SG heteromers is to transport proMMP-9 to its substrates or to other proteoglycans. Previous studies have shown that MMP-9 is bound to the plasma membrane in various cancer cell-lines and other studies have shown that it binds particularly to CD44 receptors in these surfaces [68, 158, 159]. As we know that CD44 is one of the binding partners of SG, it is easy to make a connection that perhaps, the formation of proMMP-9·CSPG/SG in monocytic cancer cell lines, might be to give proMMP-9 access to CD44 receptors and bind to the cell surfaces [23]. Since we see them in these leukemic cells, it is inevitable to question if they can also be found in complexed form in healthy

cells. If yes then, would MMP-9 still degrade SG or does this phenomenon only occurs in pathological states? Another possibility is that proMMP-9 bound to the core protein of SG involves a protection for the enzyme and under certain conditions the proMMP-9 in the complex is activated and cleave the SG core protein. The released peptide itself or a further processed form of the peptide may act as a chemokine or cytokine.

More study is required to find the importance of the MMP-9 cleaved products of SG. Mainly expressed in hematopoietic lineage cells, functionally SG is involved in the proper storage and secretion of various inflammatory mediators such as proteases, histamines, cytokines and chemokines [10]. With this in mind, it is important to question if these cleaved fragments have any similar functions in the ECM. Could they act as matrikines or chemokines? To be able to examine that, it is first important to identify the sites of the MMP-9 cleavage in SG to be able to get information about the peptide fragments. With future study on these fragments, it will also us to speculate the roles of proMMP-9·CSPG/SG complex formation. With various studies done on the sugar chains associated to various proteoglycans, this thesis is also trying to shift the focus to the functionality of core proteins in these proteoglycans.

7. Concluding remarks and future prospective

In present study, we have characterized the different domains of proMMP-9, and recognized different regions in SG, which are important in proMMP-9·CSPG/SG complex formation. We also examined the activity of different variants of the proMMP-9 in forming complexes with SG and further degrading them. These variants were tested to investigate the binding properties of MMP-9 with small substrate and two small inhibitors.

During this four-year study, we have tried to investigate most of the questions and hypothesis we had at the beginning. However, more work needs to be done to have a clearer understanding of proMMP-9, SG and their complex formation. We have managed to obtain answers to the questions and queries we had before we started this work. However, it has left us with more questions as well. Some of the works that can be done in near future are:

- Better techniques needs to be optimised for the purification of the recombinant MMP-9 variants lacking the FnII module.
- Thorough study on the molecular modelling aspect of this work is suggestable, with better models of both full MMP-9 and SG, different approach to docking studies and longer molecular dynamics simulation time.
- Degradation study by using MMP-9 variants lacking FnII module, especially MMP-9ΔFnII is necessary to give a full picture to the processing of SG.
- Cleaved fragments from the SG processed by MMP-9 could be analysed through MS to investigate their characteristics.
- Identify if these complexes are formed by other cells than monocytic cell lines.
- Find out the physiological and pathological roles of proMMP-9·CSPG/SG complexes.
- Production of exosite inhibitors could be a far future prospective.

8. References

1. Theocharis, A. D., Skandalis, S. S., Gialeli, C. & Karamanos, N. K. (2016) Extracellular matrix structure, *Advanced Drug Delivery Reviews.* **97**, 4-27.

2. Theocharis, A., Gialeli, C., Hascall, V. & Karamanos, N. K. (2012) Extracellular matrix: a functional scaffold in *Extracellular matrix: pathobiology and signaling* (Karamanos, N. K., ed) pp. 3-19, Walter de Gruyter GmbH & Co. KG, Berlin.

3. Kim, S. H., Turnbull, J. & Guimond, S. (2011) Extracellular matrix and cell signalling: the dynamic cooperation of integrin, proteoglycan and growth factor receptor, *J Endocrinol.* **209**, 139-51.

4. Cattaruzza, S. & Perris, R. (2006) Approaching the proteoglycome: molecular interactions of proteoglycans and their functional output, *Macromol Biosci.* **6**, 667-80.

5. Schaefer, L. (2012) Introduction in *Extracellular Matrix: Pathobiology and Signaling* (Karamanos, N. K., ed) pp. 135-140, Walter de Gruyter GmbH and Co. KG, Germany.

6. Kolset, S. O. & Tveit, H. (2008) Serglycin--structure and biology, *Cell Mol Life Sci.* **65**, 1073-85.

7. Krusius, T. & Ruoslahti, E. (1986) Primary structure of an extracellular matrix proteoglycan core protein deduced from cloned cDNA, *Proc Natl Acad Sci U S A.* **83**, 7683-7.

8. (1993) Proteoglycans in *Guidebook to the extracellular Matrix and Adhesion Proteins* (Kreis, T. & Vale, R., eds) pp. 12-16, Oxford University Press Inc, New York.

9. Lu, H., McDowell, L. M., Studelska, D. R. & Zhang, L. (2010) Glycosaminoglycans in Human and Bovine Serum: Detection of Twenty-Four Heparan Sulfate and Chondroitin Sulfate Motifs Including a Novel Sialic Acid-modified Chondroitin Sulfate Linkage Hexasaccharide, *Glycobiol Insights.* **2010**, 13-28.

10. Tanaka, Y., Tateishi, R. & Koike, K. (2018) Proteoglycans Are Attractive Biomarkers and Therapeutic Targets in Hepatocellular Carcinoma, *Int J Mol Sci.* **19**.

11. Perrimon, N. & Bernfield, M. (2001) Cellular functions of proteoglycans--an overview, *Seminars in cell & developmental biology.* **12**, 65-67.

12. Nikitovi, D. & Tzanakakis, G. N. (2012) Roles of sulfated and nonsulfated glycosaminoglycans in cancer growth and progression-therapeutic implications in *Extracellular Matrix: Pathobiology And Signalling* (Karamanos, N. K., ed) pp. 66-83.

13. Malla, N., Berg, E., Theocharis, A. D., Svineng, G., Uhlin-Hansen, L. & Winberg, J. O. (2013) In vitro reconstitution of complexes between pro-matrix metalloproteinase-9 and the proteoglycans serglycin and versican, *FEBS J.* **280**, 2870-87.

14. Oynebraten, I., Hansen, B., Smedsrod, B. & Uhlin-Hansen, L. (2000) Serglycin secreted by leukocytes is efficiently eliminated from the circulation by sinusoidal scavenger endothelial cells in the liver, *J Leukoc Biol.* **67**, 183-8.

15. Chang, M. Y., Chan, C. K., Braun, K. R., Green, P. S., O'Brien, K. D., Chait, A., Day, A. J. & Wight, T. N. (2012) Monocyte-to-macrophage differentiation: synthesis and secretion of a complex extracellular matrix, *J Biol Chem.* **287**, 14122-35.

16. Kolset, S. O., Mann, D. M., Uhlin-Hansen, L., Winberg, J. O. & Ruoslahti, E. (1996) Serglycin-binding proteins in activated macrophages and platelets, *J Leukoc Biol.* **59**, 545-54.

17. Scully, O. J., Chua, P. J., Harve, K. S., Bay, B. H. & Yip, G. W. (2012) Serglycin in health and diseases, *Anat Rec (Hoboken).* **295**, 1415-20.

18. Uhlin-Hansen, L., Eskeland, T. & Kolset, S. O. (1989) Modulation of the expression of chondroitin sulfate proteoglycan in stimulated human monocytes, *J Biol Chem.* **264**, 14916-22.

19. Roy, A., Femel, J., Huijbers, E. J., Spillmann, D., Larsson, E., Ringvall, M., Olsson, A. K. & Abrink, M. (2016) Targeting Serglycin Prevents Metastasis in Murine Mammary Carcinoma, *PLoS One.* **11**, e0156151.

20. Roy, A., Attarha, S., Weishaupt, H., Edqvist, P. H., Swartling, F. J., Bergqvist, M., Siebzehnrubl, F. A., Smits, A., Ponten, F. & Tchougounova, E. (2017) Serglycin as a potential biomarker for glioma: association of serglycin expression, extent of mast cell recruitment and glioblastoma progression, *Oncotarget.* **8**, 24815-24827.

21. Niemann, C. U., Kjeldsen, L., Ralfkiaer, E., Jensen, M. K. & Borregaard, N. (2007) Serglycin proteoglycan in hematologic malignancies: a marker of acute myeloid leukemia, *Leukemia.* **21**, 2406-10.

22. Edwards, I. J. (2012) Proteoglycans in prostate cancer, *Nat Rev Urol.* **9**, 196-206.

23. Korpetinou, A., Skandalis, S. S., Labropoulou, V. T., Smirlaki, G., Noulas, A., Karamanos, N. K. & Theocharis, A. D. (2014) Serglycin: at the crossroad of inflammation and malignancy, *Front Oncol.* **3**, 327.

24. Kolset, S. O. & Pejler, G. (2011) Serglycin: a structural and functional chameleon with wide impact on immune cells, *J Immunol.* **187**, 4927-33.

25. Dufour, A. (2015) Degradomics of matrix metalloproteinases in inflammatory diseases, *Front Biosci (Schol Ed).* **7**, 150-67.

26. Winberg, J. O. (2012) Introduction in *Extracellular Matrix: Pathobiology and Signaling* (Karamanos, N. K., ed) pp. 235-238, Walter de Gruyter GmnH and Co. KG, Germany.

27. Cawston, T. E. & Wilson, A. J. (2006) Understanding the role of tissue degrading enzymes and their inhibitors in development and disease, *Best Pract Res Clin Rheumatol.* **20**, 983-1002.

28. Nagase, H. & Murphy, G. (2004) Matrix Metalloproteinases in *Encyclopedia of Biological Chemistry* pp. 657-665, Elsevier

29. Huntley, G. W. (2012) Synaptic circuit remodelling by matrix metalloproteinases in health and disease, *Nat Rev Neurosci.* **13**, 743-57.

30. Hadler-Olsen, E., Fadnes, B., Sylte, I., Uhlin-Hansen, L. & Winberg, J. O. (2011) Regulation of matrix metalloproteinase activity in health and disease, *FEBS J.* **278**, 28-45.

31. Webster, N. L. & Crowe, S. M. (2006) Matrix metalloproteinases, their production by monocytes and macrophages and their potential role in HIV-related diseases, *J Leukoc Biol.* **80**, 1052-66.

32. Sylte, I., Dawadi, R., Malla, N., von Hofsten, S., Nguyen, T. M., Solli, A. I., Berg, E., Adekoya, O. A., Svineng, G. & Winberg, J. O. (2018) The selectivity of galardin and an azasugar-based hydroxamate compound for human matrix metalloproteases and bacterial metalloproteases, *PLoS One.* **13**, e0200237.

33. Nagase, H., Visse, R. & Murphy, G. (2006) Structure and function of matrix metalloproteinases and TIMPs, *Cardiovasc Res.* **69**, 562-73.

34. Nagase, H. & Woessner, J. F., Jr. (1999) Matrix metalloproteinases, *J Biol Chem.* **274**, 21491-4.

35. Massova, I., Kotra, L. P., Fridman, R. & Mobashery, S. (1998) Matrix metalloproteinases: structures, evolution, and diversification, *FASEB J.* **12**, 1075-95.

36. Jobin, P. G., Butler, G. S. & Overall, C. M. (2017) New intracellular activities of matrix metalloproteinases shine in the moonlight, *Biochim Biophys Acta Mol Cell Res.* **1864**, 2043-2055.

37. Rawlings, N. D., Waller, M., Barrett, A. J. & Bateman, A. (2014) MEROPS: the database of proteolytic enzymes, their substrates and inhibitors, *Nucleic Acids Res.* **42**, D503-9.

38. Cui, N., Hu, M. & Khalil, R. A. (2017) Biochemical and Biological Attributes of Matrix Metalloproteinases, *Prog Mol Biol Transl Sci.* **147**, 1-73.

39. Nelson, A. R., Fingleton, B., Rothenberg, M. L. & Matrisian, L. M. (2000) Matrix metalloproteinases: biologic activity and clinical implications, *J Clin Oncol.* **18**, 1135-49.

40. Westermarck, J. & Kahari, V. M. (1999) Regulation of matrix metalloproteinase expression in tumor invasion, *FASEB J.* **13**, 781-92.

41. Verma, R. P. & Hansch, C. (2007) Matrix metalloproteinases (MMPs): chemical-biological functions and (Q)SARs, *Bioorg Med Chem.* **15**, 2223-68.

42. Overall, C. M. & Lopez-Otin, C. (2002) Strategies for MMP inhibition in cancer: innovations for the post-trial era, *Nat Rev Cancer.* **2**, 657-72.

43. Fadnes, B., Hadler-Olsen, E., Sylte, I., Uhlin-Hansen, L. & Winberg, J.-O. (2012) Matrix metalloproteinase complexes and their biological significance in *Extracellular Matrix: Pathobiology and Signaling* pp. 291-314.

44. Rodriguez, D., Morrison, C. J. & Overall, C. M. (2010) Matrix metalloproteinases: what do they not do? New substrates and biological roles identified by murine models and proteomics, *Biochim Biophys Acta.* **1803**, 39-54.

45. Malemud, C. J. (2006) Matrix metalloproteinases (MMPs) in health and disease: an overview, *Front Biosci.* **11**, 1696-701.

46. Page-McCaw, A., Ewald, A. J. & Werb, Z. (2007) Matrix metalloproteinases and the regulation of tissue remodelling, *Nat Rev Mol Cell Biol.* **8**, 221-33.

47. Vu, T. H. & Werb, Z. (2000) Matrix metalloproteinases: effectors of development and normal physiology, *Genes Dev.* **14**, 2123-33.

48. Singh, D., Srivastava, S. K., Chaudhuri, T. K. & Upadhyay, G. (2015) Multifaceted role of matrix metalloproteinases (MMPs), *Front Mol Biosci.* **2**, 19.

49. Gialeli, C., Theocharis, A. D. & Karamanos, N. K. (2011) Roles of matrix metalloproteinases in cancer progression and their pharmacological targeting, *FEBS J.* **278**, 16-27.

50. Werb, Z. & Chin, J. R. (1998) Extracellular matrix remodeling during morphogenesis, *Ann N Y Acad Sci.* **857**, 110-8.

51. Gupta, V., Singh, M. K., Garg, R. K., Pant, K. K. & Khattri, S. (2014) Evaluation of peripheral matrix metalloproteinase-1 in Parkinson's disease: a case-control study, *Int J Neurosci.* **124**, 88-92.

52. Shukla, V., Kumar Shakya, A., Dhole, T. N. & Misra, U. K. (2012) Upregulated expression of matrix metalloproteinases and tissue inhibitors of matrix metalloproteinases in BALB/c mouse brain challenged with Japanese encephalitis virus, *Neuroimmunomodulation.* **19**, 241-54.

53. Collier, I. E., Wilhelm, S. M., Eisen, A. Z., Marmer, B. L., Grant, G. A., Seltzer, J. L., Kronberger, A., He, C. S., Bauer, E. A. & Goldberg, G. I. (1988) H-ras oncogene-transformed human bronchial epithelial cells (TBE-1) secrete a single metalloprotease capable of degrading basement membrane collagen, *J Biol Chem.* **263**, 6579-87.

54. Van den Steen, P. E., Van Aelst, I., Hvidberg, V., Piccard, H., Fiten, P., Jacobsen, C., Moestrup, S. K., Fry, S., Royle, L., Wormald, M. R., Wallis, R., Rudd, P. M., Dwek, R. A. & Opdenakker, G. (2006) The hemopexin and O-glycosylated domains tune gelatinase B/MMP-9 bioavailability via inhibition and binding to cargo receptors, *J Biol Chem.* **281**, 18626-37.

55. Malla, N., Sjoli, S., Winberg, J. O., Hadler-Olsen, E. & Uhlin-Hansen, L. (2008) Biological and pathobiological functions of gelatinase dimers and complexes, *Connect Tissue Res.* **49**, 180-4.

56. Goldberg, G. I., Marmer, B. L., Grant, G. A., Eisen, A. Z., Wilhelm, S. & He, C. S. (1989) Human 72-kilodalton type IV collagenase forms a complex with a tissue inhibitor of metalloproteases designated TIMP-2, *Proc Natl Acad Sci U S A.* **86**, 8207-11.

57. Strongin, A. Y., Collier, I., Bannikov, G., Marmer, B. L., Grant, G. A. & Goldberg, G. I. (1995) Mechanism of cell surface activation of 72-kDa type IV collagenase. Isolation of the activated form of the membrane metalloprotease, *J Biol Chem.* **270**, 5331-8.

58. Kurschat, P., Zigrino, P., Nischt, R., Breitkopf, K., Steurer, P., Klein, C. E., Krieg, T. & Mauch, C. (1999) Tissue inhibitor of matrix metalloproteinase-2 regulates matrix metalloproteinase-2

activation by modulation of membrane-type 1 matrix metalloproteinase activity in high and low invasive melanoma cell lines, *J Biol Chem.* **274**, 21056-62.

59. Seiki, M. (1999) Membrane-type matrix metalloproteinases, *APMIS.* **107**, 137-43.

60. Wilhelm, S. M., Collier, I. E., Marmer, B. L., Eisen, A. Z., Grant, G. A. & Goldberg, G. I. (1989) SV40-transformed human lung fibroblasts secrete a 92-kDa type IV collagenase which is identical to that secreted by normal human macrophages, *J Biol Chem.* **264**, 17213-21.

61. Brew, K. & Nagase, H. (2010) The tissue inhibitors of metalloproteinases (TIMPs): an ancient family with structural and functional diversity, *Biochim Biophys Acta.* **1803**, 55-71.

62. Goldberg, G. I., Strongin, A., Collier, I. E., Genrich, L. T. & Marmer, B. L. (1992) Interaction of 92-kDa type IV collagenase with the tissue inhibitor of metalloproteinases prevents dimerization, complex formation with interstitial collagenase, and activation of the proenzyme with stromelysin, *J Biol Chem.* **267**, 4583-91.

63. Vafadari, B., Salamian, A. & Kaczmarek, L. (2016) MMP-9 in translation: from molecule to brain physiology, pathology, and therapy, *J Neurochem.* **139 Suppl 2**, 91-114.

64. Vandooren, J., Van den Steen, P. E. & Opdenakker, G. (2013) Biochemistry and molecular biology of gelatinase B or matrix metalloproteinase-9 (MMP-9): the next decade, *Crit Rev Biochem Mol Biol.* **48**, 222-72.

65. Rudd, P. M., Mattu, T. S., Masure, S., Bratt, T., Van den Steen, P. E., Wormald, M. R., Kuster, B., Harvey, D. J., Borregaard, N., Van Damme, J., Dwek, R. A. & Opdenakker, G. (1999) Glycosylation of natural human neutrophil gelatinase B and neutrophil gelatinase B-associated lipocalin, *Biochemistry.* **38**, 13937-50.

66. Kumar, S. & Cieplak, P. (2018) Role of N-glycosylation in activation of proMMP-9. A molecular dynamics simulations study, *PLoS One.* **13**, e0191157.

67. Kotra, L. P., Zhang, L., Fridman, R., Orlando, R. & Mobashery, S. (2002) N-Glycosylation pattern of the zymogenic form of human matrix metalloproteinase-9, *Bioorg Chem.* **30**, 356-70.

68. Winberg, J. O., Kolset, S. O., Berg, E. & Uhlin-Hansen, L. (2000) Macrophages secrete matrix metalloproteinase 9 covalently linked to the core protein of chondroitin sulphate proteoglycans, *J Mol Biol.* **304**, 669-80.

69. Olson, M. W., Bernardo, M. M., Pietila, M., Gervasi, D. C., Toth, M., Kotra, L. P., Massova, I., Mobashery, S. & Fridman, R. (2000) Characterization of the monomeric and dimeric forms of latent and active matrix metalloproteinase-9. Differential rates for activation by stromelysin 1, *J Biol Chem.* **275**, 2661-8.

70. Elkins, P. A., Ho, Y. S., Smith, W. W., Janson, C. A., D'Alessio, K. J., McQueney, M. S., Cummings, M. D. & Romanic, A. M. (2002) Structure of the C-terminally truncated human ProMMP9, a gelatin-binding matrix metalloproteinase, *Acta Crystallogr D Biol Crystallogr.* **58**, 1182-92.

71. Cha, H., Kopetzki, E., Huber, R., Lanzendorfer, M. & Brandstetter, H. (2002) Structural basis of the adaptive molecular recognition by MMP9, *J Mol Biol.* **320**, 1065-79.

72. Rosenblum, G., Van den Steen, P. E., Cohen, S. R., Grossmann, J. G., Frenkel, J., Sertchook, R., Slack, N., Strange, R. W., Opdenakker, G. & Sagi, I. (2007) Insights into the structure and domain flexibility of full-length pro-matrix metalloproteinase-9/gelatinase B, *Structure.* **15**, 1227-36.

73. Piccard, H., Van den Steen, P. E. & Opdenakker, G. (2007) Hemopexin domains as multifunctional liganding modules in matrix metalloproteinases and other proteins, *J Leukoc Biol.* **81**, 870-92.

74. Helenius, A. & Aebi, M. (2001) Intracellular functions of N-linked glycans, *Science.* **291**, 2364-9.

75. Takahashi, C., Sheng, Z., Horan, T. P., Kitayama, H., Maki, M., Hitomi, K., Kitaura, Y., Takai, S., Sasahara, R. M., Horimoto, A., Ikawa, Y., Ratzkin, B. J., Arakawa, T. & Noda, M. (1998) Regulation of matrix metalloproteinase-9 and inhibition of tumor invasion by the membrane-anchored glycoprotein RECK, *Proc Natl Acad Sci U S A.* **95**, 13221-6.

76. Oh, J., Takahashi, R., Kondo, S., Mizoguchi, A., Adachi, E., Sasahara, R. M., Nishimura, S., Imamura, Y., Kitayama, H., Alexander, D. B., Ide, C., Horan, T. P., Arakawa, T., Yoshida, H., Nishikawa, S., Itoh, Y., Seiki, M., Itohara, S., Takahashi, C. & Noda, M. (2001) The membrane-anchored MMP inhibitor RECK is a key regulator of extracellular matrix integrity and angiogenesis, *Cell.* **107**, 789-800.

77. Hahn-Dantona, E., Ruiz, J. F., Bornstein, P. & Strickland, D. K. (2001) The low density lipoprotein receptor-related protein modulates levels of matrix metalloproteinase 9 (MMP-9) by mediating its cellular catabolism, *J Biol Chem.* **276**, 15498-503.

78. Swarnakar, S., Paul, S., Singh, L. P. & Reiter, R. J. (2011) Matrix metalloproteinases in health and disease: regulation by melatonin, *J Pineal Res.* **50**, 8-20.

79. Rudra, D. S., Pal, U., Maiti, N. C., Reiter, R. J. & Swarnakar, S. (2013) Melatonin inhibits matrix metalloproteinase-9 activity by binding to its active site, *J Pineal Res.* **54**, 398-405.

80. Atkinson, J. J. & Senior, R. M. (2003) Matrix metalloproteinase-9 in lung remodeling, *Am J Respir Cell Mol Biol.* **28**, 12-24.

81. Han, Y. P., Yan, C., Zhou, L., Qin, L. & Tsukamoto, H. (2007) A matrix metalloproteinase-9 activation cascade by hepatic stellate cells in trans-differentiation in the three-dimensional extracellular matrix, *J Biol Chem.* **282**, 12928-39.

82. Nakamura, H., Fujii, Y., Ohuchi, E., Yamamoto, E. & Okada, Y. (1998) Activation of the precursor of human stromelysin 2 and its interactions with other matrix metalloproteinases, *Eur J Biochem.* **253**, 67-75.

83. Knauper, V., Smith, B., Lopez-Otin, C. & Murphy, G. (1997) Activation of progelatinase B (proMMP-9) by active collagenase-3 (MMP-13), *Eur J Biochem.* **248**, 369-73.

84. Imai, K., Yokohama, Y., Nakanishi, I., Ohuchi, E., Fujii, Y., Nakai, N. & Okada, Y. (1995) Matrix metalloproteinase 7 (matrilysin) from human rectal carcinoma cells. Activation of the precursor, interaction with other matrix metalloproteinases and enzymic properties, *J Biol Chem.* **270**, 6691-7.

85. Overall, C. M., King, A. E., Sam, D. K., Ong, A. D., Lau, T. T., Wallon, U. M., DeClerck, Y. A. & Atherstone, J. (1999) Identification of the tissue inhibitor of metalloproteinases-2 (TIMP-2) binding site on the hemopexin carboxyl domain of human gelatinase A by site-directed mutagenesis. The hierarchical role in binding TIMP-2 of the unique cationic clusters of hemopexin modules III and IV, *J Biol Chem.* **274**, 4421-9.

86. Brew, K., Dinakarpandian, D. & Nagase, H. (2000) Tissue inhibitors of metalloproteinases: evolution, structure and function, *Biochim Biophys Acta.* **1477**, 267-83.

87. Vempati, P., Karagiannis, E. D. & Popel, A. S. (2007) A biochemical model of matrix metalloproteinase 9 activation and inhibition, *J Biol Chem.* **282**, 37585-96.

88. Yegneswaran, S., Tiefenbrunn, T. K., Fernandez, J. A. & Dawson, P. E. (2007) Manipulation of thrombin exosite I, by ligand-directed covalent modification, *J Thromb Haemost.* **5**, 2062-9.

89. Watanabe, Y., Hirakawa, K., Haruyama, T. & Akaike, T. (2001) Direct production of an activated matrix metalloproteinase-9 (gelatinase B) from mammalian cells, *FEBS Lett.* **502**, 63-7.

90. Birkedal-Hansen, H., Moore, W. G., Bodden, M. K., Windsor, L. J., Birkedal-Hansen, B., DeCarlo, A. & Engler, J. A. (1993) Matrix metalloproteinases: a review, *Crit Rev Oral Biol Med.* **4**, 197-250.

91. Schechter, I. & Berger, A. (1967) On the size of the active site in proteases. I. Papain, *Biochem Biophys Res Commun.* **27**, 157-62.

92. Cerda-Costa, N. & Gomis-Ruth, F. X. (2014) Architecture and function of metallopeptidase catalytic domains, *Protein Sci.* **23**, 123-44.

93. O'Farrell, T. J. & Pourmotabbed, T. (1998) The fibronectin-like domain is required for the type V and XI collagenolytic activity of gelatinase B, *Arch Biochem Biophys.* **354**, 24-30.

94. Strongin, A. Y., Collier, I. E., Krasnov, P. A., Genrich, L. T., Marmer, B. L. & Goldberg, G. I. (1993) Human 92 kDa type IV collagenase: functional analysis of fibronectin and carboxyl-end domains, *Kidney Int.* **43**, 158-62.

95. Steffensen, B., Wallon, U. M. & Overall, C. M. (1995) Extracellular matrix binding properties of recombinant fibronectin type II-like modules of human 72-kDa gelatinase/type IV collagenase. High affinity binding to native type I collagen but not native type IV collagen, *J Biol Chem.* **270**, 11555-66.

96. Allan, J. A., Docherty, A. J., Barker, P. J., Huskisson, N. S., Reynolds, J. J. & Murphy, G. (1995) Binding of gelatinases A and B to type-I collagen and other matrix components, *Biochem J.* **309 (Pt 1)**, 299-306.

97. Burg-Roderfeld, M., Roderfeld, M., Wagner, S., Henkel, C., Grotzinger, J. & Roeb, E. (2007) MMP-9-hemopexin domain hampers adhesion and migration of colorectal cancer cells, *Int J Oncol.* **30**, 985-92.

98. Hvidberg, V., Maniecki, M. B., Jacobsen, C., Hojrup, P., Moller, H. J. & Moestrup, S. K. (2005) Identification of the receptor scavenging hemopexin-heme complexes, *Blood.* **106**, 2572-9.

99. Ugarte-Berzal, E., Vandooren, J., Bailon, E., Opdenakker, G. & Garcia-Pardo, A. (2016) Inhibition of MMP-9-dependent Degradation of Gelatin, but Not Other MMP-9 Substrates, by the MMP-9 Hemopexin Domain Blades 1 and 4, *J Biol Chem.* **291**, 11751-60.

100. Dufour, A., Zucker, S., Sampson, N. S., Kuscu, C. & Cao, J. (2010) Role of matrix metalloproteinase-9 dimers in cell migration: design of inhibitory peptides, *J Biol Chem.* **285**, 35944-56.

101. Huber, R., Attili/Abedalkhader, R., Kuper, D., Hauke, L., Luns, B., Brand, K., Weissenborn, K. & Lichtinghagen, R. (2019) Cellular and Molecular Effects of High-Molecular-Weight Heparin on Matrix Metalloproteinase 9 Expression, *Int J Mol Sci.* **20**.

102. Yang, Y. & Rosenberg, G. A. (2015) Matrix metalloproteinases as therapeutic targets for stroke, *Brain Res.* **1623**, 30-8.

103. Muzzio, M. L., Miksztowicz, V., Brites, F., Aguilar, D., Repetto, E. M., Wikinski, R., Tavella, M., Schreier, L. & Berg, G. A. (2009) Metalloproteases 2 and 9, Lp-PLA(2) and lipoprotein profile in coronary patients, *Arch Med Res.* **40**, 48-53.

104. Blankenberg, S., Rupprecht, H. J., Poirier, O., Bickel, C., Smieja, M., Hafner, G., Meyer, J., Cambien, F., Tiret, L. & AtheroGene, I. (2003) Plasma concentrations and genetic variation of matrix metalloproteinase 9 and prognosis of patients with cardiovascular disease, *Circulation.* **107**, 1579-85.

105. Welsh, P., Whincup, P. H., Papacosta, O., Wannamethee, S. G., Lennon, L., Thomson, A., Rumley, A. & Lowe, G. D. (2008) Serum matrix metalloproteinase-9 and coronary heart disease: a prospective study in middle-aged men, *QJM.* **101**, 785-91.

106. Roldan, V., Marin, F., Gimeno, J. R., Ruiz-Espejo, F., Gonzalez, J., Feliu, E., Garcia-Honrubia, A., Saura, D., de la Morena, G., Valdes, M. & Vicente, V. (2008) Matrix metalloproteinases and tissue remodeling in hypertrophic cardiomyopathy, *Am Heart J.* **156**, 85-91.

107. Dhingra, R., Pencina, M. J., Schrader, P., Wang, T. J., Levy, D., Pencina, K., Siwik, D. A., Colucci, W. S., Benjamin, E. J. & Vasan, R. S. (2009) Relations of matrix remodeling biomarkers to blood pressure progression and incidence of hypertension in the community, *Circulation.* **119**, 1101-7.

108. Fang, L., Du, X. J., Gao, X. M. & Dart, A. M. (2010) Activation of peripheral blood mononuclear cells and extracellular matrix and inflammatory gene profile in acute myocardial infarction, *Clin Sci (Lond).* **119**, 175-83.

109. Ducharme, A., Frantz, S., Aikawa, M., Rabkin, E., Lindsey, M., Rohde, L. E., Schoen, F. J., Kelly, R. A., Werb, Z., Libby, P. & Lee, R. T. (2000) Targeted deletion of matrix metalloproteinase-9 attenuates left ventricular enlargement and collagen accumulation after experimental myocardial infarction, *J Clin Invest.* **106**, 55-62.

110. Yabluchanskiy, A., Ma, Y., Iyer, R. P., Hall, M. E. & Lindsey, M. L. (2013) Matrix metalloproteinase-9: Many shades of function in cardiovascular disease, *Physiology (Bethesda).* **28**, 391-403.

111. Lehoux, S., Lemarie, C. A., Esposito, B., Lijnen, H. R. & Tedgui, A. (2004) Pressure-induced matrix metalloproteinase-9 contributes to early hypertensive remodeling, *Circulation.* **109**, 1041-7.

112. Motovali-Bashi, M., Sadeghi, M. & Hemmati, S. (2010) Serum MMP-9 level associated with initiation and progression steps of breast cancer in the Iranian population, *Reprod Sci.* **17**, 585-9.

113. Rybakowski, J. K. (2009) Matrix Metalloproteinase-9 (MMP9)-A Mediating Enzyme in Cardiovascular Disease, Cancer, and Neuropsychiatric Disorders, *Cardiovasc Psychiatry Neurol.* **2009**, 904836.

114. Sakata, K., Shigemasa, K., Nagai, N. & Ohama, K. (2000) Expression of matrix metalloproteinases (MMP-2, MMP-9, MT1-MMP) and their inhibitors (TIMP-1, TIMP-2) in common epithelial tumors of the ovary, *Int J Oncol.* **17**, 673-81.

115. Wu, Z. S., Wu, Q., Yang, J. H., Wang, H. Q., Ding, X. D., Yang, F. & Xu, X. C. (2008) Prognostic significance of MMP-9 and TIMP-1 serum and tissue expression in breast cancer, *Int J Cancer.* **122**, 2050-6.

116. Holanda, A. O., Oliveira, A. R., Cruz, K. J., Severo, J. S., Morais, J. B., Silva, B. B. & Marreiro, D. D. (2017) Zinc and metalloproteinases 2 and 9: What is their relation with breast cancer?, *Rev Assoc Med Bras (1992).* **63**, 78-84.

117. Xing, L. L., Wang, Z. N., Jiang, L., Zhang, Y., Xu, Y. Y., Li, J., Luo, Y. & Zhang, X. (2007) Matrix metalloproteinase-9-1562C>T polymorphism may increase the risk of lymphatic metastasis of colorectal cancer, *World J Gastroenterol.* **13**, 4626-9.

118. Van Den Steen, P. E., Wuyts, A., Husson, S. J., Proost, P., Van Damme, J. & Opdenakker, G. (2003) Gelatinase B/MMP-9 and neutrophil collagenase/MMP-8 process the chemokines human GCP-2/CXCL6, ENA-78/CXCL5 and mouse GCP-2/LIX and modulate their physiological activities, *Eur J Biochem.* **270**, 3739-49.

119. Malla, N., Berg, E., Uhlin-Hansen, L. & Winberg, J. O. (2008) Interaction of pro-matrix metalloproteinase-9/proteoglycan heteromer with gelatin and collagen, *J Biol Chem.* **283**, 13652-65.

120. Coussens, L. M., Fingleton, B. & Matrisian, L. M. (2002) Matrix metalloproteinase inhibitors and cancer: trials and tribulations, *Science.* **295**, 2387-92.

121. Fujita-Yamaguchi, Y. (2015) Affinity Chromatography of Native and Recombinant Proteins from Receptors for Insulin and IGF-I to Recombinant Single Chain Antibodies, *Frontiers in Endocrinology.* **6**.

122. Roeb, E., Schleinkofer, K., Kernebeck, T., Potsch, S., Jansen, B., Behrmann, I., Matern, S. & Grotzinger, J. (2002) The matrix metalloproteinase 9 (mmp-9) hemopexin domain is a novel gelatin binding domain and acts as an antagonist, *J Biol Chem.* **277**, 50326-32.

123. Duong-Ly, K. & Gabelli, S. (2014) Salting out of Proteins Using Ammonium Sulfate Precipitation, *Methods in enzymology.* **541**, 85-94.

124. Scopes, R. (1993) in *Protein Purification: Principles and Practice* pp. 71-101, Springer, New York.

125. Freydell, E. J., van der Wielen, L. A., Eppink, M. H. & Ottens, M. (2010) Size-exclusion chromatographic protein refolding: fundamentals, modeling and operation, *J Chromatogr A.* **1217**, 7723-37.

126. Heussen, C. & Dowdle, E. B. (1980) Electrophoretic analysis of plasminogen activators in polyacrylamide gels containing sodium dodecyl sulfate and copolymerized substrates, *Anal Biochem.* **102**, 196-202.

127. Mahmood, T. & Yang, P. C. (2012) Western blot: technique, theory, and trouble shooting, *N Am J Med Sci.* **4**, 429-34.

128. Min, D. H. & Mrksich, M. (2004) Peptide arrays: towards routine implementation, *Curr Opin Chem Biol.* **8**, 554-8.

129. Szymczak, L. C., Kuo, H. Y. & Mrksich, M. (2018) Peptide Arrays: Development and Application, *Anal Chem.* **90**, 266-282.

130. Gromiha, M. M., Nagarajan, R. & Selvaraj, S. (2019) Protein Structural Bioinformatics: An Overview in *Encyclopedia of Bioinformatics and Computational Biology* pp. 445-459

131. Geng, C., Jung, Y., Renaud, N., Honavar, V., Bonvin, A. & Xue, L. C. (2019) iScore: A novel graph kernel-based function for scoring protein-protein docking models, *Bioinformatics*.

132. Singh, A., Vanga, S. K., Orsat, V. & Raghavan, V. (2018) Application of molecular dynamic simulation to study food proteins: A review, *Crit Rev Food Sci Nutr.* **58**, 2779-2789.

133. Roos, K., Wu, C., Damm, W., Reboul, M., Stevenson, J. M., Lu, C., Dahlgren, M. K., Mondal, S., Chen, W., Wang, L., Abel, R., Friesner, R. A. & Harder, E. D. (2019) OPLS3e: Extending Force Field Coverage for Drug-Like Small Molecules, *J Chem Theory Comput.* **15**, 1863-1874.

134. Bechet, J. J., Houadjeto, M. & d'Albis, A. (1986) Active-site titration of enzymes at high concentration. Application to myosin ATPase, *Eur J Biochem.* **161**, 343-9.

135. Morrison, J. F. (1969) Kinetics of the reversible inhibition of enzyme-catalysed reactions by tight-binding inhibitors, *Biochim Biophys Acta.* **185**, 269-86.

136. Henderson, P. J. (1972) A linear equation that describes the steady-state kinetics of enzymes and subcellular particles interacting with tightly bound inhibitors, *Biochem J.* **127**, 321-33.

137. Malla, N., Berg, E., Moens, U., Uhlin-Hansen, L. & Winberg, J. O. (2011) Biosynthesis of promatrix metalloproteinase-9/chondroitin sulphate proteoglycan heteromer involves a Rottlerin-sensitive pathway, *PLoS One.* **6**, e20616.

138. Xu, X., Chen, Z., Wang, Y., Yamada, Y. & Steffensen, B. (2005) Functional basis for the overlap in ligand interactions and substrate specificities of matrix metalloproteinases-9 and -2, *Biochem J.* **392**, 127-34.

139. Winberg, J. O., Berg, E., Kolset, S. O. & Uhlin-Hansen, L. (2003) Calcium-induced activation and truncation of promatrix metalloproteinase-9 linked to the core protein of chondroitin sulfate proteoglycans, *Eur J Biochem.* **270**, 3996-4007.

140. Collier, I. E., Krasnov, P. A., Strongin, A. Y., Birkedal-Hansen, H. & Goldberg, G. I. (1992) Alanine scanning mutagenesis and functional analysis of the fibronectin-like collagen-binding domain from human 92-kDa type IV collagenase, *J Biol Chem.* **267**, 6776-81.

141. Morgunova, E., Tuuttila, A., Bergmann, U., Isupov, M., Lindqvist, Y., Schneider, G. & Tryggvason, K. (1999) Structure of human pro-matrix metalloproteinase-2: activation mechanism revealed, *Science.* **284**, 1667-70.

142. Lauer-Fields, J. L., Juska, D. & Fields, G. B. (2002) Matrix metalloproteinases and collagen catabolism, *Biopolymers.* **66**, 19-32.

143. Woessner, J. F. & Nagase, H. (2000) in *Matrix Metalloproteinases and TIMPs* (P, I. S., ed), Oxford University Press, Oxford.

144. Bu, C. H. & Pourmotabbed, T. (1995) Mechanism of activation of human neutrophil gelatinase B. Discriminating between the role of Ca2+ in activation and catalysis, *J Biol Chem.* **270**, 18563-9.

145. Triebel, S., Blaser, J., Reinke, H., Knauper, V. & Tschesche, H. (1992) Mercurial activation of human PMN leucocyte type IV procollagenase (gelatinase), *FEBS Lett.* **298**, 280-4.

146. Bu, C. H. & Pourmotabbed, T. (1996) Mechanism of Ca2+-dependent activity of human neutrophil gelatinase B, *J Biol Chem.* **271**, 14308-15.

147. Morodomi, T., Ogata, Y., Sasaguri, Y., Morimatsu, M. & Nagase, H. (1992) Purification and characterization of matrix metalloproteinase 9 from U937 monocytic leukaemia and HT1080 fibrosarcoma cells, *Biochem J.* **285 (Pt 2)**, 603-11.

148. Ogata, Y., Itoh, Y. & Nagase, H. (1995) Steps involved in activation of the pro-matrix metalloproteinase 9 (progelatinase B)-tissue inhibitor of metalloproteinases-1 complex by 4-aminophenylmercuric acetate and proteinases, *J Biol Chem.* **270**, 18506-11.

149. Kridel, S. J., Chen, E., Kotra, L. P., Howard, E. W., Mobashery, S. & Smith, J. W. (2001) Substrate hydrolysis by matrix metalloproteinase-9, *J Biol Chem.* **276**, 20572-8.

150. Stocker, W., Grams, F., Baumann, U., Reinemer, P., Gomis-Ruth, F. X., McKay, D. B. & Bode, W. (1995) The metzincins--topological and sequential relations between the astacins, adamalysins, serralysins, and matrixins (collagenases) define a superfamily of zinc-peptidases, *Protein Sci.* **4**, 823-40.

151. Bode, W., Fernandez-Catalan, C., Tschesche, H., Grams, F., Nagase, H. & Maskos, K. (1999) Structural properties of matrix metalloproteinases, *Cell Mol Life Sci.* **55**, 639-52.

152. Murphy, G., Nguyen, Q., Cockett, M. I., Atkinson, S. J., Allan, J. A., Knight, C. G., Willenbrock, F. & Docherty, A. J. (1994) Assessment of the role of the fibronectin-like domain of gelatinase A by analysis of a deletion mutant, *J Biol Chem.* **269**, 6632-6.

153. Rowsell, S., Hawtin, P., Minshull, C. A., Jepson, H., Brockbank, S. M., Barratt, D. G., Slater, A. M., McPheat, W. L., Waterson, D., Henney, A. M. & Pauptit, R. A. (2002) Crystal structure of human MMP9 in complex with a reverse hydroxamate inhibitor, *J Mol Biol.* **319**, 173-81.

154. Tochowicz, A., Maskos, K., Huber, R., Oltenfreiter, R., Dive, V., Yiotakis, A., Zanda, M., Pourmotabbed, T., Bode, W. & Goettig, P. (2007) Crystal structures of MMP-9 complexes with five inhibitors: contribution of the flexible Arg424 side-chain to selectivity, *J Mol Biol.* **371**, 989-1006.

155. Kunder, C. A., St John, A. L., Li, G., Leong, K. W., Berwin, B., Staats, H. F. & Abraham, S. N. (2009) Mast cell-derived particles deliver peripheral signals to remote lymph nodes, *J Exp Med.* **206**, 2455-67.

156. Meen, A. J., Oynebraten, I., Reine, T. M., Duelli, A., Svennevig, K., Pejler, G., Jenssen, T. & Kolset, S. O. (2011) Serglycin is a major proteoglycan in polarized human endothelial cells and is implicated in the secretion of the chemokine GROalpha/CXCL1, *J Biol Chem.* **286**, 2636-47.

157. Woulfe, D. S., Lilliendahl, J. K., August, S., Rauova, L., Kowalska, M. A., Abrink, M., Pejler, G., White, J. G. & Schick, B. P. (2008) Serglycin proteoglycan deletion induces defects in platelet aggregation and thrombus formation in mice, *Blood.* **111**, 3458-67.

158. Bourguignon, L. Y., Gunja-Smith, Z., Iida, N., Zhu, H. B., Young, L. J., Muller, W. J. & Cardiff, R. D. (1998) CD44v(3,8-10) is involved in cytoskeleton-mediated tumor cell migration and matrix metalloproteinase (MMP-9) association in metastatic breast cancer cells, *J Cell Physiol.* **176**, 206-15.

159. Yu, Q. & Stamenkovic, I. (1999) Localization of matrix metalloproteinase 9 to the cell surface provides a mechanism for CD44-mediated tumor invasion, *Genes Dev.* **13**, 35-48.

PAPER I

Motifs and amino acids involved in the formation of complexes between pro-matrix metalloproteinase-9 and the proteoglycan serglycin core protein

Rangita Dawadi, Nabin Malla, Beate Hegge, Imin Wushur, Eli Berg, Gunbjørg Svineng, Ingebrigt Sylte and Jan-Olof Winberg*

Department of Medical Biology, Faculty of Health Sciences, UiT-The Arctic University of Norway, 9037 Tromsø, Norway.

*Corresponding author.

Abstract

Previously it was shown that the leukemic macrophage cell line THP-1 produced a part of proMMP-9 in complex with a chondroitin sulphate core protein and that the complex was SDS-stable and reduction sensitive. This complex could be reconstituted *in vitro* using purified serglycin and it was suggested that both the FnII module and the HPX domain in proMMP-9 was involved in the complex formation. It was also shown that the reduction sensitive complex did not involve inter disulphide bridges. The present work intends to give answer to questions regarding whether both the FnII and HPX regions are needed for the complex formation, which parts of the two molecules form this strong interaction and what type of binding is involved. For that purpose we expressed and purified various recombinant proMMP-9 deletion variants, isolated CSPG and serglycin from THP-1 cells, used *in vitro* reconstitution assays, peptide arrays, homology modelling, docking and molecular dynamics simulation studies. *In vitro* reconstitution studies revealed that proMMP-9 variants that lacked both the FnII module and the HPX domain could not form the proMMP-9·CSPG/SG complex. Variants that contained at least the FnII module or the HPX domain formed the complex. In serglycin, it was enough with the core protein. Peptide arrays, docking and molecular dynamic (MD) studies suggested the interactions between the two macromolecules in the complex and the dynamic of the interacting regions. The docking and MD studies using the full-length proMMP-9 also suggested that the SG core protein at the same time as it interacted with the FnII module and/or HPX domain it also interacted with parts of the catalytic region and that the complex was held together by a mixture of ionic, hydrophobic and hydrogen bond interactions.

Keywords: Serglycin, proMMP-9, proMMP-9 deletion variants, proMMP-9 complexes, *in vitro* reconstitution, peptide arrays, molecular modelling, docking, molecular dynamics simulation.

1. Introduction

The matrix metalloprotease (MMP) or matrixin family is a group of extracellular zinc and calcium dependent metallo-enzymes expressed by most cells and tissues. In humans there are 23 different MMPs, seven membrane bound and 16 secreted, where MMP-9 is one of the secreted variants[1]. The MMPs as a group, as well as individual enzymes have broad substrate specificity and together they are able to degrade almost all extracellular matrix proteins. In addition, they cleave a number of non-extracellular matrix molecules, such as cytokines, chemokines, adhesion molecules, cell receptors, proteases (including MMPs), protease inhibitors and a number of intracellular proteins [1-8]. Due to their broad substrate specificity, MMPs play a critical role in normal development, cell and tissue homeostasis, while dysregulation during disease may be either detrimental or protective to the organism. Their dual role in diseases appears to depend on various factors such as their physical location, timeframe of their activity and the substrate cleaved [1, 4-7, 9-18]. The numerous interactions between proteins and other molecules regulate their accessibility to proteolytic degradation, by either hiding protease cleavage sites or exposing new sites. Similarly, proteases form interactions with molecules in the extracellular matrix. This may affect their location, substrate specificity and catalytic efficiency [1, 19-27].

MMP-9 is secreted as an inactive proenzyme from various types of cells and like the other MMPs it contains an N-terminal prodomain, a catalytic domain and a C-terminal hemopexin-like (HPX) domain. In addition, MMP-9 contains a module in the catalytic domain of three fibronectin-II like repeats (FnII) and a unique highly glycosylated hinge domain (OG) that connects the catalytic and the HPX domains [1, 28]. This OG domain is very flexible as shown by small angle X-ray crystallography along with atomic force microscopy [29] and the likely reason why a 3D-structure of the entire protein lacks. However, the 3D-structure of the MMP-9 HPX domain is known [30] as well as for a mini-MMP-9 which consists of just the pro- and catalytic domain including the FnII module [31].

ProMMP-9 is secreted from cells as a monomer and an SDS-stable (reduction sensitive) homodimer/homotrimer [28, 32-34]. In addition, proMMP-9 is known to form heteromer complexes with various types of molecules such as TIMP-1 and -3 (tissue inhibitors of metalloproteases), lipocalin/NGAL (neutrophil gelatinase associated lipocalin), haptoglobin (Hp), proMMP-1, proMMP-8, heparin and various proteoglycan (PG) core proteins [19, 23]. THP-1 cells secrete proMMP-9 as a monomer, homodimer/homotrimer and

as heteromers with one or several chondroitin sulphate PG (CSPG) core proteins [35, 36]. Both the homodimer/homotrimer and the heteromers are SDS-stable and reduction sensitive. Addition of Ca^{2+} to the isolated proMMP-9·CSPG complex resulted in a stepwise activation and processing of proMMP-9, and release of the enzyme from the CSPG [37]. The pattern of the processing suggests that the enzyme binds to the CSPG core protein through the HPX domain, and cleave the CSPG core protein before being from the CSPG. It was also shown that the CSPG core protein in the formed proMMP-9·CSPG complex hides the region in the enzymes' FnII module that is involved in binding to gelatin [38]. This suggested that the CSPG also binds to the enzyme through the FnII module.

The proMMP-9·CSPG complexes could be reconstituted *in vitro* by mixing proMMP-9 purified from THP-1 cells with isolated CSPGs from the leukemic monocyte cell lines THP-1, U-937 and MonoMac, as well as the two purified CSPGs, serglycin (SG) from human myeloma cells and versican from normal human aortas [39]. The *in vitro* reconstitution resulted in two types of proMMP-9·CSPG complexes, one was SDS-stable and reduction sensitive, and the other was SDS-soluble. The *in vitro* reconstitution of the complexes showed that the reduction sensitive complexes were not due to a disulphide bridge between the two proteins but rather due to a mixture of ionic and hydrophobic interactions. Gelatin inhibited the formation of both type of complexes, while TIMP-1 only inhibited the formation of the SDS-soluble complex. This suggest that both the FnII module and the HPX domain are involved in the complex formation.

In the present work, we have purified proMMP-9 from THP-1 cells, produced and purified recombinant full-length proMMP-9 and five recombinant deletion variants. The deletion variants lack either the C-terminal HPX domain, the HPX and the hinge region (OG-domain) or the FnII like module. In addition one variant lacked the both the FnII module and the HPX domain and another variant lacked the FnII module in addition to the OG and HPX domains (Fig. 1). These variants have been used for *in vitro* reconstitution experiments with isolated CSPGs and purified SG to determine which regions of the enzyme are involved in the complex formation. A special focus is on the FnII module and the HPX domain in order to determine if both domains/modules are needed for the formation of the SDS-stable and SDS-soluble complexes, or if it is enough with only one of these domains/modules present. *In vitro* reconstitution experiments with recombinant His-tagged serglycin (Ht-SG) lacking GAG-chains were also performed in order to determine if CS-chains are necessary for the formation of the complexes. Peptide arrays, homology modelling, docking and molecular dynamics

(MD) simulation experiments were performed to determine which parts of the SG core protein and which parts of the FnII module and the HPX domain of proMMP-9 are involved in the complex formation.

2. Results and discussion

2.1. Expression and purification of recombinant domain variants of human proMMP-9 and full-length proMMP-9 from THP-1 cells

Production and purification of recombinant full-length proMMP-9 (rpMMP-9) were performed as described previously [40]. The recombinant deletion variants of proMMP-9 (Fig. 1A) were generated and purified as described in the Materials and Methods. Production and purification of proMMP-9 from THP-1 cells (pMMP-9) were performed as described previously [38, 40]. The purified and partly purified proMMP-9 variants were subjected to gelatin zymography (Fig. 1B), SDS-PAGE and Western blotting (Fig. 2). In addition, crude media containing proMMP-9 deletion variants were subjected to real-time gelatin zymography (Fig. 1C) and Western blotting (Fig. 2),

The variants containing the FnII module in the catalytic domain were purified on a Gelatin-Sepharose column. SDS-PAGE both under reducing and non-reducing conditions shows that the purified recombinant enzymes containing the FnII module (rpMMP-9, rpMMP-9ΔHPX and rpMMP-9ΔOGHPX), as well as the proMMP-9 purified from THP-1 cells (pMMP-9) were almost homogeneous (Fig. 2A). As we showed previously [38, 40], the purified proMMP-9 from THP-1 cells (pMMP-9) also contained a small amount of TIMP-1 (30 kDa). Gelatin binds to the FnII module in the catalytic domain [41-45]. Previously, it was suggested that gelatin also binds to the HPX domain in MMP-9 [46, 47]. In these studies, recombinant murine and human HPX-9 domains were used [46, 47]. Therefore, we first tried to purify the deletion variant that only lacked the FnII module (rpMMP-9ΔFnII) on a Gelatin-Sepharose column. However, this deletion variant did not bind to this column under the conditions used, and therefore, several other purification methods were tested. A previous study reported that full length recombinant proMMP-9 isolated from sf9 insect cells binds to Helix pomatia agglutinin (HPA) in contrast to deletion variants of MMP-9 lacking the O-glycosylated hinge region (OG) [48]. In our hands, rpMMP-9ΔFnII did not bind to HPA-linked agarose beads. Therefore, two other methods were tested. In one method, the crude media containing proMMP-9ΔFnII was applied to NH_4SO_4 precipitation followed by gel

filtration using Sephacryl S-200 as described in Materials and Methods. In the other method, the crude insect medium containing proMMP-9ΔFnII was first applied to a spin column with a 30 kDa cut-off and thereafter applied to a Heparin-Sepharose column as described in Materials and Methods. None of these two methods resulted in a pure homogeneous product as seen in Fig. 2B. Therefore, in our further experiments with this deletion variant, either the partly purified enzyme (from the HS-column or the S-200 column) or the crude unpurified media were used. Only the crude media containing the other two deletion variants that were lacking the FnII module (rpMMP-9ΔFnIIHPX and rpMMP-9ΔFnIIOGHPX) were used in the *in vitro* reconstitution experiments. As can be seen in Figs. 1C and 2C, the expressed triple deletion variant (rpMMP-9ΔFnIIOGHPX) had the expected molecular size of around 28 kDa. The rpMMP-9ΔFnIIHPX with an expected molecular size of the protein (without bound sugar chains to the OG domain) of around 35 kDa was expressed with main activity bands around 50 – 60 kDa (Fig. 1C) and Western blot showed two main MMP-9 bands, one with a molecular size of 50 kDa and the other around 55 kDa (Fig. 2C). This suggests that the glycosylation of the OG domain contributes with approximately 15 - 20 kDa to the molecular size of enzyme. In addition, several minor bands with lower molecular size appeared (Fig. 2C). The bands with a size lower than 35 kDa indicate that the enzyme has been partly processed during the expression. Noticeable, in some of the batches expressing rpMMP-9ΔFnIIHPX deletion variant, in addition to the bands at 50 - 55 kDa, a band with molecular sizes around 100 - 120 kDa also appeared (Fig. 1C, 2C). Under reducing conditions, the band around 100 - 120 kDa in the Western blot disappeared (Fig. 2C), suggesting that it is a homodimer of the rpMMP-9ΔFnIIHPX.

Both SDS-PAGE (Fig. 2A) and Western blotting (Fig. 2C) under reducing and non-reducing conditions, as well as gelatin zymography (Fig. 1B) and real-time gelatin zymography (Fig. 1C) showed that recombinant variants containing the OG domain of proMMP-9 and the proMMP-9 from THP-1 cells formed a monomer and a reduction sensitive homomultimer. The recombinant variants lacking the OG domain only formed monomers (Figs. 1B and C, Figs. 2A-C). This is consistent with a previous study of recombinant proMMP-9 deletion variants [48]. The size of the monomers of rpMMP-9ΔHPX and rpMMP-9ΔFnII deletion variants were almost identical, with a molecular size around 70 kDa. The homomultimer of the rpMMP-9ΔFnII is slightly larger than the corresponding homomultimer of rpMMP-9ΔHPX. Previously it was shown that the homomultimers were produced intracellularly and concomitantly with glycosylation [33]. The dimers/trimers could be

separated from the monomers and both forms were stable [33, 34]. The reduction sensitive homomultimer has been assumed to be a homodimer linked by a disulphide bridge [32, 33]. Recently, it was suggested that the reduction sensitive proMMP-9 multimer with a molecular size of approximately 225 kDa is not a dimer but a disulphide linked cyclic homotrimer, although the presence of disulphide bridges were not directly proven [34]. Recombinant produced HPX domain of MMP-9 (HPX-9) also forms a monomer and a reduction sensitive homodimer [30]. X-ray crystallography showed that the reduction sensitive dimer was not linked by an inter disulfide bridge, but by hydrophobic interactions and an ionic bond [30]. The reduction sensitivity occurred due to breaking the intra disulphide bridge between ^{516}C and ^{704}C. We have not tried to identify the nature of the size difference between the homomultimers formed with rpMMP-9ΔHPX and rpMMP-9ΔFnII. As expected, the proMMP-9ΔHPX variant was not detected in Western blotting using an antibody against the MMP-9HPX domain (MMP-9HPXab), while the variants containing this domain were detected (Fig. 2C). MS-MS analysis confirmed the amino acid sequences of the expressed protein variants, except for the ΔFnII variants that were not sent to MS analysis due to the presence of large impurities in these preparations that were partly purified.

2.2. Production and purification of CSPG/SG and serglycin

CSPG was produced in unstimulated THP-1 cells (monocytes) as described previously [35], and the secreted CSPG was purified as described in Materials and Methods. From the Q-Sepharose purified preparation of CSPG, SG was separated from other putative CSPGs using a Sephacryl S-400 column as described in Materials and Methods. The elution profile and the purity of the purified SG are shown in Fig. S1. Fractions II-IV contained SG, but no versican based on Western blotting. In silver stained SDS-PAGE, a main band of approximately 26 kDa occurred in the cABC treated material, corresponding to the size of the SG band(s) seen in the Western blots (Fig. S1). Previously, we showed that the purified CSPG material from THP-1 cells in addition to SG also contained versican [39]. Versican is a large proteoglycan with a $M_r \geq 1000$ kDa, consisting of a core protein with a M_r around 400 kDa and 12-15 CS-chains attached along with N- and O-linked oligosaccharides [49]. As seen from Fig. S1, if versican was present in the Q-Sepaharose purified CSPG, it should be eluted in faction I from the Sephacryl S-400 column. The amount of proteoglycans in the different fractions was determined by the Safranin O method. Based on this, the amount of proteoglycan in fraction I

is approximately 0.7% of the total amount of the produced proteoglycans. This suggests that the major secreted proteoglycan is SG. This fits well with previous studies showing that the main CSPG produced by THP-1 monocytes is SG [50, 51].

2.3. In vitro reconstitution of proMMP-9·CSPG complexes using full length and deletion variants of proMMP-9

Previously we showed that proMMP-9 forms SDS-stable and SDS-soluble complexes with purified SG and versican [39]. Because the vast majority of the secreted proteoglycan in the purified CSPG fraction is SG, we can assume that the *in vitro* reconstituted proMMP-9·CSPG complexes are with SG. Therefore, most of the *in vitro* reconstitution studies described below are with the purified CSPG, which we from here refer to as CSPG/SG. Some reconstitution experiments were performed with both CSPG/SG and SG purified from THP-1 cells, and as expected, the obtained results were identical. When we refer to the complexes obtained in the present work, they are called proMMP-9·CSPG/SG.

Previous studies suggested that both the prodomain, the FnII module and the HPX domain of proMMP-9 to some extent are involved in the formation of the proMMP-9·CSPG complexes [37-39]. In the present study, purified CSPG/SG and SG from unstimulated THP-1 cells were used. Purified CSPG from unstimulated THP-1 cells (monocytes) contains no or only a limited amount of proMMP-9·CSPG in contrast to CSPG isolated from PMA stimulated THP-1 cells (macrophages) [35]. Complexes formed by *in vitro* reconstitution with different MMP-9 variants along with CSPG/SG or SG were detected by gelatin zymography and Western blotting (Fig. 3). The full-length variants of proMMP-9 (pMMP-9 and rpMMP-9) form SDS-stable and SDS-soluble complexes with CSPG/SG (Fig. 3A). Previously it was shown that calcium, which is known to stabilize MMP-9, induced activation of proMMP-9 bound to the CSPG but not of unbound proMMP-9 [37]. This Ca^{2+}-induced activation of proMMP-9 bound to the CSPG core protein resulted in the removal of the prodomain, followed by a stepwise truncation of the HPX domain. The size of the MMP-9 fragments also suggested that parts of the CSPG core protein were cleaved, but remained bound to the truncated MMP-9. Furthermore, APMA which is an activator of proMMP-9 could not activate proMMP-9 bound to the CSPG, but instead prevented the calcium induced activation [37]. This indicates that the prodomain might be involved in the complex formation along with the FnII module. X-ray crystal structures of proMMP-9 lacking the hinge and HPX domains

showed that the N-terminal part of the prodomain interact with the third repeat of the FnII module [31]. This interaction suggests another alternative for the Ca^{2+} induced activation and truncation of the proMMP-9·CSPG complex, which is that the prodomain is not involved in the complex formation with the CSPG core protein. However, the effect of Ca^{2+} and APMA on the proMMP-9·CSPG complex may be influenced by the interaction between the prodomain and the third repeat of the FN module. To test if the enzymes' prodomain is necessary for the complex formation between proMMP-9 and the CSPG/SG core protein, proMMP-9 purified from THP-1 cells were activated by trypsin. This generated a 83 kDa form of MMP-9 (Fig. 3B) with ^{88}F as the N-terminal amino acid [52] which we previously showed to be an active protease that degrade the fluorescence quenched substrate McaPLGLDpaAR-NH_2 [40]. As an active form of MMP-9 may cleave the CSPG/SG core protein, the *in vitro* reconstitution of the complex was performed in the presence and absence of the metalloproteinase inhibitor EDTA. As shown in Fig. 3B, both SDS-stable and SDS-soluble complexes were formed, indicating that the presence of the prodomain is not necessary for the complex formation. However, it appears that the active form of MMP-9 can cleave the CSPG/SG core protein as less complex formed in the absence of EDTA than in the presence of EDTA (Fig. 3B).

Gelatin zymography showed that the HPX and OGHPX deletion variants of proMMP-9 (rpMMP-9ΔHPX and rpMMP-9ΔOGHPX) also formed SDS-stable and SDS-soluble complexes with CSPG/SG (Fig. 3A). No such complexes were detected with the FnII deletion variants (rpMMP-9ΔFn, rpMMP-9ΔFnHPX and rpMMP-9ΔFnOGHPX), using gelatin zymography as the detection method (not shown). This was the case using both partly purified (S-200 and HS) and crude media containing rpMMP-9ΔFnII. Previously it was shown that the specific activity against gelatin of active MMP-9 lacking the FnII module was only approximately 20% of the full-length variant [53]. This is similar to the active MMP-2ΔFnII, which showed activity against gelatin of approximately 10% of the active full-length variant of MMP-2 [54]. Therefore, Western blotting and an antibody detecting proMMP-9 were used to detect the formed proMMP-9·CSPG/SG complexes (Fig. 3C). *In vitro* reconstituted samples treated with DTT prior to electrophoresis showed proMMP-9·CSPG/SG complexes were formed with most proMMP-9 variants, including rpMMP-9ΔFnII. However, no complex was detected with the two deletion variants lacking both the FnII module and the HPX domain, i.e. rpMMP-9ΔFnHPX and rpMMP-9ΔFnOGHPX (data not shown). Mixing and incubating the crude media containing these two deletion variants with purified full-length

proMMP-9 and the CSPG/SG proteoglycan had no effect on the formation of the complex between the full-length proMMP-9 and CSPG/SG. Neither did this crude media affect the binding of a preformed proMMP-9·CSPG/SG complex to the Q-Sepharose column used to isolate the complex (data not shown). This shows that the lack of complex formation between these two deletion variants of proMMP-9 and the CSPG/SG proteoglycan was neither due to impurities in the crude enzyme media that prevent the complex formation nor the binding of the complex to the Q-Sepharose column, but due to the lack of both the HPX domain and the FnII module. In order to determine to which extent the formed proMMP-9·CSPG/SG complexes were of the SDS-stable or the SDS-soluble type, unreduced samples were applied to the SDS-PAGE gel. After electrophoresis and prior to blotting, the gel was incubated in 0.1 M DTT. The reason is that no CSPG or proMMP-9 bound to CSPG was transferred to the polyvinyl difluoride membrane from gels not treated with DTT prior to blotting [36]. In the presence of DTT, proMMP-9 was released from the CSPG. On the blot, MMP-9 was detected at a position corresponding to that seen in gelatin zymography [36, 39]. Fig. 3C shows that all samples that contains either the HPX domain or the FnII module form SDS-stable complexes. One complex is located in the stacking gel and the other complex just enters the separating gel similar to that seen in gelatin zymography gels. Noticeable, in these Western blots we never detect any SDS-soluble complexes, i.e. bands around 92 kDa for pMMP-9 and bands around 70 kDa for the truncated variants (rpMMP-9ΔHPX and rpMMP-9ΔFnII). This is in agreement with previous results of the isolated complex from THP-1 macrophages [36] and *in vitro* reconstituted complexes [39]. This suggests a much larger formation of the SDS-stable complexes than the SDS-soluble complex. Furthermore, the intensities of the SDS-stable and SDS-soluble complexes seen in gelatin zymography and the lack of detection of the SDS-soluble complex in Western blots suggests that the auto-activation induced by the removal of SDS from the zymography gels must be much less effective when proMMP-9 is bound to the CSPG/SG core protein. Another possibility is that the activity against gelatin is much lower for the activated MMP-9 bound to CSPG/SG than for the free MMP-9. If this is the case, there are two possibilities that may explain a lower activity. One is that the activated MMP-9 bound to the CSPG/SG core protein has a lower specific activity against gelatin than the unbound active MMP-9. Another possibility is that the CSPG/SG core protein is a MMP-9 substrate, and hence, there will be a competition between two substrates.

In conclusion, complexes between CSPG/SG and proMMP-9 were formed when proMMP-9 contained either both the HPX and FnII domains or only one of these domains.

However when both domains lacked, no complexes were formed. This indicates that the main interactions of the CSPG/SG core protein with proMMP-9 in these complexes are with the HPX domain and the FnII module, although independent of each other. Even though it appears that the pro-, the catalytic- and the OG-domains are not involved in the complex formation between proMMP-9 and the CSPG/SG core protein, it cannot be excluded that these domains may have an effect on the kinetics of the complex formation or even be involved in binding. In the latter case, the interaction is not strong enough to form the proMMP-9·CSPG/SG complex.

2.4. In vitro reconstitution of proMMP-9·Serglycin core protein complexes lacking CS-chains

To verify that pMMP-9 can bind to the core protein of SG, binding studies were performed using pMMP-9 purified from THP-1 cells and a human recombinant Ht-SG. This E-Coli produced SG contained a 25 amino acid long N-terminal His-tag (MGSSHHHHHHSSGLVPRGSHMGSHM) instead of the predomain, and lacked GAG-chains. In these binding studies, either the pMMP-9 or Ht-SG was bound to a polyvinyl difluoride membrane using a slot blot apparatus. The different membrane slots were cut out and blocked with milk powder as in Western blotting. Thereafter, relevant membrane slots were incubated with either pMMP-9 or Ht-SG. After that, the slots were washed and incubated with antibodies against either pMMP-9, SG or the His-tag as described in Materials and Methods. As shown in Fig. 4A, the MMP-9 antibody (M9Ab) detects pMMP-9 and pMMP-9 bound to the Ht-SG, but not to Ht-SG. Similarly, the antibodies against SG (SGAb) and the His-tag antibody (HtAb) detect Ht-SG and Ht-SG bound to pMMP-9, but not pMMP-9 (Figs 4 B, C). Experiments were performed to determine whether the binding of MMP-9 was to the SG core protein or to the N-terminal His-tag peptide. For this, membranes with bound pMMP-9 were incubated with either Ht-SG or a mixture of Ht-SG and a His-tag peptide (Ht-P) which is identical to the 25 N-terminal amino acids in the Ht-SG. The SG antibodies (SGAb) were used to detect binding of Ht-SG to proMMP-9. The Ht-P did not inhibit the binding of Ht-SG to pMMP-9 (Fig. 4D). This showed that pMMP-9 binds to the core protein of SG, not to the His-tag peptide part of Ht-SG.

In conclusion, these experiments show that proMMP-9 and the SG core protein can bind and form a complex. It also shows that the MMP-9 antibody does not detect the SG core protein and the antibodies against SG does not detect proMMP-9.

2.5. Peptide arrays

To gain insight into which parts in the SG core protein, the MMP-9HPX domain and MMP-9FnII module are involved in formation of the proMMP-9·SG complex, peptide arrays of these three proteins were synthesized. The first set consisted of 20-mer peptides bound on a cellulose membrane, where each peptide was obtained from a peptide walk along the entire protein sequences with two amino acid intervals. A second set of mutated peptide arrays based on the results from the first set were produced as described in Materials and Methods. Control experiments against both sets of peptide arrays were conducted both with primary and secondary antibodies to the binding protein (proMMP-9 and SG) to rule out binding contributed by the antibodies. Therefore, the data presented are only for those arrays with no interference from unspecific binding of the antibodies. In those cases with unspecific antibody binding, it was not possible to determine if there was an interaction between the peptide and the anticipated binding partner. Ht-SG was used for the binding studies of SG to the peptide arrays of the MMP-9HPX domain and the MMP-9FnII module, while only the following three proMMP-9s' purified to homogeneity (pMMP-9, rpMMP-9 and rpMMP-9ΔHPX) were used for the binding studies of proMMP-9 to the peptide arrays of SG.

2.5.1. Binding of proMMP-9 to serglycin peptide arrays

The core protein of human SG contains 131 amino acids. The mid-section contains 8 Ser-Gly repeats (amino acids 67-84) to which GAG-chains are attached (Fig. 5A), giving a peptide array containing 57 spots (Fig. 5B). Control experiments with primary and secondary antibodies revealed that they did not bind to any of the peptides in the array (data not shown). However, in one of the mutated peptide arrays, the primary antibody against MMP-9 did bind to peptide 52 and several of the mutated variants of this peptide (Fig. S2). As seen in Fig. 5, all proMMP-9 variants bind to amino acid sequences located both N-terminal and C-terminal to the GAG-attachment sites.

The two full length forms of proMMP-9 (pMMP-9 and rpMMP-9) showed an almost identical binding pattern for the SG peptide array (Figs. 5C and D). As a control of the peptides in this array, pMMP-9 was incubated with another identical array (Fig. S3). There were small differences in the intensity of the signals, which could be due to small differences in the produced batches of the peptide arrays. Binding of proMMP-9 to the region N-terminal to the GAG-attachment sites involves the following part of the SG core protein: Binding to peptide 6 suggests that the entire sequence from ^{11}V to ^{30}F is required for binding as the mutation array where the ^{11}VR and ^{29}MF amino acids were replaced did not prevent binding (data not shown). ProMMP-9 also bound to peptides 14 and 15 (Figs. 5C and D, Fig. S3). A mutation array where the putative interacting amino acids ^{29}MF and ^{45}TD were replaced (Fig. 5F), revealed that changing ^{46}D to A prevented the binding of proMMP-9. However, changing ^{29}M to G had no effect on binding. Replacing ^{30}F and ^{45}T by A and V, respectively, resulted in reduced binding of proMMP-9 to the peptide. The interactions of proMMP-9 with these two peptides, but not peptides 13 and 16 suggest a binding to the side chain of ^{46}D and likely to the side chains of ^{30}F and ^{45}T as well as the main chain amide bond of the latter two amino acids.

ProMMP-9 also seemed to bind peptides 21-27. Mutated peptide arrays of peptides 21 and 23 revealed that no single mutation prevented binding (Fig 5F), suggesting that several side chains from ^{41}P to ^{64}E are involved in binding. In these peptides, mutation of ^{46}D to A did not affect binding.

ProMMP-9 also bound to peptides 47 and 48 located C-terminal to the GAG attachment sites (Figs. 5C and D, Fig. S3). Mutation arrays of these two peptides suggested that several of the side chains from ^{93}Y to ^{114}P must be involved in binding as none of the single amino acid mutations prevented binding, but only appeared to reduce binding (Fig. 5F).

ProMMP-9ΔHPX had a similar binding as the two full-length enzymes, but did not bind peptide 21 (Fig. 5E).

2.5.2. Binding of serglycin to MMP-9 FnII peptide arrays

In order to gain information on which parts of the FnII module in proMMP-9 are involved in the binding to SG, a peptide array (Fig. 6) of the 166 amino acids in this module (^{225}A-^{390}D) was obtained as described in Materials and Methods. This gave a peptide array of 74 spots

(Fig. 6B). The primary structure of the MMP-9 FnII module is shown in Fig. 6A and the ponceau stained array is shown in Fig. 6B. Control experiments with primary and secondary antibodies revealed that they did not bind to any of the peptides in the array (data not shown). Fig. 6C shows that SG binds to several peptides, however, mutated peptide arrays revealed that the binding to peptides 41-43, 45, 46, 49, 57 and 71 appears to be artefacts (Data not shown and Fig. S4). Therefore, we conclude that SG binds to peptides 13-22 (^{249}R-^{286}K), 35 (^{293}I-^{312}R), 64 (^{351}F-^{370}R) and 65 (^{353}F-^{372}W). Peptides 13-22 comprise the FnII repeat 1, peptide 35 the first part of repeat 2 and peptides 64/65 the first part of repeat 3.

To test which amino acids in the FnII module are involved in binding of SG to peptides 13 to 22, full mutation arrays of peptides 14, 16, 19 and 22 (Fig. 6D) were performed. Mutation of amino acids ^{255}W and ^{262}Y to alanine seemed to prevent or weaken the binding of SG to peptides 14 and 16. In peptide 19 it appeared that only mutation of amino acid ^{262}Y prevented or weakened the binding. In peptide 22, mutations of several amino acids appear to weaken binding, while mutation of amino acids ^{274}E and ^{277}Y seemed to prevent binding. Also in peptide 35, mutations of several amino acids seemed to weaken binding. Only the mutation of amino acid ^{307}R appeared to prevent binding. A selected mutation peptide array of peptide 64/65 suggested that amino acids ^{353}F and ^{370}R were involved in binding of SG.

2.5.3. Binding of serglycin to MMP-9 HPX peptide arrays

In order to gain insight into which parts of the MMP-9 HPX domain are involved in the binding to SG, a peptide array (Fig. 7) of the 187 amino acid module (^{521}F-^{707}D) was obtained as described in Materials and Methods. This resulted in a peptide array of 85 spots (Fig. 7B). The primary structure of the MMP-9 HPX domain is shown in fig. 7A and the ponceau stained array is shown in fig. 7B. Control experiments with primary and secondary antibodies revealed that they did not bind to any of the peptides in the array (data not shown). Fig. 7C shows that SG bound to several peptides. Control experiments with mutated peptide arrays (Fig. S5) revealed that the binding to peptides 36, 53, 57, 78 and 82 appear to be artefacts, as the primary SG antibodies bound to these peptides. The binding to peptides 15-17 also appears to be artefacts, as SG did not bind to the mutation array of peptide 16 (data not shown). Therefore, we conclude that SG binds to the following peptides; 10-12, 18, 19, 37-38, 41, 56, 69-71, 76, 84 and 85. This suggests that binding of SG involves the end of blade 1 (peptides 10-12 and 18/19), end of blade 2 (peptides 37, 41), β-strands 2-4 blade 3 (peptide

56), end of blade 3, beginning of blade 4 (peptides 69-71) and most of the end of blade 4 (peptides 76, 84, 85).

To determine which amino acids are involved in binding of SG to peptides 10-12 of the HPX domain (Fig. 7C), a selected mutation array of peptide 11 was performed (Fig. 7D). This suggests that ^{544}E and ^{558}D are involved in the binding of the SG core protein. A selected mutation array of peptide 18/19 (Fig. 7D) suggests that the mutation of ^{573}E weakens the binding. The mutation of amino acid ^{609}D seems to prevent binding of SG to peptide 37 (Fig. 7D). Peptide 41 is at the end of blade 2 and the beginning of blade 3 and the mutation array of this peptide suggests that the mutation of ^{618}R to alanine prevents binding and so might also the mutation of ^{619}S (Fig. 7D). However, the mutation of ^{609}D did not affect the binding of the SG core protein to peptide 41. None of the mutations of peptide 56 appeared to prevent binding (Fig. 7D), suggesting that most of the amino acids in this peptide are involved in the interaction. Mutation array of peptide 69 revealed that the mutation of ^{665}F and ^{667}Y seemed to prevent binding, while the mutation of ^{672}Y and ^{673}F seemed to weaken binding (Fig. 7D). SG binding to peptide 76 seems to be prevented or weakened with a mutation of amino acid ^{685}R to an alanine (Fig. 7D). A mutation array of peptide 85 indicates that the mutation of amino acids ^{700}D and ^{701}I prevents binding (Fig. 7D). Due to the binding of the primary antibody to the peptides with the following mutated amino acids (^{694}V, ^{699}Y, ^{702}L and ^{705}P) in peptide 85 (Fig. S5), it was not possible to conclude whether these mutations affected binding or not.

The peptide arrays suggested that proMMP-9 binds to residues in SG located both N- and C-terminal to the CS-attachment sites. The arrays also suggest that SG binds to several parts of both the FnII module and the HPX domain. The *in vitro* reconstitution experiments reveal that either the FnII module or the HPX domain need to be present in order to form an SDS-stable proMMP-9·CSPG/SG complex. Several questions arise. (1) Can the FnII module or the HPX domain interact with both the N- and C-terminal part of SG at the same time? (2) Can one SG molecule at the same time bind to all sites suggested by the peptide arrays in either the FnII module or the HPX domain, or are several complexes possible with slightly different orientations of the SG? (3) Can one SG molecule bind to the FnII module and the HPX region at the same time? We have used homology modelling, docking and molecular dynamics (MD) simulations in an attempt to answer these questions.

2.6. Docking and molecular dynamic studies of the interaction of serglycin with the MMP-9 FnII module and HPX domain

In a previous *in vitro* reconstitution study of the proMMP-9·CSPG/SG complexes, it was shown that the interaction between the two macromolecules in the SDS-stable and reduction sensitive complex was not through a disulphide bond but most likely through a mixture of hydrogen bonds, hydrophobic and ionic interactions [39]. It appeared that these mixtures of interactions also occur in the formation of the SDS-soluble complex. Docking and MD simulations of the SG core protein with the proMMP-9 HPX domain and the proMMP-9 FnII module were performed in order to obtain further information about the interactions between the two molecules.

2.6.1. Homology modelling and protein-protein docking

X-ray crystallography of the cloned MMP-9 HPX domain showed a dimer [30]. To test the performance of the BioLuminate program, the HPX_B subunit was docked to the HPX_A subunit. This docking gave 67 different poses. All poses were structurally aligned with the dimeric X-ray structure. The best pose was selected based on its structural similarity with the dimer. Structural superimposing with the X-ray structure showed that the docked complex had an almost complete overlap with the X-ray structure (Fig. S6). Here, we compared the position of the amino acids in the docked structure with those in the HPX_A and HPX_B in the X-ray structure that were proposed to cause the strong interaction between the two subunits [30]. Cha et al. [30] reported that ^{707}D in HPX_A formed an ionic interaction with ^{677}R in HPX_B, while the hydrophobic cluster ^{699}Y, ^{696}Y and ^{694}V in HPX_A interacted with the hydrophobic cluster ^{696}Y, ^{678}F and ^{694}V in HPX_B. An interaction between the side chains of ^{651}D in HPX_A with ^{685}R in HPX_B was also reported. Fig. S6 showed that these residues in the docked complex are overlapping with the X-ray structure. These docking results indicate that protein-protein docking can be useful for obtaining further information about the interactions between the SG core protein and proMMP-9.

As there is no 3D structure of the SG core protein, a homology modeling of the protein was done using the Phyre^2 program as described in Materials and Methods. This predicted a model of SG based on several templates, where template c6ewvA (PDB id: 6ewv) had the highest confidence (59%). The obtained structure showed a hairpin like structure where the

Ser-Gly repeats that bind the CS-chains form a loop and the regions C- and N-terminal to the Ser-Gly repeats appear to join (Fig. 8).

The SG docking with FnII resulted in 130 poses, while the docking with HPX gave 77 poses. The best poses were selected using four steps: (1) Only poses where the energy minimization converged were considered, giving 30 poses from docking of SG and FnII and 19 poses from docking of SG and HPX. (2) Poses after step 1 were manually investigated to remove poses where the Ser-Gly repeats in SG were interacting with either the HPX or FnII part of MMP-9, which reduced the number of poses to 7 and 12, respectively, for the docking with FnII and HPX. (3) Analyze protein-protein interactions and compare the results with the results from peptide arrays. The protein interaction analysis provides a spreadsheet containing the information about interacting pairs of amino acids, atomic distances and type of interactions between interacting pairs, and putative clashes between interacting pairs. We selected poses with similar interacting regions as suggested by the peptide arrays containing at least one ionic interaction together with hydrophobic interactions and hydrogen bonds. This resulted in 3 poses from the docking of SG with FnII and 11 poses from the docking of SG with HPX. (4) Chondroitin sulphate (CS) chains were added to five of the serine residues in the Ser-Gly repeats of SG for the remaining 14 poses as described in the Materials and Methods section. To which of these eight serine residues they should be added, and the exact number of CS-chains are to our knowledge unknown. It has been suggested that four but not more than six CS-chains are attached (prof. S.O. Kolset and prof. K. Prydz, University of Oslo, Norway, personal communication) [55]. N-terminal sequencing of SG from U-937 cells gave the following sequence, SEDYXXXGFG [56]. This suggests that CS-chains are attached to the two first serine residues in the Ser-Gly repeat, i.e. ^{67}S and ^{69}S (see Fig. 5 for sequence), and was the reason that we added CS-chains to these two residues. In addition, we added CS-chains to ^{73}S, ^{77}S and ^{83}S. Adding of CS-chains to the other serines of the Ser-Gly repeat gave sterically clashes, and CS-chains were not attached to these serine residues in further studies. After CS-chains were added, we energy optimized the structure of the poses to see if these sugar chains hindered the interaction of SG with HPX and FnII. This step gave two poses from the FnII docking and four from the HPX docking that were used for MD simulations.

2.6.2. Molecular Dynamics Simulation

MD simulations were performed for the two docking complexes of SG with FnII, the four complexes of SG with HPX. Each complex was simulated twice, and in addition two simulations were performed with the docked HPX dimer and one with the X-ray dimer. The motivations for the MD simulation were to check the stability of the interactions in the docked complexes and if the structural dynamics could induce additional interactions in the complexes. First, we performed MD simulations of the HPX X-ray dimer and the best pose from the docking of HPX_B to the HPX_A subunit and compared the results. These MD simulations confirmed a large similarity between the structures of the HPX dimer from the X-ray and the docked complex (Supplement 1, Figs. S6). These results suggest that docking and MD simulations are helpful approaches for studying interactions of the SG core protein with the FnII module and the HPX domain of MMP-9.

Based on analysis of distance plots generated for interacting amino acids during MD, the most stable poses were selected as the most probable structure of the complexes. The MDs resulted in one putative model for the interaction of SG with FnII and two putative models for interaction of SG with HPX which are described further in the following. The selected amino acid pairs for all three poses are summarized in Tables 1-3 along with the information from their respective peptide arrays. Results from the MD simulations are shown in Figs. S7-S9.

2.6.3. Binding of Serglycin with FnII

The two MD simulations of each complex resulted in almost identical dynamic movements of the interacting amino acids indicating reproducibility of the simulations. Most amino acids in the FnII module that interacted with SG were found in the second repeat, while two out of fourteen amino acids were located between the first and second repeat (Fig. 9; Table 1). In SG, almost all the amino acids that interacted with FnII were present in flexible loops and the majority were present in the part of the core protein located C-terminal of the Ser-Gly repeat. The amino acid ^{227}G in the FnII module is present in a flexible loop structure that interacts with ^{38}N in SG, which is located N-terminal to the Ser-Gly repeats. The NH_2 in the side chain amide of ^{38}N formed a hydrogen bond with the main chain carbonyl of ^{227}G (Fig. S7.1). ^{280}D, ^{282}N, ^{284}D, ^{294}F, ^{295}Q, ^{306}G, ^{307}R, ^{308}S, ^{320}Y and ^{324}K, are also present in loop regions in the FnII module, where ^{282}N is at the turn of a loop structure and appeared flexible during MD.

The side chain of ^{282}N had a hydrophobic interaction with the side chain of ^{120}L in the SG, with a stable distance of around 4 Å during MD (Fig. S7.2). There was one ionic bond between ^{280}D in FnII and ^{42}R in SG (Table 1; Fig. S7.3). This bond was initially at a stable distance of 1.5 Å for the first 50 ns, and thereafter increased with time up to 16 Å (Fig. S7.3). However, there was one stable ionic interaction between ^{162}R in the catalytic domain of MMP-9 with ^{46}D in SG (Fig. S7.4). The distance between the negatively charged side chain ^{46}D and the positively charged side chain in ^{162}R was stable around 3Å during the entire MD, even though the side chains rotated. During the MD, one of the protons of the three nitrogens in ^{162}R were never at a longer distance than 3 Å from the negatively charged carboxyl group of ^{46}D. The carbonyl amide oxygen of ^{306}G formed stable hydrogen bonds with the nitrogen amides ^{96}V and ^{98}E in SG (Fig. S7.5). The side chain and main chain of ^{308}S (FnII) formed stable hydrogen bonds with the side chain of ^{98}E at a distance of approximately 2 Å for both (Fig. S7.5). The side chains of ^{294}F, ^{295}Q and ^{320}Y in FnII formed hydrophobic interactions with the side chain of ^{96}V in SG (Fig. S7.6). The interactions of ^{294}F and ^{295}Q with ^{96}V were flexible, starting with a stable distance of 3-4 Å during the first 30 ns, and thereafter increasing slowly up to 8-9 Å. ^{320}Y was initially at a distance of 5 Å with ^{96}V. After around 20 ns the distance increased up to 10 Å and remained stable around that distance for the rest of the trajectory. ^{313}W, ^{326}F and ^{328}F in FnII are present in β-strands. The side chains of ^{307}R and ^{313}W in FnII formed stable hydrogen bonds with the side chain of ^{99}S in SG at a distance around 2Å and 3-5 Å, respectively (Fig. S7.7). The hydrogens on the side chain nitrogen of ^{324}K (FnII) formed stable hydrogen bonds with the main chain carbonyl of ^{102}F in SG at a distance of around 7 Å (Fig. S7.8). The side chain of ^{326}F (FnII) formed stable hydrophobic interactions with the side chains of ^{99}S, ^{100}D and ^{101}A in SG (Fig. S7.9). The side chain of ^{328}F (FnII) also formed stable hydrophobic interactions with the side chains of ^{99}S and ^{120}L in SG (Fig. S7.10).

Binding of rpMMP-9ΔHPX to the SG peptide array indicated that the FnII module of proMMP-9 can bind amino acids located both N- and C-terminal for the Ser-Gly repeats (Fig. 5). Homology modelling of SG, docking and MD simulations of the formed complex between SG and the FnII module in proMMP-9 suggest that the FnII module at the same time can bind amino acids in SG located both N- and C-terminal to the Ser-Gly repeats. This also suggests that it is not possible for one SG molecule to bind two proMMP-9 molecules at the same time, i.e. one at both sides of the Ser-Gly repeats. SG also covers binding sites in the first and second repeat in the FnII module. Docking and molecular simulation studies also indicated

that amino acids located in peptides 41-43 in the peptide array are involved in binding, although the peptide array studies indicated that this binding might be an artefact. The only peptides from the peptide array suggested to bind the SG core protein that was not involved in the binding predicted from the docking and MD simulation were peptides 64 and 65. The docking and MD simulation studies indicated that the SG core protein covers a large part of the FnII surface and that the proMMP-9·SG complex formed by the FnII module is a result of only one complex and hence only one interacting region.

In proMMP-9·CSPG isolated from PMA-treated THP-1 cells, the CSPG core protein bind and hide epitopes in the FnII module of proMMP-9 that is involved in binding of gelatin [38]. The majority of the proMMP-9·CSPG complex did not bind gelatin, only a small fraction of the proMMP-9·CSPG complex (15-35%) binds. This binding was much weaker than the binding of gelatin to proMMP-9. The results indicated that the interaction between proMMP-9 and the core protein(s) in the CSPG has induced a new binding site for gelatin in a small part of the formed complexes. When gelatin binds to proMMP-9·CSPG complexes, proMMP-9 and proMMP-9·CSPG appear to bind to different epitopes in gelatin. This was also the case for the *in vitro* reconstituted proMMP-9·CSPG/SG SDS-stable and SDS-soluble complexes [39]. Furthermore, increasing concentrations of gelatin along with CSPG and proMMP-9 in the *in vitro* reconstitution assay resulted in decreasing formation of both the SDS-stable and SDS-soluble complexes [39]. Collier et al. [42] performed alanine scanning mutagenesis and functional analysis of gelatin binding to the FnII module in MMP-9. These studies indicated that gelatin mainly binds to the second FnII repeat and that the amino acids ^{307}R, ^{309}D, ^{319}N, ^{320}Y and ^{323}D are critical for binding. In the peptide array (Fig. 6), these amino acids are located in the peptide spots 35 and 41-46, which all bind SG. In the docking and molecular dynamic simulation studies, amino acids between ^{306}G to ^{328}F in the FnII module are involved in the binding of the SG core protein. This suggests that there are overlapping epitopes in the FnII module to which both SG and gelatin bind. Therefore, the results of the peptide arrays and the MD simulation studies are in agreement with the *in vitro* reconstitution experiments showing that gelatin inhibits the formation of the proMMP-9·CSPG/SG complex [39]. Furthermore, the results are also in agreement with the alanine scanning study of Collier et al. [42]] who determined where gelatin binds in the FnII module.

2.6.4. Binding of Serglycin with HPX

Based on the interaction patterns, we selected two models as possible for the interaction of HPX with SG. In model 1, HPX was involved entirely with the region of SG located N-terminal to the Ser-Gly repeats, while in model 2, HPX mainly interacts with the region C-terminal to the Ser-Gly repeats.

***Model 1*:** The majority of the amino acids in the HPX domain that interact with SG were from the fourth blade, while the remaining were from the third blade (Fig. 10; Table 2). SG amino acids that interacted with the HPX domain are entirely located N-terminal to the Ser-Gly repeat. The following amino acids in the HPX domain were involved in binding; ^{659}L, ^{660}D, ^{675}N, ^{676}D, ^{677}R, ^{680}W, ^{691}V, ^{695}G, ^{696}Y, ^{698}T, ^{699}Y, ^{707}D. In the peptide array, these amino acids were located in the following spots that interact with SG, 69-71 and 76-85 (Table 2, Fig. 7). ^{659}L and ^{660}D are in a loop region, and ^{675}N, ^{676}D and ^{677}R in a β-hairpin motif between two β-strands. ^{680}W, ^{691}V, ^{695}G and ^{696}Y are in β-strands, while ^{698}T, ^{699}Y, ^{707}D are in the C-terminal end region. These HPX amino acids interacted with the following amino acids in SG; ^{28}P, ^{29}M, ^{32}L, ^{33}L, ^{34}P, ^{37}S, ^{39}K, ^{41}P, ^{43}L, ^{46}D and ^{47}L. In the peptide arrays, these SG amino acids were located in the following spots that binds proMMP-9; 14, 15, 21, 23-26 (Table 2, Fig. 5).

An ionic interaction between ^{676}D in the HPX domain with ^{39}K in SG was stable around the distance of 1.8 Å during the MD simulation (Fig. S8.1). The methyl group of the ^{676}D side chain forms hydrophobic interactions with ^{41}P and ^{43}L in SG (Fig. S8.2). The side chain of ^{43}L was flexible and during the whole trajectory at least one of the methyl groups were at a distance of 7 Å from the methyl group in ^{676}D. The side chain of ^{41}P was at a stable distance of approximately 5 Å from the methyl group in ^{676}D. The carboxyl group in the side chain of ^{660}D formed hydrogen bonds with the main chain NH in ^{37}S and ^{33}L, and with the side chain OH of ^{37}S (Fig. S8.3). The carboxyl oxygens in the side chain of ^{660}D were at a stable distance of approximately 3 Å from the main chain NH of ^{37}S and 6 Å from the side chain hydroxyl group of ^{37}S, as well as 7.5 Å from the main chain NH of ^{33}L. The main chain NH of ^{660}D and the CO of ^{32}L were located at a stable distance of 7.5 Å from each other (Fig. S8.3). In addition, the methylene group of the ^{660}D side chain formed a hydrophobic interaction with the methyl groups in the side chain of ^{32}L. This is a dynamic interaction with distances around 7 Å. The side chains of ^{680}W and ^{675}Q formed hydrophobic interactions with the ^{32}L side chain (Fig. S8.4). Even though the side chains are flexible, one of the methyl groups in the side chains of ^{32}L was never at a distance longer than 4 Å from the methylene groups in ^{675}Q. In

the case of ^{680}W, the distance to ^{32}L was initially around 6 Å, and after approximately 10 ns, at least one of the methyl groups in ^{32}L was at a distance around 4 Å from the ^{680}W side chain.

The main chain NH in ^{659}L and CO in ^{32}L are at a stable dynamic distance of around 7.5 Å (Fig. S8.5). The side chain of ^{659}L formed hydrophobic interactions with the side chains of ^{32}L and ^{34}P with dynamic distances of around 10 and 7.5 Å, respectively. The side chain of ^{43}L in SG formed stable hydrophobic interactions with the methyl/methylene groups in the side chains of ^{698}T and ^{677}R in HPX (Fig. S8.6). The distance of the methyl group in ^{698}T and one of the methylene groups in ^{677}R were always at a distance of 4 Å to at least one of the methyl groups in ^{43}L. The side chain of ^{29}M in SG had dynamic fluctuations between the Cα-carbon in ^{695}G and the side chain of ^{691}V (Fig. S8.7). The sulphur and the terminal methyl group of ^{29}M were at a stable distance of around 5 Å from the Cα-carbon in ^{695}G during the first 60 ns of the trajectory and thereafter the distance increased. During the first 60 ns the distance between the sulphur and the terminal methyl group in ^{29}M were at a stable distance around 10 Å from the ^{691}V side chain. Thereafter, the distance increased and after approximately 80 ns the distance stabilized around 5 Å. The hydroxyl group of the ^{696}Y side chain formed a stable hydrogen bond to the main chain CO and NH in ^{28}P (Fig. S8.8). The distance to the CO in ^{28}P remained stable for the first 60 ns at around 2 Å and thereafter increased to 7.5 Å. The distance to the NH of ^{28}P was stable at 5 Å for the first 80 ns and thereafter increased to 7.5 Å. One of the methylene groups in the side chain of ^{28}P occurred at a stable distance of around 5 Å from the phenyl ring in ^{696}Y. The phenyl ring of ^{696}Y had hydrophobic interactions with the side chain of ^{43}L, at a stable distance around 6 Å. The main chain NH of ^{46}D and ^{47}L formed stable hydrogen bonds with the hydroxyl group in the side chain of ^{699}Y (Fig. S8.9). During the first 10 ns the distances were 5 Å and 3.7 Å, respectively. After that, the distances for both increased to around 6.2 Å and were stable for the rest of the trajectory. The side chain of ^{47}L formed a stable dynamic hydrophobic interaction with the phenyl ring of ^{699}Y at around 7 Å (Fig. S8.9). The methylene group in the side chain of ^{707}D formed a stable dynamic hydrophobic interaction with the side chain of ^{47}L with distances around 5.3 Å (Fig. S8.10).

***Model 2*:** Most amino acids of HPX that interacted with SG were from the third blade, together with some from the fourth blade (Fig. 11; Table 3). The majority of the binding amino acids in SG are located C-terminal to the Ser-Gly repeats. The following amino acids

in the HPX domain were involved in binding; ^{623}K, ^{634}R, ^{645}R, ^{646}S, ^{647}A, ^{648}S, ^{651}D, ^{652}R, ^{653}M, ^{687}E, ^{688}L, ^{690}Q and ^{691}V. In the peptide array, these amino acids were located in the following spots that interact with SG; 53, 54, 56, 57, 69-71 and 76-85 (Table 3, Fig. 7). The amino acids ^{623}K, ^{648}S, ^{674}R, ^{687}E, ^{688}L, ^{690}Q and ^{691}V are in β-strands, ^{645}R, ^{646}S and ^{647}A are in loop regions and ^{651}D, ^{652}R and ^{653}M are in a one helix-turn. These amino acids interacted with the following amino acids in SG; ^{40}I, ^{41}P, ^{42}R, ^{43}L, ^{97}D, ^{98}E, ^{113}L, ^{114}P, ^{115}S, ^{116}D, ^{117}S, ^{118}Q and ^{120}L. In the peptide arrays, these amino acids in SG are located in the following spots that binds to proMMP-9; 14, 15, 21, 47, 48 and 50-54 (Table 3, Fig. 5).

Three positively HPX amino acids and two negatively charged SG amino acids formed a cluster of ionic interactions (^{623}K, ^{634}R and ^{645}R in HPX, ^{97}D and ^{98}E in SG). These amino acids are very dynamic where at least one of the negatively charged groups were always at a close distance (< 2 Å) to one of the positively charged groups (Figs. S9.1). The side chains of ^{646}S and ^{647}A in HPX formed a cluster with hydrophobic interactions with ^{113}L and ^{114}P in SG (Fig. S9.2). The side chains of ^{647}A and ^{113}L were at a relatively stable distance of 5-6 Å. The methylene group in ^{646}S was at relatively stable distances of around 4 Å and 6 Å to the side chains of ^{114}P and ^{113}L, respectively. ^{648}S in HPX and ^{114}P in SG formed both stable hydrophobic interactions and a hydrogen bond (Fig. S9.3). The hydrogen bond was between the side chain OH in ^{648}S and the CO of ^{114}P, with a stable distance around 2 Å. The methylene group in ^{648}S was at a stable distance of around 4 Å from the ^{114}P side chain. The main chain CO in ^{651}D (HPX) and NH in ^{43}L (SG) were interacting at a distance varying from 5-8 Å, while the methylene group in ^{651}D was at a distance of 3-7.5 Å from the side chain of ^{43}L (Fig. S9.4). ^{652}R in HPX and ^{118}Q in SG formed both stable hydrophobic interactions and a stable hydrogen bond (Fig. S9.5). The hydrogen bond was between the side chain amide in ^{118}Q and the main chain CO in ^{652}R, with a stable distance of around 2 Å. At least one of the methylene groups in the two side chains was always at a distance of 4 Å. The two methylene groups in ^{652}R (HPX) also formed stable hydrophobic interactions with the methylene group in ^{115}S at a distance around 4 Å (Fig. S9.5). The side chain nitrogens of ^{652}R were at a distance of 2-7.5 Å from the OH group in the side chain of ^{115}S. The methyl group of ^{653}M (HPX) formed hydrophobic interactions with the side chain ^{114}P and the aliphatic part of ^{116}D (Fig. S9.6). The distance between the side chain of ^{643}M and the methylene group of ^{116}D were around 5 Å, while the distances to the methylene groups in ^{114}P was around 3.7 Å. A hydrophobic cluster was formed of the side chains of ^{687}E and ^{688}L in HPX and ^{42}R, ^{117}S and ^{120}L in SG (Fig. S9.7). The two methylene groups in ^{687}E were at a distance of 4.8 Å to 8 Å

from the methylene in ^{117}S, while the distance to the side chain of ^{120}L was stable around 5 Å. The side chain of ^{688}L was at a distance of around 5 Å from the methylene group of ^{117}S and around 5.8 Å to the methylene groups of ^{42}R. The side chain of ^{40}I (SG) formed hydrophobic interactions with the side chains of ^{690}Q and ^{691}V in HPX (Fig. S9.8). One of the side chain groups in ^{40}I was always at a distance around 3 - 4 Å to the ^{691}V side chain, while the distance to the ^{690}Q side chain was initially around 4 Å and rapidly increased to around 7.5 Å. Thereafter it remained stable at that distance.

Both these models seem to contain all necessary interactions for a SDS-stable and hence a reduction sensitive complex. Both models contain overlapping regions in the HPX domain that correspond to the peptide spots 69-71 and 76-85 in the peptide array (Tables 2 and 3, Fig. 7), although there are different regions in the SG core protein that interact with HPX in the two models. It is not possible to state that one of the models is more probable than the other model. In the i*n vitro* reconstituted complex, rpMMP-9ΔFnII·CSPG/SG, the proteoglycan core protein binds only to the HPX domain in MMP-9. If both models correspond to the *in vitro* formed complex, one must anticipate that there will be a competition between the two possible interaction modes of HPX and SG. This may have an effect on the amount of formed complex, depending on the kinetics and if there is a specific sequential binding of interacting regions. In the case of the complex formed with the full-length proMMP-9, two probable interaction regions in the HPX domain may also be of importance if the SG core protein can be sandwiched between the HPX domain and the FnII module due to the flexibility of the full length proMMP-9 enzyme.

2.6.5. Molecular dynamics simulations of proMMP-9 with and without bound serglycin

One of the questions that we also liked to get an answer to was if one SG molecule at the same time can bind both the FnII module and the HPX domain in proMMP-9, and if so, which parts of the two molecules are involved. As the MMP-9 is very flexible due to the long hinge region, we tried to model the 3D structure of the entire proMMP-9 molecule (^{29}V - ^{707}D). The sequence used in these experiments was without glycosylation of the MMP-9 hinge region (OG domain). The human proMMP-9 sequence (^{29}V-^{707}D) was obtained from UniProt database, with the identification code P14780. The homology modelling option in the Maestro program of the Schrödinger software was used to obtain a 3D model of this full-length proMMP-9. This resulted in a structure with an N-terminal part that could be directly overlaid

with the X-ray structure of mini-MMP-9, i.e. the pro and catalytic domain with the FnII module (PDB ID:1l6j) and the C-terminal part with the X-ray structure of the HPX domain (PDB ID:1itv). Previously it was shown by small angle X-ray crystallography in combination with atomic force microscopy that proMMP-9 is very flexible and that the two globular domains, i.e. the catalytic domain and the HPX domain, were either located closely to each other or at a long distance from each other [29]. Therefore, we used the proMMP-9 model as starting coordinates for 500 ns MD simulations in order to determine whether the simulations reflect the observations from the combined SAX and AFM study. The result was that the two globular parts moved to and from each other due to the very flexible hinge region (Movie 1). Fig. S10 shows the first and last frame of the MD simulation. In the beginning of the MD, the two globular domains were at close distance and we have designated this as the closed conformation (Fig. S10). This suggested that it should be possible to test if SG could be stably sandwiched between the FnII module and the HPX domain as well as if it was possible that SG could stably bind to either the FnII module or the HPX domain during the MD.

The SG (without CS-chains) was linked to the FnII-module as suggested by the best docking mode as described in section 2.6.3, Fig. 9. This was performed with the closed conformation of proMMP-9 as seen in Fig. S10. This model of proMMP-9 with the bound SG core protein were then applied for 500 ns MD simulations. This resulted in the SG sandwiched between the FnII-module and the HPX-domain after approximately 20-30 ns and this remained for the rest of the MD (Movie 2, Fig. S11). Amino acids in SG corresponding to those in peptides 40-57 in the peptide array interacted with amino acids in MMP-9FnII corresponding to peptides 19-28 and 32-42 in the peptide array (Table 1). SG amino acids corresponding to peptides 7-18 in the peptide array interacted with amino acids in MMP-9HPX corresponding to peptides 59-68 and 78-85 in (Table 2 and 3). Thus, the interactions seen between the full-length MMP-9 and SG in this MD simulation correspond well with the results from the peptide arrays and dockings.

We also investigated if the SG core protein could interact with proMMP-9 by placing SG between the FnII module and the HPX domain when the two domains were at different distances from each other. The MD simulations were performed for 100 ns. In two of the cases (Movies 3 and 4, Figs. S12 and S13), the SG core protein was at an equal distance from the FnII module and the HPX domain. In the third case (Movie 5, Fig. S14), the SG core protein was placed close to the FnII module. In all cases, the Ser-Gly repeats in SG were pointing away from proMMP-9. When SG was placed between the FnII module and the HPX

domain in the MMP-9 structure after 15 ns frame from Movie 1, after 10 ns the SG core protein was sandwiched between the FnII module and the HPX domain with the eight Ser-Gly repeats pointing away from MMP-9, and this remained stable during the entire MD (Movie 3, Fig. S12). Amino acids in SG corresponding to those in peptides 1-19 in the peptide array interacted with amino acids in MMP-9FnII corresponding to peptides 19-28 in the peptide array (Table 1). SG amino acids corresponding to peptides 20-29 and 40-52 in the peptide array interacted with amino acids in MMP-9HPX corresponding to peptides 4-13 and 74-85 (Tables 2 and 3). Thus, the interactions seen between the full-length MMP-9 and SG in this MD simulation correspond well with the results from the peptide arrays and dockings. After 32 ns frame from Movie 1, SG was placed between the FnII module and the HPX domain in the MMP-9 structure (Movie 4, Fig. S13). After 10 ns the SG core protein start to move towards the HPX domain and thereafter remained stably bound during the rest of the MD. Between 10-50 ns, the amino acids in the HPX domain of MMP-9 corresponding to peptides 10-20 and 28-38 in the peptide array interacted with the amino acids in SG corresponding to peptides, 10-29 and 56-57 in the peptide array (Tables 2 and 3). This fits partly with the peptide arrays (Figs. 5 and 7). From 50-100 ns, the amino acids in the MMP-9 HPX corresponding to peptides 5-14 in the peptide array interacted with the amino acids in SG corresponding to peptides 36-45 in the peptide array (Tables 2 and 3). None if these interactions were seen in the peptide arrays. After 60ns, the major part of N-terminal of SG also interacted with the OG domain in the MMP-9, which remained interacting throughout the MD as the other interactions. In the third case, the SG core protein was placed close to the FnII module in the 32 ns frame from Movie 1. The SG was oriented in a position based on the SG from the best docked model with the FnII module in MMP-9 (section 2.6.3, Fig. 9). Initially the SG moved towards the HPX domain and then remained located between the two domains, although closer to the HPX domain (Movie 5, Fig. S14). A striking feature was the N-terminal part of SG was also close to the catalytic domain and the distance seemed stable from around 8 ns. ^{134}R in the catalytic site formed an ionic bond with ^{16}D in SG and after approximately 14 ns hydrogen bonds formed between ^{128}Y and ^{160} Y in the catalytic domain with ^{37}S and ^{34}P in SG. After around 17 ns an additional ionic interaction was formed between ^{25}E in SG with ^{546}R (HPX, blade 1). This interaction was stable during the rest of the MD. After 27 ns ^{98}E and ^{97}D in SG formed an interaction with ^{685}R (HPX, blade 4). This was more dynamic with large distance variations.

In conclusion, the MD simulation using the full length proMMP-9 showed a very flexible enzyme where the hinge region (OG domain) either stretched out or coiled up, resulting in the two globular domains (catalytic and HPX domain) which were either close to each other (closed conformation) or at a longer distance from each other (stretched conformation). This may reflect the wet lab experiments using small angle X-ray crystallography along with atomic force microscopy [29]. The MD simulation also indicated that SG could either be sandwiched between the FnII module and the HPX domain or bound to only one of these domains. The interactions obtained during MD simulations reflected the interactions obtained in the peptide array experiments. Thus, the MD simulations along with the *in vitro* reconstitution experiments with the various deletion variants of proMMP-9 and the peptide arrays give a picture of the complex nature of the interactions between the two macromolecules proMMP-9 and SG that results in the formation of the SDS-stable and reduction sensitive proMMP-9·CSPG/SG complex.

2.7. Conclusion

Previous studies revealed that the leukemic monocyte cell line THP-1 when differentiated to macrophages in the presence of PMA secretes proMMP-9 both as a monomer and as SDS-stable and reduction sensitive homomultimer(s) as well as heterodimer complexes with one or several CSPG core proteins [36]. *In vitro* reconstitution studies showed that this heterodimer complex could be produced simply by mixing pure proMMP-9 with purified CSPGs from various monocytic cell lines such as THP-1, U-937 and MonoMac, as well as by mixing pure proMMP-9 with the proteoglycans SG and versican [39]. It was shown that the *in vitro* formation of these reduction sensitive complexes was not due to intramolecular disulphide bridges, but more likely due to a mixture of ionic and hydrophobic interactions along with hydrogen bonds [39]. Furthermore, in both the *in vitro* reconstituted complexes as well as in the macrophage produced complexes the gelatin binding part of proMMP-9 was hidden [38, 39]. Inhibition and activation studies indicated that both the FnII module as well as the HPX domain were involved in the complex formation [37, 39].

The *in vitro* reconstitution studies in the present work shows that when both the FnII module and the HPX domain lacks, no proMMP-9·CSPG/SG complex forms. In the presence of at least one of these two parts of proMMP-9, a complex is formed. This also shows that even if the CSPG/SG core protein interacts with the amino acids that make up the pro,

catalytic (minus the FnII part) and the OG domain, the interaction is not enough to form the SDS-stable reduction sensitive complex. This is also true with respect to the N- and O-linked glycans in the enzyme. The present work also shows that the CS-chains in SG are not involved in the complex formation.

The peptide arrays indicate that amino acids in the SG core protein located both N- and C-terminal to the central 18 amino acid Ser-Gly repeats are involved in the complex formation. It also indicates that amino acids in the first and the second repeat in the FnII module is involved in the complex formation as well as amino acids in the third and fourth blade of the HPX domain.

The docking and MD simulations suggest that the interactions between the SG core protein with the FnII module or HPX domain, involves parts on each of the two interacting molecules that are located at considerable distances from each other. Therefore, individual amino acids that appeared important for binding in the 20-mer peptide arrays may not reflect the amino acids that is involved in the binding between the full-length molecules. When the SG core protein binds to the FnII module, the results suggest that at least a part of the SG core protein binds to the same or overlapping epitopes in the FnII module that bind gelatin. This fits well with our previous studies which showed that gelatin inhibited the *in vitro* reconstitution of the proMMP-9·CSPG/SG complex(es) and that the vast majority of the complex isolated from THP-1 cells did not bind to Gelatin-Sepharose [38, 39]. The docking and MD simulations also suggest that the FnII module at the same time can interact with the parts in SG that was located both to the N- and C-terminal side of the Ser-Gly repeats. This also appear to be the case for one of the models with the HPX domain. The MD simulations of the entire proMMP-9 also suggest that the hinge region (OG-domain) is very flexible where the two globular domains in the enzyme are either at a close distance or at a longer distance from each other. These MD simulations appear to reflect previous results from small X-ray crystallography and atomic force microscopy [29]. The MD simulations also suggest that the SG core protein could be sandwiched between the FnII module and the HPX domain in the full length enzyme due to the large flexibility of the long MMP-9 hinge region. These simulations also suggest that amino acids in the catalytic domain of MMP-9 may be involved in the complex formation along with amino acids in the HPX domain and the FnII module. All over, the results in the present work shows the complexity in the formation of the proMMP-9·CSPG/SG complex(es).

3. Materials and Methods

3.1. Materials

Re-blot Plus Mild Solution (10x), TRIS, urea, guanidinium hydrochlorid, DMSO, $CaCl_2 \cdot 2H_2O$, citric acid and sodium acetate was obtained from Merck (Darmstadt, Germany). 2-Methoxy-2,4-Diphenyl-3(2H)-Furanone (MDPF), $(NH_4)_2SO_4$ and EDTA were from Fluka (Buchs, Switzerland). Acetic acid, acrylamide/bis-acrylamide, Commassie Brilliant Blue G-250 and Triton X-100 were from BDH (Poole, UK). RPMI 1640, fetal bovine serum, streptomycin, penicillin, acrylamide/Bis-acrylamide, sodium dodecyl sulphate (SDS; 20% in H_2O), dithiothreitol (DTT), safranin O (no.S-2255), ponceau S, cetylpyridinuim chloride, sodium tetraborate, phorbol 12-myristate 13-acetate (PMA), Hepes, Brij-35, trypsin, soybean trypsin inhibitor (SBTI), Silver nitrate, chondroitin sulphate C (shark cartilage CS), gelatin (porcine skin, approx. 300 Bloom) were from Sigma (St Louis, MO, USA). Proteinase free chondroitin ABC lyase (cABC) and antibody against versican (2-B-1) were from Seikagaku Kogyo Co (Tokyo, Japan). Gelatin-Sepharose, Heparin Sepharose, Q-Sepharose, Sephadex G-50 (fine), Sephadex G-200, Sephacryl S-200, Sephacryl S-400, Protein G Sepharose were from GE-Healthcare (Uppsala, Sweden). Helix pomatia agglutinin (HPA) covalently linked to agarose beads was from EY Laboratories, Inc. (San Maeo, CA, USA). Unlabelled molecular weight standards was from BioRad (Richmond, CA, USA). Magic Marker molecular weight standards were from Invitrogen (Carlsbad, CA, USA). Western Blotting Luminol reagent was from Sancta Cruz (Santa Cruz, CA, USA). HRP-conjugated goat anti-rabbit secondary antibody was from Southern Biotech (Birmingham, AL, USA) and rabbit polyclonal antibodies against C-terminal, mid-region and N-terminal part of serglycin were from Antibodies-online Inc. (Atlanta, USA). Rabbit anti-rat MMP-9 polyclonal antibody (also detect mouse and human MMP-9) was obtained from Chemicon International Inc. (Temecula, CA, USA). Silver staining kit was from Pierce (Rockford, IL, USA). Peptide arrays and the soluble His-tag peptide, were obtained from The Peptide Synthesis Core Facility, The Biotechnology Centre of Oslo, University of Oslo, Norway. Recombinant human his-tagged serglycin was from ProSpec (Ness Ziona, Israel). Vivaspin columns with a 10 and 30 kDa cut-off were from Satorius Stedim Biotech GmbH (Goettingen, Germany). Imperial blue protein stain, high range and broad range molecular weight standards were from Thermo Scientific (Rockford, Il, USA). Recombinant catalytic domain of human MMP-9 containing the FnII repeats was from AnaSpec, Inc. (Fremont, CA, USA). Biotinylated protein ladder was from Cell Signalling (Danvers, MA, USA). Polyclonal rabbit anti human MMP-9 carboxyterminal

end (HPX domain) ab38906 was from Abcam (Cambridge, UK).

3.2. Biosynthesis of proMMP-9 and CSPGs

The human leukemic monocyte cell-line THP-1 was a kind gift from Dr. K. Nilsson, Department of Pathology, University of Uppsala, Sweden. The cells were cultured in RPMI 1640 medium with 10% fetal bovine serum, 50 μg/ml of streptomycin, and 100 units/ml of penicillin. To isolate secreted cell-synthesized CSPGs and proMMP-9, the cells were washed 3 times in serum-free medium and then cultured for 72 h in serum-free RPMI 1640 medium with or without 0.1 μM PMA as described earlier [35]. Conditioned medium was harvested, loose cells were pelleted by centrifugation at 1200 rpm (200g) for 10 min. ProMMP-9 and CSPGs were thereafter isolated and detected as described below.

3.3. Detection of PG-bound CS-chains

PG-bound CS-chains were quantified spectrophotometrically by the Safranin O colour method as described previously [36].

3.4. Isolation of secreted CSPG

Secreted CSPG from unstimulated THP-1 cells (monocytes) was isolated by Q-Sepharose anion-exchange chromatography as described previously [35, 36, 39]. The amount of CSPG was based on the quantification of the GAG-chains using the safranin O method and chondroitin sulphate C (shark cartilage CS) as a standard.

3.5. Purification of serglycin

One ml of pooled CSPG (3 mg/ml) from Q-Sepharose anion-exchange chromatography was subjected to gel permeation chromatography on a Sephacryl S-400 column (90x1.6 cm) pre-equilibrated with 4 M guanidine hydrochloride, 50 mM sodium acetate, pH 6.0. The column was eluted with the same buffer, fractions collected and PGs monitored by the safranin O method and characterized by SDS-PAGE and immunoblotting. Fractions with SG were

pooled, diluted and applied to a Q-Sepharose column. Eluted material from the Q-Sepharose column was desalted on a Sephadex G-50 column and thereafter concentrated on a vacuum centrifuge (Speedvac). The amount of SG was determined by the safranin O method, using a standard curve generated from shark cartilage CS.

3.6. Chondroitin ABC lyase (cABC) treatment

The PG bound CS-chains were removed by digestion for 2 h at 37 °C with 0.2-1.0 units of cABC/ml in 0.05 M Tris-HCl, pH 8.0, containing 0.05 M sodium acetate.

3.7. Purification of proMMP-9 from the THP-1 cells

The proMMP-9 in conditioned medium from PMA stimulated THP-1 cells was partly purified as described previously [38, 40]. SDS-electrophoresis under reducing conditions, followed by either silver or Coomassie Blue staining, showed two bands, a major band at 92 kDa and a minor band at 28 kDa (Fig. 2A). Western blotting revealed that the 92 kDa band was proMMP-9 (Fig. 2C), and the 28 kDa band was TIMP-1 [38]. The amount of proMMP-9 was estimated spectrophotometrically at 280 nm using ε_{280nm} = 114.36 $mM^{-1}cm^{-1}$ [43], ignoring the contribution of TIMP-1.

ProMMP-9 was separated from TIMP-1 linked to its HPX-domain on a Sephadex G-200 column in the presence of 0.1 % SDS. The equilibration and elution buffer of the Sephadex G-200 column contained 0.1 M Hepes pH 7.5, 0.15 M NaCl, 0.1% SDS and 5.0 mM EDTA. The fractions containing pure 92 kDa proMMP-9 were concentrated on an Amicon Ultra Centrifugal Filter (Millipore) with a 10 kDa cut off. This material was passed over a Sephadex G-50 column (equilibration and elution buffer 0.1 M Hepes pH 7.5 containing 5.0 mM EDTA) to remove SDS from the pure proMMP-9. This TIMP-1 free proMMP-9 was used to produce proMMP-9 polyclonal antibodies in rabbit (Eurogentec, Liège, Belgium). The obtained polyclonal antibodies did not react with other commercially obtained MMPs (MMP-1, MMP-2 and MMP-14), TIMP-1 or His-tagged serglycin.

3.8. Activation of proMMP-9

Activation of proMMP-9 from THP-1 cells was achieved by limited proteolysis with trypsin as described previously, and the activation was stopped by adding soybean trypsin inhibitor (SBTI) [37, 40, 57]. The enzyme activity of un-activated and trypsin-activated MMP-9 was determined with the fluorescence quenched substrate Mca-PLGLDpaAR-NH_2 (10 μM) in 0.1 M Hepes pH 7.5 (containing 10 mM $CaCl_2$, 0.005% Brij-35) at 37°C in a total volume of 100 μL. The initial rate of the reaction was determined on a Perkin Elmer LS 50 Luminescence spectrometer using the FL WinLab Software Package (Perkin Elmer). The reactions were followed for one minute and during that time 600 data points were collected. The excitation and emission wavelengths were; λ_{ex}=320 nm, λ_{em}=405 nm and a slit width=10 nm at both wavelengths.

3.9. Expression of recombinant proMMP-9 variants in Sf9 and High Five Insect cells

The expression of recombinant full-length proMMP-9 (rpMMP-9) from Sf9 insect cells was performed as described previously [40]. Two deletion variants of MMP-9, one lacks the HPX domain (rpMMP-9ΔHPX) and the other lacks both the HPX and the OG domain (rpMMP-9ΔOGHPX) (Fig. 1) were generated using the purchased human preproMMP-9 cDNA (accession number: BC006093.1) cloned into the pReceiver-M02 vector (Catalogue number: EX-F0125-M02) as template. A stop codon was inserted in the sequence of MMP-9 behind the codon for ^{515}A or for ^{444}G, respectively. A two step PCR reaction was used to produce rpMMP-9ΔHPX. In the first step, a stop codon was inserted before the coding sequence of the HPX domain using the primer pairs (fwd: 5'-TAGACATG AGC CTC TGG CAG C-3', rev: 5'-GCTGGGTC*TTA*GGC ATC GTC CAC CGG ACT CAA AGG-3'). In the second step, the Invitrogen™ Gateway™ attB-sequences was inserted into the amplified PCR product using the primer pairs (fwd: 5'-GGGGACAAGTTTGTACAAAAAAGCAGGCTT CGAAGG AGATAGAAC CATGAG CCT CTGGCAGC - 3', rev: 5'-GGG GAC CAC TTT GTA CAA GAA AGC TGG GTC **TTA** GGC ATC GTC CAC C GG ACT CAA AGG-3'). Finally, BP reaction was performed to clone rpMMP-9ΔHPX into pDON 221 plasmid using Gateway® BP Clonase® II Enzyme mix (Invitrogen, Thermo Fisher Scientific Inc.), and transferred into BaculoDirect™ Linear DNA (catalogue number: 12362013) using Gateway® LR clonase® II enzyme mix. Baculoviruses were produced using Sf9 cells according to the protocol described in BaculoDirect™ Baculovirus Expression System. The P3 and P4 viral stock were used for

production of rpMMP-9ΔHPX in Sf9 cells in suspension. The following procedure was used to produce rpMMP-9ΔOGHPX. By PCR followed by a T4 ligation reaction two STOP codons were introduced before the coding sequence of the OG domain of preproMMP-9 using the primer pair (fwd: 5'- [Phos]TAA TAG CCT CGC CCT TAA CCT GAG CCA CG- 3', rev: 5'- [Phos]ACC ATA GAG GTG CCG GAT GCC A- 3'). The template of the PCR reaction was preproMMP-9 previously cloned into the Gateway® pDON 221 plasmid [40]. This rpMMP-9ΔOGHPX variant was subsequently cloned into BaculoDirect™ Linear DNA (catalogue number: 12362013) using Gateway® LR Clonase® II Enzyme mix. Baculoviruses were produced using Sf9 cells according to the protocol of the BaculoDirect™ Baculovirus Expression System. The P3 and P4 viral stocks were used for production of rpMMP-9ΔOGHPX in High Five™ cells according to protocol (Invitrogen and Thermo Fisher Scientific).

The deletion variant lacking the three FnII repeats in the catalytic site (rpMMP-9ΔFnII) (Fig. 1) was generated by the use of phosphorothioate-modified primers, a technique previously described by Stoynova et al. [58]. In this variant, amino acids 216-390 were deleted from the full length proMMP-9 by inverse PCR using phosphorothioate-modified primers (fwd: 5`- AAG GGC CAA GGA T*A*C* AGT TTG TTC CTC - 3`, rev: 5`- TCC TTG GCC CTT G*C*C* CAG GGA CCA CAA CTC - 3`). The nucleotides containing phosphorthioate are labelled with a star (*). The plasmid containing the proMMP-9 deletion was transferred into BaculoDirect™ Linear DNA (catalogue number: 12362013) using Gateway® LR clonase® II enzyme mix preserving the endogenous MMP-9 stop codon. The P3 and P4 viral stocks were used for production of this FnII deletion variant in Sf9 cells in suspension. Deletion variant rpMMP-9ΔFnIIHPX lacking the FnII repeats and the HPX domains, and rpMMP-9ΔFnIIOGHPX lacking the FnII repeats and both the HPX and the OG domain (Fig. 1) were cloned using the pDON 221 preproMMP-9ΔFnII constructs as a template for PCR. Two STOP codons were introduced behind the codon for ^{515}A for rpMMP-9ΔFnIIHPX and behind the codon for ^{444}G for rpMMP-9ΔFnIIOGHPX using the primer pairs (fwd: 5'- [Phos] CTA TTA GGC ATC GTC CAC CGG ACT C- 3', rev: 5'- [Phos] TGA AAC GTG AAC ATC TTC GAC GC- 3') and (fwd: 5'- CTA TTA TCA CTA ACC ATA GAG GTG CCG GAT GC - 3', rev: 5'- TAG TGA TAA TAG CCT CGC CCT GAA CCT GAG C - 3') respectively. The PCR for rpMMP-9ΔFnIIHPX and rpMMP-9ΔFnIIOGHPX were followed by a T4 ligation reaction. Both constructs were subsequently cloned into BaculoDirect™ Linear DNA (catalogue number: 12362013) using Gateway® LR Clonase® II

Enzyme mix. Baculoviruses were produced using Sf9 cells according to the protocol of the BaculoDirect™ Baculovirus Expression System. The P3 and P4 viral stocks were used for production of rpMMP-9ΔFnIIHPX or rpMMP-9ΔFnIIOGHPX in High Five™ cells according to protocol (Invitrogen and Thermo Fisher Scientific).

3.10. Purification of recombinant proMMP-9 variants

The purification of recombinant proMMP-9 variants containing the FnII module in the catalytic site were performed as described previously [40]. Briefly, 30 ml of serum-free medium from Sf9 and High Five insect cells infected with baculovirus containing either rpMMP-9, rpMMP-9ΔHPX or rpMMP-9ΔOGHPX was applied to a 1 ml column of Gelatin-Sepharose pre-equilibrated with 0.1 M Hepes buffer pH 7.5 containing 5.0 mM $CaCl_2$. After collecting the pass-through medium, the column was first washed with 10 column volumes of 0.1 M Hepes buffer pH 7.5 containing 5.0 mM $CaCl_2$ and 1.2 M NaCl. This was followed by a new wash with 30-40 column volumes of 0.1 M Hepes buffer pH 7.5 containing 5.0 mM $CaCl_2$. Bound proMMP-9 was eluted with a buffer containing 0.1 M Hepes pH 7.5, 5.0 mM $CaCl_2$ and 7.5% DMSO. The eluted material was concentrated and depleted of DMSO (end [DMSO] less than 0.02%) using a spin column with a cut-off of 10 kDa. The amount of proMMP-9 in the sample were determined spectrophotometrically at 280 nm using the extinction coefficient ε_{280nm} = 114.36 $mM^{-1}cm^{-1}$ [43] for the full length enzymes, ε_{280nm} = 73.185 $mM^{-1}cm^{-1}$ for the rpMMP-9ΔHPX and ε_{280nm} = 73.060 $mM^{-1}cm^{-1}$ for the rpMMP-9ΔOGHPX (calculated from the ExPASy-ProtParam tool using the amino acid sequence). Previously it was shown that determination of protein concentration based on a theoretical calculation of a proteins extinction coefficient at 280 nm from its predicted protein sequence from the DNA sequence is reliable [59]. Based on the ExPASy-ProtParam tool an extinction coefficient of 112.73 $mM^{-1}cm^{-1}$ was obtained for the full length proMMP-9, which is similar to the value of Murphy and Crabbe [43].

Purification scheme 1 of proMMP-9ΔFnII: Fifty ml of serum-free medium from Sf9 cells infected with baculovirus containing proMMP-9ΔFnII was first dialysed 2 times against 2L of 50 mM Hepes buffer with 10 mM $CaCl_2$, pH 7.5. To this dialysed material, 40 % (w/v) $(NH_4)_2SO_2$ was added and mixed in a rotator for 20 min at 4 °C. Thereafter, the mixture was centrifuged at 15000g at 4 °C for 30 min. The supernatant contained proMMP-9ΔFnII and more $(NH_4)_2SO_2$ was added to the supernatant. This resulted in a salt concentration of 55 %

(w/v) and the sample were mixed in rotator for 20 min at 4 °C, followed by centrifugation as above. The precipitate containing proMMP-9ΔFnII was dissolved in 0.5 mL of gel filtration buffer (0.1 M Hepes buffer, 10 mM $CaCl_2$ and 150 mM NaCl, pH 7.5). This material was applied to a Sephacryl-200 column (95 cm, diameter 1.2 cm) pre-equilibrated with gel filtration buffer. Fractions of 500 µL was collected, and the fractions containing proMMP-9ΔFnII (based on real-time gelatin zymography) was pooled, and applied to a centrifugal filter with a 30 kDa cut-off. This resulted in removal of contaminating proteins with molecular sizes smaller than 30 kDa and a concentrated fraction of proMMP-9ΔFnII. The amount of proMMP-9ΔFnII was determined using ε_{280nm} = 79.550 $mM^{-1}cm^{-1}$ calculated from the ExPASy-ProtParam tool using the amino acid sequence. *Purification scheme 2 of proMMP-9ΔFnII*: Fifty ml of serum-free medium from Sf9 cells infected with baculovirus containing proMMP-9ΔFnII was first desalted and concentrated on a spin column with a 30 kDa cut-off. Thereafter was 20 ml of this material applied to a 3 ml column of Heparin-Sepharose pre-equilibrated with 0.1 M Hepes buffer pH 7.5 containing 5 mM $CaCl_2$. After first collecting the pass-through medium, the column was washed with 12 column volumes of equilibration buffer. The truncated enzyme was then eluted from the column with a 30 ml NaCl gradient (0-1.0 M) in the same buffer. The pooled eluted material was concentrated and depleted of NaCl using a spin column with a 10 kDa cut-off. The amount of proMMP-9ΔFnII was determined spectrophotometrically at 280 nm.

The purified and partly purified proMMP-9 variants were applied to gelatin zymography, real-time gelatin zymography and SDS-PAGE (NuPAGE Novex 4-12% Bis-Tris gels). The SDS-PAGE gels were either further applied to Western blotting (using antibodies against MMP-9) or stained with Imperial blue where bands from the purified proMMP-9 variants containing the FnII module were cut out and sent to MS analysis at the Tromsø University Proteomics Platform (TUPP).

3.11. In vitro reconstitution of the proMMP-9·CSPG/SG heteromer

In vitro reconstitution of proMMP-9·CSPG/SG complexes were performed as described previously [39]. Briefly, purified proMMP-9 (0.05 µM) from THP-1 cells, ~ 0.05 µM trypsin activated proMMP-9, or 0.05 µM of full length or truncated recombinant proMMP-9 were incubated with 230 µg/ml of purified CSPG/SG or 80 µg/ml of purified serglycin from untreated THP-1 cells. When rpMMP-9ΔFnII was used in the reconstitution experiments, it

was assumed a purity of approximately 50%. Hence, the amount of partly purified medium used was twice as much as expected from the A_{280nm} determination to give an enzyme concentration of approximately 0.05 μM. To assure that enough amounts of rpMMP-9ΔFnIIHPX and rpMMP-9ΔFnIIOGHPX was used in the reconstitution experiments, different amounts of crude media containing these two variants and partly purified rpMMP-9ΔFnII were applied to real-time gelatin zymography. Based on that, the amount of crude media of rpMMP-9ΔFnIIHPX and rpMMP-9ΔFnIIOGHPX used in the reconstitution experiments contained approximately 3 to 5 times as much of these enzymes as that used of the rpMMP-9ΔFnII deletion variant. These mixtures were incubated for 15 min to 24 h at 37 °C in 0.1 M Hepes buffer pH 7.5. In some experiments, these mixtures also contained 10 mM EDTA. After the incubation, the mixture was passed over a small Q-Sepharose column, washed with 10 column volumes of 0.05 M sodium acetate (pH 6.0) containing 6 M urea and 0.35 M NaCl and then the bound proMMP-9·CSPG/SG complexes were eluted with the same buffer containing 1.5 M NaCl. The fractions containing proMMP-9·CSPG/SG complexes were pooled and desalted on Sephadex G-50 (fine) columns run in H_2O. The volume was reduced in a Speed Vac (Savant). The purified CSPG/SG, SG, proMMP-9·CSPG/SG and proMMP-9·SG complexes were then applied to gelatin zymography, real-time gelatin zymography or Western blotting.

3.12. In vitro reconstitution of proMMP-9·Serglycin core protein complexes lacking CS-chains

Either 100 μL of purified proMMP-9 from THP-1 cells (50 ng) or 100 μL Ht-SG (200 ng) in Western blotting buffer (48 mM TrisBase, 386 mM Glycin, 20% Methanol) 0.1 M Hepes pH 7.5 were bound to a polyvinyl difluoride membrane using a slot blot apparatus. The different slots were cut out and the membranes were blocked with milk powder as in Western blotting. Relevant membrane slots were thereafter incubated with either proMMP-9 (5 μg/ml) or Ht-SG (5 μg/ml) with or without 10 μg/ml His-tag peptide (Ht-P), washed and incubated with antibodies against proMMP-9, SG or the His-tag (1:200). The membranes were thereafter washed and treated as described for Western blotting.

3.13. Gelatin zymography and real-time gelatin zymography

SDS-substrate PAGE was done as described previously [36] with gels (7.5 cm x 8.5 cm x 0.75 mm) containing 0.1% (w/v) gelatin in both the stacking and separating gel, 4 and 7.5 % (w/v) of polyacrylamide, respectively. Gelatinase activity was evident as cleared (unstained) regions.

Real-time gelatin zymography was performed as described previously [40, 60]. Briefly, 0.1% (w/v) MDPF-fluorescent labelled gelatin was incorporated in the 7.5% SDS-PAGE separating gel and 0.2% (w/v) MDPF-fluorescent labelled gelatin was incorporated in the 4.0% SDS-PAGE separating gel. The fluorescent dye 2-methoxy-2,4-diphenyl-3(2H)-furanone was used to label gelatin to give MDPF-gelatin as described previously [60]. The main difference between normal gelatin zymography and real-time gelatin zymography is that in real-time zymography, the gel is not stained and hence it is possible to follow the degradation of the gelatin in real time without staining. Gelatinase activity was evident as dark bands against the un-degraded fluorescent background.

3.14. Western immunoblotting analysis

Purified proMMP-9 from THP-1 cells, recombinant full length and deletion variants of human proMMP-9 from Sf9 and High Five insect cells, and cABC treated purified SG from THP-1 cells with and without 0.1 M DTT were electrophoresed on SDS-polyacrylamide gel (NuPAGE Novex 4-12% Bis-Tris gels) and electroblotted to a polyvinyl difluoride membrane. After blockage of non-specific binding sites with non-fat milk in TBS-T (150 mM NaCl, 0.25% Tween-20, 20 mM Tris-HCL, pH 7.4), blots were incubated for 1 h at room temperature or 4 °C over night with either primary rabbit polyclonal antibody against human MMP-9 or rabbit polyclonal antibodies against SG (mixture of Ab against C-terminal, N-terminal and Mid-region). After washing, the blots were incubated for 1 h at room temperature with an HRP-conjugated goat anti-rabbit secondary antibody. The Blots were thereafter washed with TBS-T 3 x 5 min before visualization using Western Blotting Luminol reagent. The intensity of immunoblot bands was measured using a Luminescent Image Analyzer LAS-3000 with MultiGauge software version 3.0 (Fujifilm, Tokyo, Japan).

Non-reduced samples of purified proMMP-9·CSPG complexes with the various proMMP-9 variants were applied to SDS-PAGE (4% acrylamide in the stacking gel and 7.5% acrylamide in the separating gel; identical concentrations as in gelatin-zymography). After

electrophoresis, the polyacrylamide gels were incubated in 0.1M DTT for 1 hr at room temperature prior to blotting as described previously [36]. The gel was thereafter electro-blotted to a polyvinyl difluoride membrane, treated as described above to detect proMMP-9 variants bound to the CSPG/SG core protein. Reduced samples of purified proMMP-9·CSPG with the various proMMP-9 variants were applied to SDS-PAGE as describe above.

3.15. Peptide Arrays

Peptide arrays based on the amino acids sequences of SG (131 amino acids), the MMP-9FnII module (166 amino acids) and the MMP-9HPX domain (187 amino acids) were ordered from The Peptide Synthesis: Core Facility, The Biotechnology Centre of Oslo, University of Oslo. The first peptide in the peptide arrays was made up of the first twenty amino acids and each successive peptide had a two amino acid shift. The membranes containing the peptide arrays of SG, MMP-9FnII module and MMP-9HPX domain were first stained with 0.1% ponceau stain in 5% HAc for 5 minutes at room temperature. These membranes were then dried, marked and cut out as individual arrays of SG, MMP-9FnII module and MMP-9HPX domain. The membranes were then fitted inside a 50 ml plastic tube and the membrane was washed with water in a rotating wheel for 5 minutes. Then the membranes were washed again with 10 ml TBST for 5 minutes after which the membranes were blocked with 10 ml blocking buffer (0.5 g non-fat milk powder in 10 mL TBST) for one hour in a rotating wheel to prevent nonspecific protein binding. Thereafter, the SG array membrane was incubated in 10 ml blocking buffer containing 8.8 µl of 11.2 µg/ml proMMP-9, the arrays of the MMP-9FnII module and the MMP-9HPX domain were incubated in 10 ml blocking buffer with 10 µl of 1 ng/µl Ht-SG. These incubations were done for 1-4 hours at room temperature. The membranes were thereafter washed 3 times for 5 minutes with 10 ml TBST. Different primary antibodies according to the type of arrays were diluted in 10 ml blocking buffer and were added to the tubes with the arrays. In the tube with the SG array, 10 µl primary rabbit antibody against human MMP-9 (5.1 mg/ml) was added in 10 ml blocking buffer. Tubes with arrays of the MMP-9FnII module and the MMP-9HPX domain were incubated with 10 ml blocking buffer to which the following amounts of rabbit antibodies against human SG had been added; 2 µl of C-terminal Ab (0.25 mg/ml), 8 µl of N-terminal Ab (1 mg/ml) and 8 µl of Mid-region Ab (1 mg/ml). All membranes were incubated overnight on a rotating wheel at 4 °C. Next day the membranes were washed with 10 ml TBST, 3 times 5 minutes and then

incubated with 10 ml blocking buffer containing 10 µl HRP conjugated goat anti-rabbit secondary antibody for one hour at room temperature. Thereafter the membranes were washed with 10 ml TBST, 3 times 5 minutes. Membranes were then developed in a 1:1 ratio of Luminol reagent A and Luminol reagent B (Western Blotting Luminol reagents) for antibody detection and images were obtained by a luminescent image analyzer (Image quant LAS 4000 or Fujifilm LAS 3000).

To reuse membranes, they were stripped by first washing with 0.1M DTT in TBST for 1 hr at 37°C using a rotator. This was performed six times. After that, the membranes were incubated in Re-blot Plus Mild Solution (1x) for 1 hr at 37 °C using a rotator. Then to remove remnants of the DDT and Re-blot Plus Mild Solution, membranes were washed with TBST (5 min x 2). After this, membranes were ready to be reused.

3.16. Mutated Peptide Arrays

The amino acids selected for mutation were based on the results from the first peptide arrays. They were mutated as follows: The polar and charged amino acids serine (S), histidine (H), asparagine (N), glutamine (Q), tyrosine (Y), tryptophan (W), aspartate (D), glutamate (E), arginine (R), cysteine (C) and lysine (K) were mutated to alanine (A) since it has a small hydrophobic side chain. The polar amino acid threonine (T) was changed into valine (V). The hydrophobic amino acids Valine (V), alanine (A), isoleucine (I), methionine (M), leucine (L), proline (P) and phenylalanine (F) were mutated to glycine (G), which lacks a side chain. Glycine (G) was mutated to leucine (L).

3.17. Homology Modelling and Docking

Docking of SG into FnII and HPX domains was performed with the protein-protein docking program BioLuminate of the Schrödinger software package [61]. The X-ray structures of FnII (PDB id 1l6j; [31]) and HPX (PDB id 1itv; [30]) were gathered from the pdb database (http://www.rcb.org/pdb/), and optimized using the protein preparation wizard tool of Maestro in the Schrodinger software package [62]. The structures were prepared by capping the N and C terminus, adding missing hydrogen atoms as well as missing loops. In addition, bond orders were assigned and water molecules with less than 3 hydrogen bonds were deleted. The

structure of HPX contains only the four blades while, the structure of FnII comprises the MMP-9 prodomain, catalytic region and the three repeats of FnII.

To validate the reliability and accuracy of the protein-protein docking program for the present molecular systems, chain B (HPX_B) of the dimeric X-ray structure of HPX was docked with chain A (HPX_A) from the same structure, using HPX_A as a fixed receptor. The docking was performed with standard mode, allowing maximum 100 docking poses. Protein interaction analysis was performed to analyze the amino acid interactions between the two HPX domains of the docked dimer and compare the interactions with the amino acid interactions in the X-ray structure (1itv) [30].

PHYRE^2 [63] was used to predict the structure of SG based on its amino acid sequence. It is an online software tool, which predicts the structure based on the sequence provided and homologous structures present in the database using sequence alignments and protein/homology modeling. After the predicted SG structure was acquired, the protein preparation wizard of the Maestro program was used to prepare the structure for docking. The optimized structure was then docked to FnII and HPX, which were selected as receptors. During the docking of SG with FnII, the maximum number of poses to return was set to 150, while the maximum number during the docking with HPX was 100. After docking, three steps were taken to select the best poses for further analysis: (1) selecting poses with converged minimization during optimization, (2) selecting the poses with similarity to peptide array results and (3) checking the level of hindrances of CS-chains attached to the SG of the different poses selected after the second step.

In docking poses selected after the second step, five of the serine residues of the eight Ser-Gly repeats of SG were modified by adding the following 8 polysaccharide units, -Xyl-Gal-Gal-GlcA-GalNAc-GlcA-GalNAc-GlcA. The tetrasaccharide linker (Xyl-Gal-Gal-GlcA) was built using Maestro and linked to the tetrasaccharide CS repeat (GalNAc-GlcA-GalNAc-GlcA), extracted from the pdb structure 1RWH [64]. After adding the chain of 8 polysaccharide units to SG, the selected docking poses were optimized in Maestro. The docking pose after optimization where the added polysaccharide chain did not hinder the interaction with FnII or HPX were selected for MD.

3.18. Molecular Dynamics Simulation

The program Desmond [62, 65] was used for MD simulations of selected docking poses of HPX_A and HPX_B, and SG with HPX and FnII. First, we conducted a simulation of the best docking pose of HPX_A/HPX_B. The best pose was selected on the basis of the structural similarity with the pdb structure of the HPX dimer. This was done to test the accuracy of the structural predictions.

The selected poses were used as the initial complexes for 100 ns simulations, using the OPLS3e force field. All molecular systems were solvated with an orthorhombic box of simple point charge (SPC) water moleucles which were neutralized by adding Na^+ and Cl^- ions. The width of the box was set to 10 Å. The NaCl concentration was 0.15 M. After this, the system setup was completed molecular dynamics was performed with default settings. The ensemble class NPT (number of atoms, pressure, and temperature) was selected which allows them to keep constant during the simulation. Temperature was set at 300K and pressure at bar 1.013. The 'relax model system before simulation' was selected. Under advanced options, the time step is set at 2 fs and the cut-off radius was 9.0 Å. This is an important step as it affects the calculation speed. After the simulation was finished, 'Simulation event analysis' command was used for analyzing the output from the three simulation trajectories.

Supplementary materials:

Supplement 1: Molecular Dynamics Simulation of HPX dimer and docked HPX dimer.

Figure S1: Elution profile of Q-Sepaharose purified CSPG from THP-1 cells using a Sephacryl S-400 column.

Figure S2: Binding of pMMP-9 to a mutated SG peptide array.

Figure S3: Binding of proMMP-9 to peptides in the array of the serglcyin.

Figure S4: Binding of Ht-SG to a mutated FnII peptide array.

Figure S5: Binding of Ht-SG to a mutated HPX peptide array.

Figure S6: X-ray structure of the HPX dimer (pdb. 1itv), docking of HPX_B to HPX_A and MD simulations of both complexes.

Figure S7: Docking and molecular dynamic simulations of the interactions between the MMP-9FnII module and the SG core protein.

Figure S8: Docking and molecular dynamic simulations of the interactions between the MMP-9HPX domain and the SG core protein: Model 1.

Figure S9: Docking and molecular dynamic simulations of the interactions between the MMP-9HPX domain and the SG core protein.

Figure S10: Molecular dynamic simulations of the Full-length MMP-9.

Figure S11: Molecular dynamic simulations of the interactions between the full-length MMP-9 and the SG core protein.

Figure S12: Molecular dynamic simulations of the interactions between the full-length MMP-9 and the SG core protein.

Figure S13: Molecular dynamic simulations of the interactions between the full-length MMP-9 and the SG core protein.

Figure S14: Molecular dynamic simulations of the interactions between the full-length MMP-9 and the SG core protein based on the position from the best FnII-SG docking model.

Movie 1, Movie 2, Movie 3, Movie 4 and Movie 5

Acknowledgements: We are grateful to Dr. K. Nilsson (Department of Pathology, University of Uppsala, Sweden) for the kind gift of the THP-1 cells. This work was in part supported by grants from Tromsø Forskningsstiftelse.

Author contributions:

Conceptualization, R.D., I.S., G.S., N.M., B.H., J.-O.W.; Methology, R.D., N.M., B.H., G.S., I.W., I.S., J.-O.W.; Validation, R.D., N.M., B.H., G.S., I.S., J.-O.W.; Formal analysis, R.D, N.M., I.S., J.-O.W; Investigation, R.D., N.M., B.H., E.B., J.-O.W.; Resources, I.S., I.W., J.-O.W; Writing – Original Draft Preparation, R.D., I.S., J.-O.W.; Writing – Review & Edition, N.M., B.,H., I.W., E.B., G.S.; Visualization, R.D., J.-O.W; Supervision, I.S., I.W., J.-O.W; Project Administration, J.-O.W; Funding Acquistion, J.-O.W.

Conflicts of interest: The authors declare no conflict of interest.

References

1. Hadler-Olsen E, Fadnes B, Sylte I, Uhlin-Hansen L, Winberg JO. Regulation of matrix metalloproteinase activity in health and disease. Febs J. 2011;278(1):28-45. Epub 2010/11/23. doi: 10.1111/j.1742-4658.2010.07920.x. PubMed PMID: 21087458.
2. Butler GS, Overall CM. Updated biological roles for matrix metalloproteinases and new "intracellular" substrates revealed by degradomics. Biochemistry. 2009;48(46):10830-45. Epub 2009/10/13. doi: 10.1021/bi901656f. PubMed PMID: 19817485.
3. Cauwe B, Martens E, Proost P, Opdenakker G. Multidimensional degradomics identifies systemic autoantigens and intracellular matrix proteins as novel gelatinase B/MMP-9 substrates. Integr Biol (Camb). 2009;1(5-6):404-26. Epub 2009/12/22. doi: 10.1039/b904701h. PubMed PMID: 20023747.
4. Cauwe B, Opdenakker G. Intracellular substrate cleavage: a novel dimension in the biochemistry, biology and pathology of matrix metalloproteinases. Crit Rev Biochem Mol Biol. 2010;45(5):351-423. Epub 2010/09/04. doi: 10.3109/10409238.2010.501783. PubMed PMID: 20812779.
5. Cauwe B, Van den Steen PE, Opdenakker G. The biochemical, biological, and pathological kaleidoscope of cell surface substrates processed by matrix metalloproteinases. Crit Rev Biochem Mol Biol. 2007;42(3):113-85. Epub 2007/06/15. doi: 10.1080/10409230701340019. PubMed PMID: 17562450.
6. Nagase H, Visse R, Murphy G. Structure and function of matrix metalloproteinases and TIMPs. Cardiovasc Res. 2006;69(3):562-73. Epub 2006/01/13. doi: 10.1016/j.cardiores.2005.12.002. PubMed PMID: 16405877.
7. Ra HJ, Parks WC. Control of matrix metalloproteinase catalytic activity. Matrix Biol. 2007;26(8):587-96. Epub 2007/08/03. doi: 10.1016/j.matbio.2007.07.001. PubMed PMID: 17669641; PubMed Central PMCID: PMCPMC2246078.
8. Rodriguez D, Morrison CJ, Overall CM. Matrix metalloproteinases: what do they not do? New substrates and biological roles identified by murine models and proteomics. Biochim Biophys Acta. 2010;1803(1):39-54. Epub 2009/10/06. doi: 10.1016/j.bbamcr.2009.09.015. PubMed PMID: 19800373.
9. Alameddine HS. Matrix metalloproteinases in skeletal muscles: friends or foes? Neurobiol Dis. 2012;48(3):508-18. Epub 2012/08/14. doi: 10.1016/j.nbd.2012.07.023. PubMed PMID: 22885251.
10. De Groef L, Van Hove I, Dekeyster E, Stalmans I, Moons L. MMPs in the neuroretina and optic nerve: modulators of glaucoma pathogenesis and repair? Invest Ophthalmol Vis Sci. 2014;55(3):1953-64. Epub 2014/04/01. doi: 10.1167/iovs.13-13630. PubMed PMID: 24681977.
11. Flannery CR. MMPs and ADAMTSs: functional studies. Front Biosci. 2006;11:544-69. Epub 2005/09/09. doi: 10.2741/1818. PubMed PMID: 16146752.
12. Gialeli C, Theocharis AD, Karamanos NK. Roles of matrix metalloproteinases in cancer progression and their pharmacological targeting. Febs J. 2011;278(1):16-27. Epub 2010/11/20. doi: 10.1111/j.1742-4658.2010.07919.x. PubMed PMID: 21087457.
13. Kessenbrock K, Plaks V, Werb Z. Matrix metalloproteinases: regulators of the tumor microenvironment. Cell. 2010;141(1):52-67. Epub 2010/04/08. doi: 10.1016/j.cell.2010.03.015. PubMed PMID: 20371345; PubMed Central PMCID: PMC2862057.
14. Malemud CJ. Matrix metalloproteinases (MMPs) in health and disease: an overview. Front Biosci. 2006;11:1696-701. Epub 2005/12/22. doi: 10.2741/1915. PubMed PMID: 16368548.

15. Phillips LL, Chan JL, Doperalski AE, Reeves TM. Time dependent integration of matrix metalloproteinases and their targeted substrates directs axonal sprouting and synaptogenesis following central nervous system injury. Neural Regen Res. 2014;9(4):362-76. Epub 2014/09/11. doi: 10.4103/1673-5374.128237. PubMed PMID: 25206824; PubMed Central PMCID: PMCPMC4146196.
16. Tan RJ, Liu Y. Matrix metalloproteinases in kidney homeostasis and diseases. Am J Physiol Renal Physiol. 2012;302(11):F1351-61. Epub 2012/04/12. doi: 10.1152/ajprenal.00037.2012. PubMed PMID: 22492945; PubMed Central PMCID: PMC3774496.
17. Vilen ST, Salo T, Sorsa T, Nyberg P. Fluctuating roles of matrix metalloproteinase-9 in oral squamous cell carcinoma. ScientificWorldJournal. 2013;2013:920595. Epub 2013/02/01. doi: 10.1155/2013/920595. PubMed PMID: 23365550; PubMed Central PMCID: PMCPMC3556887.
18. Wang XX, Tan MS, Yu JT, Tan L. Matrix metalloproteinases and their multiple roles in Alzheimer's disease. Biomed Res Int. 2014;2014:908636. Epub 2014/07/23. doi: 10.1155/2014/908636. PubMed PMID: 25050378; PubMed Central PMCID: PMCPMC4094696.
19. Fadnes B, Hadler-Olsen E, Sylte I, Uhlin-Hansen L, Winberg JO. Matrix Proteinase complexes and their biological significance. In: Karamanos NK, editor. Extracellular Matrix: Pathobiology and Signaling Berlin: de Gruyter; 2012. p. 291-314.
20. Gaffney J, Solomonov I, Zehorai E, Sagi I. Multilevel regulation of matrix metalloproteinases in tissue homeostasis indicates their molecular specificity in vivo. Matrix Biol. 2015;44-46:191-9. Epub 2015/01/28. doi: 10.1016/j.matbio.2015.01.012. PubMed PMID: 25622911.
21. Kolset SO, Tveit H. Serglycin--structure and biology. Cell Mol Life Sci. 2008;65(7-8):1073-85. Epub 2007/12/11. doi: 10.1007/s00018-007-7455-6. PubMed PMID: 18066495.
22. Lee S, Jilani SM, Nikolova GV, Carpizo D, Iruela-Arispe ML. Processing of VEGF-A by matrix metalloproteinases regulates bioavailability and vascular patterning in tumors. J Cell Biol. 2005;169(4):681-91. Epub 2005/05/25. doi: 10.1083/jcb.200409115. PubMed PMID: 15911882; PubMed Central PMCID: PMCPMC2171712.
23. Malla N, Sjoli S, Winberg JO, Hadler-Olsen E, Uhlin-Hansen L. Biological and pathobiological functions of gelatinase dimers and complexes. Connect Tissue Res. 2008;49(3):180-4. Epub 2008/07/29. doi: 10.1080/03008200802151755. PubMed PMID: 18661338.
24. Overall CM, McQuibban GA, Clark-Lewis I. Discovery of chemokine substrates for matrix metalloproteinases by exosite scanning: a new tool for degradomics. Biol Chem. 2002;383(7-8):1059-66. Epub 2002/11/20. doi: 10.1515/BC.2002.114. PubMed PMID: 12437088.
25. Winberg JO. Matrix Proteinases: biological significance in health and disease. In: Karamanos NK, editor. Extracellular Matrix: Pathobiology and Signaling Berlin: de Gruyter; 2012. p. 230-8.
26. Yamamoto K, Murphy G, Troeberg L. Extracellular regulation of metalloproteinases. Matrix Biol. 2015;44-46:255-63. Epub 2015/02/24. doi: 10.1016/j.matbio.2015.02.007. PubMed PMID: 25701651.
27. Yu WH, Woessner JF, Jr. Heparin-enhanced zymographic detection of matrilysin and collagenases. Anal Biochem. 2001;293(1):38-42. Epub 2001/05/25. doi: 10.1006/abio.2001.5099. PubMed PMID: 11373076.
28. Vandooren J, Van den Steen PE, Opdenakker G. Biochemistry and molecular biology of gelatinase B or matrix metalloproteinase-9 (MMP-9): the next decade. Crit Rev Biochem

Mol Biol. 2013;48(3):222-72. Epub 2013/04/04. doi: 10.3109/10409238.2013.770819. PubMed PMID: 23547785.
29. Rosenblum G, Van den Steen PE, Cohen SR, Grossmann JG, Frenkel J, Sertchook R, et al. Insights into the structure and domain flexibility of full-length pro-matrix metalloproteinase-9/gelatinase B. Structure. 2007;15(10):1227-36. Epub 2007/10/17. doi: 10.1016/j.str.2007.07.019. PubMed PMID: 17937912.
30. Cha H, Kopetzki E, Huber R, Lanzendorfer M, Brandstetter H. Structural basis of the adaptive molecular recognition by MMP9. J Mol Biol. 2002;320(5):1065-79. Epub 2002/07/20. doi: 10.1016/s0022-2836(02)00558-2. PubMed PMID: 12126625.
31. Elkins PA, Ho YS, Smith WW, Janson CA, D'Alessio KJ, McQueney MS, et al. Structure of the C-terminally truncated human ProMMP9, a gelatin-binding matrix metalloproteinase. Acta Crystallogr D Biol Crystallogr. 2002;58(Pt 7):1182-92. Epub 2002/06/22. doi: 10.1107/s0907444902007849. PubMed PMID: 12077439.
32. Goldberg GI, Strongin A, Collier IE, Genrich LT, Marmer BL. Interaction of 92-kDa type IV collagenase with the tissue inhibitor of metalloproteinases prevents dimerization, complex formation with interstitial collagenase, and activation of the proenzyme with stromelysin. J Biol Chem. 1992;267(7):4583-91. Epub 1992/03/05. PubMed PMID: 1311314.
33. Olson MW, Bernardo MM, Pietila M, Gervasi DC, Toth M, Kotra LP, et al. Characterization of the monomeric and dimeric forms of latent and active matrix metalloproteinase-9. Differential rates for activation by stromelysin 1. J Biol Chem. 2000;275(4):2661-8. Epub 2000/01/25. doi: 10.1074/jbc.275.4.2661. PubMed PMID: 10644727.
34. Vandooren J, Born B, Solomonov I, Zajac E, Saldova R, Senske M, et al. Circular trimers of gelatinase B/matrix metalloproteinase-9 constitute a distinct population of functional enzyme molecules differentially regulated by tissue inhibitor of metalloproteinases-1. Biochem J. 2015;465(2):259-70. Epub 2014/11/02. doi: 10.1042/BJ20140418. PubMed PMID: 25360794; PubMed Central PMCID: PMCPMC4399976.
35. Malla N, Berg E, Moens U, Uhlin-Hansen L, Winberg JO. Biosynthesis of promatrix metalloproteinase-9/chondroitin sulphate proteoglycan heteromer involves a Rottlerin-sensitive pathway. PLoS One. 2011;6(6):e20616. Epub 2011/06/16. doi: 10.1371/journal.pone.0020616. PubMed PMID: 21673806; PubMed Central PMCID: PMC3105995.
36. Winberg JO, Kolset SO, Berg E, Uhlin-Hansen L. Macrophages secrete matrix metalloproteinase 9 covalently linked to the core protein of chondroitin sulphate proteoglycans. J Mol Biol. 2000;304(4):669-80. Epub 2000/12/02. doi: 10.1006/jmbi.2000.4235. PubMed PMID: 11099388.
37. Winberg JO, Berg E, Kolset SO, Uhlin-Hansen L. Calcium-induced activation and truncation of promatrix metalloproteinase-9 linked to the core protein of chondroitin sulfate proteoglycans. Eur J Biochem. 2003;270(19):3996-4007. Epub 2003/09/27. doi: 10.1046/j.1432-1033.2003.03788.x. PubMed PMID: 14511382.
38. Malla N, Berg E, Uhlin-Hansen L, Winberg JO. Interaction of pro-matrix metalloproteinase-9/proteoglycan heteromer with gelatin and collagen. The Journal of biological chemistry. 2008;283(20):13652-65. Epub 2008/03/25. doi: 10.1074/jbc.M709140200. PubMed PMID: 18359769.
39. Malla N, Berg E, Theocharis AD, Svineng G, Uhlin-Hansen L, Winberg JO. In vitro reconstitution of complexes between pro-matrix metalloproteinase-9 and the proteoglycans serglycin and versican. Febs J. 2013;280(12):2870-87. Epub 2013/04/23. doi: 10.1111/febs.12291. PubMed PMID: 23601700.
40. Sylte I, Dawadi R, Malla N, von Hofsten S, Nguyen TM, Solli AI, et al. The selectivity of galardin and an azasugar-based hydroxamate compound for human matrix

metalloproteases and bacterial metalloproteases. PLoS One. 2018;13(8):e0200237. Epub 2018/08/04. doi: 10.1371/journal.pone.0200237. PubMed PMID: 30075004; PubMed Central PMCID: PMCPMC6075749.
41. Allan JA, Docherty AJ, Barker PJ, Huskisson NS, Reynolds JJ, Murphy G. Binding of gelatinases A and B to type-I collagen and other matrix components. Biochem J. 1995;309 (Pt 1):299-306. Epub 1995/07/01. doi: 10.1042/bj3090299. PubMed PMID: 7619071; PubMed Central PMCID: PMCPMC1135833.
42. Collier IE, Krasnov PA, Strongin AY, Birkedal-Hansen H, Goldberg GI. Alanine scanning mutagenesis and functional analysis of the fibronectin-like collagen-binding domain from human 92-kDa type IV collagenase. J Biol Chem. 1992;267(10):6776-81. Epub 1992/04/05. PubMed PMID: 1313021.
43. Murphy G, Crabbe T. Gelatinases A and B. Methods Enzymol. 1995;248:470-84.
44. Strongin AY, Collier IE, Krasnov PA, Genrich LT, Marmer BL, Goldberg GI. Human 92 kDa type IV collagenase: functional analysis of fibronectin and carboxyl-end domains. Kidney Int. 1993;43(1):158-62. Epub 1993/01/01. doi: 10.1038/ki.1993.26. PubMed PMID: 8433555.
45. Xu X, Chen Z, Wang Y, Yamada Y, Steffensen B. Functional basis for the overlap in ligand interactions and substrate specificities of matrix metalloproteinases-9 and -2. Biochem J. 2005;392(Pt 1):127-34. Epub 2005/07/13. doi: 10.1042/BJ20050650. PubMed PMID: 16008524; PubMed Central PMCID: PMCPMC1317671.
46. Roeb E, Schleinkofer K, Kernebeck T, Potsch S, Jansen B, Behrmann I, et al. The matrix metalloproteinase 9 (mmp-9) hemopexin domain is a novel gelatin binding domain and acts as an antagonist. J Biol Chem. 2002;277(52):50326-32. Epub 2002/10/18. doi: 10.1074/jbc.M207446200. PubMed PMID: 12384502.
47. Ugarte-Berzal E, Vandooren J, Bailon E, Opdenakker G, Garcia-Pardo A. Inhibition of MMP-9-dependent Degradation of Gelatin, but Not Other MMP-9 Substrates, by the MMP-9 Hemopexin Domain Blades 1 and 4. J Biol Chem. 2016;291(22):11751-60. Epub 2016/04/06. doi: 10.1074/jbc.M115.708438. PubMed PMID: 27044750; PubMed Central PMCID: PMCPMC4882443.
48. Van den Steen PE, Van Aelst I, Hvidberg V, Piccard H, Fiten P, Jacobsen C, et al. The hemopexin and O-glycosylated domains tune gelatinase B/MMP-9 bioavailability via inhibition and binding to cargo receptors. J Biol Chem. 2006;281(27):18626-37. Epub 2006/05/05. doi: 10.1074/jbc.M512308200. PubMed PMID: 16672230.
49. Zimmermann DR. Versican. In: Kreis T, Vale R, editors. Guidebook to the Extracellular Matrix and Adhesion Proteins. Oxford: Oxford University Press; 1993. p. 100-1.
50. Chang MY, Chan CK, Braun KR, Green PS, O'Brien KD, Chait A, et al. Monocyte-to-macrophage differentiation: synthesis and secretion of a complex extracellular matrix. J Biol Chem. 2012;287(17):14122-35. Epub 2012/02/22. doi: 10.1074/jbc.M111.324988. PubMed PMID: 22351750; PubMed Central PMCID: PMCPMC3340194.
51. Oynebraten I, Hansen B, Smedsrod B, Uhlin-Hansen L. Serglycin secreted by leukocytes is efficiently eliminated from the circulation by sinusoidal scavenger endothelial cells in the liver. J Leukoc Biol. 2000;67(2):183-8. Epub 2000/02/12. doi: 10.1002/jlb.67.2.183. PubMed PMID: 10670578.
52. Woessner JF, Jr., Nagase H, editors. Matrix metalloproteinases and TIMPs. Oxford: Oxford Univeristy Press; 2000.
53. O'Farrell TJ, Pourmotabbed T. The fibronectin-like domain is required for the type V and XI collagenolytic activity of gelatinase B. Arch Biochem Biophys. 1998;354(1):24-30.
54. Murphy G, Nguyen Q, Cockett MI, Atkinson SJ, Allan JA, Knight CG, et al. Assessment of the role of the fibronectin-like domain of gelatinase A by analysis of a deletion mutant. J Biol Chem. 1994;269(9):6632-6. Epub 1994/03/04. PubMed PMID: 8120015.

55. Schick BP. Serglycin proteoglycan: implication for thrombosis, inflammation, artherosclerosis, and metastasis. In: Karamanos NK, editor. Extracellular Matrix: Pathobiology and Signaling Berlin: de Gruyter; 2012. p. 221-31.
56. Uhlin-Hansen L, Wik T, Kjellen L, Berg E, Forsdahl F, Kolset SO. Proteoglycan metabolism in normal and inflammatory human macrophages. Blood. 1993;82(9):2880-9. Epub 1993/11/01. PubMed PMID: 8219236.
57. Sjoli S, Solli AI, Akselsen O, Jiang Y, Berg E, Hansen TV, et al. PAC-1 and isatin derivatives are weak matrix metalloproteinase inhibitors. Biochim Biophys Acta. 2014;1840(10):3162-9. Epub 2014/07/22. doi: 10.1016/j.bbagen.2014.07.011. PubMed PMID: 25046380.
58. Stoynova L, Solorzano R, Collins ED. Generation of large deletion mutants from plasmid DNA. Biotechniques. 2004;36(3):402-4, 6. Epub 2004/03/25. doi: 10.2144/04363BM05. PubMed PMID: 15038154.
59. Gill SC, von Hippel PH. Calculation of protein extinction coefficients from amino acid sequence data. Anal Biochem. 1989;182(2):319-26. Epub 1989/11/01. doi: 10.1016/0003-2697(89)90602-7. PubMed PMID: 2610349.
60. Hadler-Olsen E, Winberg JO. Method for Determining Gelatinolytic Activity in Tissue Extracts: Real-Time Gelatin Zymography. Methods Mol Biol. 2019;1952:201-10. Epub 2019/03/03. doi: 10.1007/978-1-4939-9133-4_16. PubMed PMID: 30825176.
61. BioLuminate [Internet]. LLC. 2019. Available from: https://www.schrodinger.com/products/bioluminate.
62. Maestro [Internet]. LLC. 2019. Available from: https://www.schrodinger.com/maestro.
63. Kelley LA, Mezulis S, Yates CM, Wass MN, Sternberg MJ. The Phyre2 web portal for protein modeling, prediction and analysis. Nat Protoc. 2015;10(6):845-58. Epub 2015/05/08. doi: 10.1038/nprot.2015.053. PubMed PMID: 25950237; PubMed Central PMCID: PMCPMC5298202.
64. Lunin VV, Li Y, Linhardt RJ, Miyazono H, Kyogashima M, Kaneko T, et al. High-resolution crystal structure of Arthrobacter aurescens chondroitin AC lyase: an enzyme-substrate complex defines the catalytic mechanism. J Mol Biol. 2004;337(2):367-86. Epub 2004/03/09. doi: 10.1016/j.jmb.2003.12.071. PubMed PMID: 15003453.
65. Desmond Molecular Dynamics System New York2019. Schrödinger]. Available from: https://www.schrodinger.com/desmond.

Figure legends

Fig. 1: Schematic domain structure (A), gelatin zymography (B) and real-time gelatin zymography (C) of recombinant proMMP-9 variants. A: At the top, the full-length proMMP-9 with its domains. Above is shown the numbering of the amino acids starting with the pre-domain which is cleaved off in the endoplasmatic reticulum, and the mature proenzyme starts at amino acid 20 and ends at amino acid 707. Shown is also the amino acids at the border of the FnII module, and at the boarder of the OG and the HPX domain based on Vandooren et al. 2013 [28]. The five deletion variants with their C-terminal amino acid are shown. In the fibronectin-deleted variants, it is also shown which amino acids were linked together after the FnII deletion. The different recombinant proMMP-9 (rpMMP-9) variants were produced in sf9 and High Five insect cells with a baculoviral transfection system as described in Materials and Methods. **B**: The purified variants were applied to gelatin zymography, and the rpMMP-9ΔFnII variant is from the pooled fractions from a Sepaharose S-200 column. Under these conditions, this variant contained mainly the monomeric variant. **C**: Real-time gelatin zymography of crude media of the three ΔFnII-deleted variants. Standards in (**B** and **C**) are; std-1 (a mixture of MMP-9 (homodimer / homotrimer-225 kDa; monomeric pro-92 kDa and active-83 kDa) from THP-1 cells and MMP-2 (pro-72 kDa; active-62kDa) from skin fibroblasts), std-2 (trypsin-24 kDa) and std-3 (catalytic domain of MMP-9 containing the FnII repeats-37 kDa).

Fig. 2: SDS-PAGE and Western blot analysis of recombinant proMMP-9 variants. After purification, the different recombinant proMMP-9 (rpMMP-9) variants shown in Fig 1 were analysed by SDS-PAGE (**A, B**) and Western blotting (**C**). To determine the purity, the molecular mass as well as the presence of monomers and homomultimers, reducing (R) and non-reducing (NR) conditions were used. As a control purified pMMP-9 (proMMP-9 from THP-1 cells) was used, which also contain small amounts of TIMP-1 (30 kDa) as seen in (**A**). Std-1 and Std-2 is the high range and broad range molecular weight standards from Thermo Scientific, respectively, with the molecular weights in kDa shown (**A, B**) and Std-3 in (**C**) is the biotinylated protein ladder. In (**C**), MMP-9ab and MMP-9HPXAb is polyclonal antibodies against the entire enzyme and the C-terminal HPX domain, respectively. In (**B, C**) recombinant proMMP-9ΔFnII is purified on either a Sephacryl- S-200 column (rpMMP-9ΔFnII (S-200)) or a Heparin-Sepharose column (rpMMP-9ΔFnII (HS)) as described in Materials and Methods. In (**C**), the crude media of two FnII-deletion variants (rpMMP-9ΔFnIIHPX and rpMMP-9ΔFnIIOGHPX) are used. In (**B**) the arrowhead shows the position of the rpMMP-9ΔFnII monomer. P1 and P2 are pooled non-reduced fractions from the S-200 column, both contained rpMMP-9ΔFnII based on gelatin zymography. The same gel cut and pasted for clarity is shown by a line under the gels.

Fig. 3: *In vitro* reconstitution of complexes between proMMP-9 and proMMP-9 deletion variants with CSPG/SG. Gelatin zymography (**A, B**) and Western blots (**C**) of proMMP-9 from THP-1 cells (pMMP-9), recombinant proMMP-9 (rpMMP-9), HPX-deleted proMMP-9 (rpMMP-9ΔHPX), FnII-deleted proMMP-9 (rpMMP-9ΔFnII) and trypsin activated proMMP-9 from THP-1 cells (aMMP-9) and their complexes with CSPG/SG. Presence (+) and absence (-) of respective enzyme variants, CSPG/SG and EDTA (10 mM). The *in vitro* reconstitutions were performed as described in Materials and Methods. The arrowheads indicate the border between the stacking and separating gel. Open arrows indicate the bottom of the application wells and standard (Std.) is a mixture of MMP-9 (homodimer 225 kDa; pro-92 kDa; active-83 kDa) from THP-1 cells and MMP-2 (pro-72 kDa; active-62kDa) from skin fibroblasts (**A**, **B**). In the Western blots (**C**) samples were run under either non reducing conditions (DTT_{sample}, -) or reducing conditions (DTT_{sample}, +). Under reducing conditions, the samples were incubated with 0.1 M DTT prior to electrophoresis. When samples were run under non reducing conditions, in order to detect the bound MMP-9 to CSPG/SG, prior to blotting, the gel was incubated for 1 h in 0.1 M DTT (DTT_{gel}, +) in contrast to samples run under reducing conditions, the gel was not incubated with DTT (DTT_{gel}, -). The biotinylated protein ladder was used as M_r marker in (**C**), lanes not shown. In (**A** and **B**) the same gel cut and pasted for clarity is shown by a line under the gels.

Fig. 4: ProMMP-9·Ht-SG complex formation. Fifty ng pMMP-9 and 200 ng Ht-SG was added to a polyvinyl membrane using a slot-blot apparatus as described in methods. Briefly, the membranes were thereafter washed in TBST, incubated in blocking buffer containing milk powder (BB) for 1 h. Membrane with added pMMP-9 and Ht-SG were cut out and membrane pieces containing bound pMMP-9 were incubated with either blocking buffer (BB), 5 ng/µl (0.29 µM) Ht-SG (in BB) or 0.29 µM Ht-SG containing 0.87 µM His-tagged peptide (Ht-P). Membrane pieces with bound Ht-SG were incubated with either BB or 50 ng/µl pMMP-9 (in BB) for 2.5 hours at room temperature. After 3 times wash in TBST the membrane pieces were incubated for 24 h at 4 ˚C with either antibodies against proMMP-9 (**A**), serglycin (**B**, **D**) or serglycin His-tag (Ht Ab) (**C**). The various membranes were thereafter washed in TBST, incubated with HRP-conjugated secondary antibody, washed in TBST and antibody detection by the Luminol reagent and the Fujifilm LAS-400 system.

Fig. 5: Binding of proMMP-9 variants to SG peptide arrays. A: Primary structure of SG. **B**: Ponceau staining of the 20-mer peptides bound on a cellulose membrane, where each peptide was obtained from a peptide walk along the entire SG sequence with an interval of two amino acids. For simplicity, every fifth peptide in the array are numbered and the arrows shows the starting and ending of peptides containing the GAG binding amino acids SerGly

(amino acids 67-84) in the centre of the core protein, and underlined is the two peptides that contain the entire 8 Ser-Gly repeats. **C**: Binding of proMMP-9 purified from THP-1 cells (pMMP-9) to peptides in the SG core protein. **D**: Binding of full-length recombinant proMMP-9 (rpMMP-9) to peptides in the serglycin core protein. **E**: Binding of recombinant HPX truncated proMMP-9 (rpMMP-9ΔHPX) to peptides in the SG core protein. **F**: Binding of pMMP-9 to a SG peptide arrays containing mutated amino acids based on the interpretation of the binding to peptides observed in figs. 5C and D. Two different arrays were performed where either (1) a combination of the predicted four possible amino acids from the binding pattern obtained in figs. 5C and D were mutated or (2) where every amino acid in the peptide were mutated as described in the Materials and Methods section. Shown above each array is: (1) the number of the peptide in figs. 5C and D that is used for the mutation screen, and (2), the name and number of the parent amino acid mutated. Shown is also the position of N- and the C-terminal amino acid of the 20-mer peptides. The un-mutated control peptide is labeled with Cont.

Fig. 6: Binding of SG to MMP-9 FnII module peptide arrays. A: Primary structure of the FnII module. **B**: Ponceau staining of the 20-mer peptides bound on a cellulose membrane, where each peptide was obtained from a peptide walk along the entire MMP-9 FnII sequence with an interval of two amino acids. For simplicity, every fifth peptide in the array is numbered. **C**: Binding of recombinant Ht-SG to peptides in the FnII module. **D**: Binding of recombinant Ht-SG to FnII peptide arrays containing mutated amino acids based on the binding obtained in fig. 6C. Two different arrays were performed where either (1) a combination of the predicted four possible amino acids from the binding pattern obtained in Fig. 6C were mutated, or (2) where every amino acid in the peptide were mutated as described in the Materials and Methods section. Shown above each array is: (1) the number of the peptide in Fig. 6C that is used for the mutation screen, and (2), the name and number of the parent amino acid mutated. Shown is also the position of N- and the C-terminal amino acid of the 20-mer peptides. The un-mutated control peptide is labeled with Cont.

Fig. 7: Binding of SG to MMP-9 HPX peptide arrays. A: Primary structure of the HPX domain. **B**: Ponceau staining of the 20-mer peptides bound on a cellulose membrane, where each peptide was obtained from a peptide walk along the entire MMP-9 HPX sequence with an interval of two amino acids. For simplicity, every fifth peptide in the array is numbered. **C**: Binding of recombinant Ht-SG to peptides in the HPX domain. **D**: Binding of recombinant

Ht-SG to HPX peptide arrays containing mutated amino acids based on the binding obtained in fig. 7C. Two different arrays were performed where either (1) a combination of the predicted four possible amino acids from the binding pattern obtained in fig. 7C were mutated, or (2) where every amino acid in the peptide were mutated as described in the Materials and Methods section. Shown above each array is: (1) the number of the peptide in fig. 7C that is used for the mutation screen, and (2), the name and number of the parent amino acid mutated. Shown is also the position of N- and the C-terminal amino acid of the 20-mer peptides. The un-mutated control peptide is labeled with Cont.

Fig. 8: Predicted structure of the SG core protein. The prediction was based on the primary structure of the SG core protein using the Phyre[2] program as described in Materials and Methods. The N-terminal amino acids from 1-66 are labeled yellow, the amino acid stretch from 67-83 which contains the Ser-Gly repeats that binds the CS chains are labeled in light blue and the C-terminal stretch from amino acid 84 to 131 are labeled in orange. Shown is the eight serine residues that are the putative CS-chain attachment sites with nitrogen in blue, carbon in grey, oxygens in red and oxygen-bound hydrogen in white. The N-terminal tyrosine and the C-terminal leucine is also shown.

Fig. 9: SG docked to the FnII module in the catalytic domain of proMMP-9. The SG core protein was docked into the FnII module of proMMP-9 using the Maestro program as described in Materials and Methods. The pro and catalytic domain in MMP-9 is labelled in light green and the hemopexin module in dark green. The SG core protein is labelled as in Fig. 8 and the carbon atoms in the CS chains are coloured in grey.

Fig. 10: SG docked to the MMP-9-HPX domain, model 1: The SG core protein was docked into the MMP-9-HPX domain using the Maestro program as described in Materials and Methods. The HPX domain is labelled in light green and the SG core protein with attached CS-chains is labelled as in Figs. 8 and 9.

Fig. 11: SG docked to the MMP-9-HPX domain, model 2: The SG core protein was docked into the MMP-9-HPX domain using the Maestro program as described in Materials and Methods. The HPX domain is labelled in light green and the SG core protein with attached CS-chains is labelled as in Figs. 8 and 9.

A: Domain structure

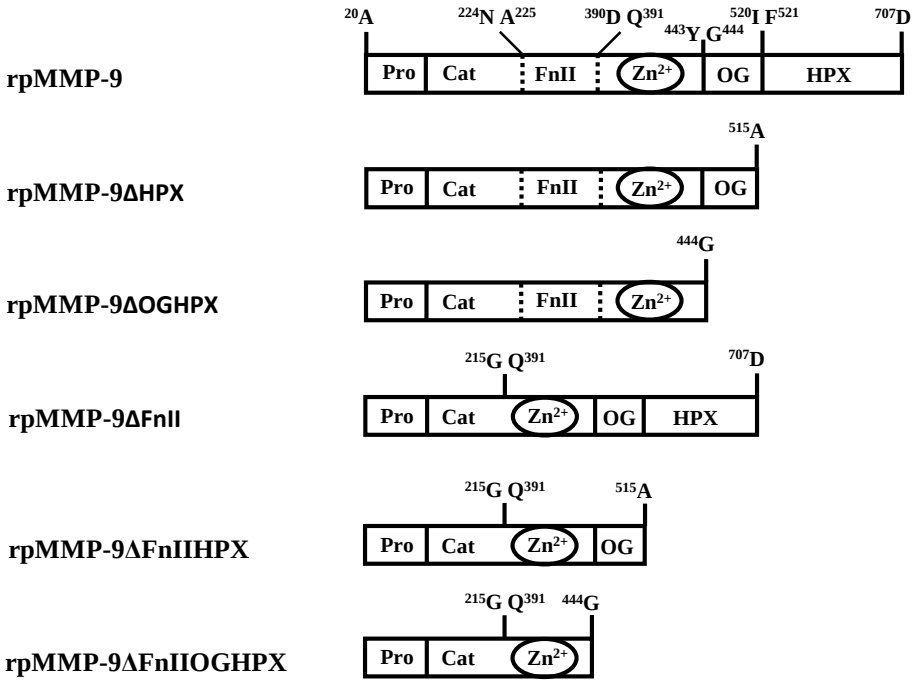

B: Gelatin zymography

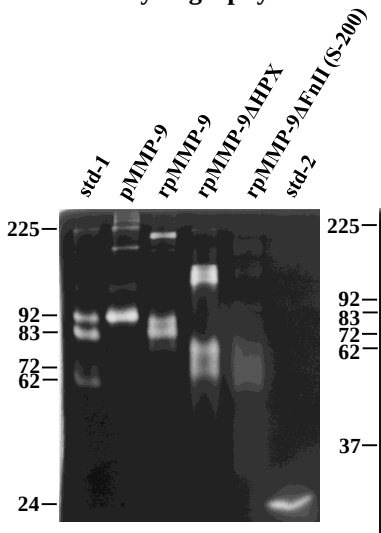

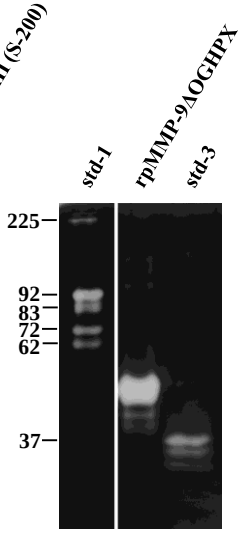

C: Real-time Gelatin zymography

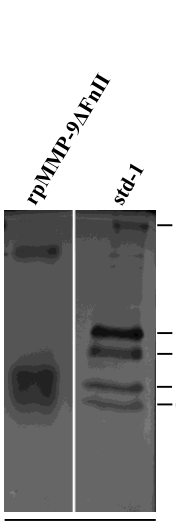

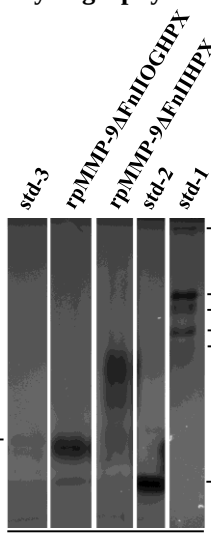

Fig. 2

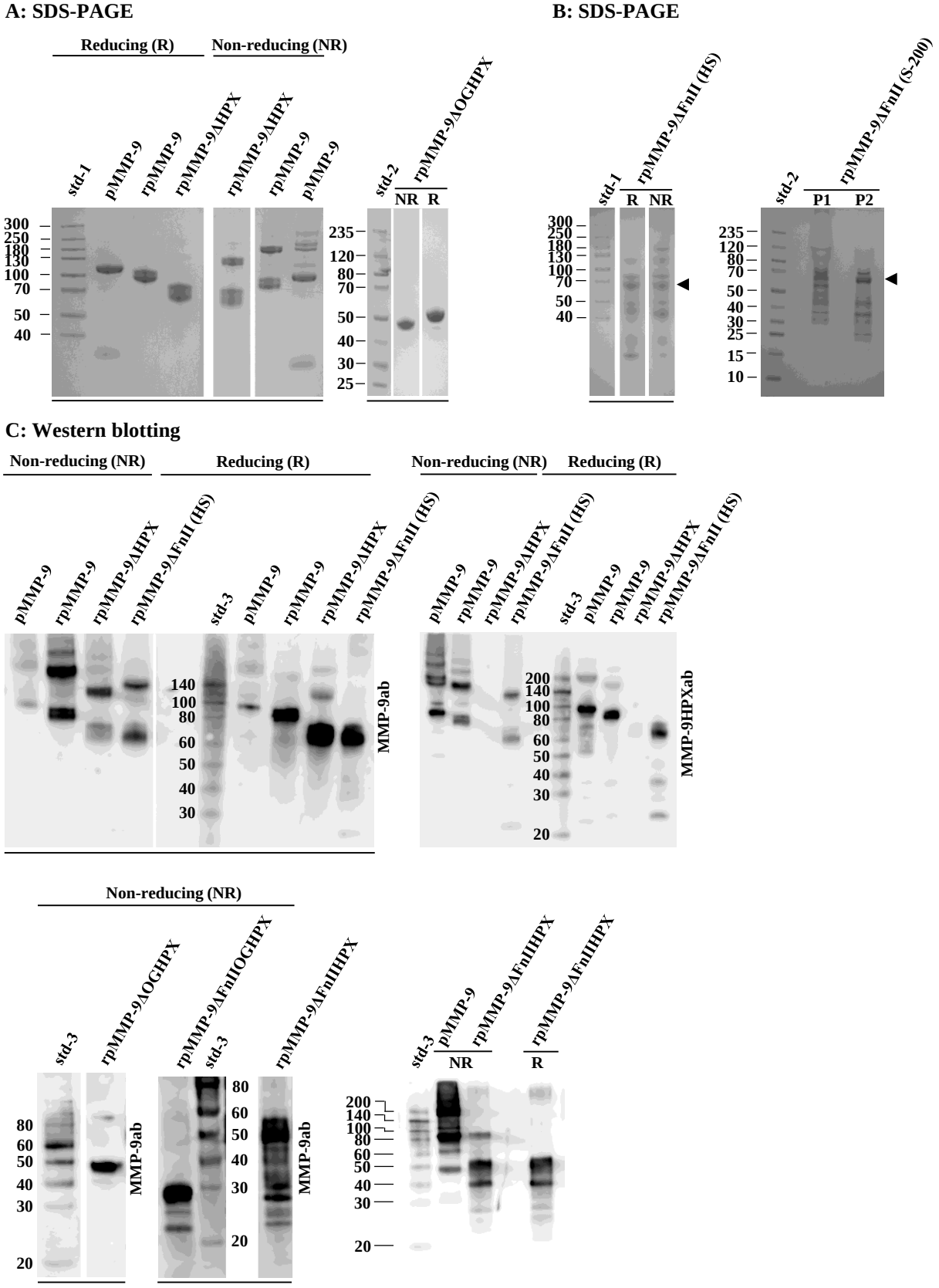
A: SDS-PAGE
Reducing (R)
Non-reducing (NR)
std-1
pMMP-9
rpMMP-9
rpMMP-9ΔHPX
rpMMP-9ΔHPX
rpMMP-9
pMMP-9
std-2
rpMMP-9ΔOGHPX
NR
R
B: SDS-PAGE
std-1
rpMMP-9ΔFnII (HS)
R
NR
std-2
rpMMP-9ΔFnII (S-200)
P1
P2
C: Western blotting
Non-reducing (NR)
Reducing (R)
pMMP-9
rpMMP-9
rpMMP-9ΔHPX
rpMMP-9ΔFnII (HS)
std-3
MMP-9ab
MMP-9HPXab
rpMMP-9ΔOGHPX
rpMMP-9ΔFnIIOGHPX
rpMMP-9ΔFnIIHPX

A: Gelatin zymography

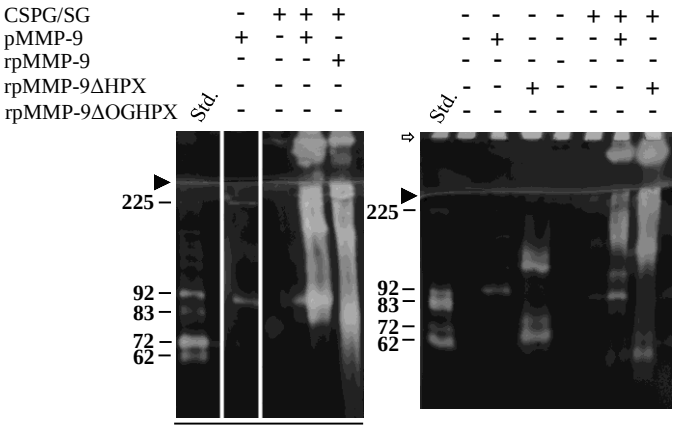

B: Gelatin zymography

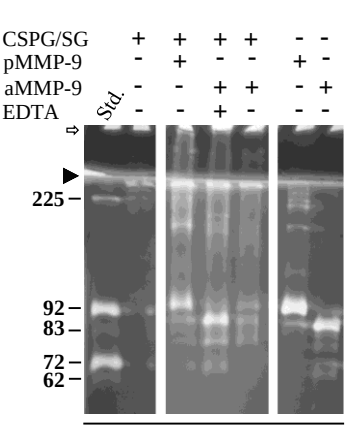

C: Western blotting

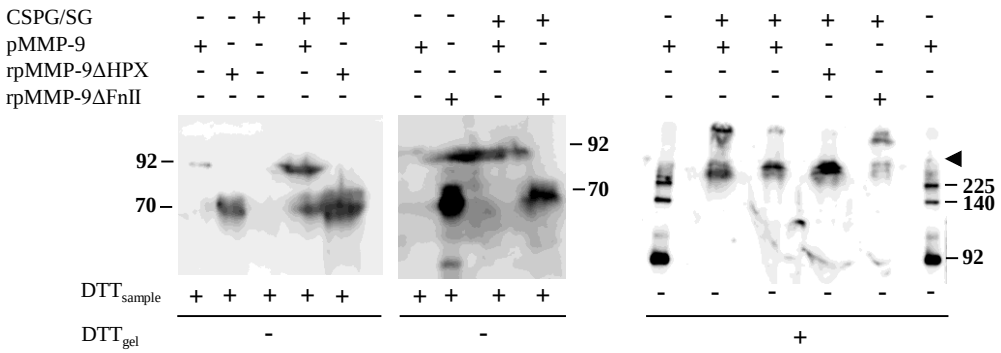

Fig. 4

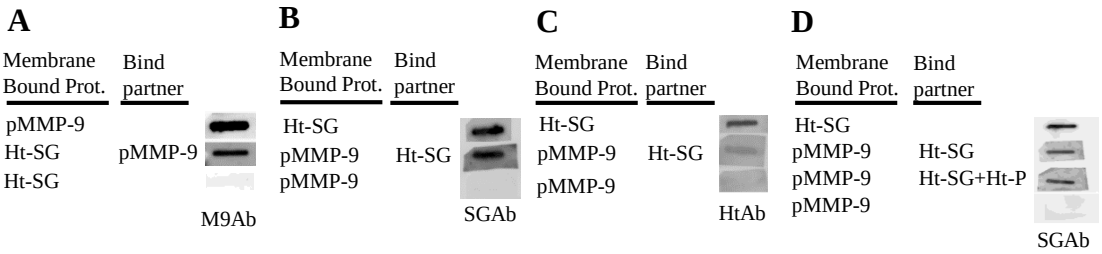
A
Membrane Bound Prot.
Bind partner
pMMP-9
Ht-SG
Ht-SG
pMMP-9
M9Ab
B
Membrane Bound Prot.
Bind partner
Ht-SG
pMMP-9
pMMP-9
Ht-SG
SGAb
C
Membrane Bound Prot.
Bind partner
Ht-SG
pMMP-9
pMMP-9
Ht-SG
HtAb
D
Membrane Bound Prot.
Bind partner
Ht-SG
pMMP-9
pMMP-9
pMMP-9
Ht-SG
Ht-SG+Ht-P
SGAb

A: Primary structure of serglycin

1 11 21
YPTRRARYQW VRCNPDSNSA NCLEEKGPMF
31 41 51
ELLPGESNKI PRLRTDLFPK TRIQDLNRIF
61 71 81
PLSEDYSGSG FGSGSGSGSG SGSGFLTEME
91 101 111
QDYQLVDESD AFHDNLRSLD RNLPSDSQDL
121
GQHGLEEDFML

B: Ponceau staining

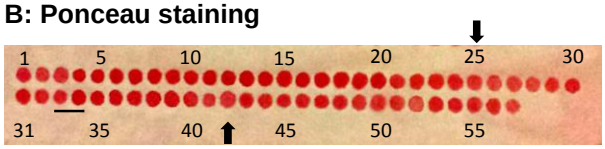

C: pMMP-9

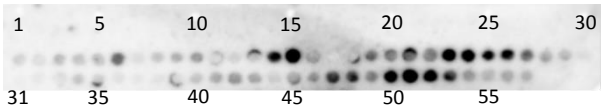

D: rpMMP-9

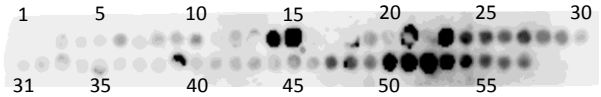

E: rpMMP-9ΔHPX

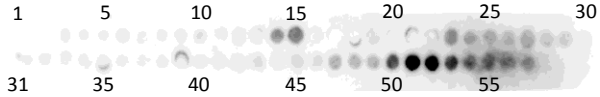

F: Serglycin mutation array

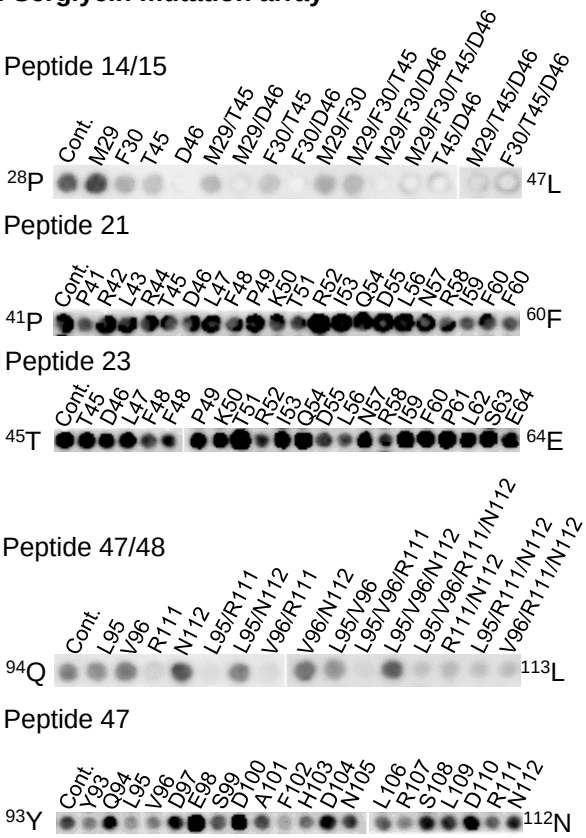

A: Primary structure of MMP-9 FnII

^{225}ADGAACHFPF^{235}IFEGRSYSAC^{245}TTDGRSDGLP
^{255}WCSTTANYDT^{265}DDRFGFCPSE^{275}RLYTQDGNAD
^{285}GKPCQFPFIF^{295}QGQSYSACTT^{305}DGRSDGYR WC
^{315}ATTANYDRDK^{325}LFGFCPTRAD^{335}STVMGGNSAG
^{345}ELCVFPFTFL^{355}GKEYSTCTSE^{365}GRGDGRLWCA
^{375}TTSNFDSDKK^{385}WGFCPD

B: Ponceau staining

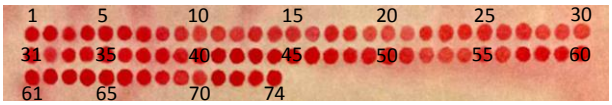

C: Serglycin

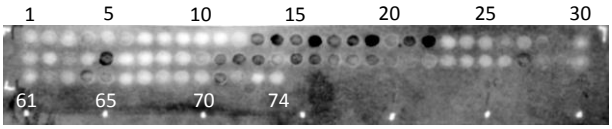

D: MMP-9 FnII mutation array

Peptide 14

Peptide 16

Peptide 19

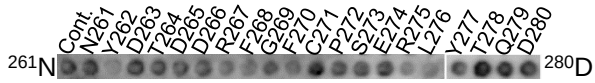

Peptide 22

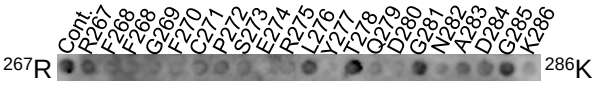

Peptide 35

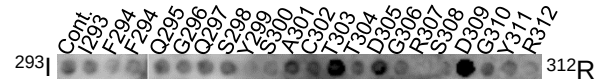

Peptide 64/65

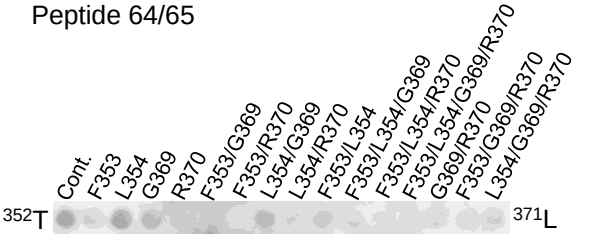

A: Primary structure of MMP-9 HPX

521 531 541
FDAIAEIGNQ LYLFKDGKYW RFSEGRGSRP
551 561 571
QGPFLIADKW PALPRKLDSV FEERLSKKLF
581 591 601
FFSGRQVWVY TGASVLGPRR LDKLGLGADV
611 621 631
AQVTGALRSG RGKMLLFSGR RLWRFDVKAQ
641 651 661
MVDPRSASEV DRMFPGVPLD THDVFQYREK
671 681 691
AYFCQDRFYW RVSSRSELNQ VDQVGYVTYD
701
ILQCPED

B: Ponceau staining

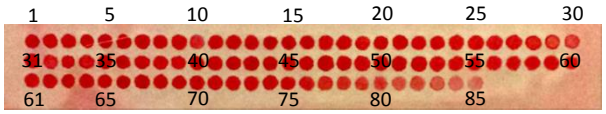

C: Serglycin

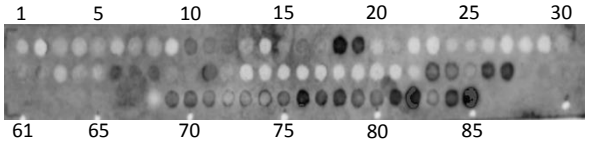

D: MMP-9 HPX mutation array

Peptide 11

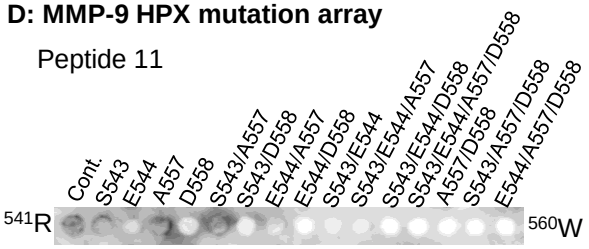

Peptide 18/19

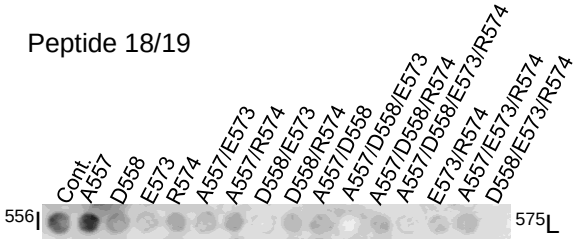

Peptide 37

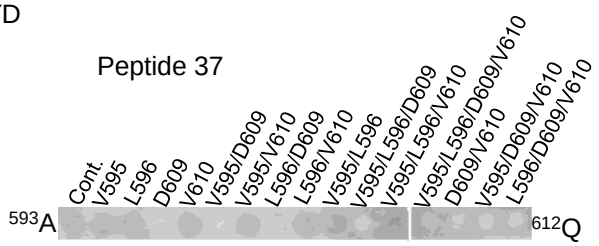

Peptide 41

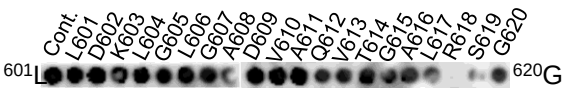

Peptide 56

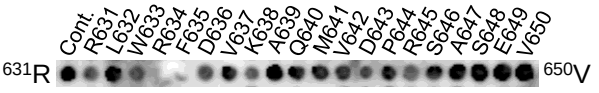

Peptide 69

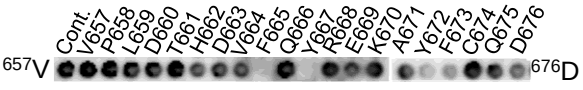

Peptide 76

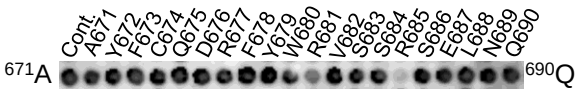

Peptide 85

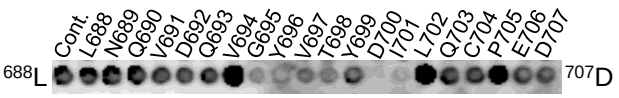

Fig. 8

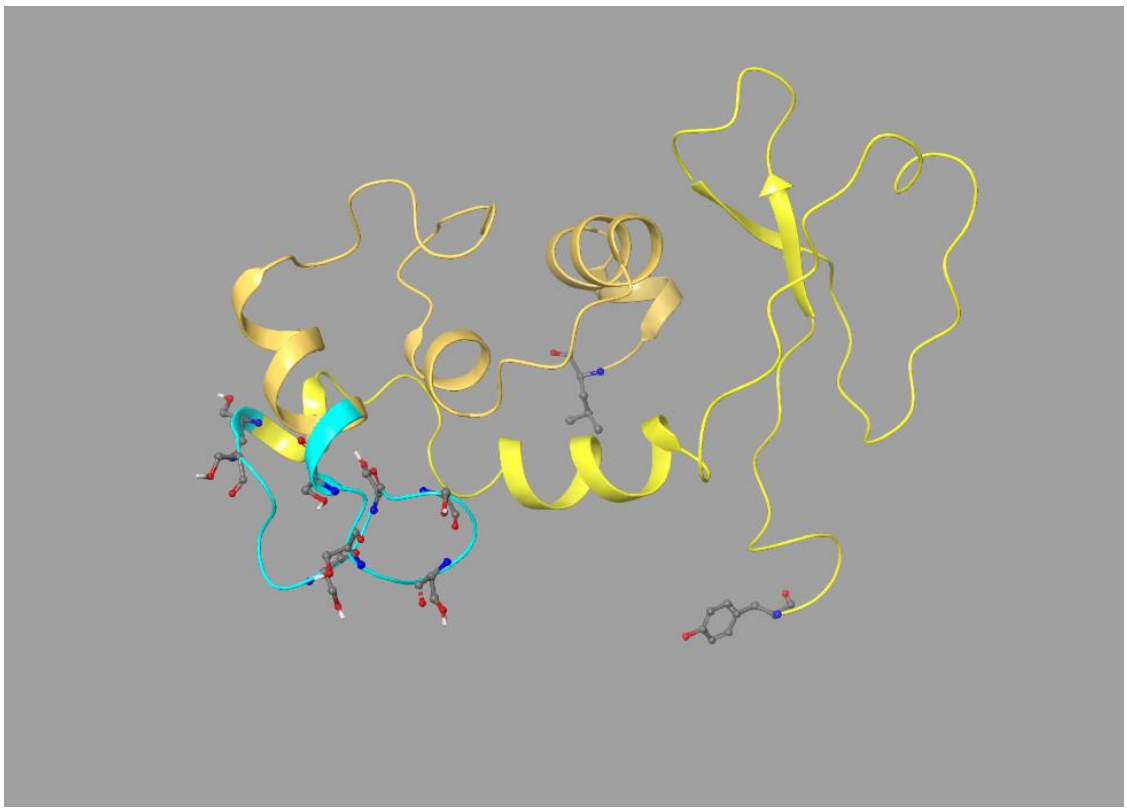

Fig. 9

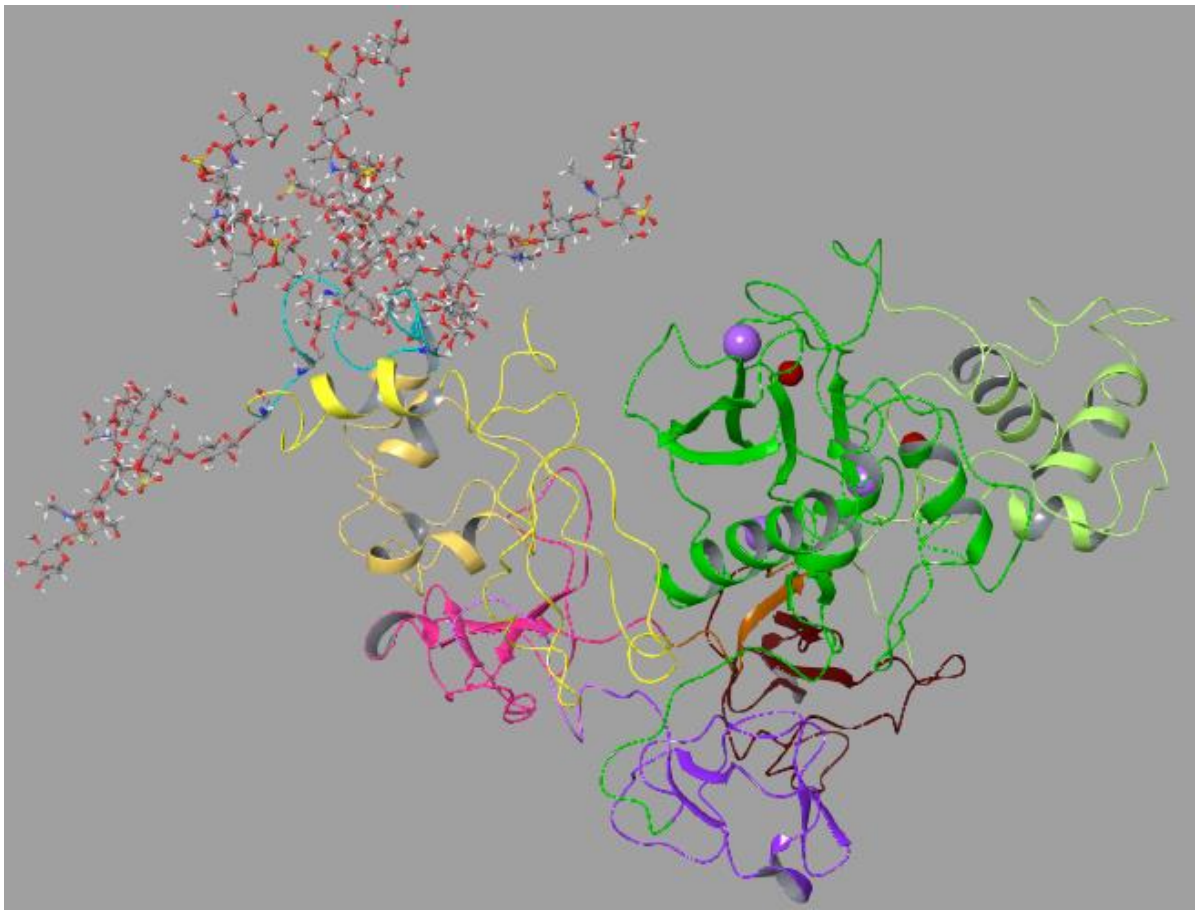

Fig. 10

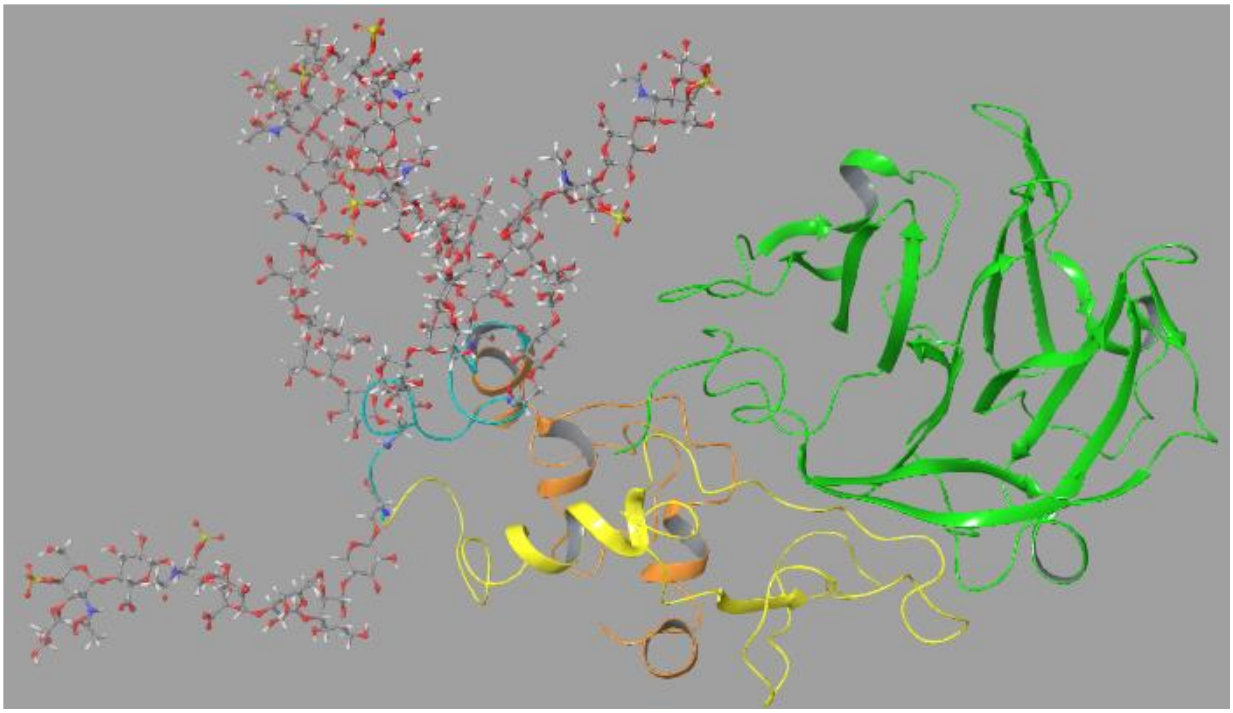

Fig. 11

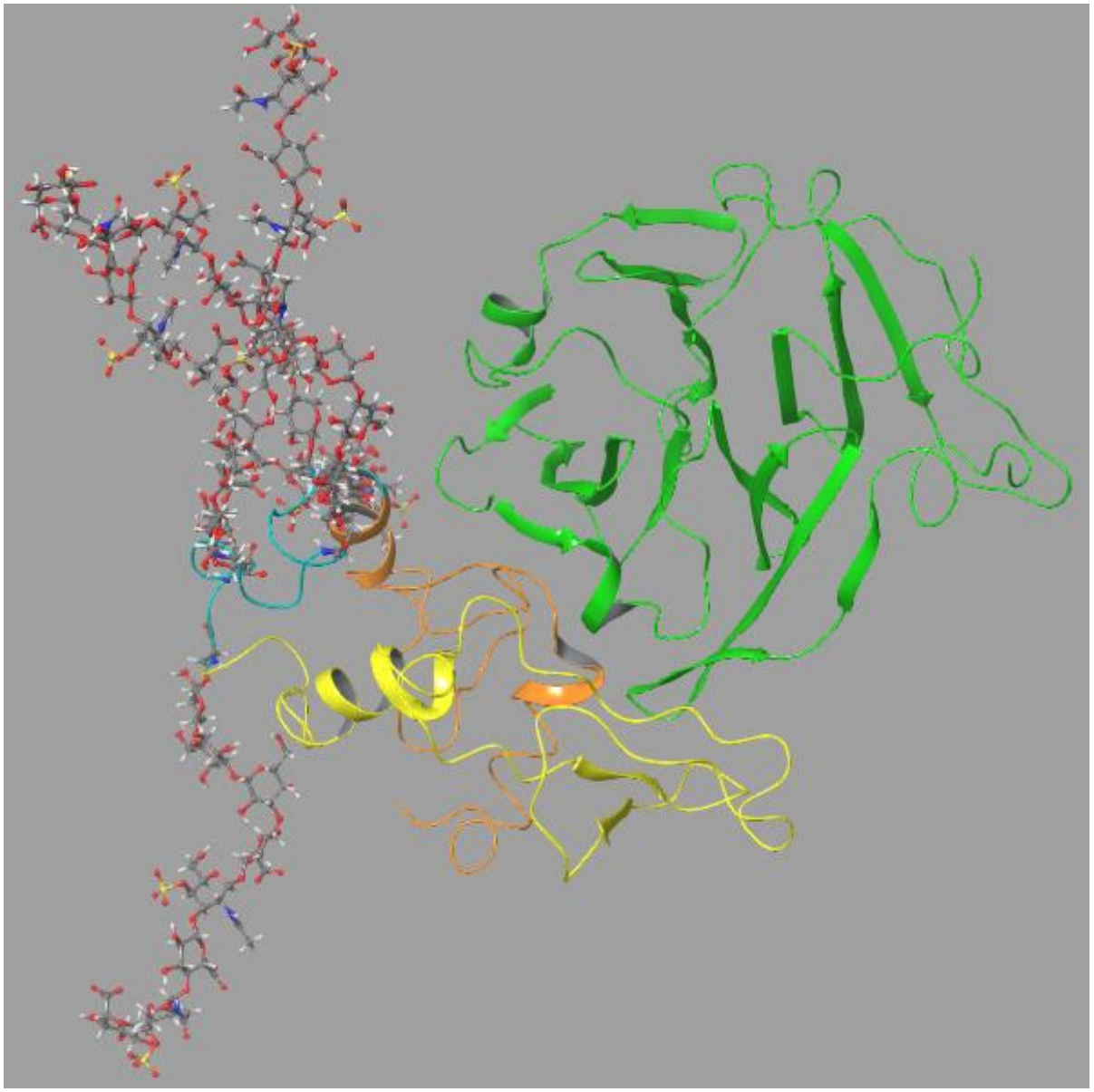

Table 1: A**mino acid interactions between FnII and SG.** Amino acid interactions between FnII and SG based on molecular modelling (docking/dynamic simulation) and the peptide arrays.

FnII				SG				Bond type[g]
Dock & Dyn Sim[a]	Peptide arrays			Dock & Dyn Sim[a]	Peptide arrays			
Amino acid	Spots contain Aa[b]	Spots bound to SG[c]	Repeat number[d]	Amino acid	Spots contain Aa[b]	Spots bound to pMMP-9[e]	N- or C-Terminal[f]	
G227(m)	1-2	-	1	N38(s)	10-19	14-15	N	Hb
D280(s)	19-28	19-22	1-2	R42(s)	12-21	14-15, 21	N	I
N282(s)	20-29	20-22	1-2	L120(s)	51-57	51-54	C	Hp
F294(s)	26-35	35	2	V96(s)	39-48	47-48	C	Hp
Q295 (s)	27-36	35	2	V96(s)	39-48	47-48	C	Hp
G306(m)	32-41	35, 41	2	V96(m) E98(m)	39-49 40-48	47-48 47-48	C C	Hb Hb
R307(s)	33-42	35,41-42	2	S99(s)	41-50	47-48	C	Hb
S308(s)(m)	33-42	35,41-42	2	E98(s)	40-49	47-48	C	Hb
W313(s)	36-45	41-43, 45	2	S99(s)	41-50	47-48	C	Hb
Y320(s)	39-48	41-43, 45-48	2	V96(s)	39-48	47-48	C	Hp
K324(s)	41-50	41-43, 45-49	2	F102(m)	42-51	47-48	C	Hb
F326(s)	42-51	41-43, 45-49	2	S99(s) D100(s) A101(Cα)	41-50 41-50 42-51	47-48 47-48 47-48	C C C	Hp Hp Hp
F328(s)	43-52	41-43, 45-49	2	S99(s) L120(s)	41-50 51-57	47-48 51-54	C C	Hp Hp

[a] Amino acids based on the time series obtained from simulation event analysis conducted on the dynamic simulation trajectory of the best docked model of FnII with SG.
[b] Amino acids belonging to the peptide spot in the peptide array of FnII and SG.
[c] Peptide spots where the amino acids in FnII are represented after incubating the peptide arrays with SG.
[d] To which FnII repeat the amino acid belongs.
[e] Peptide spots where the amino acids in SG are represented after incubating the peptide arrays with proMMP-9.
[f] The core protein of SG contains a Ser-Gly repeat zone from S67 to G84. The N-terminal represents the region before S67 and C-terminal represents the region after G84.
[g] The interaction type seen between the amino acid pairs between FnII and SG where, I is Ionic interaction, Hb is Hydrogen bond and Hp is Hydrophobic interaction.
(m): Represents the main-chain of the amino acid that is involved in the binding with another amino acid.
(s): Represents the side-chain of the amino acid that is involved in the binding with another amino acid.
(Cα): Represents the Cα-atom of the amino acid that is involved in the binding with another amino acid.
- : Spots with no intensity, which could be due to no binding or too low signal/staining.

Table 2: **Amino acid interactions between HPX and SG as seen in model 1.** Amino acid interactions between HPX and SG based on molecular modelling (docking/dynamic simulation) and the peptide arrays.

HPX				SG				Bond type[g]
Dock & Dyn Sim[a]	Peptide arrays			Dock & Dyn Sim[a]	Peptide arrays			
Amino acids	Spots contain Aa[b]	Spots bound to SG[c]	Blade number[d]	Amino acids	Spots contain Aa[b]	Spots bound to pMMP-9[e]	N- or C-Terminal[f]	
L659(s)[1](m)[2] L659(s)	61-70	69-70	3	L32(s)[1](m)[2] P34(s)	7-16 8-17	14,15 14,15	N N	Hp[1], Hb[2] Hp
D660(s)[1](m)[2] D660(s) D660(s)	61-70	69-70	3-4	L32(s)[1](m)[2] L33(m) S37(s)(m)	7-16 8-17 10-19	14,15 14,15 14,15	N N N	Hp[1], Hb[2] Hb Hb
Q675(s)	69-78	69-71, 76-78	4	L32(s)	7-16	14,15	N	Hp
D676(s)	69-78	69-71, 76-78	4	K39(s) P41(s) L43(s)	11-20 12-21 13-22	14,15 14,15,21 14,15,21	N N N	I Hp Hp
R677(s)	70-79	69-71, 76-78	4	L43(s)	13-22	14,15,21	N	Hp
W680(s)	71-80	69-71, 76-78	4	L32(s)	7-16	14,15	N	Hp
V691(s)	77-85	76-85	4	M29(s)	6-15	14,15	N	Hp
G695(Cα)	79-85	76-85	4	M29(s)	6-15	14,15	N	Hp
Y696(s)[1,2] Y696(s)	79-85	76-85	4	P28(s)[1](m)[2] L43(s)	5-14 13-22	14 14,15,21	N N	Hp[1], Hb[2] Hp
T698(s)	80-85	76-85	4	L43(s)	13-22	14,15,21	N	Hp
Y699(s) Y699(s)[1,2]	81-85	76-85	4	D46(m) L47(s)[1](m)[2]	14-23 15-24	14,15,21,23 15,21,23,24	N N	Hb Hp[1],Hb[2]
D707(s)	85	76-85	4	L47(s)	15-24	14,15, 21,23-26	N	Hp

[a] Amino acids based on the time series obtained from simulation event analysis conducted on the dynamic simulation trajectory of one of the two best docked models of HPX with SG.

[b] Amino acids belonging to the peptide spot in the peptide array of HPX and SG.

[c] Peptide spots where the amino acids in HPX are represented after incubating the peptide arrays with SG.

[d] To which HPX blade the amino acid belong to.

[e] Peptide spots where the amino acids in SG are represented after incubating the peptide arrays with proMMP-9.

[f] The core protein of SG contains a Ser-Gly repeat zone from S67 to G84. The N-terminal represents the region before S67 and C-terminal represents the region after G84.

[g] The interaction type seen between the amino acid pairs between HPX and SG where, I is Ionic interaction, Hb is Hydrogen bond and Hp is Hydrophobic interaction.

(m): Represents the main-chain of the amino acid that is involved in binding with another amino acid. The numbering ([1,2]) beside (m) correlates with the type of chain and type of interaction on the binding amino acid in the table.

(s): Represents the side-chain of the amino acid that is involved in the binding with another amino acid. The numbering ([1,2]) beside (s) correlates with the type of chain and type of interaction on the binding amino acid in the table.

(Cα): Represents the Cα-atom of the amino acid that is involved in the binding with another amino acid.

Table 3: A**mino acid interactions between HPX and SG as seen in model 2.** Amino acid interactions between HPX and SG based on molecular modelling (docking/dynamic simulation) and the peptide arrays.

HPX				SG				Bond type[g]
Dock & Dyn sym[a]	Peptide arrays			Dock & Dyn sym	Peptide arrays			
Amino acids	Spots contain Aa[b]	Spots bound to SG[c]	Blade number[d]	Amino acids	Spots contain Aa[b]	Spots bound to pMMP-9[e]	N- or C-Terminal[f]	
K623(s)	43-52	-	3	D97(s) E98(s)	40-49 40-49	47,48 47,48	C C	I I
R634(s)	48-57	53-54, 56-57	3	E98(s)	40-49	47,48	C	I
R645(s)	54-63	54, 56-57	3	E98 (s)	40-49	47,48	C	I
S646(s)	54-63	54, 56-57	3	L113(s) P114(s)	48-57 48-57	47,48,50-54 47,48,50-54	C C	Hp Hp
A647(s)	55-64	56-57	3	L113(s)	48-57	47,48, 50-54	C	Hp
S648(s)[1,2]	57-66	57	3	P114(s)[1] (m)[2]	48-57	47,48, 50-54	C	Hp[1] Hb[2]
D651(s)[1](m)[2]	57-66	57	3	L43(s)[1] (m)[2]	13-22	14,15, 21	N	Hp[1] Hb[2]
R652(s)[1](m)[2] R652(s)[1](m)[2]	57-66	57	3	S115(s)[1,2] Q118(s)[1,2]	49-57 50-57	50-54 50-54	C C	Hp[1],Hb[2] Hp[1],Hb[2]
M653(s)	58-67	-	3	P114(s) D116(s)	48-57 49-57	48,50-54 50-54	C C	Hp Hp
E687(s)	75-84	75-84	4	L120(s) S117(s)	49-57 50-57	50-54 50-54	C C	Hp Hp
L688(s)	75-85	75-85	4	S117(s) R42(s)	50-57 12-21	50-54 14-15,21	C N	Hp Hp
Q690(s)	76-85	76-85	4	I40(s)	11-20	14-15	N	Hp
V691(s)	77-85	77-85	4	I40(s)	11-20	14-15	N	Hp

[a] Amino acids based on the time series obtained from simulation event analysis conducted on the dynamic simulation trajectory of the best docked model of HPX with SG.

[b] Amino acids belonging to the peptide spot in the peptide array of HPX and SG.

[c] Peptide spots where the amino acids in HPX are represented after incubating the peptide arrays with SG.

[d] To which HPX blade the amino acid belong to.

[e] Peptide spots where the amino acids in SG are represented after incubating the peptide arrays with proMMP-9.

[f] The core protein of SG contains a Ser-Gly repeat zone from S67 to G84. The N-terminal represents the region before S67 and C-terminal represents the region after G84.

[g] The interaction type seen between the amino acid pairs between HPX and SG where, I is Ionic interaction, Hb is Hydrogen bond and Hp is Hydrophobic interaction.

(m): Represents the main-chain of the amino acid that is involved in binding with another amino acid. The numbering ([1,2]) beside (m) correlates with the type of chain and type of bond on the binding amino acid in the table.

(s): Represents the side-chain of the amino acid that is involved in the binding with another amino acid. The numbering ([1,2]) beside (s) correlates with the type of chain and type of bond on the binding amino acid in the table.

- : Spots with no intensity, which could be due to no binding or not enough staining.

Supplements

Motifs and amino acids involved in the formation of complexes between pro-matrix metalloproteinase-9 and the proteoglycan serglycin core protein

Rangita Dawadi, Nabin Malla, Beate Hegge, Imin Wushur, Eli Berg, Gunbjørg Svineng, Ingebrigt Sylte and Jan-Olof Winberg

Department of Medical Biology, Faculty of Health Sciences, UiT-The Arctic University of Norway, 9037 Tromsø, Norway.

Supplement 1

Molecular Dynamics Simulation of HPX dimer and docked HPX dimer

Molecular dynamic simulations of the HPX dimer from X-ray crystallography and the best pose from the docking of the HPX_B to the HPX_A were performed in order to compare the results and thereby evaluate the accuracy of the theoretical predictions. The ionic interaction between ^{707}D in HPX_A and ^{677}R in HPX_B was initially approximately 3 Å in both the X-ray and the docked complex (Fig. S6.2). The distance plot shows that this distance increased to around 7 Å in the X-ray structure at approximately 20 ns, while in the docked complex it increased to around 13 Å. ^{677}R in HPX_B also formed an ionic bond with ^{706}D in HPX_A. In the X-ray dimer the distance was initially around 3Å, but after 80 ns the distance gradually increased. In the docked complex this interaction was initially at around 8 Å, and after 20 ns the distance increased to approximately 12 Å. A hydrophobic cluster of ^{699}Y, ^{696}Y and ^{694}V in HPX_A and ^{696}Y, ^{678}F and ^{694}V in HPX_B showed high similarity between the X-ray and docked HPX dimer as seen in Figs. S6.3 and S6.4. The distance between ^{696}Y in HPX_A and ^{678}F in HPX_B seemed stable with dynamic movements around 6 Å in both the X-ray and docked dimer (Fig. S6.3). Similar distances were obtained between ^{699}Y in HPX_A and ^{678}F in HPX_B in both dimer complexes (Fig. S6.3). Stable dynamic movements around 6 Å during the entire 100 ns were seen for the X-ray, while the distance increased to around 9 Å during the first 30 ns and then remained at that distance for the MD of the docked dimer. The distance between the OH groups in the side chains of ^{699}Y in HPX_A and ^{696}Y in HPX_B were initially around 2 Å in the X-ray dimer and around 3 Å in the docked dimer (Fig. S6.4). The dynamic movements around these distances were stable for the first 15 ns, thereafter the distance increased to around 6 Å in the HPX X-ray dimer and to around 8 Å in the docked complex. The hydrogen bond between the side chain ^{696}Y in HPX_A and the main chain nitrogen of ^{696}Y in HPX_B showed an almost similar dynamic behavior for both HPX dimer complexes (Fig. S6.4). Another stable hydrophobic interaction was between ^{694}V in both subunits (Fig. S6.5). The distance during MD was slightly shorter in the X-ray dimer than in the docked complex. For both, the distance between the central methylene-group of the side chains was stable, at a distance of around 5 Å in the X-ray dimer and around 8Å in the docked complex. ^{651}D is located in the end of the third blade of the HPX_A and forms an interaction with ^{685}R in the HPX_B in both complexes (Fig. S6.6). This seems to be a flexible region and the distance was

quite long during MD for both the X-ray dimer and the docked complex. In the X-ray dimer, both ^{660}D and ^{651}D in HPX_A interacted with ^{685}R in HPX_B at approximately similar distances in the beginning of the MD simulations (Fig. S6.6). After approximately 30 ns the distance was reduced to approximately 5 Å and remained stable at this distance. In the docked complex the distance between ^{660}D (HPX_A) and ^{685}R (HPX_B) was shorter than between ^{651}D (HPX_A) and ^{685}R (HPX_B) (Fig. S6.6).

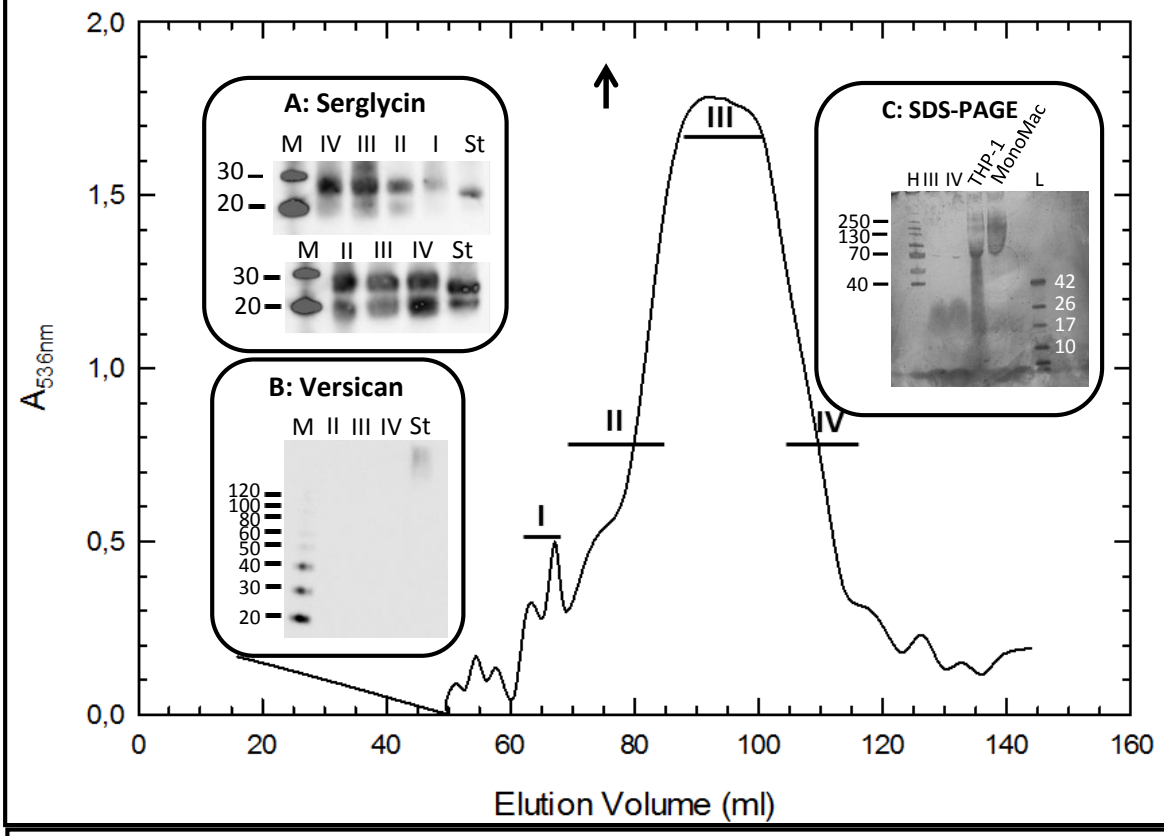

Fig. S1. Elution profile of Q-Sepaharose purified CSPG from THP-1 cells using a Sephacryl S-400 column. On the Y-axis is the absorbance at 536 nm (Safranin-O staining) and on the X-axis is the elution volume in ml. The peak of eluted proteoglycans was divided into four pools: I (fractions: 62-67 ml), II (fractions: 69-85 ml), III (fractions: 88-101 ml) and IV (fractions: 104-117 ml). These pooled fractions were further treated as described in the method section. Chondroitinase ABC treated material from each fraction was subjected to SDS-PAGE for characterization. Inserts (A-C) show gels that were either subjected to Western blotting using antibodies against serglycin (A) and versican (B) or silver stained (C). CSPG loaded per lanes were 3 µg (A), 30 µg (B) and 88.5 µg (C). In (C), Q-Sepharose purified CSPG from THP-1 cells and MonoMac cells (88.5 µg) were used as controls. Standards used in the inserts are as follows: M=Magic Marker, St= serglycin (A) and versican (B) obtained from Dr. A. Theocharis (University of Patras, Greece), H=high range ladder, L=Low range ladder, arrow = void volume (V_0) at 75ml (based on the elution of Blue Dextran). The molecular sizes of magic marker and the high and low range ladders are shown in kDa.

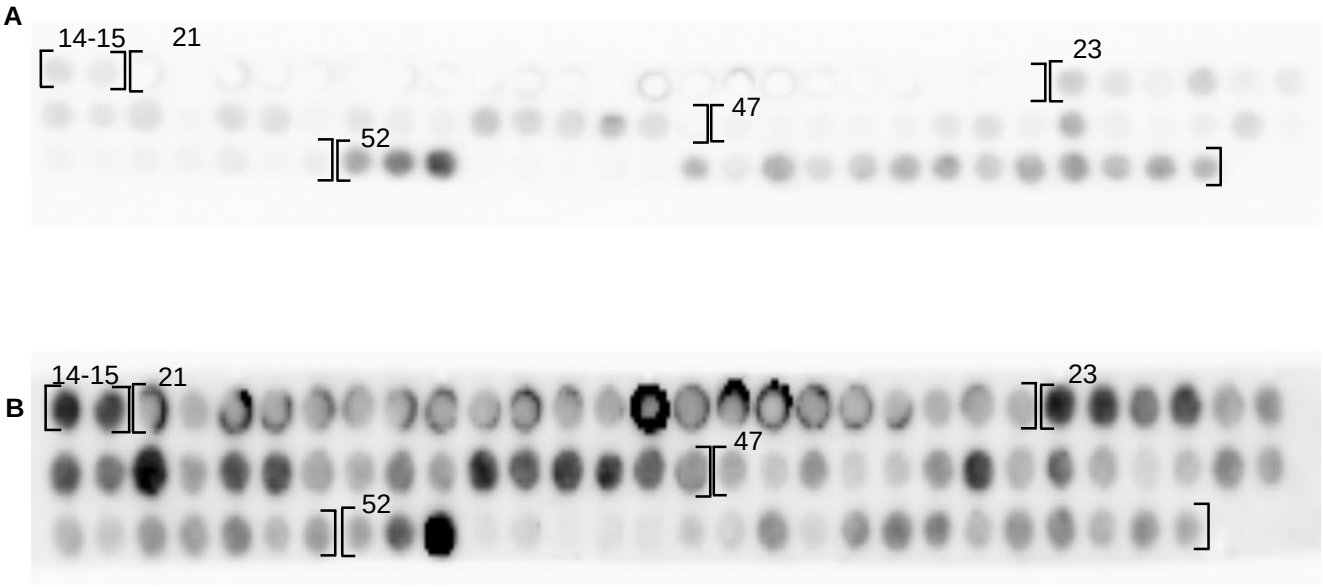

Fig. S2: Binding of pMMP-9 to a mutated SG peptide array. (A) Binding of primary MMP-9ab to a mutated SG peptide array (control of unspecific Ab binding) followed by the addition of the secondary Ab as described in Materials and Methods. **(B)** Binding of pMMP-9 to the mutated SG peptide array followed by MMP-9 Ab and secondary antibody as described in Materials and Methods. Shown is also the number of the parent peptide mutated (see Fig. 5).

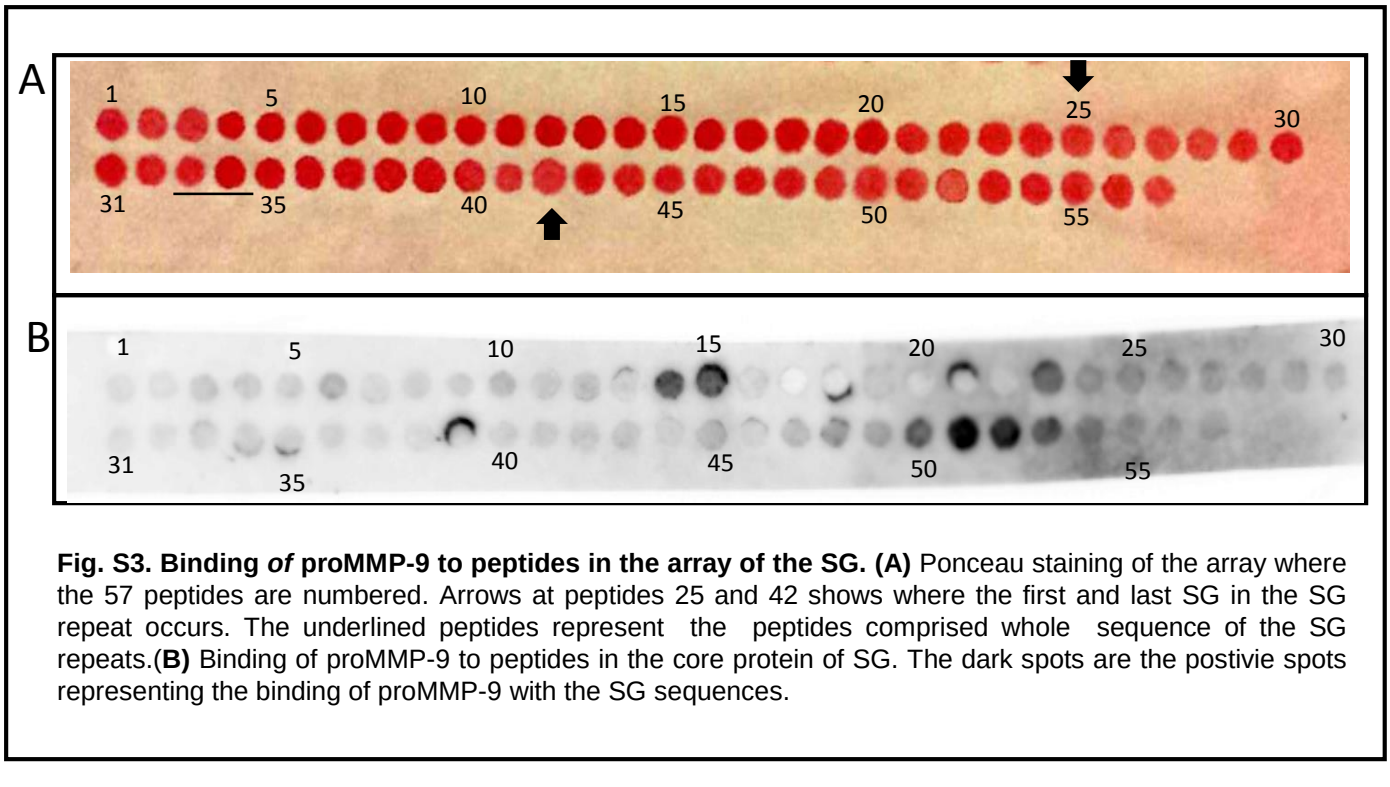

Fig. S3. Binding *of* proMMP-9 to peptides in the array of the SG. (A) Ponceau staining of the array where the 57 peptides are numbered. Arrows at peptides 25 and 42 shows where the first and last SG in the SG repeat occurs. The underlined peptides represent the peptides comprised whole sequence of the SG repeats.(**B)** Binding of proMMP-9 to peptides in the core protein of SG. The dark spots are the postivie spots representing the binding of proMMP-9 with the SG sequences.

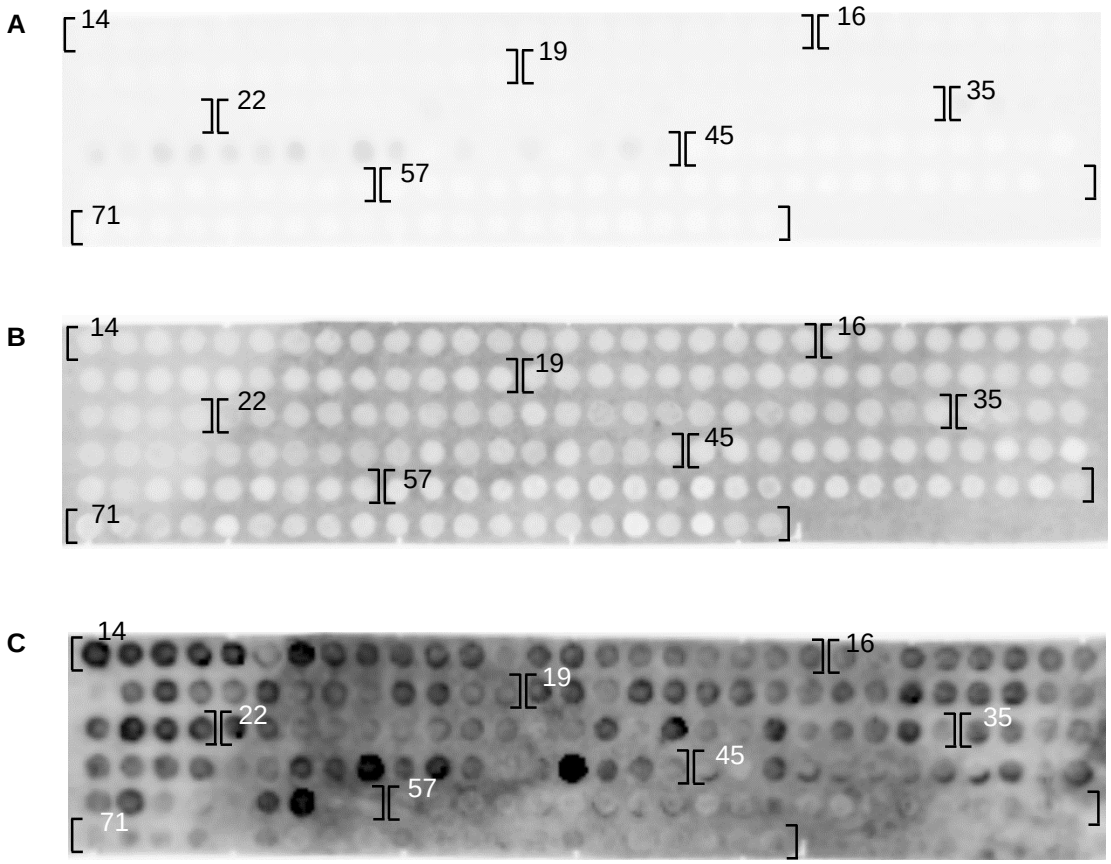

Fig. S4: Binding of Ht-SG to a mutated FnII peptide array. (A) Binding of secondary antibody to the mutated FnII peptide array (control of unspecific Ab binding), **(B)** binding of primary SG antibody to the mutated FnII peptide array (control of unspecific Ab binding) followed by the addition of the secondary Ab as described in Materials and Methods. **(C)** Binding of Ht-SG to the mutated FnII peptide array followed by primary SG antibody and secondary antibody as described in Materials and Methods. Shown is also the number of the parent peptide mutated (see Fig. 6).

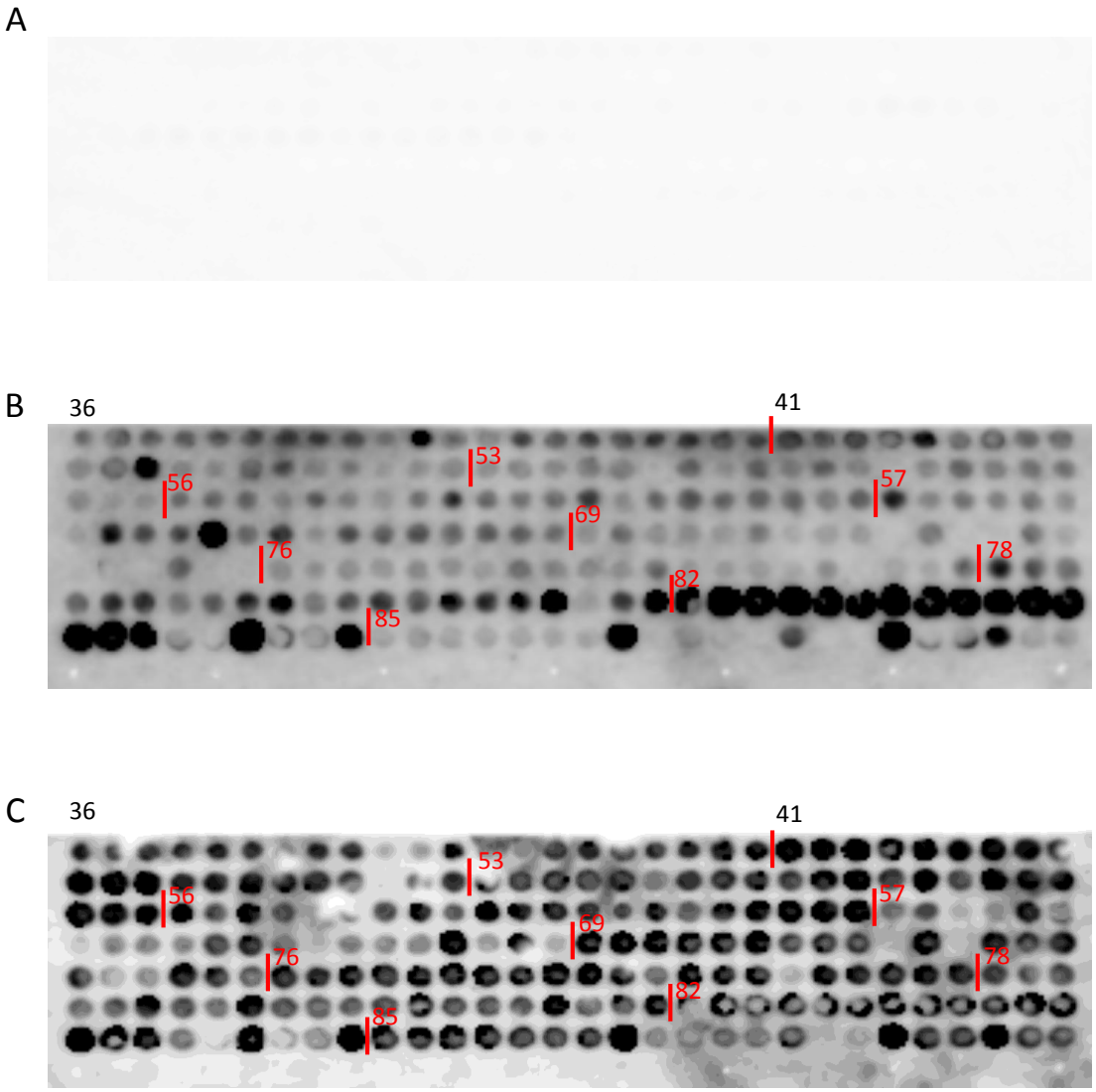

Fig. S5: Binding of Ht-SG to a mutated HPX peptide array. (A) Binding of secondary antibody to the mutated HPX peptide array (control of unspecific Ab binding), **(B)** binding of primary SG antibody to the mutated HPX peptide array (control of unspecific Ab binding) followed by the addition of the secondary Ab as described in Materials and Methods. **(C)** Binding of Ht-SG to the mutated HPX peptide array followed by primary SG antibody and secondary antibody as described in Materials and Methods. Shown is also the number of the parent peptide mutated (see Fig. 7).

Fig. S6: X-ray structure of the HPX dimer (pdb. 1itv), docking of HPX_B to HPX_A and MD simulations of both complexes.

The docked dimer is overlapped with the X-ray dimer where chain A is the fixed receptor. Molecular dynamic simulations were conducted with both complexes.

Fig. S6.1: Overview of all the amino acid side chains interacting with each other between the two subunits of HPX, in both X-ray HPX dimer and the best docked model of the dimer. The fixed chain HPX_A (green), X-ray HPX_B (blue), docked HPX_B (orange), amino acid carbons in HPX_A (green), X-ray HPX_B (blue), docked HPX_B (orange) , hydrogens (white), oxygens (red) and nitrogens (dark blue).

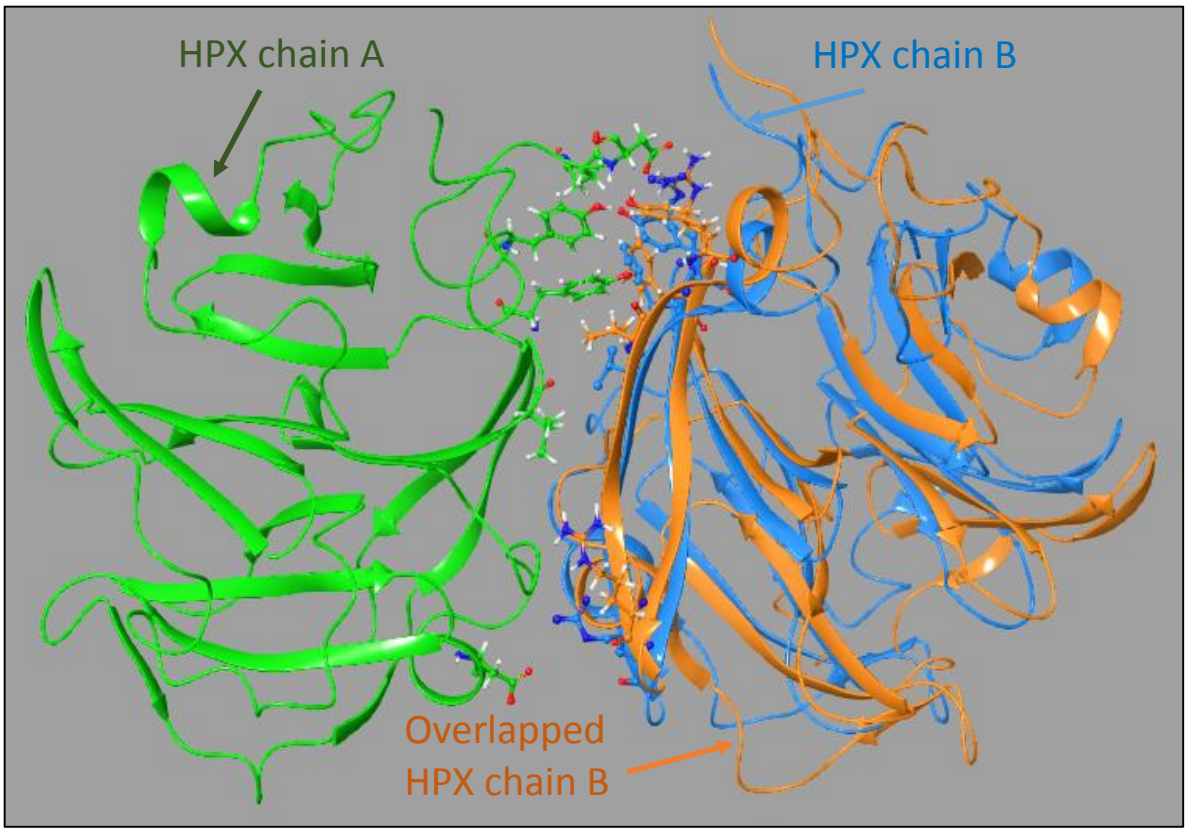

S6.2 A: Ionic interaction between E706 and D707 in chain A with the R677 in chain B, in both X-ray and best docked model of HPX dimer. Backbone chain A (dark green), chain B X-ray (blue) and docked chain B (orange). Carbons in X-ray chain A (light green), docked chain A (grey), X-ray chain B (light blue) and docked chain B (orange). Oxygens (red), nitrogens (dark blue) and hydrogens (white).

S6.2 B: The 100 ns trajectory of the interactions between the side chain oxygens in E706 and D707 with the side chain nitrogens in R677

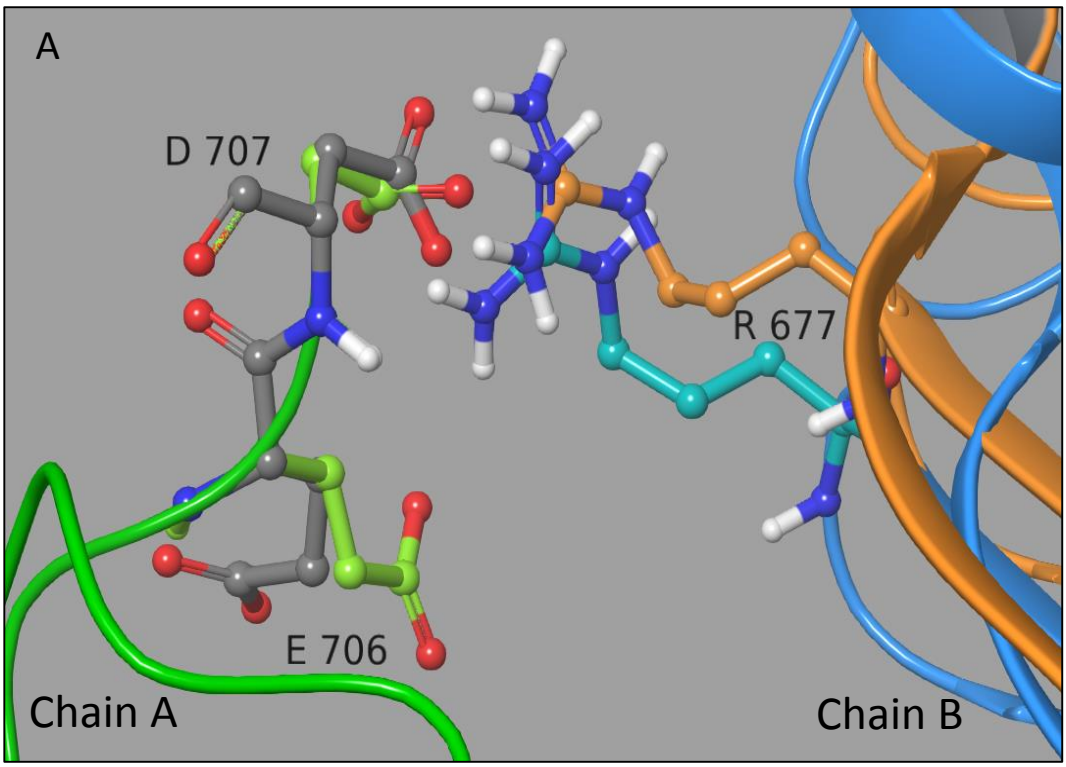

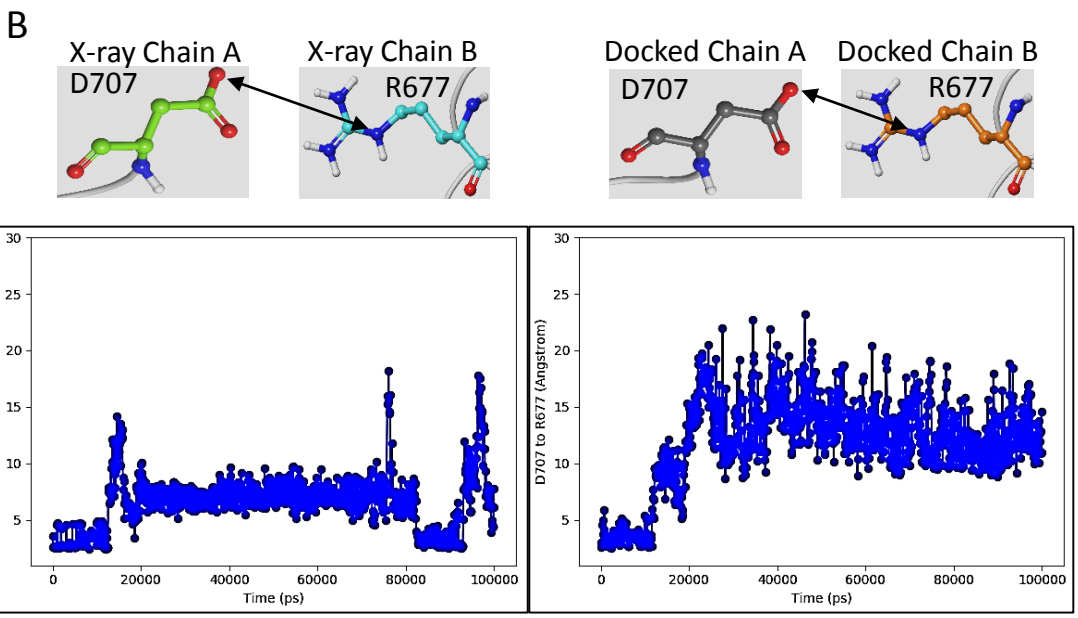

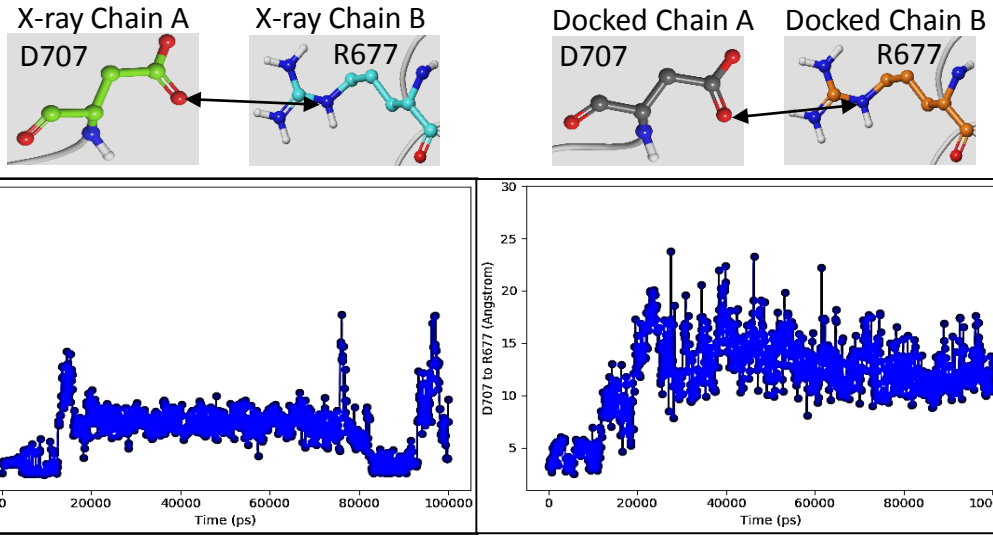
X-ray Chain A
D707
X-ray Chain B
R677
Docked Chain A
D707
Docked Chain B
R677
D707 to R677 (Angstrom)
Time (ps)
D707 to R677 (Angstrom)
Time (ps)

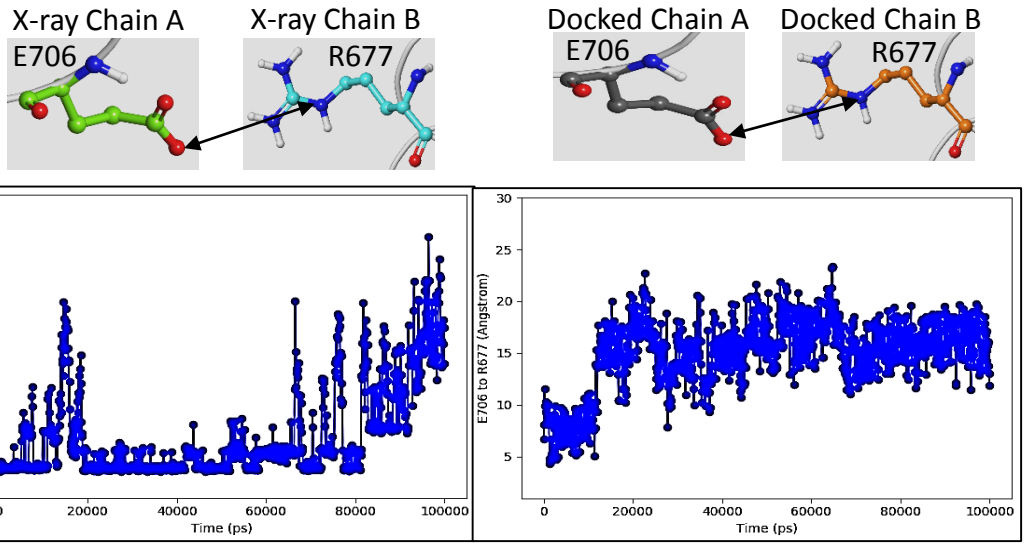
X-ray Chain A
E706
X-ray Chain B
R677
Docked Chain A
E706
Docked Chain B
R677
E706 to R677 (Angstrom)
Time (ps)
E706 to R677 (Angstrom)
Time (ps)

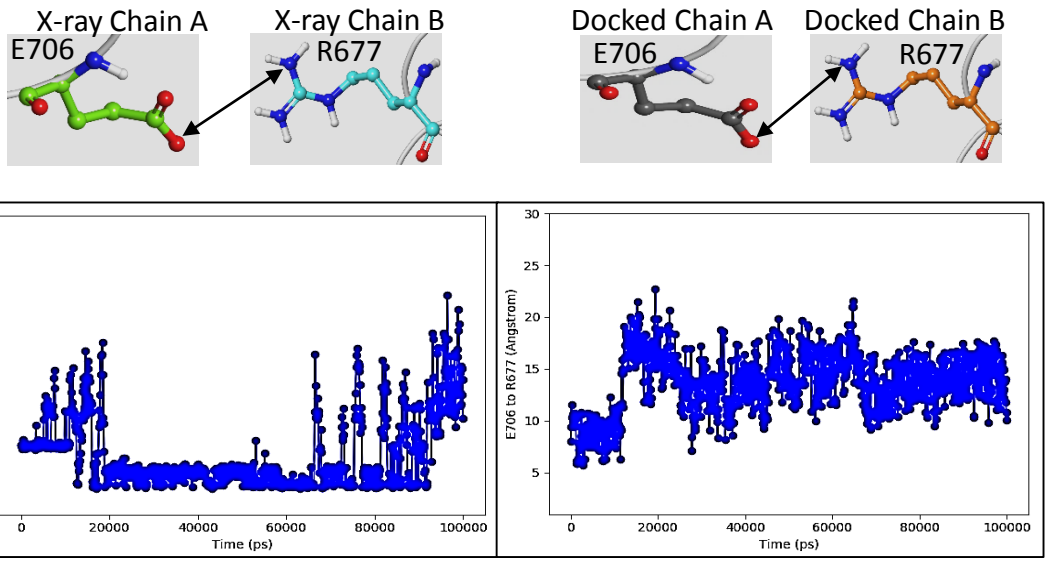
X-ray Chain A
E706
X-ray Chain B
R677
Docked Chain A
E706
Docked Chain B
R677
E706 to R677 (Angstrom)
Time (ps)
E706 to R677 (Angstrom)
Time (ps)

S6.3 A: Hydrophobic interactions between sidechains of Y696 and Y699 in chain A with the side chain of F678 in the chain B, in both X-ray and best docked model of HPX dimer. Backbone chain A (dark green), chain B X-ray (blue) and docked chain B (orange). Carbons in X-ray chain A (light green), docked chain A (grey), X-ray chain B (light blue) and docked chain B (orange). Oxygens (red), nitrogens (dark blue) and hydrogens (white).

S6.3 B: The 100 ns trajectory of the interactions of the side chain methylene in Y696 and Y699 with side chain of F678.

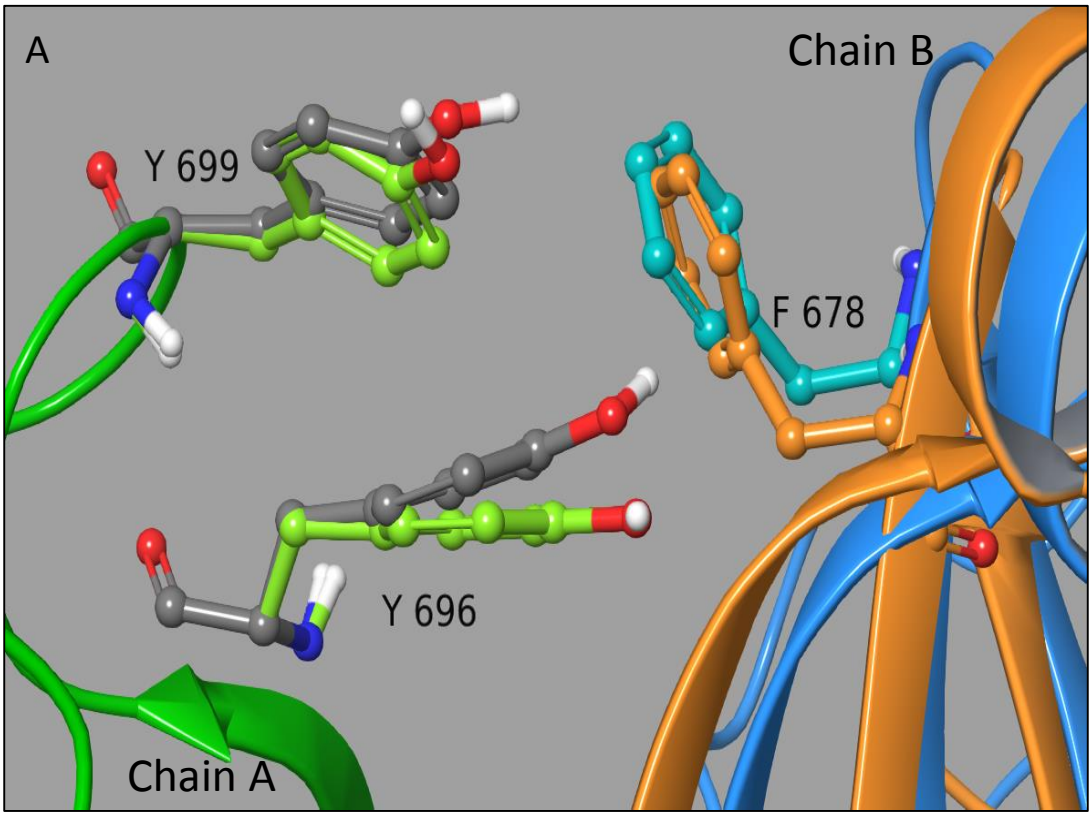

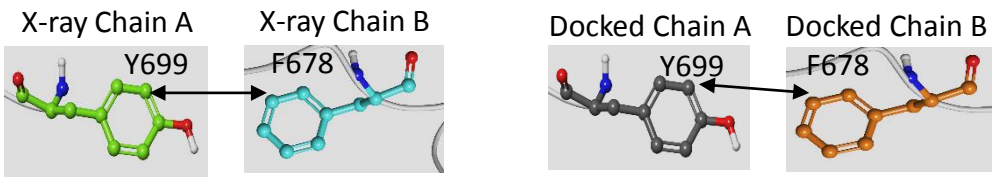

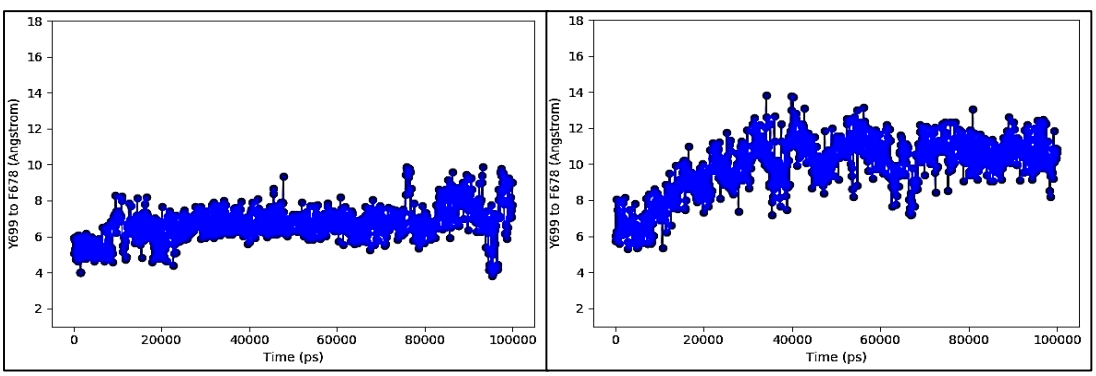

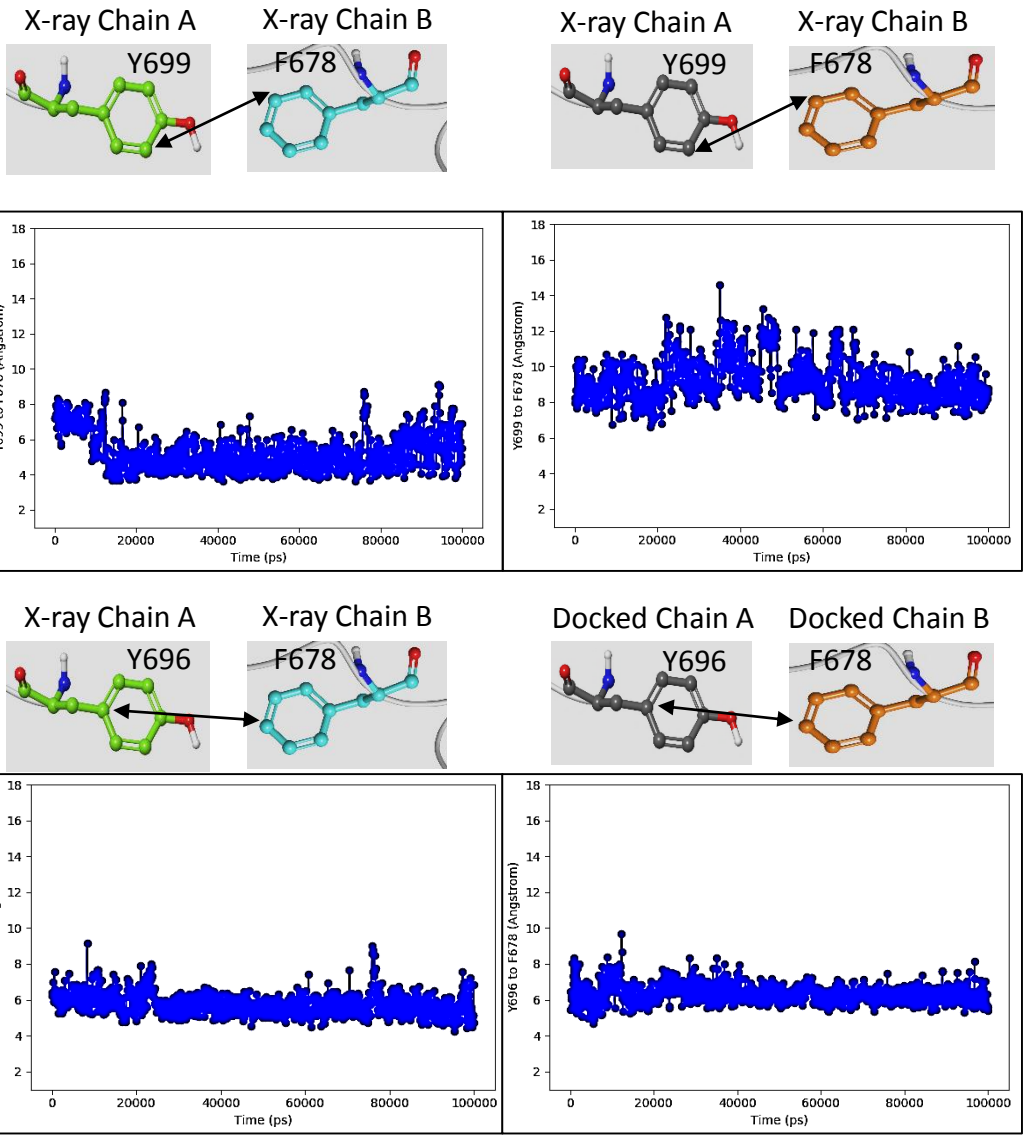
X-ray Chain A
X-ray Chain B
Y699
F678
X-ray Chain A
X-ray Chain B
Y699
F678
Y699 to F678 (Angstrom)
Time (ps)
Y699 to F678 (Angstrom)
Time (ps)
X-ray Chain A
X-ray Chain B
Y696
F678
Docked Chain A
Docked Chain B
Y696
F678
Y696 to F678 (Angstrom)
Time (ps)
Y696 to F678 (Angstrom)
Time (ps)

S6.4 A: Hydrogen bond between sidechains of Y696 and Y699 in chain A with the side chain of Y696 in the chain B, in both X-ray and best docked model of HPX dimer. Backbone chain A (dark green), chain B X-ray (blue) and docked chain B (orange). Carbons in X-ray chain A (light green), docked chain A (grey), X-ray chain B (light blue) and docked chain B (orange). Oxygens (red), nitrogens (dark blue) and hydrogens (white).

S6.4 B: The 100 ns trajectory of the interactions of the side chains in Y696 and Y699 with side chain of Y696.

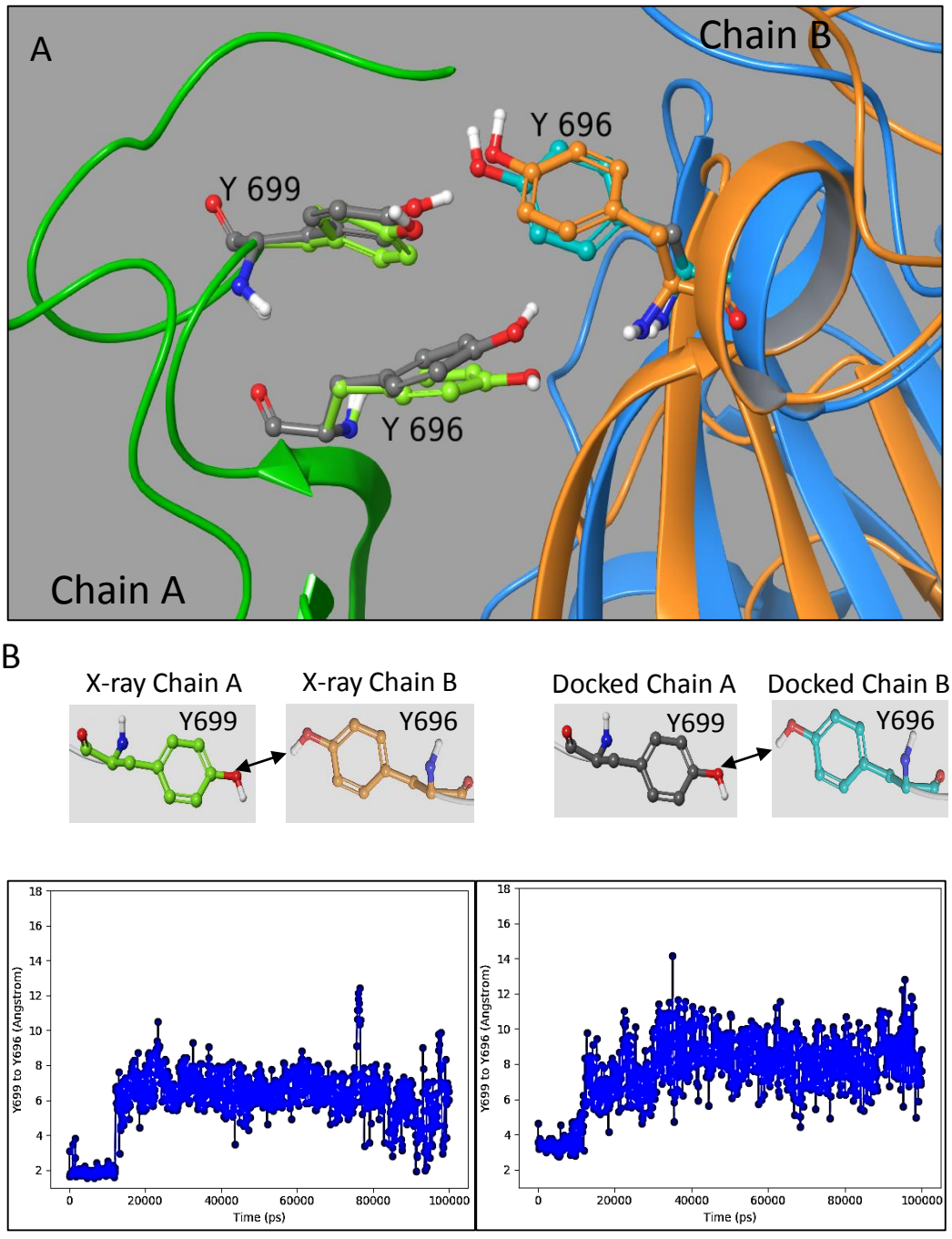

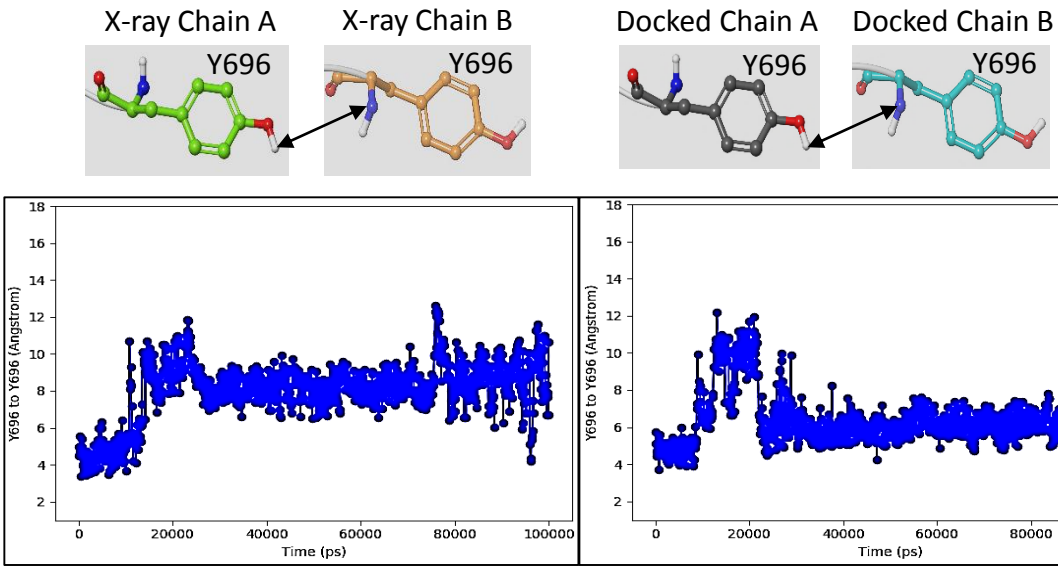
X-ray Chain A
X-ray Chain B
Docked Chain A
Docked Chain B
Y696
Y696
Y696
Y696
Y696 to Y696 (Angstrom)
Time (ps)
Y696 to Y696 (Angstrom)
Time (ps)

S6.5 A: Hydrophobic interactions between sidechain of V694 in chain A with the side chain of V694 in the chain B, in both X-ray and best docked model of HPX dimer. Backbone chain A (dark green), chain B X-ray (blue) and docked chain B (orange). Carbons in X-ray chain A (light green), docked chain A (grey), X-ray chain B (light blue) and docked chain B (orange). Oxygens (red), nitrogens (dark blue) and hydrogens (white).

S6.5 B: The 100 ns trajectory of the interactions of the side chains of both V694.

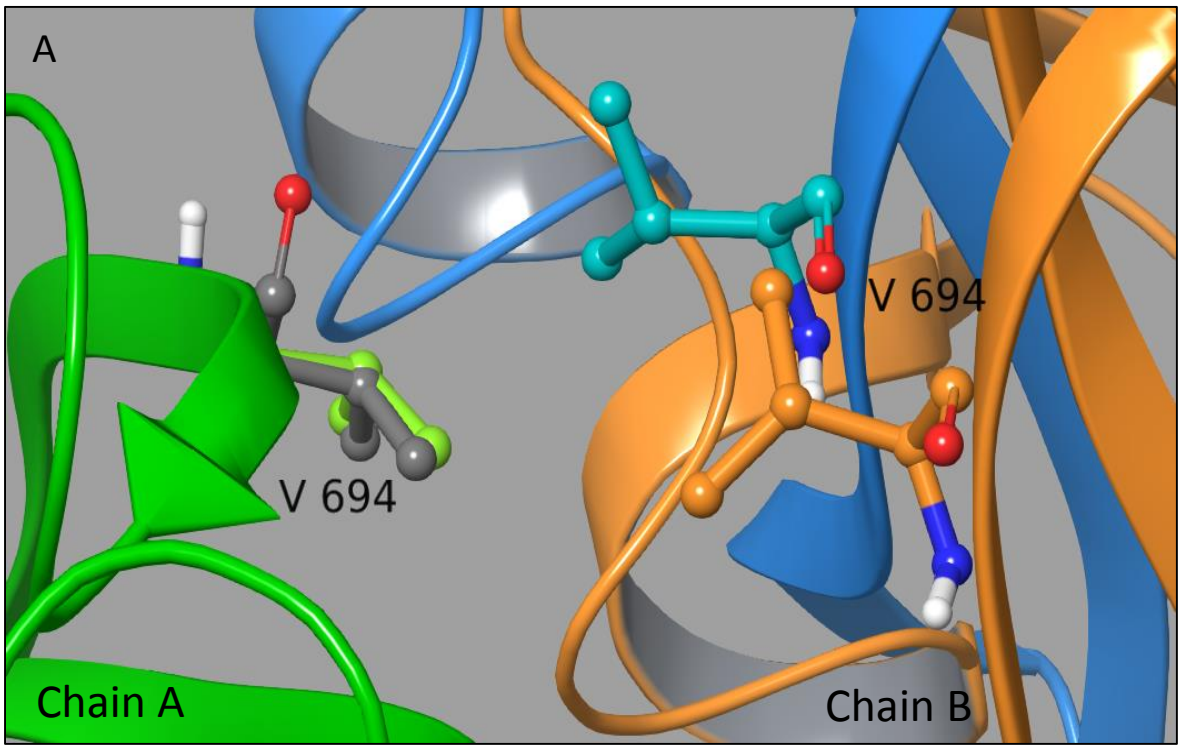

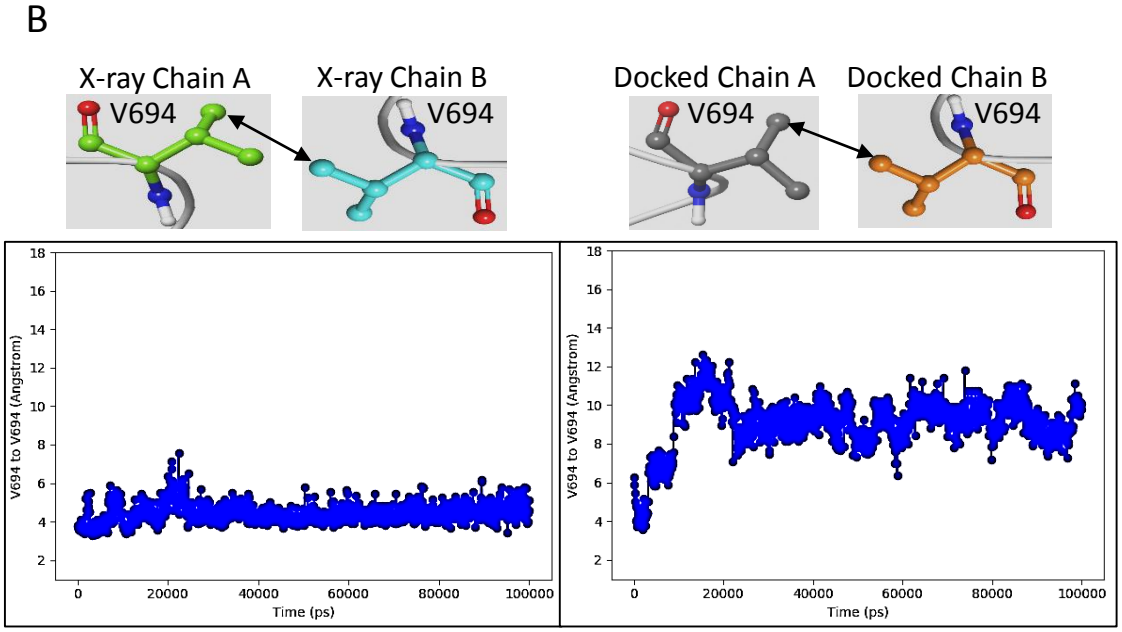

S6.6 A: Ionic interaction between D651 and D660 in chain A with the R685 in chain B, in both X-ray and best docked model of HPX dimer. Backbone chain A (dark green), chain B X-ray (blue) and docked chain B (orange). Carbons in X-ray chain A (light green), docked chain A (grey), X-ray chain B (light blue) and docked chain B (orange). Oxygens (red), nitrogens (dark blue) and hydrogens (white).

S6.6 B: The 100 ns trajectory of the interactions between the side chain oxygens in D651 and D660 with the side chain nitrogens in R685.

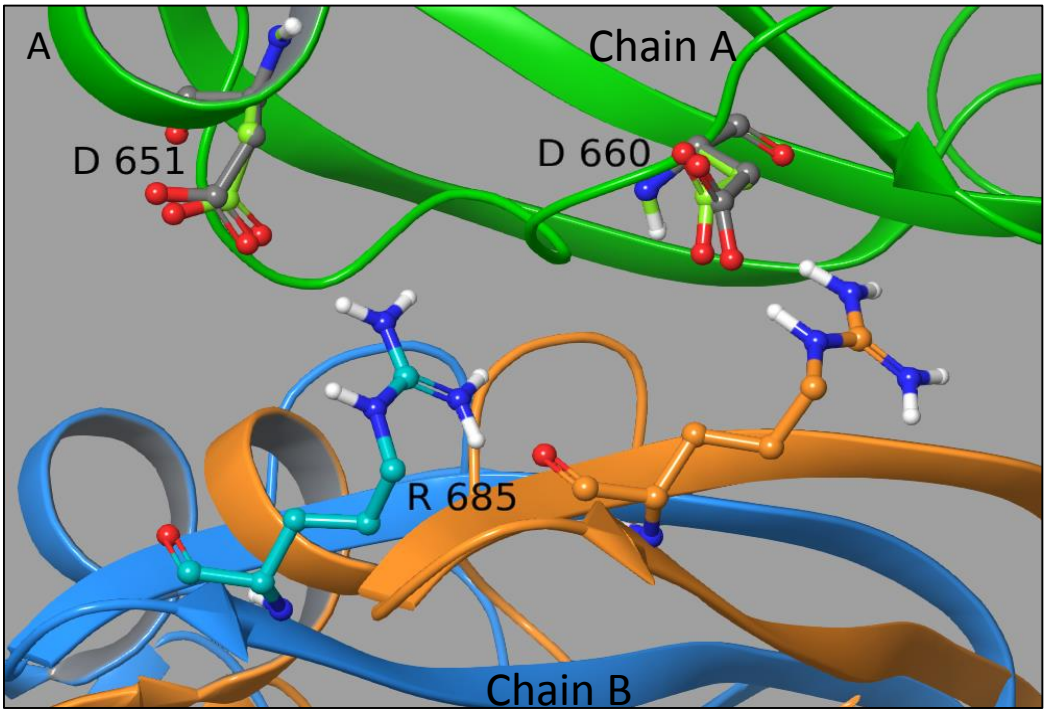

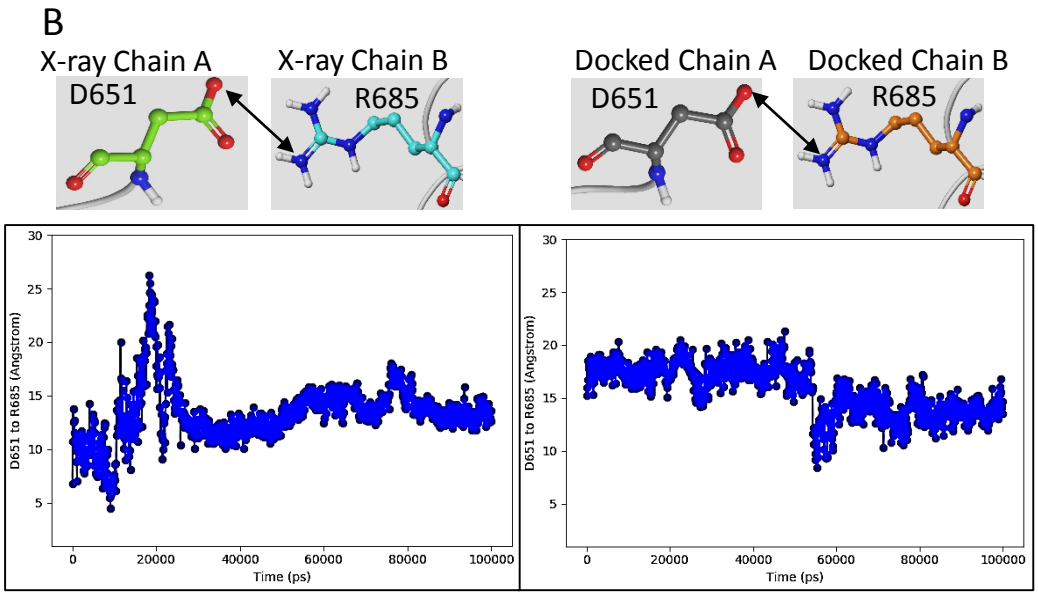

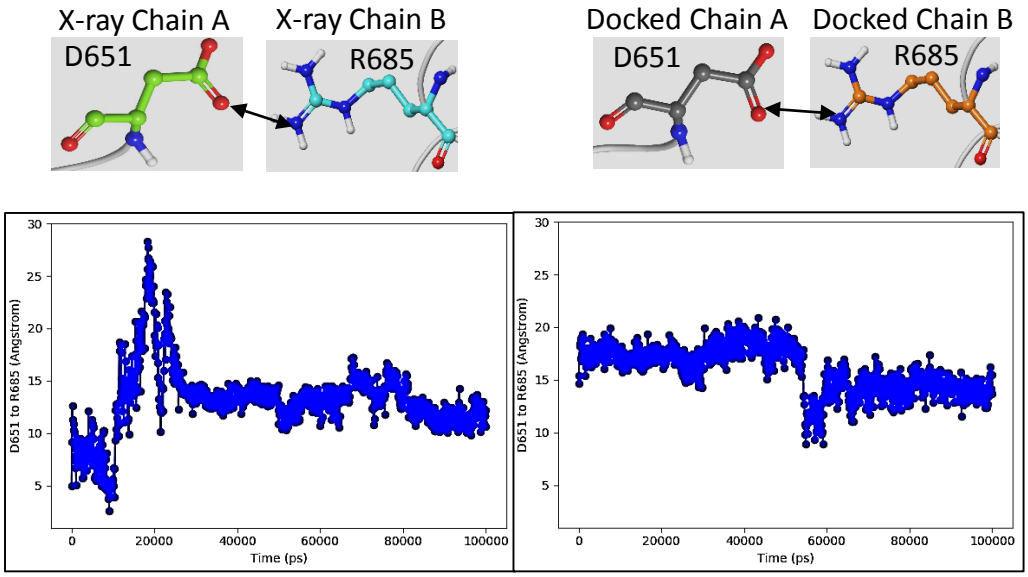
X-ray Chain A
X-ray Chain B
Docked Chain A
Docked Chain B
D651
R685
D651
R685
D651 to R685 (Angstrom)
Time (ps)
D651 to R685 (Angstrom)
Time (ps)

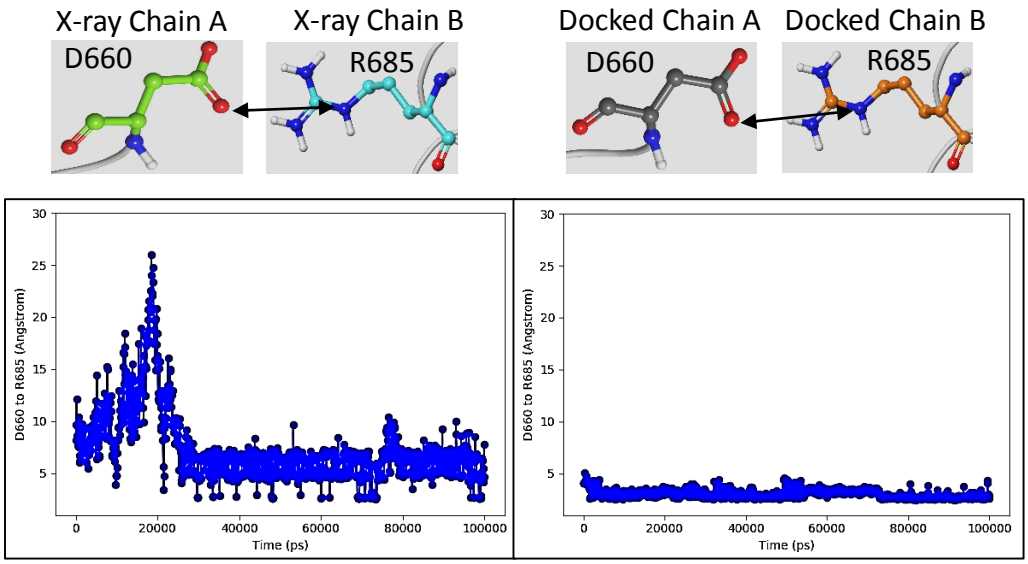
X-ray Chain A
X-ray Chain B
Docked Chain A
Docked Chain B
D660
R685
D660
R685
D660 to R685 (Angstrom)
Time (ps)
D660 to R685 (Angstrom)
Time (ps)

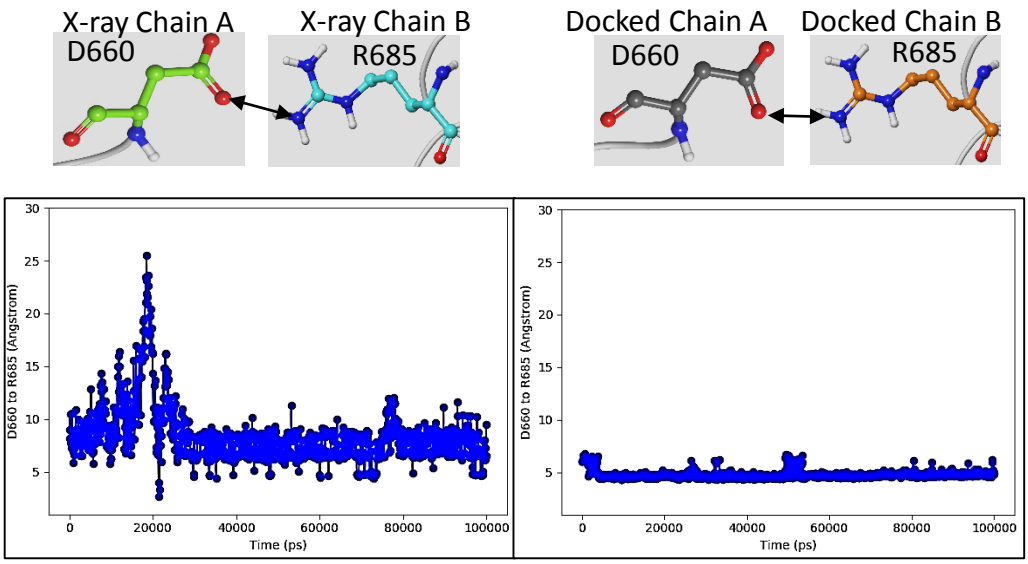
X-ray Chain A
X-ray Chain B
Docked Chain A
Docked Chain B
D660
R685
D660
R685
D660 to R685 (Angstrom)
Time (ps)
D660 to R685 (Angstrom)
Time (ps)

Fig. S7: Docking and molecular dynamic simulations of the interactions between the MMP-9FnII module and the SG core protein.

Distances between selected atoms are shown in each A-figure and the double arrows in B-figures indicate the atoms for the trajectory.

S7.1 A: Hydrogen bond between G227 main chain carbonyl oxygen in MMP-9FnII and the N38 side chain NH_2 in SG. Backbone MMP-9 catalytic domain (green), FnII repeat 1 (purple), FnII second repeat (pink) and SG N-terminal ^{1}Y-^{66}Y (yellow). Carbons in MMP-9 (orange) and SG (grey), oxygens (red), nitrogens (dark blue) and hydrogens (white).

S7.1 B: The 100 ns trajectory of the interactions of the two hydrogens on the N38 side chain with the carbonyl oxygen in G227

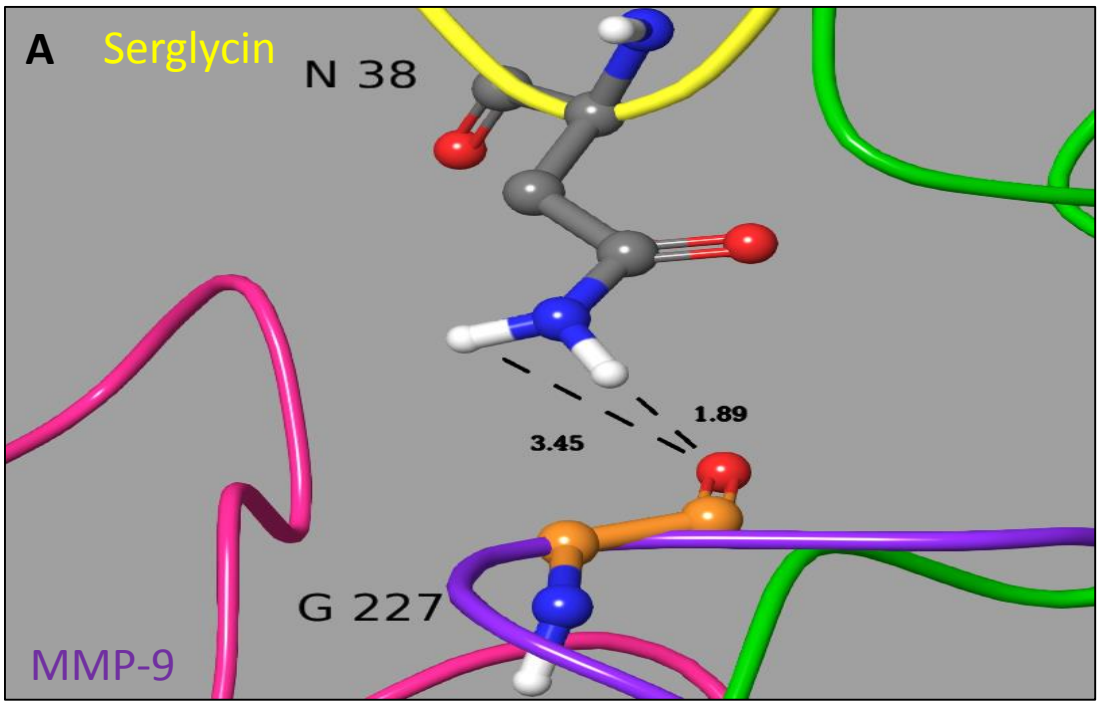

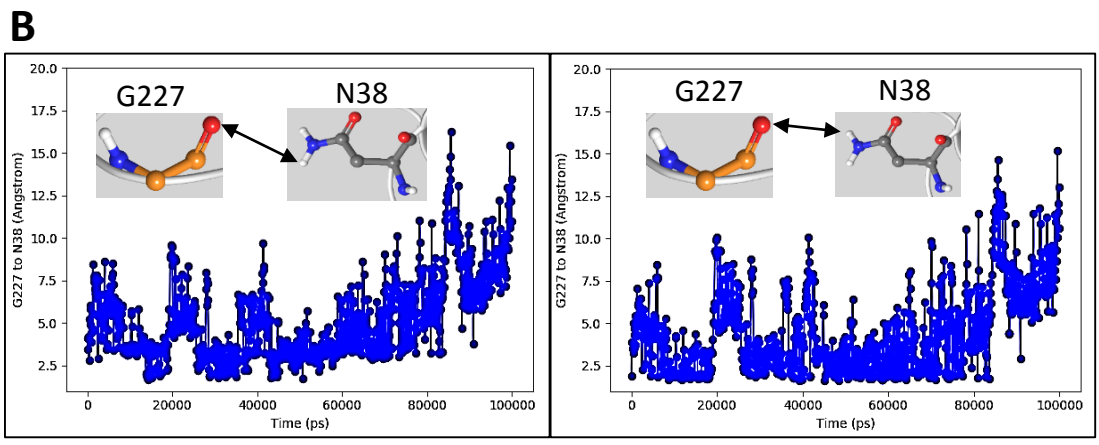

S7.2 A: Hydrophobic interactions between N282 side chain in MMP-9FnII and the L120 side chain in SG. Backbone MMP-9 FnII repeat 1 (purple), FnII second repeat (pink), SG N-terminal ^{1}Y-^{66}Y (yellow) and SG C-terminal ^{86}F-^{131}L (faded orange). Carbons in MMP-9 (orange) and SG (grey), oxygens (red), nitrogens (dark blue) and hydrogens (white).

S7.2 B: The 100 ns trajectory of the interactions of the side chain methylene in N282 with side chain of L120.

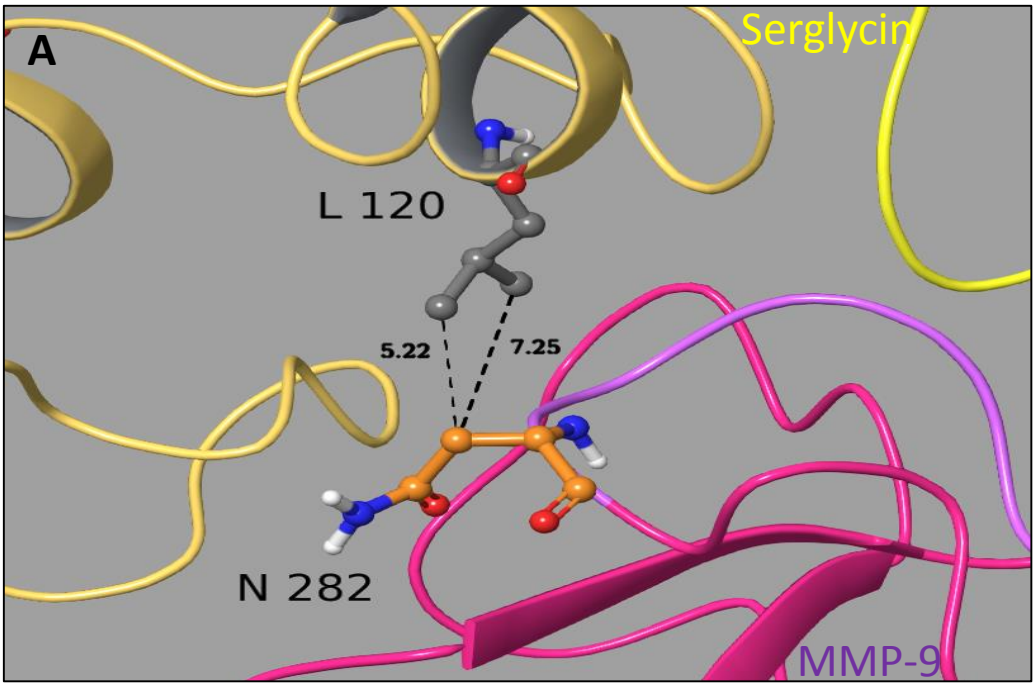

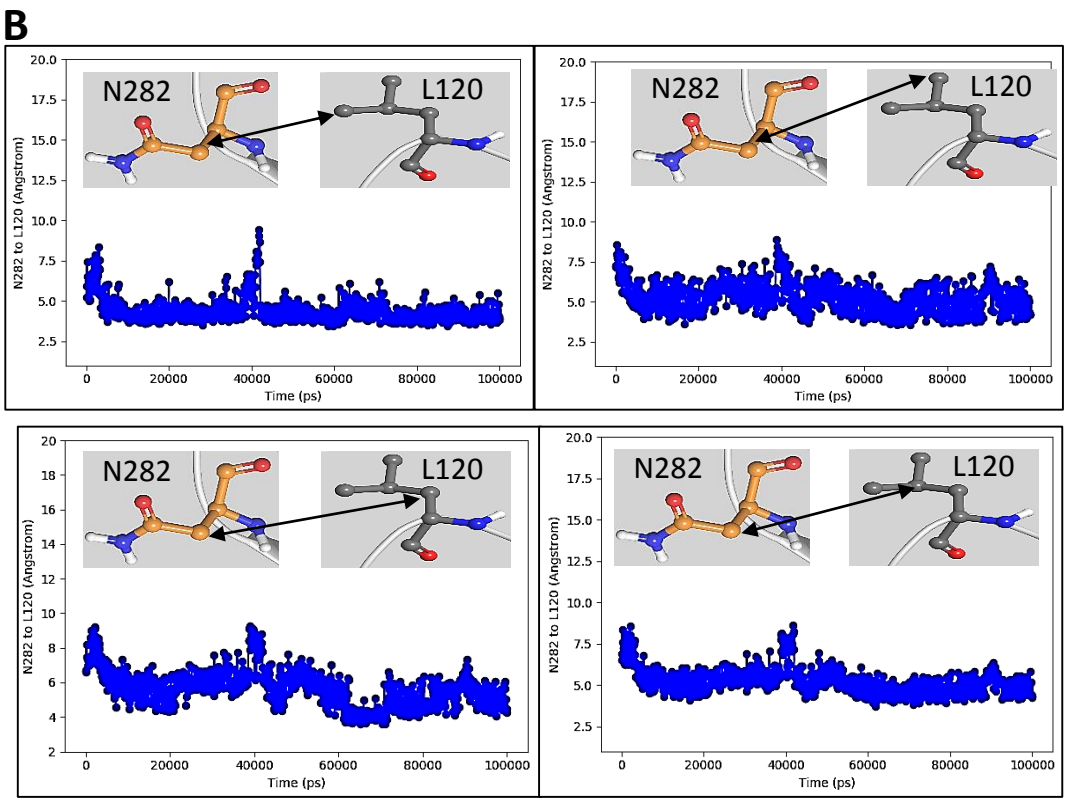

S7.3 A: Ionic interaction between D280 in MMP-9FnII and R42 in SG. Backbone MMP-9 catalytic domain (green), FnII repeat 1 (purple), FnII second repeat (pink), SG N-terminal ^{1}Y-^{66}Y (yellow) and SG C-terminal ^{86}F-^{131}L (faded orange). Carbons in MMP-9 (orange) and SG (grey), oxygens (red), nitrogens (dark blue) and hydrogens (white).

S7.3 B: The 100 ns trajectory of the interactions between the two side chain oxygens in D280 with the side chain nitrogens in R42.

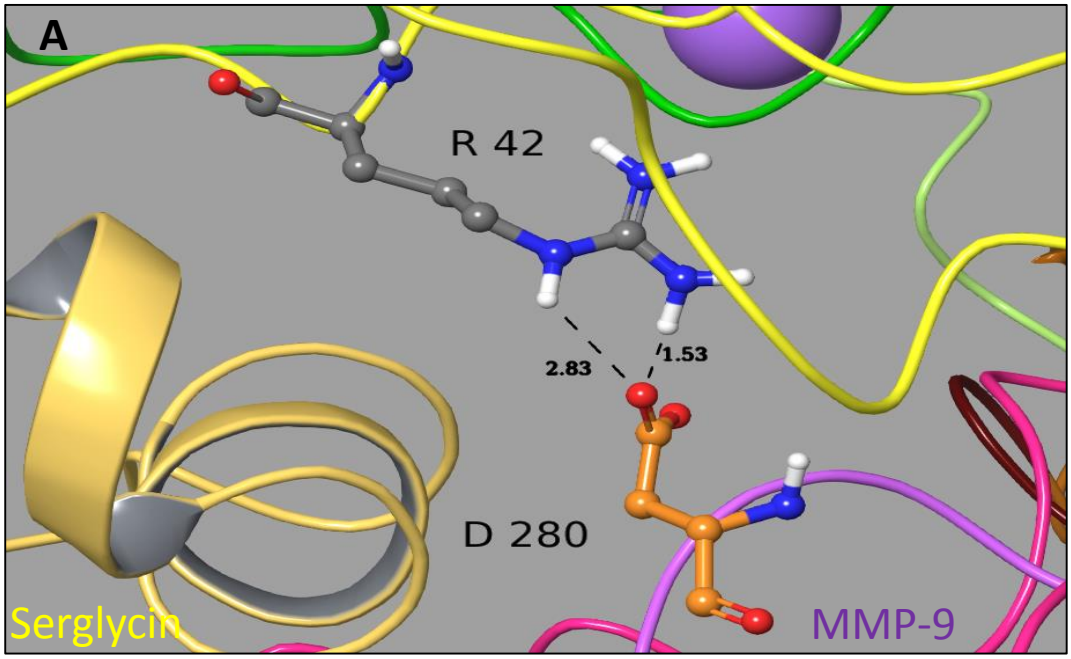

B

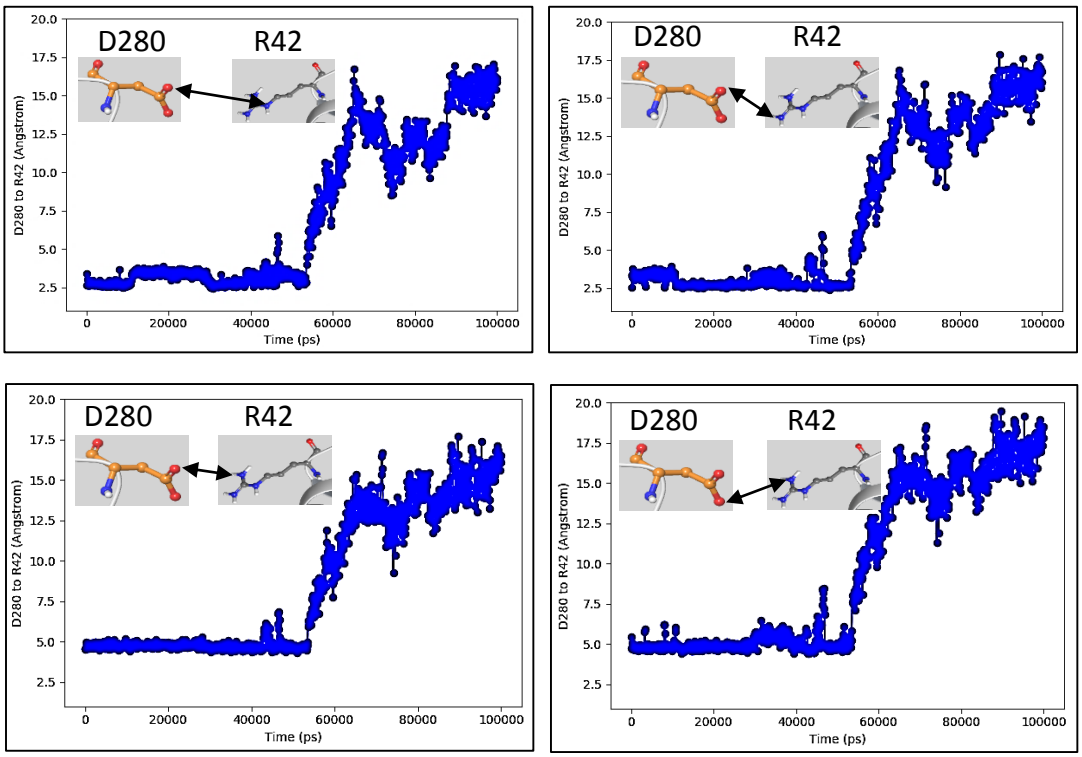

S7.4 A: Ionic interaction between R162 in MMP-9 catalytic domain and D46 in SG. Backbone MMP-9 catalytic domain (green), FnII second repeat (pink), SG N-terminal ^{1}Y-^{66}Y (yellow) and SG C-terminal ^{86}F-^{131}L (faded orange). Carbons in MMP-9 (orange) and SG (grey), oxygens (red), nitrogens (dark blue) and hydrogens (white).

S7.4 B: The 100 ns trajectory of the interactions between the side chain nitrogens in R162 and the two side chain oxygens in D46.

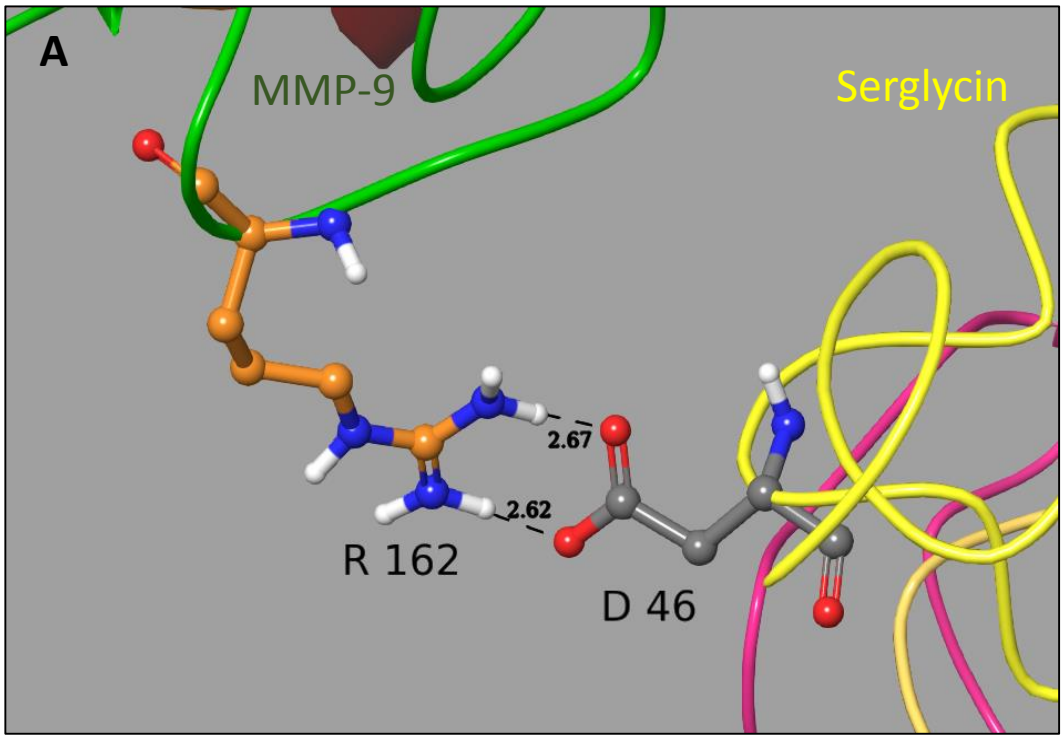

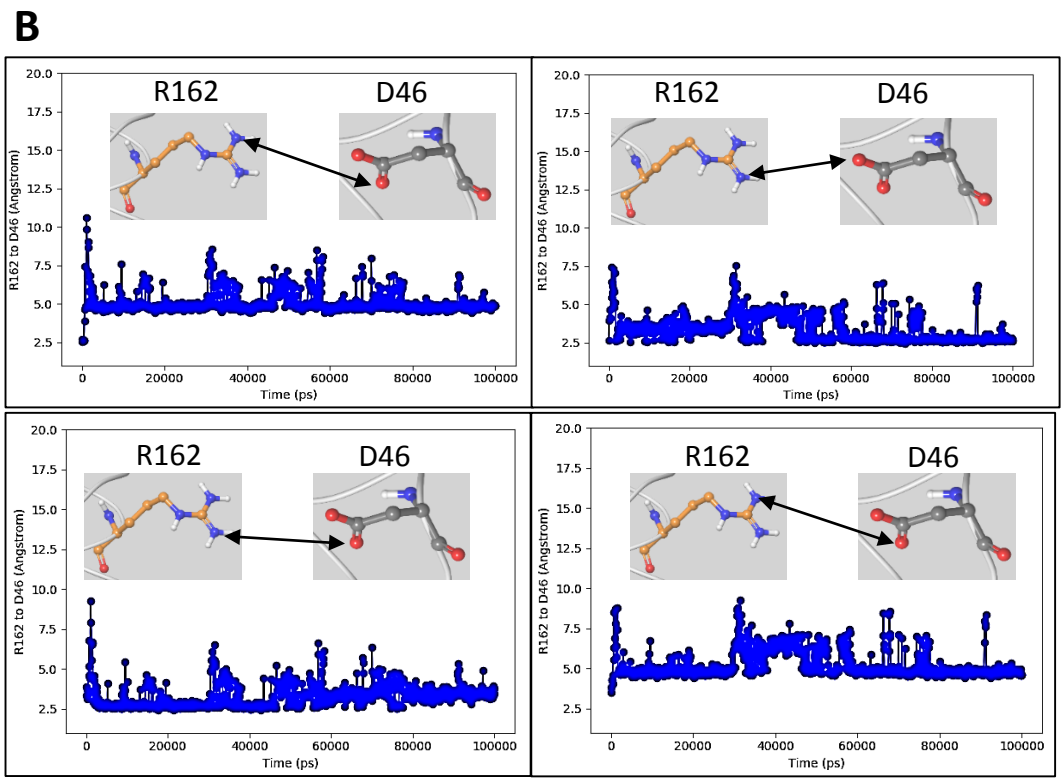

S7.5 A: Hydrogen bonds of side chain OH and main chain NH in S308 (MMP-9FnII) with side chain carboxyl in E98 (SG) and main chain carbonyl oxygen in G306 (MMP-9FnII) with main chain NH in E98 (SG) and V96 (SG). Backbone MMP-9 FnII repeat 1 (purple), FnII second repeat (pink), SG N-terminal ^{1}Y-^{66}Y (yellow) and SG C-terminal ^{86}F-^{131}L (faded orange). Carbons in MMP-9 (orange) and SG (grey), oxygens (red), nitrogens (dark blue) and hydrogens (white).

S7.5 B: The 100 ns trajectory of these interactions.

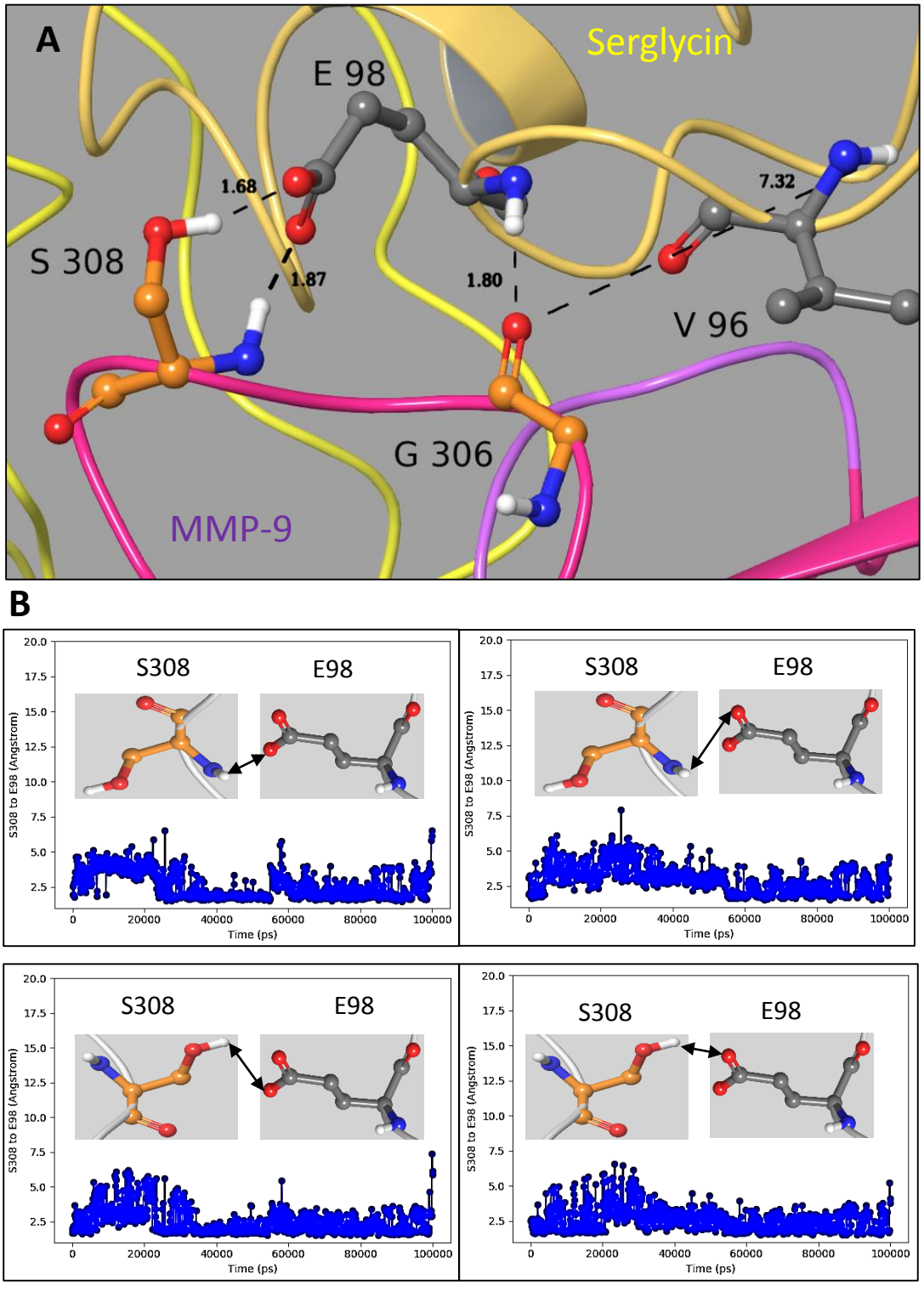

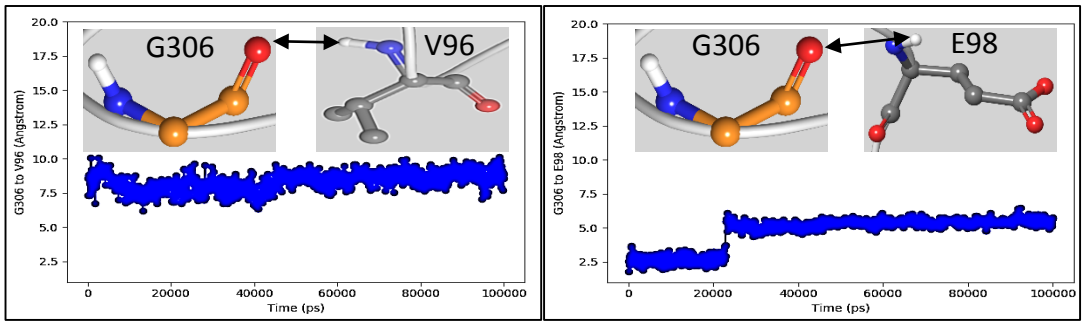
G306
V96
G306 to V96 (Angstrom)
Time (ps)
G306
E98
G306 to E98 (Angstrom)
Time (ps)

S7.6 A: Hydrophobic interactions of the side chain V96 (SG) with the hydrophobic parts of the side chains F294, Q295 and Y320 in MMP-9FnII. Backbone MMP-9 catalytic domain (green), FnII second repeat (pink), FnII third repeat (brown), SG N-terminal ^{1}Y-^{66}Y (yellow) and SG C-terminal ^{86}F-^{131}L (faded orange). Carbons in MMP-9 (orange) and SG (grey), oxygens (red), nitrogens (dark blue) and hydrogens (white).

S7.6 B: The 100 ns trajectory of these interactions.

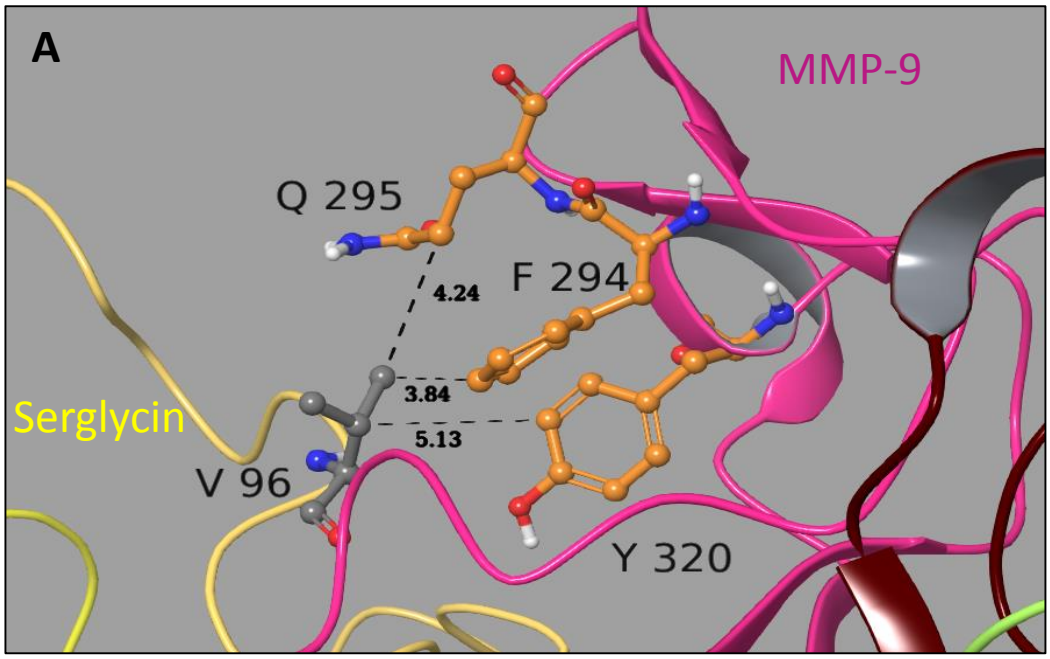

B

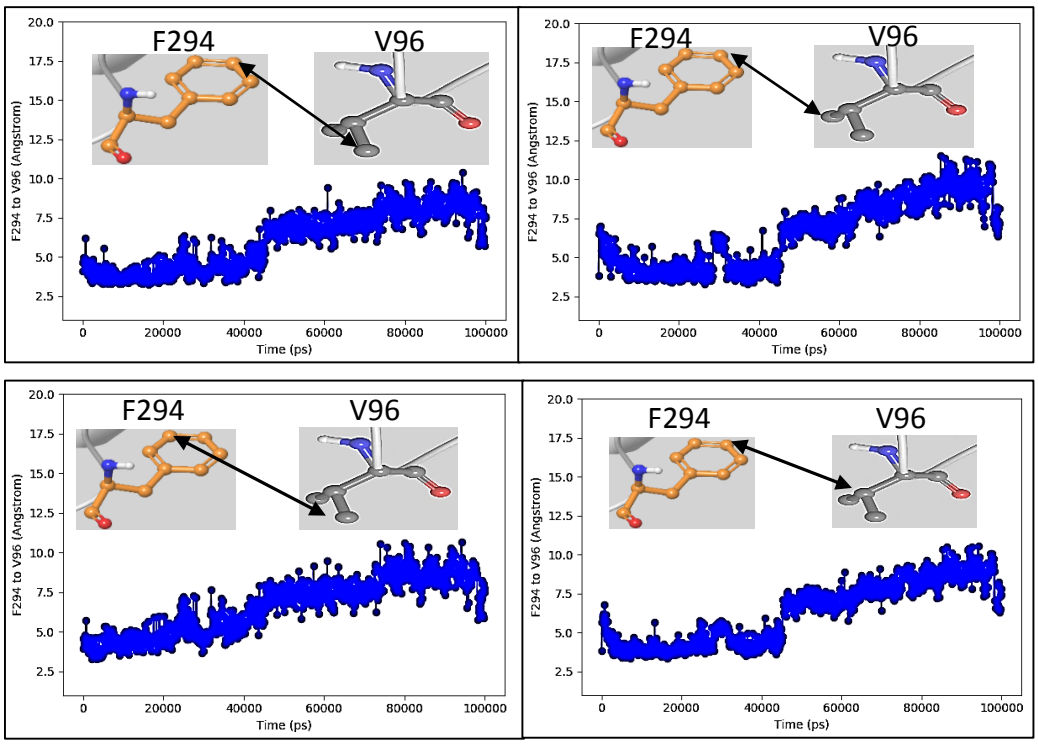

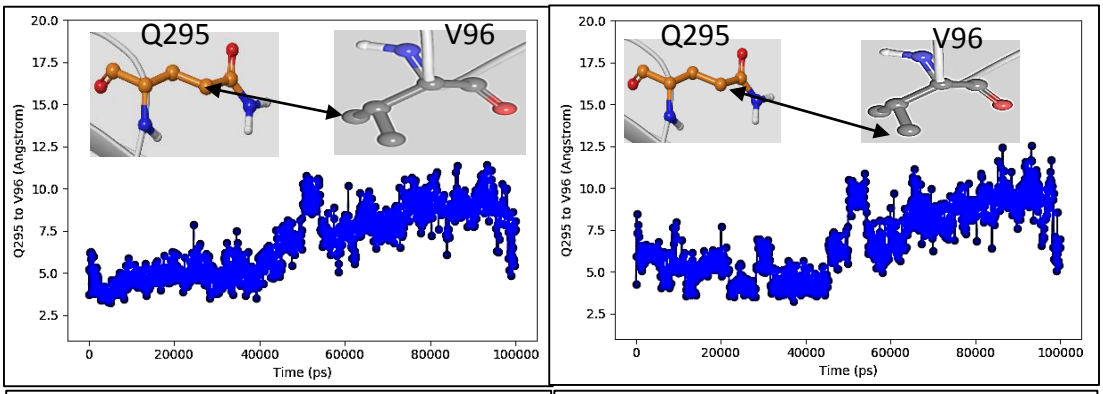
Q295
V96
Q295 to V96 (Angstrom)
Time (ps)

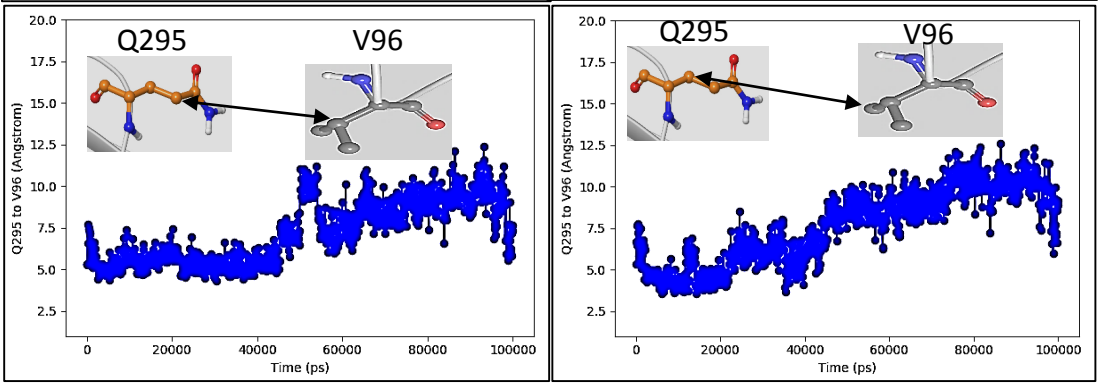
Q295
V96
Q295 to V96 (Angstrom)
Time (ps)

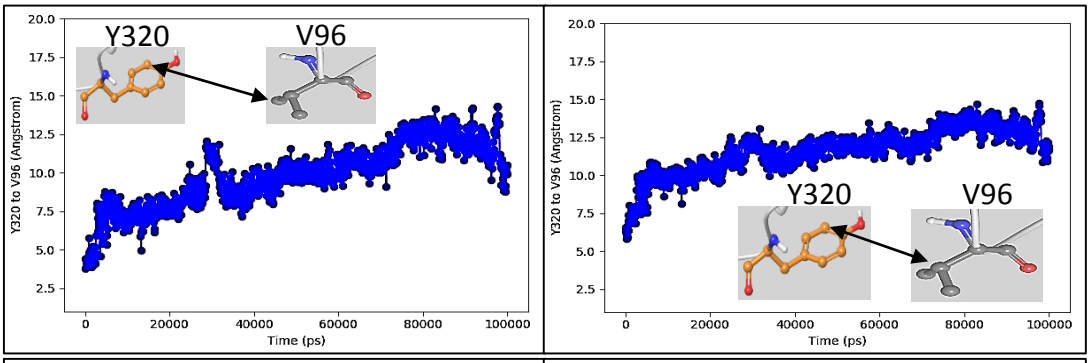
Y320
V96
Y320 to V96 (Angstrom)
Time (ps)

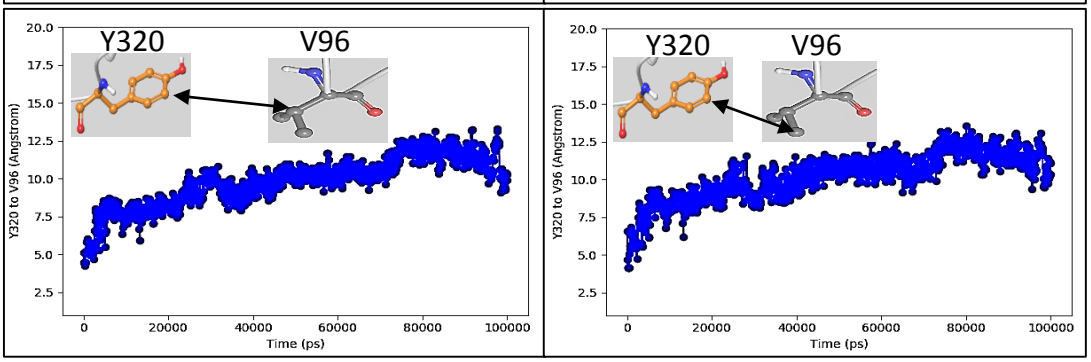
Y320
V96
Y320 to V96 (Angstrom)
Time (ps)

S7.7 A: Hydrogen bond between side chain OH of S99 in SG with side chain NH in R307 and side chain N in W313 in MMP-9FnII. Backbone MMP-9 FnII first repeat (purple), FnII second repeat (pink), SG N-terminal ^{1}Y-^{66}Y (yellow) and SG C-terminal ^{86}F-^{131}L (faded orange). Carbons in MMP-9 (orange) and SG (grey), oxygens (red), nitrogens (dark blue) and hydrogens (white).

S7.7 B: The 100 ns trajectory of these two interactions.

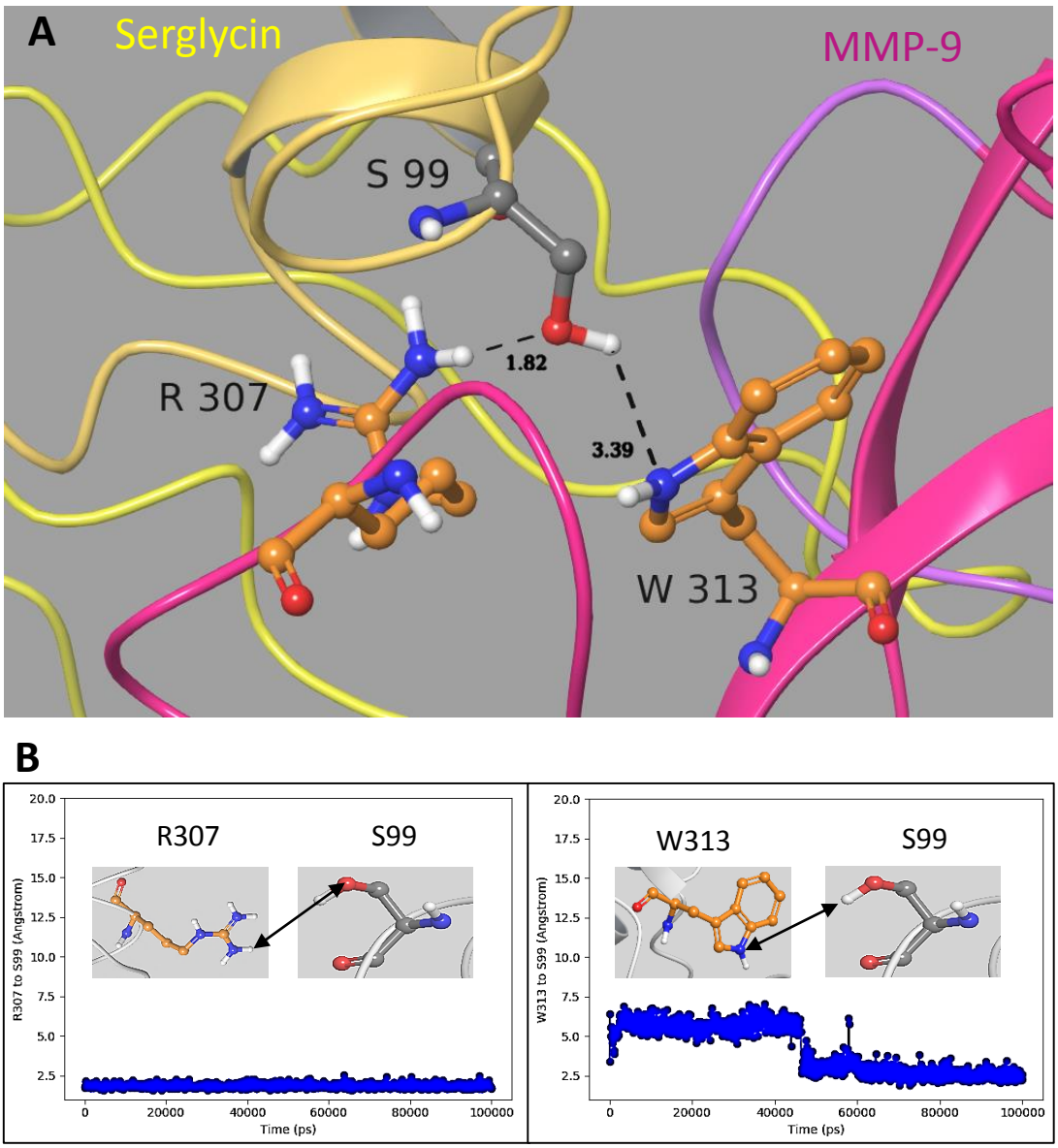

S7.8 A: Hydrogen bond between side chain NH in K324 in MMP-9FnII and main chain carbonyl oxygen in F102 (SG). Backbone MMP-9 FnII first repeat (purple), FnII second repeat (pink) and SG C-terminal ^{86}F-^{131}L (faded orange). Carbons in MMP-9 (orange) and SG (grey), oxygens (red), nitrogens (dark blue) and hydrogens (white).

S7.8 B: The 100 ns trajectory of these interactions.

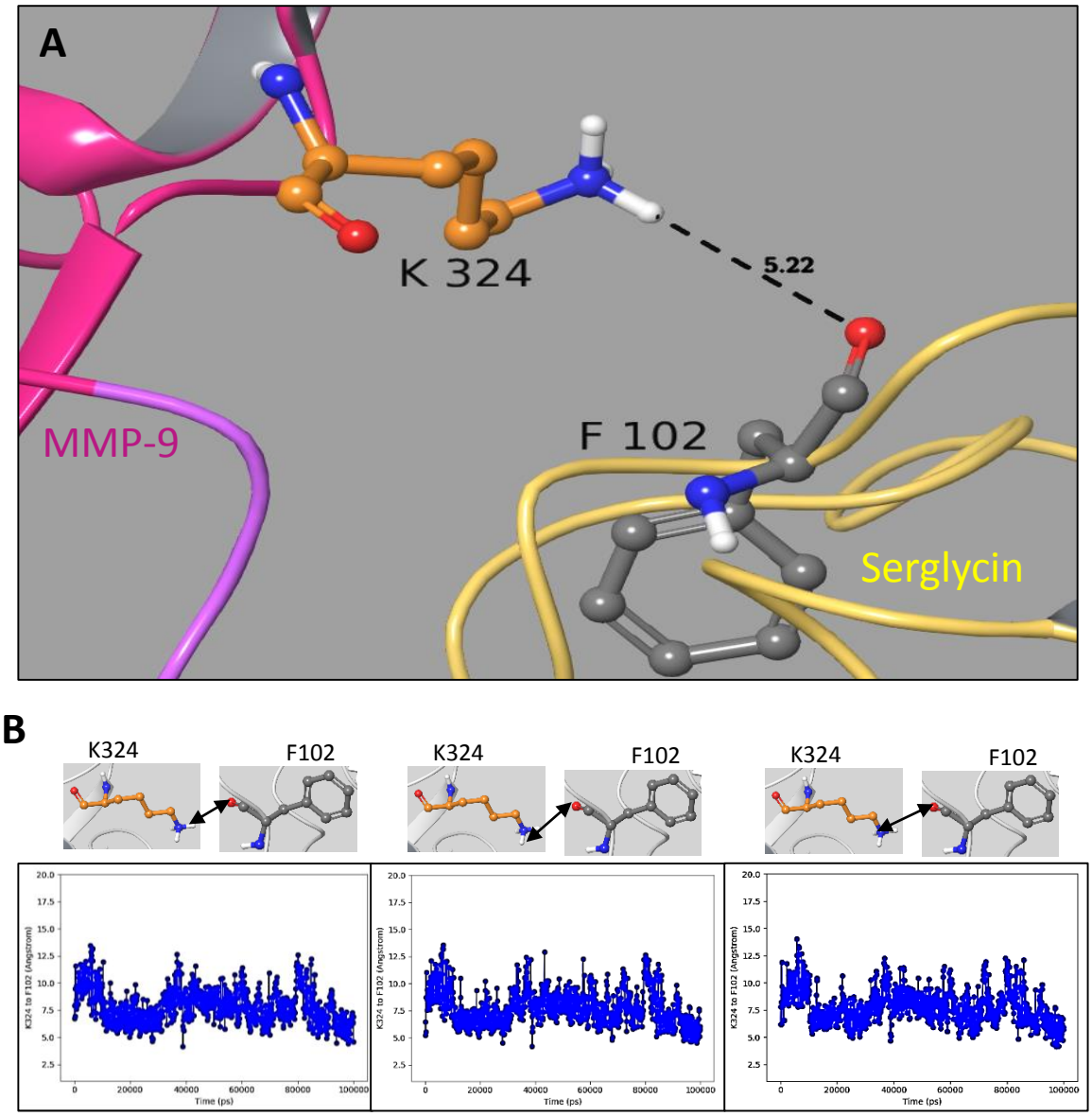

S7.9 A: Hydrophobic interactions of the side chain F326 (MMP-9FnII) with the hydrophobic parts of the side chain S99 and D100 as well as with the Cα-atom and side chain methyl of A101 in SG. Backbone MMP-9 FnII first repeat (purple), FnII second repeat (pink), SG N-terminal ^{1}Y-^{66}Y (yellow) and SG C-terminal ^{86}F-^{131}L (faded orange). Carbons in MMP-9 (orange) and SG (grey), oxygens (red), nitrogens (dark blue) and hydrogens (white).

S7.9 B: The 100 ns trajectory of these interactions.

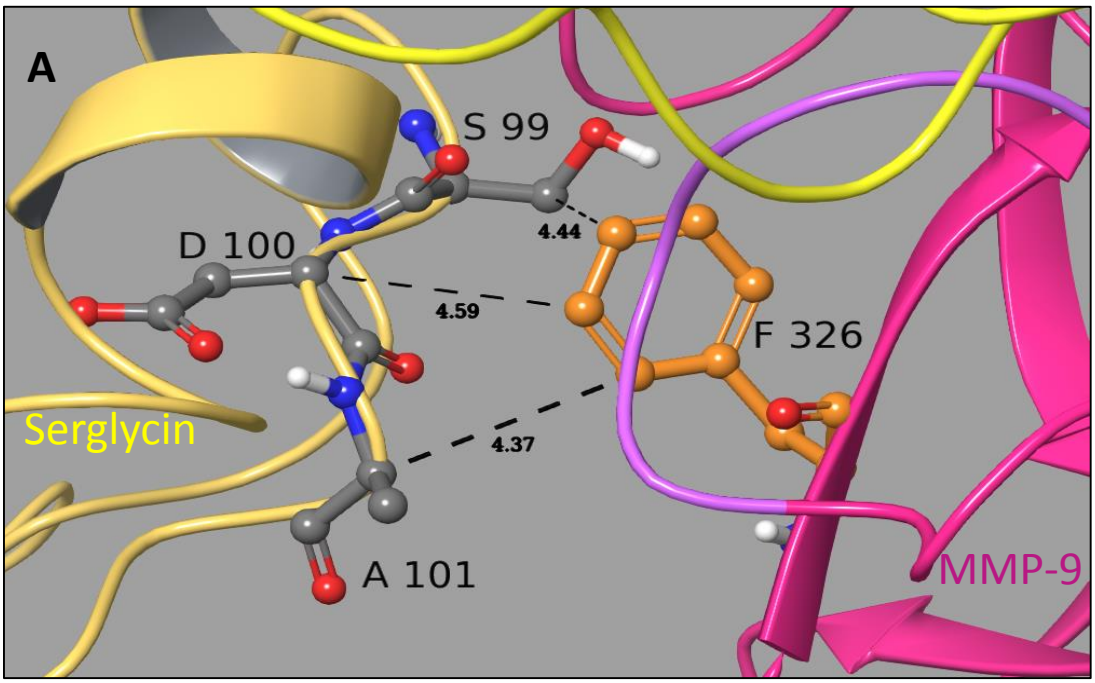

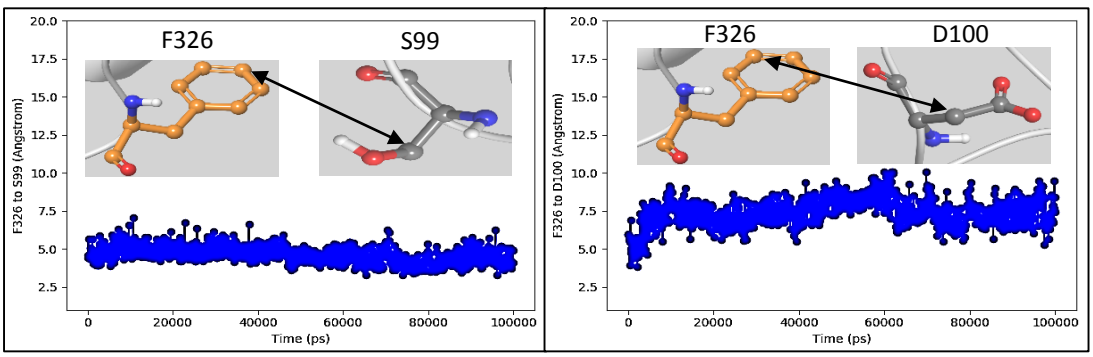

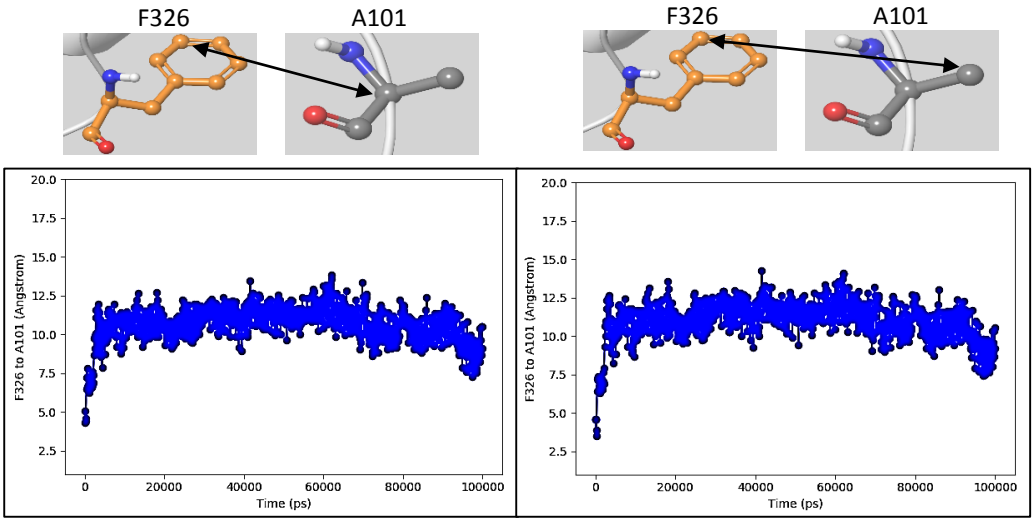
F326
A101
F326
A101
F326 to A101 (Angstrom)
Time (ps)
F326 to A101 (Angstrom)
Time (ps)

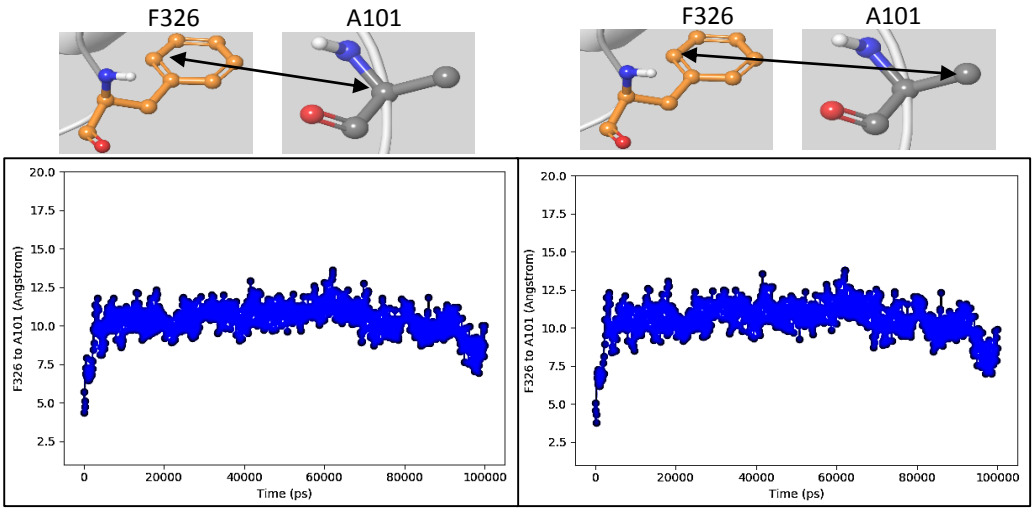
F326
A101
F326
A101
F326 to A101 (Angstrom)
Time (ps)
F326 to A101 (Angstrom)
Time (ps)

S7.10 A: Hydrophobic interactions of the side chain F328 (MMP-9FnII) with the side chain of L120 and the hydrophobic part of the side chain S99 in SG. Backbone MMP-9 catalytic domain (green), FnII first repeat (purple), FnII second repeat (pink) and SG C-terminal ^{86}F-^{131}L (faded orange). Carbons in MMP-9 (orange) and SG (grey), oxygens (red), nitrogens (dark blue) and hydrogens (white).

S7.10 B: The 100 ns trajectory of these interactions.

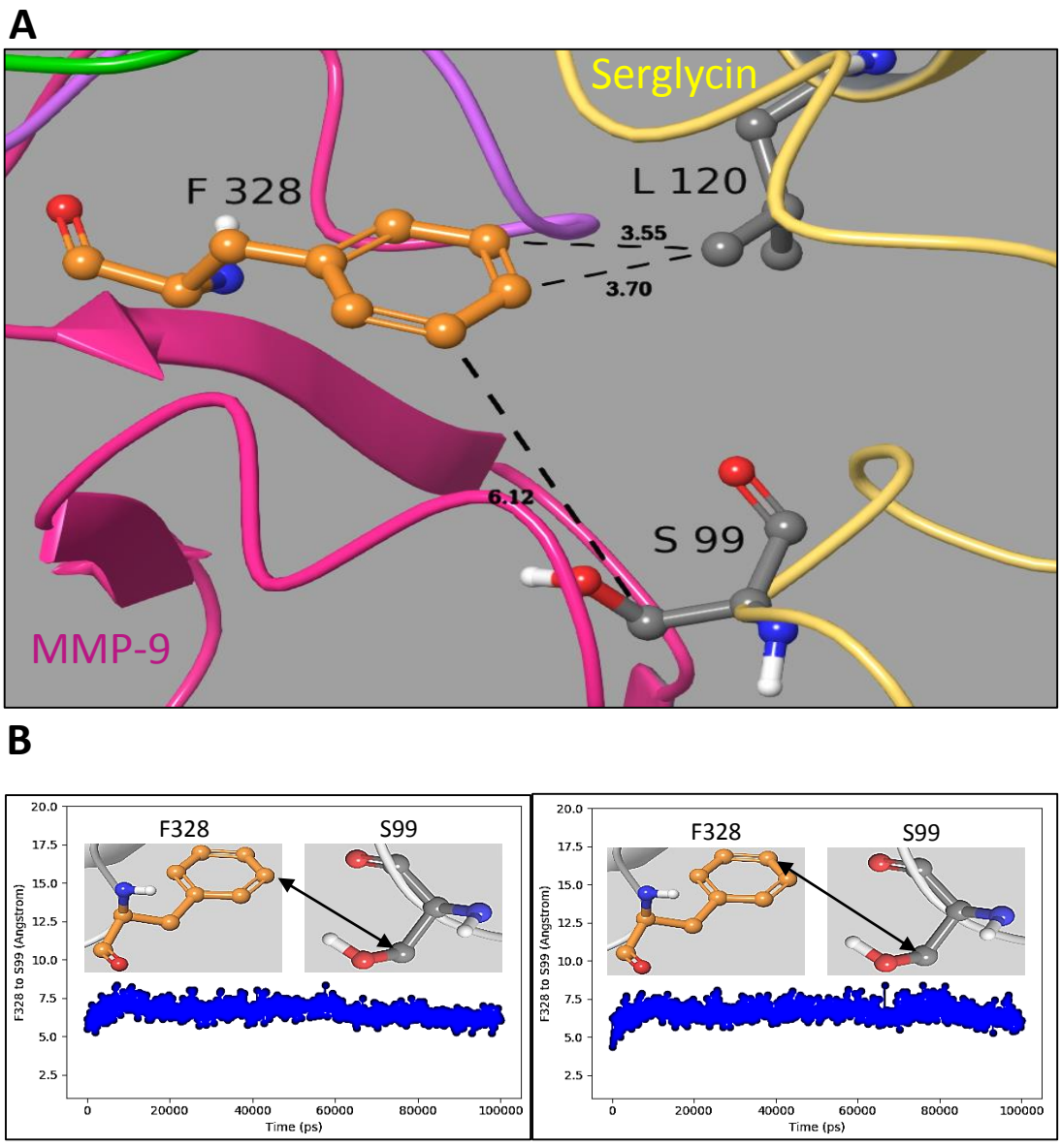

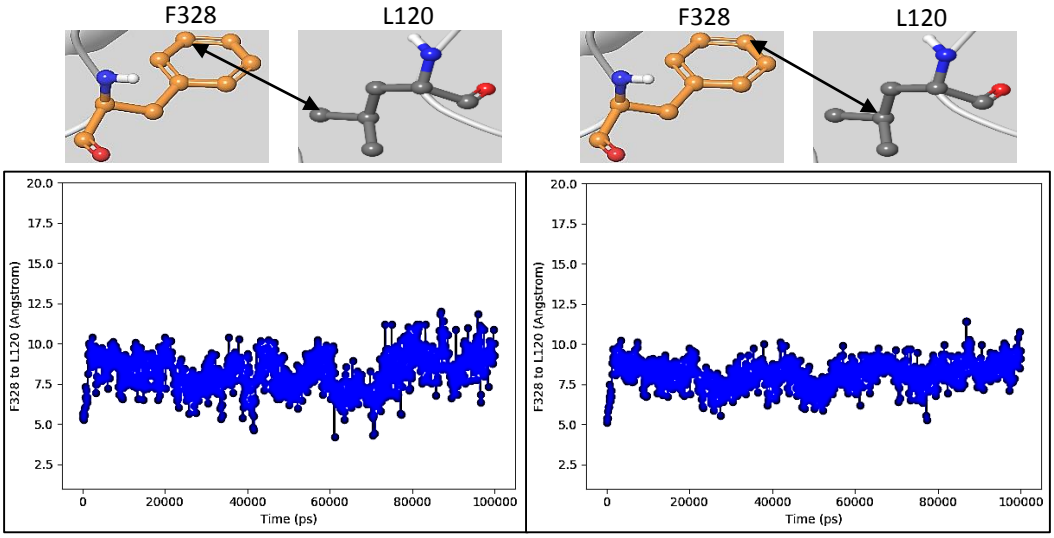
F328
L120
F328
L120
F328 to L120 (Angstrom)
Time (ps)
F328 to L120 (Angstrom)
Time (ps)

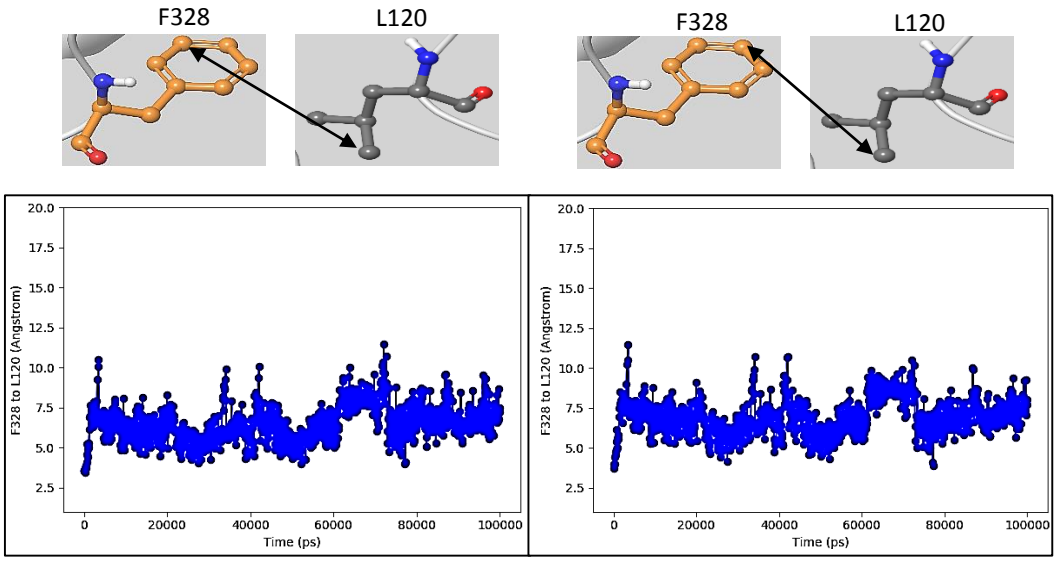
F328
L120
F328
L120
F328 to L120 (Angstrom)
Time (ps)
F328 to L120 (Angstrom)
Time (ps)

Fig. S8: Docking and molecular dynamic simulations of the interactions between the MMP-9HPX domain and the SG core protein: Model 1.

Distances between selected atoms are shown in each A-figure and the double arrows in B-figures indicate the atoms for the trajectory.

S8.1 A: Ionic interaction between D676 in MMP-9HPX and K39 in SG. Backbone MMP-9 HPX (green) and SG N-terminal ^{1}Y-^{66}Y (yellow). Carbons in MMP-9 (purple) and SG (grey), oxygens (red), nitrogens (dark blue) and hydrogens (white).

S8.1 B: The 100 ns trajectory of the interactions between the two side chain oxygens in D676 with the side chain nitrogen in K39.

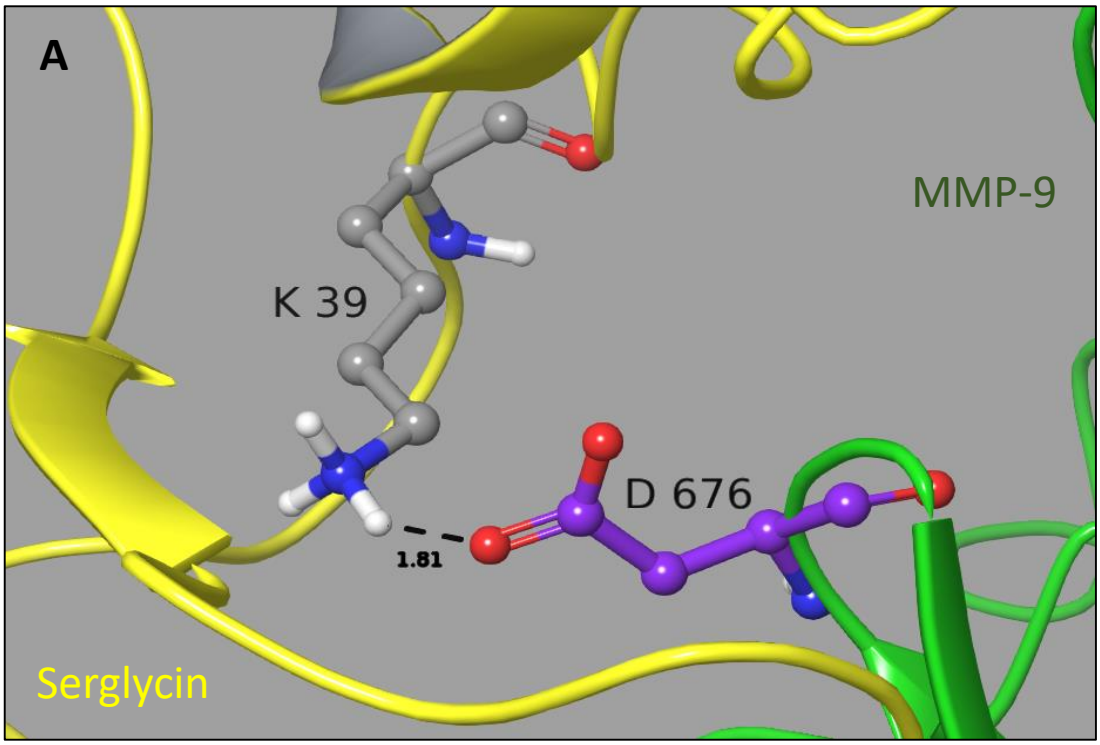

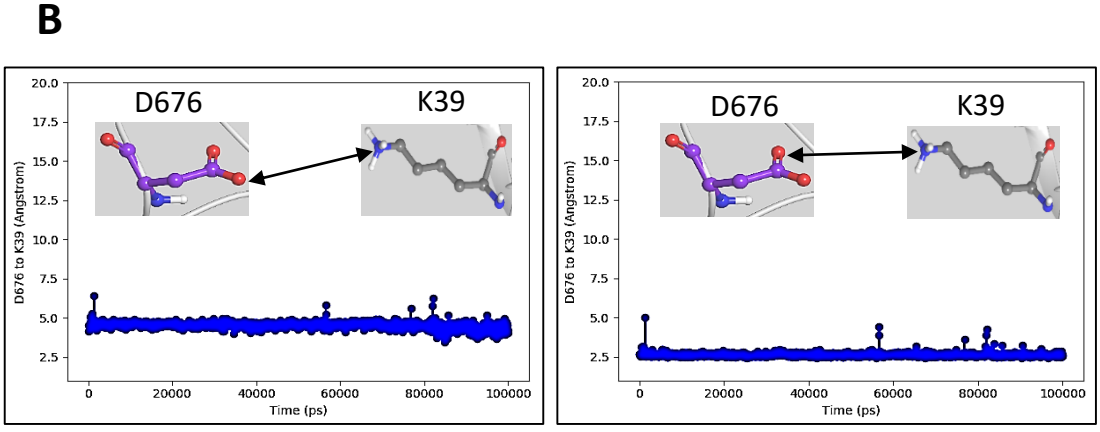

S8.2 A: Hydrophobic interactions between the methylene group in the side chain of D676 (MMP-9HPX) with side chains of P42 and L43 in SG. Backbone MMP-9 HPX (green), SG N-terminal ^{1}Y-^{66}Y (yellow) and SG C-terminal ^{86}F-^{131}L (orange). Carbons in MMP-9 (purple) and SG (grey), oxygens (red), nitrogens (dark blue) and hydrogens (white).

S8.2 B: The 100 ns trajectory of the these interactions.

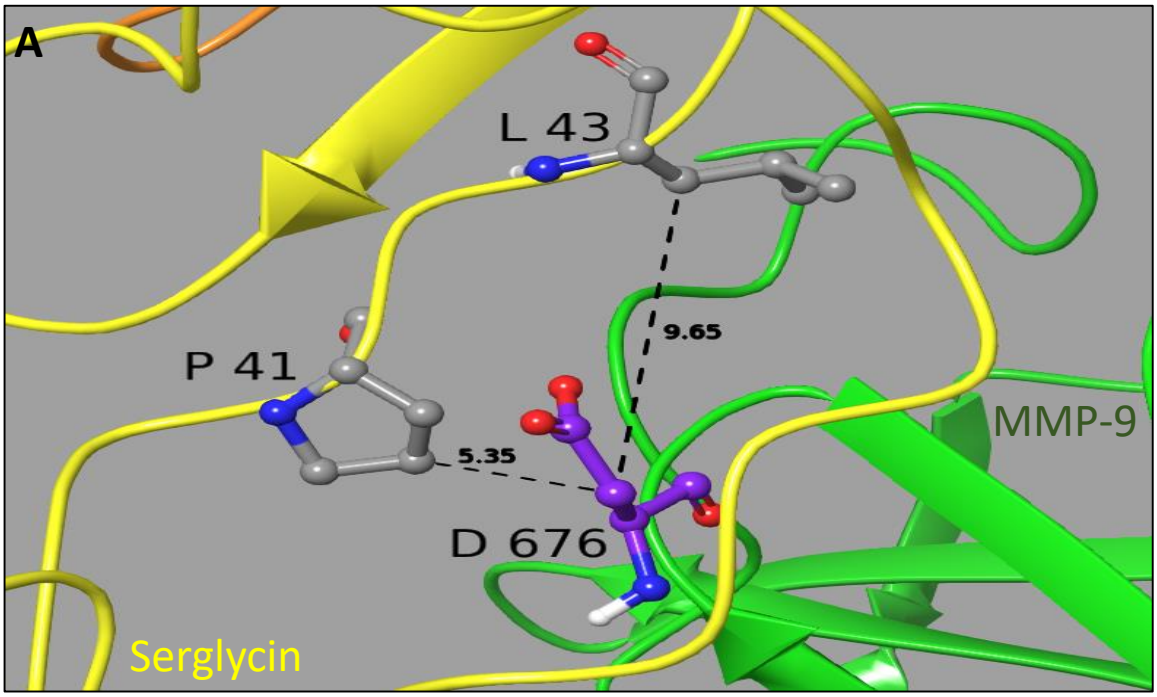

B

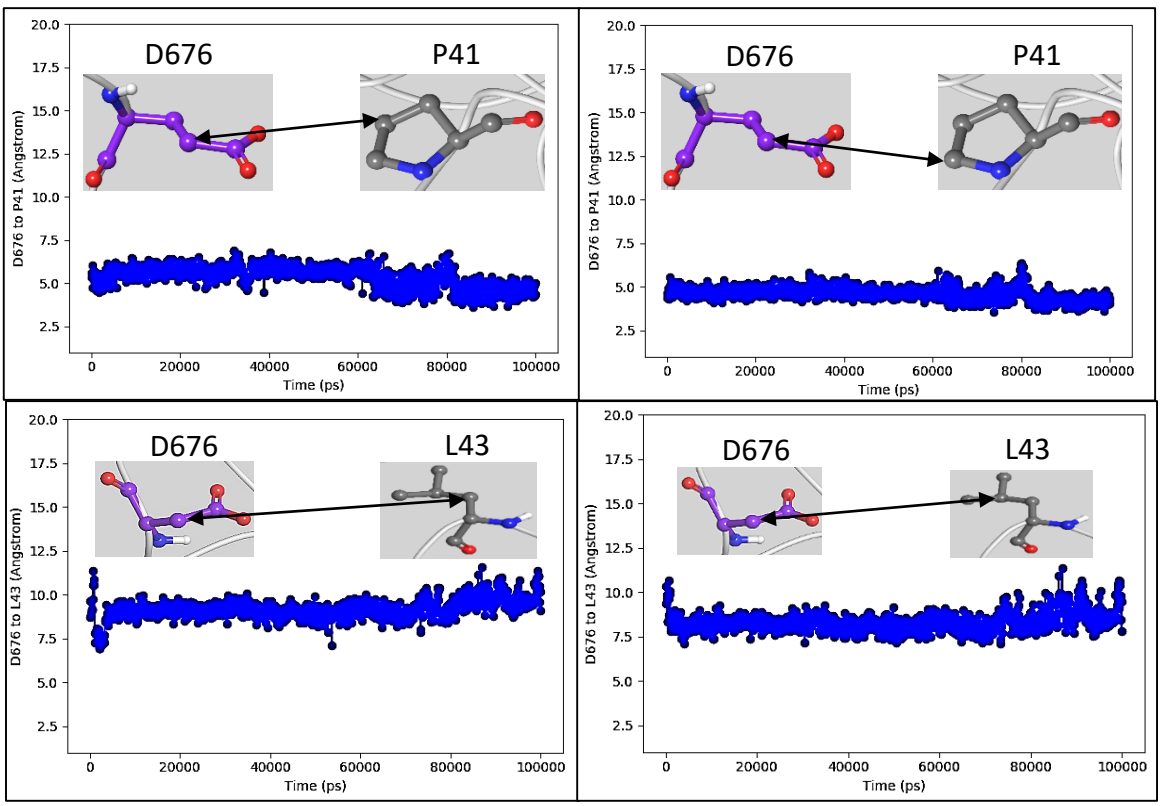

S8.3 A: Hydrogen bonds and hydrophobic interactions between the D660 (MMP-9HPX) side chain and main chain amide NH with main and side chains in L32, L33 and S37 in SG. Backbone MMP-9 HPX (green), SG N-terminal ^{1}Y-^{66}Y (yellow), SG C-terminal ^{86}F-^{131}L (orange) and SG Ser-Gly repeats ^{67}S-^{84}G (blue). Carbons in MMP-9 (purple) and SG (grey), oxygens (red), nitrogens (dark blue) and hydrogens (white).

S8.3 B: The 100 ns trajectory of these interactions.

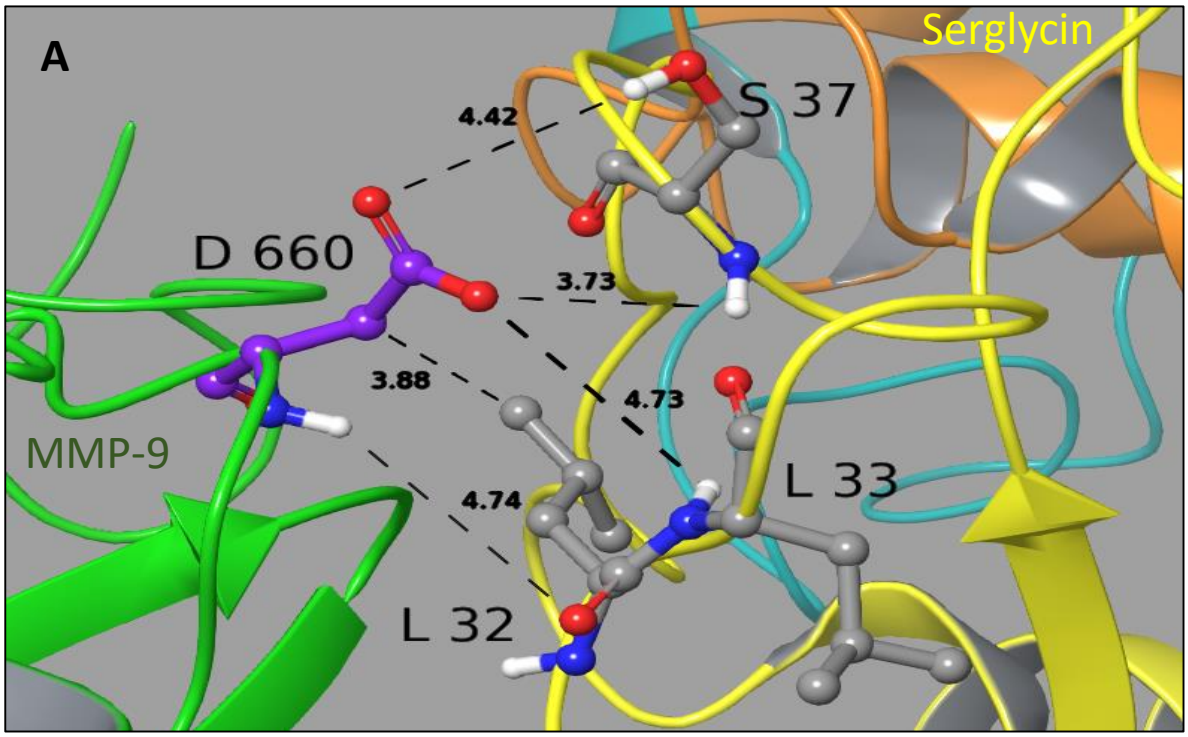

B

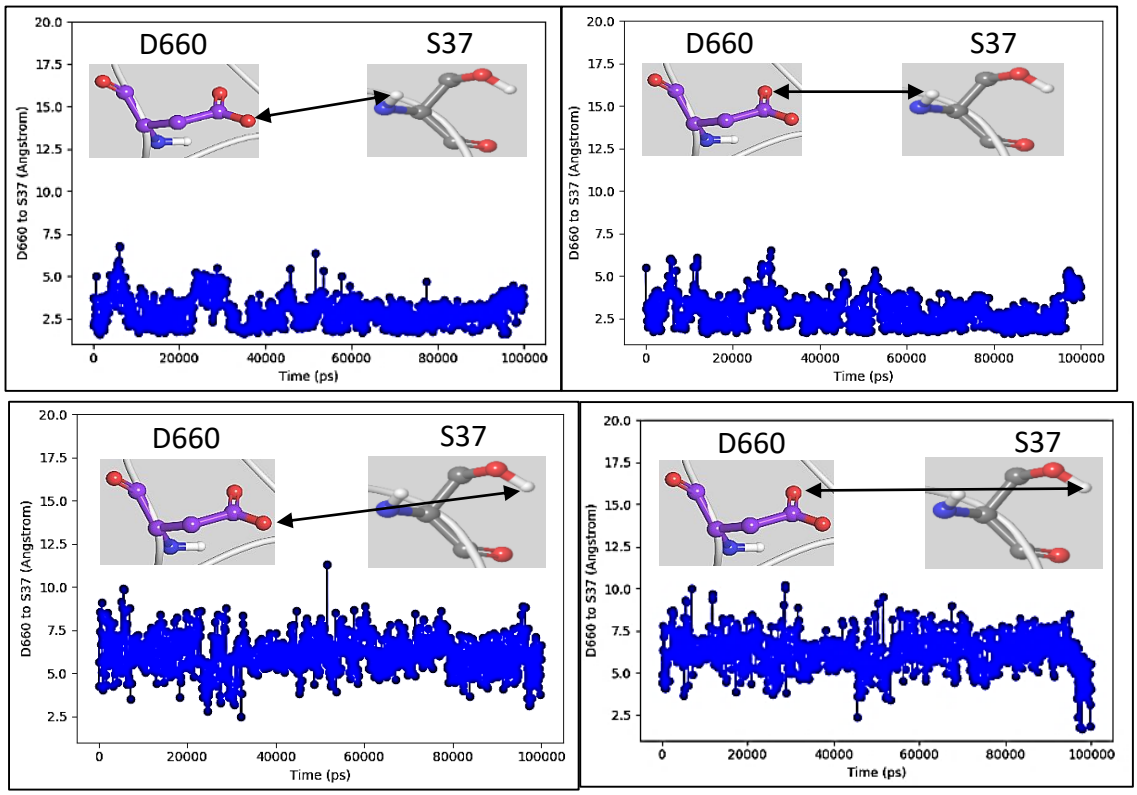

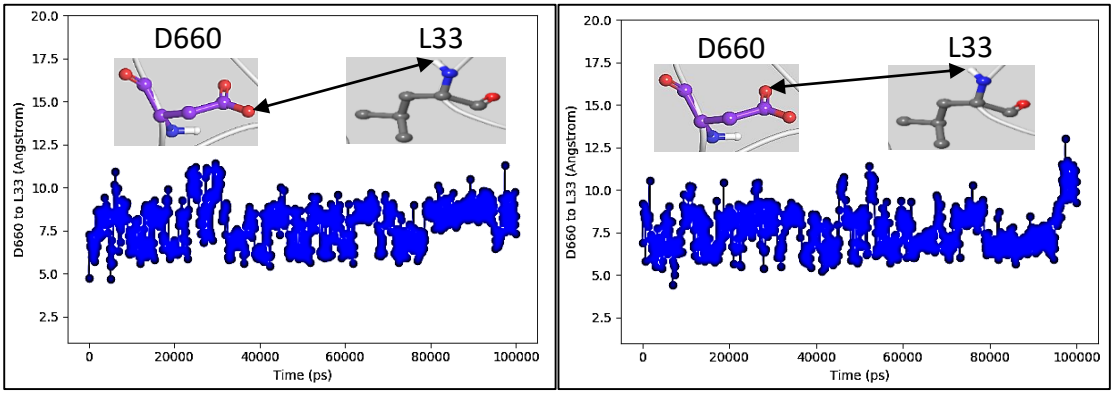
D660
L33
D660 to L33 (Angstrom)
Time (ps)
D660
L33
D660 to L33 (Angstrom)
Time (ps)

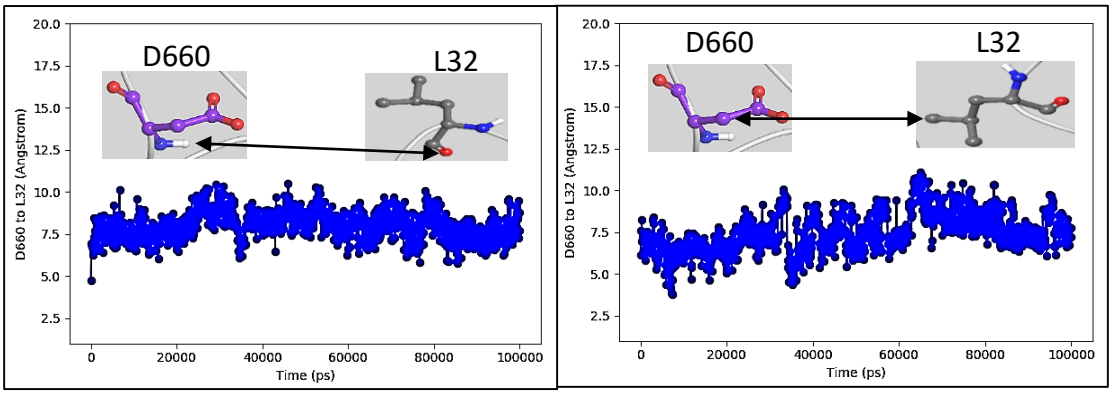
D660
L32
D660 to L32 (Angstrom)
Time (ps)
D660
L32
D660 to L32 (Angstrom)
Time (ps)

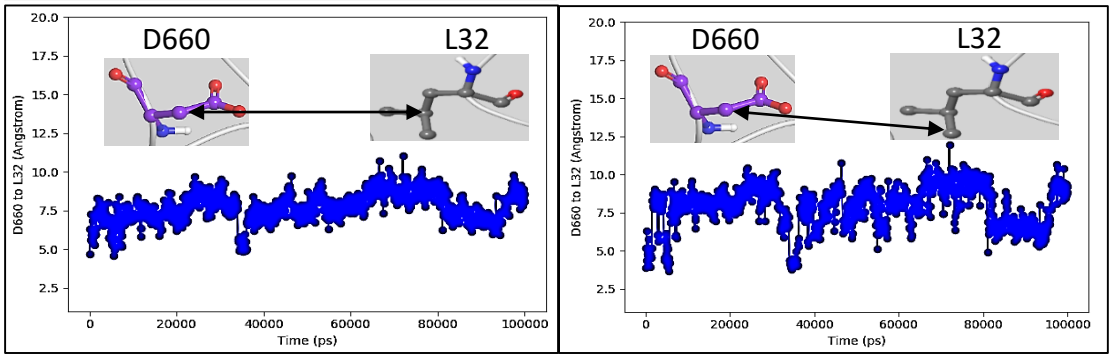
D660
L32
D660 to L32 (Angstrom)
Time (ps)
D660
L32
D660 to L32 (Angstrom)
Time (ps)

S8.4 A: Hydrophobic interactions of the side chains Q675 and W680 in MMP-9HPX with the side chain L32 in SG. Backbone MMP-9 HPX (green) and SG N-terminal ^{1}Y-^{66}Y (yellow). Carbons in MMP-9 (purple) and SG (grey), oxygens (red), nitrogens (dark blue) and hydrogens (white).

S8.4 B: The 100 ns trajectory of these interactions.

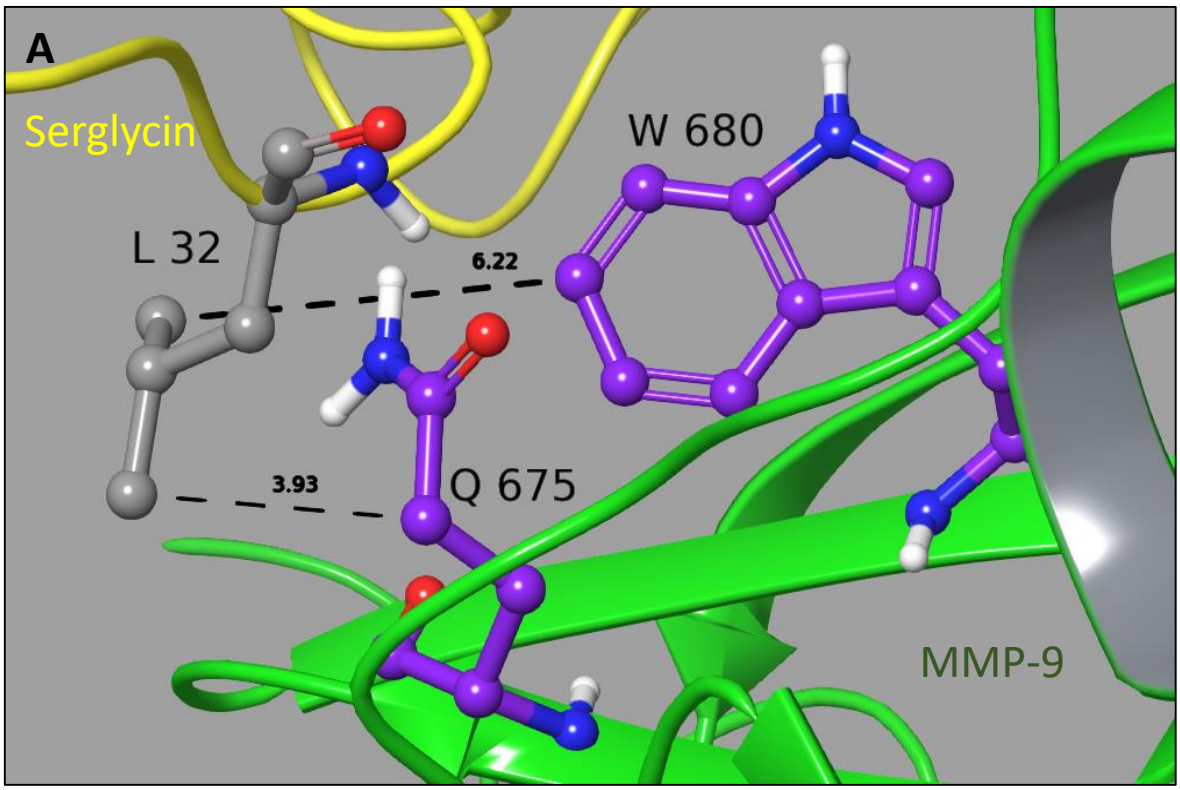

B

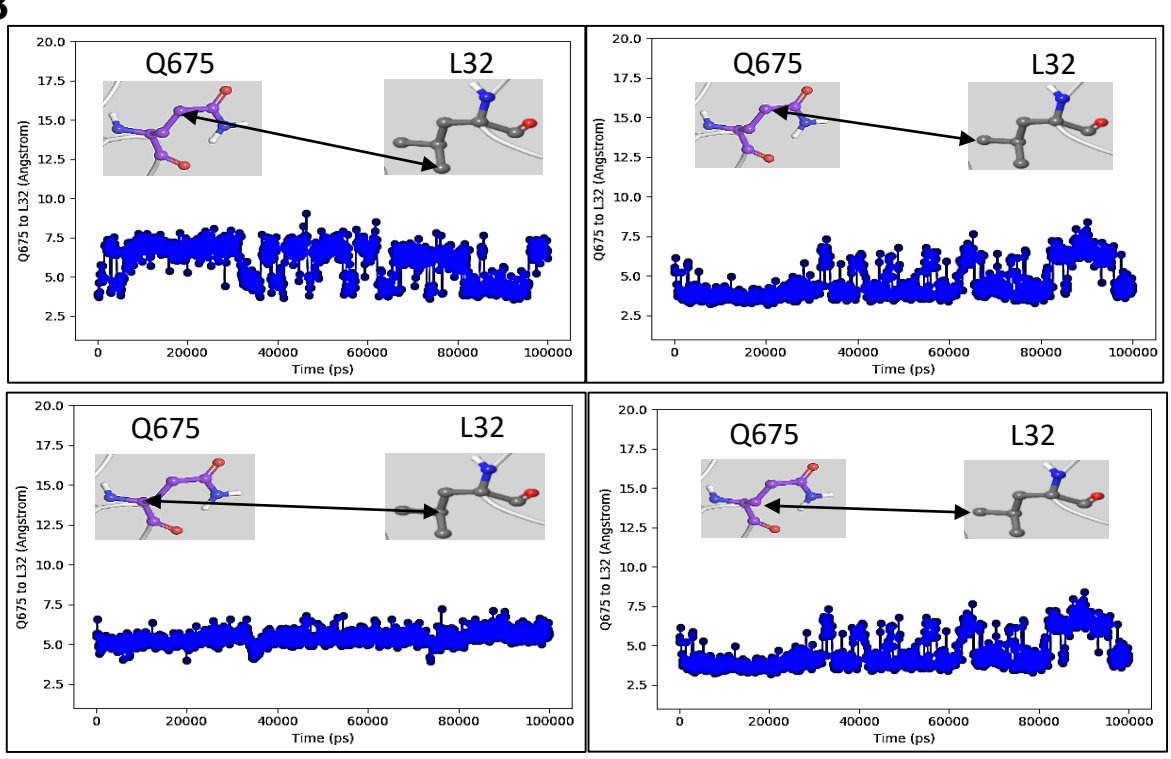

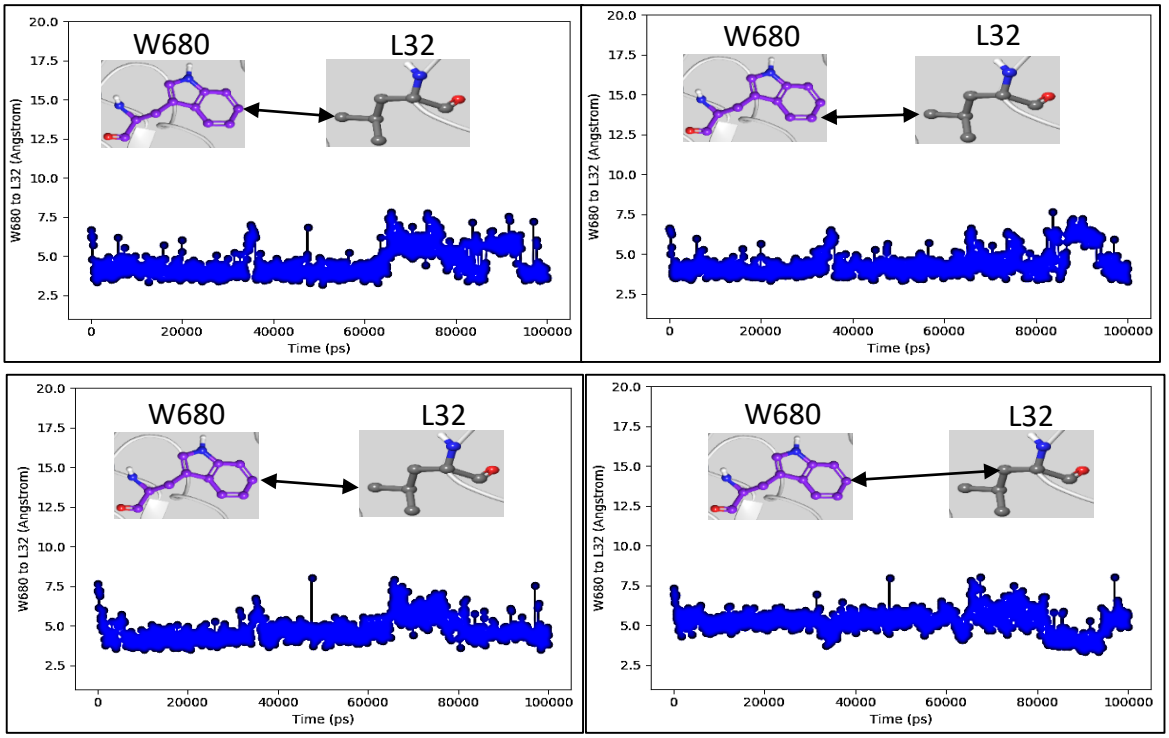
W680
L32
W680 to L32 (Angstrom)
Time (ps)
20.0
17.5
15.0
12.5
10.0
7.5
5.0
2.5
0
20000
40000
60000
80000
100000

S8.5 A: Hydrogen bond and hydrophobic interactions between the L659 (MMP-9HPX) side chain and main chain amide NH with main and side chain in L32 and P34 in SG. Backbone MMP-9 HPX (green) and SG N-terminal ^{1}Y-^{66}Y (yellow). Carbons in MMP-9 (purple) and SG (grey), oxygens (red), nitrogens (dark blue) and hydrogens (white).

S8.5 B: The 100 ns trajectory of these interactions.

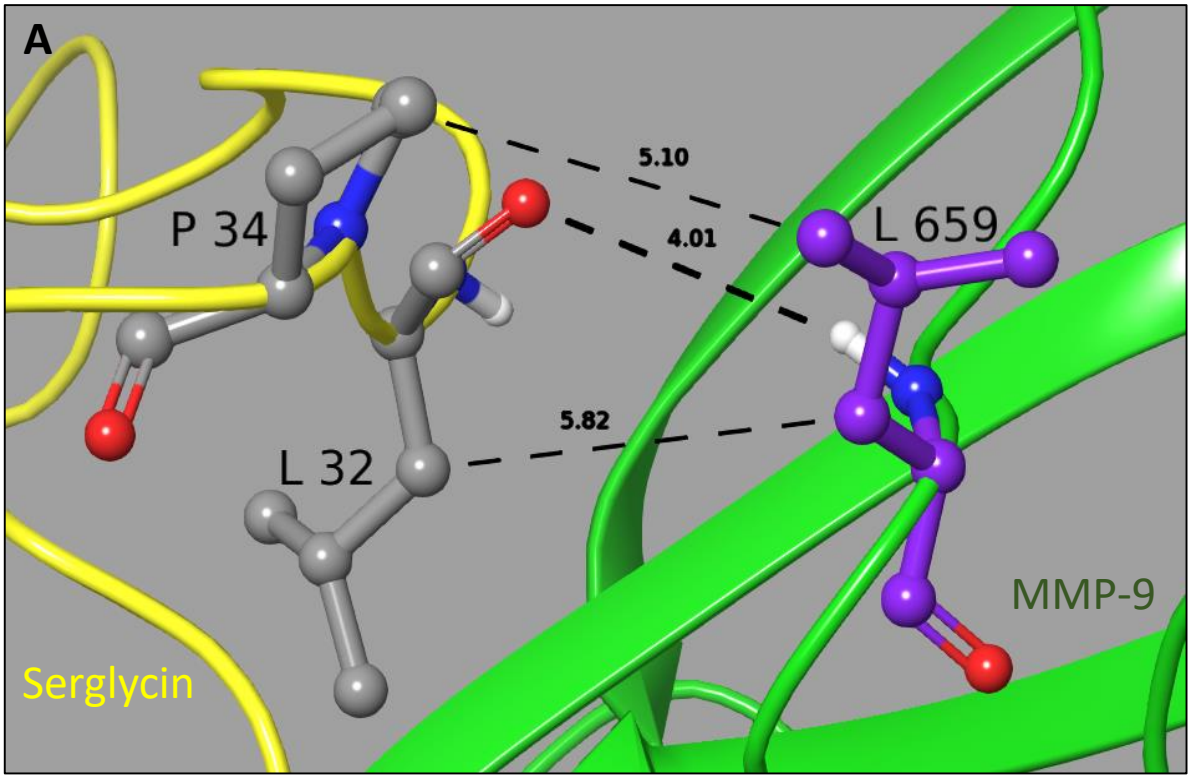

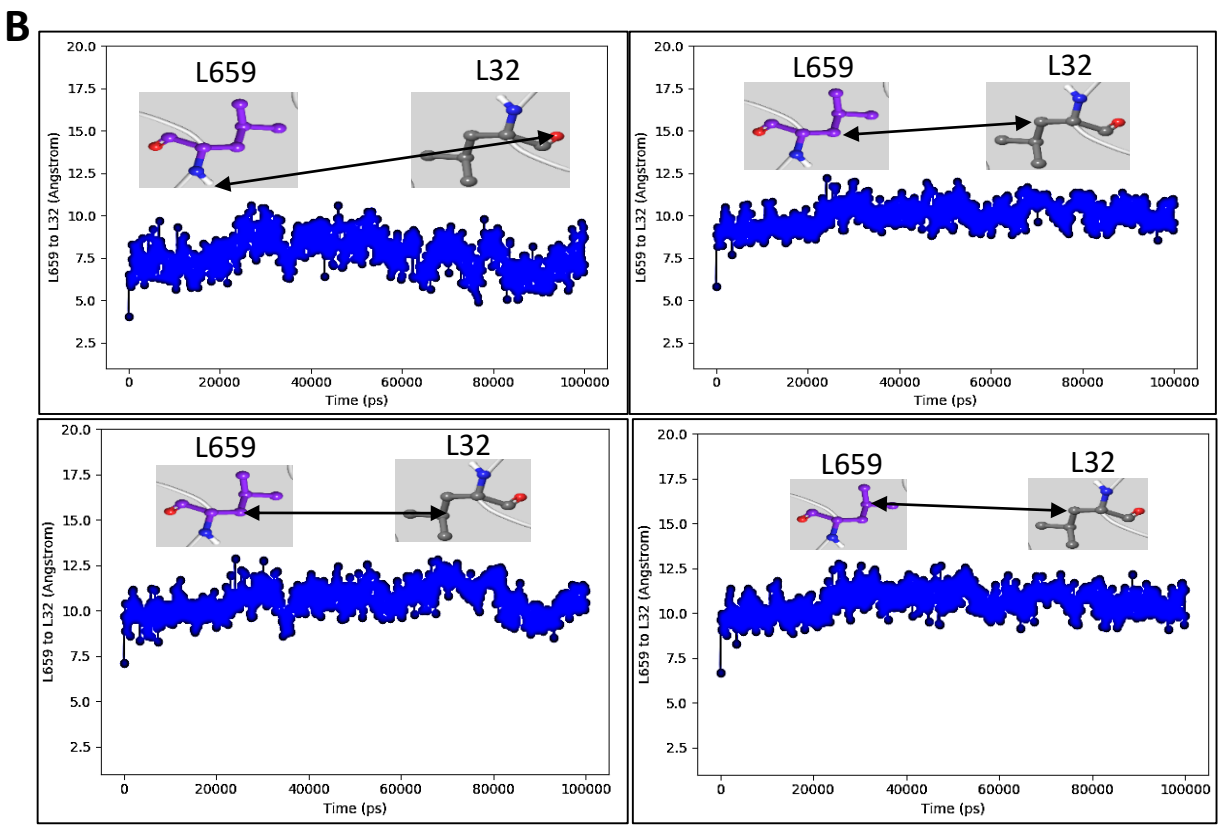

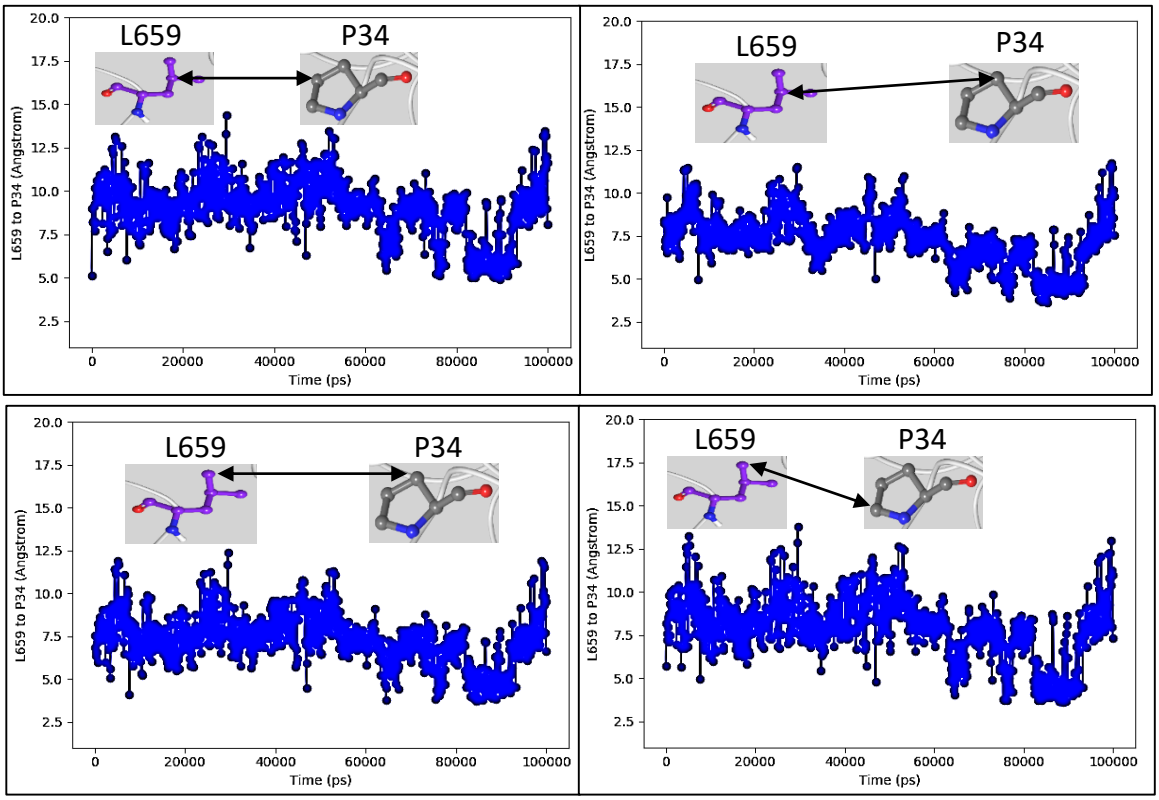
L659
P34
L659 to P34 (Angstrom)
Time (ps)
0
20000
40000
60000
80000
100000
2.5
5.0
7.5
10.0
12.5
15.0
17.5
20.0

S8.6 A: Hydrophobic interactions of the side chain L43 (SG) with the hydrophobic parts of the side chains R677 and T698 in MMP-9HPX. Backbone MMP-9 HPX (green), SG N-terminal ^{1}Y-^{66}Y (yellow) and SG C-terminal ^{86}F-^{131}L (orange). Carbons in MMP-9 (purple) and SG (grey), oxygens (red), nitrogens (dark blue) and hydrogens (white).

S8.6 B: The 100 ns trajectory of these interactions.

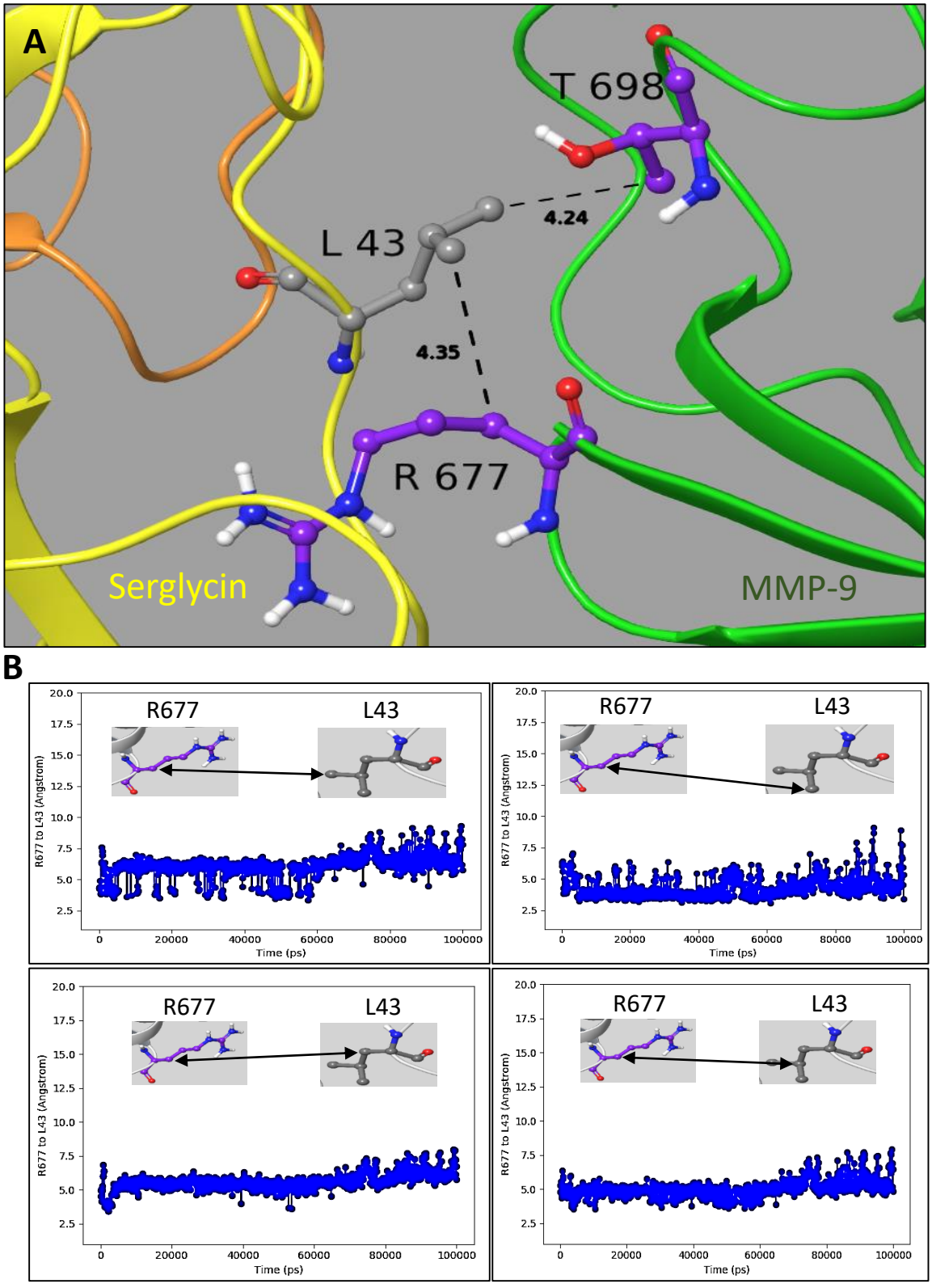

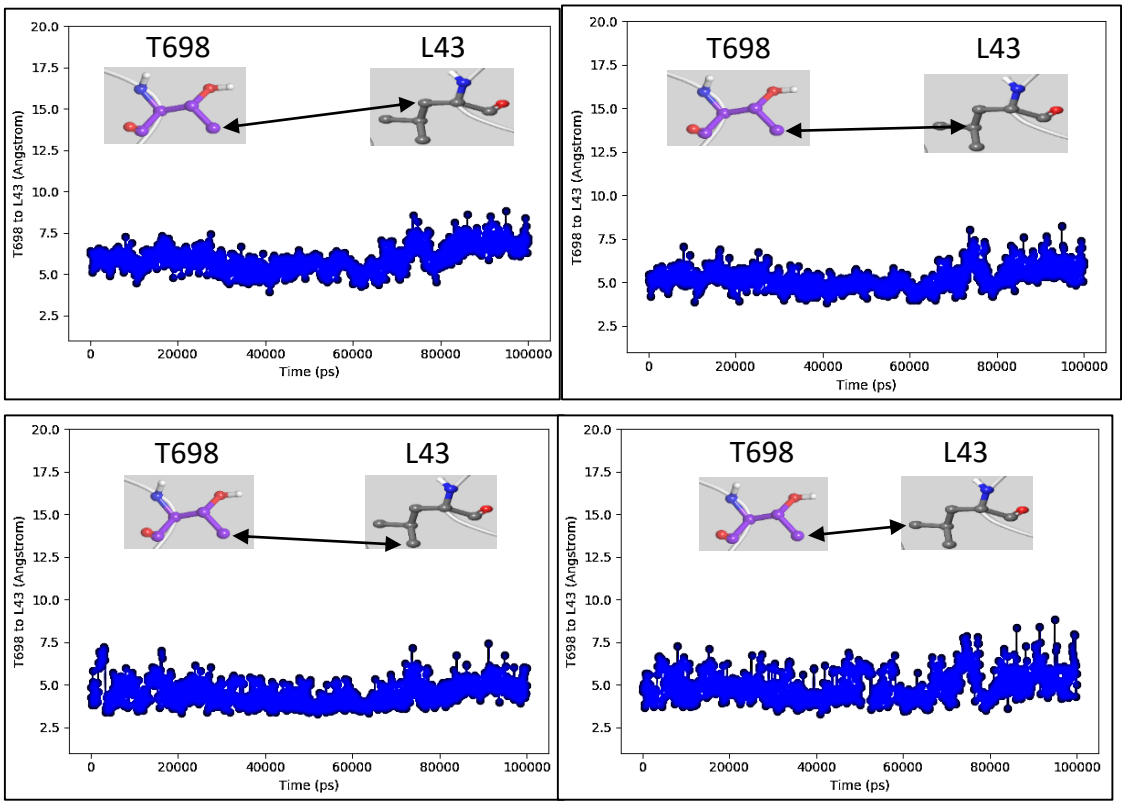
T698
L43
T698 to L43 (Angstrom)
Time (ps)
20.0
17.5
15.0
12.5
10.0
7.5
5.0
2.5
0
20000
40000
60000
80000
100000

S8.7 A: Hydrophobic interactions of the side chain M29 (SG) with the Cα-G695 and the side chain in V691 in MMP-9HPX. Backbone MMP-9 HPX (green), SG N-terminal ^{1}Y-^{66}Y (yellow) and SG C-terminal ^{86}F-^{131}L (orange). Carbons in MMP-9 (purple) and SG (grey), oxygens (red), nitrogens (dark blue) and hydrogens (white).

S8.7 B: The 100 ns trajectory of these interactions.

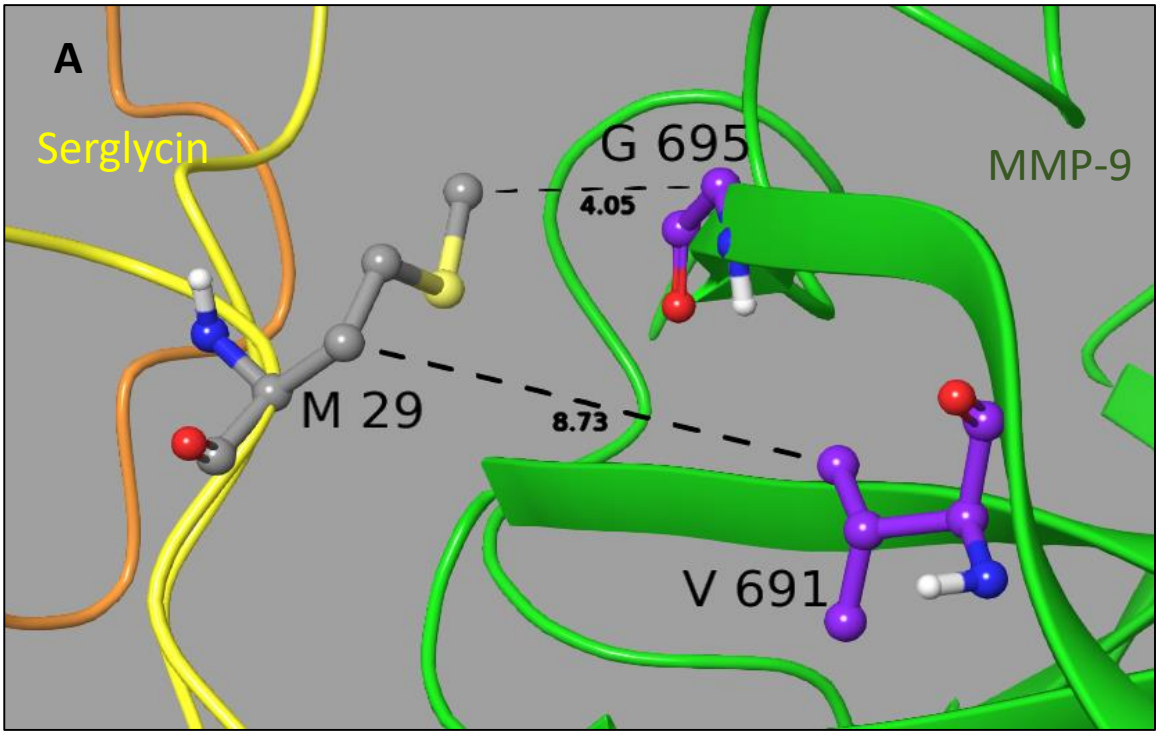

B

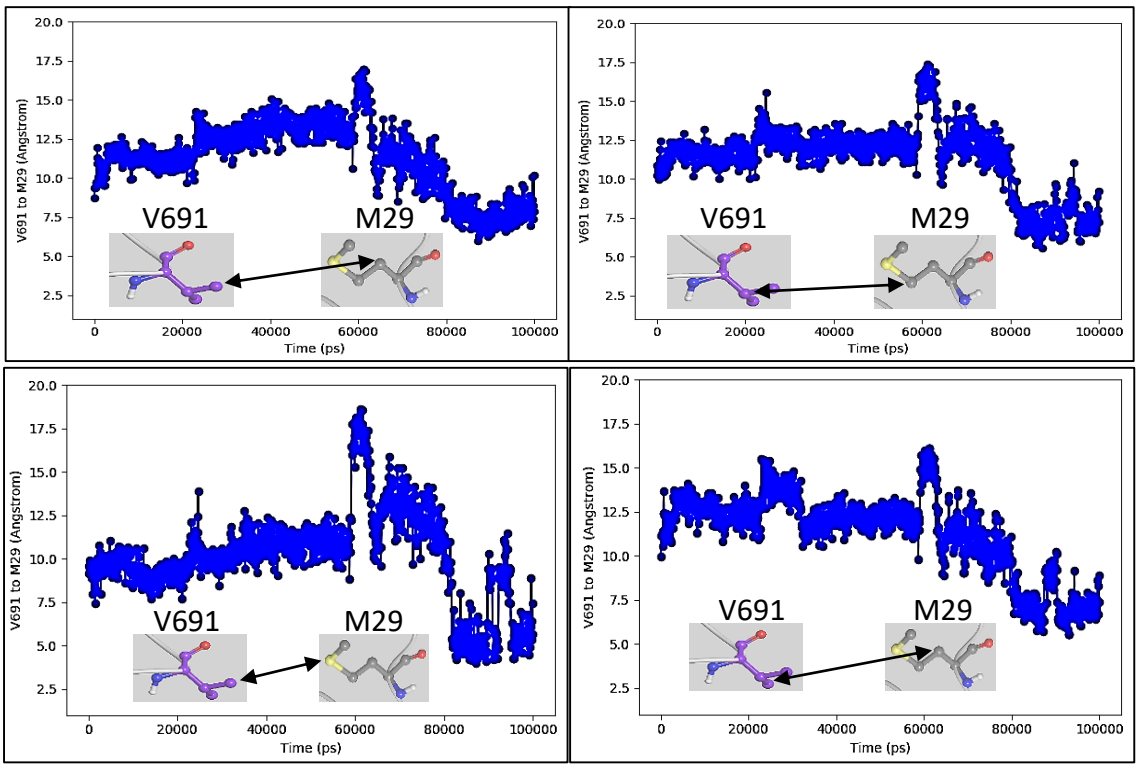

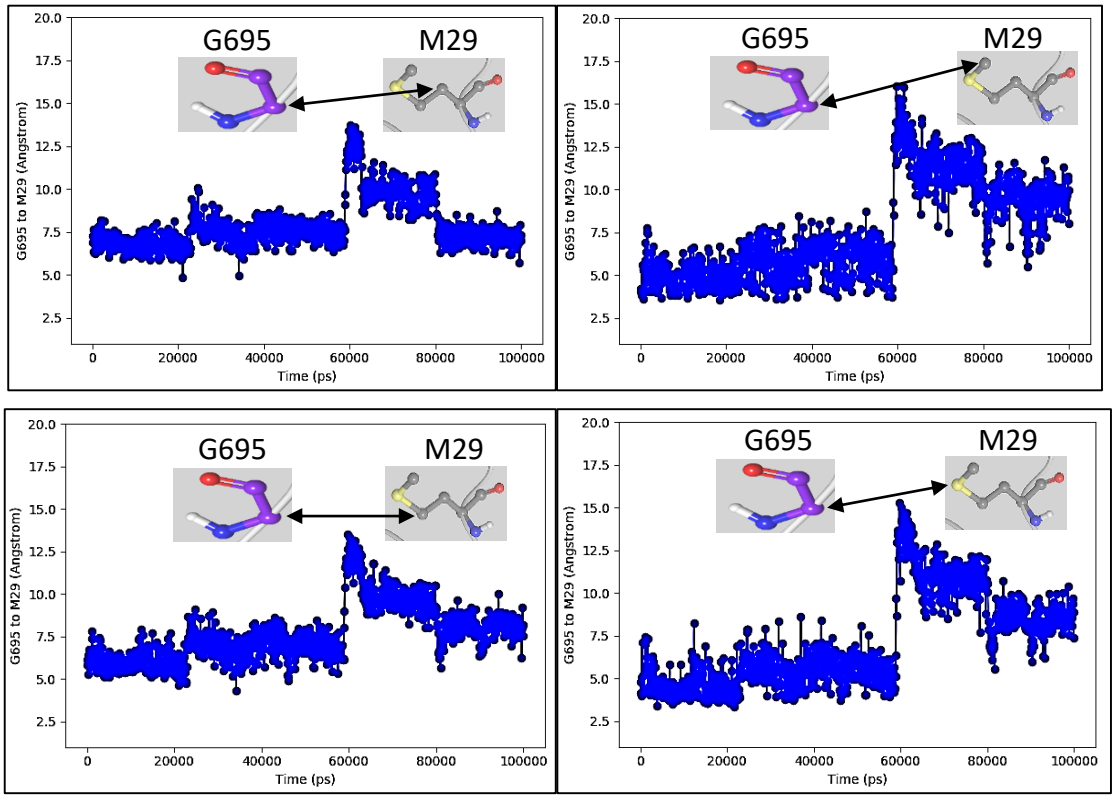
G695
M29
G695 to M29 (Angstrom)
Time (ps)
20.0
17.5
15.0
12.5
10.0
7.5
5.0
2.5
0
20000
40000
60000
80000
100000

S8.8 A: Hydrogen bond and hydrophobic interactions between the Y696 (MMP-9HPX) side chain with main and side chain in P28 and side chain of L43 in SG. Backbone MMP-9 HPX (green) and SG N-terminal ^{1}Y-^{66}Y (yellow). Carbons in MMP-9 (purple) and SG (grey), oxygens (red), nitrogens (dark blue) and hydrogens (white).

S8.8 B: The 100 ns trajectory of these interactions.

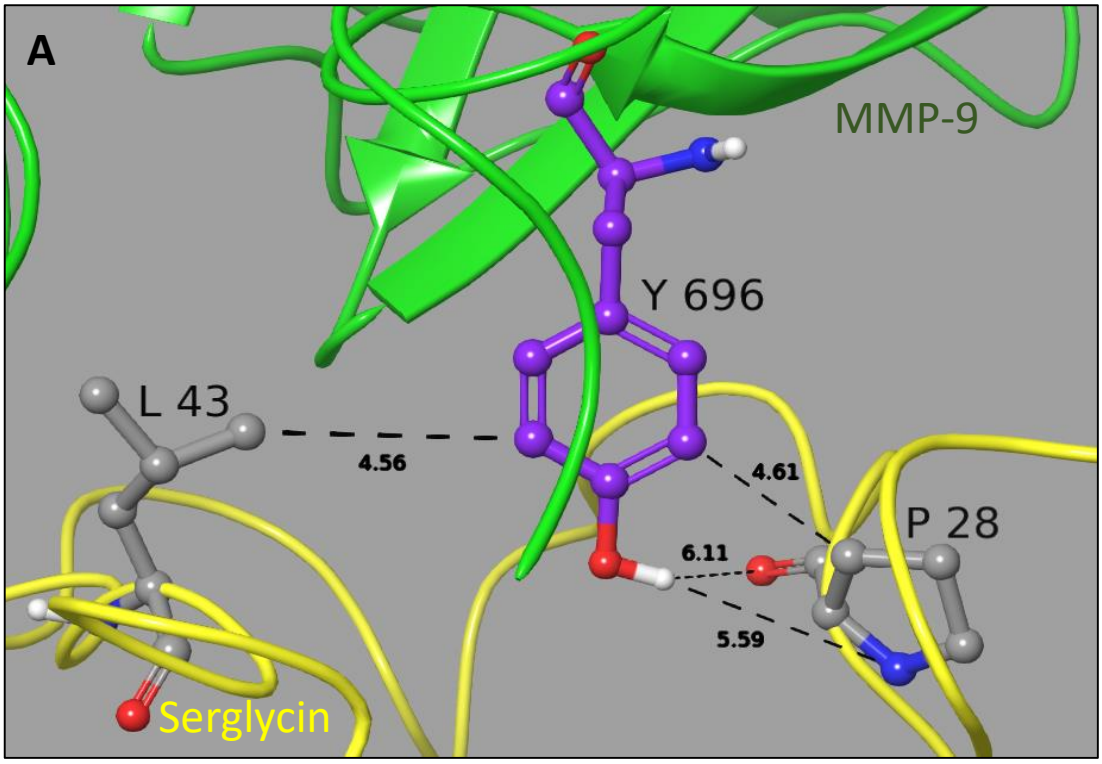

B

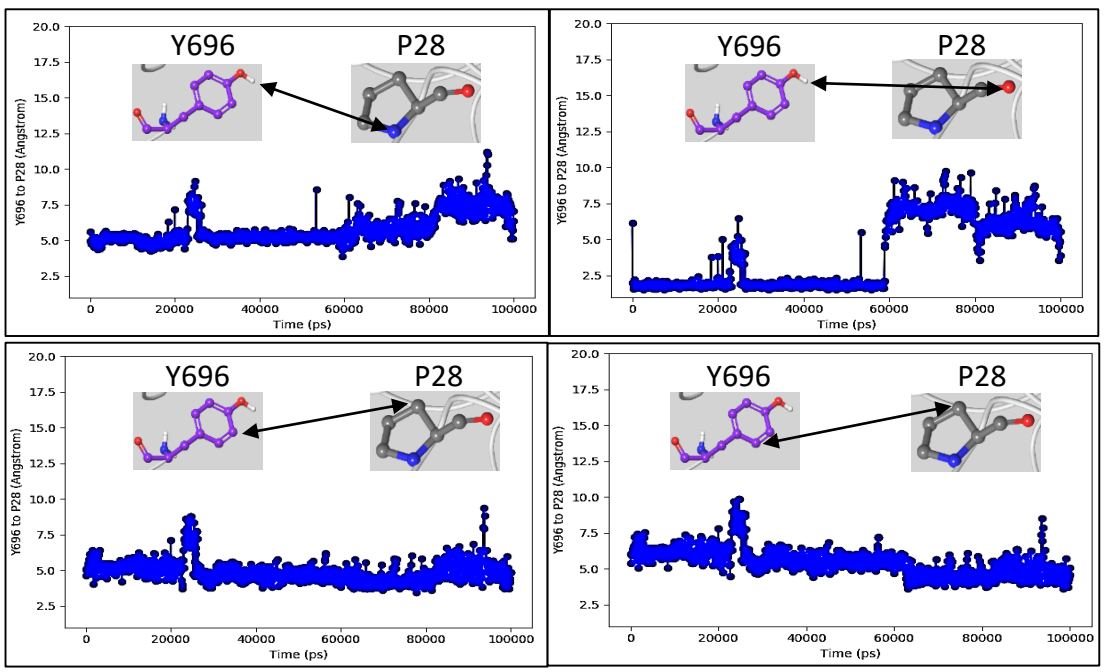

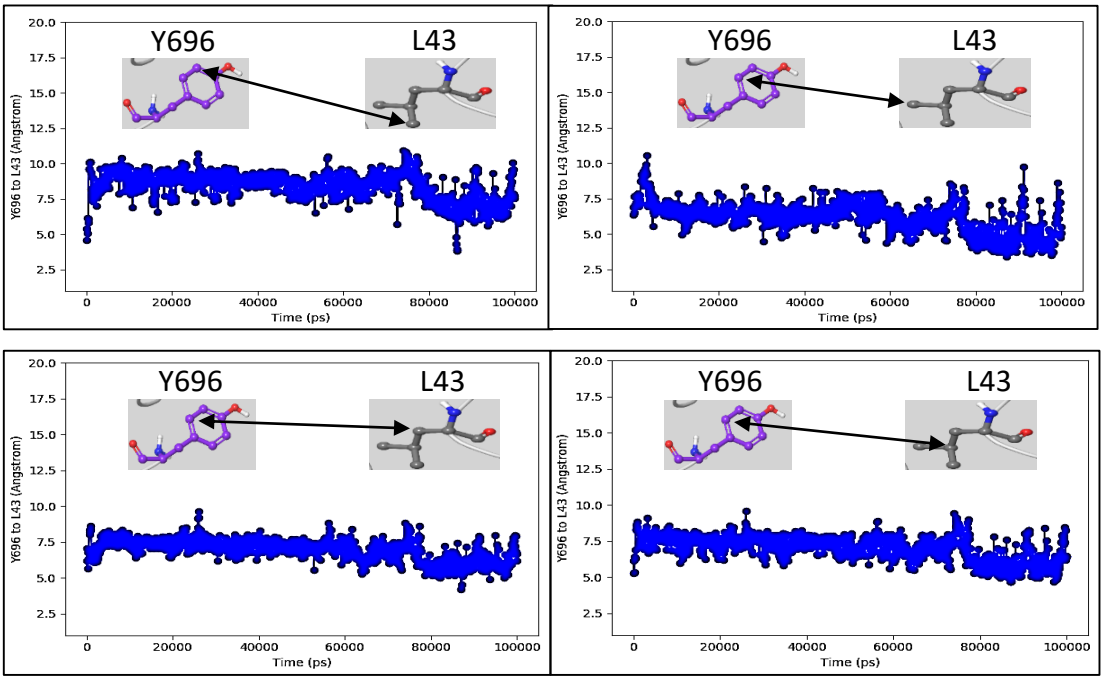
Y696
L43
Y696 to L43 (Angstrom)
Time (ps)
20.0
17.5
15.0
12.5
10.0
7.5
5.0
2.5
0
20000
40000
60000
80000
100000

S8.9 A: Hydrogen bond and hydrophobic interactions between the Y699 (MMP-9HPX) side chain with main and side chain in L47 and main chain NH of L43 in SG. Backbone MMP-9 HPX (green), SG N-terminal ^{1}Y-^{66}Y (yellow) and SG C-terminal ^{86}F-^{131}L (orange). Carbons in MMP-9 (purple) and SG (grey), oxygens (red), nitrogens (dark blue) and hydrogens (white).

S8.9 B: The 100 ns trajectory of these interactions.

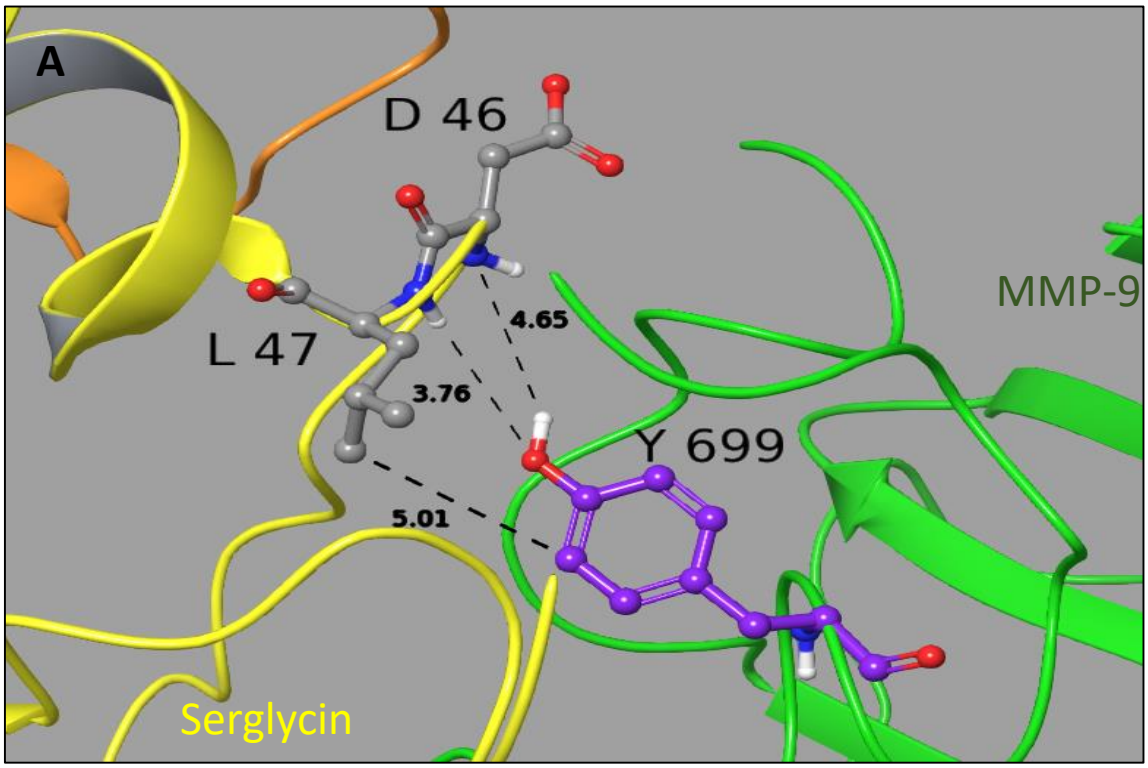

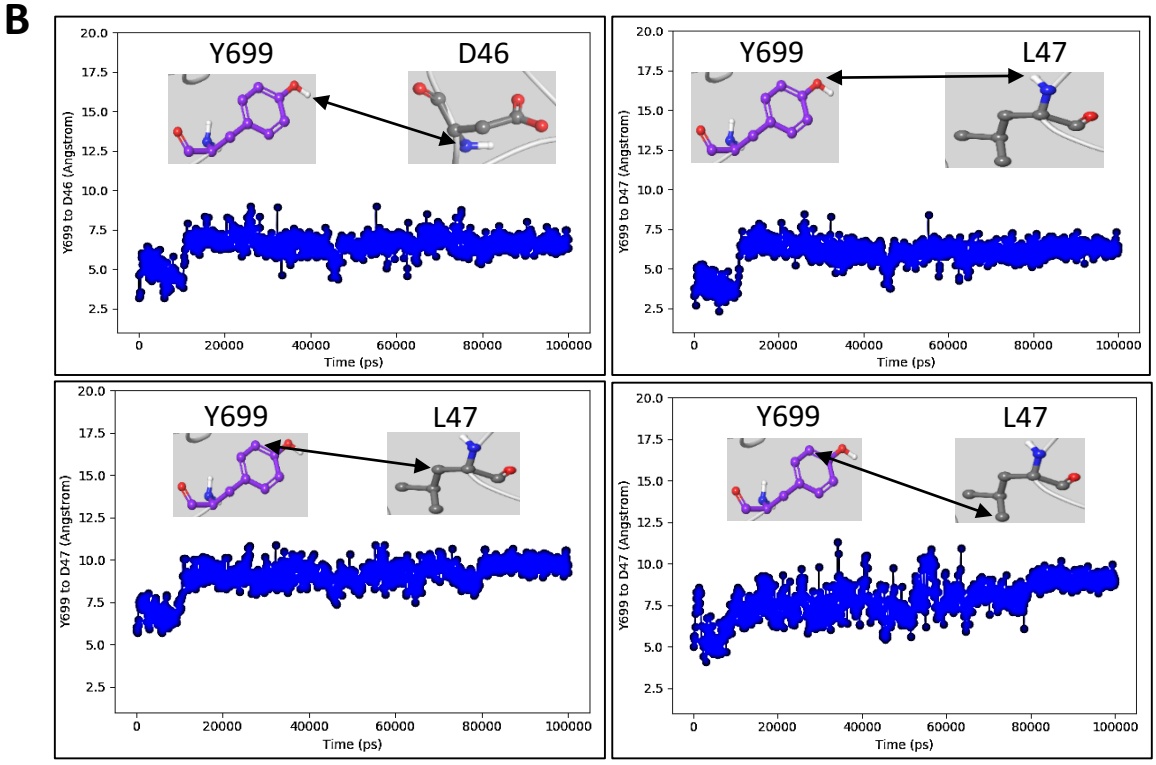

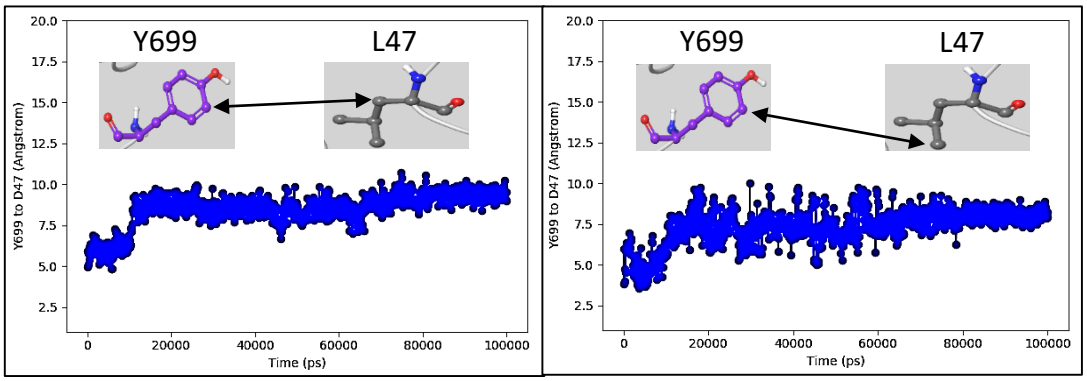
Y699
L47
Y699 to D47 (Angstrom)
Time (ps)
20.0
17.5
15.0
12.5
10.0
7.5
5.0
2.5
0
20000
40000
60000
80000
100000
Y699
L47
Y699 to D47 (Angstrom)
Time (ps)

S8.10 A: Hydrophobic interactions of the methylene group in the side chain D707 (MMP-9HPX) with side chain in L47 (SG). Backbone MMP-9 HPX (green), SG N-terminal ^{1}Y-^{66}Y (yellow), SG C-terminal ^{86}F-^{131}L (orange) and SG Ser-Gly repeats ^{67}S-^{84}G (blue). Carbons in MMP-9 (purple) and SG (grey), oxygens (red), nitrogens (dark blue) and hydrogens (white).

S8.10 B: The 100 ns trajectory of these interactions.

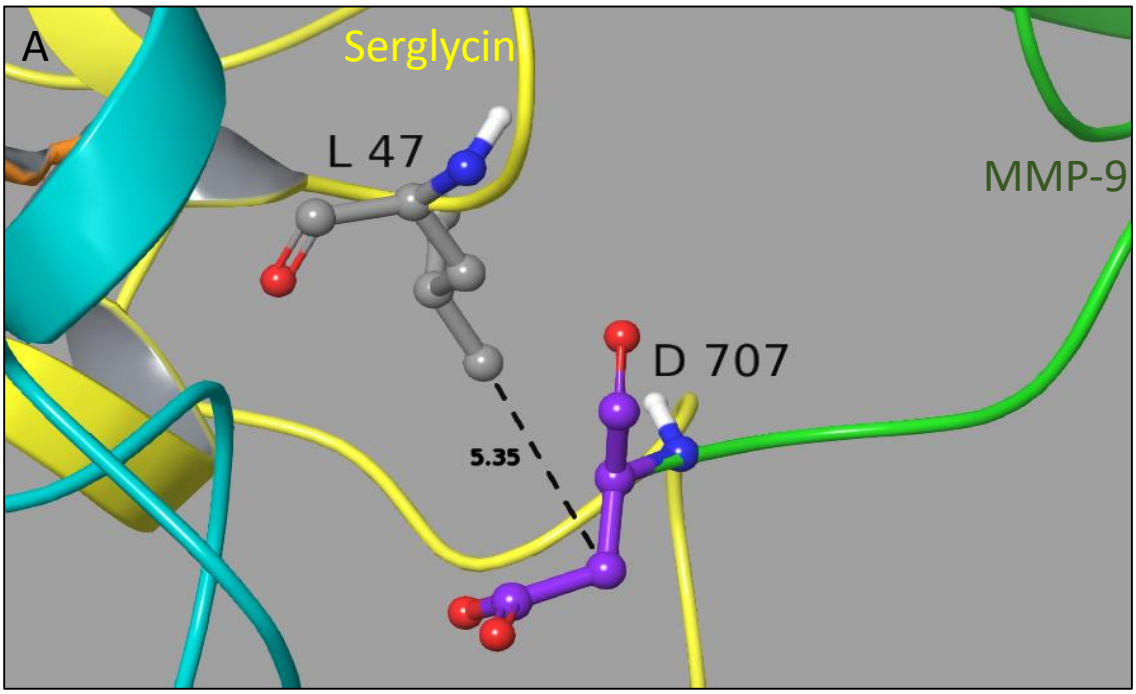

B

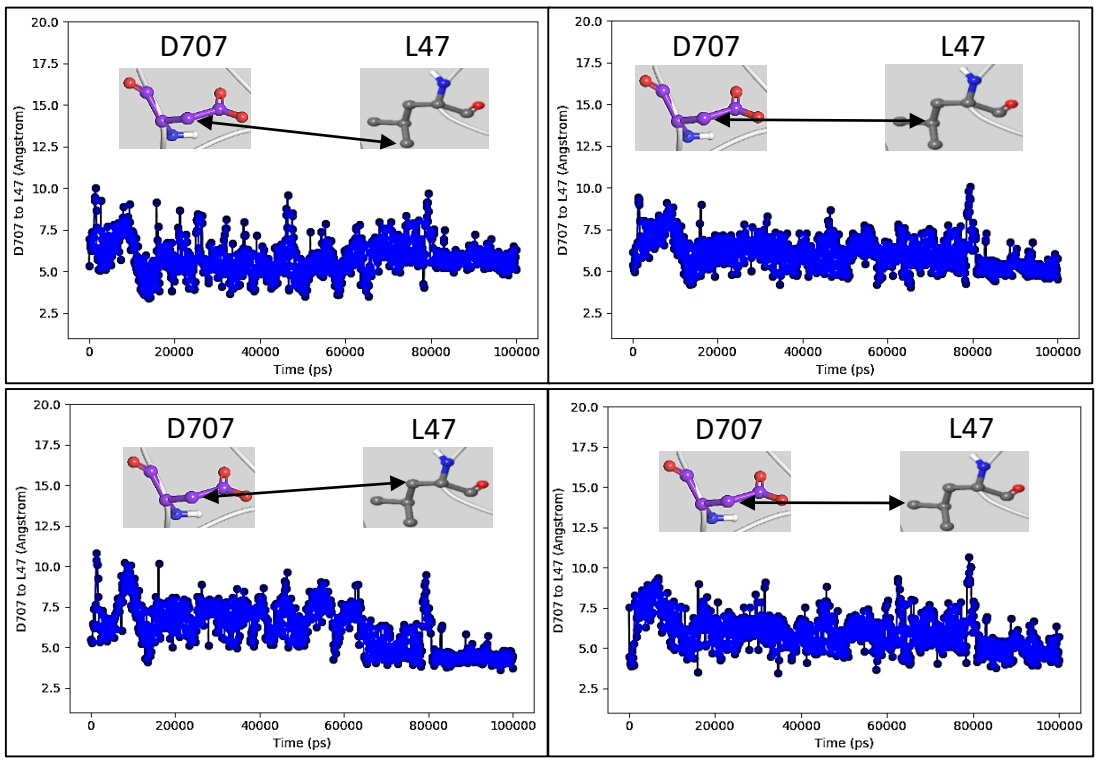

Fig. S9: Docking and molecular dynamic simulations of the interactions between the MMP-9HPX domain and the SG core protein:

Model 2. Distances between selected atoms are shown in each A-figure and the double arrows in B-figures indicate the atoms for the trajectory.

S9.1 A: Ionic interactions between K623, R634 and R645 in MMP-9HPX and D97 and E98 in SG. Shown in the upper figure is the interactions after 1 ns and in the lower figure the intereactions after 50 ns. Backbone MMP-9 HPX (green), SG N-terminal ^{1}Y-^{66}Y (yellow), SG C-terminal ^{86}F-^{131}L (orange) and SG Ser-Gly repeats ^{67}S-^{84}G (blue). Carbons in MMP-9 (purple) and SG (grey), oxygens (red), nitrogens (dark blue) and hydrogens (white).

S9.1 B: The 100 ns trajectory of these interactions.

A

Trajectory frame at 1ns

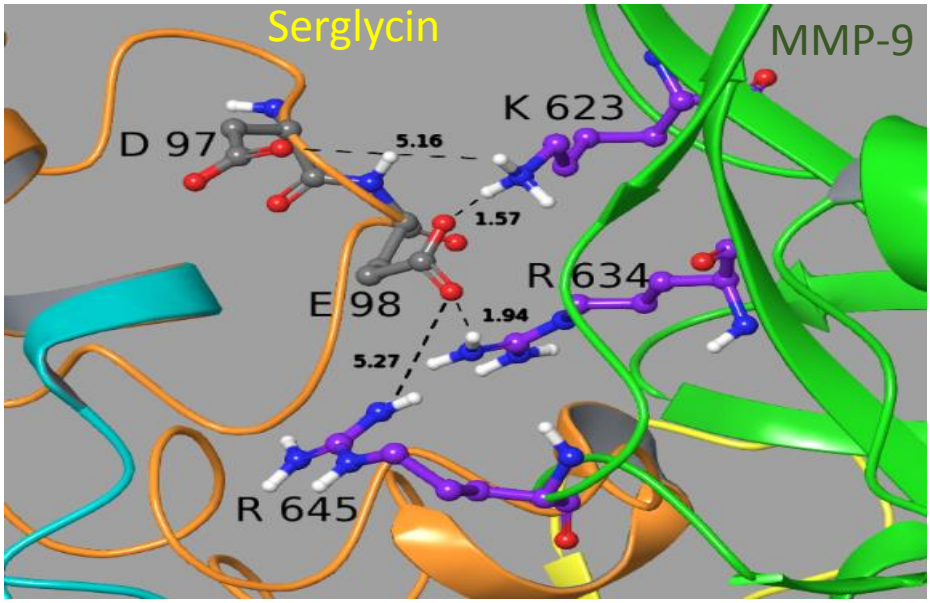

Trajectory frame at 50ns

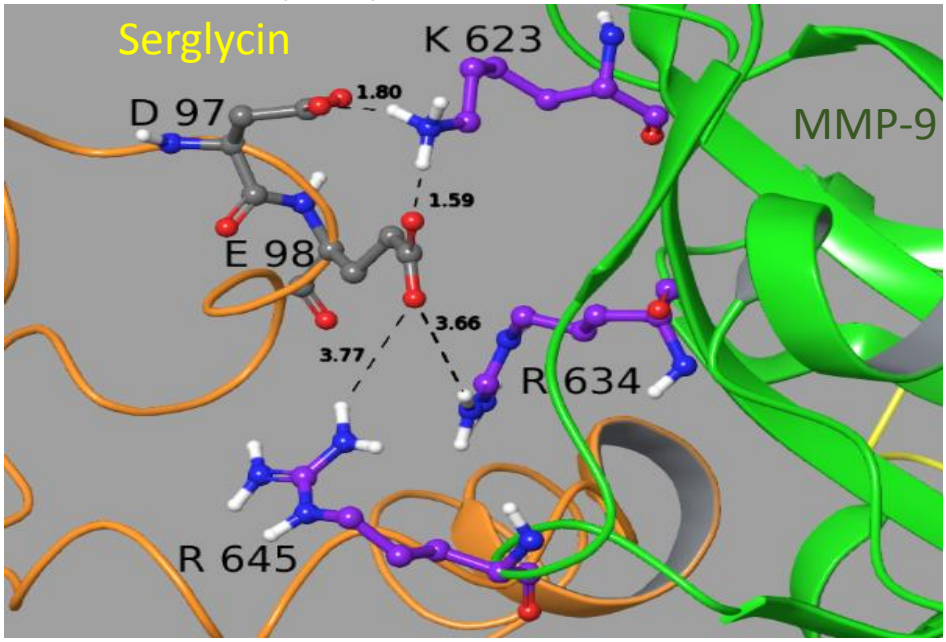

B

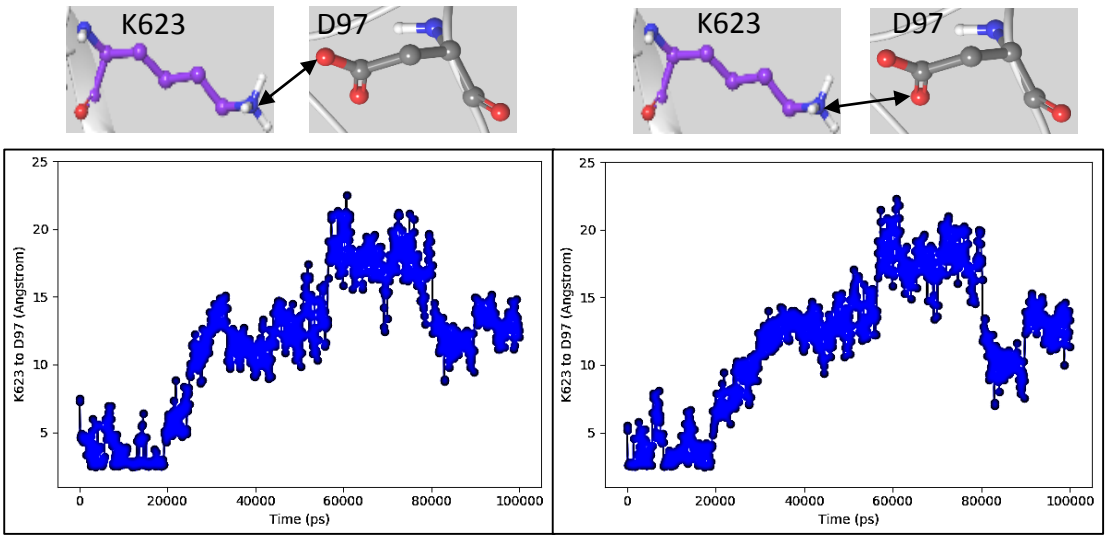
K623
D97
K623
D97
K623 to D97 (Angstrom)
Time (ps)
K623 to D97 (Angstrom)
Time (ps)

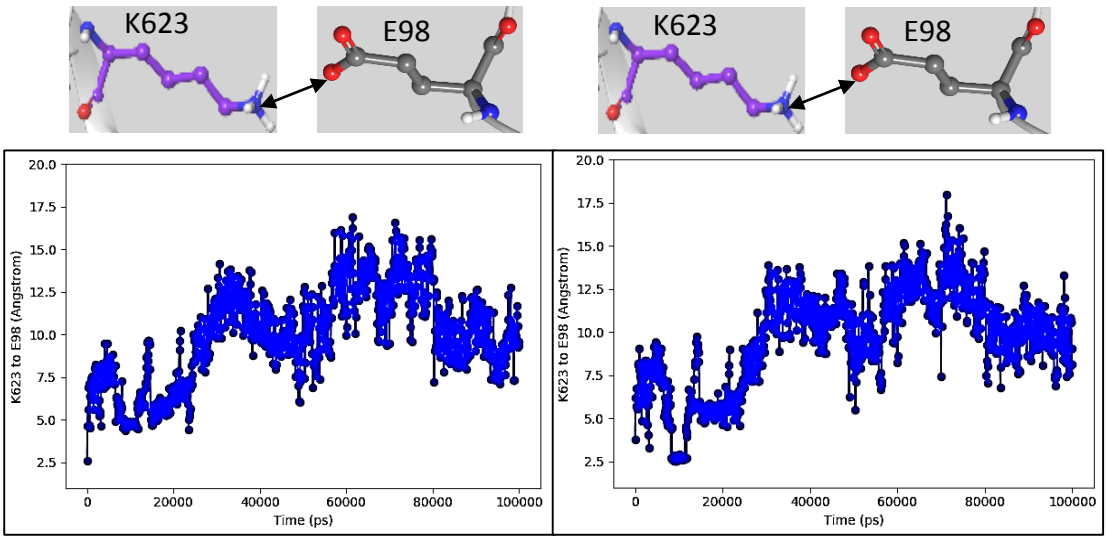
K623
E98
K623
E98
K623 to E98 (Angstrom)
Time (ps)
K623 to E98 (Angstrom)
Time (ps)

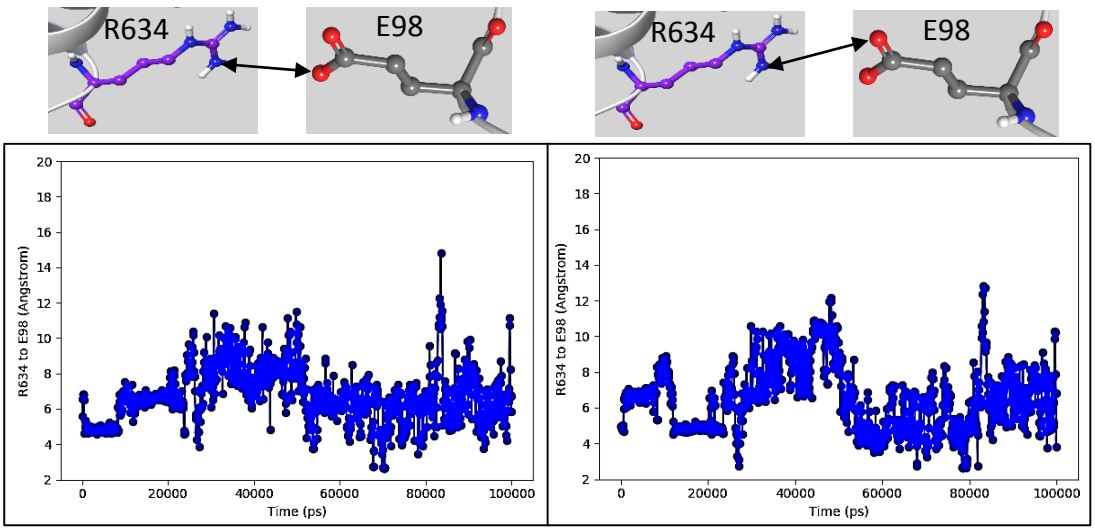
R634
E98
R634
E98
R634 to E98 (Angstrom)
Time (ps)
R634 to E98 (Angstrom)
Time (ps)

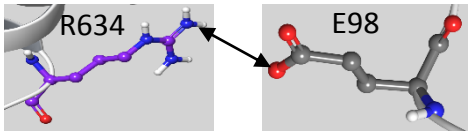
R634
E98

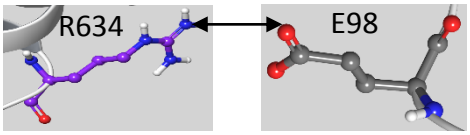
R634
E98

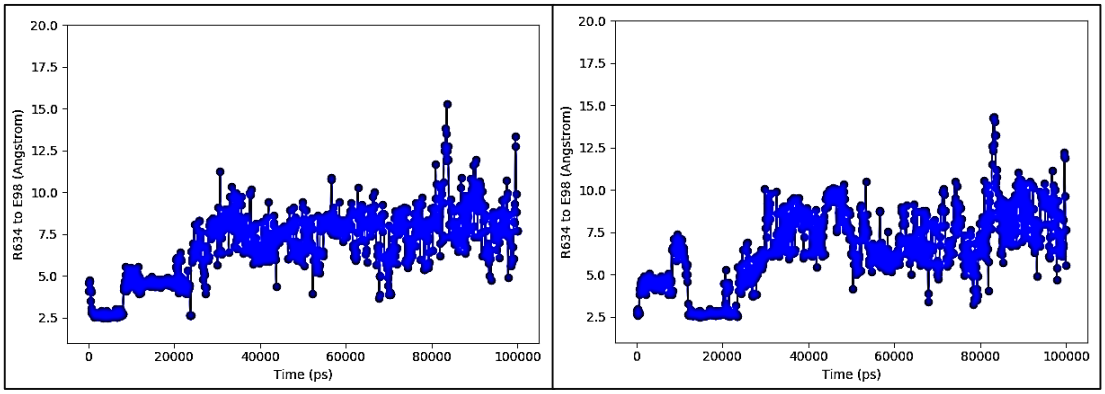
R634 to E98 (Angstrom)
Time (ps)
R634 to E98 (Angstrom)
Time (ps)

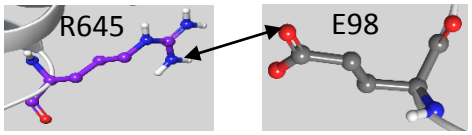
R645
E98

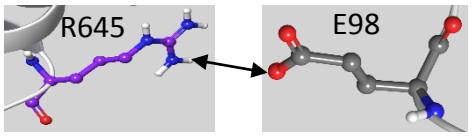
R645
E98

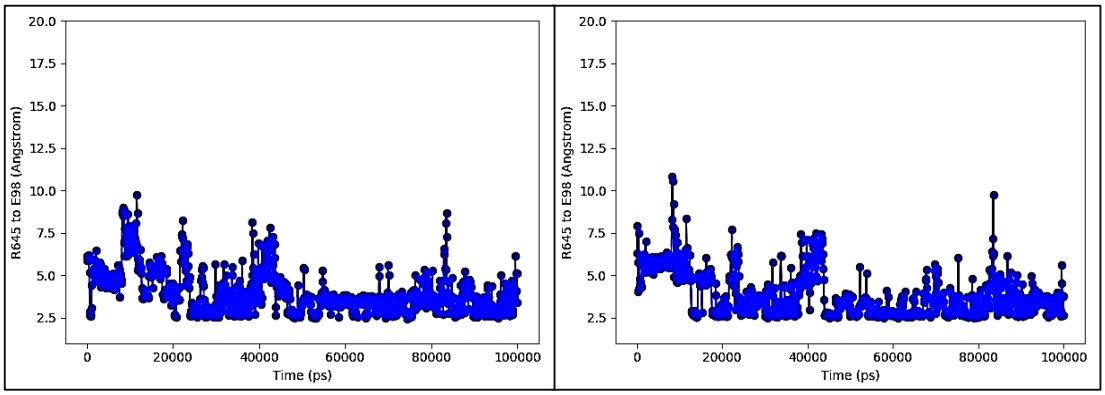
R645 to E98 (Angstrom)
Time (ps)
R645 to E98 (Angstrom)
Time (ps)

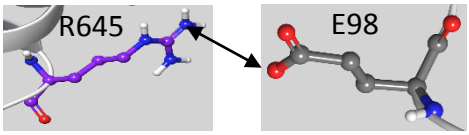
R645
E98

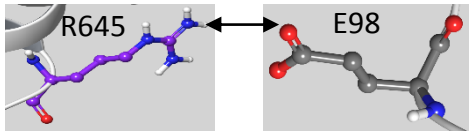
R645
E98

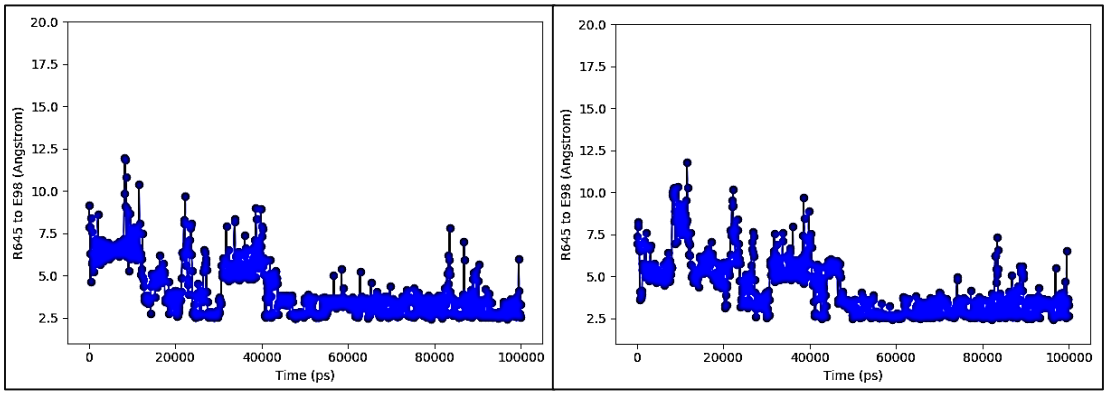
R645 to E98 (Angstrom)
Time (ps)
R645 to E98 (Angstrom)
Time (ps)

S9.2 A: Hydrophobic interactions between the methylene group in the side chain of S646 and the methyl group in A647 in MMP-9HPX with side chains of P114 and L113 in SG. Backbone MMP-9 HPX (green), SG C-terminal ^{86}F-^{131}L (orange) and SG Ser-Gly repeats ^{67}S-^{84}G (blue). Carbons in MMP-9 (purple) and SG (grey), oxygens (red), nitrogens (dark blue) and hydrogens (white).

S9.2 B: The 100 ns trajectory of the these interactions.

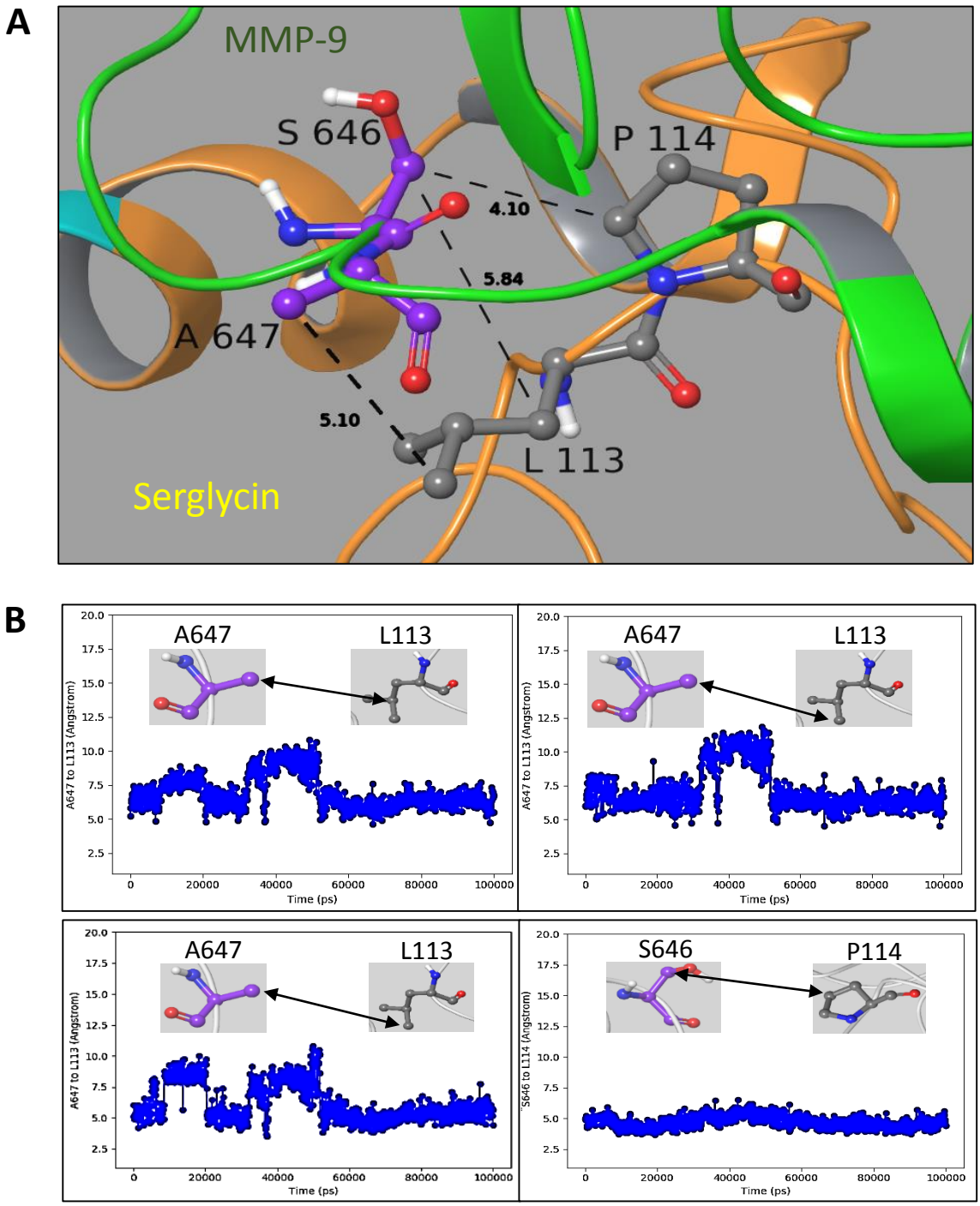

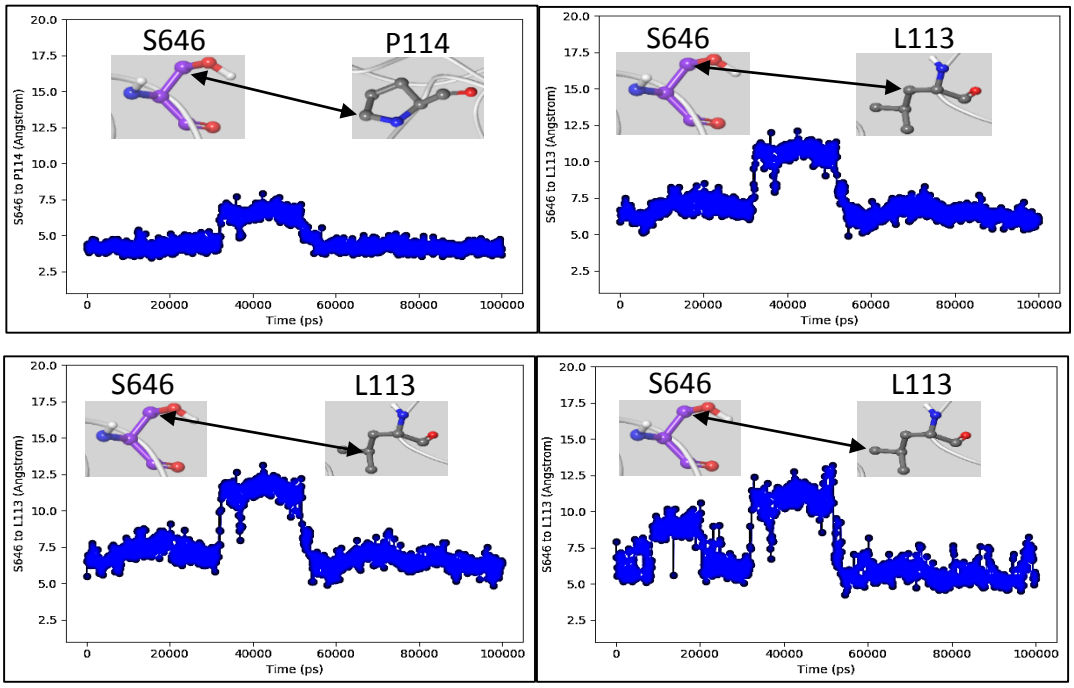
S646
P114
S646 to P114 (Angstrom)
Time (ps)
S646
L113
S646 to L113 (Angstrom)
Time (ps)
S646
L113
S646 to L113 (Angstrom)
Time (ps)
S646
L113
S646 to L113 (Angstrom)
Time (ps)

S9.3 A: A Hydrogen bond and hydrophobic interactions between the side chain in S648 (MMP-9HPX) with the side chain and the main chain amide CO in P114 (SG). Backbone MMP-9 HPX (green), SG N-terminal ^{1}Y-^{66}Y (yellow) and SG C-terminal ^{86}F-^{131}L (orange). Carbons in MMP-9 (purple) and SG (grey), oxygens (red), nitrogens (dark blue) and hydrogens (white).

S9.3 B: The 100 ns trajectory of these interactions.

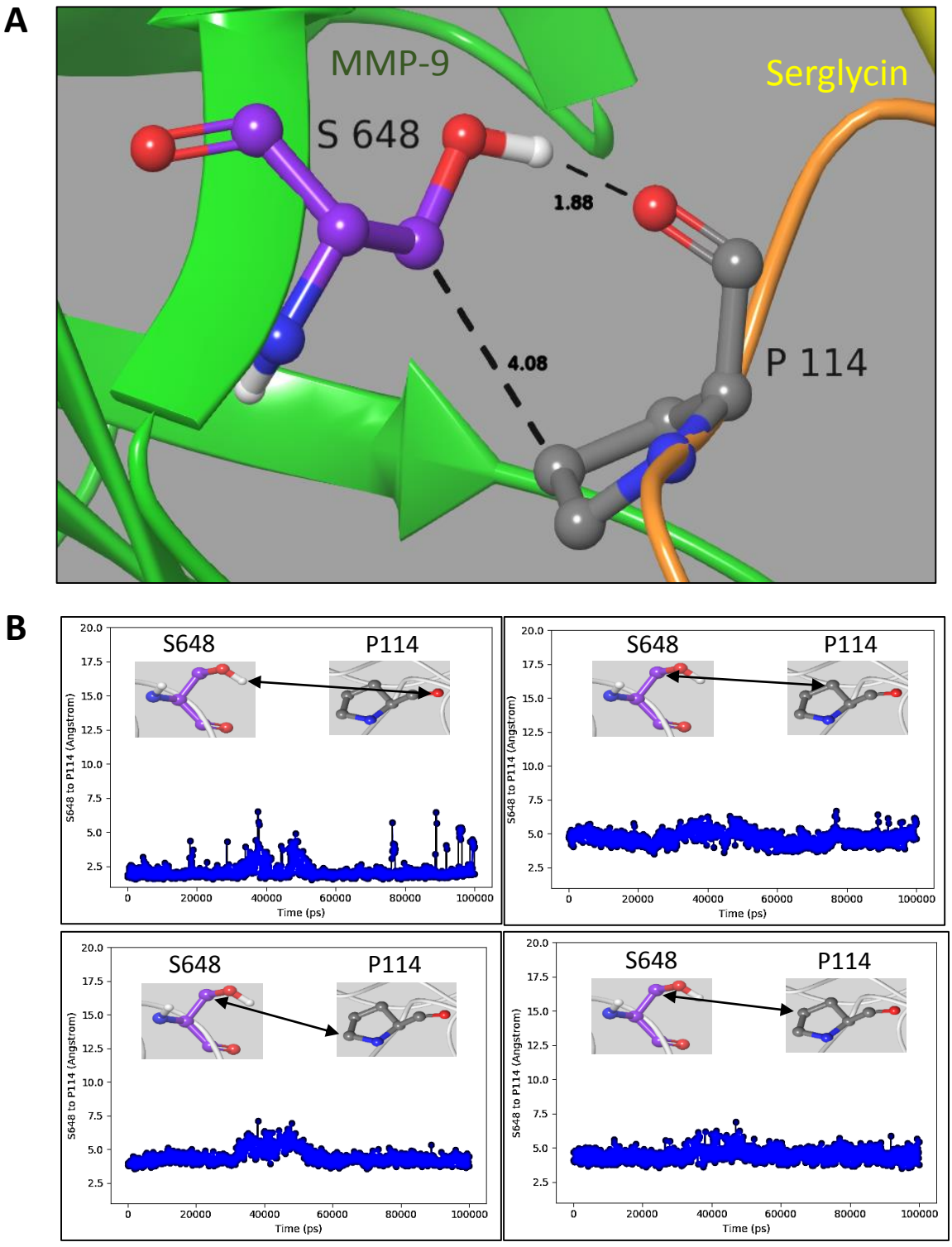

S9.4 A: A Hydrogen bond and hydrophobic interactions between the main and side chain in D651 (MMP-9HPX) with the main and side chain in L43 (SG). Backbone MMP-9 HPX (green), SG N-terminal ^{1}Y-^{66}Y (yellow) and SG Ser-Gly repeats ^{67}S-^{84}G (blue). Carbons in MMP-9 (purple) and SG (grey), oxygens (red), nitrogens (dark blue) and hydrogens (white).

S9.4 B: The 100 ns trajectory of these interactions.

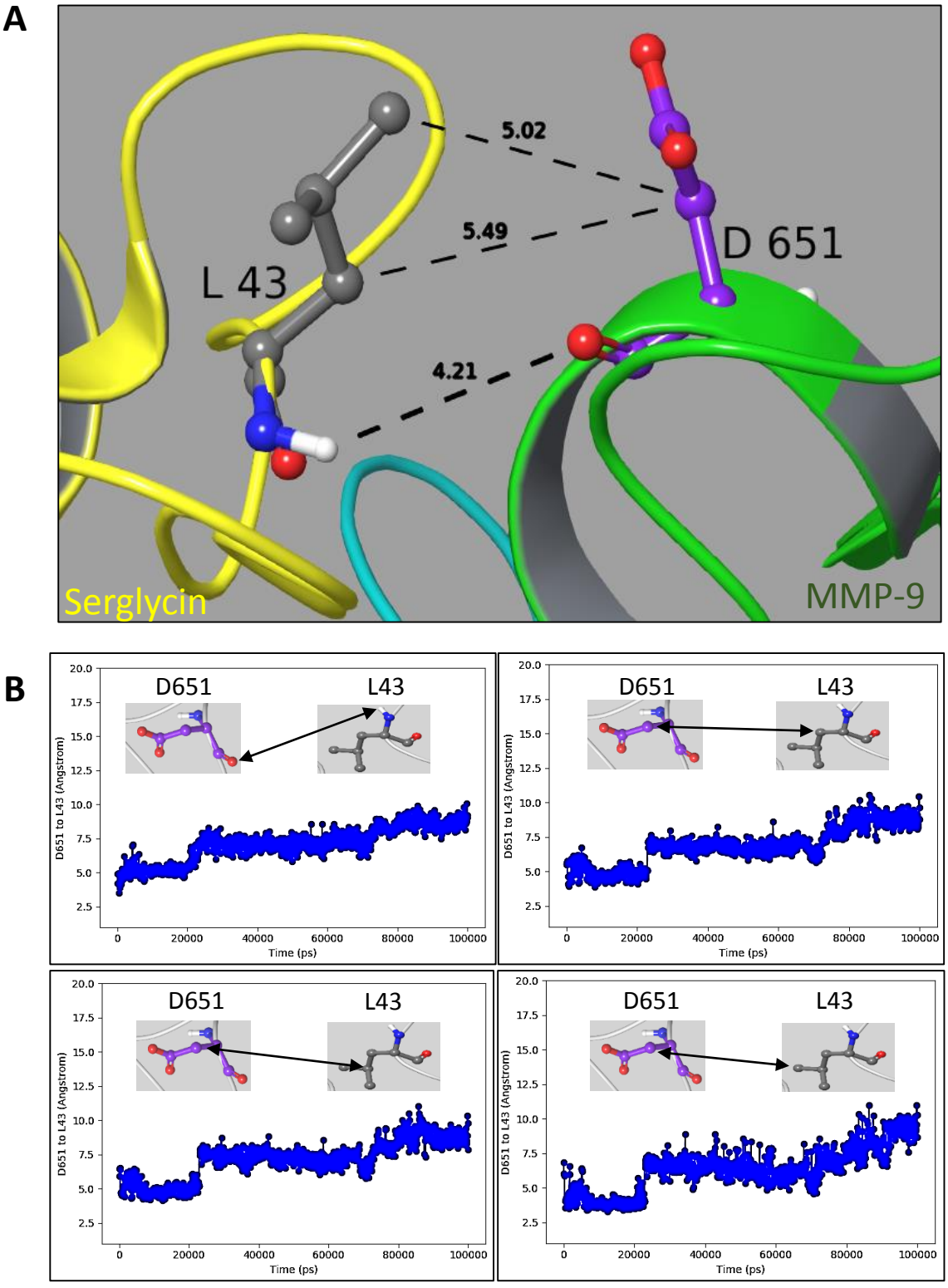

S9.5 A: Hydrogen bond and hydrophobic interactions between the main and side chain in R652 (MMP-9HPX) with the main and side chain in S115 and side chain in Q118 in SG. Backbone MMP-9 HPX (green), SG N-terminal ^{1}Y-^{66}Y (yellow) and SG C-terminal ^{86}F-^{131}L (orange). Carbons in MMP-9 (purple) and SG (grey), oxygens (red), nitrogens (dark blue) and hydrogens (white).

S9.5 B: The 100 ns trajectory of these interactions.

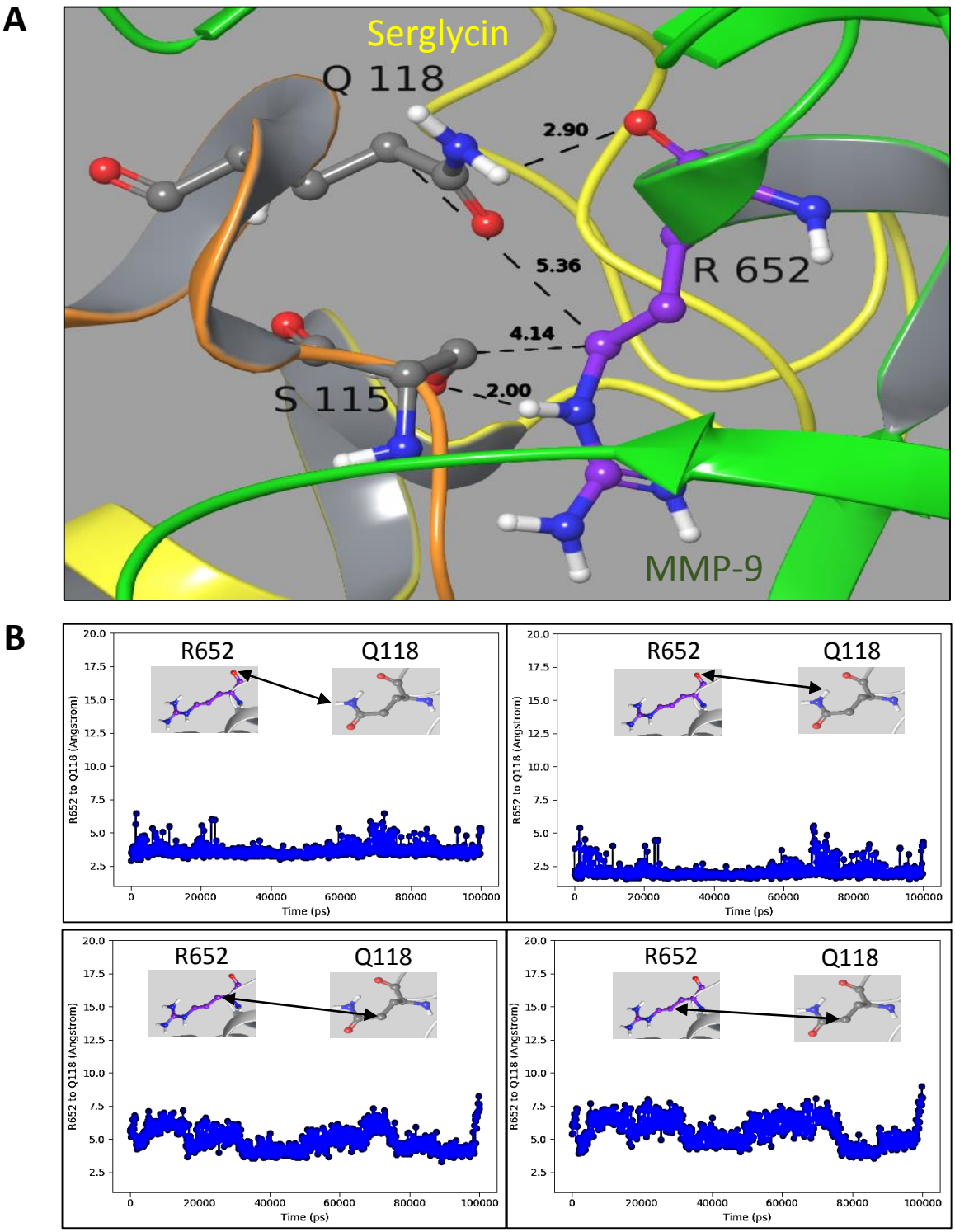

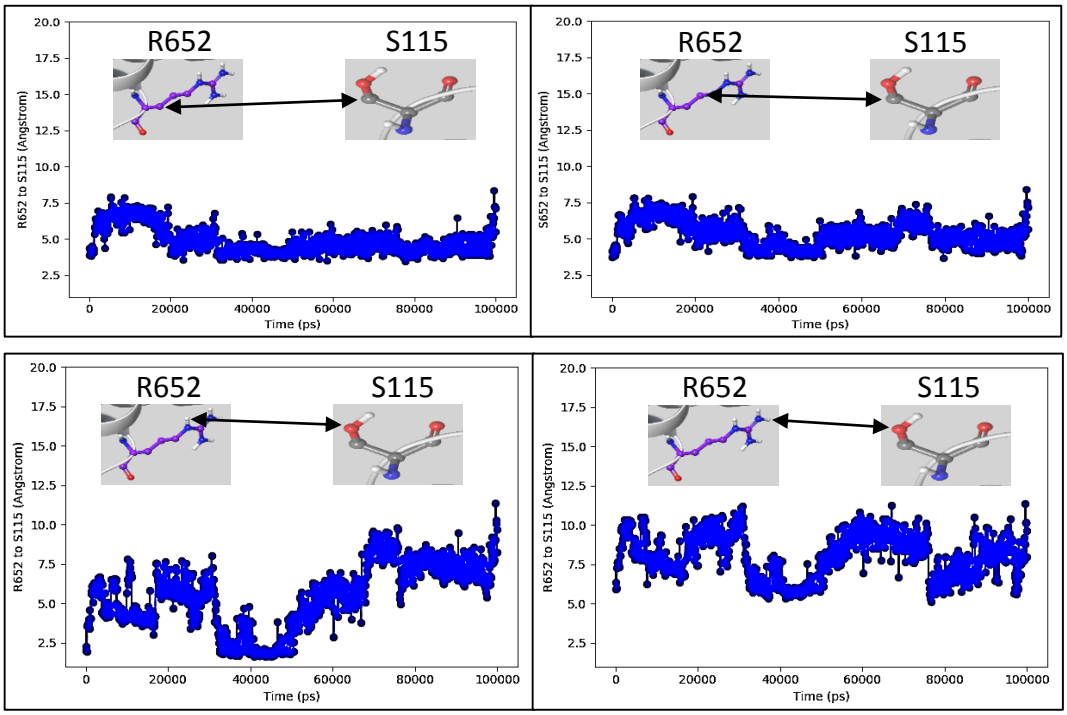
R652
S115
R652 to S115 (Angstrom)
Time (ps)
R652
S115
S652 to S115 (Angstrom)
Time (ps)
R652
S115
R652 to S115 (Angstrom)
Time (ps)
R652
S115
R652 to S115 (Angstrom)
Time (ps)

S9.6 A: Hydrophobic interactions between the methyl group in the side chain of M653 (MMP-9HPX) with side chains of P114 and D116 in SG. Backbone MMP-9 HPX (green), SG N-terminal ^{1}Y-^{66}Y (yellow) and SG C-terminal ^{86}F-^{131}L (orange). Carbons in MMP-9 (purple) and SG (grey), oxygens (red), nitrogens (dark blue) and hydrogens (white).

S9.6 B: The 100 ns trajectory of the these interactions.

A

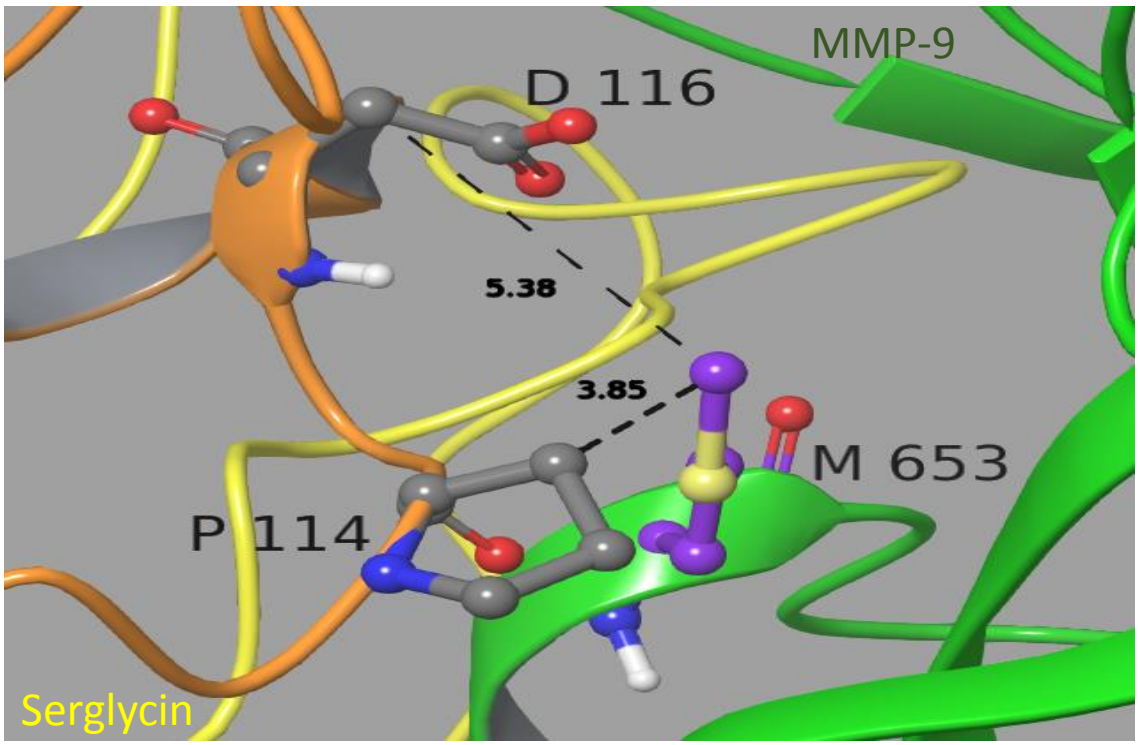

B

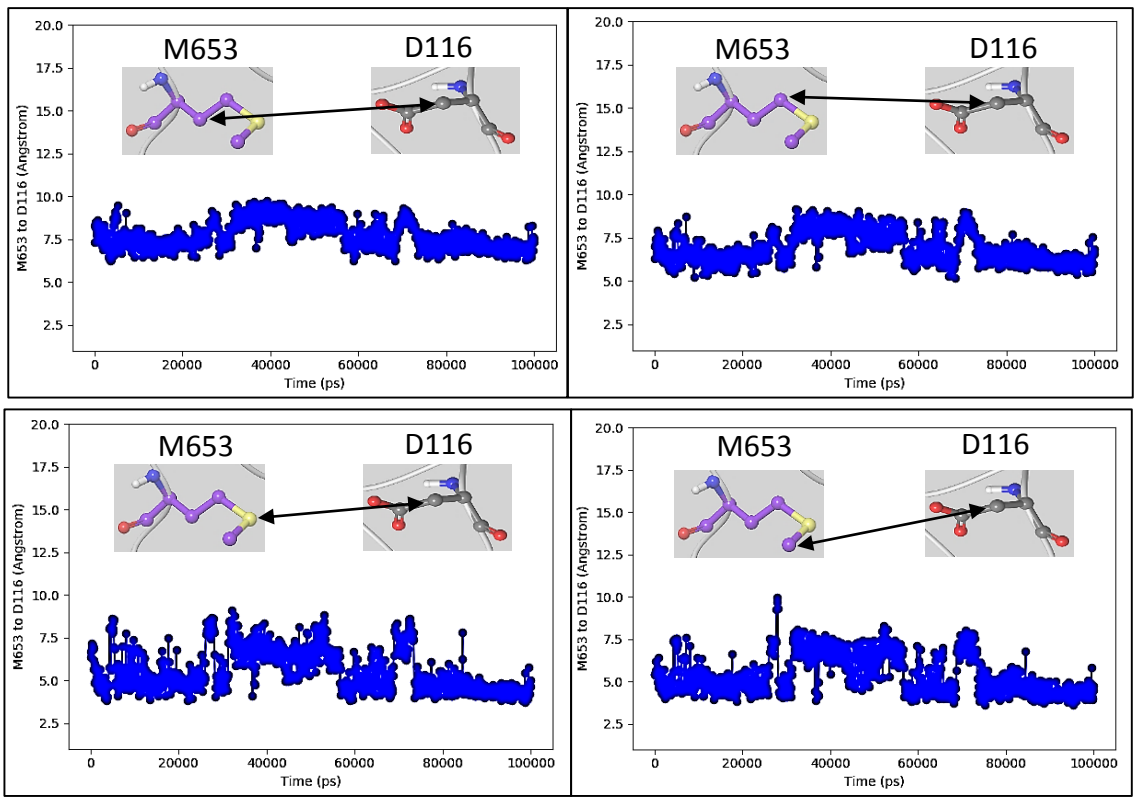

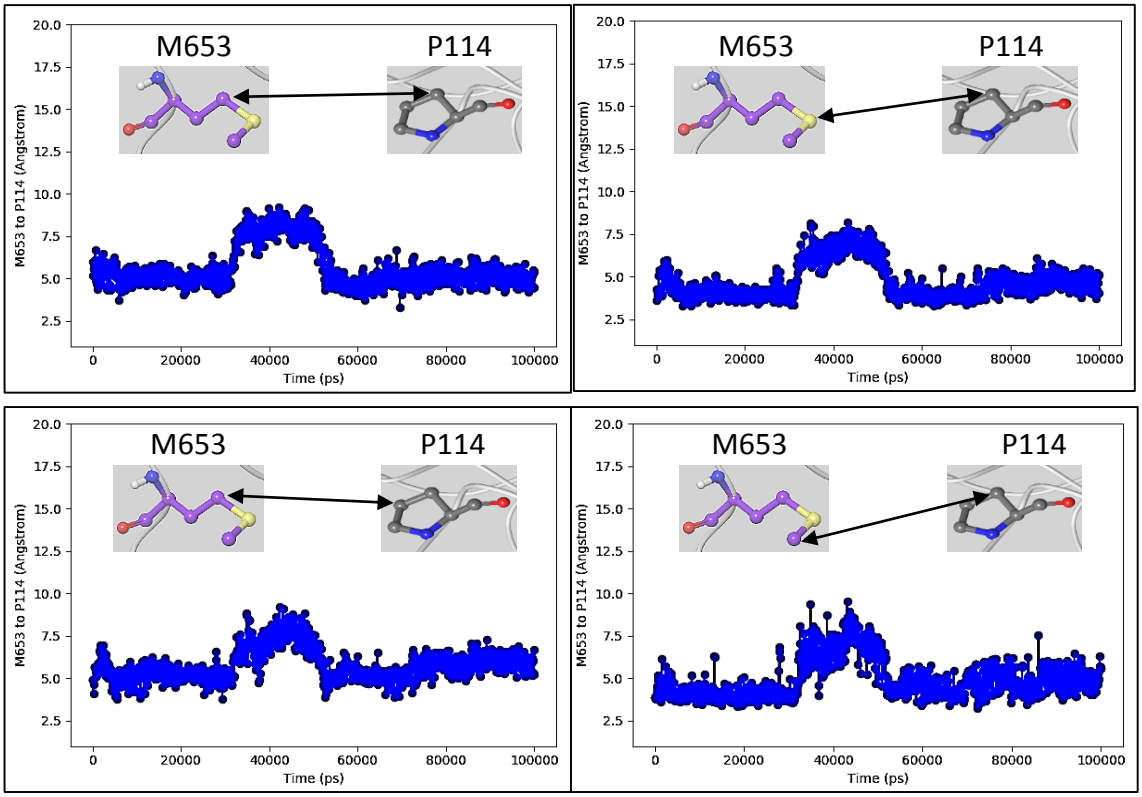
M653
P114
M653 to P114 (Angstrom)
Time (ps)
20.0
17.5
15.0
12.5
10.0
7.5
5.0
2.5
0
20000
40000
60000
80000
100000

S9.7 A: Hydrophobic interactions between the methylene groups in E687 and the side chain of L688 in MMP-9HPX with the methylene groups om R42, S117 and the side chain in L120 in SG. Backbone MMP-9 HPX (green), SG N-terminal ^{1}Y-^{66}Y (yellow) and SG C-terminal ^{86}F-^{131}L (orange). Carbons in MMP-9 (purple) and SG (grey), oxygens (red), nitrogens (dark blue) and hydrogens (white).

S9.7 B: The 100 ns trajectory of the these interactions.

A

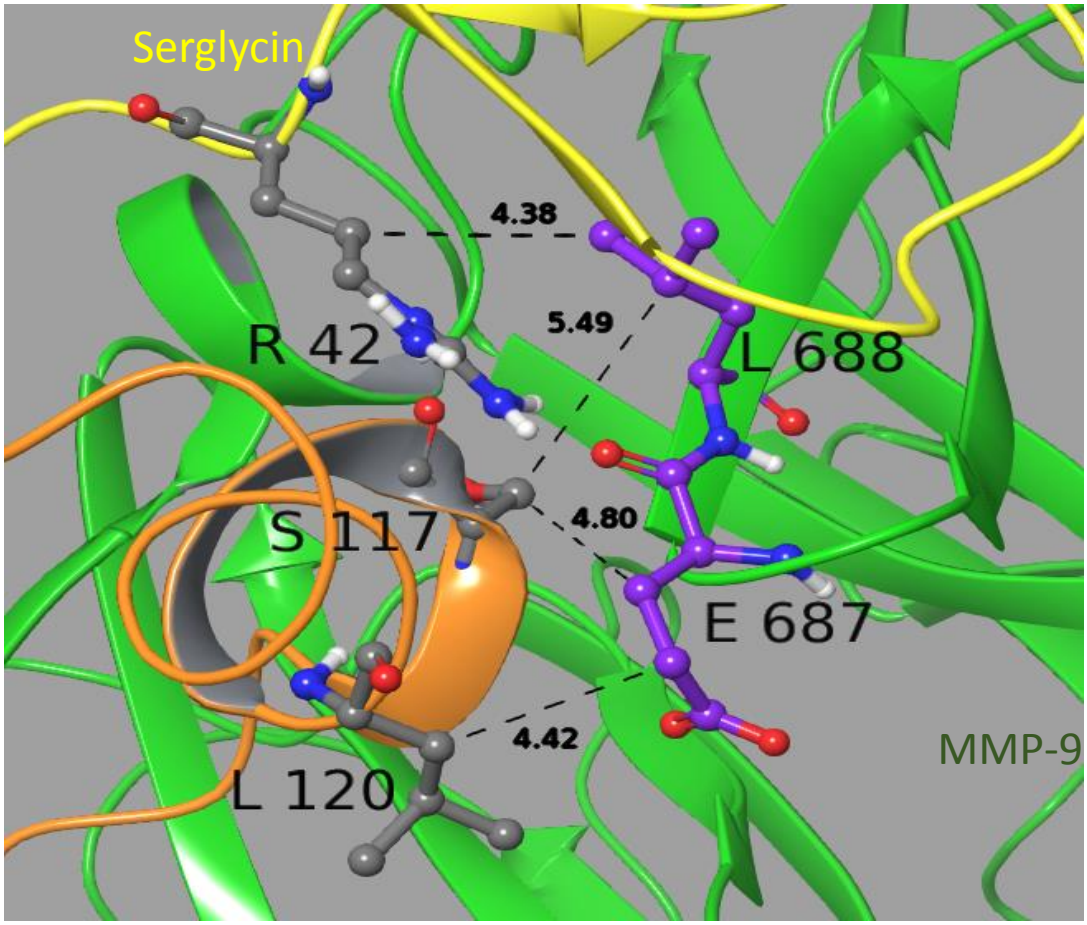

B

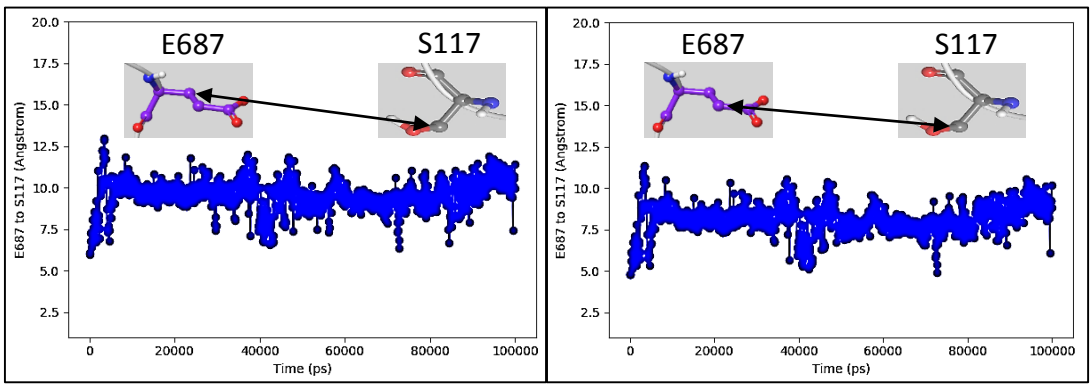

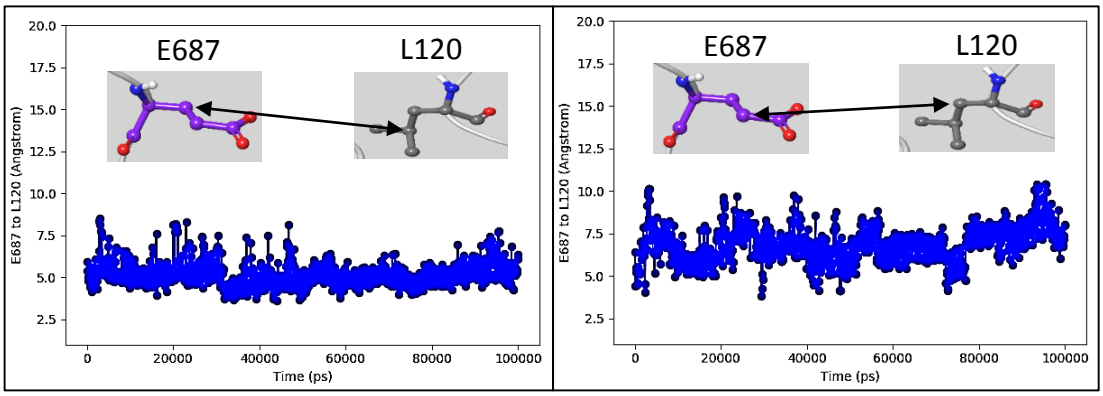
E687
L120
E687 to L120 (Angstrom)
Time (ps)

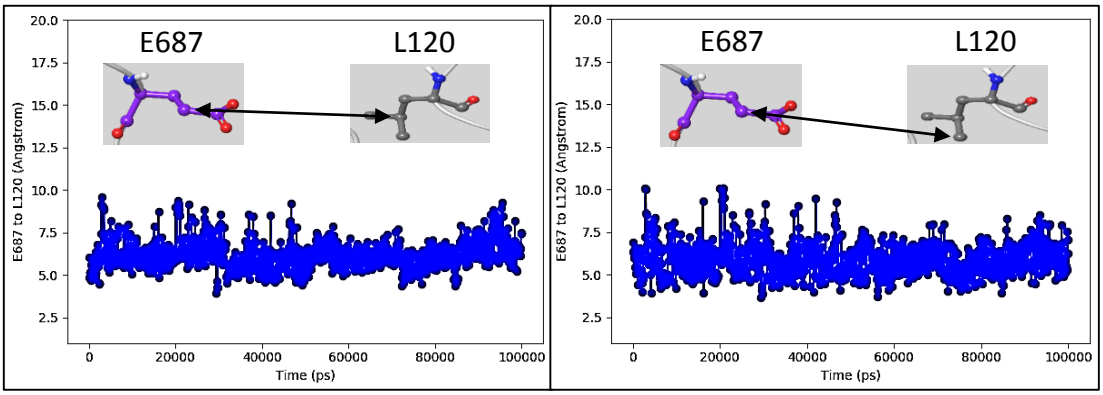
E687
L120
E687 to L120 (Angstrom)
Time (ps)

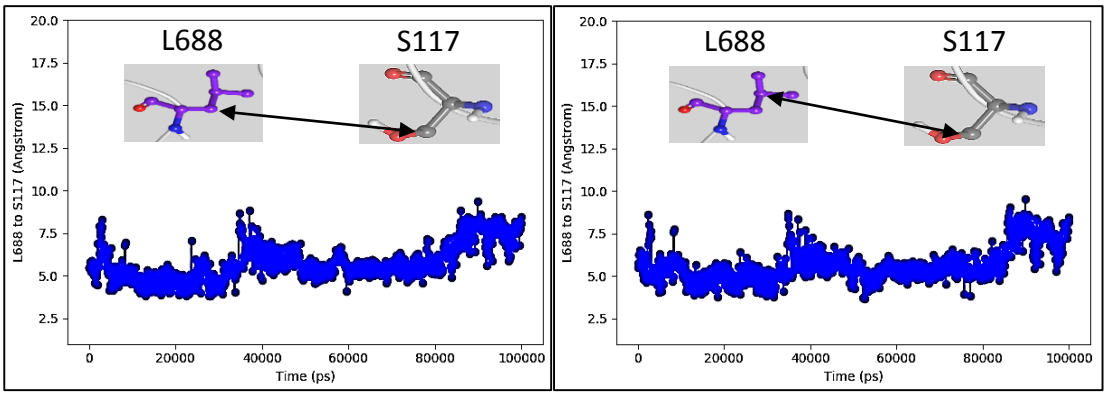
L688
S117
L688 to S117 (Angstrom)
Time (ps)

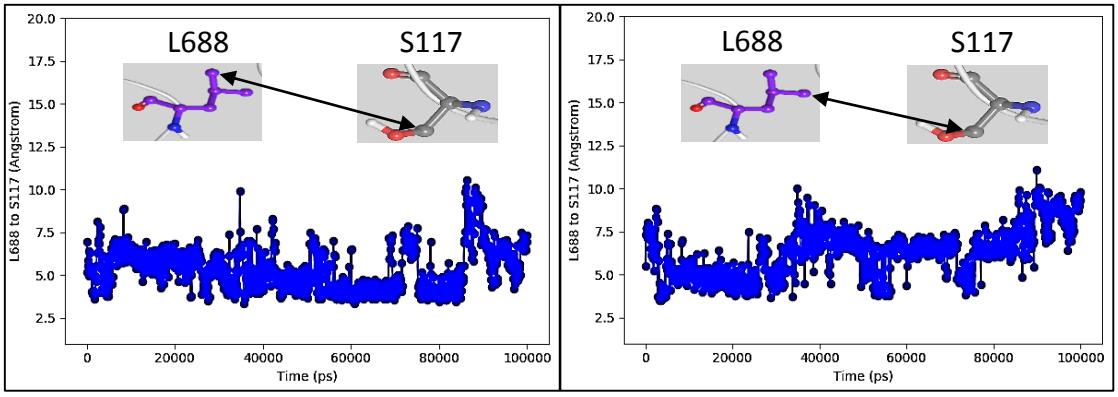
L688
S117
L688 to S117 (Angstrom)
Time (ps)

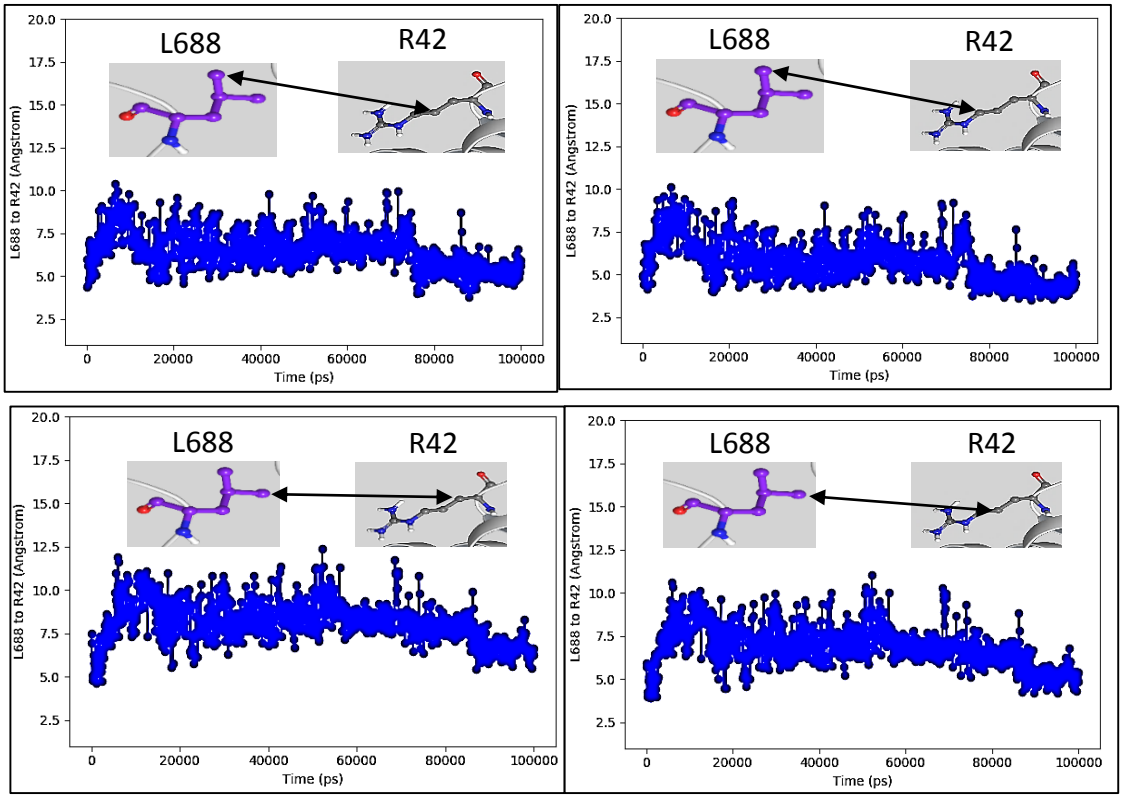
L688
R42
L688 to R42 (Angstrom)
Time (ps)
20.0
17.5
15.0
12.5
10.0
7.5
5.0
2.5
0
20000
40000
60000
80000
100000

S9.8 A: Hydrophobic interactions between Q690 and V691 in MMP-9HPX with I140 in SG. Backbone MMP-9 HPX (green), SG N-terminal ^{1}Y-^{66}Y (yellow) and SG C-terminal ^{86}F-^{131}L (orange). Carbons in MMP-9 (purple) and SG (grey), oxygens (red), nitrogens (dark blue) and hydrogens (white).

S9.8 B: The 100 ns trajectory of the these interactions.

A

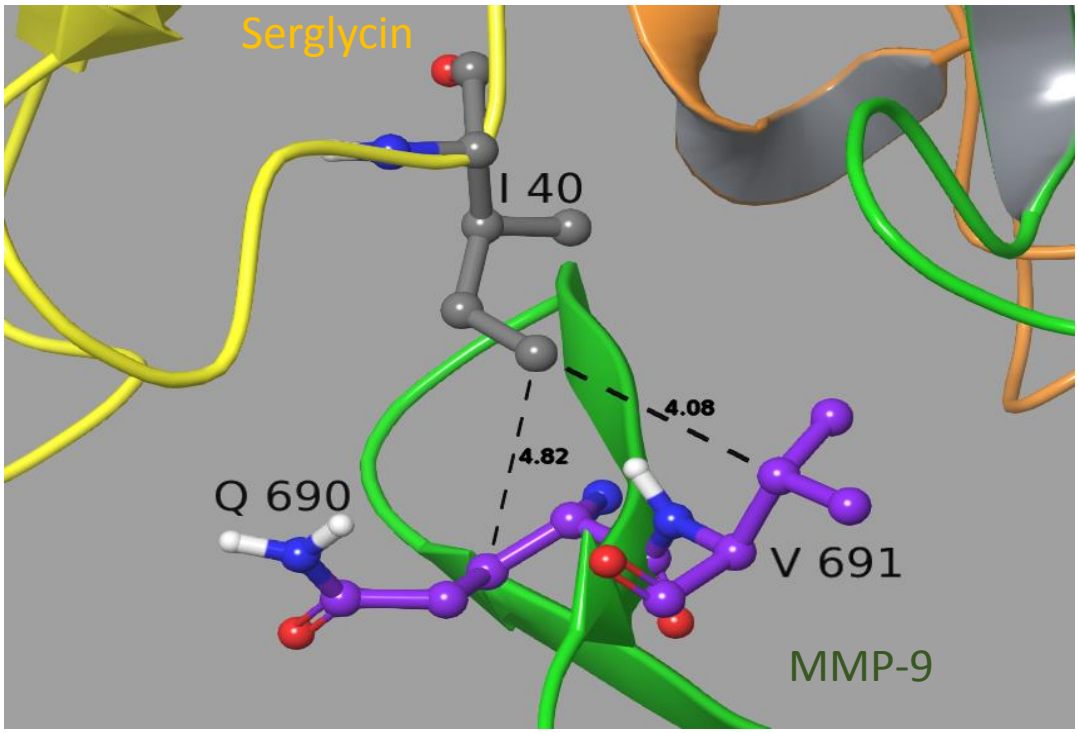

B

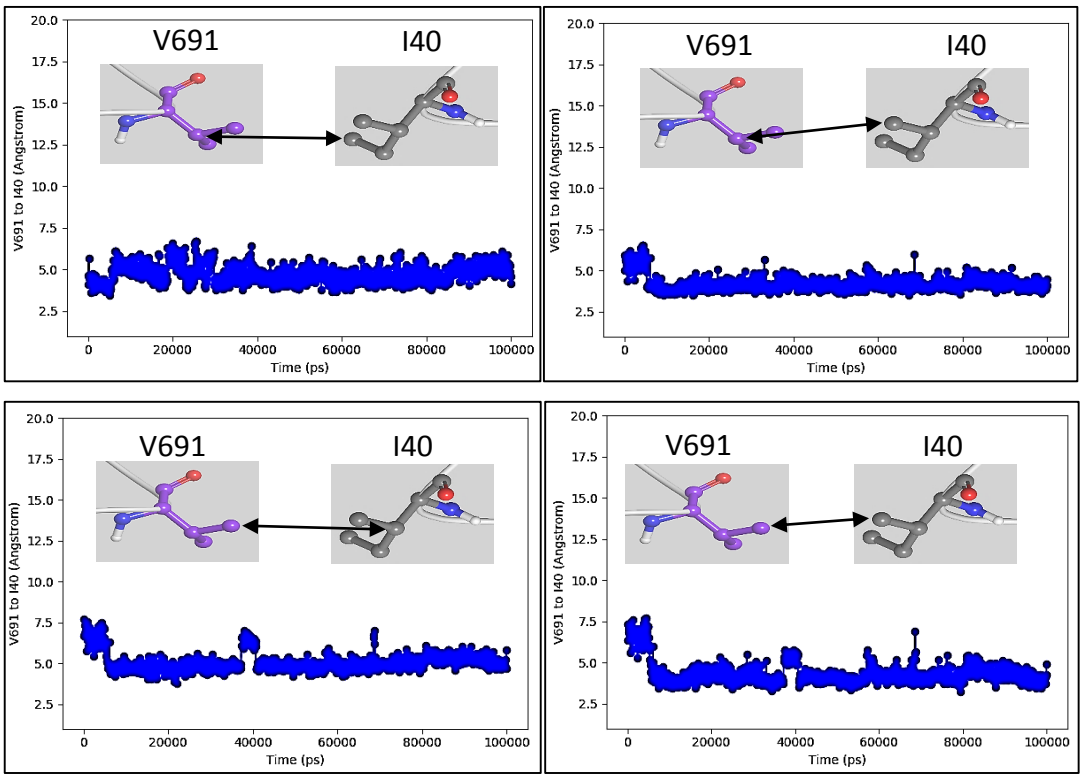

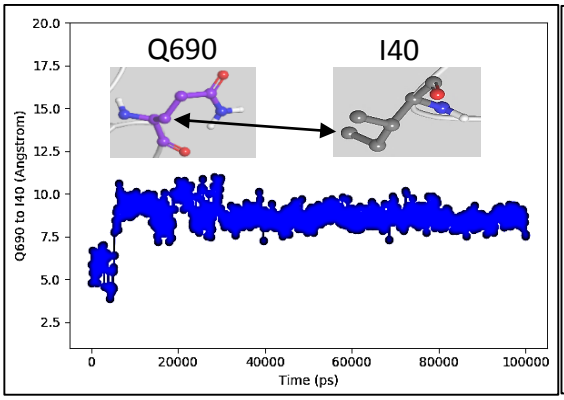
Q690
I40
Q690 to I40 (Angstrom)
Time (ps)

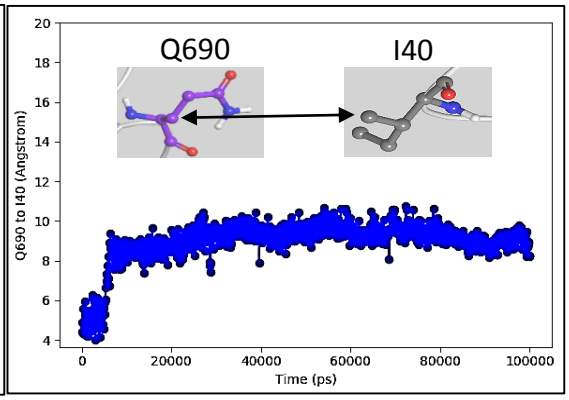
Q690
I40
Q690 to I40 (Angstrom)
Time (ps)

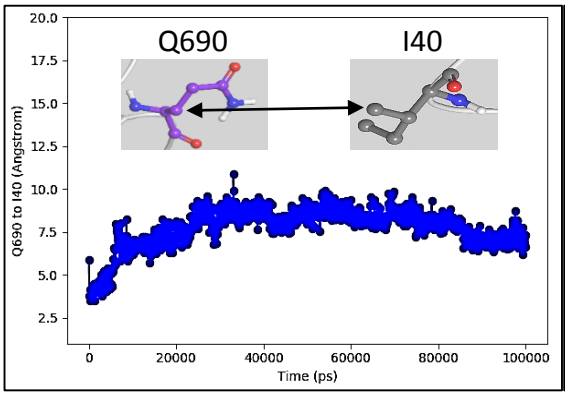
Q690
I40
Q690 to I40 (Angstrom)
Time (ps)

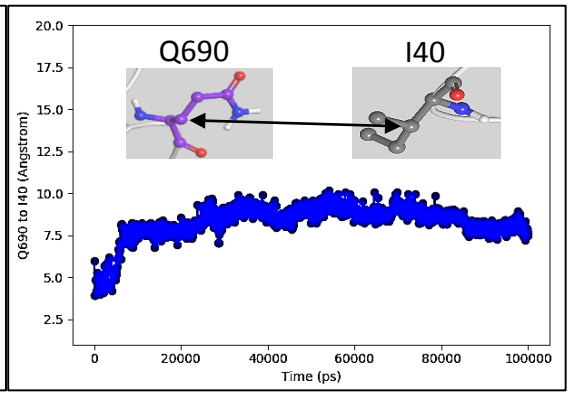
Q690
I40
Q690 to I40 (Angstrom)
Time (ps)

Fig. S10: Molecular dynamic simulations of the Full-length MMP-9.

A 500ns MD simualtion of full-length MMP-9 (Movie 1). Backbone MMP-9 pro and catalytic domain (light green), FnII repeat 1 (purple), FnII second repeat (pink), FnII third repeat (brown), OG domain (red) and HPX domain (dark green). A: the first frame of the 500ns trajectory, B: the last frame of the 500ns trajectory.

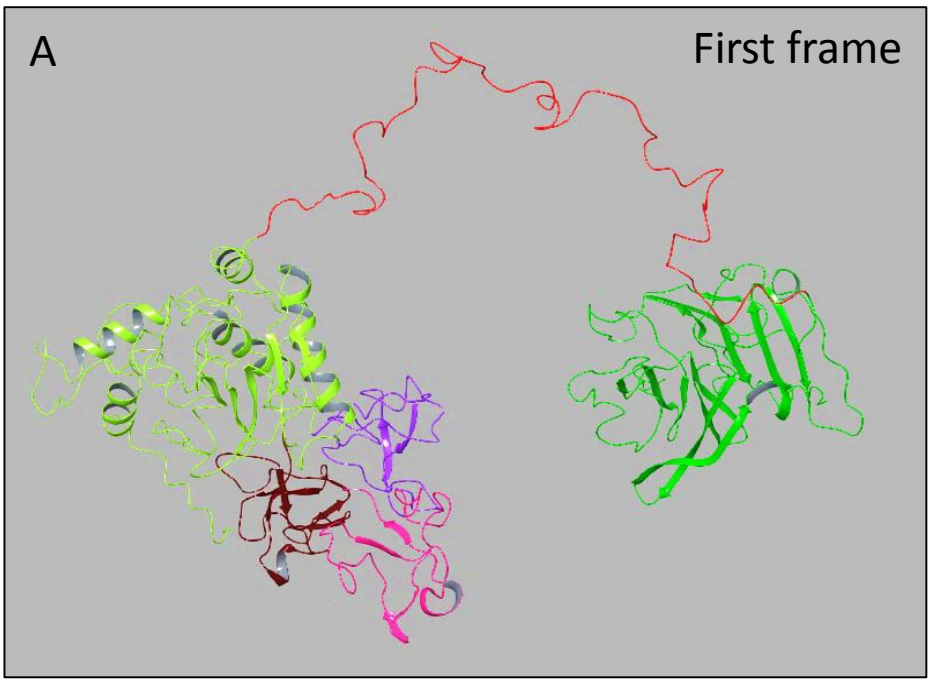

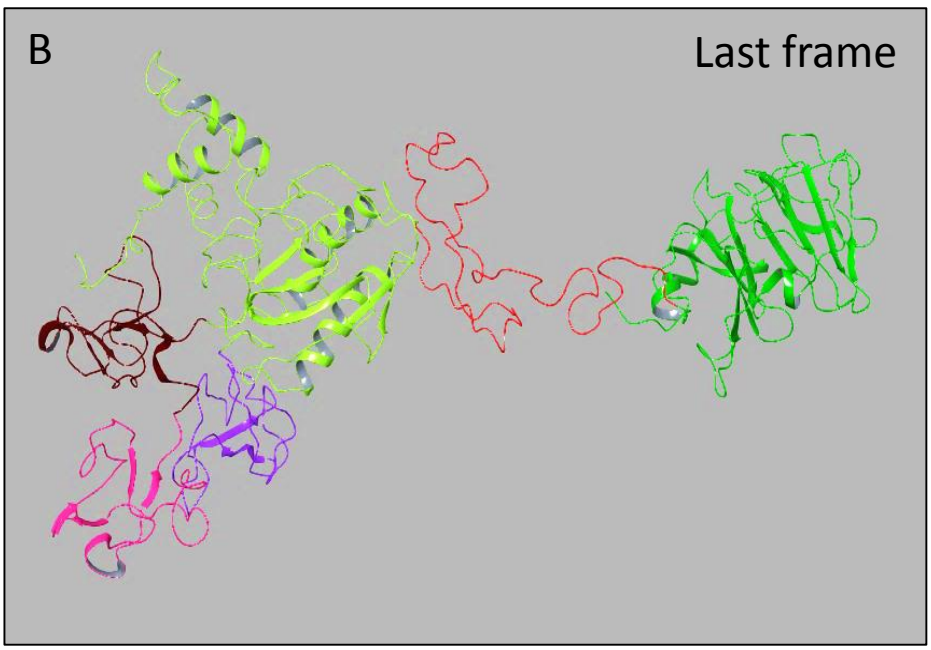

Fig. S11: Molecular dynamic simulations of the interactions between the full-length MMP-9 and the SG core protein.

MD simulation of full-length MMP-9 overlapped with SG core protein based on the binding pattern from the best docked model of MMP-9 FnII and SG core protein (Movie 2). Backbone MMP-9 pro and catalytic domain (light green), FnII repeat 1 (purple), FnII second repeat (pink) and FnII third repeat (brown), OG domain (red), HPX domain (dark green), SG N-terminal ^{1}Y-^{66}Y (yellow), SG Ser-Gly repeats ^{67}S-^{84}G (blue), SG C-terminal ^{86}F-^{131}L (orange). A: the first frame of the 500ns trajectory, B: the last frame of the 500ns trajectory.

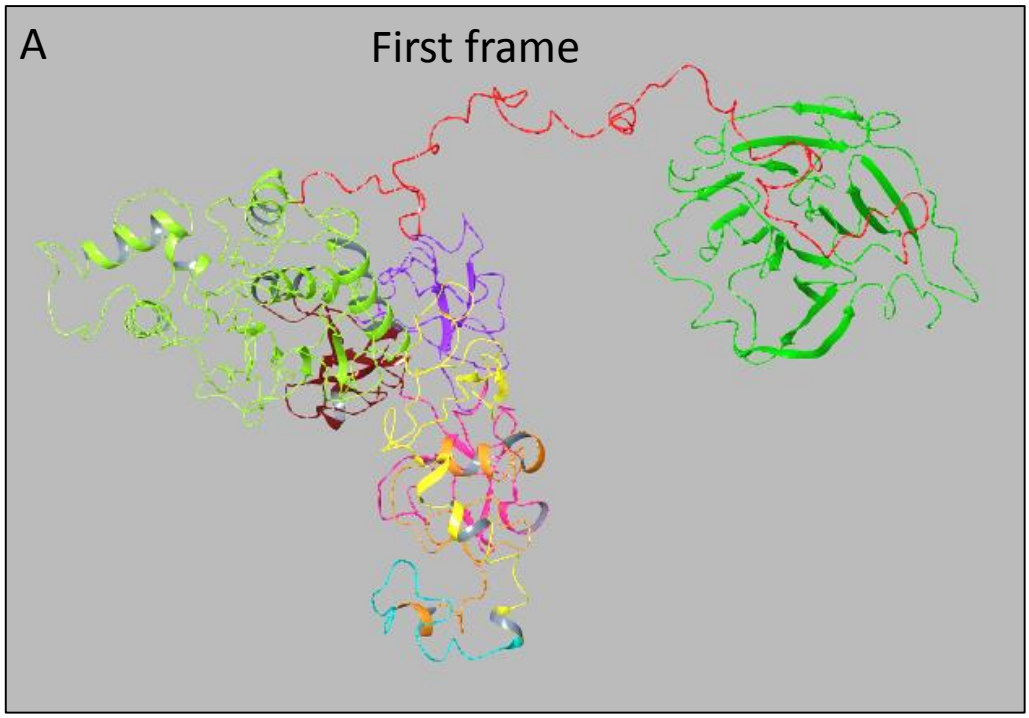

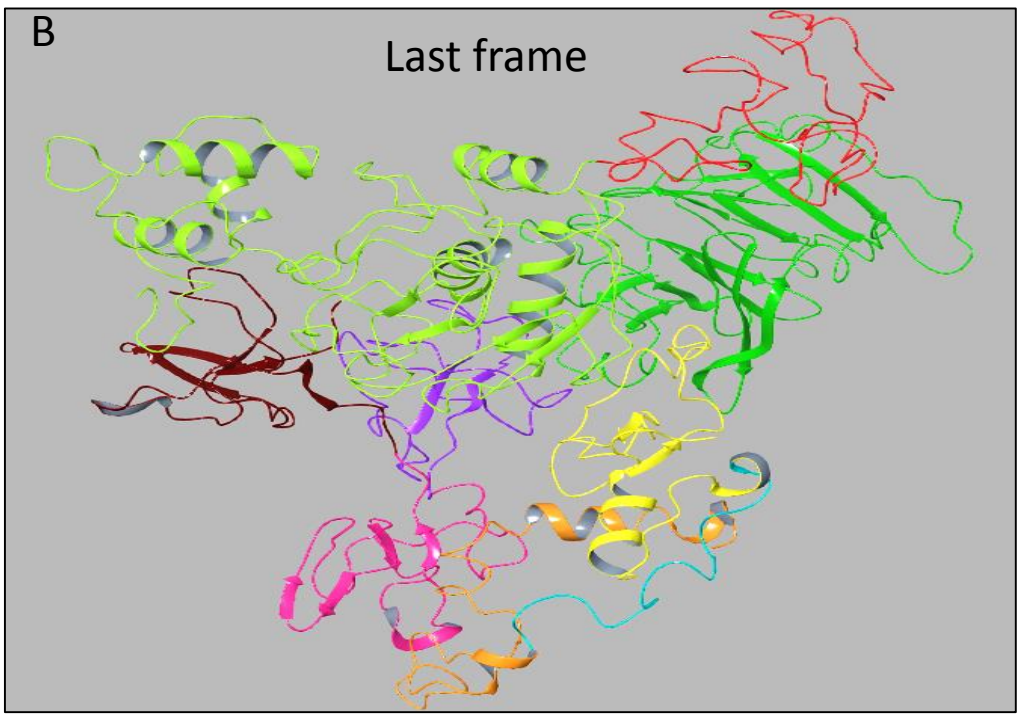

Fig. S12: Molecular dynamic simulations of the interactions between the full-length MMP-9 and the SG core protein.

MMP-9 structure of 15ns frame taken from 500ns DS (Movie 1) of full length MMP-9 used as primary structure to conduct the MD simulation with SG core protein kept between the two domains (Movie 3). Backbone MMP-9 pro and catalytic domain (light green), FnII repeat 1 (purple), FnII second repeat MMP-9 catalytic domain (light green), FnII repeat 1 (purple), FnII second repeat (pink) and FnII third repeat (brown), OG domain (red), HPX domain (dark green), SG N-terminal ^{1}Y-^{66}Y (yellow), SG Ser-Gly repeats ^{67}S-^{84}G (blue), SG C-terminal ^{86}F-^{131}L (orange). A: the first frame of the 100ns trajectory, B: the last frame of the 100ns trajectory.

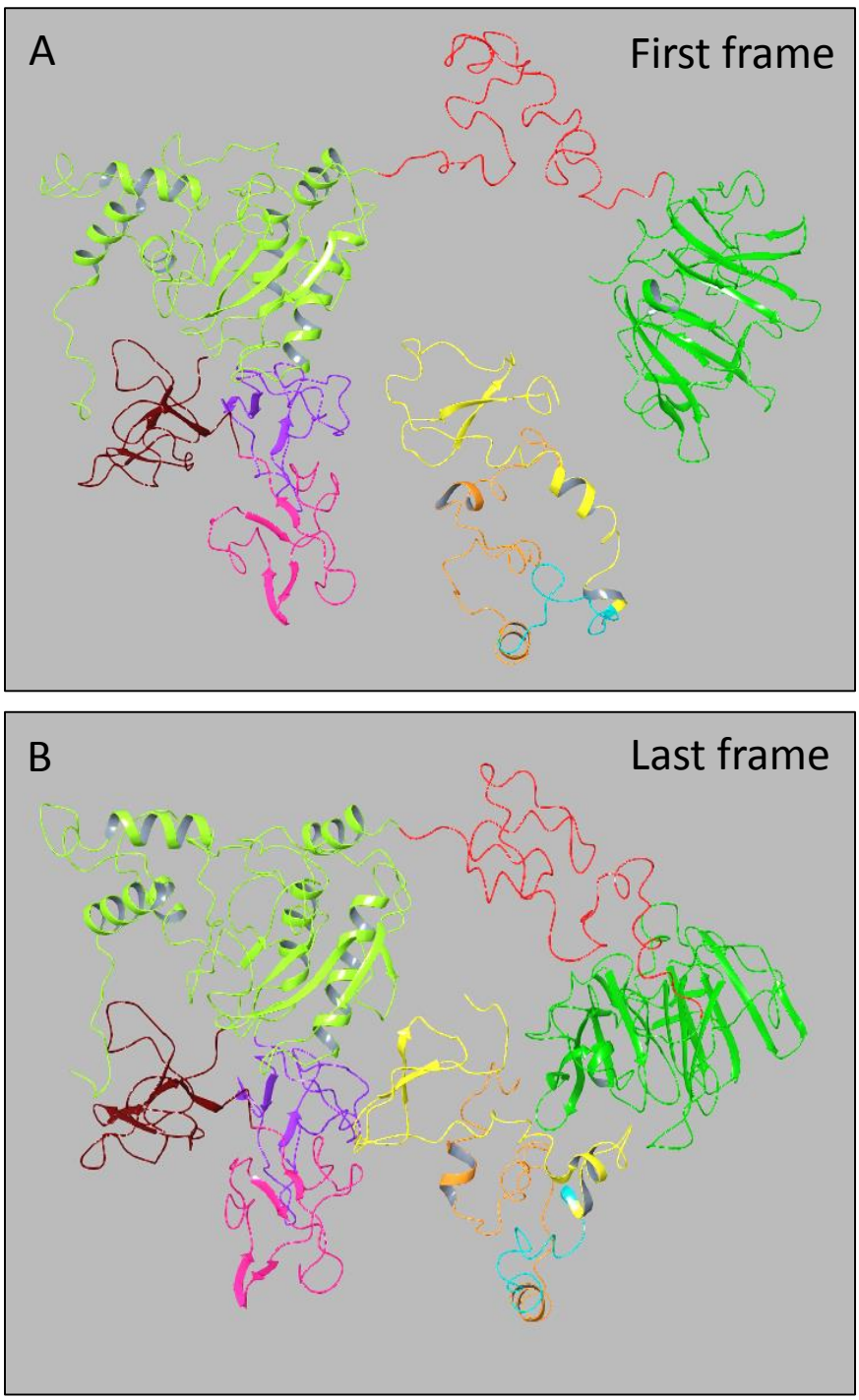

Fig. S13: Molecular dynamic simulations of the interactions between the full-length MMP-9 and the SG core protein.

MMP-9 structure of 32ns frame taken from 500ns DS (Movie 1) of full length MMP-9 used as primary structure to conduct the MD simulation with SG core protein (Movie 4). Backbone MMP-9 pro and catalytic domain (light green), FnII repeat 1 (purple), FnII second repeat MMP-9 catalytic domain (light green), FnII repeat 1 (purple), FnII second repeat (pink) and FnII third repeat (brown), OG domain (red), HPX domain (dark green), SG N-terminal ^{1}Y-^{66}Y (yellow), SG Ser-Gly repeats ^{67}S-^{84}G (blue), SG C-terminal ^{86}F-^{131}L (orange). A: the first frame of the 500ns trajectory, B: the last frame of the 100ns trajectory.

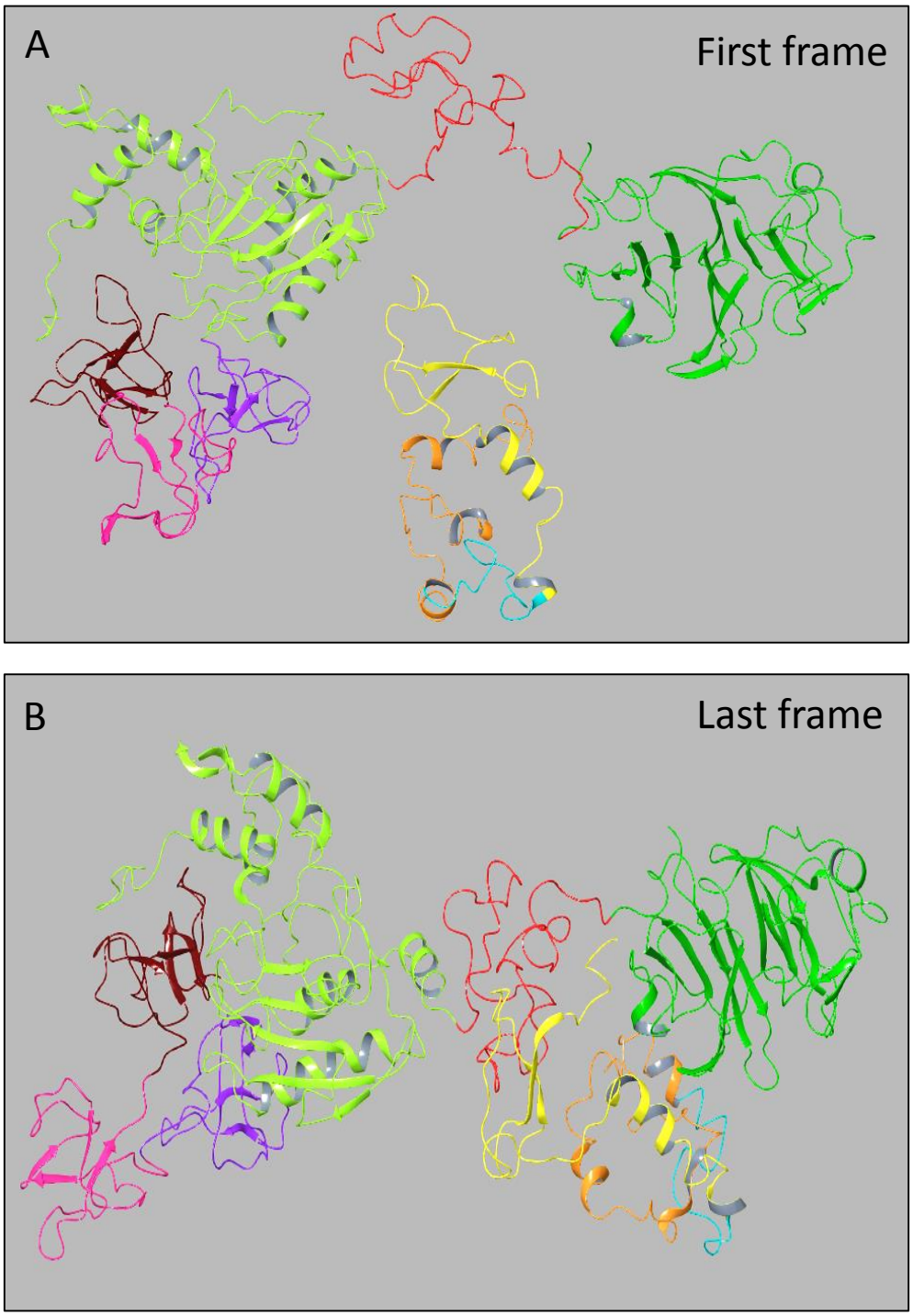

Fig. S14: Molecular dynamic simulations of the interactions between the full-length MMP-9 and the SG core protein based on the position from the best FnII-SG docking model.

MMP-9 structure of 32ns frame taken from 500ns DS (Movie 1) of full length MMP-9 used as primary structure to conduct the MD simulation with SG core protein based on the position from the best docked model between MMP-9 FnII and SG core protein (Movie 5). Backbone MMP-9 pro and catalytic domain (light green), FnII repeat 1 (purple), FnII second repeat (pink) and FnII third repeat (brown), OG domain (red), HPX domain (dark green), SG N-terminal ^{1}Y-^{66}Y (yellow), SG Ser-Gly repeats ^{67}S-^{84}G (blue), SG C-terminal ^{86}F-^{131}L (orange). A: the first frame of the 100ns trajectory, B: the last frame of the 100ns trajectory.

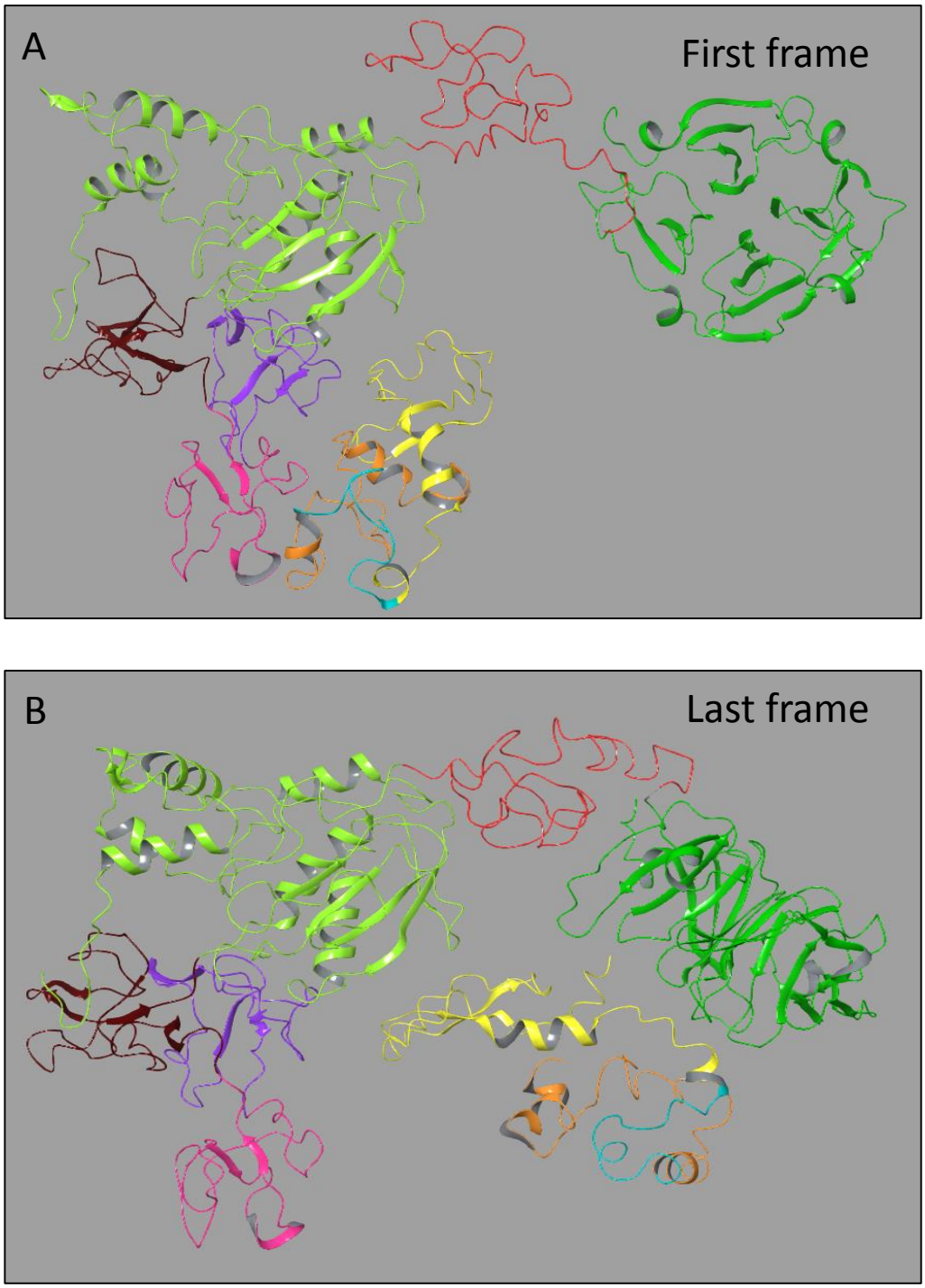

PAPER II

PLOS ONE

RESEARCH ARTICLE

The selectivity of galardin and an azasugar-based hydroxamate compound for human matrix metalloproteases and bacterial metalloproteases

Ingebrigt Sylte[1], Rangita Dawadi[1], Nabin Malla[1], Susannah von Hofsten[1], Tra-Mi Nguyen[2], Ann Iren Solli[1], Eli Berg[1], Olayiwola A. Adekoya[2], Gunbjørg Svineng[1], Jan-Olof Winberg[1]*

1 Department of Medical Biology, Faculty of Health Sciences, UiT-The Arctic University of Norway, Tromsø, Norway, **2** Department of Pharmacy, Faculty of Health Sciences, UiT-The Arctic University of Norway, Tromsø, Norway

* jan.o.winberg@uit.no

OPEN ACCESS

Citation: Sylte I, Dawadi R, Malla N, von Hofsten S, Nguyen T-M, Solli AI, et al. (2018) The selectivity of galardin and an azasugar-based hydroxamate compound for human matrix metalloproteases and bacterial metalloproteases. PLoS ONE 13(8): e0200237. https://doi.org/10.1371/journal.pone.0200237

Editor: Michael Massiah, George Washington University, UNITED STATES

Received: May 24, 2017

Accepted: June 22, 2018

Published: August 3, 2018

Data Availability Statement: All relevant data are within the paper and its Supporting Information files.

Funding: This research was funded by Tromsø Forskningsstiftelse (support to JOW). The funders had no role in study design, data collection and analysis, decision to publish, or preparation of the manuscript.

Competing interests: The authors have declared that no competing interests exist.

Abstract

Inhibitors targeting bacterial enzymes should not interfere with enzymes of the host, and knowledge about structural determinants for selectivity is important for designing inhibitors with a therapeutic potential. We have determined the binding strengths of two hydroxamate compounds, galardin and compound **1b** for the bacterial zinc metalloproteases, thermolysin, pseudolysin and auerolysin, known to be bacterial virulence factors, and the two human zinc metalloproteases MMP-9 and MMP-14. The active sites of the bacterial and human enzymes have huge similarities. In addition, we also studied the enzyme-inhibitor interactions by molecular modelling. The obtained K_i values of galardin for MMP-9 and MMP-14 and compound **1b** for MMP-9 are approximately ten times lower than previously reported. Compound **1b** binds stronger than galardin to both MMP-9 and MMP-14, and docking studies indicated that the diphenyl ether moiety of compound **1b** obtains more favourable interactions within the S'_1-subpocket than the 4-methylpentanoyl moiety of galardin. Both compounds bind stronger to MMP-9 than to MMP-14, which appears to be due to a larger S'_1-subpocket in the former enzyme. Galardin, but not **1b**, inhibits the bacterial enzymes, but the galardin K_i values were much larger than for the MMPs. The docking indicates that the S'_1-subpockets of the bacterial proteases are too small to accommodate the diphenyl ether moiety of **1b**, while the 4-methylpentanoyl moiety of galardin enters the pocket. The present study indicates that the size and shape of the ligand structural moiety entering the S'_1-subpocket is an important determinant for selectivity between the studied MMPs and bacterial MPs.

Introduction

Proteases are enzymes that cleave peptides and proteins at their N- or C-terminal ends (exopeptidases) or within the polypeptide chain (endopeptidases). They are important for all organisms, and it is estimated that there are more than 66000 different proteases [1, 2]. In

microorganisms, proteases are important for generation of nutrition, invasion into host organisms as well as growth and survival [3–9]. In vertebrates, they are involved in the regulation of various physiological processes including cell growth, cell signalling, blood pressure, coagulation, angiogenesis, reproduction, wound repair, hemostasis and homeostasis [2, 10–14]. In humans, diseases are often associated with dysregulation of one or several proteases [10, 11, 15–18] and several proteases are important targets for therapeutic intervention [19–22].

Proteases are divided into classes or clans based on residues involved in the catalytic reaction [2, 23–25]. One of these classes is the metalloproteases (MPs), where the catalytic metal most often is a zinc ion [23, 24]. The bacterial zinc-MPs thermolysin, pseudolysin and auerolysin are secreted by various types of bacteria including bacillus thermoproteolyticus, pseudomonas aeruginosa and staphylococcus aureus, and act as virulence factors [26]. These proteases belong to the M4 family of proteases. Thermolysin is one of the most studied proteases, and has become a model enzyme for the M4 family [26]. In humans, one of the most studied MP families is the matrix metalloproteases (MMPs) also called matrixins [15]. They belong to the M10 family, and in humans there are 23 different MMPs. Seven of them contain a transmembrane domain or a glycosylphosphatidyl-inosityl (GPI) moiety which links them to the cell membrane, while the other sixteen MMPs are secreted enzymes [15]. The most studied among the membrane linked is MT1-MMP (MMP-14), while MMP-9 (gelatinase B) is the most studied among the secreted MMPs [18, 27]. The reason for the intense studies of MMPs is that they are involved in a large variety of physiological processes and that they are dysregulated in a number of different malignant disorders including various types of cancer, arthritis, osteoarthritis, diabetes, cardiovascular-, eye-, brain- and nervous system diseases [15, 18].

Thermolysin, pseudolysin and auerolysin are secreted proteases classified into the clan gluzincins, i.e. their catalytic zinc ion is bound to the protein through two histidines and a glutamate (HEXXH+E) [23, 24, 26]. The fourth zinc ligand is a water molecule that is polarized by the glutamic residue next to the first histidine that binds the catalytic zinc. The catalytic sites of thermolysin and pseudolysin have been extensively studied through X-ray crystallography with various inhibitors bound and several structures are deposited in the protein database (PDB). However, for auerolysin only one X-ray structure of the free enzyme is available.

Like the majority of the MMPs, both MMP-14 and MMP-9 contain an N-terminal signal peptide followed by a pro-domain with the conserved PRCGV sequence to keep the enzyme in a latent state. This is followed by a catalytic domain linked to the C-terminal hemopexin like domain (HPX) through a hinge or linker region which varies in length and structure between the MMPs [15]. The HPX domain in MMPs is involved in complex formation with other biological molecules, activation and substrate specificity [15, 28, 29] and the 3D structure shows that this domain adopts a four bladed β-propeller where blade I is connected to blade IV through a disulphide bridge [30]. Fig 1A shows a schematic drawing of a general MMP structure with its domains and modules. MMPs belong to the clan metzincins and the catalytic zinc ion is bound to the protein through the three histidines of the segment (HEXXHXXGXXH/D+M) [23, 24]. In their inactive pro-form, the fourth zinc ligand is the cysteine of the PRCGV motif of the pro-domain [31, 32]. MMP-14 also contains a type 1 trans-membrane domain C-terminally linked to the HPX domain. At the end of the pro-domain, it contains a basic motif (RX(K/R)R). This motif is recognized by the intracellular serine protease, furin [15]. Hence MMP-14 is activated in the endoplasmatic reticulum and transported to the cell membrane as an active protease lacking its pro-domain, with the active site located in the extracellular environment [15]. MMP-9 on the other hand lacks the (RX(K/R)R) motif and is secreted from cells as an inactive pro-enzyme. This enzyme is unique among the MMPs as it contains a long and heavily O-glycosylated hinge region, also called the OG-domain. In addition, both MMP-9 and MMP-2 contain a large insert in the

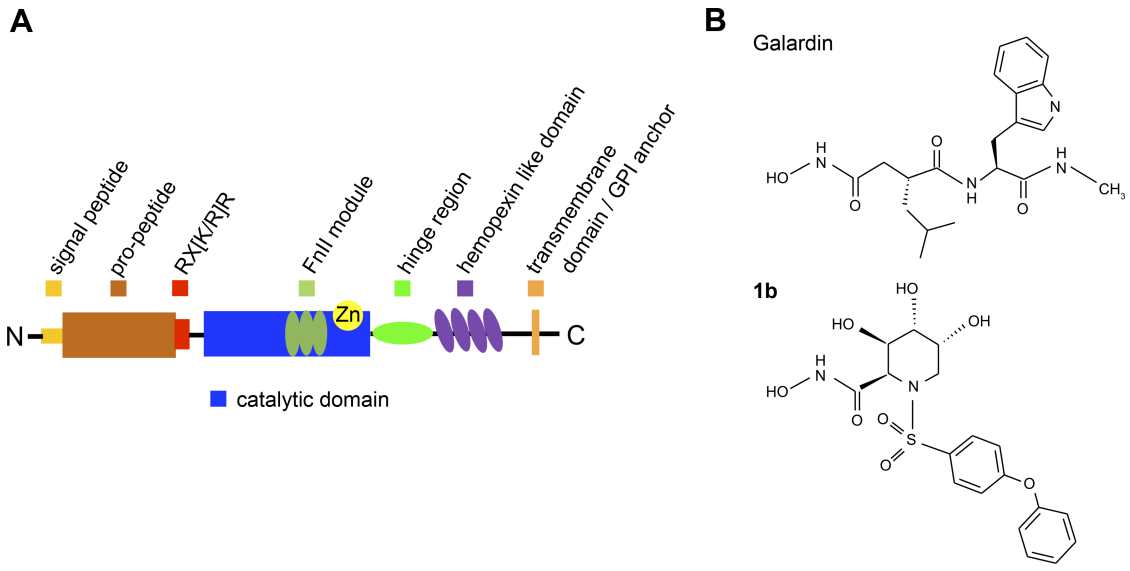

Fig 1. Domain structure of MMPs (A) and schematic representation of galardin and compound 1b (B). All MMPs contain a signal peptide (cleaved off in the endoplasmatic reticulum), a pro-peptide domain and a catalytic domain. In addition, most MMPs contain a linker (hinge-region) and a hemopexin (HPX) like domain. The hinge region in MMP-9 differs from the other MMPs as it is longer and heavily O-glycosylated, and therefore also called the OG-domain. Three secreted (MMP-11, -21, -28) and all membrane-anchored MMPs have a basic RX[K/R]R motif at the C-terminal end of their pro-domain. This motif can be cleaved inside the cells by furin-like proteases. The two gelatinases (MMP-2, -9) contain three fibronectin II like repeats (FnII module) in their catalytic domain, located N-terminal to the catalytic Zinc-binding site. Four of the six membrane-type (MT)-MMPs are anchored to the cell membranes through a type I transmembrane domain and the other two through a glycosylphosphatidylinositol (GPI) moiety.

https://doi.org/10.1371/journal.pone.0200237.g001

catalytic site, i.e. three fibronectin II-like motifs (FnII) which is important for the activity against some macromolecular substrates, such as denatured collagen (gelatin) [27, 33–38]. However, the FnII repeats have no effect on the enzymes' processing of small chromogenic peptide substrates or small inhibitors that only interact with the active site [34]. The long hinge region of MMP-9 is very flexible as shown previously by small angle X-ray crystallography combined with atomic force microscopy and is probably the reason for that the X-ray structure of the full length MMP-9 has not been solved [39]. To what extent the hinge region and the bound sugars, as well as the HPX domain of MMP-9, interact with the catalytic domain is not known. Even though these two domains did not have an effect of MMP-9's cleavage of some biological macromolecular substrates [40], it cannot be excluded that they are involved in the cleavage of other macromolecular substrates or small chromogenic substrates as well as binding of inhibitors to the catalytic site. MMP-9 can be activated in the extracellular environment by various naturally occurring proteases such as trypsin, kallikrein, MMP-2 and MMP-3. In addition, MMP-9 is also activated by organic mercurial compounds such as p-aminophenylmercuric acetate (APMA) and by bacterial proteases such as thermolysin and pseudolysin [32]. Various activators cleave the MMP-9 pro-domain at different positions resulting in enzyme structures with different N-terminals [32]. In addition, both protease activation and APMA induced auto-activation are also accompanied to various extents with further truncation of the enzyme by cleavage of the HPX domain and in some cases of the OG-domain [41–45]. Binding of inhibitors to the active site of MMP-9 and MMP-14 have been extensively investigated both by kinetic and X-ray crystallography studies [46–54]. For both, inhibitor binding is most often studied by using the recombinant

catalytic domains of MMP-14 and MMP-9. In the latter enzyme, the fibronectin II-like module in the catalytic site is lacking in most of the structures deposited in the PDB.

Many bacterial proteases like thermolysin, pseudolysin and auerolysin are virulent factors and hence putative drug targets [5–8, 55]. However, it is important that drugs targeting the bacterial enzymes not interfere with the function of the human MPs. Our focus for some time has been on MP inhibitors [56, 57]. By studying the binding of various inhibitors to bacterial and human MPs, we are aiming to obtain information about similarities and differences in the active site of these enzymes that can be used in the development of compounds that bind specifically to the bacterial enzymes. In the present work we are studying the binding of two hydroxamate containing compounds, galardin and compound **1b** (Fig 1B) to thermolysin, pseudolysin and auerolysin, and to the human MMP-9 and MMP-14. Galardin is a well studied compound that binds strongly to several MMPs including MMP-9 and MMP-14 as well as to thermolysin and pseudolysin [58–60]. Compound **1b** was developed by Moriyama and colleagues [61] and is an aza-sugar based hydroxamate that has been shown to bind strongly to MMP-1, MMP-3, MMP-9 and TACE, but have not been tested against MMP-14 or bacterial MPs. In order to assure an accurate comparison between the enzymes and between compound **1b** and galardin binding, we have thoroughly retested these compounds under the same methodological conditions against thermolysin, pseudolysin, MMP-14 and against differently activated full length MMP-9 isolated from THP-1 cells and recombinant human full length proMMP-9 produced in Sf9 insect cells. The difference between native MMP-9 and recombinant MMP-9 produced in Sf9 insect cells is the extent of glycosylation of the hinge region [40]. As the N-terminal residue of activated MMPs may affect inhibitor binding as previously seen for APMA, MMP-14 and trypsin-activated MMP-2 [62], MMP-9 was activated with three different activators (trypsin, MMP-3 (catalytic domain) and APMA) that give different N-terminal residues. Trypsin and MMP-3 are physiological activators of proMMP-9, and the small amount of TIMP-1 present in the purified proMMP-9 from various cells such as THP-1 has no or limited effects on the trypsin induced activation of proMMP-9, while in contrast the activation induced by other MMPs and APMA will be affected [42, 43, 63]. During mercury poisoning, the presence of mercury ions can result in an uncontrolled activation of proMMPs in the victim. In addition, we have performed molecular modelling studies of the two compounds interaction with the active site of the five enzymes. Comparing binding modes obtained by docking with the experimentally obtained binding strengths increases the understanding of residues and structural motifs important for binding and selectivity.

Materials and methods

Materials

TRIS, DMSO and $CaCl_2 \cdot 2H_2O$ and human recombinant MMP-3 catalytic domain were from Merck (Darmstadt, Germany). EDTA and 2-Methoxy-2,4-Diphenyl-3(2H)-Furanone (MDPF) were from Fluka (Buchs, Switzerland). Acrylamide, Commassie Brilliant Blue G-250 and Triton X-100 were from BDH (Poole, UK). RPMI 1640, streptomycin, penicillin, phorbol 12-myristate 13-acetate (PMA), Hepes, Brij-35, SDS, NaCl, p-aminophenylmercuric acetate (APMA), trypsin, soybean trypsin inhibitor (SBTI), Tween-20 and gelatin were purchased from Sigma (St Louis, MO, USA). Magnetic trypsin beads (Mag-Trypsin) were purchased from Takara (Gothenburg, Sweden). Gelatin-Sepharose, Q-Sepharose, Sephadex G-50 (fine), were from GE-Healthcare (Uppsala, Sweden). Unlabelled molecular weight standards were from BioRad (Richmond, CA, USA), while the Spectra^{TM} Multicolor High Range Protein ladder was from Pierce Biotechnology (Rockford, IL, USA). Magic Marker molecular weight standards, NuPAGE Novex 4–12% BisTris gels and Sf9 insect cells were

from Invitrogen (Carlsbad, CA, USA). Western Blotting Luminol reagent was from Sancta Cruz (Santa Cruz, CA, USA). Rabbit anti-rat MMP-9 polyclonal antibody (also detect mouse and human MMP-9) was obtained from Chemicon International Inc. (Temecula, CA, USA). HRP-conjugated goat anti-rabbit secondary antibody was from Southern Biotech (Birmingham, AL, USA). Galardin (Gm6001), pseudolysin, thermolysin and recombinant MMP-14 (catalytic domain) were from Calbiochem (San Diego, CA, USA). Spectra™ Mulitcolor High Range Protein Ladder was from Pierce (Rockford, IL, USA). Fetal bovine serum was from Biochrom AG (Berlin, Germany). Auerolysin was from BioCentrum Ltd (Kraków, Poland). The chromogenic substrates Mca-PLGLDpaAR-NH_2 (ES001) and Mca-RPPGFSAFK(Dnp)-OH (ES005) were from R&D Systems, Inc (Minneapolis, MN, USA). Azasugar-based MMP-inhibitor **1b** was a kind gift from Dr. Hideki Moriyama (Dept. Drug. Disc. Res., Carna Bioscience Inc., Kobe, Japan). Human MMP-9 (recombinant catalytic domain) was from AnaSpec (Fremont, CA, USA). Vivaspin columns with a 10 and 30 kDa cut-off were from Sartorius Stedim Biotech GmbH (Goettingen, Germany). Imperial blue protein stain was from Thermo Scientific (Rockford, Il, USA).

Production and purification of proMMP-9 from THP-1 cells

The human leukemic monocyte cell-lines THP-1 was a kind gift from Dr. K. Nilsson, Department of Pathology, University of Uppsala, Sweden. The cells were cultured in RPMI 1640 medium with 10% fetal bovine serum, 50 μg/ml of streptomycin, and 100 units/ml of penicillin. To produce proMMP-9, the cells were washed 3 times in serum-free medium and then cultured for 72 h in serum-free RPMI 1640 medium containing 0.1 μM PMA as described earlier [64]. Conditioned medium was harvested, loose cells were pelleted by centrifugation at 1200 rpm (200g) for 10 min. ProMMP-9 was first separated from Chondroitin sulphate proteoglycans (CSPG) and proMMP-9·CSPG heteromers by Q-Sepharose anion exchange chromatography and then purified by Gelatin-Sepharose affinity chromatography as described previously [65].

Production and purification of recombinant human full length proMMP-9 from Sf9 insect cells

The cDNA encoding human preproMMP-9 (accession number: BC006093.1) cloned into the pReceiver-M02 vector (catalogue number: EX-F0125-M02) was purchased from GeneCopoeia (Rockville, MD). The cDNA was flanked by Invitrogen™ Gateway™ attB-sequences (Invitrogen, Thermo Fisher Scientific Inc.) and was transferred to pDONR221 using Gateway® BP Clonase® II Enzyme mix (Invitrogen, Thermo Fisher Scientific Inc.) and subsequently to BaculoDirect™ Linear DNA (catalogue number: 12362013) using Gateway® LR Clonase® II Enzyme mix preserving the endogenous MMP-9 stop codon. Baculoviruses were produced using Sf9 cells according to the protocol of the BaculoDirect™ Baculovirus Expression System. The P3 viral stock was used for production of preproMMP-9 in Sf9 cells in suspension.

Thirty ml of serum containing medium from baculovirus infected Sf9 cells was applied to a 1 ml column of Gelatin-Sepharose pre-equilibrated with 0.1 M Hepes buffer pH 7.5 containing 5.0 mM $CaCl_2$. After collecting the pass-through medium, the column was first washed with 10 column volumes of 0.1 M M Hepes buffer pH 7.5 containing 5.0 mM $CaCl_2$ and 1.2 M NaCl. This was followed by a new wash with 30–40 column volumes of 0.1 M Hepes buffer pH 7.5 containing 5.0 mM $CaCl_2$. Bound proMMP-9 was eluted with a buffer containing 0.1 M Hepes pH 7.5, 5.0 mM $CaCl_2$ and 7.5% DMSO. The eluted material was concentrated and depleted of DMSO (end [DMSO] less than 0.02%) using a spin column with a 10 kDa cut-off. The amount of proMMP-9 in the sample was determined spectrophotometrically at 280 nm using the extinction coefficient $\varepsilon_{280nm} = 114.36\ mM^{-1}cm^{-1}$ [66]. The purified sample was

applied to SDS-PAGE (NuPAGE Novex 4–12% Bis-Tris gels). These gels were either further applied to Western blotting (using a polyclonal antibody against proMMP-9) or stained with Imperial blue where bands were cut out and sent to MS analysis at the Tromsø University Proteomics Platform (TUPP). Purified samples were also applied to Gelatin zymography.

Activation of proMMP-9

Activation of proMMP-9 through treatment of APMA (auto-activation), MMP-3 or trypsin results in a balance between activation and degradation of the enzyme and hence it is important to stop the process when the activation is at its maximum and not to allow the degradation process to go too far.

Activation of proMMP-9 from THP-1 cells was achieved by limited proteolysis with trypsin as described previously, and the activation was stopped by adding soybean trypsin inhibitor (SBTI) [67, 68].

The purified recombinant full length human proMMP-9 from Sf9 cells was activated by 1 mM of APMA at 37˚C, MMP-3 (catalytic domain) at 37˚C and trypsin covalently linked to magnetic beads (Mag-Trypsin) at room temperature (approximately 23˚C). ***Activation with APMA***: Briefly, 55 μl 1.0 mM APMA was added to 500 μl of proMMP-9 (4.6 μM). At various time points, 1.0 μl of this mixture was added to 89 μl assay buffer (0.1 M Hepes pH 7.5 containing 10 mM $CaCl_2$, 0.005% Brij-35) and 10 μl 100 μM Mca-PLGLDpaAR-NH_2. The initial rate of the reaction was determined as described under for the determination of kinetic coefficients. When it was estimated that maximal activation has occurred, the activation was stopped by adding 10 mM EDTA. Thereafter, EDTA and APMA were removed from the activated enzyme by applying the enzyme mixture to a spin column with a 10 kDa cut-off and washed with the assay buffer. ***Activation with Mag-Trypsin***: Briefly, 200 μl Mag-Trypsin was first washed with 5x1 ml of assay buffer and finally 200 μl of the same buffer were added to the beads. Then 200 μl of Mag-Trypsin was mixed with 200 μl of proMMP-9 (4.6 μM), and at various time points 0.5 μl of this mixture was added to 89.5 μl of the assay buffer and 10 μl substrate and the initial rate determined as described above. At the estimated maximal activation, Mag-Trypsin was separated from the active MMP-9 using a strong magnet and the activated MMP-9 was thereafter applied to a spin column with a 30 kDa cut-off and washed with assay buffer resulting in 125000-fold dilution of contaminating peptides. ***Activation with MMP-3 (catalytic domain)***: Briefly, 200 μl proMMP-9 (4.6 μM) was mixed with 200 μl of MMP-3 (0.05 μM) in assay buffer, and at various time points 0.25 μl of the mixture was added to 89.8 μl of assay buffer and 10 μl substrate and the initial rate determined as described above. When it was estimated that maximal activation has occurred, the activation was stopped by adding 10 mM EDTA. Thereafter, the activated MMP-9 was separated from MMP-3 by purification on a Gelatin-Sepharose column as described above, with the exception that the buffer also contained 10 mM EDTA at all washing steps and in the elution step. EDTA and DMSO were removed from the activated enzyme by applying the enzyme mixture to a spin column with a 30 kDa cut-off and washing with the assay buffer. Various dilutions of activated proMMP-9 were used for the detection of kinetic coefficients.

Gelatin zymography

SDS-substrate PAGE was done as described previously [69] with gels (7.5 cm x 8.5 cm x 0.75 mm) containing 0.1% (w/v) gelatin in both the stacking and separating gel, 4 and 7.5% (w/v) of polyacrylamide, respectively. Gelatinase activity was evident as cleared (unstained) regions.

Real-time gelatin zymography was performed as described previously for standard gelatin zymography [65, 69]. The exception was that 0.1% (w/v) MDPF-fluorescent labelled gelatin was incorporated in the 7.5% SDS-PAGE separating gel instead of 0.1% (w/v) unlabelled

gelatin. The fluorescent dye 2-methoxy-2,4-diphenyl-3(2H)-furanone was used to label gelatin to give MDPF-gelatin as described previously [70]. The main difference between normal gelatin zymography and real-time gelatin zymography is that in real-time zymography, the gel is not stained and hence it is possible to follow the degradation of the gelatin in real time without staining. Gelatinase activity was evident as dark bands against the undegraded fluorescent background.

Western blotting

Purified proMMP-9 from THP-1 cells and recombinant full length human proMMP-9 from Sf9 cells with and without 0.1 M DTT were electrophoresed on SDS-polyacrylamide gel (NuPAGE Novex 4–12% Bis-Tris gels) and electroblotted to a polyvinyl difluoride membrane. After blockage of non-specific binding sites with non-fat milk in TBS-T (150 mM NaCl, 0.25% Tween-20, 20 mM Tris-HCL, pH 7.4), blots were incubated for 1 h at room temperature with primary rabbit polyclonal antibody against human MMP-9. After washing, the blots were incubated for 1 h at room temperature with an HRP-conjugated goat anti-rabbit secondary antibody. The Blots were thereafter washed with TBS-T 3 x 5 min before visualization using Western Blotting Luminol reagent. The intensity of immunoblot bands was measured using a Luminescent Image Analyzer LAS-3000 with MultiGauge software version 3.0 (Fujifilm, Tokyo, Japan).

Determination of kinetic coefficients

To determine the kinetic and inhibitor kinetic coefficients K_m, and K_i, initial rate experiments were performed using a Perkin Elmer LS 50 Luminescence spectrometer and the FL WinLab Software Package (Perkin Elmer). The reactions were followed for one minute and during that time 600 data points were collected. The excitation and emission wavelengths for the two fluorescence quenched MMP peptide substrates, McaPLGLDpaAR-NH_2 and Mca-RPPGFSAFK (Dpn)-OH were; λ_{ex} = 320 nm, λ_{em} = 405 nm and a slit width = 10 nm at both wavelengths. All assays were performed at 37˚C in an assay buffer of 0.1 M Hepes pH 7.5, 0.005% Brij-35, 10 mM $CaCl_2$ and a total assay volume of 100 μl.

***K_m* determination.** Initial rates were determined with McaPLGLDpaAR-NH_2 and Mca-RPPGFSAFK(Dpn)-OH concentrations ranging from 0.5 to 10.0 μM, higher substrate concentrations resulted in quenching. The K_m value was calculated from non-linear regression of the Michaelis-Menten equation using the Enzyme kinetic module in GraphPad Prism 5.

***K_i* determination.** A fixed substrate concentration of 5.0 μM and / or 10 μM and a fixed enzyme concentration along with varying concentrations of potential inhibitor were used to determine the inhibitory capacity of the two compounds. From a dose response plot, v_i/v_0 vs the concentration of inhibitor [I], Eq (1) was used to determine the IC_{50} values for competitive inhibitors with $K_i > 10$ times the concentration of active enzyme in the assay ([E]) where v_i and v_0 represents the initial rate activity in the presence and absence of inhibitor (I), respectively. For a competitive inhibitor, the IC_{50} value equals $K_i(1+[S]/K_m)$. For tight binding competitive inhibitors ($K_i \leq [E]$), the values of K_i and [E] were obtained by both a dose response plot (v_i/v_0 against [I]) using the Morrison equation [71] (2) and through the linear Henderson Plot [72] (Eq 3). For tight binding inhibitors, the enzyme was pre-incubated for 15 min at 37˚C in the presence of inhibitor and the reaction was started by the addition of substrate.

Graph Pad Prism 5 was used to calculate K_i and [E] values.

$$\frac{v_i}{v_0} = \frac{1}{\left(1 + \frac{[I]}{[IC]_{50}}\right)} \quad (1)$$

$$\frac{v_i}{v_0} = 1 - \frac{\left([E] + [I] + K_i\left(1 + \frac{[S]}{K_m}\right)\right) - \sqrt{\left([E] + [I] + K_i\left(1 + \frac{[S]}{K_m}\right)\right)^2 - 4[E][I]}}{2[E]} \quad (2)$$

$$\frac{[I]}{\left(1 - \frac{v_i}{v_0}\right)} = K_i\left(1 + \frac{[S]}{K_m}\right)\left(\frac{v_0}{v_i}\right) + [E] \quad (3)$$

Ninety-six well plates and a Spectra Max Gemini EM Plate Reader controlled by the computer program Soft Max Pro version 4.3 (Molecular Devices) were used to obtain the binding strength of galardin for thermolysin and pseudolysin. Thermolysin (0.22 nM) and psudolysin (0.26 nM) were pre-incubated with galardin for 15 min at 37˚C. The final galardin concentrations in the assays varied from $2.42{\cdot}10^{-11}$ to $2.42{\cdot}10^{-5}$ M. The enzymatic reaction was started by the addition of Mca-RPPGFSAFK(Dpn)-OH (4 μM in assay), and the initial rate of the reaction was followed for 30 min at 37˚C using the same wavelengths as with the Perkin Elmer fluorimeter as described above. The IC_{50} values were determined from a dose response plot v_i/v_0 vs log [Inhibitor] as described previously [56].

Docking and scoring

Galardin and compound **1b** were docked using the Internal Coordinate Mechanics (ICM) software version 3.8–4 [73]. The compounds were docked into MMP-9, thermolysin and pseudolysin using several X-ray structures of these enzymes in complex with inhibitor. The following structures in the PDB-database were used: MMP-9; 2ovz, 4xct, 5cuh, 4h3x, thermolysin; 5dpe, 1pe5, pseudolysin; 1u4g, 3dbk. The binding modes of the inhibitors in the X-ray complexes were used to define the binding pocket in the docking process. However, X-ray structure complexes with small molecular inhibitors were not available for MMP-14 and auerolysin. For MMP-14 we used an X-ray structure of the catalytic domain of MMP-14 in complex with the tissue inhibitor of metalloproteinase-2 (TIMP-2) (PDB ID: 1bqq). Two strategies were used for identifying the binding pocket. 1: The MMP-14—TIMP-2 X-ray complex were superimposed with the MMP-9 structure in complex with an inhibitor (PDB ID: 5cuh), and the inhibitor of MMP-9 was used to define the binding pocket in MMP-14. 2: The ICM-pocket finder was used to identify the binding pocket. Both strategies gave similar results. For auerolysin the inhibitor-free X-ray structure (PDB ID: 1bqb) was used for docking. The structure was superimposed with the thermolysin-inhibitor complexes (PDB ID: 5dpe) and (PDB ID: 1pe5) and the inhibitor in these complexes were used to define the binding pocket. Crystallographic water molecules and co-crystallized small molecule inhibitors (MMP-9, thermolysin, pseudolysin) were removed and hydrogen atoms were added and optimized using the ECEPP/3 force field of ICM. Galardin and compound **1b** were built using ICM and minimized before docking. A grid map that included the active site amino acids within 5Å of co-crystallized ligand was calculated, and semi-flexible docking with flexible ligands was performed. Three parallel docking simulations were performed and the best-scored from the parallels was selected as the best orientation. The ICM virtual ligand screening (VLS) scoring function was used for scoring. The compounds were docked both with neutral and charged hydroxamate group.

Statistical analysis

To compare the obtained K_i values for the two compounds to the various MPs, a pairwise comparison was obtained by the *t*-test in SigmaPlot (SPSS Corp. Chicago, IL,USA).

Results and discussion

In the present study, enzyme kinetics and molecular modelling have been used to elucidate the binding of two hydroxamate compounds to the human zinc MPs MMP-9 and MMP-14 and the bacterial zinc MPs thermolysin, pseudolysin and auerolysin. The bacterial enzymes are secreted virulence factors, and inhibitors of these enzymes may weaken the pathogen and be a putative therapeutic strategy against bacterial infections. However, such inhibitors should not interfere with the substrate degradation of MMPs and other endogenous zinc MPs of the infected host. Knowledge about the structural determinants for selectivity is therefore important.

Synthesis, purification and activation of proMMP-9

ProMMP-9 was purified from conditioned medium of PMA stimulated THP-1 cells by first passing the medium through a Q-Sepharose column to remove chondroitin sulphate proteoglycans (CSPG) and CSPG associated proMMP-9 (proMMP-9·CSPG) from free proMMP-9 [65]. The pass through fraction from this column contained free proMMP-9, free TIMP-1, TIMP-1 linked to proMMP-9 and other proteins that was applied to a Gelatin-Sepharose column and eluted with 10% DMSO as described earlier [65]. This gave rise to two bands in SDS-PAGE under reducing conditions, a major band at 92 kDa (proMMP-9) and a minor band at 28 kDa (TIMP-1) (Fig 2A). TIMP-1 does not bind to the Gelatin-Sepharose column, but TIMP-1 binds through its C-terminal domain to the C-terminal HPX-domain of proMMP-9 [42, 63, 74, 75] and hence purified proMMP-9 from THP-1 cells will always contain some TIMP-1. The bound TIMP-1 has its N-terminal domain free, the domain that interacts with the active site in MMPs and inhibits the activity. Hence, the presence of proMMP-9·TIMP-1 complexes will affect the activation of proMMP-9 by other active MMPs such as MMP-3. TIMP-1 binds to the active site of these MMPs and form ternary proMMP-9·TIMP-1·MMP and MMP-9·TIMP-1·MMP complexes [63, 74]. The presence of TIMP-1 will not interfere with trypsin during the activation of proMMP-9, but the inhibitor will bind to the active site of the activated MMP-9. TIMPs are slow, tight-binding reversible inhibitors with dissociation constants in the pico-molar region and low dissociation rates of the formed complex [32, 76]. A detailed study of the binding of TIMP-2 to MMP-2 revealed a dissociation constant (K_i) of 0.6 fM and a rate constant for the dissociation of the MMP-2•TIMP-2 complex of $2x10^{-8}$ s^{-1}, i.e. a half-life of approximately 1 year [77]. Similar detailed studies have not been performed for the binding of TIMP-1 to the full length MMP-9, and reliable K_i values could not be obtained with conventional methods due to the strong binding (low pico-molar region) [78]. The level of MMP-9 activity depends on the amount of TIMP-1 compared to the amount of active MMP-9. With such tight complexes and extremely slow dissociation rates it is fair to assume that the presence of TIMP-1 in the MMP-9 preparation will not affect the K_m value for a substrate or the K_i value of an inhibitor compared to an enzyme preparation without TIMP-1 present. Trypsin activation gave rise to a main active form of MMP-9 with a molecular size of approximately 84 kDa, and three minor bands of lower molecular size ranging between 62–80 kDa (Fig 2B). Previously it has been shown that trypsin activated MMP-9 has lost the pro-domain and has F107 (sequence numbering includes the pre-sequence of 19 amino acids) as its N-terminal amino acid residue, and hence the zinc binding motif (97-PRCGVPD) has been removed [32]. The purified proMMP-9 was also treated with 1 mM APMA at 37°C up to 24h. Zymography revealed that most of the 92 kDa pro-form of MMP-9

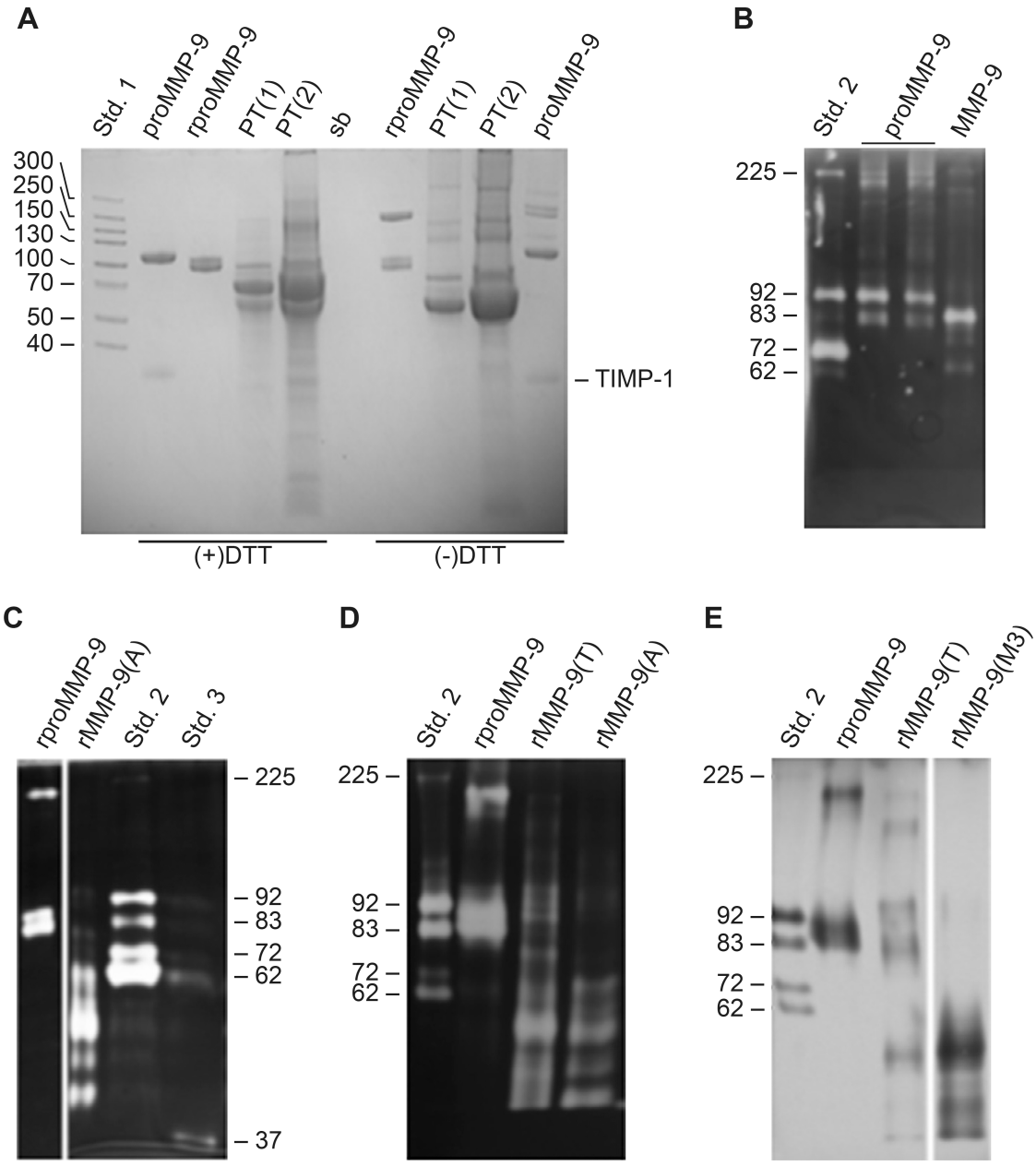

Fig 2. Purification and activation of proMMP-9. (**A**) Imperial stained SDS-PAGE showing the purity of purified recombinant human full length proMMP-9 expressed in Sf9 cells (rproMMP-9) and of proMMP-9 purified from THP-1 cells (proMMP-9) as described in the Materials and Methods section. PT is the pass through fraction from Gelatin-Sepharose Chromatography of the recombinant enzyme, and 4 times more protein was loaded to the gel in the lanes labelled PT(2) compared to the lanes labelled PT (1). Std. 1 is the molecular size marker Spectra^{TM} Mulitcolor High Range Protein Ladder and sb is sample buffer. Prior to electrophoresis, samples were either treated (+) or not treated (-) with DTT. Gelatin (**B-D**) and real-time gelatin (**E**) zymography of purified proMMP-9, trypsin activated (MMP-9) proMMP-9 from THP-1 cells, purified rproMMP-9, AMPA (rMMP-9(A)), trypsin (rMMP-9(T)) and MMP-3 (rMMP-9(M3)) activated recombinant proMMP-9. Std.2 in (**B-E**) is a mixture of proMMP-9 from THP-1 cells and proMMP-2 from human skin fibroblasts. Std. 3 is the 37 kDa catalytic domain of human MMP-9.

https://doi.org/10.1371/journal.pone.0200237.g002

had been converted to an 84 kDa form, but no activity could be detected by the rate assay (data not shown). APMA activated MMP-9 has an intact zinc binding motif (97-PRCGVPD) in the pro-domain with M94 (sequence numbering includes the pre-sequence of 19 amino acids) as its

N-terminal amino acid residue [32, 41, 43, 45, 79, 80]. The lack of activity is expected, as the enzyme in addition must be C-terminally truncated in order to be active [41, 42, 74].

TIMP-1 free recombinant full length human proMMP-9 was expressed in baculovirus infected Sf9 cells and purified from the serum-containing medium in a one-step procedure using a Gelatin-Sepharose column. This gave rise to three bands in non-reducing SDS-PAGE (Fig 2A) and gelatin zymography (Fig 2C), a band at 205 kDa and two bands at 87 and 83 kDa. SDS-PAGE under reducing and non-reducing conditions (Fig 2A) revealed that the band of 205 kDa was either a homodimer or a homotrimer as recently shown by Vandooren et al. 2015 [81] and Western blotting along with mass spectroscopy (MS) confirmed that all three bands were proMMP-9 (data not shown). The slightly lower molecular size of the recombinant proMMP-9 compared to the native proMMP-9 is most likely due to difference in glycosylation of the hinge region [40]. APMA activation of purified recombinant proMMP-9 in the presence of 10 mM of $CaCl_2$ resulted in a main form of active MMP-9 with a molecular size of 54 kDa and three minor forms with molecular sizes of 61, 49 and 45 kDa (Fig 2C). Previously it has been shown that APMA activated MMP-9 has an intact zinc binding motif (97-PRCGVPD) in the pro-domain with M94 (sequence numbering includes the pre-sequence of 19 amino acids) as its N-terminal amino acid residue and parts of the HPX-domain removed [32, 41, 43, 45, 79, 80]. Mercury ion induced auto-cleavage of the MMP-9 HPX domain occurred between E687 and L688 in the end of blade 4 and between Ala526 and Glu527 in the beginning of blade 1 [45]. A disulphide bridge link between C516 and C704 link blade 1 and blade 4 [27, 30]. This suggests that in the 54 kDa active rMMP-9, almost the entire HPX domain is removed, but with the last amino acids in the HPX C-terminal domain (L688—D707) retained linked to the processed enzyme through the disulphide bridge between C516 and C704. Previously it was suggested that the presence of Ca^{2+} resulted in C-terminal truncation and a conformational change that unblocked the catalytic site and hence resulted in an enzyme with full enzymatic activity [79].

Trypsin activation of the purified recombinant proMMP-9 resulted in a zymography pattern similar to the APMA activated enzyme (Fig 2D), with a main form of active MMP-9 with a molecular size slightly larger than 54 kDa. Thus, trypsin induced activation of the recombinant proMMP-9 resulted in both the removal of the N-terminal pro-domain as well as large parts or almost the entire C-terminal HPX-domain similar to the APMA activated enzyme.

As for the trypsin induced activation of the recombinant proMMP-9, MMP-3(catalytic domain) induced activation also resulted in a combination of N- and C-terminal truncation of the recombinant proMMP-9 (S1 Fig). This is in agreement with previous reports on MMP-3 induced activation of proMMP-9 [43, 80]. The fully MMP-3 activated MMP-9 (rMMP-9(M3)) after removal of MMP-3, contaminating peptides, EDTA and DMSO, has a major band at approximately 54 kDa, and two minor bands with lower molecular size (Fig 2E). As for the APMA and trypsin activated MMP-9, the MMP3 activated form also lacks large parts or the entire C-terminal HPX-domain. Previously it was shown that MMP-3 and trypsin-activated MMP-9 has identical N-terminal residue, F107 [32].

K_m determination

In order to study the binding strength of inhibitors to an enzyme, it is first necessary to determine the enzyme's K_m value for the substrate under the conditions used to study inhibitory binding. The quenched fluorescence substrate Mca-PLGLDpaAR-NH_2 was used for the studies with MMP-9 and MMP-14. For trypsin activated MMP-9 from THP-1 cells a K_m value of 3.0 ± 0.7 μM was obtained, while for APMA, trypsin and MMP-3 activated recombinant human MMP-9 (rMMP-9(A), rMMP-9(T) and rMMP-9(M3)) K_m values of 3.2 ± 0.2, 3.1 ± 0.4

and 4.5 ± 0.4 μM, respectively, were obtained. Thus, there was no significant variation in the obtained K_m values in spite of differences in their N- and C-terminal amino acid residues. This is in contrast to trypsin and APMA activated MMP-2, where the differences in N- and C-terminal amino acid residues had an effect on the K_m value for the substrate [62].

The obtained K_m value for MMP-14 was 6.9 ± 0.9 μM. The K_m values obtained for MMP-9 and MMP-14 are similar to our previous K_m values (4 ± 1 μM and 6 ± 1 μM) determined under almost identical conditions, with the exception that the assay in our previous study also contained 5% DMSO [67].

With the bacterial MPs, the quenched fluorescence substrate Mca-RPPGFSAFK(Dnp)-OH was used. The obtained K_m values for auerolysin, thermolysin and pseudolysin were 47 ± 41 μM, 6 ± 1 μM and 24 ± 8 μM, respectively. For auerolysin and pseudolysin, the K_m values are far above the highest concentration that could be used in the assay due to quenching at concentrations higher than 10 μM. In spite of the low precision of the obtained K_m values for auerolysin and pseudolysin, it can be concluded that the substrate concentration of 5.0 μM and 4.0 μM used in the inhibition experiments is far lower than the K_m value, and hence the obtained IC_{50} and K_i^{app} values are close to the real K_i values.

K_i determination

To be able to compare the binding strength of different inhibitors for a given enzyme and of a given inhibitor for different enzymes, it is important that the reported K_i values are obtained under the same conditions and with the same methods. For tight binding inhibitors, it is necessary to know the amount of active enzyme in the assay in order to obtain a correct K_i value. As the two inhibitory compounds studied here contain a strong zinc binding residue, the hydroxamate group, the two compounds are believed to be competitive inhibitors. To assure that the obtained K_i values for the two compounds are as correct as possible and competitive with the substrate, we have varied the concentration of the inhibitors in a series of experiments. Two different concentrations of enzyme have been used, and in some cases also two different substrate concentrations. We have compared the obtained results from two plotting and estimation methods, which determine both the concentration of active enzyme ([E]) in the assay and the K_i value. One method is using the Morrison equation [71] (Eq 2 in the Materials and Methods section) to fit the results to a plot v_i/v_0 vs [I], while the other is the Henderson plot [72] (Eq 3 in the Materials and Methods section) which is based on a linearized form of the Morrison equation.

***K_i* MMP-14.** Galardin (Gm6001) inhibits the MMP-14 (catalytic domain) with a reported IC_{50} value of 13.4 nM [60], while the IC_{50} value is not reported for compound **1b.** Fig 3A shows a typical dose response plot (v_i/v_0 vs [Gm6001]) using two different enzyme concentrations and Fig 3B a typical Henderson plot where one experiment contained twice as high concentration of both MMP-14 and substrate as the other experiment. In the Henderson plot the concentration of MMP-14 in the assay can be directly determined from the regression lines crossing of the y-axis. Furthermore, the slope in a Henderson plot gives an apparent K_i (K_i^{app}) value. For a competitive inhibitor, K_i^{app} equals $K_i(1+[S]/K_m)$ and hence, the slope increases with increasing substrate concentrations. As expected, this is the case for the galardin inhibition of MMP-14 (Fig 3B). Table 1 shows the obtained average K_i value from the different Henderson plots. Although there were some differences in the results obtained from the Henderson plot and the Morrison equation for an individual experiment (S1 Table and Fig 3), the average K_i value for galardin was the same, 0.87 nM.

The inhibitory effects of compound **1b** on MMP-14 are shown in Fig 3C and 3D. Although the K_i values obtained from the Morrison equation are slightly higher than the values obtained

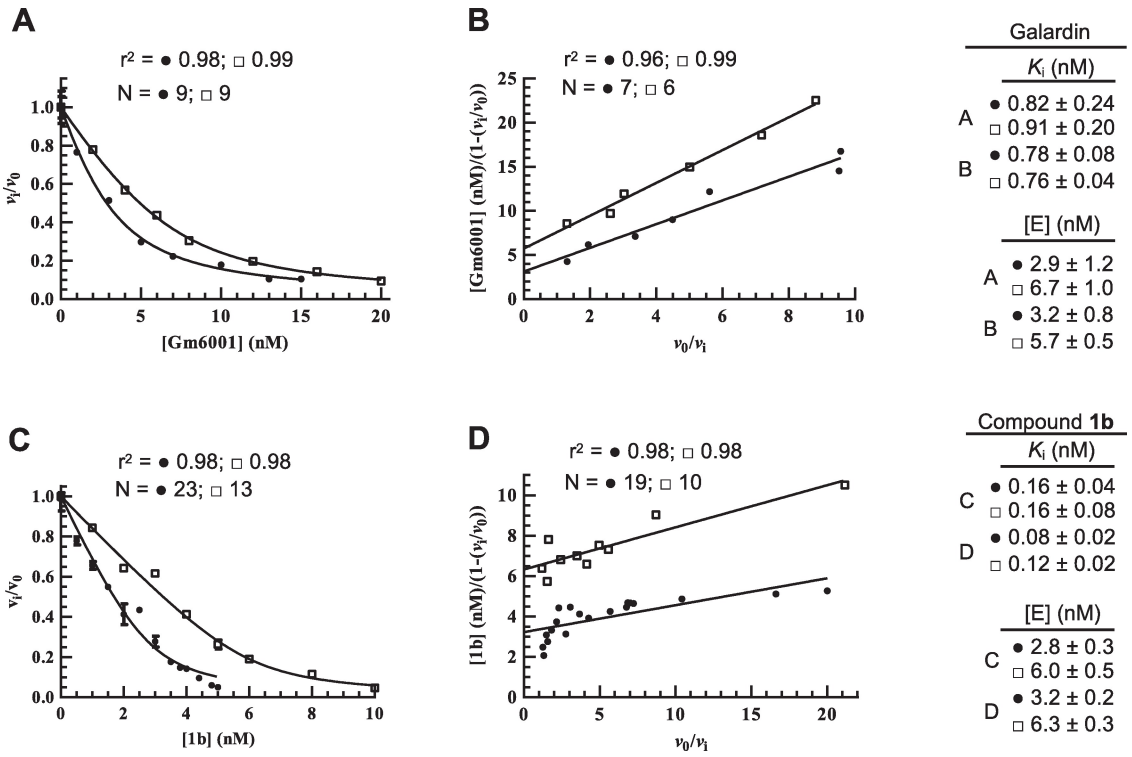

Fig 3. Inhibition of MMP-14 by galardin (A, B) and compound 1b (C, D). The inhibition constant K_i and [MMP-14] in assay were obtained from dose response plots v_i/v_0 vs [I] using the Morrison Eq (2) (**A, C**) and Henderson plots (**B, D**). In all plots, [MMP-14] was twice as high for experiments labelled (□) as for those labelled (●). The [S] is 5.0 μM except in the experiment in (**B**) labelled (□) where it is 10.0 μM. Shown in the figures is also the obtained K_i and [E] values (mean ± SD), in addition to the regression coefficient r^2 and the number of individual assays (N) for each curve.

https://doi.org/10.1371/journal.pone.0200237.g003

Table 1. Inhibitory activity of galardin and compound 1b against human and bacterial metalloproteases.

Protease	K_i (nM)	
	Galardin	1b
MMP-14	0.870 ± 0.070 (5)	0.090 ± 0.020 (4)
rMMP-9(A)	0.051 ± 0.003 (5)	0.011 ± 0.001 (2)
rMMP-9(T)	0.069 ± 0.001 (5)	N.D.[a]
rMMP-9(M3)	0.063 ± 0.008 (3)	N.D.
MMP-9(T)	0.067 ± 0.006 (4)	0.006 ± 0.000 (2)
Auerolysin	452 ± 35 (1)[b]	N.I.[c]
Thermolysin	20[d]	N.I.
Pseudolysin	20[d]	N.I.

The K_i values were obtained through Henderson plots as described in materials and methods. Presented is the K_i ± S.E.M. and in parenthesis the number of independent individual experiments that has given rise to the presented values. The results shown are for recombinant human MMP-14 catalytic domain, recombinant human MMP-9 activated with APMA (rMMP-9(A)), magnetic trypsin beads (rMMP-9 (T)), MMP-3 (rMMP-9(M3), trypsin activated human MMP-9 isolated from THP-1 cells (MMP-9 (T)), auerolysin, thermolysin and pseudolysin.

[a]N.D., not done;

[b]Values from dose response plot using Eq (1) in methods;

[c]N.I., no inhibition up to 100 μM of inhibitor;

[d]Values from Grobelny D et al. [58].

https://doi.org/10.1371/journal.pone.0200237.t001

from the Henderson plots of the same experiment (S2 Table), it can be concluded that compound **1b** is a significantly stronger MMP-14 binder than galardin ($p<0.001$; Table 1).

***K_i* MMP-9.** Previous works showed that both galardin and compound **1b** are tight binding inhibitors of MMP-9. The obtained IC_{50} and K_i values for galardin were 0.5 nM and 0.18 nM, respectively [59, 60] and a K_i value for compound **1b** of 0.097 nM [61]. An MMP may be activated by several different compounds, including various proteases and organo-mercurial compounds like APMA. This often results in removal of non-identical parts from the pro-domain of the given MMP, giving a different N-terminal residue of the activated forms. Differences in N-terminal residue of the activated forms may affect both inhibitor binding and degradation of biological and small chromogenic substrates. Previously we have shown that APMA and trypsin activated MMP-2 have different capacity to bind TIMP-1 as well as different ability to cleave both gelatin and the quenched fluorescence substrate Mca-PLGLDpaAR-NH_2 [62]. We have therefore tested the binding of galardin to APMA, MMP-3 and trypsin activated MMP-9 and compound **1b** to both APMA and trypsin activated MMP-9. As shown in Tables 1 and S1, galardin binds with similar strength to the four forms of activated MMP-9 (0.051–0.069 nM, Henderson plot; 0.057–0.074 nM, Morrison equation). Furthermore, the K_i values calculated from the Morrison equation were similar and not statistically different from the values obtained by the Henderson plot (S1 Table). It was only the K_i value obtained by APMA activated rMMP-9 that was slightly lower than the values for the other activated forms. Disregarding this slight difference in binding strength, it can be concluded that the difference in N- and C-terminal amino acid residues in the different activated rMMP-9 species, the presence of the HPX-domain and small amounts of TIMP-1 (MMP-9) as well as differences in O-glycosylation of the hinge region (rMMP-9 vs MMP-9) have no significant effect on the enzyme's affinity for galardin.

Compound **1b** binds significantly stronger to both APMA and trypsin activated MMP-9 than galardin ($p<0.003$; Tables 1, S1 and S2). Furthermore, the K_i values of compound **1b** calculated from the Morrison equation (0.016 ± 0.001; 0.008 ± 0.003) was not statistically different from the values obtained from the Henderson plots (0.011 ± 0.001; 0.006 ± 0.002) (S2 Table). Furthermore, the difference in K_i for compound **1b** between rMMP-9 and MMP-9 was not statistically significant (Tables 1 and S2).

***K_i* bacterial metalloproteases.** Previous studies showed that galardin is a strong inhibitor of thermolysin and pseudolysin (Table 1) [58]. In initial scanning experiments of various inhibitors in our laboratory, galardin was used as a control compound. The obtained K_i values (data not shown) were similar to those obtained by Grobelny et al [58]. Galardin was also a strong inhibitor of auerolysin with a K_i value much larger than the 3.6 nM of enzyme used in the assay. The line in the Henderson plot crossed at origo. The K_i^{app} value from the slope of the curve was 0.50 ± 0.06 μM ($r^2 = 0.84$; N = 16), giving a K_i value of 0.45 ± 0.05 μM. A dose response plot v_i/v_0 vs [galardin] using Eq (1) in the Materials and Methods section resulted in an IC_{50} value of 0.50 ± 0.04 μM ($r^2 = 0.96$; N = 18) giving a K_i value of 0.45 μM (Table 1). Thus, the binding of galardin to auerolysin is about 25 times weaker than the binding to thermolysin and pseudolysin.

Notable, up to the highest concentration tested of compound **1b** (100 μM), no inhibitory effect of the three bacterial MPs was detected (Table 1).

Docking and molecular modelling

In order to elucidate the structural reasons for the differences in binding affinity for the studied MPs, we have examined the binding modes of galardin and **1b** by docking. Furthermore, it was suggested that the NHOH group of a hydroxamate compound may lose its proton at or close to the physiological pH and generate a negatively charged group (NHO^-)

[82]. Protonation/deprotonation of the NHO(H) moiety may influence the zinc binding properties of hydroxamate compounds, and therefore, **1b** and galardin were docked both with protonated and deprotonated NHO(H) moiety. When available, the compounds were docked into several structures of the enzyme. In that way, target structural flexibility to some extent was taken into account in the docking process. The docking studies indicated that the protonated and deprotonated inhibitors had almost similar binding modes at the active sites. Further, the docking showed that the protonated galardin and **1b** had better docking scores than the deprotonated forms for all enzymes, which is contradictory to a previous docking study of other hydroxamates for the MMP-9, indicating that the deprotonated hydroxamates in general scored better than the protonated [83].

MMP-9

Four MMP-9 complexes from the PDB database were used for docking of both protonated and deprotonated variants of galardin and **1b**. The best scoring values were obtained with the 5cuh (PDB ID) structure. This structure is obtained from a truncated recombinant MMP-9 variant, that is lacking the pro, hinge and C-terminal HPX domains in addition to the FnII module in the catalytic site, and the PDB file is numbered from amino acids G106 to G269. The N-terminal of this recombinant variant is starting at the 106-GFQT segment. The G residue is not present in the natural variant [25, 27] and in trypsin and MMP-3 activated MMP-9 the N-terminal is 107-FQT [32]. In the full-length enzyme, the 175 amino acid long FnII module is present between amino acids V216 and G217 and we therefore used the numbering given in the Merops data base [25] for the amino acids. The X-ray structure of the human proMMP-9 has been resolved at 2.5 Å resolution (PDB id: 1L6J). The structure includes the pro-domain, the catalytic domain and the FnII module. The docking was performed into X-ray complexes with small molecular inhibitors that were used to define the binding region of the inhibitors during docking. A grid map that included all amino acids within 5Å of the co-crystallized inhibitor were used in the docking. The FnII module may influence inhibitor binding, but Fig 4 indicates that the FnII domain is located far from the binding site of small molecular inhibitors, and that the grid map used for docking should not be influenced by the presence of the FnII module. The lack of FnII module in the 5cuh structure should therefore not affect the docking of the molecules in the present study.

For protonated compound **1b**, both the oxygens on the NHO(H) and CO groups of the hydroxamate moiety binds to the catalytic zinc (Fig 5). In addition, the hydroxamate forms hydrogen bonds between the hydroxyl hydrogen of the NHO(H) moiety and the side chain of E402, while the nitrogen hydrogen of the NHO(H) moiety forms a hydrogen bond with the backbone CO of A189. The heterocyclic ring with its three OH-groups points into the opening of the active site cavity and appears not to have direct interactions with residues of the enzyme. One of the oxygens of the SO_2 group forms a hydrogen bond with the backbone NH of L188. The diphenyl ether moiety is located within the S'_1-subpocket (Fig 6) having interactions with the side chains of L188, L397, V398, H401, Y423 and T426 (Figs 5 and 6). Compound **1b** also has van-der Waals interactions with many main chain residues including H401, M422 and R424. In summary, in addition to large van-der Waals interactions, compound **1b** forms 3 hydrogen bonds with the enzyme and 2 ionic interactions with the catalytic zinc ion. The de-protonated form of compound **1b** overlapped with the protonated form and the main difference was that the de-protonated variant lacked the hydrogen bond to the E402 side chain (not shown).

The binding mode of galardin to MMP-9 was similar to that of compound **1b** (Fig 5). The CO and NHO(H) moieties interact with the zinc, E402 and A189 similarly to compound **1b**. The 4-methylpentanoyl moiety in galardin was located in the S'_1-subpocket, but not as deep

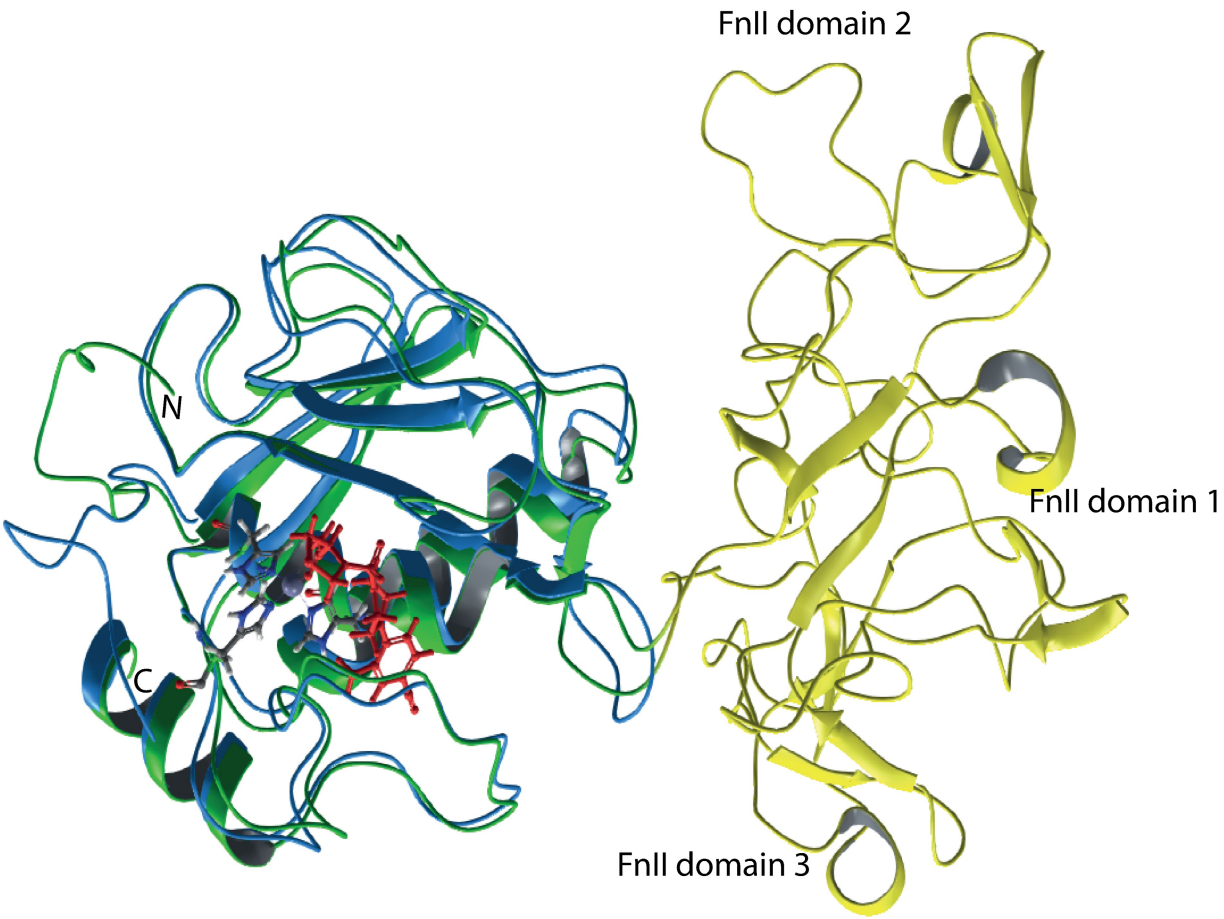

Fig 4. Structural superimposition (backbone) of the 5cuh and the 1l6j x-ray structures of MMP-9. The 1l6j structure contains the FnII domains (yellow) and the catalytic domain (green), while the 5cuh only contains the catalytic domain (blue). The pro-domain has been deleted from 1l6j, such that the sequence starts at F107. The co-crystallized hydroxamate inhibitor LT4 of the 5cuh in red, while the catalytic zinc and the coordinating histidines are in grey. The position of the co-crystallized inhibitor was used to define the docking grid during docking of galardin and compound **1b**, and the figure shows that the docking into a structure lacking the FnII domains (5cuh) should not affect the docking results.

https://doi.org/10.1371/journal.pone.0200237.g004

into the pocket and with less interaction than the diphenyl ether of compound **1b** (Fig 6). The main interactions of this hydrophobic moiety of galardin are with the side chains of H401, V398, P421 and Y423 (Fig 5). The oxygen of the CO neighbour of the 4-methylpentanoyl moiety and the oxygen on the tryptophan methylamide form hydrogen bonds with the main chain NH of L188 and Y423, respectively. The tryptophan moiety points into the opening of the active site cavity and appears to have no direct interactions with the enzyme. The docking indicates that both protonated **1b** and galardin forms two ionic interactions with the zinc, and three hydrogen bonds with the enzyme. The main difference is that the diphenyl ether moiety of compound **1b** penetrates deeper into the S'_1-subpocket than the 4-methylpentanoyl moiety of galardin (Fig 6). This appears to be the main explanation for the approximately 5 to 10 times stronger interaction of MMP-9 with compound **1b** than with galardin.

MMP-14

The docking indicated that compound **1b** and galardin bind MMP-14 in similar binding modes as for MMP-9 (Fig 5). The compounds were docked using two different approaches to

MMP-9
Galardin

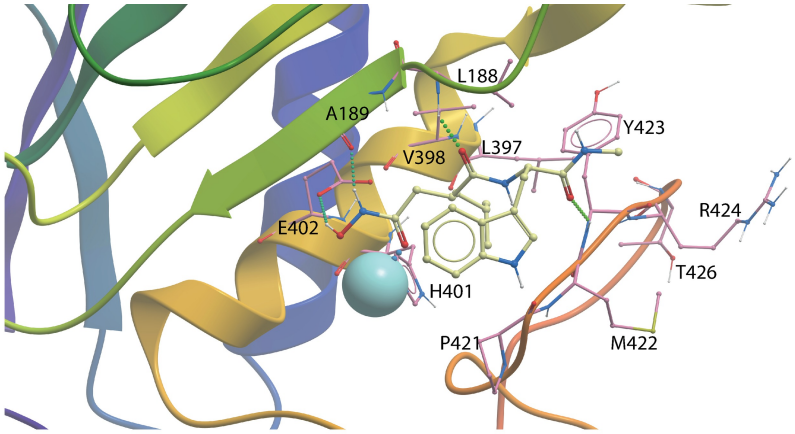

MMP-9
1b

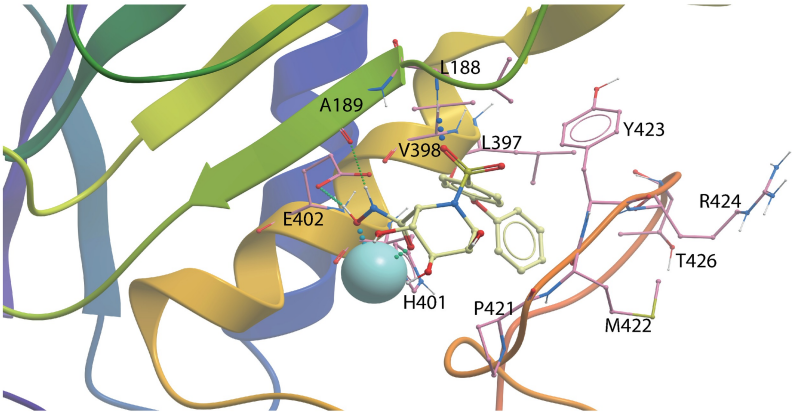

MMP-14
Galardin

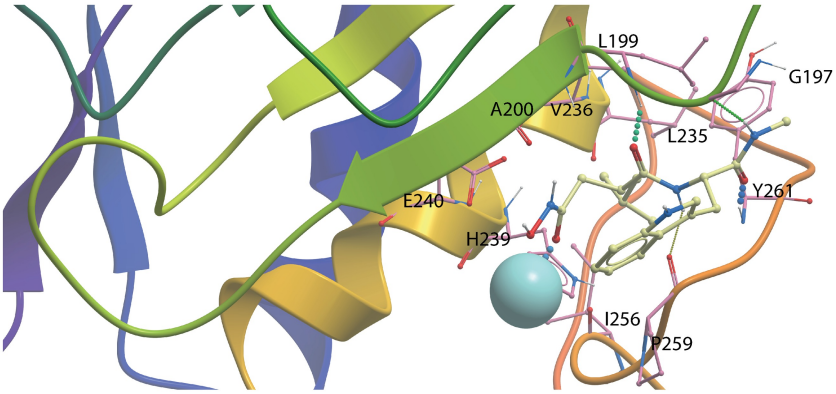

MMP-14
1b

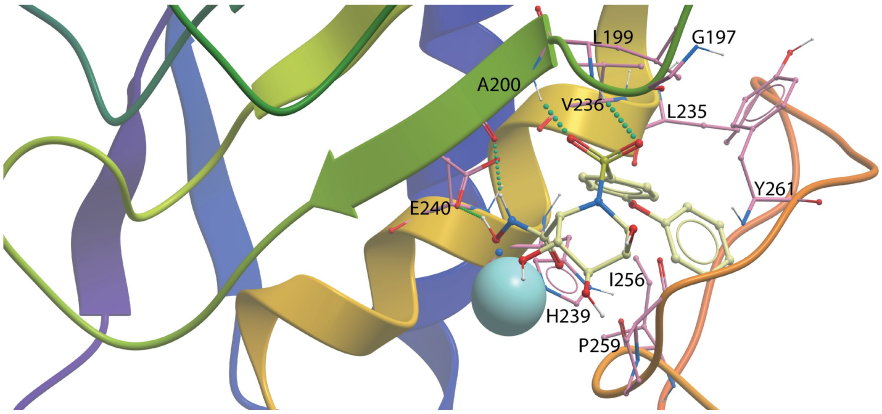

Fig 5. Galardin and compound 1b docked into the catalytic site of MMP-9 and MMP-14. The figure shows close ups of the active site region with the compound structures (xsticks), secondary structure elements and the most important amino acids for ligand binding (xsticks) indicated. Colour coding of atoms of amino acids and ligands: oxygen; red, nitrogen; blue, hydrogen; white, sulphur; yellow, carbon atoms of ligands; yellow, carbon atoms of amino acid side chains; pink, the zinc ion; light blue. The secondary structures elements are coloured from the N- to the C-terminal such that corresponding secondary elements of MMP-9 and MMP-14 obtain similar colour.

https://doi.org/10.1371/journal.pone.0200237.g005

define the binding pocket (ICM pocket finder and superimposing with a MMP-9 inhibitor complex), and both approaches gave similar results. Both protonated and un-protonated compounds had quite similar binding modes, however, with some differences.

Protonated **1b** formed more hydrogen bonds with the enzyme than deprotonated **1b** and had better scoring values. In the highest scored binding mode of compound **1b** the two oxygen atoms in the CONHO(H) moiety formed strong interactions with the catalytic zinc. However, due to protonation, the position of the CONHOH is slightly disturbed compared with the deprotonated counterpart, such that the hydroxyl hydrogen of the NHOH forms a hydrogen bond with the side chain of E240, while NH forms a hydrogen bond with the main chain CO of A200 (Fig 5). Such hydrogen bonds are not observed for the deprotonated **1b**. The three OH-groups of the heterocyclic ring point into the opening of the active site cavity without direct interactions with the enzyme. The SO_2 group of protonated **1b** forms two hydrogen bonds with the main chain NH of residues A200 and L199 (Fig 5), while the SO_2 of the deprotonated **1b** forms a hydrogen bond with the backbone NH of A200, only. The diphenyl ether moiety is filling up large parts of the S'_1-subpocket as seen for MMP-9 (Fig 6), having interactions with the side chains of L199, L235, V236, H239, I256, P259 and Y261. The ether oxygen is close to the Nd1 atom of H239. One of the main reasons for the slightly weaker binding of compound **1b** to MMP-14 than to MMP-9 seems to be that the size of the S'_1-subpocket is larger in MMP-9 (based on calculations by ICM pocket finder) and hence allows for more freedom of the ligand to obtain optimal interactions.

Galardin binds MMP-14 very similar to compound **1b**. The hydroxamate forms two ionic interactions with the catalytic zinc ion, one through the carbonyl oxygen and the other through the oxygen at the NHO(H) group (Fig 5). The hydroxyl hydrogen of the protonated NHO(H) moiety has a hydrogen bond with the side chain of E240. The nitrogen proton at NHO(H) forms a hydrogen bond with the CO of A200. The 4-methylpentanoyl moiety was located in the entrance of S'_1-subpocket and interacted with the side chains of H239, Y261(Me), L199(cd1) and V236. The amide neighbour of the 4-methylpentanoyl moiety forms two hydrogen bonds, one between the CO oxygen and main chain NH of L199, and the other between the NH and the CO on P259. The methylamide moiety also forms two hydrogen bonds to the main chain of the enzyme, one between the CO group and the NH of Y261 and the other between the NH moiety and the CO of G197. The tryptophan moiety points into the opening of the active site cavity having minimal interactions with the enzyme. The most likely explanation for the 10 times stronger interaction of compound **1b** with the enzyme compared to the interaction with galardin is that the diphenyl ether moiety in the former compound has a larger interaction surface with the S'_1-subpocket than the 4-methylpentanoyl moiety of galardin.

Bacterial metalloproteases

The binding studies indicated that galardin binds quite strongly to thermolysin and pseudolysin and somewhat weaker to aeurolysin, while inhibition of these enzyme by compound **1b** was not observed. These results were also confirmed by the docking studies. Galardin fits into the binding pocket of these enzymes with ionic interactions between the oxygen atoms of the CONHO(H)-moiety and the zinc ion (Fig 7), and with the 4-methylpentanoyl moiety into S'_1-

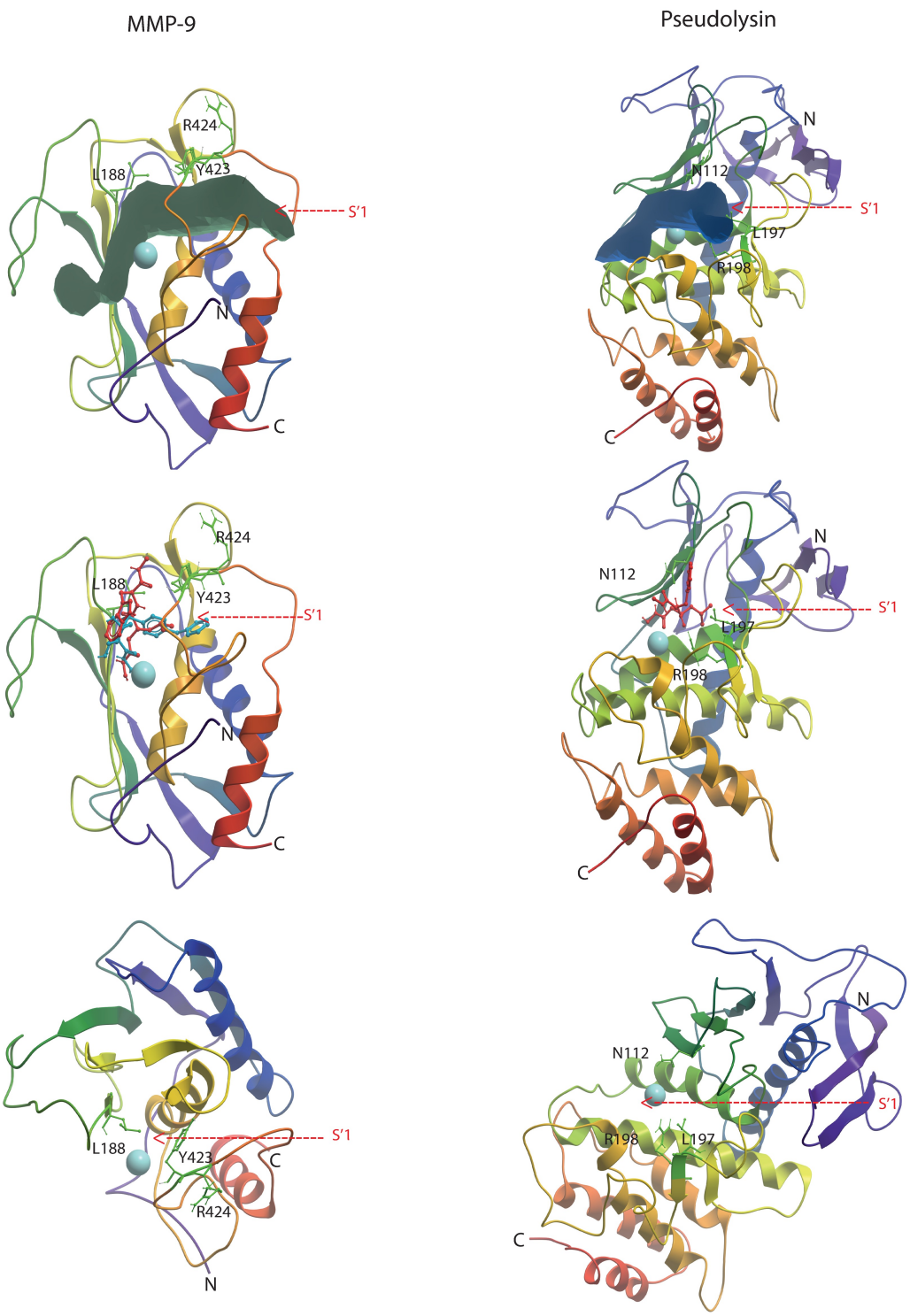

Fig 6. Galardin and compound 1b docked into MMP-9 and galardin docked into pseudolysin. Upper panel: The backbones of MMP-9 (5cuh) and pseudolysin (3dbk). The volume of the full binding pocket identified by the ICM Pocketfinder is displayed for both enzymes, with the S'_1-subpocket indicated by an arrow. Middle panel: Galardin (red) and compound **1b** (blue) docked into the binding pocket of MMP-9 and galardin (red) docked into pseudolysin. The panel shows that compounds may enter the S'_1-subpocket of MMP-9 in a region between the side chains of Y423 and L188 on one side and the zinc. The corresponding entrance in pseudolysin is partly hindered by the side chain of R198. Lower panel: The complex from the middle section rotated 90 degrees and the ligands removed. The panel shows that the

side chains of L188 and Y423 are located close to each other and hinder the entrance into the S'$_1$-subpocket from the region above the zinc, while the corresponding region in pseudolysin is wider (side chains of N112 and L197).

https://doi.org/10.1371/journal.pone.0200237.g006

subpocket (Figs 6 and 7). However, compound **1b,** did not fit into the binding site of the bacterial enzymes, and reasonable binding modes were not obtained in any of the bacterial enzymes. The docking indicates that the diphenyl ether moiety of **1b** is too big for a proper fitting into the S´$_1$-subpocket as observed for compound **1b** in the MMPs. The S´$_1$-subpocket of the bacterial enzymes seems much more rigid than that of the MMPs. An important reason for that is an arginine (corresponding to R198 of pseudolysin), which is located at the end of a β-strand at the border between the S´$_1$- and S´$_2$-subpockets and is pointing into the binding site. This arginine interacts with galardin, but does not hinder the smaller 4-methylpentanoyl moiety of galardin to enter the S´$_1$-subpocket (Figs 6 and 7), while the diphenyl ether moiety of **1b** is hindered. However, the arginine hinders galardin to penetrate deeply into the pocket. The corresponding region of the studied MMPs constitutes a structurally more flexible loop region (methionine loop) that more easily can adopt to the inhibitor structure.

For thermolysin, the binding mode of protonated and deprotonated galardin were similar. The best scoring was obtained with the X-ray structure 5dpe (PDB ID). The CONHO(H)-moiety forms two ionic interactions with the zinc (Fig 7). The NH group of the hydroxamate is hydrogen bonded with E143 (corresponding to E402 in MMP-9 and E240 in MMP-14), while the CO group is also hydrogen bonded with the side chain of H231 (NH in the ring). The 4-methylpentanoyl was located in the S´$_1$-subpocket, while the CO oxygen next to the 4-methylpentanoyl formed two hydrogen bonds with the side chain of R203 (Fig 7). Both the CO and the NH of the tryptophan methylamide are both engaged in hydrogen bonds with the side chain of N112. The NH of the tryptophan ring forms a hydrogen bond with the CO at the backbone of N111.

Most of the interactions of galardin with thermoysin are similar to those in pseudolysin (Fig 7). The amino acids corresponding to E143, H231, R203, N111, and N112 are conserved between the enzymes. The only differences between the highest scored binding mode in thermolysin and pseudolysin was that the NH of the CONHO(H)-moiety was located a bit more distantly from E141 (corresponding to E143 in thermolysin), and that H223 (corresponding to H231 in thermolysin) did not form a hydrogen bond with the CO of the hydroxamate.

The binding mode of galardin with auerolysin (Fig 7) is very similar to the binding modes in thermolysin and pseudolysin, however, there are some differences. Protonated and deprotonated galardin have similar binding modes, but protonated galardin scores better than deprotonated. The CONHO(H)-moiety forms two ionic interactions with zinc, while the protonated OH of the hydroxamate has a hydrogen bond with the side chain of E145 (corresponding to E143 in thermolysin and E141 in pseudolysin). The NH group of the hydroxamate has a hydrogen bond to the backbone CO of A115. The 4-methylpentanoyl is pointing into the S´$_1$-subpocket, while the CO oxygen next to the 4-methylpentanoyl forms a hydrogen bond with the side chain of R200 (corresponding to R203 in thermolysin and R198 in pseudolysin). However, the CO and the NH of the tryptophan methylamide are not involved in hydrogen bonding with the enzymes, which may explain the lower binding affinity of galardin for aeurolysin than for thermolysin and pseudolysin.

Conclusions

Activation of the rproMMP-9 resulted in a largely truncated form in all scenarios, lacking most of or the entire HPX-domain but appearing to contain the entire O-glycosylated hinge region. The main difference between the three activated variants of rMMP-9 seems to be in the

Thermolysin

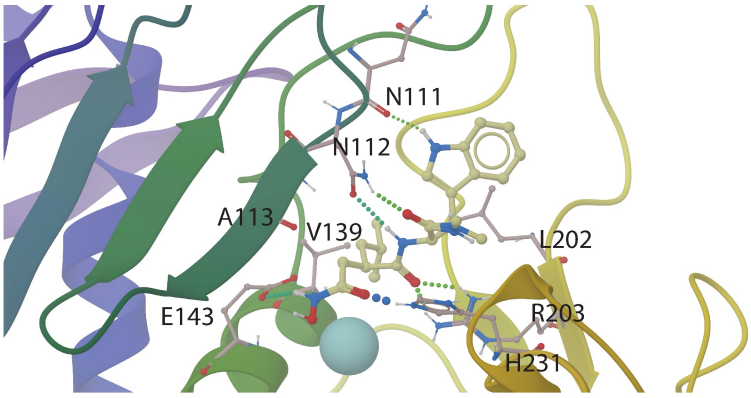

Pseudolysin

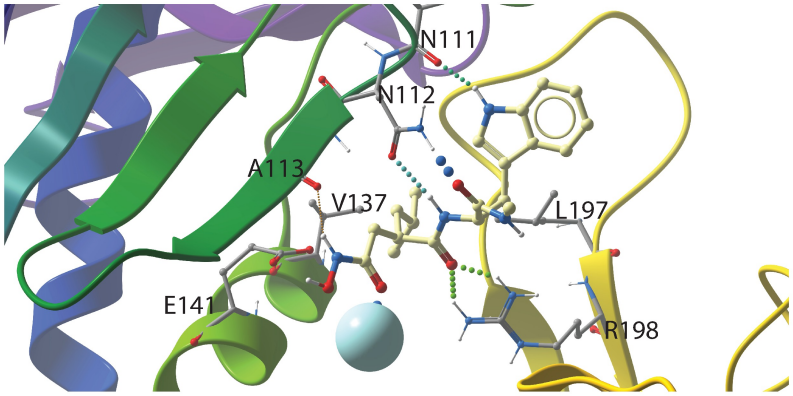

Auerolysin

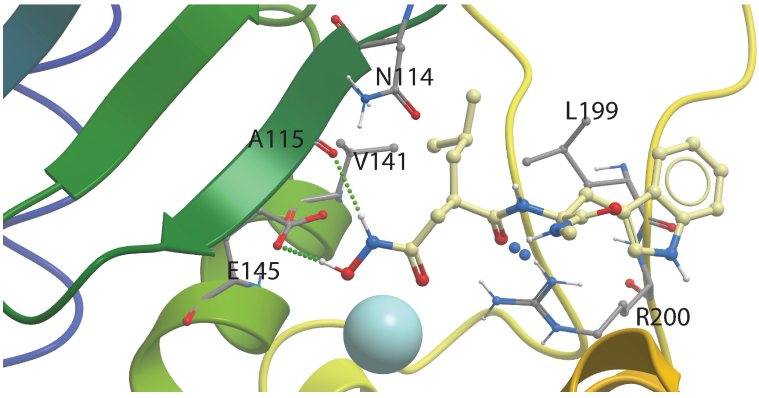

Fig 7. Galardin docked into the catalytic site of thermolysin, pseudolysin and auerolysin. The figure shows close ups of the active site region with the compound structures (xsticks), secondary structure elements and the most important amino acids for ligand binding (xsticks) indicated. Colour coding of atoms of amino acids and ligands:

oxygen; red, nitrogen; blue, hydrogen; white, carbon atoms of ligands; yellow, carbon atoms of amino acid side chains; grey, the zinc ion; light blue.

https://doi.org/10.1371/journal.pone.0200237.g007

N-terminal region. The trypsin and MMP-3 activated forms have F107 and the APMA activated form M94 as the N-terminal residue. The major form of the trypsin activated MMP-9 from THP-1 cells retained its C-terminal HPX-domain due to the presence of some TIMP-1 in the purified enzyme, with F107 as its N-terminal residue. In spite of all these differences, these four differently processed and activated forms had an almost identical K_m value for the quenched fluorescence substrate Mca-PLGLDpaAR-NH_2 and K_i values for galardin and compound **1b**. This suggests that it is possible to compare the average binding strength of the two compounds to each other as well as between the enzymes.

The previously presented binding strength of galardin to MMP-9 and MMP-14 and compound **1b** to MMP-9 appears to be slightly under-estimated compared to the results of the present study. The reason is most likely that these compounds previously have been tested in a series of a large number of compounds against several MPs, and hence detailed kinetic constants were not obtained. An exception is the study of Pourmotabbed et al [59] who studied the binding of galardin to wild-type and mutated un-glycosylated human MMP-9 produced in *E coli*. Both our study and the previous studies show that galardin has a stronger interaction with MMP-9 than with MMP-14. Our study also shows that compound **1b** binds stronger to MMP-9 than to MMP-14 ($p<0.002$; Tables 1 and S2). An important difference between these two compounds is that compound **1b** binds stronger than galardin to the two human MMPs (Tables 1, S1 and S2), and the docking studies indicated that this could be explained by that the diphenyl ether moiety of compound **1b** has a larger interaction surface with the S'_1-subpocket than the 4-methylpentanoyl moiety in galardin. Our studies show that galardin binds quite strongly to all the bacterial MPs, but weaker than to the MMPs, while compound **1b** did not bind the bacterial MPs at all. The size and structural rigidity of the S'_1-subpocket explains why the MMPs more easily adopt to the structure of the inhibitors than do the bacterial MPs. The docking indicated that the diphenyl ether moiety of compound **1b** could not fit into the S'_1-subpocket of thermolysin, pseudolysin and auerolysin as observed for the MMPs, while the smaller 4-methylpentanoyl moiety of galardin could enter the S'_1-subpocket. The entrance from the top of the S'_1-subpocket of the MMPs is quite narrow due to side chain of Y423 and L188 (MMP-9 numbering) as previously explained [56, 57]. However, both galardin and compound **1b** may enter the pocket between the zinc atom and H401 (MMP-9 numbering) on one side and the tyrosine and leucine side chains in the other side. The pocket is also structurally quite flexible since the methionine loop constitutes a large part of the pocket, and therefore the pocket may adopt quite big ligand entities. The entrance from the top of the S'_1-subpocket of the bacterial enzymes is wider than that of the MMPs. However, an arginine side chain located at the border between the S'_1 and S'_2-subpockets is pointing into the binding site and interacts with galardin, and hinders the compound to penetrate deeply into the subpocket (Fig 6). This arginine is located at a rigid β strand, while the corresponding region of the MMPs is in the methionine loop. The docking also indicated that the reason for stronger binding of galardin to thermolysin and pseudolysin than to auerolysin could be explained by hydrogen bonding interactions between the tryptophan methylamide moiety of galardin with two aspargines in pseudolysin and thermolysin (Fig 7). Such interactions were not seen with auerolysin. The present study indicates that the size and shape of the ligand structural moiety entering the S'_1-subpocket is an important determinant for selectivity between the studied MMPs and bacterial MPs. Compounds with less interaction with the S'_1- subpocket, but occupy other subpockets may bind more selectively to the bacterial enzymes than to the MMPs.

Supporting information

S1 Fig. Activation of full length recombinant human proMMP-9 with MMP-3(catalytic domain). (A) Twenty μL of 4.6 μM proMMP-9 was mixed with 20 μL of 0.05 μM MMP-3 at 37˚C. At different time points either 0.5 μL (up to 30 min) or 0.25 μL (from 40 min) of activation mixture was added to 99 μL of 10 μM substrate (in assay buffer) and the enzyme activity (initial rate) was determined as described in methods. **(B)** At the same time points as in (A), 0.5 μL of activation mixture was mixed with 19.5 μL of 10 mM EDTA (in assay buffer). This mixture was further diluted (12.5 times) and mixed with sample buffer and applied to real-time gelatin zymography as described in methods. The molecular size standards used were proMMP-9 purified from THP-1 cells (proMMP-9), recombinant human full length proMMP-9 purified (rproMMP-9) from sf9 cells, the 37 kDa catalytic domain of MMP-9 (Std 3) and a mixture of proMMP-9 from THP-1 cells and proMMP-2 from human skin fibroblasts (St 2).
(PDF)

S1 Table. Inhibitory constant K_i of galardin against human metalloproteases. The K_i ± s.d. values for each experiment were obtained through both Henderson plots and the Morrison equation as described in materials and methods. Shown is also the average $\bar{x}$ ± S.E.M. value for each enzyme and plot. The results shown are for recombinant human MMP-14 catalytic domain, recombinant human MMP-9 activated with APMA (rMMP-9(A)), magnetic trypsin beads (rMMP-9 (T)), MMP-3 (rMMP-9(M3) and trypsin activated human MMP-9 isolated from THP-1 cells (MMP-9 (T)).
(PDF)

S2 Table. Inhibitory constant K_i of compound 1b against human metalloproteases. The K_i ± s.d. values for each experiment were obtained through both Henderson plots and the Morrison equation as described in materials and methods. The average $\bar{x}$ ± S.E.M. values for each enzyme and plot are also shown. The results shown are for recombinant human MMP-14 catalytic domain, recombinant human MMP-9 activated with APMA (rMMP-9(A)) and trypsin activated human MMP-9 isolated from THP-1 cells (MMP-9(T)).
(PDF)

Acknowledgments

We are grateful to Dr. K. Nilsson (Department of Phatology, University of Uppsala, Sweden) for the kind gift of THP-1 cells and Dr. Hideki Moriyama (Dept. Drug. Disc. Res., Carna Bioscience Inc., Kobe, Japan) for the kind gift of compound **1b**. We also would like to thank Rod Wolstenholme (Faculty of Health Sciences, UiT-The Arctic University of Norway) for help with drawing and generating Figs 1–3 into EPS and TIF files and Dr. Imin Wushur for help with drawing and generating Fig 4. We are grateful to Dr. P. McCourt for reading the manuscript.

Author Contributions

Conceptualization: Ingebrigt Sylte, Rangita Dawadi, Nabin Malla, Gunbjørg Svineng, Jan-Olof Winberg.

Formal analysis: Ingebrigt Sylte, Nabin Malla, Jan-Olof Winberg.

Investigation: Ingebrigt Sylte, Rangita Dawadi, Nabin Malla, Susannah von Hofsten, Tra-Mi Nguyen, Ann Iren Solli, Eli Berg, Jan-Olof Winberg.

Methodology: Ingebrigt Sylte, Nabin Malla, Gunbjørg Svineng, Jan-Olof Winberg.

Resources: Ingebrigt Sylte, Olayiwola A. Adekoya, Jan-Olof Winberg.

Supervision: Ingebrigt Sylte, Jan-Olof Winberg.

Validation: Ingebrigt Sylte, Nabin Malla, Gunbjørg Svineng, Jan-Olof Winberg.

Writing – original draft: Ingebrigt Sylte, Jan-Olof Winberg.

Writing – review & editing: Rangita Dawadi, Nabin Malla, Susannah von Hofsten, Tra-Mi Nguyen, Ann Iren Solli, Eli Berg, Olayiwola A. Adekoya, Gunbjørg Svineng.

References

1. Artenstein AW, Opal SM. Proprotein convertases in health and disease. N Engl J Med. 2011; 365 (26):2507–18. Epub 2011/12/30. https://doi.org/10.1056/NEJMra1106700 PMID: 22204726.
2. Winberg JO. Matrix Proteinases: biological significance in health and disease. In: Karamanos NK, editor. Extracellular Matrix: Pathobiology and Signaling Berlin: de Gruyter; 2012. p. 230–8.
3. Ballok AE, O'Toole GA. Pouring salt on a wound: Pseudomonas aeruginosa virulence factors alter Na+ and Cl- flux in the lung. J Bacteriol. 2013; 195(18):4013–9. Epub 2013/07/10. https://doi.org/10.1128/JB.00339-13 PMID: 23836869; PubMed Central PMCID: PMC3754746.
4. Dubin G. Extracellular proteases of Staphylococcus spp. Biol Chem. 2002; 383(7–8):1075–86. Epub 2002/11/20. https://doi.org/10.1515/BC.2002.116 PMID: 12437090.
5. Jensen LM, Walker EJ, Jans DA, Ghildyal R. Proteases of human rhinovirus: role in infection. Methods Mol Biol. 2015; 1221:129–41. Epub 2014/09/28. https://doi.org/10.1007/978-1-4939-1571-2_10 PMID: 25261311.
6. Maeda H. Role of microbial proteases in pathogenesis. Microbiol Immunol. 1996; 40(10):685–99. Epub 1996/01/01 8981341. PMID: 8981341
7. Matsumoto K. Role of bacterial proteases in pseudomonal and serratial keratitis. Biol Chem. 2004; 385 (11):1007–16. Epub 2004/12/04. https://doi.org/10.1515/BC.2004.131 PMID: 15576320.
8. Shinoda S, Miyoshi S. Proteases produced by vibrios. Biocontrol Sci. 2011; 16(1):1–11. Epub 2011/04/07 PMID: 21467624.
9. Silva-Almeida M, Pereira BA, Ribeiro-Guimaraes ML, Alves CR. Proteinases as virulence factors in Leishmania spp. infection in mammals. Parasit Vectors. 2012; 5:160. Epub 2012/08/09. https://doi.org/10.1186/1756-3305-5-160 PMID: 22871236; PubMed Central PMCID: PMC3436776.
10. De Groef L, Van Hove I, Dekeyster E, Stalmans I, Moons L. MMPs in the neuroretina and optic nerve: modulators of glaucoma pathogenesis and repair? Invest Ophthalmol Vis Sci. 2014; 55(3):1953–64. Epub 2014/04/01. https://doi.org/10.1167/iovs.13-13630 PMID: 24681977.
11. Quiros PM, Langer T, Lopez-Otin C. New roles for mitochondrial proteases in health, ageing and disease. Nat Rev Mol Cell Biol. 2015; 16(6):345–59. Epub 2015/05/15. https://doi.org/10.1038/nrm3984 PMID: 25970558.
12. Ricard-Blum S, Vallet SD. Proteases decode the extracellular matrix cryptome. Biochimie. 2016; 122:300–13. Epub 2015/09/19. https://doi.org/10.1016/j.biochi.2015.09.016 PMID: 26382969.
13. Rodriguez D, Morrison CJ, Overall CM. Matrix metalloproteinases: what do they not do? New substrates and biological roles identified by murine models and proteomics. Biochim Biophys Acta. 2010; 1803(1):39–54. Epub 2009/10/06. https://doi.org/10.1016/j.bbamcr.2009.09.015 PMID: 19800373.
14. Wolberg AS, Mast AE. Tissue factor and factor VIIa—hemostasis and beyond. Thromb Res. 2012; 129 Suppl 2:S1–4. Epub 2012/03/16. https://doi.org/10.1016/j.thromres.2012.02.017 PMID: 22417944; PubMed Central PMCID: PMC3336011.
15. Hadler-Olsen E, Fadnes B, Sylte I, Uhlin-Hansen L, Winberg JO. Regulation of matrix metalloproteinase activity in health and disease. FEBS J. 2011; 278(1):28–45. Epub 2010/11/23. https://doi.org/10.1111/j.1742-4658.2010.07920.x PMID: 21087458.
16. Hadler-Olsen E, Winberg JO, Uhlin-Hansen L. Matrix metalloproteinases in cancer: their value as diagnostic and prognostic markers and therapeutic targets. Tumour Biol. 2013; 34(4):2041–51. Epub 2013/05/18. https://doi.org/10.1007/s13277-013-0842-8 PMID: 23681802.
17. Kessenbrock K, Plaks V, Werb Z. Matrix metalloproteinases: regulators of the tumor microenvironment. Cell. 2010; 141(1):52–67. Epub 2010/04/08. https://doi.org/10.1016/j.cell.2010.03.015 PMID: 20371345; PubMed Central PMCID: PMC2862057.
18. Sbardella D, Fasciglione GF, Gioia M, Ciaccio C, Tundo GR, Marini S, et al. Human matrix metalloproteinases: an ubiquitarian class of enzymes involved in several pathological processes. Mol Aspects

Med. 2012; 33(2):119–208. Epub 2011/11/22. https://doi.org/10.1016/j.mam.2011.10.015 PMID: 22100792.

19. Geurts N, Opdenakker G, Van den Steen PE. Matrix metalloproteinases as therapeutic targets in protozoan parasitic infections. Pharmacol Ther. 2012; 133(3):257–79. Epub 2011/12/06. https://doi.org/10.1016/j.pharmthera.2011.11.008 PMID: 22138604.

20. Gialeli C, Theocharis AD, Karamanos NK. Roles of matrix metalloproteinases in cancer progression and their pharmacological targeting. FEBS J. 2011; 278(1):16–27. Epub 2010/11/20. https://doi.org/10.1111/j.1742-4658.2010.07919.x PMID: 21087457.

21. Vandenbroucke RE, Libert C. Is there new hope for therapeutic matrix metalloproteinase inhibition? Nat Rev Drug Discov. 2014; 13(12):904–27. Epub 2014/11/08. https://doi.org/10.1038/nrd4390 PMID: 25376097.

22. Yadav L, Puri N, Rastogi V, Satpute P, Ahmad R, Kaur G. Matrix metalloproteinases and cancer—roles in threat and therapy. Asian Pac J Cancer Prev. 2014; 15(3):1085–91. Epub 2014/03/13 PMID: 24606423.

23. Cerda-Costa N, Gomis-Ruth FX. Architecture and function of metallopeptidase catalytic domains. Protein Sci. 2014; 23(2):123–44. Epub 2014/03/07 https://doi.org/10.1002/pro.2400 PMID: 24596965; PubMed Central PMCID: PMC3926739.

24. Gomis-Ruth FX, Botelho TO, Bode W. A standard orientation for metallopeptidases. Biochim Biophys Acta. 2012; 1824(1):157–63. Epub 2011/05/12. https://doi.org/10.1016/j.bbapap.2011.04.014 PMID: 21558023.

25. Rawlings ND, Barrett AJ, Finn R. Twenty years of the MEROPS database of proteolytic enzymes, their substrates and inhibitors. Nucleic Acids Res. 2016; 44(D1):D343–50. Epub 2015/11/04. https://doi.org/10.1093/nar/gkv1118 PMID: 26527717; PubMed Central PMCID: PMC4702814.

26. Adekoya OA, Sylte I. The thermolysin family (M4) of enzymes: therapeutic and biotechnological potential. Chem Biol Drug Des. 2009; 73(1):7–16. Epub 2009/01/21. https://doi.org/10.1111/j.1747-0285.2008.00757.x PMID: 19152630.

27. Vandooren J, Van den Steen PE, Opdenakker G. Biochemistry and molecular biology of gelatinase B or matrix metalloproteinase-9 (MMP-9): the next decade. Crit Rev Biochem Mol Biol. 2013; 48(3):222–72. Epub 2013/04/04. https://doi.org/10.3109/10409238.2013.770819 PMID: 23547785.

28. Fadnes B, Hadler-Olsen E, Sylte I, Uhlin-Hansen L, Winberg JO. Matrix metalloproteinase complexes and their biological significance. In: Karamanos NK, editor. Extracellular Matrix: Pathobiology and Signaling Berlin: de Gruyter; 2012. p. 291–314.

29. Malla N, Sjoli S, Winberg JO, Hadler-Olsen E, Uhlin-Hansen L. Biological and pathobiological functions of gelatinase dimers and complexes. Connect Tissue Res. 2008; 49(3):180–4. Epub 2008/07/29. https://doi.org/10.1080/03008200802151755 PMID: 18661338.

30. Cha H, Kopetzki E, Huber R, Lanzendorfer M, Brandstetter H. Structural basis of the adaptive molecular recognition by MMP9. J Mol Biol. 2002; 320(5):1065–79. Epub 2002/07/20 PMID: 12126625.

31. Nagase H, Woessner JF Jr. Matrix metalloproteinases. J Biol Chem. 1999; 274(31):21491–4. PMID: 10419448

32. Woessner JF Jr., Nagase H. Matrix metalloproteinases and TIMPs. In: Sheterline P, editor. Protein Profile. Oxford: Oxford Univeristy Press; 2000.

33. Collier IE, Krasnov PA, Strongin AY, Birkedal-Hansen H, Goldberg GI. Alanine scanning mutagenesis and functional analysis of the fibronectin-like collagen-binding domain from human 92-kDa type IV collagenase. J Biol Chem. 1992; 267(10):6776–81. Epub 1992/04/05 PMID: 1313021.

34. Murphy G, Nguyen Q, Cockett MI, Atkinson SJ, Allan JA, Knight CG, et al. Assessment of the role of the fibronectin-like domain of gelatinase A by analysis of a deletion mutant. J Biol Chem. 1994; 269(9):6632–6. Epub 1994/03/04 PMID: 8120015.

35. O'Farrell TJ, Pourmotabbed T. The fibronectin-like domain is required for the type V and XI collagenolytic activity of gelatinase B. Arch Biochem Biophys. 1998; 354(1):24–30. https://doi.org/10.1006/abbi.1998.0662 PMID: 9633594

36. Pourmotabbed T. Relation between substrate specificity and domain structure of 92-kDa type IV collagenase. Ann N Y Acad Sci. 1994; 732:372–4. Epub 1994/09/06 PMID: 7978812.

37. Shipley JM, Doyle GA, Fliszar CJ, Ye QZ, Johnson LL, Shapiro SD, et al. The structural basis for the elastolytic activity of the 92-kDa and 72- kDa gelatinases. Role of the fibronectin type II-like repeats. J Biol Chem. 1996; 271(8):4335–41. PMID: 8626782

38. Xu X, Chen Z, Wang Y, Yamada Y, Steffensen B. Functional basis for the overlap in ligand interactions and substrate specificities of matrix metalloproteinases-9 and -2. Biochem J. 2005; 392(Pt 1):127–34. Epub 2005/07/13. BJ20050650 [pii] https://doi.org/10.1042/BJ20050650 PMID: 16008524; PubMed Central PMCID: PMC1317671.

39. Rosenblum G, Van den Steen PE, Cohen SR, Grossmann JG, Frenkel J, Sertchook R, et al. Insights into the structure and domain flexibility of full-length pro-matrix metalloproteinase-9/gelatinase B. Structure. 2007; 15(10):1227–36. Epub 2007/10/17. https://doi.org/10.1016/j.str.2007.07.019 PMID: 17937912.

40. Van den Steen PE, Van Aelst I, Hvidberg V, Piccard H, Fiten P, Jacobsen C, et al. The hemopexin and O-glycosylated domains tune gelatinase B/MMP-9 bioavailability via inhibition and binding to cargo receptors. J Biol Chem. 2006; 281(27):18626–37. Epub 2006/05/05. https://doi.org/10.1074/jbc.M512308200 PMID: 16672230.

41. Bu CH, Pourmotabbed T. Mechanism of activation of human neutrophil gelatinase B. Discriminating between the role of Ca2+ in activation and catalysis. J Biol Chem. 1995; 270(31):18563–9. Epub 1995/08/04 PMID: 7629187.

42. Morodomi T, Ogata Y, Sasaguri Y, Morimatsu M, Nagase H. Purification and characterization of matrix metalloproteinase 9 from U937 monocytic leukaemia and HT1080 fibrosarcoma cells. Biochem J. 1992; 285 (Pt 2):603–11. Epub 1992/07/15 PMID: 1379048; PubMed Central PMCID: PMCPMC1132831.

43. Okada Y, Gonoji Y, Naka K, Tomita K, Nakanishi I, Iwata K, et al. Matrix metalloproteinase 9 (92-kDa gelatinase/type IV collagenase) from HT 1080 human fibrosarcoma cells. Purification and activation of the precursor and enzymic properties. J Biol Chem. 1992; 267(30):21712–9. Epub 1992/10/25 PMID: 1400481.

44. Sang QX, Birkedal-Hansen H, Van Wart HE. Proteolytic and non-proteolytic activation of human neutrophil progelatinase B. Biochim Biophys Acta. 1995; 1251(2):99–108. Epub 1995/09/06 PMID: 7669817.

45. Triebel S, Blaser J, Reinke H, Knauper V, Tschesche H. Mercurial activation of human PMN leucocyte type IV procollagenase (gelatinase). FEBS Lett. 1992; 298(2–3):280–4. Epub 1992/02/24 PMID: 1312026.

46. Antoni C, Vera L, Devel L, Catalani MP, Czarny B, Cassar-Lajeunesse E, et al. Crystallization of bi-functional ligand protein complexes. J Struct Biol. 2013; 182(3):246–54. Epub 2013/04/10. https://doi.org/10.1016/j.jsb.2013.03.015 PMID: 23567804.

47. Fernandez-Catalan C, Bode W, Huber R, Turk D, Calvete JJ, Lichte A, et al. Crystal structure of the complex formed by the membrane type 1-matrix metalloproteinase with the tissue inhibitor of metalloproteinases-2, the soluble progelatinase A receptor. EMBO J. 1998; 17(17):5238–48. Epub 1998/09/02. https://doi.org/10.1093/emboj/17.17.5238 PMID: 9724659; PubMed Central PMCID: PMC1170851.

48. Grossman M, Tworowski D, Dym O, Lee MH, Levy Y, Murphy G, et al. The intrinsic protein flexibility of endogenous protease inhibitor TIMP-1 controls its binding interface and affects its function. Biochemistry. 2010; 49(29):6184–92. Epub 2010/06/16. https://doi.org/10.1021/bi902141x PMID: 20545310.

49. Nuti E, Cantelmo AR, Gallo C, Bruno A, Bassani B, Camodeca C, et al. N-O-Isopropyl Sulfonamido-Based Hydroxamates as Matrix Metalloproteinase Inhibitors: Hit Selection and in Vivo Antiangiogenic Activity. J Med Chem. 2015; 58(18):7224–40. Epub 2015/08/12. https://doi.org/10.1021/acs.jmedchem.5b00367 PMID: 26263024.

50. Nuti E, Casalini F, Avramova SI, Santamaria S, Cercignani G, Marinelli L, et al. N-O-isopropyl sulfonamido-based hydroxamates: design, synthesis and biological evaluation of selective matrix metalloproteinase-13 inhibitors as potential therapeutic agents for osteoarthritis. J Med Chem. 2009; 52 (15):4757–73. Epub 2009/07/18. https://doi.org/10.1021/jm900261f PMID: 19606871.

51. Nuti E, Casalini F, Avramova SI, Santamaria S, Fabbi M, Ferrini S, et al. Potent arylsulfonamide inhibitors of tumor necrosis factor-alpha converting enzyme able to reduce activated leukocyte cell adhesion molecule shedding in cancer cell models. J Med Chem. 2010; 53(6):2622–35. Epub 2010/02/26. https://doi.org/10.1021/jm901868z PMID: 20180536.

52. Nuti E, Panelli L, Casalini F, Avramova SI, Orlandini E, Santamaria S, et al. Design, synthesis, biological evaluation, and NMR studies of a new series of arylsulfones as selective and potent matrix metalloproteinase-12 inhibitors. J Med Chem. 2009; 52(20):6347–61. Epub 2009/09/25. https://doi.org/10.1021/jm900335a PMID: 19775099.

53. Rowsell S, Hawtin P, Minshull CA, Jepson H, Brockbank SM, Barratt DG, et al. Crystal structure of human MMP9 in complex with a reverse hydroxamate inhibitor. J Mol Biol. 2002; 319(1):173–81. Epub 2002/06/08. https://doi.org/10.1016/S0022-2836(02)00262-0 PMID: 12051944.

54. Tochowicz A, Maskos K, Huber R, Oltenfreiter R, Dive V, Yiotakis A, et al. Crystal structures of MMP-9 complexes with five inhibitors: contribution of the flexible Arg424 side-chain to selectivity. J Mol Biol. 2007; 371(4):989–1006. Epub 2007/06/30. https://doi.org/10.1016/j.jmb.2007.05.068 PMID: 17599356.

55. Brotz-Oesterhelt H, Sass P. Bacterial caseinolytic proteases as novel targets for antibacterial treatment. Int J Med Microbiol. 2014; 304(1):23–30. Epub 2013/10/15. https://doi.org/10.1016/j.ijmm.2013.09.001 PMID: 24119566.

56. Adekoya OA, Sjoli S, Wuxiuer Y, Bilto I, Marques SM, Santos MA, et al. Inhibition of pseudolysin and thermolysin by hydroxamate-based MMP inhibitors. Eur J Med Chem. 2015; 89:340–8. Epub 2014/12/03. https://doi.org/10.1016/j.ejmech.2014.10.009 PMID: 25462250.

57. Sjoli S, Nuti E, Camodeca C, Bilto I, Rossello A, Winberg JO, et al. Synthesis, experimental evaluation and molecular modelling of hydroxamate derivatives as zinc metalloproteinase inhibitors. Eur J Med Chem. 2016; 108:141–53. Epub 2015/12/08. https://doi.org/10.1016/j.ejmech.2015.11.019 PMID: 26638045.

58. Grobelny D, Poncz L, Galardy RE. Inhibition of human skin fibroblast collagenase, thermolysin, and Pseudomonas aeruginosa elastase by peptide hydroxamic acids. Biochemistry. 1992; 31(31):7152–4. Epub 1992/08/11 PMID: 1322694.

59. Pourmotabbed T, Aelion JA, Tyrrell D, Hasty KA, Bu CH, Mainardi CL. Role of the conserved histidine and aspartic acid residues in activity and stabilization of human gelatinase B: an example of matrix metalloproteinases. J Protein Chem. 1995; 14(7):527–35. Epub 1995/10/01 PMID: 8561849.

60. Yamamoto M, Tsujishita H, Hori N, Ohishi Y, Inoue S, Ikeda S, et al. Inhibition of membrane-type 1 matrix metalloproteinase by hydroxamate inhibitors: an examination of the subsite pocket. J Med Chem. 1998; 41(8):1209–17. Epub 1998/05/09. https://doi.org/10.1021/jm970404a PMID: 9548812.

61. Moriyama H, Tsukida T, Inoue Y, Yokota K, Yoshino K, Kondo H, et al. Azasugar-based MMP/ADAM inhibitors as antipsoriatic agents. J Med Chem. 2004; 47(8):1930–8. Epub 2004/04/02. https://doi.org/10.1021/jm0304313 PMID: 15055993.

62. Lindstad RI, Sylte I, Mikalsen SO, Seglen PO, Berg E, Winberg JO. Pancreatic trypsin activates human promatrix metalloproteinase-2. J Mol Biol. 2005; 350(4):682–98. Epub 2005/06/14. https://doi.org/10.1016/j.jmb.2005.05.018 PMID: 15950241.

63. Goldberg GI, Strongin A, Collier IE, Genrich LT, Marmer BL. Interaction of 92-kDa type IV collagenase with the tissue inhibitor of metalloproteinases prevents dimerization, complex formation with interstitial collagenase, and activation of the proenzyme with stromelysin. J Biol Chem. 1992; 267(7):4583–91. Epub 1992/03/05 PMID: 1311314.

64. Malla N, Berg E, Moens U, Uhlin-Hansen L, Winberg JO. Biosynthesis of promatrix metalloproteinase-9/chondroitin sulphate proteoglycan heteromer involves a Rottlerin-sensitive pathway. PLoS One. 2011; 6(6):e20616. Epub 2011/06/16. https://doi.org/10.1371/journal.pone.0020616 PMID: 21673806; PubMed Central PMCID: PMC3105995.

65. Malla N, Berg E, Uhlin-Hansen L, Winberg JO. Interaction of pro-matrix metalloproteinase-9/proteoglycan heteromer with gelatin and collagen. J Biol Chem. 2008; 283(20):13652–65. Epub 2008/03/25. https://doi.org/10.1074/jbc.M709140200 PMID: 18359769.

66. Murphy G, Crabbe T. Gelatinases A and B. Methods Enzymol. 1995; 248:470–84. PMID: 7674939

67. Sjoli S, Solli AI, Akselsen O, Jiang Y, Berg E, Hansen TV, et al. PAC-1 and isatin derivatives are weak matrix metalloproteinase inhibitors. Biochim Biophys Acta. 2014; 1840(10):3162–9. Epub 2014/07/22. https://doi.org/10.1016/j.bbagen.2014.07.011 PMID: 25046380.

68. Winberg JO, Berg E, Kolset SO, Uhlin-Hansen L. Calcium-induced activation and truncation of promatrix metalloproteinase-9 linked to the core protein of chondroitin sulfate proteoglycans. Eur J Biochem. 2003; 270(19):3996–4007. Epub 2003/09/27. 3788 [pii] PMID: 14511382.

69. Malla N, Berg E, Theocharis AD, Svineng G, Uhlin-Hansen L, Winberg JO. In vitro reconstitution of complexes between pro-matrix metalloproteinase-9 and the proteoglycans serglycin and versican. FEBS J. 2013; 280(12):2870–87. Epub 2013/04/23. https://doi.org/10.1111/febs.12291 PMID: 23601700.

70. Mathisen B, Lindstad RI, Hansen J, El-Gewely SA, Maelandsmo GM, Hovig E, et al. S100A4 regulates membrane induced activation of matrix metalloproteinase-2 in osteosarcoma cells. Clin Exp Metastasis. 2003; 20(8):701–11. Epub 2004/01/10 PMID: 14713104.

71. Morrison JF. Kinetics of the reversible inhibition of enzyme-catalysed reactions by tight-binding inhibitors. Biochim Biophys Acta. 1969; 185(2):269–86. Epub 1969/01/01 PMID: 4980133.

72. Henderson PJ. A linear equation that describes the steady-state kinetics of enzymes and subcellular particles interacting with tightly bound inhibitors. Biochem J. 1972; 127(2):321–33. Epub 1972/04/01 PMID: 4263188; PubMed Central PMCID: PMC1178592.

73. Neves MA, Totrov M, Abagyan R. Docking and scoring with ICM: the benchmarking results and strategies for improvement. J Comput Aided Mol Des. 2012; 26(6):675–86. Epub 2012/05/10. https://doi.org/10.1007/s10822-012-9547-0 PMID: 22569591; PubMed Central PMCID: PMC3398187.

74. Ogata Y, Itoh Y, Nagase H. Steps involved in activation of the pro-matrix metalloproteinase 9 (progelatinase B)-tissue inhibitor of metalloproteinases-1 complex by 4-aminophenylmercuric acetate and proteinases. J Biol Chem. 1995; 270(31):18506–11. Epub 1995/08/04 PMID: 7629179.

75. Wilhelm SM, Collier IE, Marmer BL, Eisen AZ, Grant GA, Goldberg GI. SV40-transformed human lung fibroblasts secrete a 92-kDa type IV collagenase which is identical to that secreted by normal human macrophages. J Biol Chem. 1989; 264(29):17213–21. Epub 1989/10/15 PMID: 2551898.

76. Brew K, Dinakarpandian D, Nagase H. Tissue inhibitors of metalloproteinases: evolution, structure and function. Biochim Biophys Acta. 2000; 1477(1–2):267–83. Epub 2000/03/10 PMID: 10708863.

77. Hutton M, Willenbrock F, Brocklehurst K, Murphy G. Kinetic analysis of the mechanism of interaction of full-length TIMP-2 and gelatinase A: evidence for the existence of a low-affinity intermediate. Biochemistry. 1998; 37(28):10094–8. Epub 1998/07/17. https://doi.org/10.1021/bi980616p PMID: 9665714.

78. O'Connell JP, Willenbrock F, Docherty AJ, Eaton D, Murphy G. Analysis of the role of the COOH-terminal domain in the activation, proteolytic activity, and tissue inhibitor of metalloproteinase interactions of gelatinase B. J Biol Chem. 1994; 269(21):14967–73. Epub 1994/05/27 PMID: 8195131.

79. Bu CH, Pourmotabbed T. Mechanism of Ca2+-dependent activity of human neutrophil gelatinase B. J Biol Chem. 1996; 271(24):14308–15. Epub 1996/06/14 PMID: 8662913.

80. Shapiro SD, Fliszar CJ, Broekelmann TJ, Mecham RP, Senior RM, Welgus HG. Activation of the 92-kDa gelatinase by stromelysin and 4-aminophenylmercuric acetate. Differential processing and stabilization of the carboxyl-terminal domain by tissue inhibitor of metalloproteinases (TIMP). J Biol Chem. 1995; 270(11):6351–6. Epub 1995/03/17 PMID: 7890773.

81. Vandooren J, Born B, Solomonov I, Zajac E, Saldova R, Senske M, et al. Circular trimers of gelatinase B/matrix metalloproteinase-9 constitute a distinct population of functional enzyme molecules differentially regulated by tissue inhibitor of metalloproteinases-1. Biochem J. 2015; 465(2):259–70. Epub 2014/11/02. https://doi.org/10.1042/BJ20140418 PMID: 25360794; PubMed Central PMCID: PMCPMC4399976.

82. Shrivastava A, Ghosh KK, Dubey DK. Determination of pK(a)'s of hydroxamic acids by nucleophilic substitution reaction. Indian J Chem A. 2007; 46(10):1630–4 ISI:000250310900012.

83. Zhong H, Wees MA, Faure TD, Carrillo C, Arbiser J, Bowen JP. The impact of ionization States of matrix metalloproteinase inhibitors on docking-based inhibitor design. ACS Med Chem Lett. 2011; 2(6):455–60. Epub 2011/06/09. https://doi.org/10.1021/ml200031m PMID: 24900330; PubMed Central PMCID: PMC4018105.

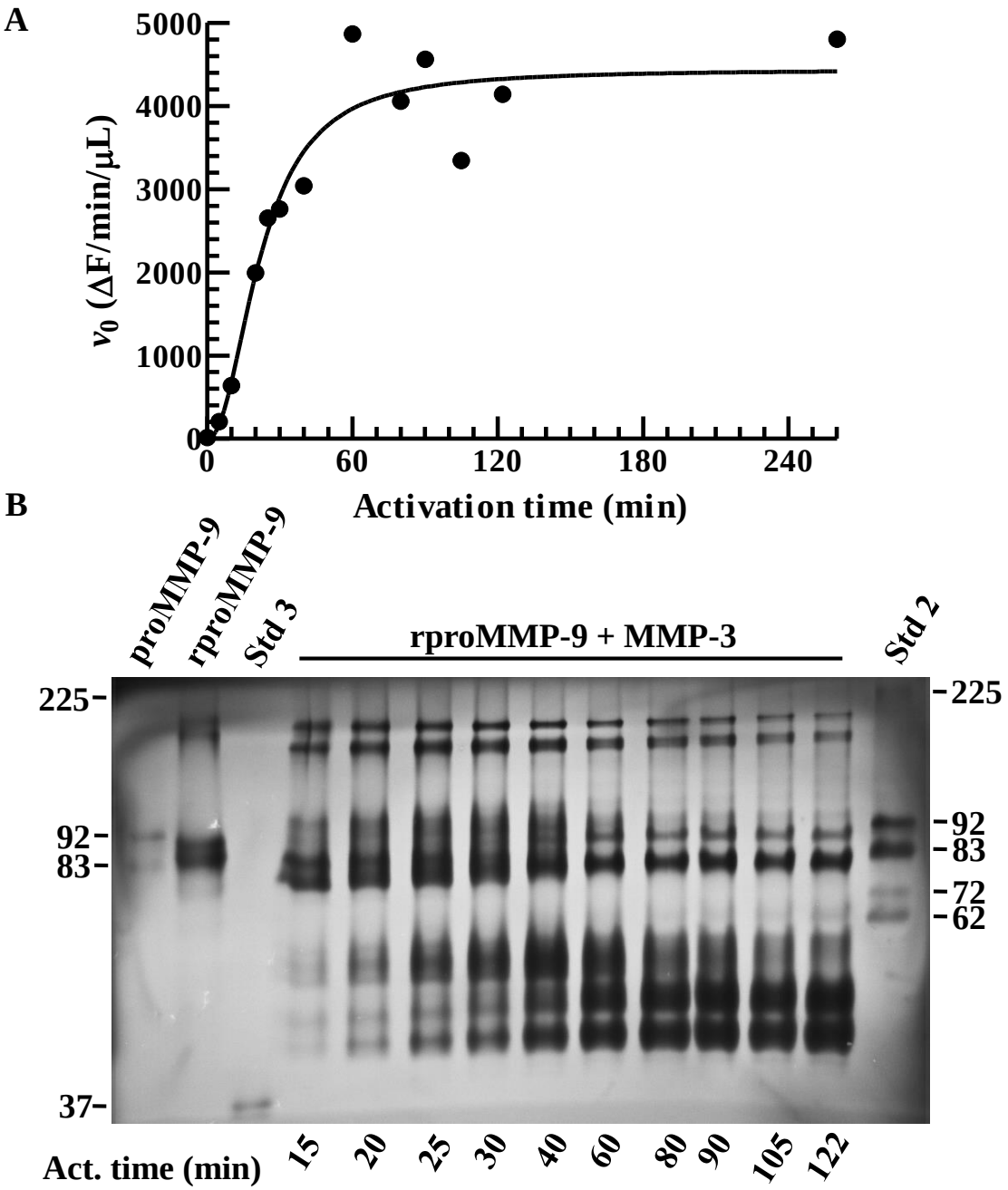

S1 Fig. Activation of full length recombinant human proMMP-9 with MMP-3(catalytic domain). (A) Twenty μL of 4.6 μM proMMP-9 was mixed with 20 μL of 0.05 μM MMP-3 at 37 °C. At different time points either 0.5 μL (up to 30 min) or 0.25 μL (from 40 min) of activation mixture was added to 99 μL of 10 μM substrate (in assay buffer) and the enzyme activity (initial rate) was determined as described in methods. **(B)** At the same time points as in (A), 0.5 μL of activation mixture was mixed with 19.5 μL of 10 mM EDTA (in assay buffer). This mixture was further diluted (12.5 times) and mixed with sample buffer and applied to real-time gelatin zymography as described in methods. The molecular size standards used were proMMP-9 purified from THP-1 cells (proMMP-9), recombinant human full length proMMP-9 purified (rproMMP-9) from sf9 cells, the 37 kDa catalytic domain of MMP-9 (Std 3) and a mixture of proMMP-9 from THP-1 cells and proMMP-2 from human skin fibroblasts (St 2).

S1 Table. Inhibitory constant K_i of galardin against human metalloproteases.

Protease	Experiment	Galardin K_i (nM)	
		Henderson Plot	Morrison equation
MMP-14	1	0.78 ± 0.08	0.82 ± 0.24
	2	0.86 ± 0.05	0.91 ± 0.20
	3	0.76 ± 0.04	0.89 ± 0.27
	4	0.78 ± 0.05	0.95 ± 0.15
	5	1.16 ± 0.04	0.78 ± 0.13
	$\bar{x}$ ± S.E.M.	0.87 ± 0.07	0.87 ± 0.03
rMMP-9 (A)	1	0.046 ± 0.002	0.053 ± 0.004
	2	0.061 ± 0.011	0.053 ± 0.012
	3	0.045 ± 0.010	0.044 ± 0.002
	4	0.051 ± 0.010	0.064 ± 0.020
	5	0.053 ± 0.012	0.070 ± 0.019
	$\bar{x}$ ± S.E.M.	0.051 ± 0.003	0.057 ± 0.005
rMMP-9 (T)	1	0.065 ± 0.013	0.068 ± 0.022
	2	0.068 ± 0.004	0.067 ± 0.005
	3	0.071 ± 0.005	0.081 ± 0.009
	4	0.071 ± 0.016	0.062 ± 0.022
	5	0.070 ± 0.010	0.075 ± 0.016
	$\bar{x}$ ± S.E.M.	0.069 ± 0.001	0.071 ± 0.003
rMMP-9 (M3)	1	0.057 ± 0.004	0.076 ± 0.008
	2	0.054 ± 0.003	0.058 ± 0.004
	3	0.078 ± 0.008	0.088 ± 0.005
	$\bar{x}$ ± S.E.M.	0.063 ± 0.008	0.074 ± 0.009
MMP-9 (T)	1	0.075 ± 0.005	0.078 ± 0.007
	2	0.075 ± 0.010	0.074 ± 0.027
	3	0.065 ± 0.004	0.075 ± 0.009
	4	0.051 ± 0.001	0.067 ± 0.009
	$\bar{x}$ ± S.E.M.	0.067 ± 0.006	0.074 ± 0.002

The K_i ± s.d. values for each experiment were obtained through both Henderson plots and the Morrison equation as described in materials and methods. Shown is also the average $\bar{x}$ ± S.E.M. value for each enzyme and plot. The results shown are for recombinant human MMP-14 catalytic domain, recombinant human MMP-9 activated with APMA (rMMP-9(A)), magnetic trypsin beads (rMMP-9 (T)), MMP-3 (rMMP-9(M3) and trypsin activated human MMP-9 isolated from THP-1 cells (MMP-9 (T)).

S2 Table. Inhibitory constant K_i of compound 1b against human metalloproteases.

Protease	Experiment	1b	
		K_i (nM)	
		Henderson Plot	Morrison equation
MMP-14	1	0.074 ± 0.015	0.16 ± 0.04
	2	0.128 ± 0.023	0.16 ± 0.08
	3	0.081 ± 0.029	0.10 ± 0.06
	4	0.070 ± 0.047	0.21 ± 0.12
	$\bar{x}$ ± S.E.M.	0.088 ± 0.015	0.16 ± 0.02
rMMP-9 (A)	1	0.010 ± 0.006	0.015 ± 0.009
	2	0.012 ± 0.006	0.017 ± 0.013
	$\bar{x}$ ± S.E.M.	0.011 ± 0.001	0.016 ± 0.001
MMP-9 (T)	1	0.006 ± 0.002	0.006 ± 0.002
	2	0.006 ± 0.002	0.010 ± 0.004
	$\bar{x}$ ± S.E.M.	0.006 ± 0.000	0.008 ± 0.002

The K_i ± s.d. values for each experiment were obtained through both Henderson plots and the Morrison equation as described in materials and methods. The average $\bar{x}$ ± S.E.M. values for each enzyme and plot are also shown. The results shown are for recombinant human MMP-14 catalytic domain, recombinant human MMP-9 activated with APMA (rMMP-9(A)) and trypsin activated human MMP-9 isolated from THP-1 cells (MMP-9(T)).

PAPER III

The Proteoglycan Serglycin is Cleaved by Matrix Metalloprotease-9

Rangita Dawadi, Nabin Malla, Beate Hegge, Eli Berg, Gunbjørg Svineng and Jan-Olof Winberg

Department of Medical Biology, Faculty of Health Sciences, UiT-The Arctic University of Norway, 9037 Tromsø, Norway.

Abstract

Previous studies of *in vitro* reconstitution of proMMP-9·CSPG/SG complexes and treatment of THP-1 cell produced complex by calcium suggested that active MMP-9 may cleave the core protein of serglycin. In the present work we have investigated if various activated forms of recombinant full-length and truncated variants of MMP-9 as well as trysin-activated MMP-9 from THP-1 cells can cleave the core protein of serglycin. MMP-9 were tested against a commercial his-tagged serglycin produced in E-Coli and hence lack attached glycosamino-glycan chains. The enzyme was also tested against intact serglycin purified from THP-1 cells and cABC-treated serglycin, which only contains a short stub of attached chondroitin sulphate chains. The methods used were trypsin- and APMA-activation of various proMMP-9 variants, real-time gelatin zymography, active-site titration and determination of the kinetic coefficient K_m for a peptide quenched chromogenic substrate and K_i for the slow tight binding inhibitor galardin, SDS-PAGE and Western blotting. MMP-9 cleaved the His-tagged serglycin at several places and generated products with M_r that ranged from approximately 3 - 21 kDa. The active enzyme also cleaved the intact and cABC-treated serglycin from THP-1 cells and generated a product of approximately 10 kDa, which was further cleaved. Activated variants of recombinant full-length and truncated variants of MMP-9 cleaved His-tagged serglycin and the degradation pattern appeared identical. Only the trypsin-activated MMP-9 from THP-1 cells had a distinct degradation product compared to the activated recombinant MMP-9 variants. This suggest that binding of serglycin to the enzymes HPX domain have altered the degradation pattern and hence, this domain may contain an exosite for serglycin. This is possible due to the flexibility of the long hinge region that links the HPX domain to the catalytic domain.

Keywords: Serglycin, proMMP-9, proMMP-9 deletion variants, activation, active site titration, proteolytic degradation, inhibitor binding.

Introduction

The proteoglycan serglycin (SG) is produced by various cell types such as hematopoetic and endothelic cells [1-5]. SG has functions under physiological conditions in the immune system, hemostasis, cell growth, apoptosis and reproduction as well as in diseases such as cancer, inflammatory disorders as well as platelet-associated disorders [6-15]. SG is either constitutively secreted from the cells, or stored in intracellular secretory granules and secreted upon stimulation [2]. The glycosaminoglycan (GAG)-chains associated to the core protein is either chondroitin sulphate (CS), heparin/heparan sulphate (HS) or a mixture of the two depending on the cell type [2]. In hematopoetic cells like the leukocytic monocyte cell line THP-1, the GAG-chains associated to the proteoglycan core protein is CS [2, 16]. The main CSPG produced by THP-1 monocytes is SG and it contributes to more than 95% of the secreted CSPGs [17, 18]. SG has a small core protein and in humans containing 131 amino acids with a M_r of approximately 14 kDa [2]. SG has been cloned and sequenced from human, mouse and rat cells. In addition the sequence has been predicted from several other species. In all cases, the GAG-chains are attached to serine residues which are clustered as Ser-Gly repeats in the center of the core protein and varies in size from 5 to 24 repeats [2, 19]. In human and mouse cells, the SG core protein is transcribed from three exons where exon 1 codes for the pre-domain (amino acid 1-27) which is removed during secretion [2, 10, 19]. In humans, exon 2 codes for amino acids 28-76 and exon 3 for amino acids 77-158 and the eight Ser-Gly repeats are from amino acids 94-111 [2]. In some cells like neutrophils and various cancer cell lines, a part of the produced SG contains a shorter core protein due to an alternative splice variant lacking exon 2 [2, 10].

The matrix metalloprotease (MMP) or the matrixin family is a group of extracellular zinc and calcium dependent metallo-proteases expressed by most cells and tissues. In humans there are 23 different MMPs, seven membrane bound and 16 secreted, where MMP-9 is one of the secreted variants [20]. MMP-9 is produced by many cell types such as keratinocytes, monocytes, macrophages, polymorphonuclear leukocytes, brain cells and a variety of malignant cells [21-23]. MMP-9 has important functions in health and disease. This enzyme is involved in physiological functions such as apoptosis, reproduction, growth and development as well as in inflammation and wound healing [22-35]. MMP-9 also has a role in several pathological conditions including various types of cancer, inflammatory, proliferative, vascular, degenerative, infectious diseases and in pathologic bone resorption as well as in premature rupture of amniotic membranes [22, 23, 33, 36-40]. As the majority of the other

members of the MMP family, MMP-9 consists of a pre-, pro-, catalytic, hinge and a C-terminal HPX-domain [20, 22, 23]. Like MMP-2, this enzyme also contains three fibronectin-like (FnII) repeats in the catalytic domain. MMP-9 also differs from the other MMPs as it has a longer and heavily O-glycosylated hinge region, OG domain [20, 22, 23]. Like the other members of the MMP family, MMP-9 has a broad substrate specificity [21, 31, 34, 37, 39-45] and for some substrates it has also been reported that sites outside the catalytic cleft (exosites) are important for its function. These sites are localized in the FnII module and in the HPX domain [46-51].

Previously we have shown that a part of the proMMP-9 secreted from PMA stimulated THP-1 cells occurs in complex with a CSPG core protein [16, 52, 53] and that the CSPG is most likely SG. We have also shown that this proMMP-9·CSPG complex can be reconstituted *in vitro* using purified proMMP-9 and isolated CSPG from unstimulated THP-1 cells, i.e. leukemic monocytes [54]. Previous studies showed that the main CSPG produced by THP-1 monocytes is SG [17, 18]. *In vitro* reconstitution also showed that proMMP-9 and purified SG formed a proMMP-9·SG complex [54]. Calcium ions that normally stabilizes MMPs like MMP-9 had the opposite effect on the formed proMMP-9·CSPG/SG complex. Addition of Ca^{2+} ions to the purified proMMP-9·CSPG/SG complex resulted in an auto-activation of the enzyme, followed by release of the active MMP-9 from the CSPG/SG by first cleaving the CSPG/SG core protein and then a successive C-terminal truncation of MMP-9 [55]. Another indirect evidence that active MMP-9 can cleave the CSPG/SG core protein was that the *in vitro* reconstitution of a MMP-9·CSPG/SG complex using trypsin-activated MMP-9 from THP-1 cells required the presence of EDTA [56]. All this suggests that the core protein of SG is a substrate for MMP-9. In the present work, we have used trypsin- and APMA-activated full-length MMP-9 isolated from THP-1 cells, and recombinant full-length proMMP-9 as well as recombinant HPX and OGHPX deleted MMP-9 variants produced in insect cells. The activated MMP-9 variants were used against recombinant His-tagged SG (Ht-SG) produced in E-Coli (lack attached GAG-chains) and SG isolated from unstimulated THP-1 cells. We show that active MMP-9 can cleave both recombinant Ht-SG at several places as well as intact SG isolated from unstimulated THP-1 cells (monocytes) and cABC treated CSPG/SG from THP-1 cells (i.e. CSPG/SG with most of the CS chains removed). This is shown by SDS-PAGE and Western blots.

Materials and Methods

Materials

TRIS, urea, DMSO, citric acid, Na_2HPO_4, guanidinium hydrochlorid, $CaCl_2 \cdot 2H_2O$, and sodium acetate were obtained from Merck (Darmstadt, Germany). 2-Methoxy-2,4-Diphenyl-3(2H)-Furanone (MDPF) and EDTA were from Fluka (Buchs, Switzerland). Acetic acid, sodium chloride, acrylamide/bis-acrylamide, Commassie Brilliant Blue G-250 and Triton X-100 were from BDH (Poole, UK). Tween-20, RPMI 1640, fetal bovine serum, streptomycin, penicillin, cetylpyridinuim chloride, safranin O (no.S-2255), sodium dodecyl sulphate (SDS; 20% in H_2O), dithiothreitol (DTT), phorbol 12-myristate 13-acetate (PMA), Hepes, Brij-35, chondroitin sulphate C (shark cartilage CS), gelatin (type A: porcine skin, approx. 300 blom) and p-aminiphenylmercuric acetate (APMA) were from Sigma (St Louis, MO, USA). Proteinase free chondroitin ABC lyase (cABC) was from Seikagaku Kogyo Co (Tokyo, Japan). Gelatin-Sepharose, Q-Sepharose, Sephadex G-50 (fine), Sephadex 200 and Sephacryl S-400 were from GE-Healthcare (Uppsala, Sweden). Unlabelled molecular weight standards was from BioRad (Richmond, CA, USA). Imperial™ protein stain, SeeBlue prestained protein standard and Spectra™ multicolor low range protein ladder were from Thermo Fisher Scientfic, (Rockford, Il, USA). Biotinylated protein ladder was from Cell Signalling (Danvers, MA, USA). Western Blotting Luminol reagent was from Sancta Cruz (Santa Cruz, CA, USA). HRP-conjugated goat anti-rabbit secondary antibody was from Southern Biotech (Birmingham, AL, USA). Rabbit polyclonal antibodies against a human full length serglycin produced in E-Coli (amino acids 28-158) and a human C-terminal serglycin peptide (amino acids 118-148) were from Antibodies-Online GmbH (Aachen, Germany). Recombinant human his-tagged serglycin (Ht-SG) produced in E-Coli was from ProSpec (Ness Ziona, Israel). The chromogenic substrate Mca-PLGLDpaAR-NH_2 was from R&D Systems, Inc ((Minneapolis, MN, USA). Magnetic trypsin beads (Mag-Trypsin) was from Takara (Gothenburg, Sweden). NuPAGE Novex 4-12% Bis-Tris gels and Sf9 insect cells were from Invitrogen (Carlsbad, CA, USA). Galardin (Gm6001) was from Calbiochem (San Diego, CA, USA).

Biosynthesis of CSPGs

The human leukemic monocyte cell-line THP-1 was a kind gift from Dr. K. Nilsson,

Department of Pathology, University of Uppsala, Sweden. The cells were cultured in RPMI 1640 medium with 10% fetal bovine serum, 50 μg/ml of streptomycin, and 100 units/ml of penicillin. To isolate secreted cell-synthesized CSPG/SG the cells were washed 3 times in serum-free medium and then cultured for 72 h in serum-free RPMI 1640 medium without PMA as described earlier [52]. Conditioned medium was harvested, loose cells were pelleted by centrifugation at 1200 rpm (200g) for 10 min. CSPG/SG was thereafter isolated and detected as described below.

Detection of PG-bound CS-chains

PG-bound CS-chains were quantified spectrophotometrically by the Safranin O colour method as described previously [53].

Isolation of secreted CSPG/SG

Secreted CSPG/SG was isolated by Q-Sepharose anion-exchange chromatography as described previously [52-54]. The amount of CSPG was based on the quantification of the GAG-chains using the safranin O method and shark cartilage CS (chondroitin sulphate C) as a standard.

Purification of serglycin

One ml of pooled CSPG (3 mg/ml) from Q-Sepharose anion-exchange chromatography was subjected to gel permeation chromatography on a Sephacryl S-400 column (90x1.6 cm) pre-equilibrated with 4 M guanidine hydrochloride, 50 mM sodium acetate, pH 6.0. The column was eluted with the same buffer, fractions collected and PGs monitored by the safranin O method and characterized by SDS-PAGE and immunoblotting. Fractions with SG were pooled, diluted and applied to a Q-Sepharose column. Eluted material from the Q-Sepharose column was desalted on a Sephadex G-50 column and thereafter concentrated on a vacuum centrifuge (Speedvac). The amount of SG was determined by the safranin O method, using a standard curve generated from shark cartilage CS (chondroitin sulphate C) and the presence of SG was determined by Western blotting.

Chondroitin ABC lyase (cABC) treatment

The PG bound CS-chains were removed by digestion for 2 h at 37 °C with 0.2-1.0 units of cABC/ml in 0.05 M Tris-HCl, pH 8.0, containing 0.05 M sodium acetate.

Expression and Purification of recombinant proMMP-9 in Sf9 Insect cells

The expression and purification of recombinant full-length proMMP-9 (rpMMP-9) from Sf9 insect cells was performed as described previously [58]. Recombinant proMMP-9 lacking the HPX domain (rpMMP-9ΔHPX) or the OG and HPX domains (rpMMP-9ΔOGHPX) were produced as described previously [56].

The purification of the recombinant full-length and deletion variants of proMMP-9 was performed as described previously [56, 58]. The amount of purified proMMP-9 variants were determined by measuring the absorbance at 280 nm and using the extinction coefficients as described previously [56].

Activation of recombinant proMMP-9 variants

Activation of the various recombinant proMMP-9 variants was performed with both APMA (auto-activation) and Mag-Trypsin as described previously [58].

Production, purification and activation of proMMP-9 from THP-1 cells

The biosynthesis, purification and activation of proMMP-9 from the human leukemic monocyte cell-line THP-1 was performed as described previously [16, 52, 54, 55, 59]. The amount of purified proMMP-9 was estimated spectrophotometrically at 280 nm using ε_{280nm} = 114.36 $mM^{-1}cm^{-1}$ [60], ignoring the contribution of TIMP-1.

Gelatin zymography and real-time gelatin zymography

SDS-substrate PAGE was done as described previously [53] with gels (7.5 cm x 8.5 cm x 0.75 mm) containing 0.1% (w/v) gelatin in both the stacking and separating gel, 4 and 7.5 % (w/v)

of polyacrylamide, respectively. Gelatinase activity was evident as cleared (unstained) regions.

Real-time gelatin zymography was performed as described previously [58, 61]. Briefly, 0.1 % (w/v) MDPF-fluorescent labelled gelatin was incorporated in the 7.5 % SDS-PAGE separating gel and 0.2 % (w/v) MDPF-fluorescent labelled gelatin was incorporated in the 4.0 % SDS-PAGE separating gel. The fluorescent dye 2-methoxy-2,4-diphenyl-3(2H)-furanone was used to label gelatin to give MDPF-gelatin as described previously [61]. The main difference between normal gelatin zymography and real-time gelatin zymography is that in real-time zymography, the gel is not stained and hence it is possible to follow the degradation of the gelatin in real time without staining. Gelatinase activity was evident as dark bands against the undegraded fluorescent background.

Western immunoblotting analysis

Purified proMMP-9 from THP-1 cells, recombinant full length and deletion variants of human proMMP-9 from Sf9 cells and cABC treated purified CSPG/SG from THP-1 cells with and without 0.1 M DTT were electrophoresed on SDS-polyacrylamide gel (NuPAGE Novex 4-12% Bis-Tris gels) and electroblotted to a polyvinyl difluoride membrane. After blockage of non-specific binding sites with non-fat milk in TBS-T (150 mM NaCl, 0.25% Tween-20, 20 mM Tris-HCL, pH 7.4), blots were incubated for 1 h at room temperature or 4 °C over night with rabbit polyclonal antibodies against either human full-length serglycin (amino acids 28-158) or human C-terminal serglycin (amino acids 118-148). After washing, the blots were incubated for 1 h at room temperature with an HRP-conjugated goat anti-rabbit secondary antibody. The Blots were thereafter washed with TBS-T 3 x 5 min before visualization using Western Blotting Luminol reagent. The intensity of immunoblot bands was measured using a Luminescent Image Analyzer LAS-3000 with MultiGauge software version 3.0 (Fujifilm, Tokyo, Japan).

Determination of MMP-9 activity and kinetic coefficients

To determine the MMP-9 activity (v_0), concentration of active MMP-9 (active site titration), kinetic and inhibitor kinetic coefficients K_m, and K_i, initial rate experiments were performed using a Perkin Elmer LS 50 Luminescence spectrometer and the FL WinLab Software

Package (Perkin Elmer). The reactions were followed for one minute and during that time, 600 data points were collected. The excitation and emission wavelengths for the fluorescence quenched MMP peptide substrate, McaPLGLDpaAR-NH_2, were; λ_{ex}=320 nm, λ_{em}=405 nm and a slit width=10 nm at both wavelengths. All assays were performed at 37°C in an assay buffer of 0.1 M Hepes pH 7.5, 0.005 % Brij-35, 10 mM $CaCl_2$ and a total assay volume of 100 µl.

Active-site titration

Active-site titration was used to determine the concentration of activate MMP-9 and the binding coefficient (K_i) for galardin (Gm6001). This was performed as described previously [58]. Briefly, a fixed amount of activate MMP-9 was mixed with varying concentrations of the slow tight binding substrate competitive inhibitor galardin (Gm6001). This mixture was incubated for 15 min at 37 °C and thereafter was a fixed concentration of substrate added and the enzymatic activity/velocity was determined fluorimetrically as described above. The concentration of substrate ([S]) was either 5.0 µM or 10 µM. The concentration of activate MMP-9 in the assay and the binding coefficient (K_i) for galardin (Gm6001) were determined from both a dose response plot, v_i/v_0 vs the concentration of inhibitor [I], using the Morrison equation (1) [62], and through the linear Henderson Plot (equation 2) [63]. The velocities v_i and v_0 represents the initial rate activity in the presence and absence of inhibitor (I), respectively. Graph Pad Prism 5 was used to calculate K_i and [E] values.

$$\frac{v_i}{v_0} = 1 - \frac{([E] + [I] + K_i\left(1 + \frac{[S]}{K_m}\right)) - \sqrt{\left([E] + [I] + K_i\left(1 + \frac{[S]}{K_m}\right)\right)^2 - 4[E][I]}}{2[E]} \quad (1)$$

$$\frac{[I]}{(1 - \frac{v_i}{v_0})} = K_i\left(1 + \frac{[S]}{K_m}\right)\left(\frac{v_0}{v_i}\right) + [E] \quad (2)$$

K_m determination

Initial rates were determined with McaPLGLDpaAR-NH_2 concentrations ranging from 0.5 to 10.0 µM, higher substrate concentrations resulted in quenching. The K_m value was calculated from non-linear regression of the Michaelis-Menten equation using the Enzyme kinetic module in GraphPad Prism 5.

MMP-9 processing of serglycin

One ml Ht-SG (1 mg/ml) was dialysed against three changes of 1 l 0.1 M Hepes buffer, pH 7.5 in order to remove DTT. The activity of MMP-9 is inhibited by DTT. To process Ht-SG, 2-3 µg of this protein was mixed with various concentrations (18-50 nM) of either APMA- or trypsin-activated proMMP-9 variants in 0.1 M Hepes buffer pH 7.5 containing 10 mM $CaCl_2$ and 0.005% Brij-35. These mixtures were incubated for various time points at 37 °C. The amount of active MMP-9 used was based on active site titration of the various activated variants. The enzymatic activity was stopped by adding EDTA to a concentration of 10 mM or galardin to a concentration of approximately 500 nM.

To process intact CSPG/SG or SG, approximately 50 nM of APMA-activated recombinant full length MMP-9 was mixed with either 0.4-10 µg of intact CSPG/SG or SG from THP-1 cells. All assays were performed in 0.1 M Hepes buffer pH 7.5 containing 10 mM $CaCl_2$ and 0.005% Brij-35, and were incubated for various time points at 37 °C. The enzymatic activity was stopped by adding EDTA to a concentration of 10 mM or galardin to a concentration of approximately 500 nM. In some experiments the CS-chains of CSPG/SG or SG were removed by cABC (protease free) prior to addition of active MMP-9.

Results and Discussion

Synthesis and purification of CSPG/SG and SG from THP-1 monocytes

CSPG/SG was produced and purified from unstimulated THP-1 cells (monocytes) as described previously [52, 56] and in Materials and Methods. From the Q-Sepharose purified preparation of CSPG/SG, SG was separated from other putative CSPGs using a Sephacryl S-400 column as described previously [56] and in Materials and Methods.

Synthesis and purification of recombinant proMMP-9 variants

The various recombinant proMMP-9 variants were expressed and purified as described previously [56, 58]. All variants contain the FnII-module in the catalytic domain and were purified to homogeneity. The only exception is the proMMP-9 purified from THP-1 cells that also contains a small amount of TIMP-1 bound to the enzymes' HPX domain [16, 56, 58].

Activation of the proMMP-9 variants

Activation of the various proMMP-9 variants with APMA, trypsin and MagTrypsin was performed as described previously [58] and in Materials and Methods. Both APMA and MagTrypsin activation of rpMMP-9 results in activated variants that has lost a large part of the HPX domain as shown and discussed previously [58]. However, in the trypsin-activated proMMP-9 from THP-1 cells is the HPX domain retained as described and discussed previously [58]. During activation, the HPX bound TIMP-1 will bind to the active MMP-9 and form a very strong complex. As the amount of TIMP-1 is less than the amount of MMP-9, only a part of the active MMP-9 binds to TIMP-1 and hence the TIMP-1 free MMP-9 is active. That a fraction of the activated MMP-9 contains TIMP-1 bound to the active site does not affect its activity against substrates or binding of inhibitors like galardin (Gm6001) or the determination of kinetic coefficients as described and discussed previously [58]. This is due to the strong binding of the inhibitor to the active site of the enzyme and a very slow dissociation rate of the complex. Fig. 1 shows real-time gelatin zymography of the activated variants along with the unactivated proforms. In this figure rpMMP-9, APMA- and trypsin-activation of this variant are shown in order to compare the size of the activated rpMMP-9 deletion variants. The molecular size of the APMA- and trypsin-activated rpMMP-9 (rMMP-9(A) and rMMP-

9(T)) (Fig. 1B) corresponded well with those in our previous work [58]. The rpMMP-9ΔOGHPX has a molecular size around 47 kDa and trypsin-activation of rpMMP-9ΔOGHPX (rMMP-9ΔOGHPX(T)) resulted in two activated forms, a major form with molecular size of approximately 39 kDa and a minor form of approximately 38 kDa (Fig. 1A). Trypsin-activation should result in an active enzyme with ^{107}F as the N-terminal amino acid [64] and hence a truncation of approximately 10 kDa. The homodimer of rpMMP-9ΔHPX shows a doublet with molecular sizes around 135 and 122 kDa and a monomer with a molecular size of around 75 kDa (Figs. 1A and B). In addition, a weak band was seen around 67 kDa, which is likely an auto-activated form. APMA-activation of rpMMP-9ΔHPX (rMMP-9ΔHPX(A)) results in a strong band with a molecular size of 118 kDa (Figs. 1A and B) indicating that both subunits in the homodimer has lost its prodomain. Previously it has been shown that APMA-activation of MMP-9 results in ^{94}M as the N-terminal amino acid and hence the zinc binding region of the prodomain (^{97}PRCGVPD) remains [64]. This suggest that approximately 8 kDa of the prodomain was lost from each subunit. Previously when the full-length proMMP-9 was activated by APMA in the presence of calcium, in addition to lose 8 kDa of the prodomain a C-terminal truncation occurred. It was suggested that a conformational change due to the C-terminal truncation resulted in an unblocked catalytic site that could account for the full activity of the activated enzyme [65]. APMA-activation of rpMMP-9ΔHPX also resulted in four main forms with molecular size smaller than the 75 kDa monomer (Figs. 1A and B). The molecular size of the four truncated forms are 67, 54, 48 and 42 kDa. The 67 kDa form has most likely just lost 8 kDa of the prodomain, while the smaller forms in addition has lost different parts of the C-terminal OG domain. These activated forms appear slightly smaller than the trypsin- and APMA-activated rpMMP-9 (rMMP-9(T) and rMMP-9(A)) (Fig. 1B). The APMA-activated variants has ^{94}M and the trypsin-activated variants ^{107}F as the N-terminal residue. All the activated forms appear to have similar but not identical C-terminal residues. It was previously suggested that the APMA- and trypsin-activated rMMP-9 has lost most of its C-terminal HPX domain [58].

K_m determination, active-site titration and K_i determination of the activated MMP-9 variants

The K_m values for the different MMP-9 variants were determined against the quenched fluorescence substrate Mca-PLGLDpaAR-NH_2. Previously the following K_m values were

obtained for trypsin-activated MMP-9 from THP-1 cells and rMMP-9, as well as for APMA-activated rMMP-9; 3.0 ± 0.7, 3.2 ± 0.2 and 3.1 ± 0.4 μM [58]. Here we obtained the following K_m values for APMA-activated rMMP-9ΔHPX and trypsin-activated rMMP-9ΔOGHPX; 4.7 ± 1.2 and 2.7 ± 0.5 μM. This shows that there are no drastic differences in the obtained K_m values for the various activated MMP-9 variants. Hence, the difference in N- and C-terminal residues in these MMP-9 variants has a minimal effect on the K_m value for this fluorescence quenched small peptide substrate. The obtained K_m values were used to calculate the dissociation constant (K_i) of Gm6001 for the various MMP-9 variants as well as for the determination of the [E] in the active-site titration experiments when the Morrison equation (1) is used.

Activation of full-length proMMP-9 and proMMP-9 deletion variants through treatment of trypsin or APMA (auto-activation) results in a balance between activation and degradation. Therefore, it is important to determine the concentration of active enzyme in the activated batches of the MMP-9 variants. For that purpose, active-site titration of the various activated MMP-9 variants were performed as described in Materials and Methods, using the zinc chelating tight binding inhibitor galardin (Gm6001). Two different plots and equations were used to determine the concentration of active enzyme in the assay ($[E]_{assay}$) and the K_i value for the binding of Gm6001 to the enzymes. One plot is a dose response curve (v_i/v_0 against [Gm6001]) using the Morrison equation (1) [62] and the other is through the linear Henderson plot (eqn. 2) [63]. Fig. 2 shows typical dose response plots using the Morrison equation (Figs. 2A, C and E) and Henderson plots (i.e. the linearized form of the Morrison equation) (Figs. 2B, D and F) for trypsin-activated rMMP-9 (Figs. 2A and B) and rMMP-9ΔOGHPX (Figs. 2E and F) as well as for APMA-activated rMMP-9ΔHPX (Figs. 2C and D). Shown in the figure is also the obtained values of $[E]_{assay}$ and K_i of the respective plot. Previously we showed that the correlation and precision of the obtained $[E]_{assay}$ and K_i values for these two types of plot are very good and most often, almost identical or very similar values were obtained from the two plots [58]. The presented K_i values for trypsin-activated rMMP-9 (Figs. 2A and B) are those for experiment 2 in the supplementary table S1 in our previous article [58]. The mean K_i values for Gm6001 with rMMP-9ΔHPX(A) and rMMP-9ΔOGHPX(T) are 67 ± 14 and 55 ± 9 pM. These values are similar to those obtained earlier for the APMA- and trypsin-activated full-length rMMP-9 and the trypsin-activated MMP-9 from THP-1 cells [58]. The obtained mean values for the $[E]_{assay}$ was used to calculate the concentration of active enzyme in the activated stock solutions in order to use similar or

identical amount of the activated enzymes when comparing their ability to process Ht-SG. Various activity tests and repeated active-site titrations at various time points showed that the activated MMP-9 variants are stable when stored at -70 ºC.

MMP-9 cleave and degrade His-tagged serglycin

In the commercially obtained E-Coli produced His-tagged SG (Ht-SG), the 27 amino acid predomain was replaced by a 25 amino acid long His-tag (Fig. 3). This Ht-SG lack attached GAG-chains. In the text, we will use the numbering of the SG starting with the predomain, not the His-tag. In various experiments, Ht-SG was mixed with either various concentrations of APMA-activated recombinant human MMP-9 or a single concentration of the enzyme. The enzymatic reactions performed at 37 ºC were stopped at various time points by adding either EDTA or galardin, as described in Materials and Methods. The intact Ht-SG and its degradation products were subjected to SDS-PAGE. In some experiments the intact Ht-SG and the degradation products were detected by Imperial blue staining of the gel or in other experiments detected with Western blotting using either a rabbit polyclonal antibody against the entire recombinant human SG (amino acids 28 – 158) or a rabbit polyclonal antibody against a recombinant C-terminal peptide of SG (amino acids 118 – 148). As seen in Fig. 4A, MMP-9 cleave the Ht-SG into several products with molecular size that range from approximately 3 - 21 kDa. The polyclonal antibody against the entire SG core protein detected several bands from approximately 8 to 21 kDa, including the un-cleaved Ht-SG with a M_r estimated to be around 23 kDa (Fig. 4B). The polyclonal antibody against the C-terminal peptide detected in addition to the un-cleaved Ht-SG, only processed Ht-SG fragments with molecular size from 16 to 21 kDa, but no fragments with lower molecular size (Fig. 4C). In order to detect which fragments that contain the His-tag of the cleaved SG substrate, samples withdrawn at the different time points of the incubation with MMP-9 were applied to talon beads. His-tagged proteins bind to the beads as described in Materials and Methods. Fig. 4D shows that almost all of the un-treated Ht-SG binds to the column. The cleaved band at 21 kDa appear to be a mixture of a peptide that has just lost the N-terminal part of the His-tag and another peptide that has lost the end part of its C-terminal. Most of the peptides in the cleaved band at 18 kDa appear to lack its N-terminal His-tag (Fig. 4D), while it still contain most or all of the C-terminal sequence (Aa 118-148) detected by the antibody against the SG C-terminal (Fig. 4C). Only a minor part of this band contain the N-terminal His-tag. The three

weaker bands with M_r around 12-16 kDa (Figs. 4B) seem to lack both the His-tag and the C-terminal part of the peptide detected by the antibody against the C-terminal SG (Figs. 4C and D). The strong intermediate band that appears just above 10 kDa and the band just under 10 kDa both seems to be a mixture of peptides where some contain the His-tag and while the other peptides lack the His-tag (Fig. 4D). The peptides in both bands lack the C-terminal part detected by the antibody against the C-terminal SG (Fig. 4B). Fig. 4A shows that these bands also are detected in imperial blue stained SDS-PAGE gels. The cleaved band at around 3-5 kDa that is detected at large amounts already after 10 min incubation with MMP-9 is most likely the N-terminal His-tagged fragment as it is not detected by any of the antibodies against SG used.

Galardin (Gm6001) is a slow tight binding inhibitor of various MMPs and showed a K_i value from 50-70 pM against APMA-, trypsin- and MMP-3-activated recombinant MMP-9 as well as against trypsin-activated MMP-9 from THP-1 cells [58]. When MMP-9 was mixed with galardin along with SG and the mixture incubated from 15 to 180 minutes, the enzyme did not cleave SG (Fig. 5A). When galardin was added after 15 min incubation of SG with MMP-9 and the mixture (with and without galardin) further incubated for 180 min at 37 ºC, the inhibitor totally blocked further degradation (Fig. 5B). When small amounts of the MMP inhibitor EDTA was added (much less than needed for full inhibition), only limited inhibition was obtained after 180 min (Fig. 5A). In the presence of 10 mM EDTA, full inhibition was obtained (data not shown). This proves that the processing of Ht-SG is through active MMP-9.

MMP-9 cleave intact and cABC treated serglycin isolated from THP-1 cells

Previous studies showed that the main CSPG produced by THP-1 monocytes is SG [17, 18]. These authors also detected three minor bands with a molecular size between 26 and 53 kDa. In our study, we obtain a main SG band at around 25 kDa in the purified CSPG/SG material after cABC treatment (Fig. 6B). In addition, minor bands with a molecular size between 30 to 50 kDa were detected as well as a band of approximately 140 kDa. The 140 kDa band was not detected in all batches and it was necessary to load a large amount of CSPG in order to detect the band. This suggest that the cABC used prior to SDS-PAGE did not uniformly remove the CS-chains from the SG core protein. In addition, SG may also contain hetero and homo dimer/ multimers involving the two cysteines (^{40}C and ^{49}C) in the N-terminal region of the protein.

Various concentrations of intact CSPG/SG as well as cABC treated CSPG/SG were mixed with various concentrations of either APMA-activated or Mag-trypsin activated recombinant proMMP-9. The enzymatic reactions performed at 37 ºC were stopped at various time-points by adding either EDTA or Galardin as described in Materials and Methods. Intact CSPG/SG, SG and the degradation products were subjected to SDS-PAGE and detected with Western blotting. Antibodies used were either a rabbit polyclonal antibody against the entire recombinant human SG core protein (amino acids 28 – 158) or a rabbit polyclonal antibody against a recombinant C-terminal peptide of SG (amino acids 118 – 148). In experiments were CSPG/SG and purified SG were used simultaneously in order to compare the results, these were almost similar (data not shown).

APMA activated recombinant MMP-9 was incubated with SG purified from THP-1 cells for various time points at 37 ºC. Western blots (Fig. 6A) showed that the SG core protein was cleaved and a fragment around 10 kDa appeared after incubation with MMP-9. Notable, no bands were seen in the control wells containing just SG. This band around 10 kDa also appeared if SG was treated with cABC either after or before incubation with MMP-9 (Figs. 6B and C), while this band did not appear in the wells with un-treated SG. This also showed that cABC (protease free) did not cleave the SG core protein and release a 10 kDa peptide fragment. Furthermore, the SG antibody reacts with a band around 140 kDa in the cABC treated SG and this SG fraction was processed by MMP-9. Altogether, these experiments indicate that 10 kDa SG fragment released by MMP-9 do not contain any CS-chains and that the cleavage is either on the N- or C-terminal side of the Ser-Gly repeats that contain the CS-chains.

We also used different dilutions of CSPG/SG to see if MMP-9 also degraded the fragments around 25 kDa, which is the expected size of SG after cABC treatment. As shown in Figs. 6D and E, both the rabbit polyclonal antibody against the entire recombinant human SG (amino acids 28 – 158) and the rabbit polyclonal antibody against the recombinant C-terminal peptide of SG (amino acids 118 – 148) detected the SG band at around 25 kDa in cABC treated CSPG/SG. The antibody against the full length SG also detected a band around 20 kDa that is much weaker than the 25 kDa band (Fig. 6D). In contrast to this, the antibody against the C-terminal part of SG did not detect this band (Fig. 6E). This indicates that at least a part of the C-terminal region lacks in the 20 kDa species. Both the 25 and the 20 kDa SG species were processed and two new bands with M_r around 10 and 8 kDa appeared (Fig. 6D). These bands were further cleaved, as the intensity of the bands decreased with increasing

incubation time in the presence of MMP-9. The two bands (8 and 10 kDa) appeared to lack a large part of the C-terminal domain, as the antibody that just recognizes the SG C-terminal fragment did not detect the bands. All this shows that active MMP-9 also cleave the SG core-protein whether it contains intact CS-chains or just a stub of the CS-chains due to cABC treatment. Both MMP-9 and SG are inflammatory proteins and both are also expressed in various diseases like cancer. Based on the results in the present *in vitro* study, one would expect that when active MMP-9 and SG are present in the same tissue, MMP-9 would be able to process the SG core protein. It is hard to predict whether this will have an effect on the biological function of SG, as studies on SG so far has mainly focused on the role of the GAG-chains. These chains bind various factors including growth factors, cytokines and various type of enzymes including MMPs [2, 8, 66]. A possibility is that the fragments released from SG core protein after MMP-9 cleavage can act as chemokines, cytokines or growth factors alone or if they are further processed by other proteases. One such example is the processing of collagen I by MMP-8 and MMP-9 that releases a fragment that is further processed by a prolyl endopeptidase that releases a three amino acid peptide (PGP) that acts as a chemo attractant [67, 68]. Future biological studies will reveal whether the peptide fragments released from SG by MMP-9 processing has a biological *in vivo* effect. If so, what is the biological and physiological importance and consequences?

Degradation of His-Tagged serglycin by active recombinant deletion variants of MMP-9

Previously it was shown that CSPG/SG and SG form stable complexes with proMMP-9 isolated from THP-1 cells, as well as with recombinant full length and deletion variants of proMMP-9 [54, 56]. The complex formation involves both the HPX domain and the FnII module of proMMP-9. We have therefore also determined to which extent the presence of various domains (HPX and OG) affect the degradation of SG. In these experiments we did not use our produced FnII-deletion variants, as we so far has not been able to purify them to homogeneity [56]. Trypsin-activation of proMMP-9 from THP-1 cells results in an active MMP-9 that has lost its prodomain, but most if not all of the HPX domain is retained [58]. This is in contrast to APMA- and trypsin-activated recombinant proMMP-9 expressed and purified from insect cells, which has lost its prodomain as well as most of its HPX domain [58]. When Ht-SG was incubated for different time-points at 37 ºC with approximately the same amount of APMA-activated recombinant MMP-9 and trypsin-activated MMP-9 from

THP-1 cells, the degradation pattern are similar but not identical (Figs. 7A and B). With APMA-activated MMP-9 a band at approximately 17 kDa appeared. This band was not seen in the trypsin-activated MMP-9, and the opposite is the case for a band that appeared just under 17 kDa. Likewise, the bands just below 10 kDa were not identical (Figs. 7B). In the APMA-activated MMP-9 the band at around 5 kDa appeared early and remains fairly stable throughout the incubation time, while this band successively was converted to a peptide with lower molecular size and thereafter disappeared when Ht-SG was treated with trypsin-activated MMP-9 from THP-1 cells (Fig. 7B). All this suggests that the presence of the HPX domain to some extent may have an effect of the processing of the SG core protein. One reason that the HPX domain could affect the processing of SG is that SG is known to bind to the HPX domain [56] and that MMP-9 is a very flexible enzyme [56, 69]. Hence, the presence of the HPX domain may affect the binding of the SG to the catalytic site and hence the cleavage site in the core protein. It is not possible to exclude that also the differences in the N-terminal region between these two enzymes may have caused the changes in cleavage patterns, even though it did not have an effect on the binding of galardin (K_i value) or the K_m value for the small fluorescence quenched substrate Mca-PLGLDpaAR-NH_2. Previously it was shown that activation of the two collagenases MMP-1 and MMP-8 by various activators resulted in different N-terminal residues. One single amino acid difference had striking effect on these enzymes catalytic capacity [70-72]. We need more experiments to determine if the two MMP-9 variants different cleavage patterns of Ht-SG is due to the presence and absence of the HPX-domain or different N-terminal residues.

We have also studied the processing of Ht-SG with various truncated recombinant variants of MMP-9. The variants used were trypsin-activated rMMP-9ΔOGHPX and rMMP-9 as well as APMA-activated recombinant MMP-9ΔHPX (Fig. 8). There are no striking differences in the peptide pattern of the processed Ht-SG, except the 18 kDa band could not be seen in the Ht-SG processed by rMMP-9ΔHPX(A). This is not likely due to the different N-terminal residues in APMA and trypsin activated variants as this band is detected when APMA-activated rMMP-9 was used to cleave Ht-SG (Fig. 4). Previously, we also showed that compounds that only interact with the catalytic domain of APMA- and trypsin-activated rMMP-9 had almost identical kinetic parameters such as the K_m value for the small fluorescence quenched substrate (Mca-PLGLDpaAR-NH_2) and the K_i value for galardin [58]. If the difference in SG processing is real, it must be due to differences in the C-terminal

region. More work is needed in order to verify whether there is a difference between the various activated and truncated rMMP-9 variants ability to process Ht-SG.

The FnII module in the catalytic site of proMMP-9 bind gelatin and based on this, the protease are purified on a Gelatin-Sepharose column [58, 60, 73-76]. The enzyme is removed from the column by the addition of DMSO (7-10%). Active MMP-9 lacking the FnII module has only 20% of the activity against gelatin compared to the enzyme containing this module [48], suggesting that the FnII-module contain an exosite that presents gelatin to the catalytic site of the enzyme. Similar to this, we showed that DMSO inhibits the degradation of gelatin [59]. However, the effect of DMSO on the degradation of the fluorescence quenched peptide substrate (McaPLGLDpaAR-NH_2) is limited, and this small peptide substrate just binds to the active site cleft of the catalytic domain [59]. Furthermore, SG form a complex with proMMP-9 that involves the FnII-module of the protease [56]. Gelatin and SG share overlapping epitopes in the FnII-module and gelatin inhibits the formation of the proMMP-9·CSPG/SG complex [54, 56]. However, DMSO (10%) did not inhibit the formation of the proMMP-9·CSPG/SG complex, nor did DMSO dissolve the complex [54]. In spite of this, it cannot be excluded that during the cleavage of Ht-SG by MMP-9, a part of the Ht-SG bind the FnII module in such a way that DMSO can affect the binding and the processing of the Ht-SG. Therefore, it was of interest to determine if DMSO affect the degradation of SG. It was shown that DMSO has a limited effect on the MMP-9 cleavage of Ht-SG (Fig. 9) and the effect are similar to its effect on MMP-9 cleavage of the McaPLGLDpaAR-NH_2 substrate. This is in agreement with the results that show that DMSO had no effect on the proMMP-9·CSPG/SG complex formation. This result does not exclude or suggest that the FnII module is involved in binding and presenting the SG core protein to the catalytic site of MMP-9. Therefore, it will be interesting to determine the processing of SG with active MMP-9 deletion variants that lack the FnII module and compare the degradation pattern with the MMP-9 variants that contains the FnII module.

Conclusion

SG is resistant to protease cleavage due to the dense clustering of GAG-chains [8]. The present work shows that MMP-9 can cleave the core protein both in intact SG with bound CS-chains as wells as in SG that lacks CS-chains. Our results also suggest the presence of an SG exocite in the HPX domain of MMP-9 that is involved in presenting the SG core protein to the

enzymes' active site. Whether the FnII module in the catalytic site of MMP-9 also contain an exosite that presents the SG core protein to the enzymes catalytic site remains to be determined. To what extent MMP-9 can process the SG core protein during *in vivo* conditions remain to be investigated.

References

1. Castronuevo, P., Thornton, M. A., McCarthy, L. E., Klimas, J. & Schick, B. P. (2003) DNase I hypersensitivity patterns of the serglycin proteoglycan gene in resting and phorbol 12-myristate 13-acetate-stimulated human erythroleukemia (HEL), CHRF 288-11, and HL-60 cells compared with neutrophils and human umbilical vein endothelial cells, *J Biol Chem.* **278**, 48704-12.
2. Kolset, S. O. & Tveit, H. (2008) Serglycin--structure and biology, *Cell Mol Life Sci.* **65**, 1073-85.
3. Roy, A., Attarha, S., Weishaupt, H., Edqvist, P. H., Swartling, F. J., Bergqvist, M., Siebzehnrubl, F. A., Smits, A., Ponten, F. & Tchougounova, E. (2017) Serglycin as a potential biomarker for glioma: association of serglycin expression, extent of mast cell recruitment and glioblastoma progression, *Oncotarget.* **8**, 24815-24827.
4. Schick, B. P. (2012) Serglycin proteoglycan: implication for thrombosis, inflammation, artherosclerosis, and metastasis in *Extracellular Matrix: Pathobiology and Signaling* (Karamanos, N. K., ed) pp. 221-231, de Gruyter, Berlin.
5. Schick, B. P., Ho, H. C., Brodbeck, K. C., Wrigley, C. W. & Klimas, J. (2003) Serglycin proteoglycan expression and synthesis in embryonic stem cells, *Biochim Biophys Acta.* **1593**, 259-67.
6. He, L., Zhou, X., Qu, C., Tang, Y., Zhang, Q. & Hong, J. (2013) Serglycin (SRGN) overexpression predicts poor prognosis in hepatocellular carcinoma patients, *Med Oncol.* **30**, 707.
7. Imoto-Tsubakimoto, H., Takahashi, T., Ueyama, T., Ogata, T., Adachi, A., Nakanishi, N., Mizushima, K., Naito, Y. & Matsubara, H. (2013) Serglycin is a novel adipocytokine highly expressed in epicardial adipose tissue, *Biochem Biophys Res Commun.* **432**, 105-10.
8. Kolset, S. O. & Pejler, G. (2011) Serglycin: a structural and functional chameleon with wide impact on immune cells, *J Immunol.* **187**, 4927-33.
9. Korpetinou, A., Papachristou, D. J., Lampropoulou, A., Bouris, P., Labropoulou, V. T., Noulas, A., Karamanos, N. K. & Theocharis, A. D. (2015) Increased Expression of Serglycin in Specific Carcinomas and Aggressive Cancer Cell Lines, *Biomed Res Int.* **2015**, 690721.
10. Korpetinou, A., Skandalis, S. S., Labropoulou, V. T., Smirlaki, G., Noulas, A., Karamanos, N. K. & Theocharis, A. D. (2014) Serglycin: at the crossroad of inflammation and malignancy, *Front Oncol.* **3**, 327.
11. Korpetinou, A., Skandalis, S. S., Moustakas, A., Happonen, K. E., Tveit, H., Prydz, K., Labropoulou, V. T., Giannopoulou, E., Kalofonos, H. P., Blom, A. M., Karamanos, N. K. & Theocharis, A. D. (2013) Serglycin is implicated in the promotion of aggressive phenotype of breast cancer cells, *PLoS One.* **8**, e78157.
12. Li, X. J., Ong, C. K., Cao, Y., Xiang, Y. Q., Shao, J. Y., Ooi, A., Peng, L. X., Lu, W. H., Zhang, Z., Petillo, D., Qin, L., Bao, Y. N., Zheng, F. J., Chia, C. S., Iyer, N. G., Kang, T. B., Zeng, Y. X., Soo, K. C., Trent, J. M., Teh, B. T. & Qian, C. N. (2011) Serglycin is a theranostic target in nasopharyngeal carcinoma that promotes metastasis, *Cancer Res.* **71**, 3162-72.
13. Li, X. J. & Qian, C. N. (2011) Serglycin in human cancers, *Chin J Cancer.* **30**, 585-9.
14. Scully, O. J., Chua, P. J., Harve, K. S., Bay, B. H. & Yip, G. W. (2012) Serglycin in health and diseases, *Anat Rec (Hoboken).* **295**, 1415-20.
15. Skliris, A., Labropoulou, V. T., Papachristou, D. J., Aletras, A., Karamanos, N. K. & Theocharis, A. D. (2013) Cell-surface serglycin promotes adhesion of myeloma cells to collagen type I and affects the expression of matrix metalloproteinases, *Febs J.* **280**, 2342-52.

16. Malla, N., Berg, E., Uhlin-Hansen, L. & Winberg, J. O. (2008) Interaction of pro-matrix metalloproteinase-9/proteoglycan heteromer with gelatin and collagen, *J Biol Chem.* **283**, 13652-65.
17. Chang, M. Y., Chan, C. K., Braun, K. R., Green, P. S., O'Brien, K. D., Chait, A., Day, A. J. & Wight, T. N. (2012) Monocyte-to-macrophage differentiation: synthesis and secretion of a complex extracellular matrix, *J Biol Chem.* **287**, 14122-35.
18. Oynebraten, I., Hansen, B., Smedsrod, B. & Uhlin-Hansen, L. (2000) Serglycin secreted by leukocytes is efficiently eliminated from the circulation by sinusoidal scavenger endothelial cells in the liver, *J Leukoc Biol.* **67**, 183-8.
19. Angerth, T., Huang, R. Y., Aveskogh, M., Pettersson, I., Kjellen, L. & Hellman, L. (1990) Cloning and structural analysis of a gene encoding a mouse mastocytoma proteoglycan core protein; analysis of its evolutionary relation to three cross hybridizing regions in the mouse genome, *Gene.* **93**, 235-40.
20. Hadler-Olsen, E., Fadnes, B., Sylte, I., Uhlin-Hansen, L. & Winberg, J. O. (2011) Regulation of matrix metalloproteinase activity in health and disease, *Febs J.* **278**, 28-45.
21. Iyer, R. P., Patterson, N. L., Fields, G. B. & Lindsey, M. L. (2012) The history of matrix metalloproteinases: milestones, myths, and misperceptions, *Am J Physiol Heart Circ Physiol.* **303**, H919-30.
22. Van den Steen, P. E., Dubois, B., Nelissen, I., Rudd, P. M., Dwek, R. A. & Opdenakker, G. (2002) Biochemistry and molecular biology of gelatinase B or matrix metalloproteinase-9 (MMP-9), *Crit Rev Biochem Mol Biol.* **37**, 375-536.
23. Vandooren, J., Van den Steen, P. E. & Opdenakker, G. (2013) Biochemistry and molecular biology of gelatinase B or matrix metalloproteinase-9 (MMP-9): the next decade, *Crit Rev Biochem Mol Biol.* **48**, 222-72.
24. Arnould, C., Lelievre-Pegorier, M., Ronco, P. & Lelongt, B. (2009) MMP9 limits apoptosis and stimulates branching morphogenesis during kidney development, *J Am Soc Nephrol.* **20**, 2171-80.
25. Bengatta, S., Arnould, C., Letavernier, E., Monge, M., de Preneuf, H. M., Werb, Z., Ronco, P. & Lelongt, B. (2009) MMP9 and SCF protect from apoptosis in acute kidney injury, *J Am Soc Nephrol.* **20**, 787-97.
26. Camp, T. M., Tyagi, S. C., Senior, R. M., Hayden, M. R. & Tyagi, S. C. (2003) Gelatinase B(MMP-9) an apoptotic factor in diabetic transgenic mice, *Diabetologia.* **46**, 1438-45.
27. Choi, Y. A., Kim, D. K., Bang, O. S., Kang, S. S. & Jin, E. J. (2009) Secretory phospholipase A2 promotes MMP-9-mediated cell death by degrading type I collagen via the ERK pathway at an early stage of chondrogenesis, *Biol Cell.* **102**, 107-19.
28. Fatunmbi, M., Shelton, J. & Aronica, S. M. (2012) MMP-9 increases HER2/neu expression and alters apoptosis levels in human mammary epithelial cells (HMEC), *Breast Cancer Res Treat.* **135**, 519-30.
29. Kolaczkowska, E., Koziol, A., Plytycz, B., Arnold, B. & Opdenakker, G. (2009) Altered apoptosis of inflammatory neutrophils in MMP-9-deficient mice is due to lower expression and activity of caspase-3, *Immunol Lett.* **126**, 73-82.
30. Kowluru, R. A., Mohammad, G., dos Santos, J. M. & Zhong, Q. (2011) Abrogation of MMP-9 gene protects against the development of retinopathy in diabetic mice by preventing mitochondrial damage, *Diabetes.* **60**, 3023-33.
31. Nissinen, L. & Kahari, V. M. (2014) Matrix metalloproteinases in inflammation, *Biochim Biophys Acta.* **1840**, 2571-80.
32. Sun, M. H., Chen, K. J., Tsao, Y. P., Kao, L. Y., Han, W. H., Lin, K. K. & Pang, J. H. (2011) Down-regulation of matrix metalloproteinase-9 by pyrrolidine dithiocarbamate

prevented retinal ganglion cell death after transection of optic nerve in rats, *Curr Eye Res.* **36**, 1053-63.
33. Vafadari, B., Salamian, A. & Kaczmarek, L. (2016) MMP-9 in translation: from molecule to brain physiology, pathology, and therapy, *J Neurochem.* **139 Suppl 2**, 91-114.
34. Verslegers, M., Lemmens, K., Van Hove, I. & Moons, L. (2013) Matrix metalloproteinase-2 and -9 as promising benefactors in development, plasticity and repair of the nervous system, *Prog Neurobiol.* **105**, 60-78.
35. Xu, J., Liu, H., Wu, Y., Gong, X., Zhou, Q. & Qiao, F. (2011) Proapoptotic effect of metalloproteinase 9 secreted by trophoblasts on endothelial cells, *J Obstet Gynaecol Res.* **37**, 187-94.
36. De Groef, L., Van Hove, I., Dekeyster, E., Stalmans, I. & Moons, L. (2014) MMPs in the neuroretina and optic nerve: modulators of glaucoma pathogenesis and repair?, *Invest Ophthalmol Vis Sci.* **55**, 1953-64.
37. Farina, A. R. & Mackay, A. R. (2014) Gelatinase B/MMP-9 in Tumour Pathogenesis and Progression, *Cancers (Basel).* **6**, 240-96.
38. Tokito, A. & Jougasaki, M. (2016) Matrix Metalloproteinases in Non-Neoplastic Disorders, *Int J Mol Sci.* **17**.
39. Vilen, S. T., Salo, T., Sorsa, T. & Nyberg, P. (2013) Fluctuating roles of matrix metalloproteinase-9 in oral squamous cell carcinoma, *ScientificWorldJournal.* **2013**, 920595.
40. Yabluchanskiy, A., Ma, Y., Iyer, R. P., Hall, M. E. & Lindsey, M. L. (2013) Matrix metalloproteinase-9: Many shades of function in cardiovascular disease, *Physiology (Bethesda).* **28**, 391-403.
41. Butler, G. S. & Overall, C. M. (2009) Updated biological roles for matrix metalloproteinases and new "intracellular" substrates revealed by degradomics, *Biochemistry.* **48**, 10830-45.
42. Cauwe, B. & Opdenakker, G. (2010) Intracellular substrate cleavage: a novel dimension in the biochemistry, biology and pathology of matrix metalloproteinases, *Crit Rev Biochem Mol Biol.* **45**, 351-423.
43. Cauwe, B., Van den Steen, P. E. & Opdenakker, G. (2007) The biochemical, biological, and pathological kaleidoscope of cell surface substrates processed by matrix metalloproteinases, *Crit Rev Biochem Mol Biol.* **42**, 113-85.
44. Hernandez-Guillamon, M., Mawhirt, S., Blais, S., Montaner, J., Neubert, T. A., Rostagno, A. & Ghiso, J. (2015) Sequential Amyloid-beta Degradation by the Matrix Metalloproteases MMP-2 and MMP-9, *J Biol Chem.* **290**, 15078-91.
45. Opdenakker, G., Van den Steen, P. E., Dubois, B., Nelissen, I., Van Coillie, E., Masure, S., Proost, P. & Van Damme, J. (2001) Gelatinase B functions as regulator and effector in leukocyte biology, *J Leukoc Biol.* **69**, 851-9.
46. Fields, G. B. (2015) New strategies for targeting matrix metalloproteinases, *Matrix Biol.* **44-46**, 239-46.
47. Lauer-Fields, J. L., Whitehead, J. K., Li, S., Hammer, R. P., Brew, K. & Fields, G. B. (2008) Selective modulation of matrix metalloproteinase 9 (MMP-9) functions via exosite inhibition, *J Biol Chem.* **283**, 20087-95.
48. O'Farrell, T. J. & Pourmotabbed, T. (1998) The fibronectin-like domain is required for the type V and XI collagenolytic activity of gelatinase B, *Arch Biochem Biophys.* **354**, 24-30.
49. O'Farrell, T. J. & Pourmotabbed, T. (2000) Identification of structural elements important for matrix metalloproteinase type V collagenolytic activity as revealed by chimeric enzymes. Role of fibronectin-like domain and active site of gelatinase B, *J Biol Chem.* **275**, 27964-72.
50. Overall, C. M. (2002) Molecular determinants of metalloproteinase substrate specificity: matrix metalloproteinase substrate binding domains, modules, and exosites, *Mol Biotechnol.* **22**, 51-86.

51. Shipley, J. M., Doyle, G. A., Fliszar, C. J., Ye, Q. Z., Johnson, L. L., Shapiro, S. D., Welgus, H. G. & Senior, R. M. (1996) The structural basis for the elastolytic activity of the 92-kDa and 72-kDa gelatinases. Role of the fibronectin type II-like repeats, *J Biol Chem.* **271**, 4335-41.
52. Malla, N., Berg, E., Moens, U., Uhlin-Hansen, L. & Winberg, J. O. (2011) Biosynthesis of promatrix metalloproteinase-9/chondroitin sulphate proteoglycan heteromer involves a Rottlerin-sensitive pathway, *PLoS One.* **6**, e20616.
53. Winberg, J. O., Kolset, S. O., Berg, E. & Uhlin-Hansen, L. (2000) Macrophages secrete matrix metalloproteinase 9 covalently linked to the core protein of chondroitin sulphate proteoglycans, *J Mol Biol.* **304**, 669-80.
54. Malla, N., Berg, E., Theocharis, A. D., Svineng, G., Uhlin-Hansen, L. & Winberg, J. O. (2013) In vitro reconstitution of complexes between pro-matrix metalloproteinase-9 and the proteoglycans serglycin and versican, *Febs J.* **280**, 2870-87.
55. Winberg, J. O., Berg, E., Kolset, S. O. & Uhlin-Hansen, L. (2003) Calcium-induced activation and truncation of promatrix metalloproteinase-9 linked to the core protein of chondroitin sulfate proteoglycans, *Eur J Biochem.* **270**, 3996-4007.
56. Dawadi, R., Malla, N., Hegge, B., Wushur, I., Berg, E., Svineng, G., Sylte, I. & Winberg, J. O. (2020) Motifs and amino acids involved in the formation of complexes between pro-matrix metalloproteinase and the proteoglycan serglycin core protein, *Unpublished, Manuscript 1*.
57. Theocharis, A. D., Seidel, C., Borset, M., Dobra, K., Baykov, V., Labropoulou, V., Kanakis, I., Dalas, E., Karamanos, N. K., Sundan, A. & Hjerpe, A. (2006) Serglycin constitutively secreted by myeloma plasma cells is a potent inhibitor of bone mineralization in vitro, *J Biol Chem.* **281**, 35116-28.
58. Sylte, I., Dawadi, R., Malla, N., von Hofsten, S., Nguyen, T. M., Solli, A. I., Berg, E., Adekoya, O. A., Svineng, G. & Winberg, J. O. (2018) The selectivity of galardin and an azasugar-based hydroxamate compound for human matrix metalloproteases and bacterial metalloproteases, *PLoS One.* **13**, e0200237.
59. Sjoli, S., Solli, A. I., Akselsen, O., Jiang, Y., Berg, E., Hansen, T. V., Sylte, I. & Winberg, J. O. (2014) PAC-1 and isatin derivatives are weak matrix metalloproteinase inhibitors, *Biochim Biophys Acta.* **1840**, 3162-9.
60. Murphy, G. & Crabbe, T. (1995) Gelatinases A and B, *Methods Enzymol.* **248**, 470-84.
61. Hadler-Olsen, E. & Winberg, J. O. (2019) Method for Determining Gelatinolytic Activity in Tissue Extracts: Real-Time Gelatin Zymography, *Methods Mol Biol.* **1952**, 201-210.
62. Morrison, J. F. (1969) Kinetics of the reversible inhibition of enzyme-catalysed reactions by tight-binding inhibitors, *Biochim Biophys Acta.* **185**, 269-86.
63. Henderson, P. J. (1972) A linear equation that describes the steady-state kinetics of enzymes and subcellular particles interacting with tightly bound inhibitors, *Biochem J.* **127**, 321-33.
64. Woessner, J. F., Jr. & Nagase, H. (2000) *Matrix metalloproteinases and TIMPs*, Oxford Univeristy Press, Oxford.
65. Bu, C. H. & Pourmotabbed, T. (1996) Mechanism of Ca2+-dependent activity of human neutrophil gelatinase B, *J Biol Chem.* **271**, 14308-15.
66. Kolset, S. O., Mann, D. M., Uhlin-Hansen, L., Winberg, J. O. & Ruoslahti, E. (1996) Serglycin-binding proteins in activated macrophages and platelets, *J Leukoc Biol.* **59**, 545-54.
67. Burgess, J. K. & Weckmann, M. (2012) Matrikines and the lungs, *Pharmacol Ther.* **134**, 317-37.
68. Ricard-Blum, S. & Vallet, S. D. (2016) Proteases decode the extracellular matrix cryptome, *Biochimie.* **122**, 300-13.

69. Rosenblum, G., Van den Steen, P. E., Cohen, S. R., Grossmann, J. G., Frenkel, J., Sertchook, R., Slack, N., Strange, R. W., Opdenakker, G. & Sagi, I. (2007) Insights into the structure and domain flexibility of full-length pro-matrix metalloproteinase-9/gelatinase B, *Structure.* **15**, 1227-36.
70. Farr, M., Pieper, M., Calvete, J. & Tschesche, H. (1999) The N-terminus of collagenase MMP-8 determines superactivity and inhibition: a relation of structure and function analyzed by biomolecular interaction analysis, *Biochemistry.* **38**, 7332-8.
71. Knauper, V., Wilhelm, S. M., Seperack, P. K., DeClerck, Y. A., Langley, K. E., Osthues, A. & Tschesche, H. (1993) Direct activation of human neutrophil procollagenase by recombinant stromelysin, *Biochem J.* **295 (Pt 2)**, 581-6.
72. Suzuki, K., Enghild, J. J., Morodomi, T., Salvesen, G. & Nagase, H. (1990) Mechanisms of activation of tissue procollagenase by matrix metalloproteinase 3 (stromelysin), *Biochemistry.* **29**, 10261-70.
73. Allan, J. A., Docherty, A. J., Barker, P. J., Huskisson, N. S., Reynolds, J. J. & Murphy, G. (1995) Binding of gelatinases A and B to type-I collagen and other matrix components, *Biochem J.* **309 (Pt 1)**, 299-306.
74. Collier, I. E., Krasnov, P. A., Strongin, A. Y., Birkedal-Hansen, H. & Goldberg, G. I. (1992) Alanine scanning mutagenesis and functional analysis of the fibronectin-like collagen-binding domain from human 92-kDa type IV collagenase, *J Biol Chem.* **267**, 6776-81.
75. Strongin, A. Y., Collier, I. E., Krasnov, P. A., Genrich, L. T., Marmer, B. L. & Goldberg, G. I. (1993) Human 92 kDa type IV collagenase: functional analysis of fibronectin and carboxyl-end domains, *Kidney Int.* **43**, 158-62.
76. Xu, X., Chen, Z., Wang, Y., Yamada, Y. & Steffensen, B. (2005) Functional basis for the overlap in ligand interactions and substrate specificities of matrix metalloproteinases-9 and -2, *Biochem J.* **392**, 127-34.

Figure Legends

Fig. 1. Real-time gelatin zymography of pro- and activated MMP-9 variants. Shown is both trypsin (T) and APMA (A) activated full length rMMP-9 (rMMP-9(A), rMMP-9(T), rMMP-9 deletion variants lacking the HPX domain (rMMP-9ΔHPX(A)) and the OG and HPX domains (rMMP-9ΔOGHPX(T) along with their unactivated proforms (rpMMP-9, rpMMP-9ΔHPX and rpMMP-9ΔOGHPX). Std. 1 is the 24 kDa trypsin, Std. 2 is the 37 kDa catalytic domain of human MMP-9 and std. 3 is a mixture of proMMP-9 from THP-1 cells (92 kDa pro and 83 kDa active) and proMMP-2 from human skin fibroblasts (72 kDa pro and 62 kDa active). The line under the figures indicate that it is from the same gel. Gel in (**A**) was incubated for 2.5 hr at 37 °C and gel in (**B**) for 2 hr at 37 °C.

Fig. 2. Active-site titration and K_i determination of galardin with three active recombinant MMP-9 variants. The concentration of active MMP-9 in the assays ($[E]_{assay}$) and the inhibition constant K_i for galardin (Gm6001) were obtained from dose response plots v_i/v_0 vs [Gm6001] using the Morrison eq. (1) (**A**, **C**, **E**) and Henderson plots eq. (2) (**B**, **D**, **F**) of trypsin-activated full length MMP-9 (rMMP-9(T) (**A, B**), APMA- and trypsin-activated deletion variants rMMP-9ΔHPX(A) (**C, D**) and rMMP-9ΔOGHPX (**E, F**). Shown in the figures is also the obtained $[E]_{assay}$ and K_i values (mean ± SD) in addition to the regression coefficient r^2 and the number of individual assays (N) for each curve.

Fig. 3. Amino acid sequence of human SG. Shown is the SG sequence starting with the 27 amino acid long predomain (underlined) and the numbering starts with the first amino acid of the predomain. Shown above the predomain is the 25 amino acid long His-tag (underlined) that replaces the predomain in the His-tag SG produced in E-Coli.

Fig. 4: Degradation of Ht-SG by activated recombinant full-length proMMP-9. (**A**) Three µg of Ht-SG in 3 µl 0.1 M Hepes buffer pH 7.5 was mixed with either 7 µl buffer or 7 µl APMA activated rMMP-9 (~50 nM in assay) and incubated at 37 °C at different time points as described in the figure. Samples were applied to SDS-PAGE and after electrophoresis was the gel stained with Imperial protein stain. Western blot using a

polyclonal antibody against entire SG core protein (amino acids 28-158) (**B**, **D**) and a polyclonal antibody against C-terminal part (amino acids 118-148) of SG (**C**). (**B, C**) 248 ng Ht-SG in 9 µl 0.1 M Hepes buffer pH 7.5 was mixed with either 13 µl buffer (-) or 13 µl APMA activated MMP-9 (~50 nM in assay). (**D**) 200 ng Ht-SG in 2 µl 0.1 M Hepes buffer pH 7.5 was mixed with either 6 µl buffer or 6 µl APMA activated MMP-9 (~50 nM in assay) and incubated at 37 °C at different time points as described in the figure. The enzyme activity was stopped by adding 1 µl 100 mM EDTA. Thereafter, samples were added to Talon beads added as described in Materials and Methods. In **C-D**, 100 ng of Ht-SG was loaded to each lane. St.1 is the SeeBlue prestained protein standard, St.2 is the biotinylated protein ladder and St.3 is the Spectra^{TM} multicolor low range protein ladder.

Fig. 5. Effect of galardin (Gm6001) on MMP-9 cleavage of Ht-SG. Three µg of Ht-SG in 3 µl 0.1 M Hepes buffer pH 7.5 was mixed with either 6 µl 0.1 M Hepes buffer pH 7.5 or 6 µl APMA activated recombinant full length MMP-9 (~50 nM in assay). (**A**) Before adding enzyme to SG, either 1 µl buffer pH 7.5, 1 µl 2.5 mM EDTA or 1 µl 5.0 µM Gm6001 was added to SG. Total assay volume is 10 ul and the different mixtures were incubated at 37 ºC for the time points shown in the figure. In (**B**), MMP-9 was allowed to degrade Ht-SG for 15 min at 37 ºC. After that, one batch was added directly to sample buffer for SDS-PAGE analysis, and two other batches were either mixed with 1 µl buffer or 1 µl 5.0 µM Gm6001 and further incubated for 180 min as shown in the figure. St is the Spectra^{TM} multicolor low range protein ladder. Gels were stained with Imperial protein stain.

Fig. 6. Degradation of SG by activated recombinant full-length proMMP-9. (**A, B**) Ten µg of SG purified from THP-1 cells in 5 µl of 0.1 M Hepes buffer pH 7.5 was mixed with either 6 µl buffer (control (-)) or 6 µl APMA-activated recombinant MMP-9 (+) (~50 nM in assay) and incubated for different time points at 37 ºC. Enzyme activity was stopped with 20 mM EDTA. In (**B**), all samples were treated with cABC prior to loading on SDS-PAGE gels followed by Western blotting. In (**C**), all samples were treated with cABC prior to treatment with MMP-9. In (**D, E**), 0.43 µg of CSPG/SG isolated from THP-1 cells in 6 µl of 0.1 M Hepes buffer was mixed with either 8 µl buffer (control (-)) or 8 µl of APMA-activated MMP-9 (+) (~50 nM in assay). The mixture of CSPG/SG with MMP-9 was incubated for various time points at 37 ºC and the reaction was stopped by the addition of 1 µl of 0.25 M EDTA. All

samples were treated with cABC, followed by SDS-PAGE and Western blotting. The antibodies used was a rabbit polyclonal antibody against the entire recombinant human SG core protein (amino acids 28 – 158) (**A-D**) and a rabbit polyclonal antibody against a recombinant C-terminal peptide of SG (amino acids 118 – 148) (**E**). St is the biotinylated protein ladder and sb is sample buffer.

Fig. 7. Degradation of Ht-SG by APMA activated recombinant full-length proMMP-9 and trypsin activated MMP-9 isolated from THP-1 cells. Three µg of Ht-SG in 3 µl 0.1 M Hepes buffer pH 7.5 was mixed with either 12 µl buffer (-) or 12 µl trypsin-activated MMP-9 (+) or 10.8 µl buffer pH 7.5 and 1.2 µl APMA activated rMMP-9 (+). These mixtures were incubated for different time points at 37 °C as indicated in (**A** and **B**). The amount of active enzyme in the assays were similar, ~18 nM of both enzymes. The enzymatic reaction was stopped by adding 2.7 µl SDS-sample buffer containing 0.1 M DTT. The gels were stained by Imperial protein stain as described in Materials and Methods. St.1 is the Spectra^{TM} multicolor low range protein ladder and St.2 is the SeeBlue prestained protein standard.

Fig. 8. Degradation of Ht-SG by MMP-9 deletion variants. 250 ng Ht-SG in 3 µl 0.1 M Hepes buffer pH 7.5 was mixed with either 7 µl buffer or 7 µl trypsin-activated full-length rMMP-9 (rMMP-9(T)), APMA-activated rMMP-9ΔHPX (rMMP-9ΔHPX(A)) or trypsin-activate rMMP-9ΔOGHPX (rMMP-9ΔOGHPX(T)). This gave an assay concentration of the various MMP-9 variants of 50 nM based on active site titration. The mixture of enzymes and Ht-SG was incubated at 37 °C for various time points as described in the figure. The enzyme activity was stopped by adding 6 µl 1.3 µM galardin. Samples were applied to SDS-PAGE and after electrophoresis, the gel were applied to Western blot using the polyclonal antibody against the entire SG core protein (amino acids 28-158). St is the biotinylated protein ladder.

Fig. 9. Effect of DMSO on rMMP-9 cleavage of Ht-SG. Two µg Ht-SG in 2 µl 0.1 M Hepes buffer was mixed with either 8 µl buffer, or 3 µl APMA-activated full-length rMMP-9 (25 nM in assay) and 3 µl buffer containing no or different [DMSO]. The [DMSO] in the assays and the incubation time of the assay mixtures are shown in the figure. The enzymatic reaction was stopped by mixing samples with sample buffer and applied to SDS-PAGE. Gels were stained

with Imperial protein staine as described on Materials and Methods. St.1 is the Spectra^{TM} multicolor low range protein ladder.

Fig. 1

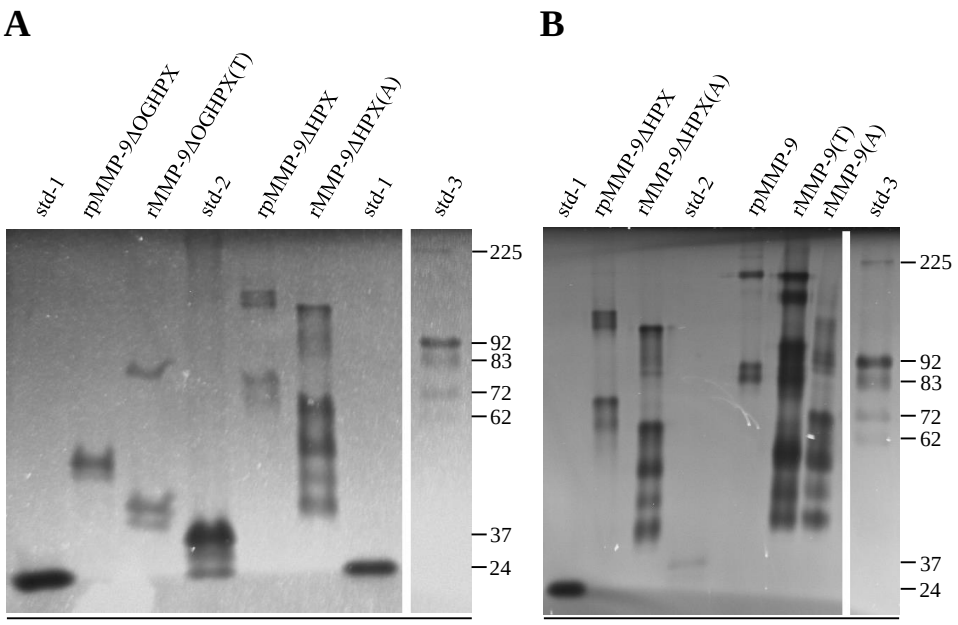
A
std-1
rpMMP-9ΔOGHPX
rMMP-9ΔOGHPX(T)
std-2
rpMMP-9ΔHPX
rMMP-9ΔHPX(A)
std-1
std-3
225
92
83
72
62
37
24
B
std-1
rpMMP-9ΔHPX
rMMP-9ΔHPX(A)
std-2
rpMMP-9
rMMP-9(T)
rMMP-9(A)
std-3
225
92
83
72
62
37
24

Fig. 2

rMMP-9(T)

A

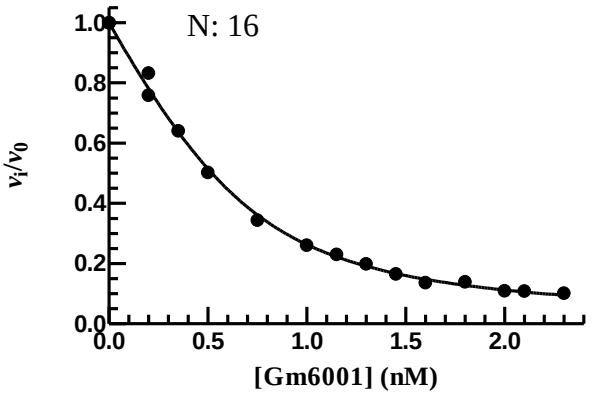

B

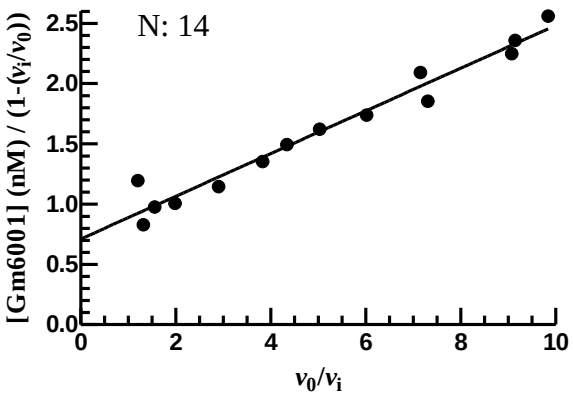

rMMP-9ΔHPX(A)

C

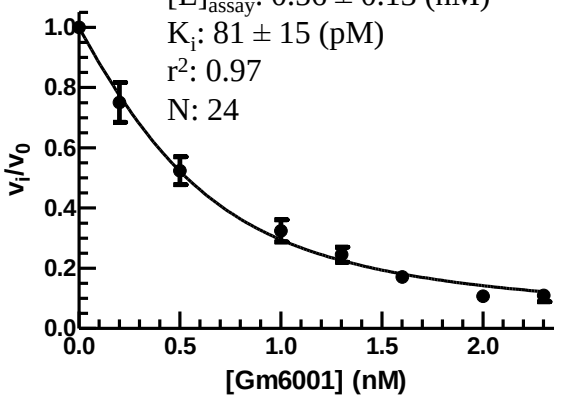

D

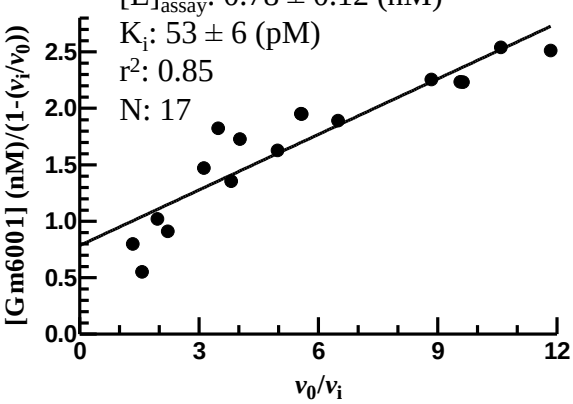

rMMP-9ΔOGHPX(T)

E

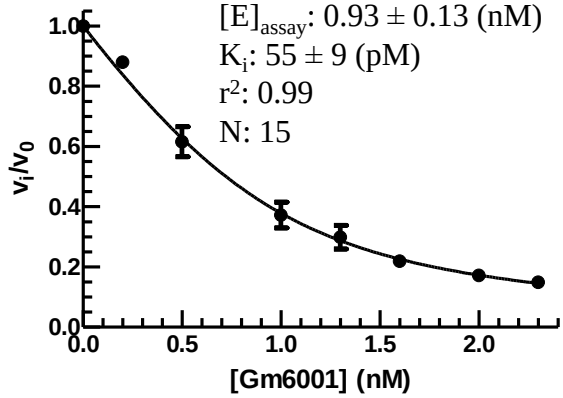

F

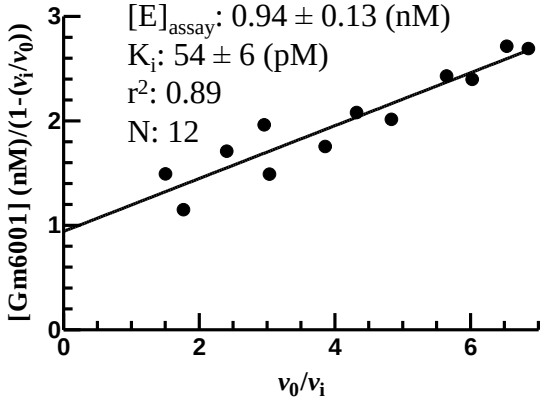

Fig. 3

```
                  10                  20
MGSSHHHHHH SSGLVPRGSH MGSHM

                  10                  20                  30                  40                  50
MMQKLLKCSR LVLALALILV LESSVQGYPT RRARYQWVRC NPDSNSANCL

                  60                  70                  80                  90                 100
EEKGPMFELL PGESNKIPRL RTDLFPKTRI QDLNRIFPLS EDYSGSGFGS

                 110                 120                 130                 140                 150
GSGSGSGSGS GFLTEMEQDY QLVDESDAFH DNLRSLDRNL PSDSQDLGQH

                 158
GLEEDFML
```

Fig. 4

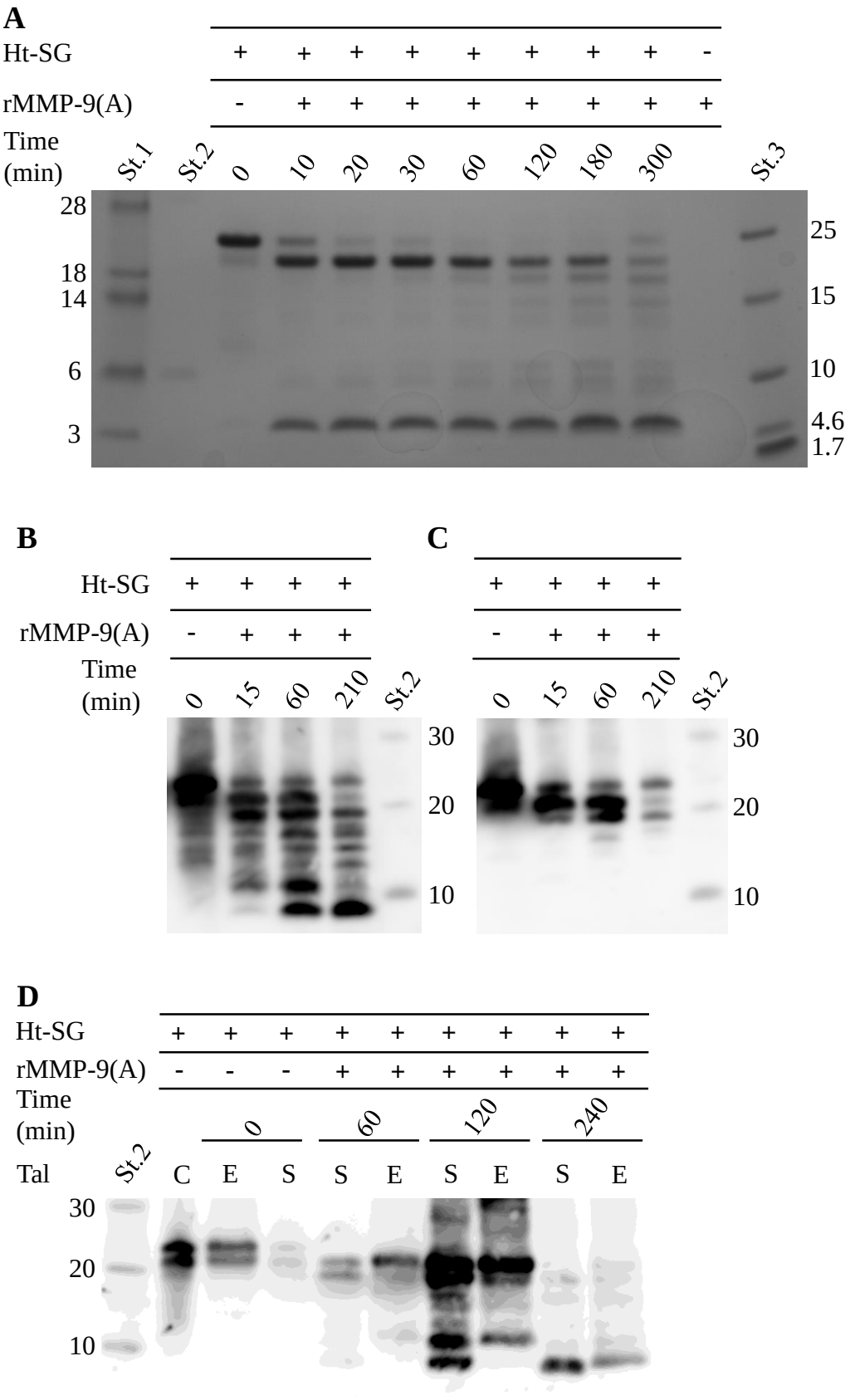
A
Ht-SG
rMMP-9(A)
Time (min)
St.1
St.2
0
10
20
30
60
120
180
300
St.3
28
18
14
6
3
25
15
10
4.6
1.7
B
C
Ht-SG
rMMP-9(A)
Time (min)
0
15
60
210
St.2
30
20
10
D
Ht-SG
rMMP-9(A)
Time (min)
0
60
120
240
Tal
St.2
C
E
S
30
20
10

Fig. 5

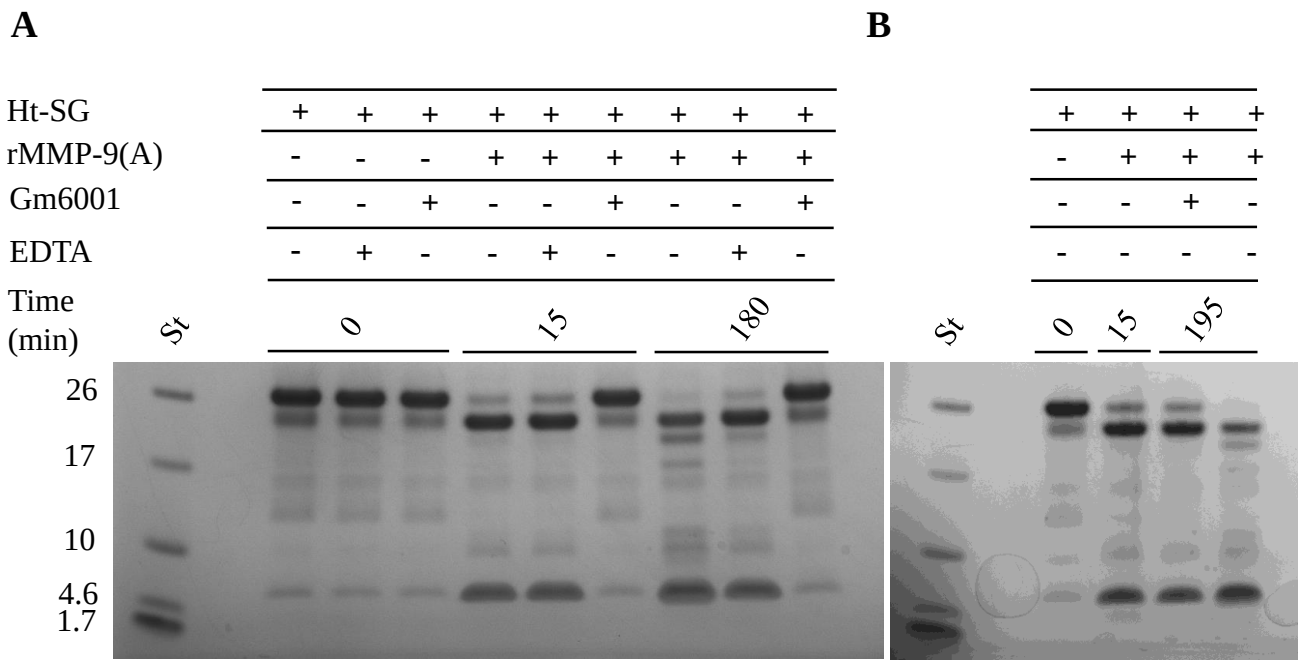
A
B
Ht-SG
rMMP-9(A)
Gm6001
EDTA
Time (min)
St
0
15
180
195
26
17
10
4.6
1.7

Fig. 6

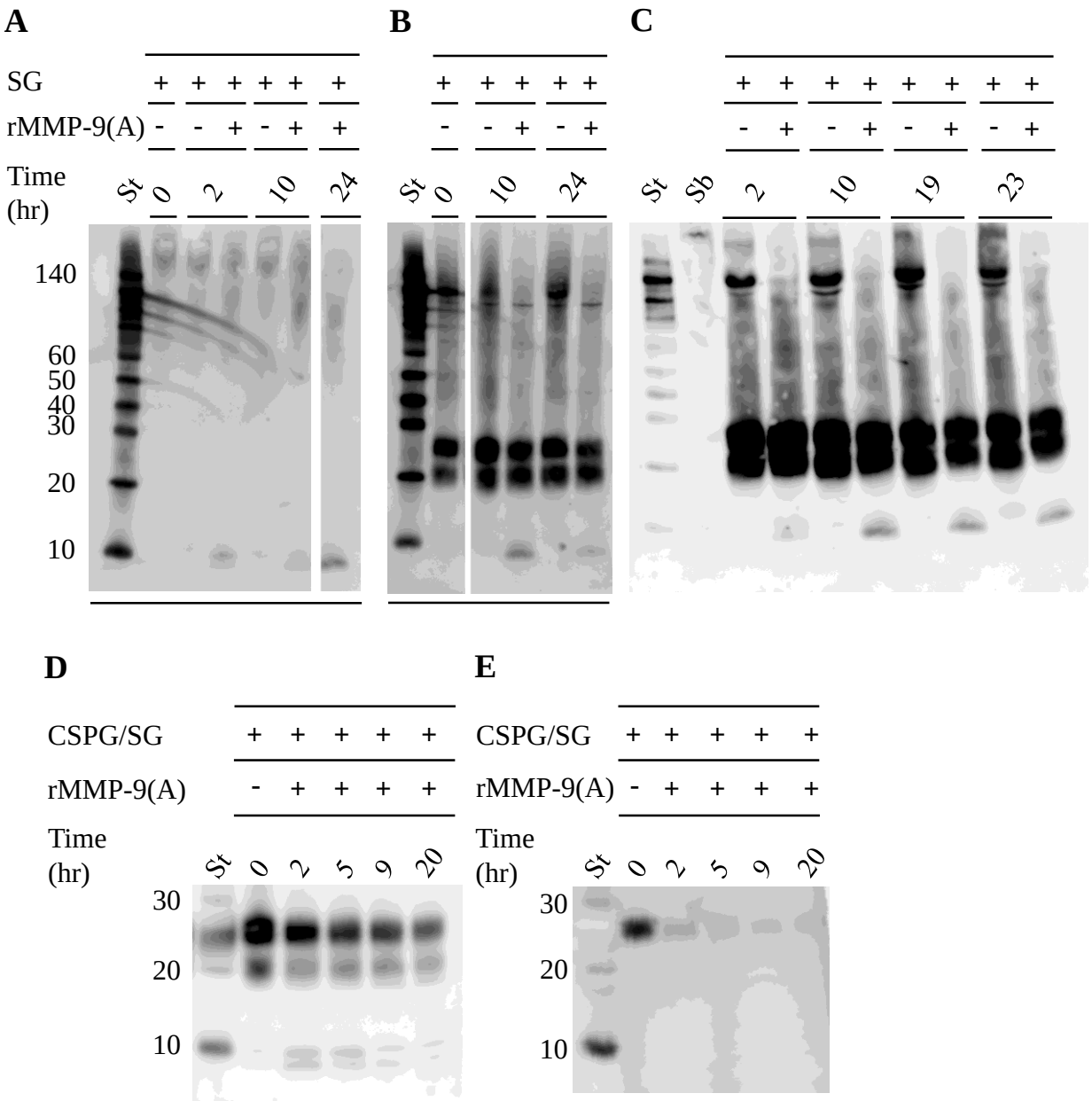
A
B
C
SG
rMMP-9(A)
Time (hr)
St
0
2
10
24
Sb
19
23
140
60
50
40
30
20
10
D
E
CSPG/SG
rMMP-9(A)
Time (hr)
5
9

Fig. 7

A

Ht-SG	+	+	+	+	+	+	+
MMP-9 (T)	-	+	+	+	-	-	-
rMMP-9 (A)	-	-	-	-	+	+	+
Time (h)	St.1	0	1	6.3	18	1	6.3	18

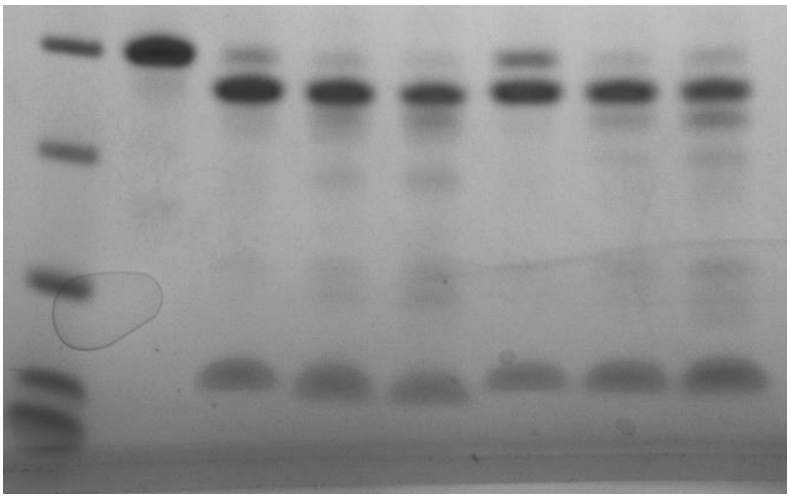

B

Ht-SG	+	+	+	+	+	+	+	
MMP-9 (T)	-	+	+	+	-	-	-	
rMMP-9 (A)	-	-	-	-	+	+	+	
Time (h)	St.1	0	1	20	24	1	20	24	St.2

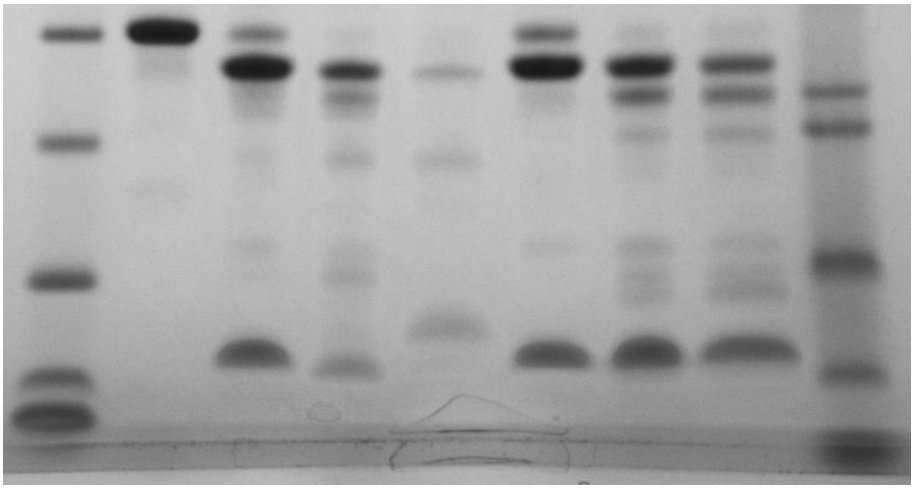

Fig. 8

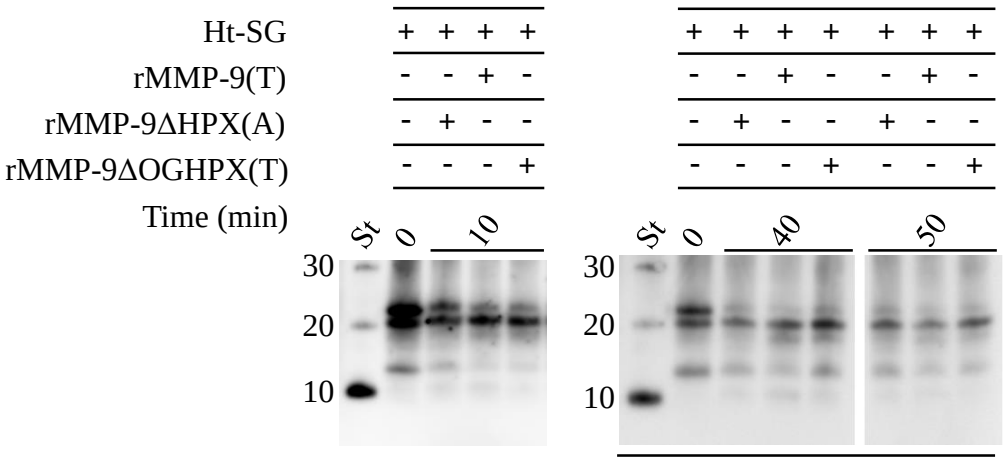
Ht-SG
rMMP-9(T)
rMMP-9ΔHPX(A)
rMMP-9ΔOGHPX(T)
Time (min)
St
0
10
40
50
30
20
10

Fig. 9

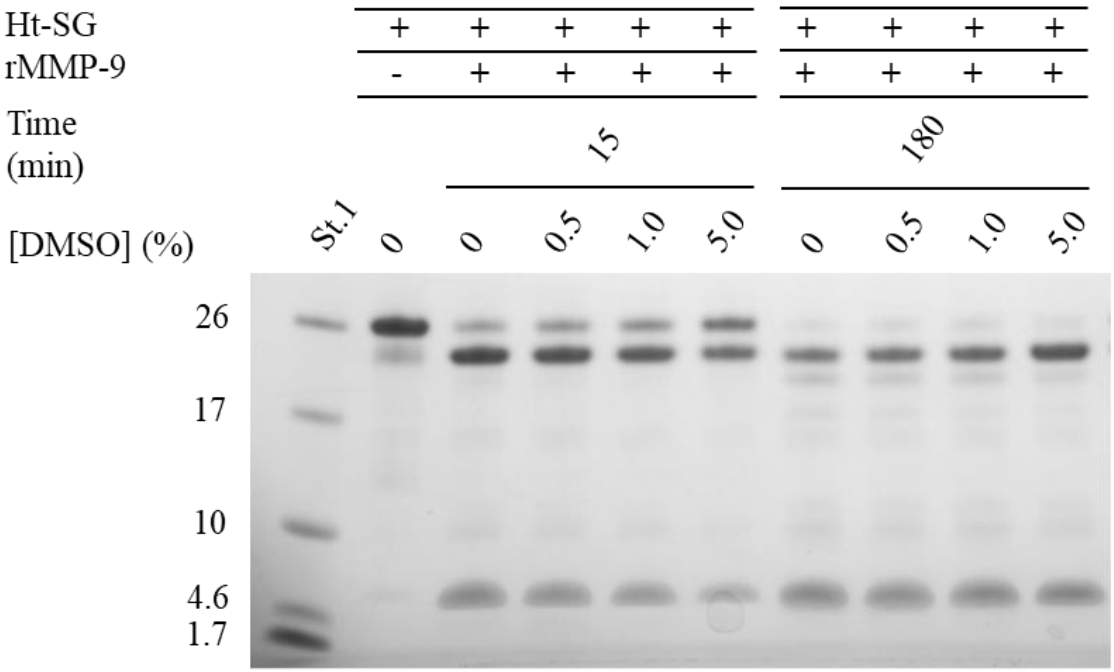
Ht-SG
rMMP-9
Time (min)
[DMSO] (%)
St.1
0
0
0.5
1.0
5.0
0
0.5
1.0
5.0
15
180
26
17
10
4.6
1.7